Sequence-Controlled Polymers via Thiol-ene Step-Growth Polymerization of Precision Macromonomers

Inaugural dissertation

for the attainment of the title of doctor
in the Faculty of Mathematics and Natural Sciences
at the Heinrich-Heine-University Düsseldorf

presented by

Christoph Gerke

from Uslar

Düsseldorf, August 2018

from the Institute of Organic Chemistry and Macromolecular Chemistry
at the Heinrich-Heine-University Düsseldorf

Published by permission of the
Faculty of Mathematics and Natural Sciences at
Heinrich-Heine-University Düsseldorf

Supervisor: Prof. Dr. Laura Hartmann
Co-supervisor: Priv.-Doz. Dr. Klaus Schaper

Date of the oral examination: 25.02.2019

Declaration of authorship

I hereby declare that the thesis submitted is my own work without making use of impermissible aids, considering the "Rules on the Principles for Safeguarding Good Scientific Practice at Heinrich-Heine University Düsseldorf". All direct or indirect sources used are acknowledged in the bibliography as references. I further declare that I have not submitted this nor a similar thesis at any other examination board in order to obtain a degree.

Düsseldorf, the 29th of August 2018

_____

(Christoph Gerke)

Table of contents

Summary

The inspiration from Nature's perfection of complex macromolecules subsequently resulting in a specific function led to a pursuit of precision in artificial materials, opening the field of well-defined polymers. Biopolymers with a specific function in the living organism, such as proteins or DNA, are high molecular weight compounds which are monodisperse with a precise monomer sequence. Despite the challenges, a variety of new synthetic approaches have been developed within the last decades to synthesize well-defined polymers with either a narrow molecular weight distribution, a controlled primary structure, or even both. Whereas many approaches show high control over molecular weight distribution, the control over monomer arrangement is often only achieved to a certain extent, obtaining multiblock, alternating or gradient copolymers. Most powerful approaches towards polymers with an exact monomer arrangement are based on the multistep-growth approach, applying a stepwise coupling of single monomer units onto a supporting material, which was first introduced for the synthesis of peptides by Merrifield. However, the final molecular weight of the assembled compound is significantly below the reached molecular weight using other chain- or step-growth polymerization methods.

In this thesis, a synthetic approach is presented to further increase the molecular weight of oligoamides with a precise monomer sequence derived from a multistep-growth assembly on a solid support (solid phase synthesis (SPS)) by their subsequent polymerization. The polymerization is realized using a photoinduced thiol-ene click (TEC) coupling reaction by functionalizing the defined macromonomers from SPS with terminal thiol and alkene moieties. Applying UV irradiation, the telechelic macromonomers are subsequently polymerized in step-growth fashion. Thereby, the defined sequences from the macromonomers are translated into the final sequence of the resulting high molecular weight polymers, realizing a new class of sequence-controlled polymers.

As monomer units in SPS, so-called building blocks are used which, similar to amino acids for solid phase peptide synthesis, contain an Fmoc-protected amine as well as a carboxylic acid group which allow for their iterative assembly (see **Figure 1A**). A library of different building blocks was successfully developed in previous studies, giving the possibility to specifically tune the backbone properties, the architecture as well as to introduce specific bioactive binding motifs in the side chain. As binding motifs, especially carbohydrates are of interest, allowing for the synthesis of well-defined glycomimetics for the investigation of carbohydrate – protein interactions.

In the first part of this thesis, two sequence-defined oligoamides derived from SPS, one containing two terminal thiol moieties and the other two terminal alkene moieties, were polymerized by TEC. Using this AA/BB approach, the two macromonomers are assembled in a strictly alternating fashion, therefore forming a multiblock copolymer (see **Figure 1B**). Special focus was devoted to the determination of optimal reaction conditions, reaching highest possible degrees of polymerization ($\bar{X}_n$) by changing different reaction parameters.

The optimized polymerization procedure was subsequently applied to polymerize four sequence-defined glycomacromonomers, carrying between one and five α-D-mannopyranoside (Man) moieties in their side-chain, with a hydrophilic spacing macromonomer, not presenting binding ligands. The achieved glycopolymers as well as the glycomacromolecules were applied in clustering and binding studies towards the Man-recognizing protein Concanavalin A (Con A) to obtain insights in multivalent binding mechanisms, especially in the effect of carbohydrate spacing introduced by the hydrophilic spacing macromonomer. With the first set of glycopolymers as well as macromonomers, only a strong correlation between Man valency and no influence of the Man spacing or the overall molecular weight on the Con A clustering or binding was observed.

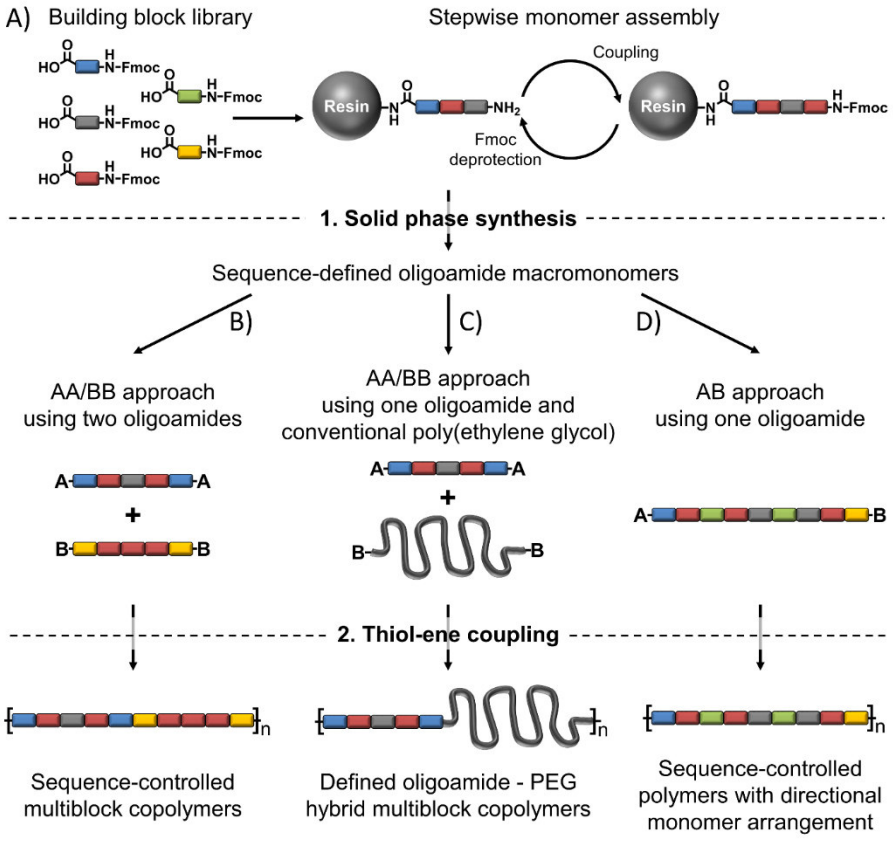

Figure 1: Schematic overview of different synthetic approaches towards sequence-controlled polymers using monodisperse precision macromonomers derived from solid phase synthesis. Showing in A) the concept of a stepwise monomer assembly by solid phase synthesis using tailor-made building blocks, B) an AA/BB approach using two homofunctionalized macromonomers, C) an AA/BB approach using one homofunctionalized macromonomer as well as a homofunctionalized poly(ethylene glycol), D) an AB approach using one heterofunctionalized macromonomer.

In the second part, the concept of subsequently polymerizing macromonomers derived from SPS via TEC in a step-growth polymerization was extended, aiming to further increase the molecular weights of the glycopolymers. Therefore, a more reactive alkene moiety for photoinduced TEC coupling as well as a dithiol-poly(ethylene glycol) ($PEG(SH)_2$-6000) with a number average molecular weight ($\bar{M}_n$) of 6000 Da as second macromonomer were introduced (see **Figure 1C**), successfully increasing $\bar{X}_n$ and $\bar{M}_n$ of the final glycopolymers. Besides that, an additional motivation using the $PEG(SH)_2$-6000 was to further increase the spacing between the Man binding motifs since so far no influence on Con A binding was observed when using the hydrophilic spacing blocks.

Five glycomacromonomers carrying between one and three Man moieties as well as different spacing between the carbohydrates were synthesized via SPS. After their polymerization and a series of purification procedures a total of 12 different glyco(oligoamide) – PEG multiblock copolymers were obtained which were again subjected to Con A binding assays. Although the glyco(oligoamide) – PEG multiblock copolymers presented a higher amount of Man moieties in comparison to most sequence-controlled glycopolymers from the first series, significantly weaker binding affinities to Con A were observed, which can be attributed to the high molecular weight PEG block.

The third part focused on the synthesis of periodic sequence-controlled polymers with a regularly recurring monomer sequence in one direction along the polymeric backbone using an AB approach by polymerizing one heterofunctionalized macromonomer in step-growth fashion performing TEC (see **Figure 1D**). Due to self-initiation of monomers presenting both, a thiol as well as an alkene moiety, an AB approach was so far not successful, and therefore the polymerization was limited to the use of two symmetrical, homofunctionalized monomers which do not exhibit a directional controlled incorporation into the final polymer. An uncontrolled polymerization was successfully prevented by the introduction of a nitrobenzyl based photolabile protecting group which was coupled to the reactive thiol moiety. The final thiol-protected, heterofunctionalized macromonomer was polymerized in a two-step approach, first removing the protecting group and thereby liberating the reactive thiol moiety followed by its polymerization resulting in a periodic copolymer with a directional monomer sequence along the polymeric backbone.

Overall, a novel synthetic approach based on a combination of SPS and TEC step-growth polymerization towards sequence-controlled polymers was developed, thereby contributing in the field of well-defined polymers. The approach ensures control over the final polymer sequence in two levels: first, during the precise monomer arrangement in SPS and second during the specific linkage in the step-growth assembly of the defined macromonomers. The here presented novel class of sequence-controlled polymers can give, in addition to the stated glycomimetics, access to a broad range of bioactive or biomimetic polymers since a large variety of biological relevant motifs can be introduced into the macromonomer sequence via SPS. Furthermore, the TEC polymerization method tolerates various functional groups and solvents, thereby further emphasizing its great potential for application, due to only a few limitations of the polymerized macromonomers regarding their chemical nature. Besides the synthetic aspect, further insights about the effect of Man density and spacing as well as the overall molecular weight of glycomimetics towards the interaction with Con A were obtained, thereby contributing in the elucidation of specific binding mechanisms during multivalent carbohydrate – protein interactions.

Zusammenfassung

Die Natur dient oftmals als Vorbild für innovativen Fortschritt in vielen Bereichen der Technik, Architektur und Naturwissenschaft. Inspiriert durch komplexe, natürliche Makromoleküle, die eine spezifische Funktion erfüllen, entwickelte sich ein Streben nach Präzision in synthetischen Materialien, was schließlich zur Etablierung des Forschungsgebiets der wohldefinierten Polymere führte. Biopolymere, die als Vorbild dienen, wie zum Beispiel Proteine und DNA, sind hochmolekulare aber monodisperse Strukturen mit einer präzisen Monomeranordnung. Trotz der synthetisch anspruchsvollen Aufgabe wurde in den letzten Jahrzehnten eine Vielzahl von Synthesemethoden zur Herstellung wohldefinierter Polymere, mit einer engen Molmassenverteilung, einer definierten Monomersequenz, oder sogar beiden, entwickelt. Während mit vielen Methoden eine enge Molmassenverteilung erzielt werden kann, ist die Kontrolle der Primärstruktur oft nur zu einem geringen Maß möglich. Mit konventionellen Polymerisationsmethoden sind unter anderem Multiblock-, Alternierende- oder Gradient-Copolymere zugänglich, welche bei weitem nicht die Komplexität der natürlichen Vorbilder erreichen. Die geeignetsten Methoden zur Synthese von Polymeren mit einer definierten Monomersequenz basieren auf mehrstufigen Wachstumsreaktionen, bei denen Monomereinheiten separat an ein Trägermaterial gekuppelt werden. Mit dieser von Merrifield erstmals zur Herstellung von Peptiden entwickelten Methode kann allerdings nur ein, im Vergleich zu andren geläufigen Ketten- oder Stufenwachstumsreaktionen, niedriges Molekulargewicht erreicht werden.

In dieser Dissertation wird ein Syntheseansatz zur Steigerung des Molekulargewichts von sequenzdefinierten Oligoamiden, die mittels einer mehrstufigen Wachstumsreaktion (Festphasensynthese) hergestellt werden, präsentiert, indem sie in einer anschließenden Reaktion weiter polymerisiert werden. Als Polymerisationsmethode wird eine photoinduzierte Thiol-En Kupplung gewählt, bei der durch UV Bestrahlung die terminal mit Thiol oder Alken Gruppen funktionalisierten telechelen Oligoamide in einer Stufenwachstumsreaktion weiter verknüpft werden. Bei der Polymerisation wird die definierte Monomersequenz des Oligoamids in die finale Sequenz des hochmolekularen Polymers übertragen, wodurch eine neue Klasse von sequenzkontrollierten Polymeren geschaffen wird.

Während der Festphasensynthese werden sogenannte Bausteine als Monomereinheiten verwendet, welche, ähnlich zu den Aminosäuren in der Festphasen-Peptidsynthese, ein Fmoc-geschütztes Amin und eine Carbonsäure tragen und somit iterativ gekuppelt werden können (siehe **Abbildung 1A**). In vorherigen Projekten wurde erfolgreich eine Bibliothek von verschiedenen Bausteinen erstellt, welche es ermöglicht die Eigenschaften des Polymerrückrads, die Architektur der Oligoamide, oder die Anbringung verschiedener bioaktiver Liganden in der Haupt- oder Seitenkette gezielt zu steuern. Zur Herstellung sequenzdefinierter Glykomimetika können beispielsweise Kohlenhydrate als mögliche bioaktive Liganden in die Oligoamid-Struktur eingebracht werden, welche anschließend zur Untersuchung von Kohlenhydrat – Protein Wechselwirkung eingesetzt werden können.

In dem ersten Teil der Dissertation wurden zwei mittels Festphasensynthese hergestellte sequenzdefinierte Oligoamide, eins mit terminalen Thiolen und das andere mit terminalen Alken Gruppen, durch eine Thiol-En Stufenwachstumsreaktion polymerisiert. Durch den AA/BB Ansatz werden die beiden telechelen Makromonomere streng alternierend miteinander verknüpft, wodurch sich ein Multiblock-Copolymer bildet (siehe **Abbildung 1B**). Der Fokus des ersten Teils lag auf der Bestimmung optimaler Reaktionsbedingungen, indem verschiedene Reaktionsparameter variiert wurden, um einen höchstmöglichen Polymerisationsgrad ($\bar{X}_n$) zu erreichen.

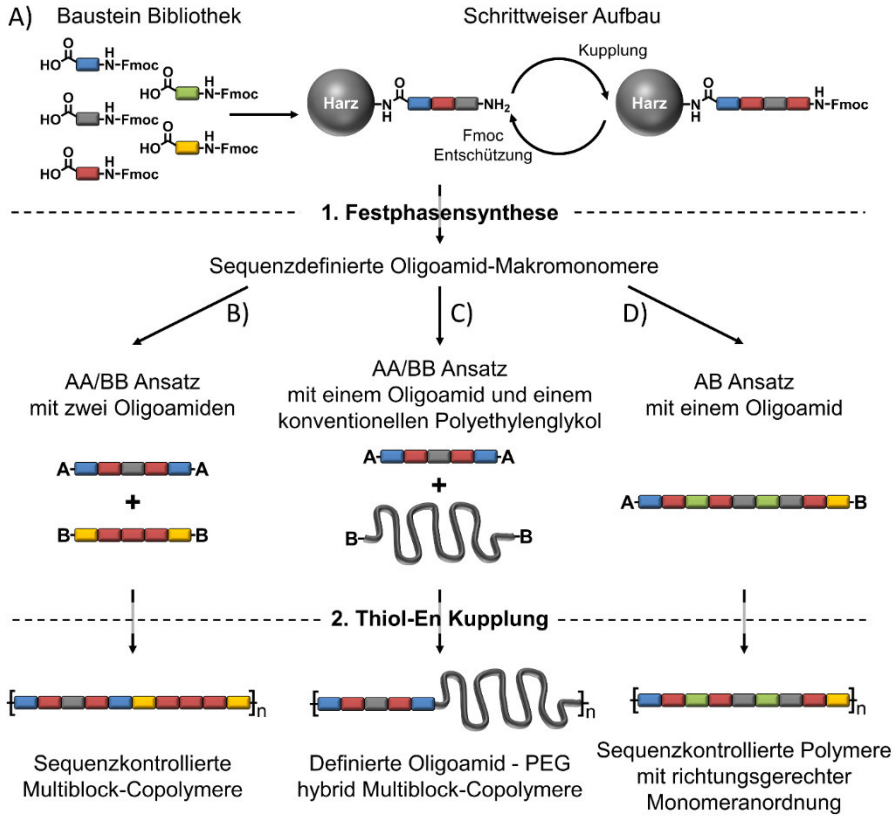

Abbildung 1: Schematische Übersicht der synthetischen Ansätze zur Herstellung von sequenzkontrollierten Polymeren durch die Polymerisation monodisperser Präzisionsmakromonomere, gewonnen mittels Festphasensynthese. Dargestellt in A) das Konzept des schrittweisen Aufbaus eines Oligoamids an einer Festphase unter Verwendung von selbst hergestellten Bausteinen, B) einen AA/BB Ansatz mit zwei homofunktionalisierten Makromonomeren, C) einen AA/BB Ansatz mit einem homofunktionalisierten Makromonomer und einem homofunktionalisierten Polyethylenglykol, D) einen AB Ansatz mit einem heterofunktionalisierten Makromonomer.

Die optimierte Polymerisationsmethode wurde anschließend zur Polymerisation von vier sequenzdefinierten Glykomakromonomeren, die zwischen einem und fünf α-D-Mannopyranose (Man) Liganden in deren Seitenketten tragen, angewendet. Um einen Abstand zwischen den Man Liganden einzuführen wurden die Glykomakromonomere jeweils mit einem hydrophilen, unfunktionalisierten Makromonomer copolymerisiert. Die hergestellten Glykopolymere, wie auch die Glykomakromonomere, wurden anschließend in Rezeptor-Clustering und Rezeptor-Bindungsstudien mit dem Man-spezifischen Lektin Concanavalin A (Con A) getestet und somit die multivalenten Bindungsmechanismen von Kohlenhydrat – Lektin Wechselwirkungen studiert. Besonderes Interesse lag auf der Untersuchung des Einflusses des Abstands zwischen den bindenden Man Liganden, welcher durch das hydrophile, unfunktionalisierte Makromonomer eingeführt wurde.

Mit der ersten Reihe von Glykopolymeren und Glykomakromonomeren wurde lediglich eine starke Korrelation zwischen der Man Valenz und kein Einfluss des Man Abstands oder des Molekulargewichts der Liganden auf Con A Clustering oder Bindung beobachtet.

In dem zweiten Teil der Dissertation wurde das entwickelte Konzept der anschließenden Thiol-En Stufenwachstumsreaktion von Makromonomeren, die mittels Festphasensynthese hergestellt wurden, erweitert. Dabei wurde besonders eine weitere Steigerung der zuvor erzielten Molekulargewichte der Glykopolymere angestrebt. Aus diesem Grund wurde zum einen eine reaktivere Alken Endgruppe für photoinduzierte Thiol-En Kupplung und zum anderen ein Polyethylenglykol-dithiol (PEG$(SH)_2$-6000) mit einer zahlenmittleren Molmasse ($\bar{M}_n$) von 6000 Da als zweites Makromonomer verwendet (siehe **Abbildung 1C**). Durch die beiden Veränderungen wurden erfolgreich der $\bar{X}_n$ wie auch der $\bar{M}_n$ der Glykopolymere weiter erhöht. Ein zusätzlicher Grund für die Verwendung des PEG$(SH)_2$-6000 war die weitere Vergrößerung des Abstands zwischen den Man Liganden, da durch den Abstand des vorher verwendeten hydrophilen Makromonomers kein Einfluss auf die Wechselwirkung mit Con A beobachtet werden konnte. Fünf Glykomakromonomere, die zwischen einem und drei Man Liganden mit unterschiedlichen Abständen zueinander tragen, wurden per Festphasensynthese hergestellt und mit PEG$(SH)_2$-6000 copolymerisiert. Nach der Polymerisation und einer Reihe von Aufreinigungsschritten wurden 12 verschiedene Glyko(oligoamid) – PEG Multiblock-Copolymere erhalten, welche erneut in Wechselwirkungsstudien mit dem Lektin Con A eingesetzt wurden. Trotz deutlich höherer Man Valenzen im Vergleich zu den meisten Glykopolymeren der ersten Reihe, wurden erheblich geringere Bindungsaffinitäten zu Con A bestimmt, was der hochmolekularen PEG Einheit zugeschrieben wurde.

Der dritte und abschließende Teil der Dissertation beschäftigt sich mit der Synthese eines sequenzkontrollierten Polymers mit einer periodisch wiederkehrenden Monomersequenz in eine definierte Richtung entlang des Polymerrückrads. Dazu wurde anstatt eines AA/BB Ansatzes ein AB Ansatz gewählt, bei dem ein heterofunktionalisiertes Makromonomer in einer Thiol-En Stufenwachstumsreaktion polymerisiert wurde (siehe **Abbildung 1D**). Aufgrund der auftretenden Selbstinitiation von heterofunktionalisierten Makromonomeren, die sowohl ein reaktives Thiol als auch ein Alken tragen, war ein AB Ansatz bisher nicht durchführbar. Demzufolge war die Polymerisation lediglich auf symmetrische, homofunktionalisierte Makromonomere limitiert, da ein Einbau in eine definierte Richtung in das Polymerrückrad bei einem AA/BB Ansatz nicht möglich ist. Mit Hilfe einer auf Nitrobenzyl basierenden photolabilen Schutzgruppe, welche an die reaktive Thiol Endgruppe angebracht wurde, konnte eine unkontrollierte Initiation der Polymerisation erfolgreich verhindert werden. Das Thiol-geschützte, heterofunktionalisierte Makromonomer wurde anschließend in einem zweistufigen Prozess polymerisiert, indem zuerst die photolabile Thiol-Schutzgruppe entfernt und anschließend die Makromonomere mit beiden reaktiven Endgruppen miteinander verknüpft wurden, was zu einem periodischen sequenzkontrollierten Polymer mit einer richtungsgerechten Monomersequenz entlang des Polymerrückrads führte.

Im Allgemeinen wurde eine Methode zur Synthese von sequenzkontrollierten Polymeren entwickelt, die Festphasensynthese und eine anschließende Thiol-En Stufenwachstumsreaktion miteinander verbindet, womit eine Beitrag im Bereich der wohldefinierten Polymere geleistet wurde. Mit dem Ansatz kann die Kontrolle über die Monomersequenz auf zwei Ebenen gewährleistet werden: erstens während des präzisen, schrittweisen Aufbaus in der Festphasensynthese und zweitens während der spezifischen Verknüpfung der Makromonomere in der anschließenden Stufenwachstumsreaktion. Die präsentierte neue Klasse von sequenzkontrollierten Polymeren ermöglicht es, zusätzlich zu den hier genannten Glykopolymeren, eine große Reihe bioaktiver oder biomimetischer Polymere zugänglich zu machen, da eine vielfältige Auswahl von biologisch relevanten Motiven während der Festphasensynthese in die Makromonomere eingebracht werden können. Darüber hinaus ist die entwickelte Thiol-En Stufenwachstumsreaktion tolerant gegenüber vielen funktionellen Gruppen und Lösungsmitteln. Diese geringe Limitierung in der chemischen Natur der eingesetzten Makomonomere zeigt das große Potential der vielzähligen Anwendung der Methode auf. Zusätzlich zu den synthetischen Aspekten wurden neue Erkenntnisse bezüglich des Einflusses des Abstands und der Dichte von Man Liganden, sowie des Molekulargewichts von Glykomimetika auf die Wechselwirkungen mit Con A erlangt. Mit den neuen Erkenntnissen wurde zur Aufklärung der spezifischen Mechanismen, die bei multivalenten Kohlenhydrat – Lektin Wechselwirkungen auftreten, beigetragen.

List of publications

Publications included in this thesis

Sequence-Controlled Glycopolymers via Step-Growth Polymerization of Precision Glycomacromolecules for Lectin Receptor Clustering

C. Gerke, M. F. Ebbesen, D. Jansen, S. Boden, T. Freichel and L. Hartmann

Biomacromolecules, **2017**, 18, (3), 787-796

Sequence-Controlled High Molecular Weight Glyco(oligoamide) – PEG Multiblock Copolymers as Ligands and Inhibitors in Lectin Binding

C. Gerke, F. Jacobi, L. E. Goodwin, F. Pieper, S. Schmidt, L. Hartmann

Macromolecules, **2018**, 51, (15), 5608−5619

Enabling Directional Sequence-Control via Step-Growth Polymerization of Heterofunctionalized Precision Macromonomers

C. Gerke, P. Siegfeld, K. Schaper, L. Hartmann

Macromolecular Rapid Communications, **2019**, 40, (3), 1800735

Publications not included in this thesis

Biodegradable poly(amidoamine)s with uniform degradation fragments via sequence-controlled macromonomers

M. F. Ebbesen, C. Gerke, P. Hartwig and L. Hartmann

Polymer Chemistry **2016,** 7, (46), 7086-7093

Recent developments in solid phase strategies towards synthetic, sequence-defined macromolecules

S. A. Hill, C. Gerke and L. Hartmann

Chemistry - An Asian Journal, **2018**, 13, (23), 3611-3622

Multivalent interactions of polyamide based sequence-controlled glycomacromolecules with concanavalin A

A. Camaleño de la Calle, C. Gerke, X. J. Chang, A. Grafmüller, L. Hartmann and S. Schmidt

Submitted in *Macromolecular Bioscience*

Oral and poster presentations:

Sequence-controlled polymeric glycomimetics for the investigation of epitope spacing on multivalent ligand/receptor interactions

C. Gerke, M. F. Ebbesen, D. Jansen, S. Boden, T. Freichel, L. Goodwin, F. Pieper, A. C. de la Calle, S. Schmidt and L. Hartmann

Abstracts of Papers of The American Chemical Society (254th National Meeting & Exposition). PMSE-577. 1155 16TH ST, NW, Washington, DC 20036 USA: Amer Chemical Soc **2017**

From Sequence-Defined Glycooligomers to Multiblock Glycopolymers: Precision Glycopolymers for the Investigation of Multivalent Ligand/Receptor Interactions

C. Gerke, M. F. Ebbesen, D. Jansen, S. Boden, T. Freichel and L. Hartmann

20th European Symposium on Organic Chemistry, **2017**

1 General introduction

Nature! … She is the only artist; working-up the most uniform material into utter opposites; arriving, without a trace of effort, at perfection, at the most exact precision, though always veiled under a certain softness.[1]

– Johann Wolfgang von Goethe –

Nature permanently served as an example for mankind, promoting scientific and technological progress which led to novel functional materials as well as innovative designs in a broad range of industrial fields. Also at a molecular level, Nature continuously inspires scientists especially by precisely constructed macromolecules and their specific physiological function. The defined arrangement of amino acids in proteins results in unique properties such as catalytic properties of enzymes or strong interactions of antibodies with exogenous pathogens, naming just two famous examples. Other properties realized by proteins include antifreeze[2, 3] or fluorescent[4, 5] properties, the formation of structural elements by triggered self-assembly[6, 7] as well as strong adhesion[8, 9] or high toxicity[10, 11]. The inspiration from Nature's perfection of complex macromolecules subsequently resulting in a specific function led to a pursuit of precision in artificial materials, opening the field of well-defined polymers. Whereas Nature achieves complete control over monomer sequence, molecular weight as well as molecular weight distribution for a majority of biopolymers using elegant enzymatic coupling procedures, synthesis of well-defined artificial polymers remains a challenge today but holds the promise of creating new, highly functional materials.[12-14]

1.1 Well-defined polymeric materials: Synthetic strategies

In the field of well-defined polymers, different levels of control are targeted, mainly depending on the required needs of the functional material that is synthesized. In general, the two primary levels of control that are aimed for are a narrow molecular weight distribution and a controlled primary structure (monomer sequence) of the polymer. Different synthetic strategies have been developed in the last decades, ensuring one or even both of these two parameters. Polymers with a controlled monomer sequence but with non-uniform molecular weight distribution are generally referred to as sequence-controlled polymers, whereas polymers with both, a defined monomer sequence as well as a uniform distribution, are called sequence-defined polymers.[12]

For the synthesis of polymers with narrow molecular weight distributions, achieving dispersities of 1.01, a variety of chain-growth polymerization methods were developed (see **Figure 2**, top for a schematic illustration of a chain-growth polymerization). The so-called living or controlled polymerization was first introduced by Michael Szwarc in 1956[15, 16] performing an anionic polymerization of styrene leading to polymers with significantly lower distributions compared to conventional free radical polymerization methods. The primary reason for reaching a narrow distribution by living polymerizations is the absence of chain termination as well as chain transfer steps, which was already observed by Ziegler in 1936.[17] Further, their higher initiation than propagation rates result in a simultaneous formation of all active species and thus in a much more constant chain-growth. Besides that, the chain-growth is linear over the reaction time, and therefore the molecular weight of the final polymer can be predicted. A further important characteristic of living polymerizations is the remaining activity of the reactive polymer chain ends which allows for continuous addition of different monomers and thus also for a certain control of the monomer sequence by synthesizing multiblock type copolymers.

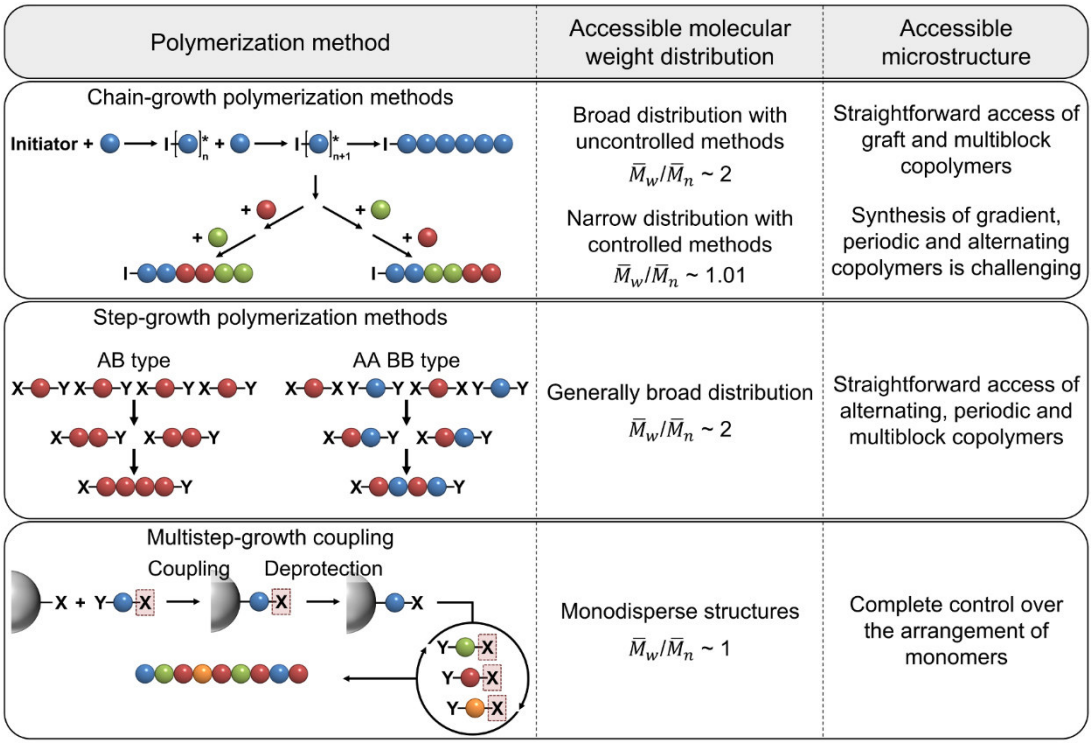

Figure 2: Adapted and modified from Jean-Francois Lutz[12], showing three different approaches for the synthesis of polymers: Chain-growth polymerization methods (top), step-growth polymerization methods (center) and multistep-growth coupling here shown on a solid support (bottom) as well as accessible molecular weight distributions and sequential monomer arrangements for each approach.

Also with other conventional polymerization methods, the sequential arrangement of monomers is only possible to a limited extent. By copolymerization of more than one monomer using chain- or step-growth polymerization methods, simple chain microstructures such as multiblock, periodic, graft or strictly alternating copolymers can be obtained, however, by far not achieving the structural complexity of biopolymers.

With the invention of Nylon 6,6 by Carothers in the 1930th, the strictly alternating copolymers are probably the first example of synthetic polymers with a simple level of a controlled arrangement of monomers.[18] The polyamide is synthesized by a step-growth polycondensation of the two homofunctionalized comonomers hexamethylenediamine and adipic acid (see **Figure 2**, center for a schematic illustration of a step-growth polymerization).

Although the field of synthesizing artificial polymers with a well-defined monomer sequence beyond these of simple copolymers is a current evolving area, in other research fields, such as biology and biochemistry, the regulation of monomer sequence is thoroughly studied for several decades. A variety of methods were implemented for the synthesis of biopolymers like peptides or deoxyribonucleic acid (DNA) and ribonucleic acid (RNA). These existing synthesis approaches for biopolymers, especially solid phase peptide synthesis (SPPS) (as shown in **Figure 2**, bottom for a schematic illustration for a multistep-growth polymerization similar to SPPS), and also methods from other areas like organic chemistry and engineering were adapted and used for the synthesis of manmade polymers with narrow molecular weight distributions and/or a defined monomer sequence. Currently, relevant controlled polymerization methods as well as recent examples for the synthesis of sequence-controlled polymers are introduced in the next subchapters.

1.1.1 Living and controlled chain-growth polymerizations

The decisive difference in the absence of chain termination or chain transfer steps in living when compared to conventional chain-growth polymerizations can be achieved in various ways. Primary developed living polymerization techniques were based on ionic propagating species, such as the anionic living polymerization pioneered by Szwarc[15, 16] as well as cationic polymerizations which were developed by Higashimura and Kishiro[19] in the late 1970th. A termination of two active chain ends is precluded in ionic based living polymerizations due to electrostatic repulsion.[20] Even though excellent dispersities can be achieved with living anionic and cationic polymerization, both techniques are sensitive towards impurities and not compatible with certain solvents. The highly reactive end-groups can undergo chain transfer steps with trace amounts of impurities or some, especially polar, solvents, resulting in a termination of the polymerization. For the same reason, the methods are not compatible with several functional groups, thus limiting a high variety of side chain motifs.[21] Due to these restrictions, further techniques were developed which are also based on the principle of eliminating chain termination and transfer but allow for a broader variety of functional groups and solvents making them more relevant in current polymer science than ionic living polymerizations. In general, two further main classes of more robust controlled polymerizations were developed, first being the class of controlled radical polymerizations (CRP)[22-25] and second being specific ring-opening polymerization (ROP)[26-29] techniques.

Technically speaking, the class of CRP reactions cannot be considered as truly living polymerizations since chain terminations are possible but suppressed. In controlled radical polymerizations, the growing free radical chain end is in equilibrium with a so-called dormant species which does not propagate. Besides the dormant species are non-propagating species, a chain transfer or termination at this state is also not possible. The equilibrium lies on the side of the dormant species, thereby suppressing chain termination steps resulting in narrow molecular weight distributions similar to those of truly living ionic polymerizations. The suppression of chain termination steps by the presence of a deactivated dormant species can be achieved in different ways, and at present-day, three established methods are widely used which can be applied to polymerize a broad range of monomers. The three approaches are the stable free radical polymerizations (SFRP)[22, 30, 31], with the nitroxide mediated polymerization (NMP)[22, 32, 33] being a well-established example, metal catalyzed atom transfer radical polymerization (ATRP)[34-36] and reversible addition-fragmentation chain transfer (RAFT) polymerization[22, 37, 38].

1.1.1.1 Chain-growth approaches for the synthesis of sequence-controlled polymers

Even though narrow molecular weight distributions can be achieved with controlled chain-growth polymerizations, control over the monomer sequence is still challenging. Generally, only one monomer is polymerized at a time, but due to the remaining activity of the reactive chain end, an addition of a different monomer after complete consumption of the first monomer leads to multiblock like copolymers with blocks of a defined length of one incorporated monomer.[39-41] A simultaneous polymerization of two monomers will generally result in a random or statistical copolymer if both monomers exhibit similar reactivity, which is usually the case. When choosing two monomers with different reactivity, an instantaneous incorporation of the more reactive monomer in the polymer scaffold after its addition can be achieved. An example of a copolymerization of monomers with different reactivity in a controlled chain-growth polymerization was introduced by the group of Lutz, copolymerizing styrene with more reactive maleic anhydride monomers.[42] The maleic anhydride, which is referred to as acceptor comonomer, is incorporated after its addition in a narrow region of the polystyrene backbone that is built up out of the donor monomer when the acceptor monomer concentration decreases. A variety of *N*-functionalized maleic anhydride monomers were developed, presenting hydrophobic or hydrophilic as well as basic or acidic substituents, giving access to multiblock copolymers with specific functional blocks.[43] Further examples for controlling the monomer sequence in a controlled chain-growth polymerization were developed by the group of Ouchi and Sawamoto working on so-called template initiators as well as template monomers. A template initiator is a specific monomer-recognizing moiety that is rigidly fixed on a polymerizable initiator and thus promotes the incorporation of a template interacting monomer due to its resulting proximity to the initiator.[44, 45] Template monomers, on the other hand, are monomers that are fixed prior to their polymerization, generally covalently[46] but also using metal complexes[47], and are due to their proximity polymerized subsequently. The template moiety connecting the monomers is removable, and after its cleavage strictly alternating or periodic copolymers can be obtained.

Since two or even three polymerizable moieties are presented on one template monomer, the polymerization is generally performed under highly diluted conditions to prevent cross-linking. First published template monomer was a 1,8-functionalized naphthalene containing an acrylate and a methacrylate, respectively, resulting in a highly alternating methacrylate-acrylate copolymer after its polymerization and subsequent removal of the naphthalene.[46] Two elegant approaches for the synthesis of periodic copolymers by chain-growth polymerization were introduced by the group of Hawker[48] as well as the group of Hillmyer[49]. Both groups performed ring-opening metathesis polymerization (ROMP) of macrocycles with a defined sequence of five and four functional groups, respectively, which are after their polymerization represented in the polymer backbone as periodically repeating sequence.

1.1.2 Step-growth polymerization methods

In contrast to chain-growth polymerization techniques, the step-growth polymerization approach is generally used when a controlled primary structure is targeted, rather than a narrow molecular weight distribution. As described by Flory, who together with Carothers was one of the pioneers of step-growth polymerization, the molecular weight distribution of a linear step-growth polymerization with almost complete conversion approaches a value of 2.[50, 51] Besides this, the poor control of molecular weight or even the difficulty of achieving high molecular weights are significant disadvantages in comparison to chain-growth polymerizations. In contrast to chain-growth polymerization, high molecular weights are only obtained at high monomer conversion as studied by Carothers.[52] The previous reaction step in a polymerization of one heterofunctionalized monomer or two homofunctionalized monomers results in the formation of dimeric structures although half of the reactive end-groups are converted. Subsequently, a conversion of 95% of the reactive end-group only results in a polymer with twenty repeating units and a conversion of 99% in 100 repeating units.[52] The prerequisite of high conversion implies a choice of a quantitative coupling reaction as well as an equimolar ratio of the reactive end-groups. However, when meeting the requirements, step-growth approaches are straightforward methods to achieve polymers with a strictly alternating monomer sequence.

Furthermore, due to the possibility of separating the reactive end-groups of the monomer by a long spacing block, supposedly a block with a specific arrangement of functional groups, periodic polymers can be synthesized with well-defined repeating units. The group of Wagner first performed this approach of polymerizing defined telechelic macromonomers in 2004 for the synthesis of a defined ethylene/1-butene copolymer[53], and it quickly became a widely used method. Click reactions (see **Chapter 1.2**) are extensively used as coupling reaction due to their quantitative conversion and lack of side reactions. To name some, the groups of Lutz[54], Guan[55] and Kopecek[56] used copper (I) mediated azide-alkyne cycloaddition (CuAAC) coupling (see **Chapter 1.2.1**) whereas the groups of Tew[57], Junkers[58] or Du Prez[59] made use of thiol-ene coupling (TEC) reactions (see **Chapter 1.2.2**) to couple well-defined telechelic macromonomers in order to obtain periodic copolymers via such a step-growth polymerization method.

1.1.3 Multistep-growth coupling

The currently most precise approach controlling the primary structure of synthetic polymers is the multistep-growth coupling procedure, consisting of a stepwise coupling of single monomer units onto a supporting material; primary a solid particle. The origin of this procedure goes back to the year 1963 when Bruce Merrifield published his work on solid phase peptide synthesis (SPPS)[60] introducing a straightforward method to control the amino acid sequence of peptides. A variety of novel approaches synthesizing artificial polymers today are based on the fundamental principles of this "bio-inspired" procedure.

1.1.3.1 Solid phase peptide synthesis

Merrifield's general idea was to significantly accelerate the previously developed synthesis procedure of peptides in solution, first performed by Fischer and Fourneau[61], which implied complex purification steps. The concept of peptide synthesis consists of a condensation reaction of a carboxylic acid and an amine group of two amino acids, connecting both under formation of an amide linkage. To prevent the polymerization of the bifunctional amino acids in a step-growth fashion (see **Chapter 1.1.2**), Bergmann and Zervas[62] were the first to introduce a temporary protecting group for one of the reactive end-groups. Beside the end-groups, also the reactive side chain functionalities need to be protected to prevent side reactions (see **Figure 3,** Protecting groups). Side chain protecting groups are generally orthogonal to those of the reactive end-groups.[63] A crucial characteristic is that the protecting group can be quantitatively removed to liberate all reactive end-groups, allowing for coupling of another amino acid. A further milestone in peptide synthesis was the development of coupling reagents since the amide bond formation is not favored at room temperature, because the carboxylic acid is mainly present in its highly unreactive carboxylate form in the reaction mixture containing basic amines.[64, 65] Most noteworthy invention was probably the discovery of the class of carbodiimides by Sheehan and Hess[66] in 1955 (see **Figure 3**, Coupling reagents, top), activating the carboxylic acid group under formation of an *O*-acyl isourea intermediate which is a good leaving group and can be easily displaced by the primary amine during nucleophilic substitution. With a significant increase in yield for each coupling step when using coupling reagents, the amount of deletion sequences was reduced. However, despite decreasing the amount of side-products with both of the stated accomplishments in peptide synthesis, the isolation of the target structure from an excess of remaining starting material and coupling reagents was still time-consuming and potentially problematic, e.g., due to a drastic loss in yields.[65] By attaching one end of the peptide to a solid support and building up the amino acid sequence from the accessible end in a stepwise fashion, remaining reagents after each coupling step can be easily removed by filtration and extensive washing of the solid material. The covalently bound target structure remains on the solid support until its final amino acids sequence is obtained and is cleaved. Due to the ease of separating the reaction solution from the target compound, also a significantly higher excess of the coupled amino acid as well as coupling reagents can be used, driving the coupling step almost to completion.[65]

As solid support, or so-called resin, Merrifield used a hydrophobic copolymer network based on styrene which is cross-linked using *para*-divinylbenzene (DVB) (see **Figure 3**, Examples for resins, top).[60] On the solid support, a specific linker, allowing for a covalent anchoring of the first amino acid is present. The original Merrifield resin contained chloromethyl groups to which the C-terminal end of the first amino acid can be linked via a benzyl ester (see **Figure 3**, Examples for linkers, top). The ester linkages can be cleaved under basic or acidic conditions, releasing the final product from the resin.[60] Because of the hydrophobic nature of the polystyrene resin, long peptide chains tend to aggregate on the solid support.[67] In an aggregated state, the reactive end-groups are less accessible, and lower yields for subsequent coupling steps are often observed which lead to the development of new, more hydrophilic resins. One example is the TentaGel® resin, which contains additional poly(ethylene glycol) (PEG) chains, thereby increasing the hydrophilicity and also the flexibility of the resin. The structures of an original Merrifield resin as well as a PS-PEG resin such as a TentaGel® resin are shown in **Figure 3** (Examples for resins, top for PS and bottom for PS-PEG resin).

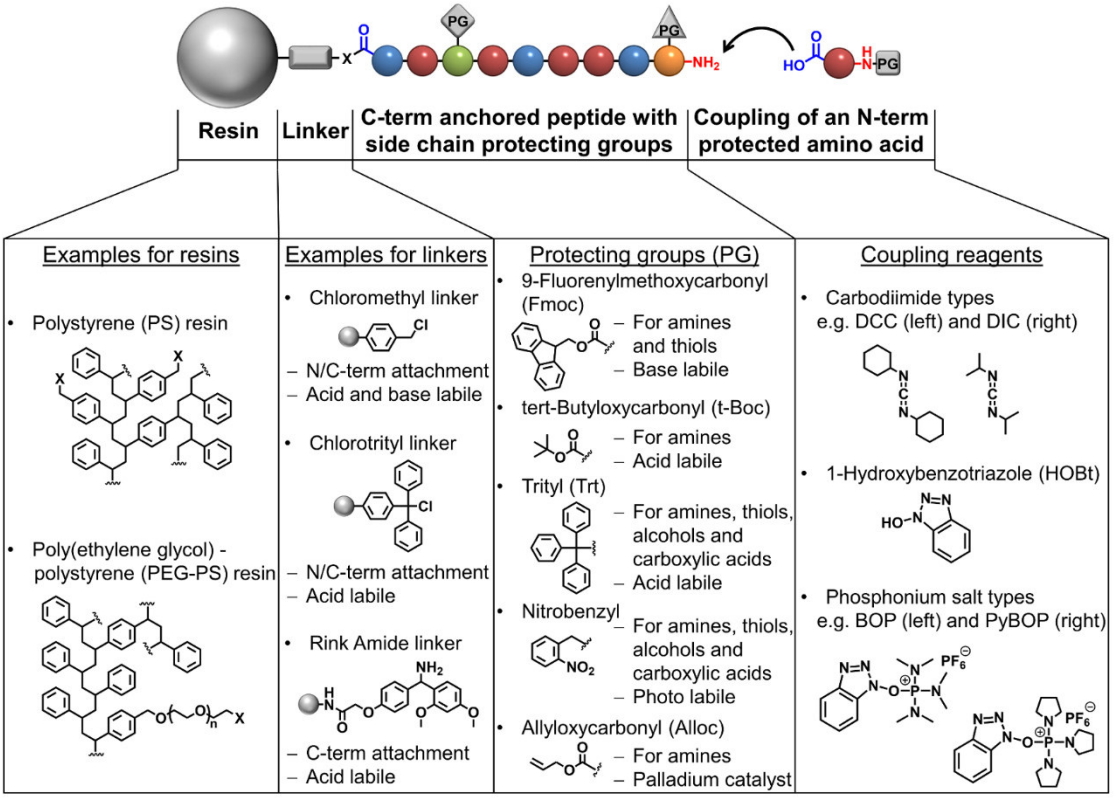

Figure 3: Schematic illustration of a C-terminal anchored peptide on a solid support with side chain protecting groups as well as a coupling of an N-terminal protected amino acid. Exemplary structures of widely used resins, linkers, protecting groups and coupling reagents are shown.

Not only the composition and the properties of the resin but also of the linker that connects the amino acid to the solid support were further modified and optimized. Today, researchers can choose from a large variety of linkers that can be cleaved under different conditions such as basic or acidic conditions but also under reductive conditions[68] or using UV irradiation[69]. Furthermore, the chosen linker also determines the terminal functional end-groups of the compound after cleavage.

One of the most prominent anchoring points to the resin are chlorotrityl linkers which are acid cleavable linkers.[67] The bound compound can be cleaved from these linkers by addition of low amounts (generally 1-5vol%[67]) of trifluoroacetic acid (TFA), depending on the functionalization of the trityl group. A further example for a commonly used linker is the Rink Amide linker which is also an acid cleavable type linker, but requires up to 95vol% of TFA for a quantitative liberation of the product.[67] Structures of a chlorotrityl as well as the Rink Amide linker are shown in **Figure 3** (Examples for linkers, center for chlorotrityl and bottom for Rink Amide linker).

In general, most common linkers in SPPS are acid labile, mainly connecting the C-terminal end of the amino acid to the resin. Therefore, the fluorenylmethyloxycarbonyl (Fmoc) protecting group, which can be removed under basic conditions, was established over the years as the primary protecting group for the reactive amino end-group. The quantitative liberation of the N-terminal end of a previously coupled amino acid does thus not result in a cleavage from the resin. The Fmoc group can be specifically removed under mild basic conditions, generally using 20vol% of piperidine.[63] Besides the Fmoc group also the acid labile *tert*-butyloxycarbonyl (*t*-Boc) group is a widely used α-amino protecting group which is one of the first protecting groups that were developed.[70] *t*-Boc protecting groups can be used in combination with linkers that are stable under acidic conditions but also with those that need very harsh acidic conditions for their cleavage. In the early stage of SPPS, for example, the *t*-Boc group was used in combination with the benzyl ester anchoring via chloromethyl groups which need hydrofluoric acid (HF) for their liberation. Therefore, an orthogonal removal of the *t*-Boc group using 30-50vol% TFA with only minimal loss of product was possible.[70] A further acid labile protecting group that can be cleaved at milder conditions compared to the *t*-Boc group is the trityl (Trt) group which can be removed using a TFA concertation between 1-5vol%.[63] Similar to the developed resin linkers also protecting groups other than those that can be cleaved under acidic or basic conditions were established. Here, especially the allyloxycarbonyl (Alloc) group and the nitrobenzyl derivatives are often used. The Alloc group can be specifically removed using a palladium-catalyzed allyl transfer[63, 71] whereas nitrobenzyl groups can be cleaved under UV irradiation[72, 73]. Due to their stability at different pH, temperature or under reductive conditions, they present excellent orthogonality towards other common protecting groups.[63, 74, 75] Structures, suitable functional groups and cleavage conditions of all the presented protecting groups are given in **Figure 3** (Protecting groups).

The stability of the side and especially the main chain protecting group throughout the stepwise synthesis is crucial in order to achieve high yields and purities. In addition to that, also a quantitative coupling of one monomer unit is of utter importance. The amide bond formation is mainly realized by activating the carboxylic acid in terms of the addition of a good leaving group. There are many possible approaches based on this concept, e.g., their conversion into acyl halides or azides as well as mixed anhydrides.[76] However, most of these approaches are not suitable for SPPS since they may lead to the cleavage of certain protecting groups and linkers as well as rearrangements or the activated intermediates hydrolyze quickly.[76]

A variety of coupling reagents were implemented over time, first different carbodiimides derivatives such as *N,N'*-dicyclohexylcarbodiimide (DCC) or *N,N'*-diisopropylcarbodiimide (DIC).[66] The structures of DCC and DIC are shown in **Figure 3** (Coupling reagents). After formation of the *O*-acyl isourea, the primary amine can attack the carbonyl group, displacing a urea derivative, as shown in **Scheme 1** (top and center). However, when using carbodiimide reagents racemization and side reactions were observed, one being the formation of a stable *N*-acyl urea by rearrangement of the *O*-acyl isourea (see **Scheme 1**, center).[76]

Scheme 1: Mechanism of the coupling of an Fmoc-protected amino acid to the primary amine of a peptide chain on a solid support using a carbodiimide type coupling reagent. With top showing the formation of the reactive *O*-acyl isourea intermediate, center showing the nucleophilic attack of the primary amine to the *O*-acyl isourea and bottom showing the coupling under the addition of the strong nucleophile HOBt, the formation of an active Obt ester intermediate as well as its attack by the primary amine.

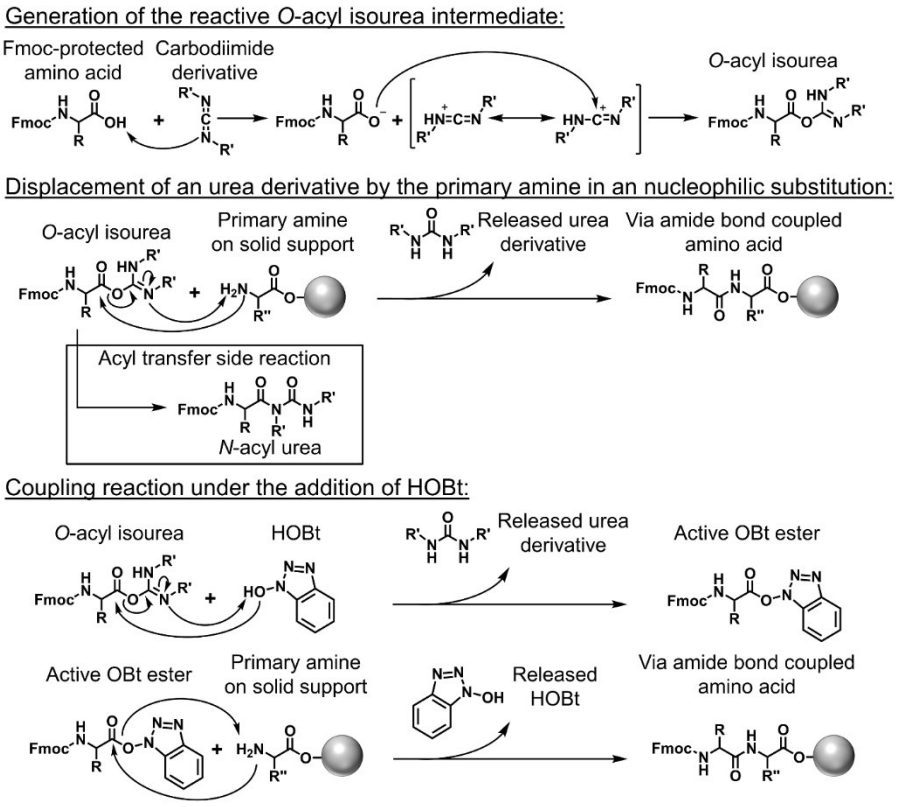

An approach to suppress the acyl transfer is the addition of a further nucleophile which is highly reactive and attacks the *O*-acyl isourea faster than it rearranges. The activity of the formed intermediate has to be still sufficiently high for the addition of the amino group. An example of a nucleophile ensuring this is hydroxybenzotriazole (HOBt) (see **Scheme 1**, bottom) generating an active ester on the C-terminal end of the amino acid. The formed active Obt ester can be subsequently attacked by the primary amine of the peptide on the solid support under liberation of the HOBt moiety, resulting in the final amide linkage. In addition to the suppression of the rearrangement, its use also reduces racemization.[76] The reaction mechanism of the coupling using a carbodiimide under the addition of HOBt is exemplarily shown in **Scheme 1** (bottom).

A further reduction in racemization was achieved by using phosphonium salt type coupling reagents which contain an internal HOBt moiety that is released *in situ* in the first step of the coupling reaction. The first published coupling reagent of this class was benzotriazol-1-yl-oxy-tris-(dimethylamino)-phosphonium hexafluorophosphate (BOP), also known under the name Castro's reagent, in 1975.[77] For the coupling, the addition of a base, generally *N,N*-diisopropylethylamine (DIEA), is necessary to deprotonate the carboxylic acid.

Scheme 2: Mechanism of the coupling of an Fmoc-protected amino acid to the primary amine of a peptide chain on a solid support using a phosphonium salt type coupling reagent. With top showing the formation of the reactive acyl phosphonium intermediate, center showing the nucleophilic attack of previously released Obt$^-$ to the acyl phosphonium intermediate and the formation of an active Obt ester and bottom the attack of the primary amine to the active Obt ester.

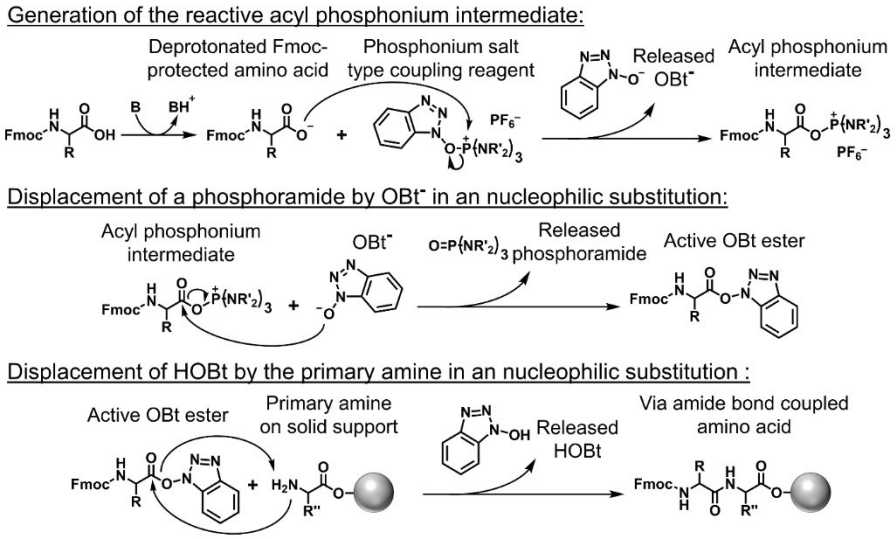

The carboxylate can then attack the positively charged phosphonium ion under formation of an activated acyl phosphonium intermediate and deprotonated HOBt, as shown in **Scheme 2** (top). Subsequently, the Obt anion reacts with the activated acyl, forming again the active Obt ester which allows for a quantitative substitution by the amino group (see **Scheme 2** center and bottom).[76] A disadvantage of BOP is the release of carcinogenic hexamethylphosphoric acid triamide (HMPA) which is the reason for the BOP reagent being replaced by the benzotriazol-1-yl-oxy-tris-(pyrrolidino)-phosphonium hexafluorophosphate (PyBOP) not releasing a harmful side-product.[78] The structures of the introduced coupling reagents BOP and PyBOP with the highlighted internal HOBt moiety are shown in **Figure 3** (Coupling reagents).

1.1.3.2 Solid phase synthesis of oligoamides

After its intentional invention for the synthesis of peptides, the powerful method of solid phase synthesis was soon further extended to other systems, first within the field of biopolymers for nucleic acids[79] and carbohydrates[80] but in the later 1990s[81, 82] also for the synthesis of unnatural, artificial oligomeric compounds. In general, the method can be adapted to all types of monomers, having a bifunctional character with a temporary protecting group on one of the two functionalities. Besides that, also the type of coupling reaction can be varied with the only premise of resulting in a quantitative linkage, if necessary also by means of coupling reagents.

In the group of Hartmann, the concept of SPPS was applied to synthesize monodisperse, sequence-defined oligomers based on an amide backbone. Instead of using amino acids, tailor-made building blocks with different main and side chain motifs were established giving access to a vast range of macromolecules with precisely tuned physicochemical properties as well as architectures.[83-86] Similar to conventional amino acids used for SPPS, the artificial building blocks contain an Fmoc protected primary amine as well as a carboxylic acid functionality and can therefore be coupled applying optimized coupling procedures. Additionally, it is also possible to include amino acids within the oligoamide backbone to introduce a certain functional side chain group or a selectively cleavable main chain motif.[87, 88] The well-defined oligoamides are used as synthetic biomimetic compounds, presenting biological relevant ligands for the investigation of biological processes. For that, a monodisperse compound with a defined primary structure is of utter importance to gain unambiguous structure-activity correlations. A particular emphasis in the group of Hartmann is devoted to the synthesis of precision glycomacromolecules with an exact amount and positioning of carbohydrate motifs as well as a precise architecture, for example, varying between linear and branched structures.[85, 86, 89, 90] A broad variety of different building blocks was developed over the years which can be generally divided into two different types, the functional and the spacing building blocks. Functional building blocks carry a specific side chain functionality, which allows introducing a binding motif, such as a carbohydrate, but can also serve as a branching point.[83, 85] The spacing-type building blocks can be used to achieve spacing between binding ligands, to adjust the overall contour length and molecular weight of the oligomer as well as to tune the hydrophobicity or rigidity of the backbone.[83, 90, 91] Structures of the building blocks from the current library are shown in **Figure 4**.

Most functional building blocks are based on a diethylenetriamine moiety with a functional side chain on its centered secondary amine. The two primary amines are Fmoc-protected and succinylated, respectively. Each building block is termed with a specific letter code, generally consisting out of three letters. The essential diethylenetriamine as well as the succinyl group are always stated in the nomenclature as the last letters, which are DS (D for diethylene triamine and S for succinyl). The first letter gives information about the functional group of the side chain. Most relevant functional building block so far is TDS[83], presenting an alkyne group (T for triple bond) on its side chain.

The alkyne moiety can be used to attach an azide-functionalized ligand by CuAAC reaction (see **Chapter 1.2.1**), e.g., carbohydrates such as 2-azidoethyl-α-D-mannopyranoside or 2-azidoethyl-β-D-galactopyranoside.[83, 86] In contrast to TDS, the BADS[85] building block (BA for benzyl azide) can be also used for CuAAC but to attach alkyne-functionalized carbohydrates, which are often more easily accessible as their azide-functionalized counterparts.

Further building blocks that allow for an introduction of ligands are the DDS[92] and MDS[89] building blocks with a double bond and a protected carboxylic acid (M for methyl succinyl) group in their side chain, respectively. To the DDS block, a coupling of thiol-functionalized ligands by TEC[92] reaction (see **Chapter 1.2.2**) is possible whereas azide- or amine-functionalized ligands can be coupled to the MDS block by Staudinger ligation[89] or amide formation using the appropriate coupling reagents. The two building blocks BDS[84] and ADS[84] contain an orthogonal protecting group on the centered secondary amine, a *t*-Boc protecting group for BDS as well as an Alloc group for ADS, which can both be selectively cleaved on the resin. They can be applied to introduce branching points during backbone synthesis, allowing for a successive coupling of a further building block to the liberated secondary amine as well as for the synthesis of oligoamides with free amines to generate positively charged backbones.[84]

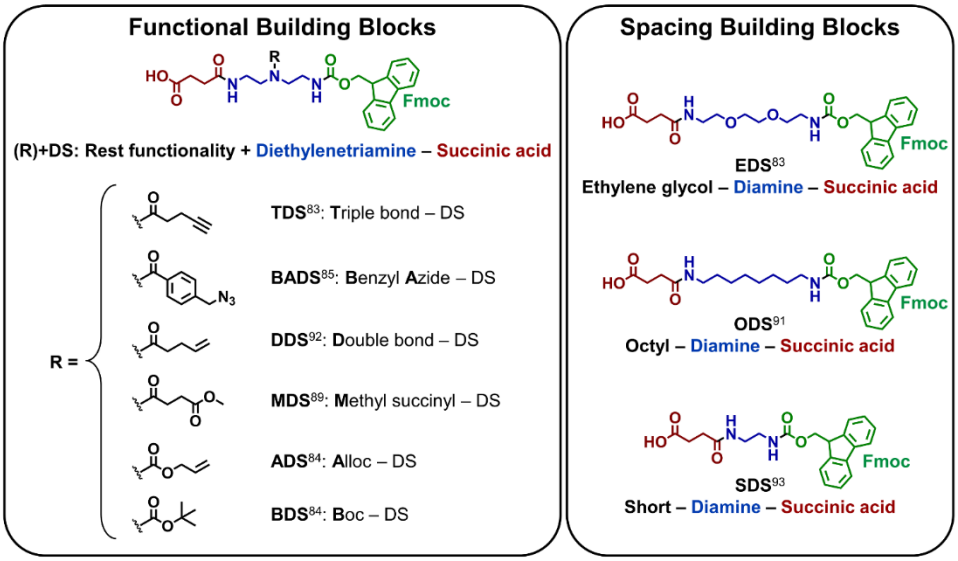

Figure 4: Examples from the current library of tailor-made building blocks for solid phase synthesis from the group of Hartmann showing functional (left) as well as spacing (right) building blocks. The essential carboxylic acid and Fmoc group for solid phase synthesis are highlighted in red and green, respectively. The centered diethylenetriamines for the functional as well as the different name-giving diamines for the spacing building blocks are highlighted in blue.

The spacing building blocks are mainly based on a diamine moiety which makes up the most substantial part of the final building block and thus also determines the final physicochemical properties as well as the size and molecular weight of the building block. Similar to the functional building blocks, one of the primary amines is protected with an Fmoc group whereas the other is functionalized with a succinyl group. Their nomenclature is also comparable to that of the functional building blocks, likewise terminating the three letter code with DS. However, other than for the functional building blocks the D stands for diamine. The first letter gives information about the used diamine.

EDS[83] for example, which is the most used spacing building block, contains with 2,2′-(ethylenedioxy)bis(ethylamine) a centered ethylene glycol-like diamine and is thus abbreviated with an E. The use of EDS provides a good solubility in aqueous buffers but also in organic solvents as well as a high flexibility of the oligoamides. The ODS[91] building block is the hydrophobic counterpart of EDS, containing a 1,8-diaminooctane (O for octyl), which has a similar contour length and molecular weight compared to EDS. The SDS[93] building block with an ethylenediamine moiety, which is the shortest possible aliphatic center (S for short), completes the current library of spacer building blocks.

1.1.3.3 Multistep-growth approaches for the synthesis of sequence-defined polymers

The multistep-growth technique has gained high popularity in the field of well-defined polymers since it is currently the most accurate approach of regulating monomer arrangement. The majority of groups focus on a repetitive coupling and reactive end-group generation cycles. The reactive end-group generation step can be the removal of a protecting group[94] but also the successive formation of a reactive functionality in a further reaction step[59, 95]. Besides that, it is also possible to use not only one coupling reaction but two, thus functionalizing each monomer with two orthogonal reactive end-groups to prevent their polymerization in a step-growth fashion.[96]

Similar to the group of Hartmann, the groups of Lutz[96, 97] and Du Prez[98] also make use of a solid supporting material for the multistep-growth assembly. The group of Lutz focuses on the synthesis of encoded polymers carrying information in terms of an exact arrangement of two monomers, comparable to a binary code. They developed different synthetic approaches, one approach consisting in an iterative coupling of dimethoxytrityl (DMT) protected phosphoramidites followed by the deprotection of the DMT group[97] and another approach involving an iterative coupling of two monomers with orthogonal reactivity. The first monomer was functionalized with a carboxylic acid as well as an alkyne group while the other with an amine and an azide group.[96] Thus, an amide bond formation using coupling reagents followed by CuAAC coupling reaction (see **Chapter 1.2.1**) were possible for their alternating assembly resulting in sequence-defined polymers. Du Prez and co-workers also worked with protecting-group-free approaches on solid support, performing a two-step coupling procedure. First, an isocyanate functionalized thiolactone is coupled to an alcohol group presented on the solid support. In a following so-called amine-thiol-ene conjugation reaction, the thiolactone is opened by an amine which also carries an additional alcohol group thus generating a further reactive end-group. The liberated thiol group is simultaneously functionalized with an alkene in a TEC reaction (see **Chapter 1.2.2**). By varying the side chain of the alkene, it is possible to introduce a specific functionality at a defined position within the polymer backbone.[98]

Instead of using a solid support for multistep-growth assembly, also approaches using a soluble supporting material were developed, as by the group of Alabi.[99] In their work, they made use of a fluorous tag onto which the well-defined polymer was assembled in an iterative fashion.

After the coupling of a monomeric unit, the excess of remaining starting material was separated using fluorous solid phase extraction, similar to the washing step in solid phase synthesis. As coupling reaction, they used orthogonal thiol-ene chemistry (see **Chapter 1.2.2**), performing one photoinduced thiol-ene coupling reaction with an allyl group followed by a phosphine catalyzed, Michael type thiol-ene coupling, with an electron deficient acrylamide. A variety of different allyl acrylamide monomers, carrying a specific functional group on the centered nitrogen atom, were synthesized which were able to be precisely arranged by the iterative coupling.[99]

Further examples of groups that developed procedures to synthesize polymers with a defined monomer arrangement but without the use of a supporting material are the groups of Johnson[94, 100] and Meier[95]. The group of Johnson developed the so-called iterative exponential growth (IEG) approach which consists in the coupling of one heteroprotected monomer in an automated flow reactor. Before coupling, the monomer is separated in two equal parts, where each part undergoes a targeted removal of one of the protecting groups. After their complementary deprotections, the two intermediated are combined and coupled resulting in a heteroprotected dimer. The dimer can subsequently undergo the same procedure. In each coupling step the molecular weight is doubled which is why the method is referred to as exponential growth. The initial monomer contains a triisopropylsilyl (TIPS) protected alkyne as well as an alkyl bromide moiety. After its separation in two parts, for one of the parts, the TIPS protecting groups is removed whereas the second fraction undergoes a substitution reaction of the bromide by an azide. The combined fractions can subsequently react in a CuAAC coupling reaction (see **Chapter 1.2.1**).[94, 100] In contrast to the published work from Johnson, the group of Meier introduced an example of a protecting-group-free multistep-growth assembly without a supporting material. In their approach, they first performed an UGI four-component reaction of a carboxylic acid, an aldehyde, an isocyanide and an amine, where the aldehyde was additionally functionalized with an alkene moiety. In the following TEC reaction (see **Chapter 1.2.2**) using 4-mercaptopropionic acid, a carboxylic acid moiety is added which allows for a further UGI reaction step. By variation of the amine as well as the isocyanide, different functional side chains can be introduced during each UGI reaction step thus allowing for a precise arrangement of distinct functionalities during the stepwise assembly.[95]

Even though the control over monomer arrangement is excellent by multistep-growth approaches, these procedures are generally highly complex and time-consuming. Besides that, the accessible molecular weights as well as the amount of synthesized material are still limiting factors.

1.2 Click coupling reactions

The term click reactions was first introduced by Sharpless[101] in the early 2000s and in general refers to high yielding chemical reactions that have rapid reaction rates, a high thermodynamic driving force, high regio- and sterospecificty as well as no formation of side-products. Besides that, the reactions should at best proceed under mild reaction conditions. The implementation of this novel concept was a milestone in synthetic chemistry, changing the way of solving synthetic problems and serving as new inspiration for design strategies. The fundamental idea of modularity combined with orthogonality leads to the possibility of easily combining the previously functionalized components into final structures which is often more efficient compared to their total synthesis. Besides this, the flexibility of interchanging one functionalized compound gives faster access to a broad range of structures.[102]

A variety of different fast proceeding reactions were analyzed and categorized as click reactions by the group of Sharpless, including cycloaddition reaction such as the Diels-Alder reaction, carbonyl chemistry reactions or nucleophilic substitutions on strained heterocycles. However, the reaction fulfilling most established characteristics of a click coupling reaction is the CuAAC coupling.[101]

1.2.1 Copper (I) mediated azide-alkyne cycloaddition

The CuAAC reaction is a copper-catalyzed and stereospecific variety of the (2+3)-cycloaddition reaction of an azide and an alkyne forming a 1,2,3-triazole which was first introduced by Huisgen in 1967.[103]

Scheme 3: Postulated ligand-free copper (I) mediated azide-alkyne cycloaddition mechanism via a dinuclear copper intermediate.[104, 105]

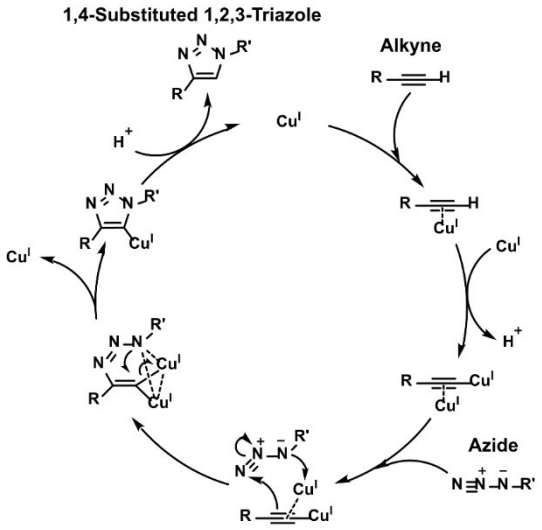

The initially performed reaction by Huisgen, besides its lack of stereospecificity, was also a very slowly proceeding reaction which required high temperatures. Under the addition of a copper catalyst, the reaction rate was increased significantly, with the reaction almost reaching completion even at room temperature and exclusively forming the 1,4-functionalized triazole.[101, 106, 107]

Furthermore, CuAAC is tolerant towards almost all functional groups as well as solvents and generates no side-products. Because of these facts, it was referred to as “cream of the crop” of click reactions by Sharpless, matching all defined characteristics.[101] The stereospecificity can be explained by the proposed reaction mechanism which is shown in **Scheme 3**. When using a ruthenium (II) catalyst instead of copper (I), exclusively the 1,5-adduct is formed.[108]

Since only copper (I) serves as catalyst, which is sensitive towards oxidation, a reducing agent is generally added to the reaction mixture. As reducing agent, sodium ascorbate has been widely established.[107] During the reaction, two Cu (I) cations coordinate onto the terminal alkyne moiety under its deprotonation. The ring formation with the azide occurs under the release of one of the coordinated transition metals. In the last step, the second Cu (I) which is attached in the position 5 of the triazole is replaced by a hydrogen, generating the final 1,4-functionalized 1,2,3-triazole as well as the Cu (I) catalyst which can serve in a further cycloaddition.[104, 105] Although CuAAC is such a powerful method, the need of metallic catalyst is one of its few drawbacks which is why the further development of different click type reactions is still relevant.

1.2.2 Thiol-ene click coupling

The reaction of thiols with carbon-carbon double bonds leading to the formation of thioethers (see **Scheme 4**) is a highly efficient and fast proceeding reaction which was first investigated in the early 1900s.[109] However, the TEC reaction did not gain much importance before the groundbreaking work of Sharpless implementing the novel concept of click-reactions.[101]

Scheme 4: Overview of TEC from a thiol and alkene leading in a thioether either radical or base mediated.

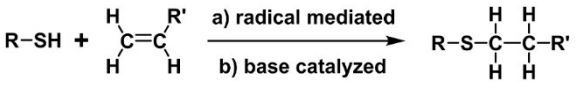

With the increased focus on click reactions and their broad applications also the thiol-ene reaction, fitting several of the defined characteristics, was exploited for its use in synthesis and material development.[110] Besides the primarily introduced click reactions, the TEC reaction gained increasing importance providing a further alternative for similar applications but with different orthogonality towards specific functional groups or different possibilities regarding the choice of solvents and catalysts. Especially in terms of catalyst, the TEC has advantages over the widely used CuAAC reaction.[101] Despite its unique reaction kinetics and the exclusive formation of one product, the need of copper catalysts is a limiting factor when applying CuAAC on biologically relevant structures due to its toxicity for living organisms. Therefore, after being the method of choice for several years in bioconjugation reactions, the CuAAC was displaced by TEC because of the better physiological compatibility.[111] Here, especially the possibility of directly using present thiol groups from the naturally occurring amino acid cysteine is a further advantage for the functionalization of proteins.

The TEC can proceed according to two different mechanisms: a radical-mediated anti-Markovnikov addition to alkenes via a thiyl radical intermediate as well as a base catalyzed thiol-Michael addition via a thiolate anion intermediate.

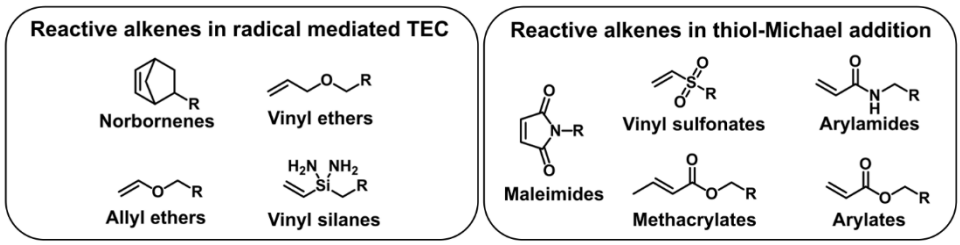

Figure 5: Structures of different reactive alkene moieties, either electron rich or stained alkenes for radical-mediated thiol-ene coupling[112] (left) or electron deficient alkenes for thiol-Michael addition[113] (right).

Both types of TEC have similar efficiencies but react with different alkene moieties. Whereas the radical-mediated pathways need electron rich or strained alkene moieties, the base-mediated pathways exclusively react via electron poor Michael acceptors, thus introducing additional orthogonality even among TEC reactions. Examples for electron rich or strained alkenes are vinyl ethers, allyl ethers, vinyl silanes and norbornenes used in radical-mediated TEC[112], whereas electron deficient maleimides, acrylates, acrylamides, methacrylates and vinyl sulfones are used in thiol-Michael addition reaction[113]. The structures of the stated alkene moieties are shown in **Figure 5**.

1.2.2.1 Photoinduced thiol-ene coupling

The radical-mediated TEC starts with the formation of a thiyl radical via hydrogen abstraction using an adequate initiator system. Here, the use of photo-, thermic- as well as redox-initiators are common.[114] Besides the use of a radical initiator, also a homolytic cleavage of the sulfur-hydrogen bond by UV irradiation is possible therefore having the opportunity to work without an initiator.[115, 116] However, the possible self-initiation even by sunlight also results in difficulties of handling samples containing thiols and alkene moieties simultaneously[117, 118].

The next reaction step is the addition of the thiyl radical to the present alkene moiety. The addition occurs in an anti-Markovnikov manner, leading to a higher substitute and therefore more stable carbon-centered radical. From the carbon radical, two pathways are theoretically possible, a step-growth as well as a chain-growth pathway.[112] When proceeding in a step-growth fashion, the following reaction step is the abstraction of a hydrogen atom from a further thiol group generation a new thiyl radical as well as the final thioether which is from then on inert. The thiyl radical can then propagate to a further alkene moiety followed again by a chain-transfer step. In the chain-growth pathway, the carbon-centered radical undergoes a reaction with another alkene moiety again resulting in a carbon-centered radical with the possibility of following either the step-growth or chain-growth pathways.

Whether a radical-mediated TEC follows a step-growth or chain-growth pathway depends on the reaction rate of the propagation and the chain transfer step. For an ideal purely step-growth TEC reaction the rates of propagation (k_p) and chain transfer (k_{CT}) have to be identical thus neither the thiyl nor the carbon-centered radical accumulates during the reaction process (equation (1) in **Scheme 5**). In case of the chain transfer being the rate-limiting reaction step, a chain-growth polymerization is likely due to the high excess of carbon-centered radicals (equation (2) in **Scheme 5**). A slow propagation reaction is generally caused by a low reactivity of the alkene moiety, which would then lead to accumulation of thiyl radicals and a potential termination of the reaction by recombination resulting in the formation of disulfides (equation (3) in **Scheme 5**).

Scheme 5: Thiol-ene reaction mechanism following a step or a chain-growth pathway as well as correlations between propagation and chain transfer rates.

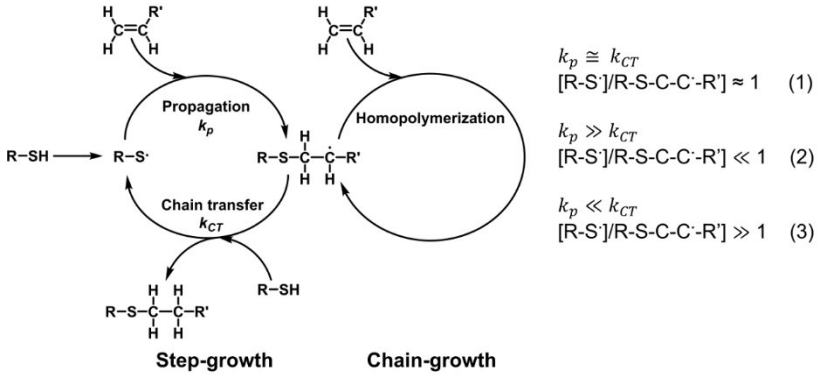

The reaction rates of propagation and chain transfer highly depend on the nature of the alkene as well as the carbon-centered radical but also on the ability of the used thiol to abstract a hydrogen atom. The group of Bowman investigated different alkene moieties in terms of their reaction rates in radical TEC reaction.[119, 120] They found that especially norbornenes and vinyl ethers have almost equal reaction rate constants for the propagation (k_p) and chain transfer step (k_{CT}), thus being selective for the step-growth TEC reaction with almost no possibility of homopolymerization. For allyl ethers and acrylates on the other hand, the rate constant for the propagation step is larger than for the chain transfer, resulting in a mixture of TEC and homopolymerization, allowing a different interesting application in mixed-mode photopolymerization.[121-123]

Not only is the low possibility of homopolymerization a crucial advantage of norbornene moieties in radical-mediated TEC but also the fact that it is one of the most reactive alkene moieties for this reaction. The addition of the thiyl radical towards the norbornene has a very low propagation barrier due to the release of ring strain. However, after the propagation step, there is no further driving force to lower the chain transfer barrier which would theoretically mean that the chain transfer step is slower compared to the propagation step and thus an accumulation of carbon-centered radicals is possible (equation (2) in **Scheme 5**). The fact that a homopolymerization still does not occur may be explained by a low steric accessibility of the carbon-centered radical by a further norbornene moiety.[112]

1.2.2.2 Thiol-Michael click coupling

In contrast to the radical mechanism, the reactive species during thiol-Michael addition is a thiolate anion which is mainly generated in the presence of a base, for example, triethylamine (TEA). Besides the addition of a base, an initiation using a nucleophile such as a phosphine is also a widely used approach.[113, 124] An initiation by a metals[125] or Lewis acids[126] is also possible but not as common. In comparison to the base catalyzed approach, other initiations generally amount in more side-products.[124]

Scheme 6: Base-catalyzed mechanism (left) as well as the nucleophile initiated mechanism (right) of a thiol-Michael addition reaction. B standing for base, Nu for nucleophile and EWG for electron withdrawing group.

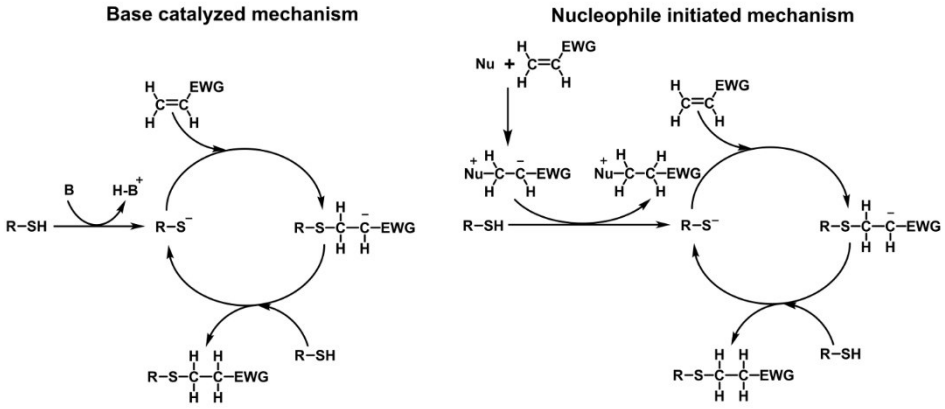

Whereas the formation of the reactive thiolate species is simply achieved via deprotonation using a base in case of the base catalyzed approach (see **Scheme 6**, left), its formation using a nucleophile for initiation is a two-step process. In the first step, the nucleophile used for initiation attacks onto an electron deficient alkene moiety under formation of a zwitterionic intermediate. Its subsequent protonation occurs via a hydrogen abstraction from a thiol moiety, generating the reactive thiolate species as well as a positively charged nucleophile adduct of a previous alkene moiety (see **Scheme 6**, right). The nucleophile adduct is a common side-product in the nucleophile initiated approach.[113, 124]

After initiation, either via a base or a nucleophile, the generated thiolate can subsequently attack an electron deficient alkene moiety leading to the formation of a strong carbanion intermediate which can deprotonate a further thiol as chain transfer step. In contrast to the radical-mediated thiol-ene reaction, a homopolymerization does not occur due to the high probability to protonate the carbanion either by a present thiol but also by solvent molecules or the protonated base present in the reaction mixture when applying the base-catalyzed approach.[113, 124]

1.3 Glycobiology: The role of carbohydrates in Nature

The monomeric units of carbohydrates, the so-called monosaccharides, are, besides nucleotides, amino acids and lipids, one of the four main building blocks in biology, each one contributing essential properties and functions within a living organism. The field of glycobiology covers the study of carbohydrates in biological processes but also the elucidation of their structures, their biosynthesis as well as their linkage to proteins or lipids.[127] The term was first introduced by the group of Dwek in 1988[128] after the importance of carbohydrates in living organisms, besides their role in energy supply and storage or as a structural element, became more evident. In addition to the previously thought to be more relevant classes of nucleotides and amino acids, or rather their biopolymeric counterparts the DNA and RNA as well as the proteins, in processes such as storage and delivery of information, signal transduction and pathogen recognition, the carbohydrates were observed to also take part in a variety of these processes.[129] These findings resulted in an increasing interest to investigate the functions of carbohydrates which was previously highly underestimated. At present day, evidence for the importance of carbohydrates in cell communication[130, 131], cell adhesion[132, 133], signal transduction[134, 135] and pathogen recognition[136-138] such as bacterial[139, 140] or viral[141, 142] infection were gathered. Especially due to the contribution in bacterial and viral infection processes, further knowledge about their exact role and mechanism of action becomes extremely important to potentially develop novel antibiotic or antiviral treatments.

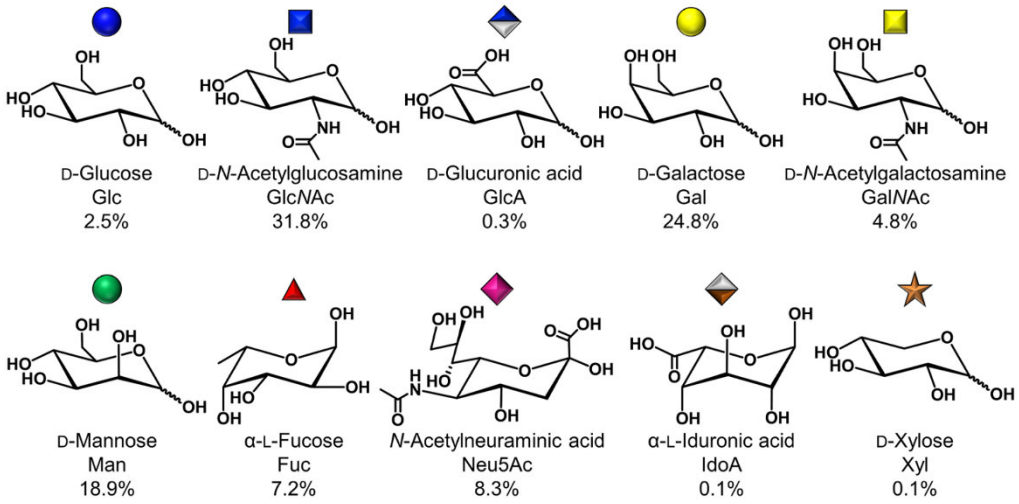

Figure 6: Structures of the ten most abundant monosaccharides in mammalian cell surfaces oligosaccharides relevant in carbohydrate – proteins interactions for cell communication, cell adhesion, signal transduction and pathogen recognition processes. The abundance of each monosaccharide as determined by the group of Seeberger is stated.[143] Besides their structures also their common abbreviation and their symbols as defined by the Consortium for Functional Glycomics are given.

Compared to the progress made investigating the role of proteins as well as DNA and RNA, new information about carbohydrates in biological processes is gained rather slowly which is associated with the high structural complexity of the carbohydrates in comparison to that of the other main classes of biopolymers.[144, 145]

Whereas amino acids or nucleotides only have one possible connection point resulting in a linear arrangement within the biopolymer, two monosaccharides can be connected at various position since each hydroxyl group could potentially serve as a glycosidic linkage. Besides that, also conformational differences for some linkage position or different sizes of the formed heterocycle are possible. Overall, the coupling of just two monosaccharides can already result in sixteen different disaccharides. Extending this concept and considering that in a living organism twenty relevant monosaccharides are present, the coupling of three monosaccharides already leads to almost 27.000 different trisaccharide structures.[143, 144] The possibility of linking the same monomeric units in a variety of diverse arrangements gives access to a large number of structures carrying specific information. However, for their investigation, it is extremely challenging, both in terms of synthesizing as well as isolating such oligosaccharides.

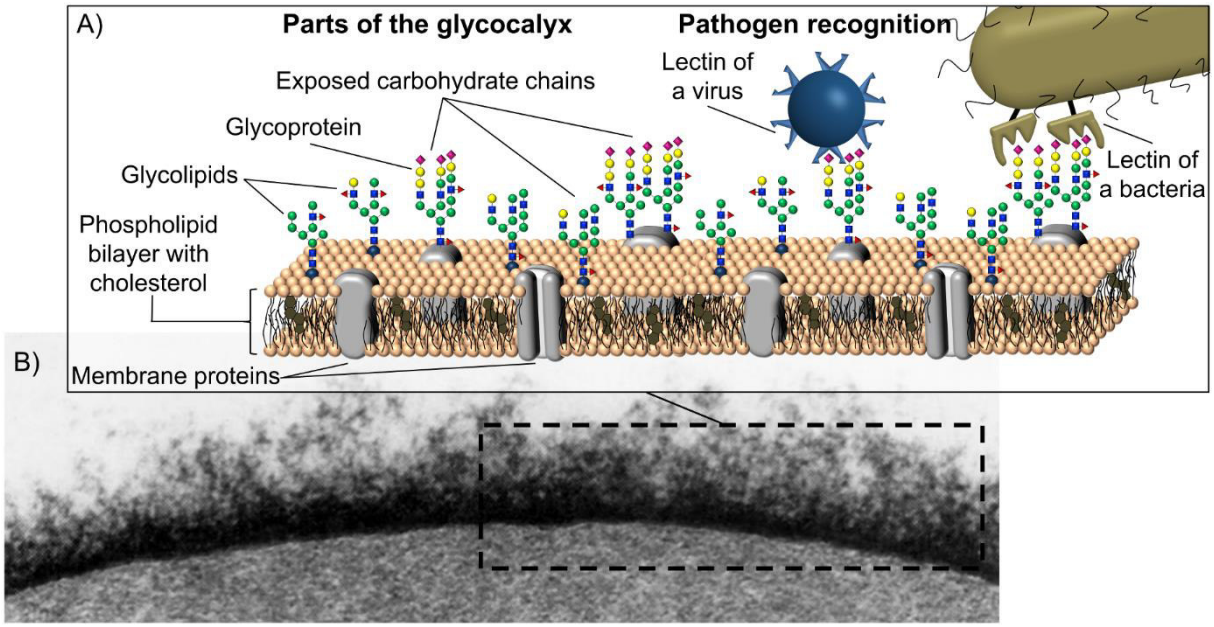

Figure 7: A): Schematic illustration of a cell membrane out of a phospholipid bilayer containing cholesterol and membrane proteins as well as exposed carbohydrates fixed in the membrane in terms of glycolipids or glycoproteins which assemble the glycocalyx. The interactions of a virus and a bacteria via cell surface carbohydrates with lectin receptors of the pathogens is also shown. B): Electron microscope image of a stained glycocalyx of an erythrocyte.[146]

In an organism, the oligosaccharides are mainly presented on the outside of the cell membrane, generally attached to proteins or lipids as glycoconjugates within the lipid bilayer. Most abundant monosaccharides are *N*-acetylglucosamine (Glc*N*Ac), galactose (Gal) and mannose (Man) summing approximately 75% of the entire oligosaccharides of mammalian cell surfaces.[143] However, most exposed monosaccharides and therefore probably most relevant in the stated biological processes are *N*-acetylneuraminic acid (Neu5Ac), fucose (Fuc) and Gal with approximately 26.1%, 23.8%, and 23.0%, respectively.[143] The structure, abbreviation, symbol as well as abundance of the ten most common monosaccharides in mammalian cell surface oligosaccharides are given in **Figure 6**.

The oligosaccharide presentation is highly dense, resulting in a carbohydrate capsule, referred to as glycocalyx, which surrounds almost every cell.[147, 148] A schematic illustration of a cell membrane containing exposed carbohydrates as well as an electron microscope image of an erythrocyte with its dense glycocalyx are shown in **Figure 7**.[146] The type of presented carbohydrates is characteristic for each organism but also for the type of cell or its developmental stage within the same organism. Whereas it was first assumed that the glycocalyx forms a structural border towards mechanical stress as well as a hydrophilic area for the accumulation of nutrients, it is now known that the glycocalyx plays a fundamental role as mediator between cells and also for recognition of exogenous compounds or cells, as shown schematically for the interaction with a virus or a bacteria with exposed carbohydrates of a cell surface in **Figure 7**.[147-149]

The interactions of the presented carbohydrates are mainly towards carbohydrate recognizing receptor proteins, the so-called lectins, which are reversible and of non-covalent nature similar to well-known protein – protein interactions.[150] In contrast to the thoroughly studied protein – protein interactions such as the majority of antibody – antigen recognition processes, carbohydrate – protein interactions are generally much weaker. For most protein-based antibody – antigen interactions, dissociation constants (K_D) in the nanomolar range can be achieved[151, 152], whereas the K_D lies in the millimolar range for the interaction of a monosaccharide with its corresponding lectin.[153]

1.3.1 Carbohydrate – lectin interactions

First discoveries of proteins that specifically bind to carbohydrate ligands were already made in 1860, observing the agglutination of erythrocytes after the addition of rattlesnake venom.[154] The agglutination was determined to occur due to the interaction of the blood type antigens on the erythrocyte surface with proteins in the venom, which is also why these proteins were initially referred to as hemagglutinins. First evidence for the interaction being based on carbohydrates was not made before 1936 after Sumner and Howell thoroughly studied the precipitation of the plant lectin Concanavalin A (Con A) with glycogen and starch which lead to the assumption that the agglutination of erythrocytes is also caused by interaction with glycoproteins.[155] Their postulation was unambiguously confirmed in 1952 by Watkins and Morgan after showing that the interaction can be inhibited by the addition of a specific monosaccharide.[156] In 1954, Boyd and Shapleigh first introduced the term lectin, from the Latin word lectus which means to choose, after discovering that some of such proteins can be applied to distinguish between different blood type antigens but differentiating them from other immunoglobulins based on protein – protein interactions.[157, 158] Due to the specific agglutination they took a significant role in the elucidation of blood group specificity after their discovery. Besides that, the ability to inhibit lectin-induced agglutination were subsequently used to determine the specific binding monosaccharide of isolated lectins. Over time the ubiquitous existence of lectins became evident and a vast variety was isolated and studied, first from plants and later also from animals or microorganisms.[159]

Also, first discoveries of carbohydrate – lectin interactions in diseases were made, when a more pronounced agglutination of malignant in comparison to healthy cells after the addition of lectins was observed, leading to the assumption that a modification of the exposed carbohydrates on the cell surface of cancer cells occurs.[160, 161] Their role in bacterial infection was first observed in 1977 by Ofek[162], encouraging researchers to strive for novel antibiotic treatment based on carbohydrates.

The plant lectin Con A, which was first isolated from jack beans (*canavalia ensiformis*), became a model lectin to fundamentally study the interaction with carbohydrates on a molecular basis since it was the first lectin with a known primary as well as quaternary structure.[163, 164] It specifically binds to α-D-mannopyranoside (Man) as well as α-D-glucopyranoside (Glc), whereas the binding affinity is approximately four times lower towards the latter. Under neutral conditions, Con A predominantly adopts a tetrameric conformation out of four identical coassembled peptide subunits with one carbohydrate recognition domain (CRD) each allowing for carbohydrate ligand binding. Under acidic conditions, it mainly consists of two subunits. The binding domains are approximately 68 Å apart. The crystal structure of Con A in its tetrameric form with the four subunits highlighted in different colors is shown in **Figure 8** (left).[165, 166] The monovalent binding behavior of a single monosaccharide ligand was studied using Con A, giving valuable insights into the binding mechanism as well as indications why carbohydrate – lectin interactions are generally weak.

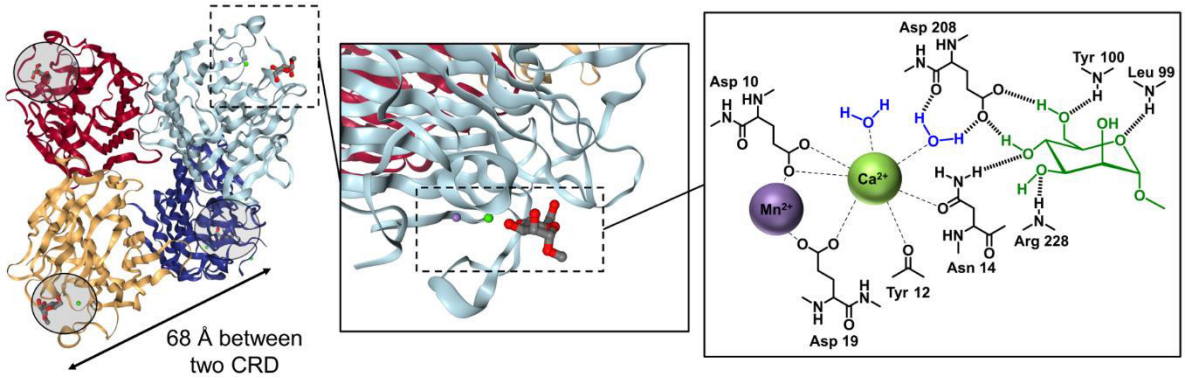

Figure 8: Crystal structure of Con A with its four subunits highlighted in different colors, showing one methyl-α-D-mannopyranoside as well as one calcium and one manganese cation coordinated to each of the four carbohydrate recognition domains (left).[165, 166] A close up of one CRD with the three coordinated compounds (center)[165, 166] as well as the coordination of the monosaccharide binding ligand on a molecular level with formed hydrogen bonds towards amino acids residues, solvent molecules and the cations (right)[165] are also shown.

It was observed that the binding is mainly based on hydrogen bonding since carbohydrates present many hydroxyl groups whose oxygens can interact with hydrogen donating amides of the protein backbone. Hydroxyl groups that do not directly undergo hydrogen bonding with amino acids of the protein are generally solvent exposed and coordinate water molecules, indirectly mediating hydrogen boding towards surrounding amino acids. Besides the formation of hydrogen bonds, also hydrophobic interactions play a role during binding.

Although carbohydrates are generally hydrophilic, they also contain hydrophobic carbon – hydrogen bonds or in some cases even a rather hydrophobic side, when hydroxyl groups are exposed to one side exclusively, which can than interact with hydrophobic amino acid residues.[167] Some lectins, including Con A, use metal coordination to increase the binding affinity. Con A contains a strongly bound calcium cation (Ca^{2+}) as well as a manganese cation (Mn^{2+}) in its CRD. It was observed that they coordinate amino acids within the CRD as well as surrounding solvent molecules which subsequently coordinate to the bound monosaccharide. The coordination of one methyl-α-D-mannopyranoside ligand in one CRD and the interactions it undergoes with surrounding amino acid residues, the coordinated calcium and manganese cations as well as solvent molecules are shown in **Figure 8** (right).[165] The CRD of Con A and also many other lectins is presented on the surface of the protein in a rather shallow depression which is highly accessible to solvent. Therefore the hydrogen bonds towards the corresponding amino acids of the protein can be easily interrupted by competing coordination of water molecules explaining the rather weak binding of carbohydrates with lectins.[168]

To overcome such a weak binding, the affinity is increased by a simultaneous binding of multiple carbohydrates with various protein receptors, which is referred to as multivalent binding. In protein – protein interaction, the concept of multivalency also exists but is by far not as pronounced. Multivalent binding also implies that carbohydrate – protein interactions are more complex binding events compared to protein – protein interactions which, in addition to the structural complexity of the carbohydrates, further increases the difficulty investigating the role of carbohydrates in biological processes. There are a variety of different mechanisms that take part in the multivalent binding which still need to be further understood.

1.3.2 The concept of multivalency

Multivalent binding is an essential principle in Nature which is applied to combine single, generally weak, ligand – receptor binding events in additive fashion resulting in an increase in avidity and specificity, yet being reversible. The vast increase in avidity can be explained by four main mechanisms that are relevant during the multivalent binding event which are explained here using the example of carbohydrate – lectin interaction with Con A as model lectin. These are receptor clustering, chelate effect, statistical rebinding and steric shielding.[169] A schematic illustration of the four mechanisms on the tetrameric Con A are shown in **Figure 9**.

Since most of the lectins have multiple CRD which allow binding of one specific sugar moiety each, they can act as cross-linkers when interacting with one or more multivalent carbohydrate ligands. The overall avidity is simply increased due to additive effects.[170] The clustering of multiple lectins by a multivalent carbohydrate is also referred to as the cluster glycoside effect.[171, 172] Especially for membrane receptors, the cluster glycoside effect is of utter importance, often triggering signal transductions by a conformational change after clustering.[173-175]

Besides the intermolecular binding of multiple CRD also the intramolecular binding by one multivalent carbohydrate ligand is possible, which is also known as chelate effect. The enhanced stability of chelate complexes in comparison to complexes with separate ligands bound to each binding site is well known and generally associated with the entropic effects of the binding event due to the release of a maximal amount of compounds that can freely move in solution.[174] Besides that, during each binding event an entropic penalty caused by the loss of rotational, transformational as well as conformational degrees of freedom of the binding ligand are paid. During chelate binding, the majority of this entropic contribution is assumed to be made for the first binding event exclusively and not for the subsequent, chelating event. In total, the stated entropic effects make a possible chelate binding highly favorable, assuming to increase binding affinity by at least 10^4 orders of magnitude.[174, 176, 177] However, chelate binding strongly depends on the backbone properties and the distance between two binding sugar moieties permitting to span two CRD of the lectin.[174, 178]

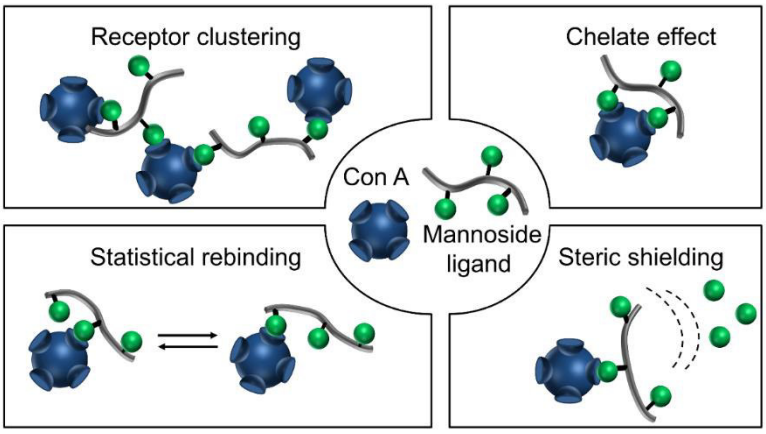

Figure 9: Schematic illustration of the four possible binding mechanisms during the interaction of a multivalent carbohydrate ligand with a lectin receptor containing multiple CRD on the example of tetravalent Con A and a trivalent mannoside ligand.

The third important mechanism during a multivalent binding is the statistical rebinding effect.[175, 179] The weak interaction of one sugar moiety with the binding site of the lectin results in rapid dissociation rates. However, due to the high accessibility of the CRD, association rates are also generally high. When a high local concentration of possible binding partners is present in close proximity of the binding site of the lectin, the probability of a quick re-association of a different ligand after the dissociation of a previously bound ligand is increased which also results in an increase in the overall binding avidity. Due to the course of the binding event, this mechanism is also referred to as bind-and-slide-effect.[180]

The last mechanism takes the components of the ligand that do not directly take part in the current binding event into account. These components can be non-binding sugar moieties, different scaffolds such as proteins or lipids but also binding sugars that temporarily do not take part in a binding event. Although they do not directly interact with the CRD of the lectin, they have a significant influence on the stability of the carbohydrate – lectin complex, serving as a steric shield, protecting the complex towards competing ligands that could potentially also bind to the CRD of the lectin.

This so-called steric shielding effect enhances the overall binding affinity by stabilizing and therefore preserving the formed complex and highly depends on the size of the carbohydrate ligand, especially its non-binding components.[170, 181]

Although some of the mechanistic processes of multivalent carbohydrate – lectin interaction were revealed over the years, there is still a lack of information especially required for the targeted synthesis of pharmaceutically active compounds that use multivalent binding. One opportunity to gain novel insights into the underlying multivalent interactions but also the design of novel bioactive compounds making use of multivalent effects is the use of simplified artificial multivalent carbohydrate ligands, the so-called glycomimetics.[169, 175, 182-184]

1.3.3 Artificial multivalent glycomimetics

To simplify the complexity of investigating carbohydrate – lectin interaction, synthetic chemist developed the concept of carbohydrate presenting macromolecules that mimic structural properties of their natural counterparts. They cannot only serve as model compounds in mechanistic studies, but they also represent novel pharmaceutically active compounds.[184, 185]

In most cases, only the most exposed sugar moieties on an oligosaccharide construct can be assumed to be interacting ligands towards the lectin. The importance of the remaining carbohydrate scaffold is still under debate. Since a variety of the saccharides in the oligosaccharide core do not show binding to lectins, they are generally assumed to serve as supporting scaffold. However, some researchers postulate that they are also relevant during the lectin binding event, for example, increasing specificity as well as promoting an exact conformational exposure of the binding sugar or increasing steric shielding.[186]

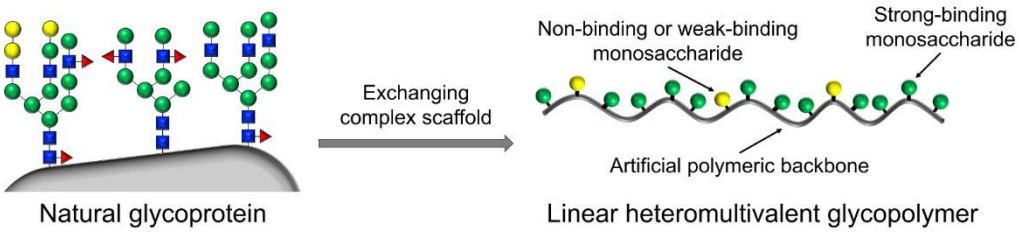

Figure 10: Concept of glycomimetics, exchanging the complex oligosaccharide scaffold of a natural carbohydrate ligand by an artificial polymeric scaffold which carries the smallest carbohydrate binding motif. Here a heteromultivalent linear glycopolymer is shown, carrying higher and lower affinity carbohydrate moieties.

An approach to simplify the structural complexity of these carbohydrate ligands is the removal of all unnecessary sugar moieties that do not show binding towards a lectin and replacing them by an artificial scaffold which is less complex compared to natural oligosaccharides and therefore easier accessible during synthesis (see **Figure 10**). Considering this, multiple copies of the smallest binding epitope, which is generally a monosaccharide but can also be a di- or trisaccharide, are fixed onto the synthetic scaffold resulting in a multivalent glycomimetic.

If more than one type of binding epitope is relevant for binding, simultaneous presentation, e.g., of different binding monosaccharides is possible, as shown in **Figure 10** for a schematic linear heteromultivalent glycopolymer, presenting two different sugar moieties. Such heteromultivalent structures can also be assembled by combining binding and non-binding ligands, with later also being non-carbohydrate based structures.[182, 187]

Over the years, a great number of different glycomimetics were introduced, especially varying the architecture to investigate the influence of sugar presentation as well as the physicochemical properties of the scaffold. They range from low molecular weight compounds presenting only a few copies of binding ligands, to high molecular weight, multivalent polymers, and densely functionalized surfaces.[169, 188] In terms of architecture, glycodendrimers[189-191] as well as liner[192-195], star shaped[196, 197] or brush glycopolymers[198, 199] were synthesized, whereas the scaffold properties were, for example, varied from flexible to more rigid scaffolds[200-202] but also hydrophobic and hydrophilic scaffolds[203-205] were compared. An attachment of carbohydrates onto nano- or microparticles is another important approach, mimicking an entire cell with a simplified glycocalyx.[91, 206-208] Also glycolipids or block copolymers, which subsequently self-assembly to supramolecular micelles, were proven to be good mimetics of a simplified cell with an exposed carbohydrate shell.[209-211] Selected examples of different glycomimetic architectures are shown in **Figure 11**.

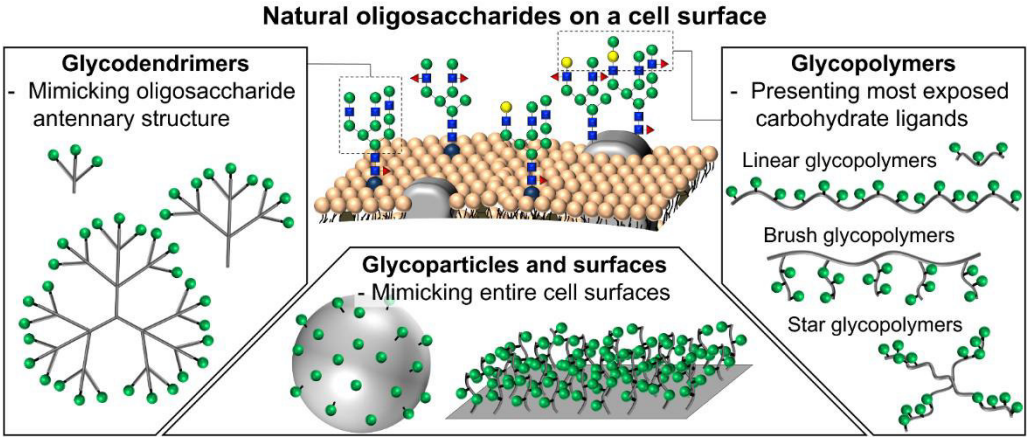

Figure 11: Examples for glycomimetics showing: Left) Glycodendrimers mimicking the branched antennary structures of a natural oligosaccharide. Right) Linear, brush and star glycopolymers presenting only the most exposed saccharides of a natural oligosaccharide on an artificial scaffold. Bottom) Glycoparticles and functionalized surfaces mimicking entire cells and their glycocalyx.

Due to the simplified structure of the glycomimetics, a further elucidation of the carbohydrate – lectin binding mechanisms is usually less complex than for the natural constructs. Besides that, the structure of the glycomimetic can be selectively adapted to potentially target one of the four mentioned binding mechanisms and thereby tune the resulting biological properties. For example, the chelate effect is often targeted as main binding mechanism, trying to precisely tune the distance between two binding sugar moieties through the chosen scaffold, spanning two binding sites and thus allowing for a simultaneous binding of two CRD of the investigated lectin.

The groups of Wittmann and Pieters were able to show a significant increase in binding affinity after precisely bridging the distance between two binding sites in wheat germ agglutinin (WGA), LecA and Shiga-like toxins.[212] It could also be shown that the backbone properties are of great importance when targeting chelate binding. Rigid scaffolds show the best binding if the distance between the two carbohydrate ligands is consistent with the distance of two CRD since they are entropically more favored over flexible scaffolds which have higher degrees of freedom.[174, 178, 212] If this is not the case, a chelate binding does not occur due to an excessive deformation of the backbone, and more flexible scaffold are more suitable.[185] For these studies, especially low molecular weight glycomimetics with a low valency of binding carbohydrates were used. Besides the chelate effect, also steric shielding, statistical rebinding, and cluster formation were studied on the basis of low molecular weight glycomimetics[83, 86] but also of higher molecular weight glycopolymers presenting high amounts of specific sugar residues to further investigate multivalent binding effects of glycomimetics.[182, 187]

When working with high molecular weight glycomimetics achieved by polymerization, a well-defined polymeric structure with a known composition is of utter importance to obtain an unambiguous structure-activity correlation from performed binding studies. As previously described in **Chapter 1.1**, this can either reflect in polymers with a narrow molecular weight distribution or polymers with a well-defined monomer arrangement. Controlled radical polymerization methods as well as ring-opening polymerization methods are widely used, generally polymerizing carbohydrate bearing monomers, alone or in the presence of an additional comonomer.[40, 192-197] Such approaches give access to linear or star glycopolymers with narrow molecular weight distributions as well as controlled molecular weight and degree of polymerization which also determine the final carbohydrate valency. When using additional comonomers also the carbohydrate density can be controlled or heteromultivalent glycopolymers, carrying different sugar moieties, are accessible. Due to the ease of synthesizing multivalent glycopolymers with straightforward polymerization procedures, a broad variety of this class of glycomimetics was synthesized to get insight into the influence of different architectural features in lectin binding or inhibition. Special focus was devoted to the elucidation of the influence of carbohydrate valency and density, the flexibility of the polymeric backbone or the molecular weight of the glycopolymers.[169, 185, 192, 195, 196, 213] It is generally agreed on that a high amount of binding ligands, especially in a highly dense fashion, is not beneficial for effective lectin binding since not all ligands can simultaneously take part during a binding event.[169, 185, 192, 196] Besides that, it was found that the binding affinity towards a lectin decreases for increasing molecular weight of the glycopolymer which can be explained by an increased conformational entropy as well as steric repulsion.[169, 192, 196] In an inhibition event however, an increasing molecular weight and size may have a positive effect, thereby increasing steric shielding towards competing binding ligands.[169, 192, 214, 215]

In general, there are still many open questions for the synthesis of synthetic glycomimetics for biomedical applications. If the triggering of a specific biological process is aimed, especially a specific and strong binder is required to potentially achieve a signal transduction. For this objective, characteristics such as the carbohydrate valency and distance between carbohydrate ligands are of importance which could potentially lead to a directed chelate formation, receptor clustering as well as a high probability of statistical rebinding. Developing a pharmaceutical compound with targeted inhibitory potential, potentially blocking a pathogen from interacting with a healthy cell, especially the steric shielding has to be taken into account, minimizing the accessibility and thus the risk of harmful contact towards the healthy cell.[185] To determine whether an artificial glycomimetic is a strong lectin binder or inhibitor, a variety of assays were established, ranging from simple turbidity assays[169, 192, 216] over sensitive instrumental assays[86, 191, 196, 212] to *in vitro* cell or bacterial assays[90, 195, 217].

1.3.4 Methods to determine multivalent carbohydrate – lectin interactions

A broad range of assays which can be used to determine the binding affinity of a carbohydrate ligand towards a lectin receptor were devolved or adapted from other research areas over the years. The assays vary in their setup, especially in terms of the ligand or receptor presentation or whether the assay is performed in a dynamic or rather static environment. Depending on the setup of the assay, some mechanistic binding events prevail more than others which has to be taken into account during assay choice and data evaluation.

Since most lectin receptors have multiple CRD, a receptor clustering after the addition of a corresponding multivalent carbohydrate ligand is leading to the formation of a cross-linked network of the two binding partners which subsequently precipitates. The observation of an occurring turbidity due to the formation of the insoluble precipitate was the first method to identify carbohydrate – lectin interactions[154-156] and the phenomenon was further exploited to quantify interactions, thereby allowing for comparison of different carbohydrate ligands. Possible approaches to quantify the formation of a precipitate are, for example, by a kinetic type assay determining the rate of precipitation (k_i) after the addition of a carbohydrate ligand[196, 209, 218, 219] or by a quantitative precipitation assay giving access to the receptor – ligand ration in the formed precipitate[169, 190, 192, 216]. The stated kinetic turbidity and quantitative precipitation assay are the most common turbidity based assays which can additionally provide further parameters, such as the maximal precipitate formation and the time ($t_{½}$) or carbohydrate ligand concentration required to reach half maximal precipitation.[169, 192, 196]

The turbidity based assays, in which both binding partners are presented in solution, are generally straightforward and rapid to perform, giving first indications about the glycomimetic's potential as lectin binder, especially their receptor clustering potential. However, for a more precise comparison of different glycomimetics, a broad range of more sensitive instrumental assays was developed, giving access to association and dissociation rate constants (k_{on} and k_{off}) when performing kinetic type assays or dissociation and binding constants (K_D and K_A) when performing saturation type assays.[220]

Besides that, also thermodynamic parameters such as the Gibbs free energy change, molar enthalpy change or entropy change (ΔG, ΔH, and ΔS) of binding events are often determined, for example, by isothermal titration calorimetry (ITC)[90, 221, 222], or single dissociation/rupture forces of a ligand – receptor pair using single-molecule atomic force microscopy (SM-AFM)[223-225] are accessible.

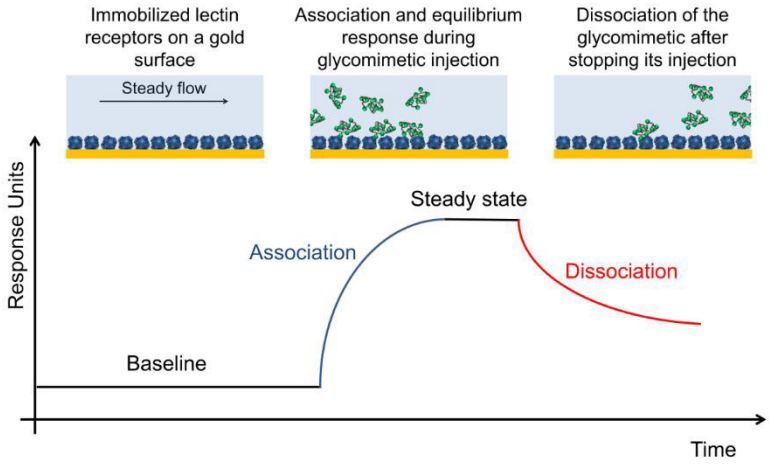

Figure 12: Overview of an SPR sensorgram obtained from a direct binding SPR assay with surface immobilized lectin receptors injecting glycomimetics in the liquid phases passing over the functionalized surface. Association (blue), steady state (black) and dissociation phase (red) of the sensorgram are assigned.

One of the most powerful methods used to determine carbohydrate – lectin interactions is surface plasmon resonance (SPR) which allows conducting both, kinetic as well as saturation experiments, therefore giving access to k_{on}, k_{off}, K_D and K_A values. In SPR assays, one binding partner is attached to a surface whereas the other is in a fluidic phase passing by the surface with a steady flow (see **Figure 12**). When the ligand is captured by the surface attached receptors or vice versa, a mass increase on the surface is obtained which is subsequently detected by a change in refractive index of the surface.[226, 227] The refractive index of the surface is constantly monitored and its change, after the injection of the binding ligand for a specific time until the injection is stopped, results in an SPR sensorgram. The sensorgram primarily shows an increase in response units (RU) due to the carbohydrate ligand interaction with the lectins on the surface (association phase) followed by a steady state phase when the association and dissociation events are in equilibrium (equilibrium response) and finally a decrease in RU after stopping the ligand injection, thereby washing off the ligand from the surface with the attached receptors (dissociation phase) (see **Figure 12**). Since the mass increase also depends on the molecular weight and size of the glycomimetic binding ligands, in a direct binding SPR assay the ligand is injected at different concentrations until saturation of the surface is reached (maximal response (R_{max})). The required ligand concentration to reach half maximum saturation of the receptor surface ($R_{max}/2$) is the dissociation constant (K_D), which is molecular weight or size independent and can be used to directly compare different carbohydrate ligands. Additionally, when analyzing the shape of the association and dissociation phases of an SPR sensorgram, information about the kinetics (rate constants k_{on} and k_{off}) of the ongoing interaction of the two binding partners can be deduced from the same set of data obtained from the SPR assay.

A further assay to determine carbohydrate – lectin direct binding events is the soft colloidal probe – reflection interference contrast microscopy (SCP-RICM) which reflects a binding event of two highly multivalent interfaces.[207, 228] The assay is based on the determination of the adhesion energy of ligand or receptor functionalized PEG particle (soft colloidal probes) towards a glass surface functionalized with the corresponding binding partner. The adhesion energy can be obtained by evaluating the mechanical deformation of the PEG particle when bound to the surface.[207, 229] Due to the ligand and receptor presentation as well as the size and properties of the applied probes, the SCP-RICM assay mimics a natural situation of two interacting cells, providing an interesting platform compared to other interaction assays which generally do not represent a natural situation to such extent.[230]

Besides the assays performed to quantify avidity, also inhibition assays were developed, determining the potency of a glycomimetic to inhibit carbohydrate – lectin interactions.[170, 174, 185, 231] In general, it is possible to perform inhibition assays with the majority of the introduced direct binding approaches under the addition of a competing carbohydrate binding ligand, for example, a binding monosaccharide derivative. The competing ligands can be incubated with the lectin receptors prior or after the addition of the glycomimetic, thereby distinguishing between the glycomimetic's potential to inhibit an ongoing binding event or to block the lectin from competing ligands. A variety of established assays are based on a successive titration of carbohydrate ligand towards an already ongoing carbohydrate – lectin interaction until a complete inhibition is obtained. The carbohydrate ligand concentration needed to inhibit half of the maximal inhibition (half maximum inhibitory concentration (IC_{50})) is obtained which can be subsequently used to compare different glycomimetics regarding their inhibitory potency.[83, 86, 170, 174]

2 Aims and outline

Significant progress in the field of well-defined polymers was achieved in the last decades, aiming for novel functional polymeric materials with unique properties such as polymeric biomimetics targeting biomedical applications.[12, 232, 233] Especially for the interaction with biological systems and potential applications in medicine, it is crucial to apply polymers with a well-defined structure, thereby obtaining unambiguous structure-activity correlations.[213, 234, 235]

A synthetic approach towards well-defined glycomimetics, performing a stepwise assembly of single monomer units onto a solid support has been described by the group of Hartmann, resulting in monodisperse as well as sequence-defined carbohydrate presenting oligoamides.[83, 85, 86, 89, 92] The concept is based on solid phase peptide synthesis, applying established amide coupling procedures, however not making use of amino acids but tailor-made building blocks bearing terminal carboxylic acids and protected-amine moieties. Different types of building blocks were developed: functional building blocks, e.g., allowing for the introduction of carbohydrates at a specific position and spacer building blocks, e.g., allowing for variation of the spacing between the carbohydrate moieties or an increase of the overall length of the polymeric scaffold.[83, 85, 89, 92] With this approach, different glycomimetic systems based on such glyco(oligoamides) were synthesized, deriving fundamental information on their biological properties, specifically their interactions with carbohydrate-recognizing proteins, the lectins.[83, 86, 207] However, due to a general synthetic limitation of SPS approaches, the defined compounds were of lower molecular weight with a maximum of ten carbohydrate moieties[90] so far. In Nature, carbohydrate ligands of various molecular weights exist, smaller such as mono- or oligosaccharides, but also larger in the form of polysaccharides or glycan conjugates where multiple copies of an oligosaccharide are attached to a protein scaffold. In order to also mimic such higher molecular weight carbohydrate ligands, the primary objective of this thesis will be the development of a synthetic approach towards high molecular weight glycomimetics with a multivalent carbohydrate presentation which still exhibit a precise monomer and thus carbohydrate arrangement.

To achieve this objective, a polymerization of defined oligoamides from SPS will be targeted, which is the most promising approach to achieve a highly controlled monomer arrangement in the final polymer when compared to other polymerization methods. The oligoamides will therefore be functionalized with reactive end-groups as telechelic macromonomers which can be subsequently further polymerized in a step-growth type reaction. The defined sequence from the macromonomer is thereby translated into the final sequence of the polymer, resulting in a sequence-controlled polymer with a periodically recurring sequence. The reaction used for polymerization needs to be fast proceeding without the formation of side-products, especially in the presence of various functional groups such as the hydroxyl groups from carbohydrate ligands. The method of choice will therefore be the click-type, radical-mediated, thiol-ene coupling reaction which fulfills the stated requirements.

In a first approach, an AA/BB system will be targeted where two homofunctionalized macromonomers can be polymerized, one carrying two terminal thiol end-groups and the other two terminal alkene end-groups, as required for thiol-ene coupling. This system will be used to establish a reproducible polymerization method looking at the highest possible conversion and thus the highest possible degree of polymerization and molecular weight. In particular, the effects of irradiation time, solvent, photoinitiator and reducing agent, which is potentially needed for the reduction of formed disulfides, will be investigated. After establishing a suitable polymerization procedure, this can then be adapted to a set of different glycomacromonomers creating a first series of sequence-controlled glycopolymers allowing for the investigation of multivalent binding mechanisms in carbohydrate – lectin interactions.

In a second part of the project, the previously developed protocol will also be applied to non-SPS derived macromonomers such as commercially available PEG systems. This will allow for the synthesis of a next generation of glycopolymers with increased valency, ligand spacing and overall molecular weights suitable for further studies of their lectin binding. Furthermore, this also should show the potential applicability of the overall synthetic strategy to other polymeric systems beyond glycomimetics.

In a third part, novel strategies to implement an AB approach during polyaddition reaction, and thereby allowing for directional control during polymerization will be explored. When using macromonomers with non-symmetrical sequences along the scaffold in the initially applied AA/BB approach, control over the orientation of the monomer sequence would be lost. When changing to an AB approach, such directional control along the backbone can be re-installed further increasing the complexity of sequences achievable via the here presented methods.

3 Conclusion

Successful implementation of a novel synthetic approach towards sequence-controlled multiblock glycopolymers was achieved by polymerizing sequence-defined macromonomers derived from SPS in a step-growth polymerization via TEC coupling as schematically shown in **Scheme 7**.

Scheme 7: Schematic overview of the synthetic approach towards sequence-controlled multiblock glycopolymers via a combination of SPS (left) and step-growth TEC polymerization (right). The reaction mechanism of the TEC step-growth polymerization was adapted from Bowman and coworkers.[110] Adapted with permission from C. Gerke, M. F. Ebbesen, D. Jansen, S. Boden, T. Freichel and L. Hartmann, Sequence-Controlled Glycopolymers via Step-Growth Polymerization of Precision Glycomacromolecules for Lectin Receptor Clustering, *Biomacromolecules*, **2017**, 18, (3), 787-796. Copyright © 2017 American Chemical Society.

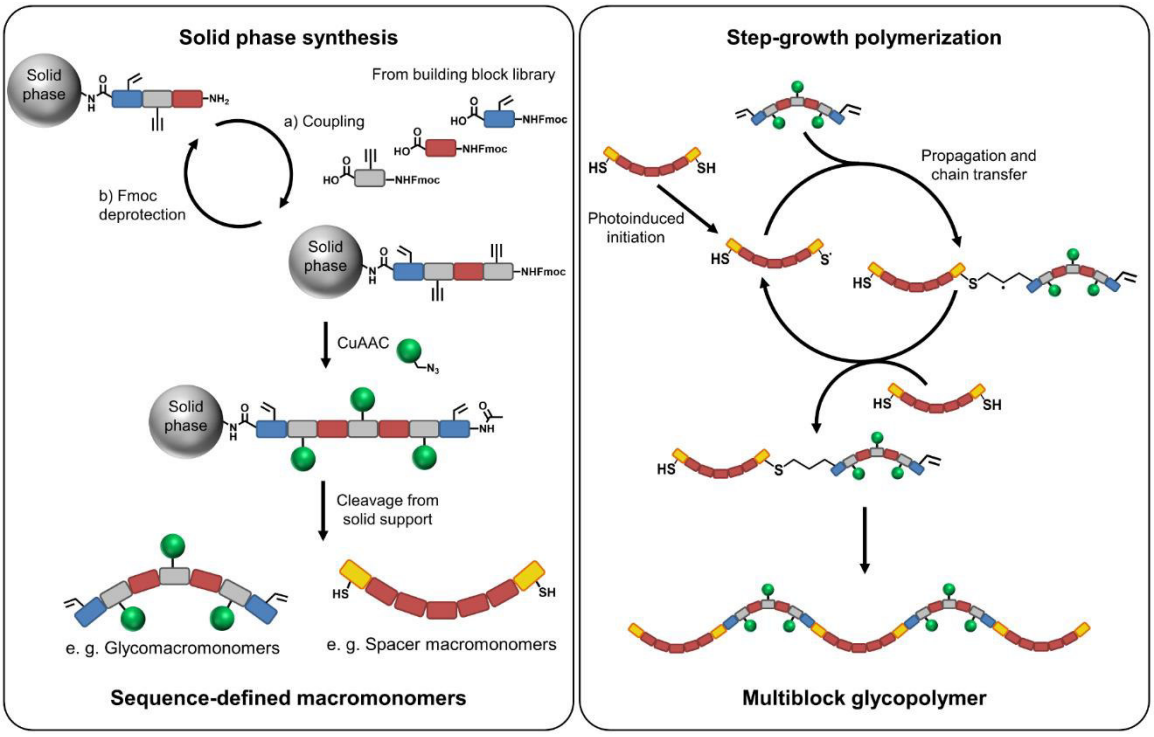

In the first part of the thesis, a reproducible polymerization method of two homofunctionalized macromonomers, one presenting terminal thiol groups and the other terminal alkene moieties, was developed. The thiol groups were introduced by the amino acid L-cysteine (Cys) whereas the terminal alkene groups were incorporated using the established building block DDS[92]. For the method development, both macromonomers contained five ethylene glycol based EDS[83] building blocks, as shown in **Figure 13A**. The two telechelic macromonomers were polymerized in an AA/BB approach and were therefore combined in an equimolar ratio which is crucial to achieve high conversion in a step-growth polymerization. Besides that, both macromonomers were used in a high concentration of 50 mM. Different reaction parameters were varied to achieve the best reaction outcome, which was reaching the highest possible degrees of polymerization ($\bar{X}_n$), as determined by GPC-RI-LS analysis. Applying MALDI-TOF and ^{1}H NMR analysis, assisted in monitoring the formation of side-products.

After choosing DMSO as an adequate solvent, ensuring good solubility of macromonomers (at 50 mM concentration) as well as additional reactants during the entire course of the reaction, the first parameter which was optimized was the photoinitiator. A total of five different initiators were tested, including cleavage (Type I) and H-abstraction (Type II) type initiators with absorption maxima below as well as close to the emitted wavelength of the used medium pressure mercury (Hg) UV lamp (365 nm). Comparing the reaction outcome of each of the five initiators, the highest $\bar{X}_n$ was achieved with the acetophenone derivative 2,2-dimethoxy-2-phenylacetophenone (DMPA), confirming the findings from the group of Yagci who also determined DMPA to be the most suitable initiator for photoinduced TEC.[114] During optimization, the amount of DMPA was varied between 25 and 75 mM, observing that an equimolar amount of 50 mM provides the best results of the TEC polymerization, reaching $\bar{X}_n$ between 9 and 10. Besides the five stated initiators, also a batch without the addition of a photoinitiator was tested, reaching only a low $\bar{X}_n$ of 5, thereby showing the essential need of the photoinitiator for a good polymerization outcome. The achieved number and mass average molecular weights ($\bar{M}_n$ and $\bar{M}_w$), molecular weight distributions ($\bar{M}_w/\bar{M}_n$) as well as $\bar{X}_n$ varying the DMPA concentrations are shown in **Figure 13B**.

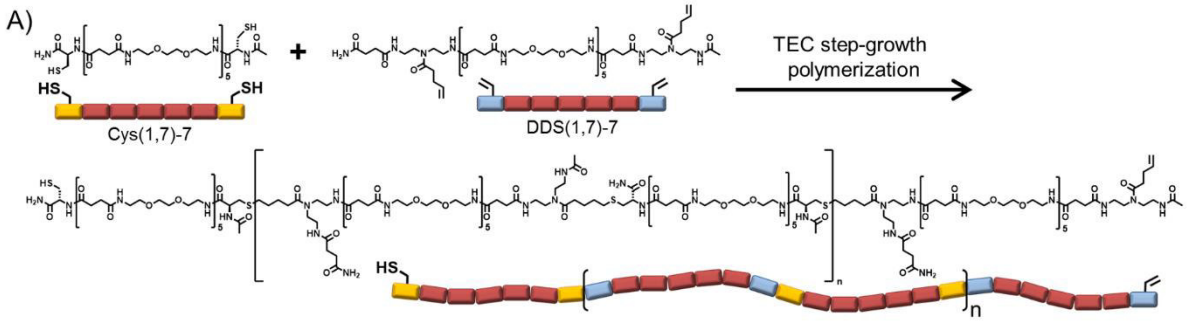

DMPA [equiv]	TCEP [equiv]	$\bar{M}_w$ [kDa]	$\bar{M}_n$ [kDa]	$\bar{M}_w/\bar{M}_n$	$\bar{X}_n$
0	0.01	16.1	7.80	2.06	5
0.5	0	26.5	10.8	2.46	7
	0.01	22.5	12.6	1.79	8
	0.1	21.9	8.70	2.52	6
1.0	0	32.6	14.5	2.24	9
	0.01	**29.0**	**16.0**	**1.81**	**10**
	0.1	26.4	14.5	1.82	9
1.5	0	29.1	14.8	1.97	9
	0.01	28.9	14.9	1.94	9
	0.1	23.8	11.7	2.04	7

Figure 13: A) Reaction overview of the step-growth polymerization via thiol-ene coupling using two macromonomers with five central EDS spacing building blocks, one containing two terminal thiol groups (Cys(1,7)-7) and the other two terminal alkene moieties (DDS(1,7)-7). B) Overview of the achieved $\bar{M}_w$, $\bar{M}_n$, $\bar{M}_w/\bar{M}_n$ and $\bar{X}_n$ after varying the DMPA as well as the TCEP concentration during the TEC polymerization. C) GPC-RI-LS data from the analysis of the multiblock polymer with the highest achieved $\bar{X}_n$ during method development and its corresponding precursor macromonomers. Columns: Suprema Lux (2 × 100 and 1000 Å). Buffer: 50 mM NaH_2PO_4, 150 mM NaCl, 250 ppm of NaN_3 (pH 7.2), 30% ACN. Flow: 1 mL/min.

Since the reactive thiol end-groups tend to oxidize, resulting in disulfides which cannot further react during the TEC polymerization, the effect of an added reducing agent to the reaction mixture was evaluated. As reducing agent, tris(2-carboxyethyl)phosphine hydrochloride (TCEP) was chosen, being one of few reducing agents that are not thiol-based as well as providing good solubility in the reaction solvent. Since phosphines can undergo concurrent side-reactions with both, the reactive alkene[236-238] as well as the thiol[239-242] end-groups under UV irradiation, the concentration of the reducing agent was varied, limiting the possibility of side-reactions but still providing the possibility for disulfide reduction. The optimal amount was determined to be 0.01 equiv (0.5 mM), reaching the highest possible $\bar{X}_n$ between 8 and 10 as determined by GPC analysis (see **Figure 13B**). Specific side-products formed when using higher amounts of TCEP were not determined by MALDI-TOF analysis with the optimized concentration. Since water is needed during the reduction of disulfides using TCEP, a mixture of DMSO and water with a ratio of 9/1 was used for the polymerization.

A final parameter investigated was the duration of UV irradiation. Investigations determined 60 min as the optimal, even though almost no further increase in conversion was observed after 30 min. However, the polymerization outcome was more reproducible after the increase in the irradiation time. After optimization, a final $\bar{X}_n$ of 10 was achieved when irradiating an equimolar amount of two macromonomers for 60 min under the presence of 1 equiv of photoinitiator DMPA as well as 0.01 equiv of reducing agent TCEP using a total of 200 µL of a mixture of DMSO and water in a ratio of 9/1. The $\bar{M}_n$, $\bar{M}_w$, $\bar{M}_w/\bar{M}_n$ as well as $\bar{X}_n$ of different method development procedures are given in **Figure 13B**. The reaction conditions which lead to highest $\bar{X}_n$ are highlighted in bold. A GPC elugram of the polymer with highest $\bar{X}_n$ as well as of the two used macromonomers are shown in **Figure 13C**.

After establishing a reproducible polymerization method, a series of four different glycomacromonomers was polymerized with a hydrophilic spacing macromonomer built out of EDS-centered building blocks. The glycomacromonomers were functionalized with terminal alkene moieties whereas the same dithiol macromonomer, as used during method development, was applied in the synthesis of the multiblock glycopolymers. The glycomacromonomers presented different amounts of Man ligands, varying from one to five moieties as shown in **Scheme 8A**. After their polymerization, for all four multiblock glycopolymers an $\bar{X}_n$ of 8 was achieved, corresponding to $\bar{M}_n$ between 13.4 and 17.5 kDa, depending on the molecular weight of the incorporated glycomacromonomer. The $\bar{X}_n$ was therefore slightly below that achieved during method development, which indicates that the glycomacromonomers seem to be less reactive in the TEC step-growth polymerization when compared to the unfunctionalized macromonomer only containing EDS building blocks. The lower reactivity could be explained by a different polarity of the macromonomers or a different accessibility of the reactive alkene end-groups.

With an achieved $\bar{X}_n$ of 8, each carbohydrate carrying macromonomer is incorporated four times in the final multiblock glycopolymer, therefore obtaining glycopolymers with final average Man valencies between 4 and 20. The structures of the multiblock glycopolymers as well as the achieved $\bar{M}_n$, and the average Man valency are shown in **Scheme 8A**.

Scheme 8: Overview of the multiblock copolymers synthesized showing in A) the first set, assembled out of two oligoamides derived from SPS using DDS as reactive alkene bearing building block and in B) the second set, assembled out of an oligoamide and a functionalized PEG using NDS as reactive alkene bearing building block. For all obtained multiblock copolymers, the final $\bar{M}_n$ as well as average Man valency are stated. **F1** – **F3** in B) stand for the different fractions separated after preparative GPC fractionation.

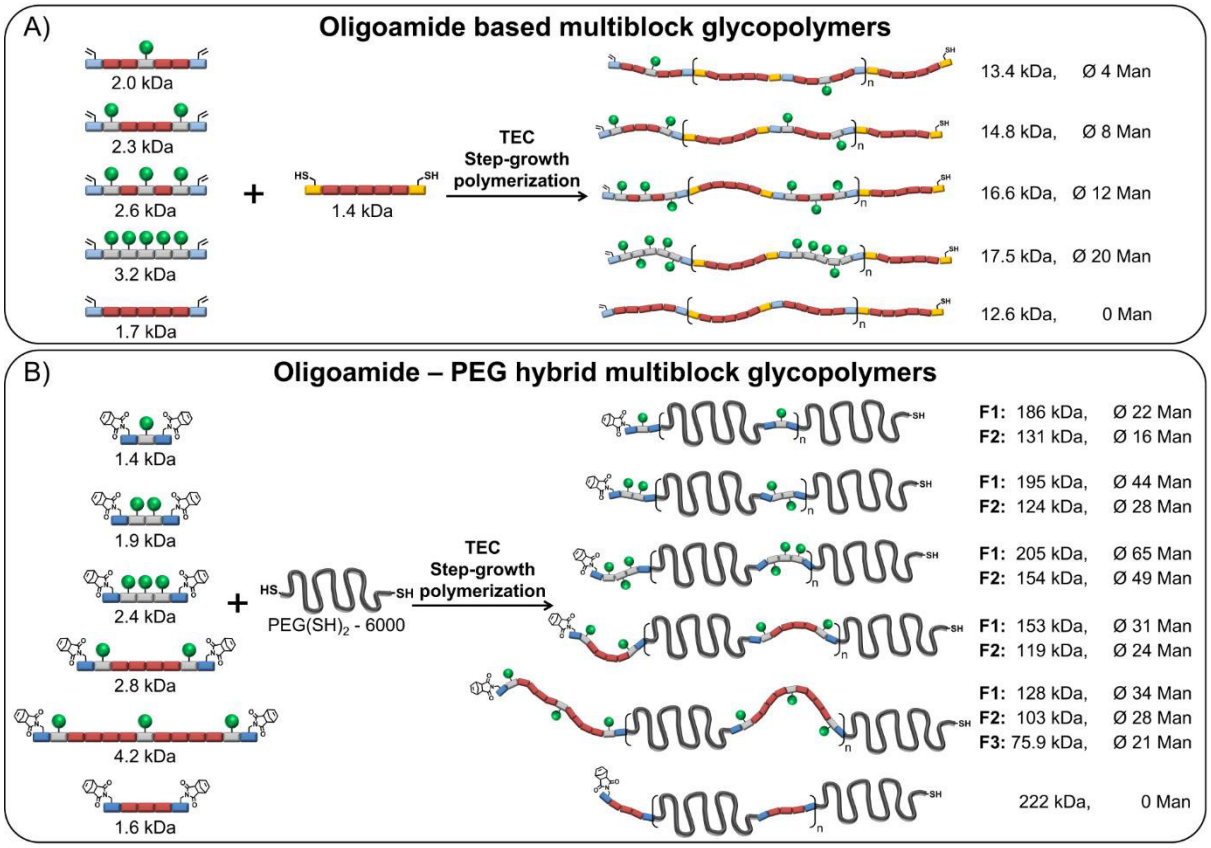

In the second part of this thesis, the goal was to further increase the molecular weights and the overall Man valency of multiblock glycopolymers. For this task, a more reactive alkene moiety was introduced by developing a novel building block. As alkene moiety a norbornene group was chosen, which is known to be highly reactive in radical-mediated TEC.[112] Due to the higher reactivity when compared to the vinyl group of the previously used DDS, a higher conversion and thus higher $\bar{X}_n$ could be expected. The novel NDS building block was successfully synthesized using a similar synthetic approach as for previously introduced functional building blocks, starting from the heteroprotected diethylenetriamine key intermediate.[83] The centered secondary amine was used to introduce a norbornene bearing linker. As linker, an *N*-propionic acid functionalized nadicimide was chosen. Its carboxylic acid group was subsequently coupled onto the centered secondary amine of the key intermediate via the acid chloride derivative. The final NDS building block was obtained in high purity (> 98%) adapting established synthetic procedures[83] for the following two reaction steps, exchanging the trifluoroacetamide by an Fmoc group and the trityl by a succinyl group.

The final synthetic pathway towards the novel NDS building block is shown in **Scheme 9**. By synthesizing two similar glyco(oligoamides), one with terminal DDS and the other with the novel NDS building blocks, their reactivity in radical-mediated TEC was compared. Therefore, both oligoamides were polymerized with the dithiol functionalized spacing macromonomer used during method development as well as for the first set of glycopolymers, by applying the optimized reaction conditions. It was observed that a 40% higher $\bar{X}_n$ was accessible when using the novel NDS building block, proving the assumption of further increasing $\bar{X}_n$ due to the higher reactivity.

Scheme 9: Synthetic overview of the synthesis of the novel norbornene bearing NDS building block, starting from the key intermediate and the acid chloride of *N*-propionic acid functionalized nadicimide, followed by two protecting group exchanges analog to the synthetic pathway of other functional building blocks.

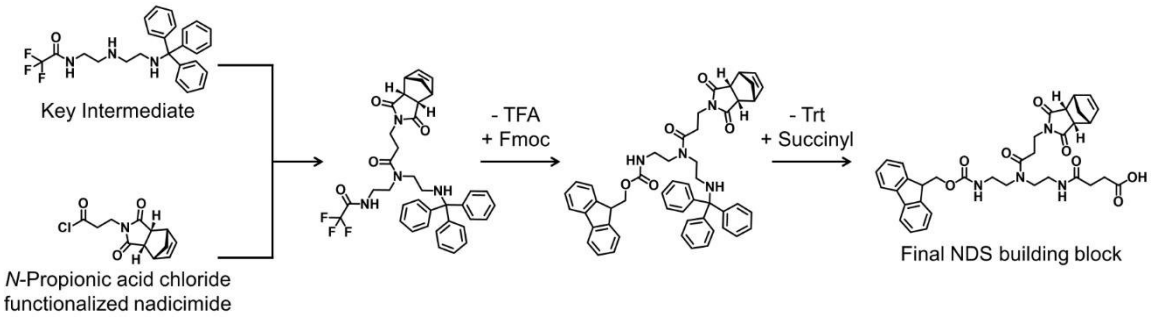

Therefore, a second set of glycomacromonomers with terminal NDS building blocks was synthesized by SPS, obtaining a total of five Man functionalized structures carrying between one and three Man moieties. Two different glycomacromonomers with a Man valency of two and three were synthesized, one without spacing between the carbohydrates and another with a spacing of four EDS blocks between the Man moieties as shown in **Scheme 8B**. Besides the five glycomacromonomers, one macromonomer not carrying Man moieties to be used as negative control in later binding studies was synthesized. In contrast to the first set of glycomacromonomers, the second set was not copolymerized with a defined oligoamide from SPS but with a commercially available end-functionalized poly(ethylene glycol) with an $\bar{M}_n$ of 6000 Da, presenting two terminal thiol moieties (PEG(SH)$_2$-6000) (see **Scheme 8B**). Thereby, the final molecular weight of the resulting glycopolymers but also the spacing between the Man bearing binding blocks were further increased. The reaction conditions for the polymerization of the six macromonomers derived from SPS with PEG(SH)$_2$-6000 had to be slightly adapted due to the low solubility of the formed oligoamide – PEG copolymers at room temperature using a DMSO and water mixture in a ratio of 9/1. After starting the UV irradiation, an instant solidification of the reaction mixture was observed. Therefore, the solvent, the concentration of the macromonomers as well as the reaction temperature were adapted from the previous protocol. As final reaction conditions, an equal ratio of DMSO and water was used and the final concentration of the macromonomers was reduced to 25 mM. The reaction temperature was set at 50 °C, ensuring complete solubility of the macromonomers and additional reagents over the entire reaction time of 60 min. With the adapted reaction conditions, all six macromonomers were polymerized with PEG(SH)$_2$-6000.

Average $\bar{X}_n$ values of 45 were achieved, which was significantly higher compared to those reached for the previously synthesized multiblock copolymers. This is attributed to the more reactive NDS building blocks as well as the higher reaction temperature. The increased temperature could be potentially beneficial for the diffusion rate of the macromonomers and also for a reduced viscosity during the course of the polymerization. However, besides the TEC step-growth, a further concurrent side-reaction was observed, which became especially evident when evaluating the GPC elugrams of the final polymers showing multimodal distributions and a nonlinear slope in the molecular weight vs. elution volume plot, as shown in the GPC elugram in **Figure 14A**. By a series of control experiments, the side-reaction was identified to be a pronounced oxidation of the thiol groups to disulfides, thereby linking various PEG(SH)$_2$-6000 chains together to form high molecular weight PEG-based polymers, as shown in **Figure 14A**. Since the PEG-based side-product only incorporated low amounts of the Man-bearing glyco(oligoamide) block, the side-product was successfully removed by performing an affinity chromatography using a Sepharose 4B resin with immobilized Con A receptors (see **Figure 14B**).

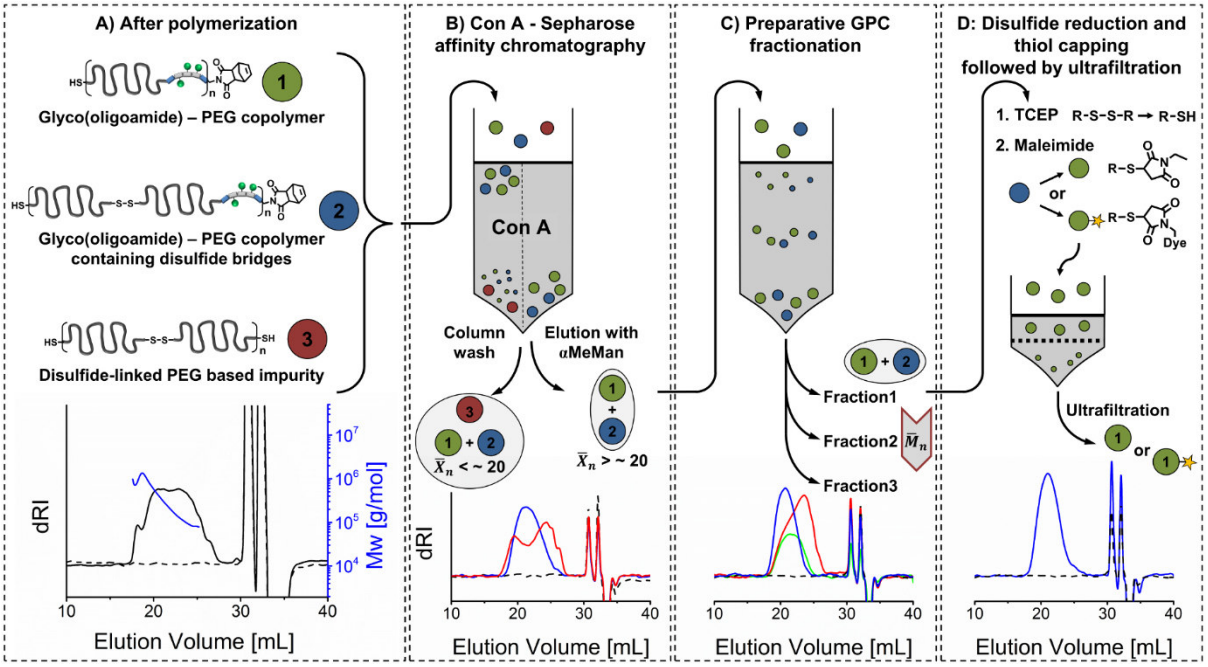

Figure 14: Overview of formed compounds using the example of the glyco(oligoamide) – PEG multiblock copolymer obtained after polymerizing a trivalent glyco(oligoamide) with PEG(SH)$_2$-6000 as well as the separation of the two impurities applying different purification procedures. The purification procedures are illustrated schematically and the separation of a specific species is stated. Exemplary GPC-RI-LS elugrams after each purification step are shown. A) Structure of desired product (1) as well as the two major side products (2 + 3) and GPC elugram (black) as well as the molecular weight plot (blue). B) Illustration of purification by affinity chromatography and GPC elugrams after the washing (red) and elution (blue) process. C) Illustration of fractionation procedure by preparative GPC and GPC elugrams of the three separated fractions 1, 2 and 3 (blue, green and red). D) Illustration of disulfide reduction and thiol capping procedure and GPC elugram of the final purified glyco(oligoamide) – PEG multiblock copolymer (blue). GPC-RI-LS setup: Columns: Suprema Lux (2 × 100 and 1 × 1000 Å). Buffer: 50 mM NaH_2PO_4, 150 mM NaCl, 250 ppm of NaN_3 (pH 7.2), 30% ACN. Flow: 0.8 mL/min. Adapted with permission from C. Gerke, F. Jacobi, L. E. Goodwin, F. Pieper, S. Schmidt, L. Hartmann, Sequence-Controlled High Molecular Weight Glyco(oligoamide) – PEG Multiblock Copolymers as Ligands and Inhibitors in Lectin Binding, *Macromolecules*, **2018**, 51, (15), 5608−5619. Copyright © 2018 American Chemical Society.

After applying the obtained polymer mixture to the Sepharose Con A column, the glyco(oligoamide) – PEG multiblock copolymers bound to the immobilized Con A on the column due to an interaction of the Man moieties, whereas the PEG-based side product could be washed off the column. After excessive washing, the bound glyco(oligoamide) – PEG copolymers were eluted from the column by adding a solution containing methyl-α-D-mannopyranoside (αMeMan). After the affinity chromatography, the molecular weight distribution was further reduced by performing an additional purification step by preparative GPC fractionation (see **Figure 14C**). For each glyco(oligoamide) – PEG multiblock copolymer, three fractions were collected and fractions with an $\bar{M}_w/\bar{M}_n$ below 1.7 were used in the following procedures. As a final purification step, the remaining disulfide bonds in the glyco(oligoamide) – PEG multiblock copolymers were reduced by incubation in a solution of TCEP and the liberated thiol moieties were capped with a maleimide reagent to prevent a subsequent oxidation to disulfides. Besides the remaining reducing reagent and maleimide, also low molecular weight cleavage fragments, formed after disulfide reduction, were removed by ultrafiltration (see **Figure 14D**). An overview of the three purification steps, presenting exemplary structures for the final glyco(oligoamide) – PEG multiblock copolymers as well as the formed side-products is shown in **Figure 14** along with GPC elugrams of the separated fractions. In total, 12 oligoamide – PEG multiblock copolymers were isolated, exhibiting $\bar{X}_n$ between 14 and 56 corresponding to $\bar{M}_n$ between 75.9 and 222 kDa, thereby successfully further increasing both values as initially targeted by the introduction of the NDS building block and the $PEG(SH)_2$-6000 chain. The average Man valencies varied between 16 and 65 moieties and were therefore also further increased compared to those of the first generation of multiblock glycopolymers. The structures as well as the achieved $\bar{M}_n$, and the average Man valency for different isolated fractions of each polymer by preparative GPC fractionation are shown in **Scheme 8B**.

The glycopolymers obtained from both approaches were subjected to binding assays with the Man specific lectin Con A. In total, 15 different glycopolymers were achieved with a broad range of final $\bar{M}_n$ as well as average Man valencies. The glycopolymers from the first series have $\bar{M}_n$ up to 17.5 kDa whereas the $\bar{M}_n$ of the PEG hybrid glycopolymers are with a maximum value of 222 kDa more than tenfold higher. Also, the Man valencies of the majority of the glyco(oligoamide) – PEG copolymers (16 – 65 Man) are above those of the first set of glycopolymers (4 – 20 Man). Besides the synthesized glycopolymers, also the glycomacromolecules used as macromonomers for the first set of polymers were applied in lectin binding studies, thereby including low molecular weight (1.8 – 3.2 kDa) carbohydrate ligands presenting a few Man moieties (1 – 5 Man). In addition to the glycopolymers, a total of 19 Man bearing ligands were available to further investigate specific multivalent binding mechanisms. The polymeric ligands were specifically designed to focus on the effect of carbohydrate density and spacing on receptor binding and clustering, presenting a spacing between Man-bearing blocks either by a hydrophilic spacing block out of five EDS or a significantly larger PEG-6000 chain. In previous studies by other research groups, it was shown that a high carbohydrate valency is not necessarily beneficial for effective lectin binding and clustering, which is mainly attributed to an excessive carbohydrate density rather than valency.[169, 185, 192, 196, 216]

To investigate whether the introduced spacing affects the interactions towards Con A, a total of four different assays were performed. Two assays are based on the formation of an insoluble precipitate due to a cross-linking of multiple lectin receptors after the addition of carbohydrate ligands, therefore obtaining information about effective receptor clustering. In the first assay, the carbohydrate ligands are titrated into a solution with a fixed Con A concentration and the required ligand concentration to reach half-maximal turbidity (conc. $½T_{Max}$) can be obtained. The reciprocal value (1/ conc. $½T_{Max}$) is subsequently used to compare the ligands clustering potential. In the second assay, the amount of Con A in a formed precipitate after the addition of a fixed ligand concentration is determined photometrically. The thereby resulting receptor/ligand ratio in the formed precipitate can be used to compare the different carbohydrate ligands. The two turbidity assays were only performed for the first set of multiblock glycopolymers as well as their precursor glycomacromolecules. The results from both turbidity based assays are shown in **Figure 15**.

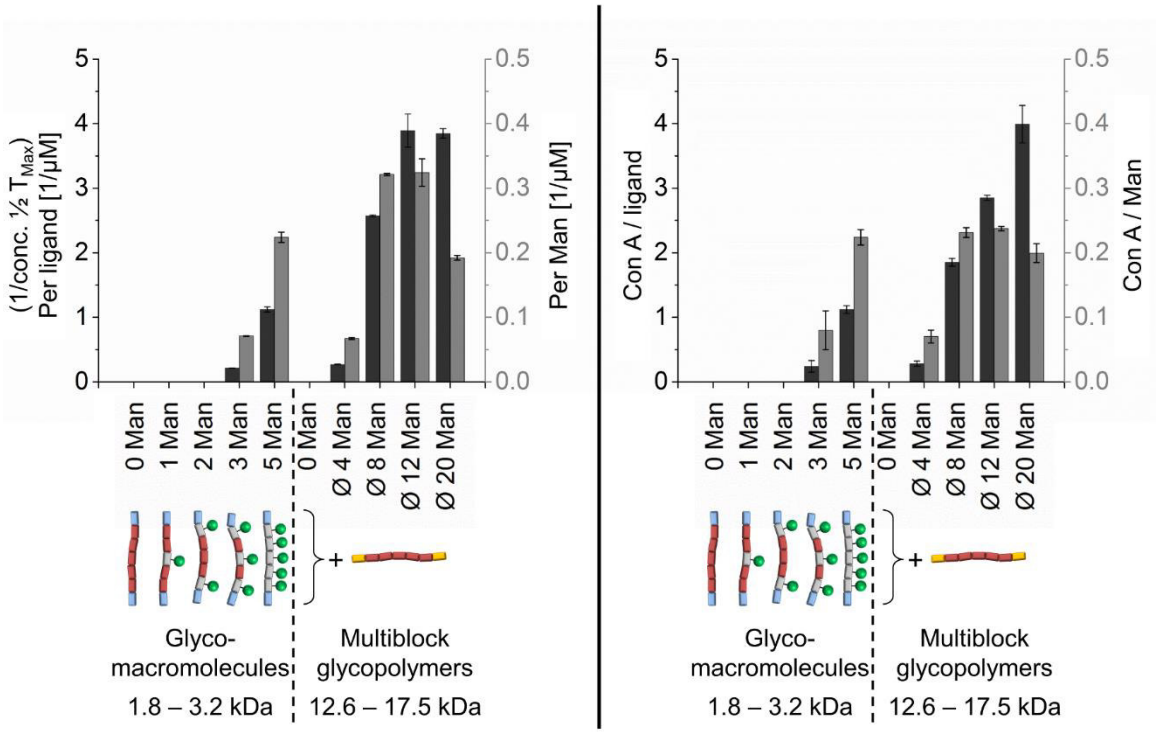

Figure 15: Results from the two turbidity based assays showing left the reciprocal value of the required ligand concentration for half-maximal turbidity (black bars) as well as the normalized values per Man moiety giving the reciprocal values of the required Man concentration for half-maximal turbidity (grey bars) and right the determined Con A/ligand ratios in the formed precipitate (black bard) as well as the normalized values per Man giving the ratio of Con A/Man in the precipitate.

It was found that the clustering potential was mainly dependent on the Man valency. However, when reaching higher Man valencies, the increase in clustering efficiency stalls and in one of the two turbidity assays even decreased for the glycopolymer with the highest Man valency (20 Man) (see **Figure 15** (black bars) and **Figure 17A** (right)). This is in agreement with the previously described hypothesis which states that not every carbohydrate moiety on a multivalent scaffold takes part during the interaction towards a lectin receptor.[169, 192, 196] To further evaluate this finding, the contribution of one Man moiety of the carbohydrate ligands on the receptor clustering was determined by normalizing the measured values onto the number of Man moieties on the scaffold.

After normalization, the assertion becomes even more evident, now showing a decrease in clustering efficiency per Man moiety in both performed turbidity assays. Highest values were achieved for the glycopolymers with 8 and 12 Man moieties with decreasing clustering efficiency when further increasing Man valency (see **Figure 15**, grey bars).

After the evaluation of the Man valency in the turbidity based assays, the effect of the molecular weight and Man spacing were assessed. Even though the molecular weight of the glycomacromolecules containing 3 and 5 Man moieties is with 3 kDa approximately five times below that of the glycopolymer presenting an average of 4 Man moieties (13.4 kDa) and also that their interligand spacing exhibit significant differences, surprisingly similar values in their receptor clustering potential were obtained (see **Figure 15**, black bars). At first, it was assumed that the accessible Man density in solution might be similar for the three stated glycomimetics due to the formation of a highly coiled conformation of the glycopolymer containing 4 Man moieties, thereby explaining their similar clustering potential. However, as determined by DLS measurements, the hydrodynamic radii (R_h) of the glycomacromonomers are with values of 1.5 and 1.4 nm, respectively, approximately four times lower when compared to the glycopolymer, exhibiting an R_h of 5.8 nm. Due to these findings, the similar clustering potential is assumed to be obtained by different ongoing mechanisms when comparing the low molecular weight glycomacromonomers with the high molecular weight glycopolymer. Whereas the glycomacromonomers are not able to simultaneously bind two CRD of one Con A receptor, a chelate formation by the glycopolymer is possible, thereby increasing binding affinity towards one Con A receptor. In contrast to that, the possibility of an initial binding event and statistical rebinding are more likely for the glycomacromonomers due to the higher density of Man binding ligands when compared to the glycopolymer. Although both mechanisms are probably only targeted to a certain extent since the clustering potential of the three compared carbohydrate ligands is rather low when compared to the higher-valent ligands, it can be assumed that the influence of the two different binding mechanisms result in a similar overall Con A binding affinity of the two glycomacromolecules and the glycopolymer which may result in similar stabilities of the formed Con A clusters (see **Figure 17A** (left)).

A further assay performed to evaluate the interaction with Con A, which included all 19 carbohydrate ligands, was an SPR direct binding assay to determine the K_A values for each ligand. For the multiblock glycopolymers from the first set, similar to the results from the turbidity assays, an increased binding affinity for an increasing Man valency was observed. The most pronounced increase in binding affinity is achieved after exceeding a valency of 5 Man moieties. In contrast to the turbidity assays, in the direct binding assay, no subsequent decrease was observed after passing through a maximum, showing highest K_A for the glycopolymer with 20 Man moieties (see **Figure 16**, black bars). Additionally for the Man normalized values, the affinity is continuously increasing, although not as pronounced (see **Figure 16**, grey bars). A reason for the observed differences between the results from the turbidity and the direct binding assays may be again explained by the different influence of ongoing binding mechanisms due to the different setup of the assays.

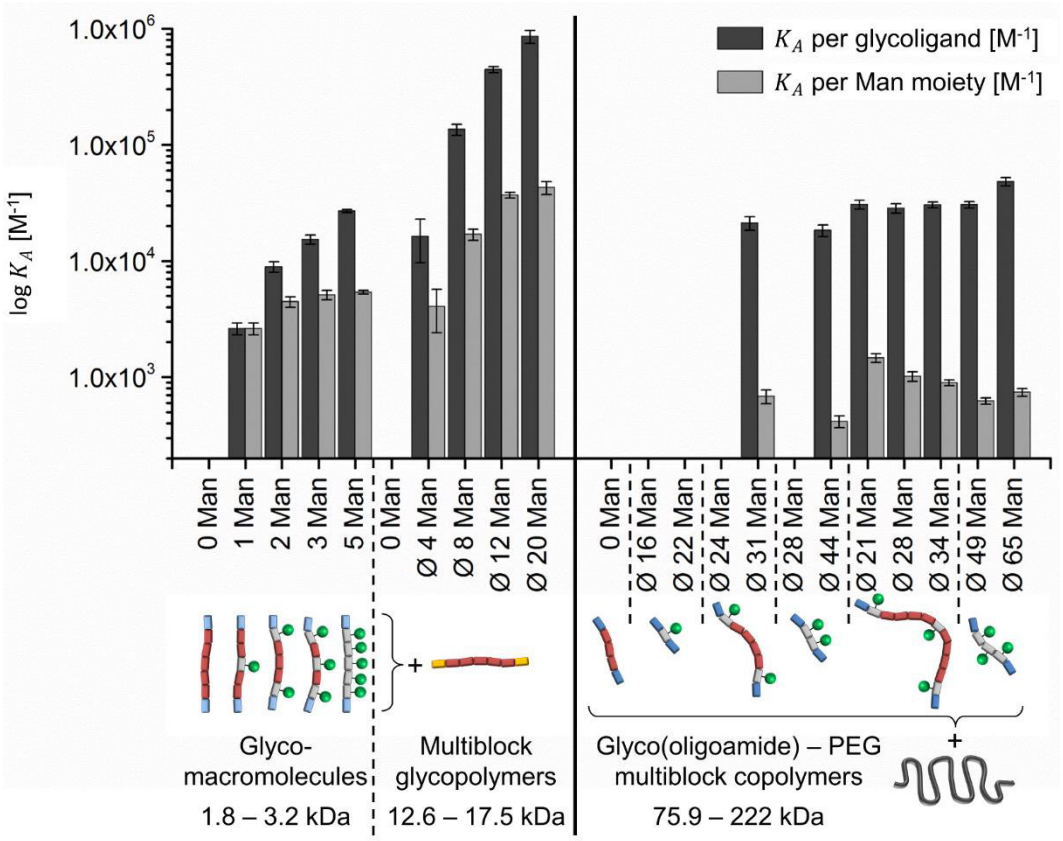

Figure 16: Results from the SPR direct binding assay showing the determined K_A per ligand (black bars) as well as per Man moiety (grey bars) for all 19 carbohydrate ligands synthesized as well as three negative controls not presenting Man moieties.

Here, especially statistical rebinding and conformational changes of the carbohydrate ligands are likely, which are assumed to have a significantly higher effect in the direct binding SPR assay, representing a binding situation in solution with a constant movement of ligands, compared to a turbidity assay during which a solid precipitate is formed. After the formation of a solid precipitate and the resulting low movement of the ligands and Con A receptors, an unbinding followed by a subsequent rebinding of a different Man binding moiety in close proximity is not as pronounced and relevant for the overall affinity. Also conformational changes of the carbohydrate ligands, thereby subsequently obtaining accessibility of previously screened Man moieties, is rather not possible after a solid precipitate is formed. In the direct binding SPR however, statistical rebinding and constant conformational changes of the ligand are likely which can explain the further increase in K_A with increasing Man valency and the higher contribution of one Man moiety during binding. In the turbidity assays, the Con A binding sites are assumed to be saturated after exceeding 12 Man moieties per carbohydrate ligand and a further increase in Man moieties is not beneficial for effective Con A clustering. On the contrary, it seems even to have a negative influence for the glycopolymer presenting an average of 20 Man moieties, supposedly due to the close positioning of the Man ligands and their potential steric hindrance during Con A binding (see **Figure 17A** (right) and **B** (top right)).

When again comparing the two glycomacromolecules with 3 and 5 Man moieties with the glycopolymers presenting an average of 4 Man moieties, this time in terms of their binding affinity, a similar behavior as in the previously stated turbidity assays can be observed (see **Figure 16**, black bars). Also in this assay, no influence of the carbohydrate spacing or overall molecular weight of the carbohydrate ligands towards their binding affinity is observed, probably due to the same reason of different influences of ongoing binding mechanisms (statistical rebinding vs. chelate binding) (see **Figure 17A** (left) and **B** (top left)).

The introduced spacing using the EDS based hydrophilic spacing block is supposedly still too short to have a significant influence on lectin binding as well as clustering by the spanning of multiple CRD. Therefore, the second set of glyco(oligoamide) – PEG multiblock copolymers was synthesized to increase the spacing between the carbohydrate binding blocks further and applied in a similar SPR direct binding assay, as the glycomacromolecules and glycopolymers from the previous series. A glycopolymer from the first set was included in the assay, obtaining the same value for K_A as in the previously performed SPR experiment, which therefore allows for direct comparison of the structures from the first and the second set of carbohydrate ligands synthesized. Since the glyco(oligoamide) – PEG copolymers exhibit significantly higher average Man valencies (16 – 65 Man), K_A values were expected to lie in the same range or even above that of the multiblock glycopolymer with highest Man valency (20 Man) from the first set. However, surprisingly the measured K_A values were at least a factor 20 below the determined value for the highest affinity binding multiblock glycopolymer from the first set and rather in a range of the low molecular weight and low-valent glycomacromolecules, despite their significantly higher Man valency (see **Figure 16**, black bars). Whereas the spacing seems to have had a relatively low influence for the first set of glycopolymers, the high molecular weight PEG block in the second series seems to significantly decrease binding affinity towards Con A, which is also in agreement with previous findings of other groups working with similar PEGylated carbohydrate ligands.[243] The low binding affinity can be explained by the decrease of carbohydrate density below a certain threshold but also by an increased steric repulsion of the carbohydrate ligands during binding due to their elevated molecular weight, which was also discussed by other groups.[90, 169, 192, 196] In addition to the high molecular weight of the ligands, also the flexibility of the PEG chain may have a negative influence on the binding, as already determined in previous works using flexible carbohydrate functionalized PEG particles[228, 230], thereby increasing the conformational entropy (see **Figure 17B** (bottom left)). Furthermore, by GPC analysis, a highly coiled conformation of the glyco(oligoamide) – PEG copolymers in solution was determined, which supports the assumption that a great number of Man moieties are not accessible for lectin binding, due to a pronounced shielding by the PEG chains. When calculating the K_A per Man moiety for the glyco(oligoamide) – PEG copolymers, the low contribution of one Man moiety becomes evident. The Man normalized K_A values of all glyco(oligoamide) – PEG copolymers were even lower when compared to the value of the monovalent glycomacromolecule (see **Figure 16**, grey bars).

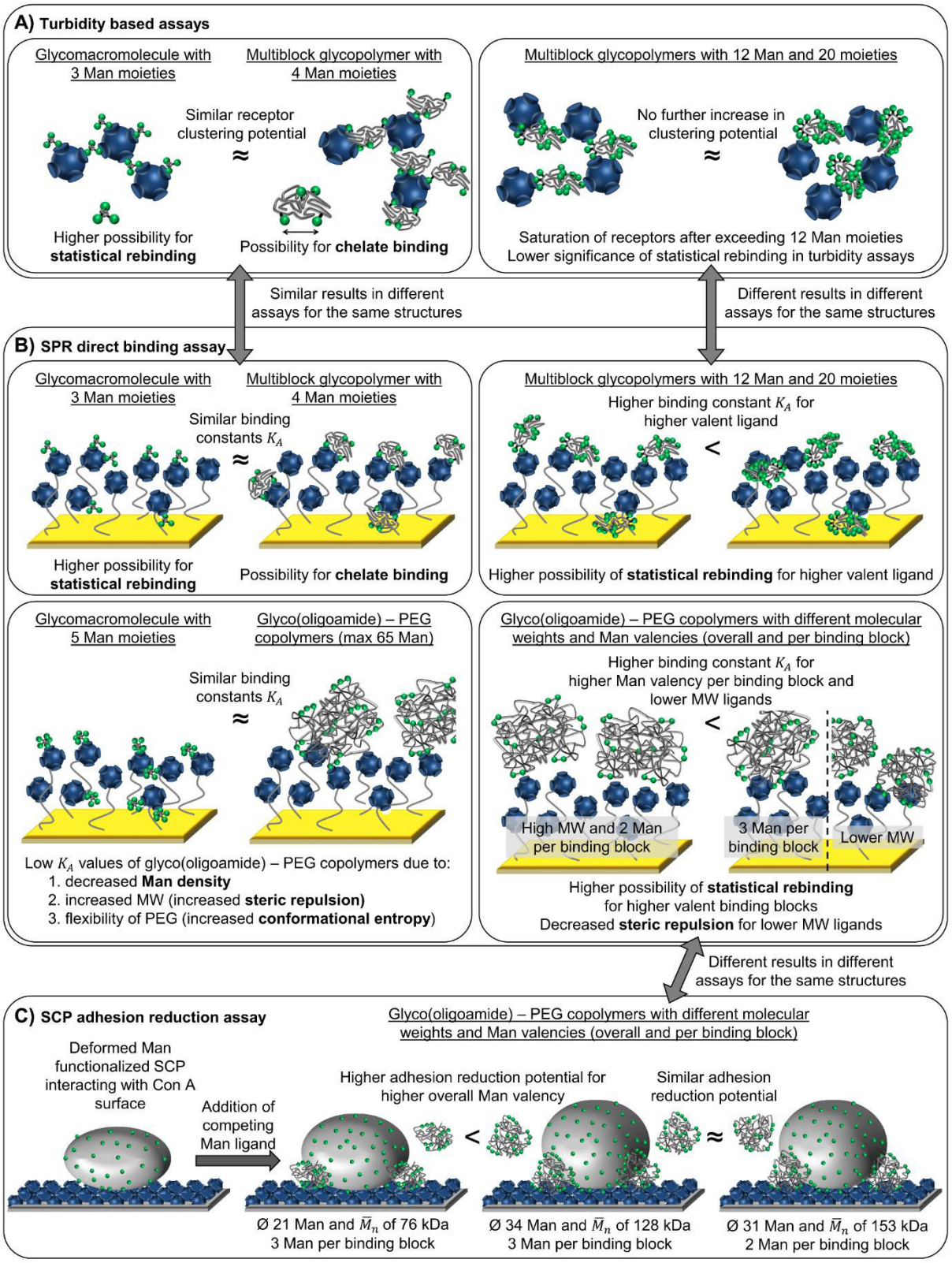

Figure 17: Schematic overview summarizing the most important results obtained from A) the turbidity based assays, B) the SPR direct binding assays and C) the SCP adhesion reduction assay, comparing different Man presenting ligands and discussing potential multivalent effects of macromolecular carbohydrate ligands that could explain the observations made in this thesis.

Besides the decrease in binding affinity with increasing molecular weight, a further correlation between an architectural feature of the different glyco(oligoamide) – PEG copolymers and lectin binding which can be observed among the series is that of Man valency within one binding block. Highest K_A values were determined for the glycopolymers derived from the trivalent glyco(oligoamides) followed by the divalent ones, whereas no K_A was able to be measured for the polymer derived out of the monovalent glyco(oligoamide), as shown in **Figure 16** (black bars). Since various glycopolymers, for which no or only very low K_A values were determined, have a similar overall average Man valency and molecular weight compared to those with higher binding affinities, the difference was attributed to the Man valency within the incorporated binding block. It can be assumed that a higher local concentration is beneficial for lectin binding, enhancing the probability for an initial binding event as well as statistical rebinding when a binding block is eventually exposed and not shielded by the PEG chain (see **Figure 17B** (bottom right)).

As further method, investigating the potential to inhibit carbohydrate – lectin interactions, a recently introduced assay based on the adhesion of Man functionalized PEG-microparticle, so-called soft colloidal probes (SCP), on a Con A functionalized glass surface, as shown in **Figure 17C** (left), was performed.[86, 207] Thereby the reduction in the adhesion energy of the SCP on the surface after the addition of a fixed concentration of glyco(oligoamide) – PEG copolymer was measured. The adhesion reduction assay was only performed for seven selected structures of the glyco(oligoamide) – PEG copolymers and results indicated that an inhibition is exclusively dependent on the Man valency rather than the interligand spacing, molecular weight or amount of Man moieties within the binding block, which were determined to be important parameters during the direct binding interaction. Especially an increase in molecular weight, which was stated to have a significantly negative influence during a direct binding event associated with an increasing steric repulsion, contributes differently in an inhibition based assay as also observed by other working groups.[169, 192, 195] In an inhibition event, an increasing molecular weight is even stated to be beneficial, thereby increasing a possible steric shielding of competing binding ligands.[174, 185] For the obtained results of the adhesion reduction assay, a positive influence of the molecular weight was not observed, supposedly because all synthesized glyco(oligoamide) – PEG copolymers already exceed a molecular weight for maximum steric shielding, which can be supported by findings of other groups also investigating the inhibition potential of synthetic glycopolymers towards Con A.[196, 214] Therefore, for the here applied glycopolymers, an exclusive direct correlation between increasing Man valency and adhesion reduction potential can be observed (see **Figure 17C**).

Overall, looking at the series of binding studies, it can be summarized that the structural design of multivalent carbohydrate ligands have distinct effects in each assay since various multivalent binding mechanisms are of importance and, depending on the assay, prevail to a different extent. Here, especially the differences between a direct binding in comparison to an inhibition assay are to mention. An increasing molecular weight of the glycopolymers results in a drastic decrease in binding affinity whereas the molecular weight seems not to have such a negative influence in the inhibition competition assay.

The same is true for a locally high concentration of binding ligands, thereby increasing statistical rebinding events which are crucial for a high affinity in a lectin direct binding event but are assumed to be less relevant in inhibition assays. Furthermore, slightly different results for the same carbohydrate ligands were observed from the turbidity assays when compared to the SPR direct binding assay. In the turbidity assays, a maximum Man valency for highest possible clustering potential was determined, whereas the direct binding assay showed a steady increase in binding efficiency with increasing Man valency for the first set of multiblock glycopolymers. The reason for this difference could be also based on the statistical rebinding effect, which is in the case of the turbidity assays only relevant to a low extent in the solidified complex when cross-linked.

In the third and final part of this thesis, an additional synthetic approach towards periodic sequence-controlled polymers with a regularly recurring monomer sequence along the polymeric backbone in one direction was successfully implemented. Similar to the synthesis of the multiblock copolymers, the approach combines SPS and a subsequent TEC step-growth polymerization. In contrast to the previously established procedure, an AB approach was applied, using a heterofunctionalized macromonomer, carrying both, the reactive alkene as well as the thiol moiety, in the same compound. Due to a self-initiation of heterofunctionalized macromonomers for TEC, the developed step-growth polymerization method was primarily limited to an AA/BB approach using two homofunctionalized macromonomers, which also implies the use of symmetrical sequences within the macromonomers to control the periodically recurring sequence completely. In addition to the terminal Cys as well as NDS for the introduction of the reactive end-groups, as non-symmetrical sequence for the AB approach, a combination of EDS building blocks and different amino acids (L-glycine (Gly), L-leucine (Leu), L-histidine (His), L-phenylalanine (Phe), L-serine (Ser), L-lysine (Lys)), displaying the initials of the participating researchers, was chosen (see **Scheme 10**).

Scheme 10: Schematic illustration of the two-step polymerization of the heterofunctionalized macromonomer with the MBNB protecting group towards a periodic copolymer with a regularly recurring monomer sequence along the polymeric backbone in one direction (the five structural repeating units stated on the brackets in the final polymer refer to the $\bar{X}_n$ achieved in the polymerization and does not imply the formation of a uniform end-product). Adapted with permission from C. Gerke, P. Siegfeld, K. Schaper, L. Hartmann, Enabling Directional Sequence-Control via Step-Growth Polymerization of Heterofunctionalized Precision Macromonomers, *Macromol. Rapid Commun.*, **2019**, 40, (3), 1800735. Copyright © 2019 John Wiley & Sons.

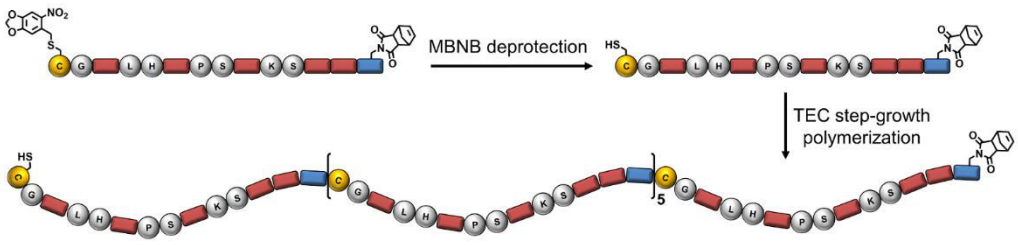

The uncontrolled self-initiation was prevented by the introduction of a photolabile protecting group which was attached to the reactive thiol end-group. As protecting group, 3,4-methylenebisoxy-6-nitrobenzyl (MBNB) was used which was successfully coupled to the thiol group as its bromide derivative, performing a nucleophilic substitution reaction directly on the solid support.

The MBNB group was chosen since this nitrobenzyl derivative shows a high absorption coefficient at a wavelength of 365 nm. The used medium pressure Hg UV lamp for polymerization also shows a strong band of emission. Therefore, an *in situ* liberation of the thiol group followed by a direct polymerization via TEC should theoretically be possible, however, so far proved not successful in the lab. Therefore, the step-growth polymerization of the heterofunctionalized macromonomer was conducted in a two-step procedure as shown in **Scheme 10**, first cleaving the MBNB group using an UV-LED lamp, followed by its polymerization using the medium pressure Hg UV lamp, applying the developed reaction condition used for the synthesis of the first set of multiblock glycopolymers.

A successful polymerization was achieved, reaching an $\bar{M}_n$ of 18.2 kDa for the periodic copolymer, corresponding to an $\bar{X}_n$ of 7 for the used macromonomer, which is in the same range as the first set of multiblock glycopolymers (see **Figure 13**). However, higher $\bar{X}_n$ were expected due to the use of the highly reactive norbornene end-group as well as an equimolar ratio of the reactive end-groups in an AB approach, which is crucial to reach high $\bar{X}_n$ in a step-growth polymerization. A further observation for the polymerization of the heterofunctionalized macromonomer was a pronounced formation of a macrocyclic compound, caused by an intramolecular TEC reaction of the macromonomer. Both, the low $\bar{X}_n$ as well as the formation of cyclic side-product, are assumed to be promoted due to a lower concentration of reactive end-groups in comparison to previously performed polymerizations. Furthermore, an increase in the reaction temperature could potentially further increase the $\bar{X}_n$, as observed during the synthesis of the glyco(oligoamide) – PEG multiblock copolymers. To remove the cyclic side-product as well as low molecular weight polymers, the periodic copolymer was purified via ultrafiltration using a membrane with a molecular weight cut off (MWCO) of 10 kDa, thereby successfully increasing the $\bar{X}_n$ to 10 corresponding to an $\bar{M}_n$ of 23.8 kDa.

Overall, the results of this thesis promote further progress within the field of sequence-controlled polymers, showing novel approaches towards multiblock copolymers as well as periodic copolymers with an additional directional control of the monomer sequence along the polymeric backbone. Combining SPS and TEC gives access to polymers exclusively based on oligoamides but also to hybrid polymers with incorporated conventional polymers, as shown for the PEG copolymer. In addition to the synthetic progress, new insights about the design and properties of polymeric glycomimetics were obtained. Specifically, the influence of carbohydrate spacing during multivalent binding towards the lectin Con A was evaluated, showing no influence when using a short spacing in terms of an EDS based oligoamide between the binding Man moieties and a drastic decrease in binding affinity when further increasing the spacing by a high molecular weight PEG chain.

Based on the presented novel synthetic approach, the scope of synthesizing bioactive sequence-controlled multiblock copolymers will be further extended in future studies. Due to the ease of introducing different biological relevant motifs in the macromonomer sequence during SPS and the high tolerance of the TEC polymerization procedure towards functional groups or solvents, the approach has great potential for a broad range of applications.

Possible examples potentially permitting the implementation of the presented synthetic approach could be in the field of degradable polymers with defined degradation pattern, polymeric drug delivery systems, but also high molecular weight pharmaceutically active compounds. Additionally, the demonstrated possibility of incorporating a conventional, end-functionalized polymer into the polymeric scaffold gives access to different hybrid block copolymers, potentially developing novel functional materials with unique properties. Besides the application of the synthetic procedure, the influence of the molecular weight as well as interligand spacing on multivalent binding mechanisms during lectin interaction will be further investigated, introducing a spacing size in between the here used hydrophilic spacing oligoamide and the PEG-6000 block, which were assumed either to be insufficient or excessive. Besides that, applying the approach using a photolabile protecting group, glycopolymers with a non-symmetrical carbohydrate presentation along the polymeric backbone are accessible which could allow for the investigation of the influence of a further structural feature of a glycomimetic on multivalent lectin binding.

4 References

1. Huxley, T. H., Nature: Aphorisms by Goethe. *Nature* **1869,** 1, 9-11.
2. Biggs, C. I.; Bailey, T. L.; Ben, G.; Stubbs, C.; Fayter, A.; Gibson, M. I., Polymer mimics of biomacromolecular antifreezes. *Nat. Commun.* **2017,** 8, (1), 1546.
3. Lv, J.; Song, Y.; Jiang, L.; Wang, J., Bio-Inspired Strategies for Anti-Icing. *ACS Nano* **2014,** 8, (4), 3152-3169.
4. Chalfie, M.; Tu, Y.; Euskirchen, G.; Ward, W.; Prasher, D., Green fluorescent protein as a marker for gene expression. *Science* **1994,** 263, (5148), 802-805.
5. Tsien, R. Y., The Green Fluorescent Protein. *Annu. Rev. Biochem.* **1998,** 67, (1), 509-544.
6. Jain, G.; Pendola, M.; Huang, Y.-C.; Juan Colas, J.; Gebauer, D.; Johnson, S.; Evans, J. S., Functional Prioritization and Hydrogel Regulation Phenomena Created by a Combinatorial Pearl-Associated Two-Protein Biomineralization Model System. *Biochemistry* **2017,** 56, (28), 3607-3618.
7. Bergström, L.; Sturm, E. V.; Salazar-Alvarez, G.; Cölfen, H., Mesocrystals in Biominerals and Colloidal Arrays. *Acc. Chem. Res.* **2015,** 48, (5), 1391-1402.
8. Schmidt, S.; Reinecke, A.; Wojcik, F.; Pussak, D.; Hartmann, L.; Harrington, M. J., Metal-Mediated Molecular Self-Healing in Histidine-Rich Mussel Peptides. *Biomacromolecules* **2014,** 15, (5), 1644-1652.
9. Baer, A.; Schmidt, S.; Haensch, S.; Eder, M.; Mayer, G.; Harrington, M. J., Mechanoresponsive lipid-protein nanoglobules facilitate reversible fibre formation in velvet worm slime. *Nat. Commun.* **2017,** 8, (1), 974.
10. Lalli, G.; Bohnert, S.; Deinhardt, K.; Verastegui, C.; Schiavo, G., The journey of tetanus and botulinum neurotoxins in neurons. *Trends Microbiol.* **2003,** 11, (9), 431-437.
11. Lacy, D. B.; Tepp, W.; Cohen, A. C.; DasGupta, B. R.; Stevens, R. C., Crystal structure of botulinum neurotoxin type A and implications for toxicity. *Nat. Struct. Biol.* **1998,** 5, 898.
12. Lutz, J.-F., Defining the Field of Sequence-Controlled Polymers. *Macromol. Rapid Commun.* **2017,** 38, (24), 1700582.
13. Martens, S.; Holloway, J. O.; Du Prez, F. E., Click and Click-Inspired Chemistry for the Design of Sequence-Controlled Polymers. *Macromol. Rapid Commun.* **2017,** 38, (24), 1700469.
14. Ouchi, M.; Sawamoto, M., Sequence-controlled polymers via reversible-deactivation radical polymerization. *Polym. J.* **2017,** 50, 83-94.
15. Szwarc, M., 'Living' Polymers. *Nature* **1956,** 178, 1168.
16. Szwarc, M.; Levy, M.; Milkovich, R., Polymerization Initiated By Electron Transfer To Monomer. A New Method of Formation of Block Polymers. *J. Am. Chem. Soc.* **1956,** 78, (11), 2656-2657.
17. Ziegler, K., Die Bedeutung der alkalimetallorganischen Verbindungen für die Synthese. *Angew. Chem.* **1936,** 49, (30), 499-502.
18. Ndiaye, P. A., *Nylon and Bombs: DuPont and the March of Modern America*. Johns Hopkins University Press: Baltimore, 2007.
19. Higashimura, T.; Kishiro, O., Possible Formation of Living Polymers of *p*-Methoxystyrene by Iodine. *Polym. J.* **1977,** 9, 87-93.
20. Young, R. J.; Lovell, P. A., *Introduction to polymers*. CRC press: Boca Raton, 2011.
21. Ishizone, T.; Tsuchiya, J.; Hirao, A.; Nakahama, S., Anionic polymerization of monomers containing functional groups. 4. Anionic living polymerization of *N*,*N*-dialkyl-4-vinylbenzenesulfonamides. *Macromolecules* **1992,** 25, (19), 4840-4847.
22. Braunecker, W. A.; Matyjaszewski, K., Controlled/living radical polymerization: Features, developments, and perspectives. *Prog. Polym. Sci.* **2007,** 32, (1), 93-146.
23. Grubbs, R. B.; Grubbs, R. H., 50th Anniversary Perspective: Living Polymerization—Emphasizing the Molecule in Macromolecules. *Macromolecules* **2017,** 50, (18), 6979-6997.
24. di Lena, F.; Matyjaszewski, K., Transition metal catalysts for controlled radical polymerization. *Prog. Polym. Sci.* **2010,** 35, (8), 959-1021.
25. Chen, M.; Zhong, M.; Johnson, J. A., Light-Controlled Radical Polymerization: Mechanisms, Methods, and Applications. *Chem. Rev.* **2016,** 116, (17), 10167-10211.
26. Albertsson, A.-C.; Varma, I. K., Recent Developments in Ring Opening Polymerization of Lactones for Biomedical Applications. *Biomacromolecules* **2003,** 4, (6), 1466-1486.

27. Mespouille, L.; Coulembier, O.; Kawalec, M.; Dove, A. P.; Dubois, P., Implementation of metal-free ring-opening polymerization in the preparation of aliphatic polycarbonate materials. *Prog. Polym. Sci.* **2014,** 39, (6), 1144-1164.
28. Nguyen, S. T.; Johnson, L. K.; Grubbs, R. H.; Ziller, J. W., Ring-opening metathesis polymerization (ROMP) of norbornene by a Group VIII carbene complex in protic media. *J. Am. Chem. Soc.* **1992,** 114, (10), 3974-3975.
29. Bielawski, C. W.; Grubbs, R. H., Living ring-opening metathesis polymerization. *Prog. Polym. Sci.* **2007,** 32, (1), 1-29.
30. Matyjaszewski, K.; Woodworth, B. E.; Zhang, X.; Gaynor, S. G.; Metzner, Z., Simple and Efficient Synthesis of Various Alkoxyamines for Stable Free Radical Polymerization. *Macromolecules* **1998,** 31, (17), 5955-5957.
31. Listigovers, N. A.; Georges, M. K.; Odell, P. G.; Keoshkerian, B., Narrow-Polydispersity Diblock and Triblock Copolymers of Alkyl Acrylates by a "Living" Stable Free Radical Polymerization. *Macromolecules* **1996,** 29, (27), 8992-8993.
32. Hawker, C. J.; Bosman, A. W.; Harth, E., New Polymer Synthesis by Nitroxide Mediated Living Radical Polymerizations. *Chem. Rev.* **2001,** 101, (12), 3661-3688.
33. Nicolas, J.; Guillaneuf, Y.; Lefay, C.; Bertin, D.; Gigmes, D.; Charleux, B., Nitroxide-mediated polymerization. *Prog. Polym. Sci.* **2013,** 38, (1), 63-235.
34. Matyjaszewski, K.; Xia, J., Atom Transfer Radical Polymerization. *Chem. Rev.* **2001,** 101, (9), 2921-2990.
35. Matyjaszewski, K., Atom Transfer Radical Polymerization (ATRP): Current Status and Future Perspectives. *Macromolecules* **2012,** 45, (10), 4015-4039.
36. Wang, J.-S.; Matyjaszewski, K., Controlled/"living" radical polymerization. atom transfer radical polymerization in the presence of transition-metal complexes. *J. Am. Chem. Soc.* **1995,** 117, (20), 5614-5615.
37. Chiefari, J.; Chong, Y. K.; Ercole, F.; Krstina, J.; Jeffery, J.; Le, T. P. T.; Mayadunne, R. T. A.; Meijs, G. F.; Moad, C. L.; Moad, G.; Rizzardo, E.; Thang, S. H., Living Free-Radical Polymerization by Reversible Addition-Fragmentation Chain Transfer: The RAFT Process. *Macromolecules* **1998,** 31, (16), 5559-5562.
38. Moad, G.; Rizzardo, E.; Thang, S. H., Radical addition-fragmentation chemistry in polymer synthesis. *Polymer* **2008,** 49, (5), 1079-1131.
39. Percec, V.; Guliashvili, T.; Ladislaw, J. S.; Wistrand, A.; Stjerndahl, A.; Sienkowska, M. J.; Monteiro, M. J.; Sahoo, S., Ultrafast Synthesis of Ultrahigh Molar Mass Polymers by Metal-Catalyzed Living Radical Polymerization of Acrylates, Methacrylates, and Vinyl Chloride Mediated by SET at 25 °C. *J. Am. Chem. Soc.* **2006,** 128, (43), 14156-14165.
40. Zhang, Q.; Collins, J.; Anastasaki, A.; Wallis, R.; Mitchell, D. A.; Becer, C. R.; Haddleton, D. M., Sequence-Controlled Multi-Block Glycopolymers to Inhibit DC-SIGN-gp120 Binding. *Angew. Chem. Int. Ed.* **2013,** 52, (16), 4435-4439.
41. Matsuo, Y.; Konno, R.; Ishizone, T.; Goseki, R.; Hirao, A., Precise Synthesis of Block Polymers Composed of Three or More Blocks by Specially Designed Linking Methodologies in Conjunction with Living Anionic Polymerization System. *Polymers* **2013,** 5, (3), 1012-1040.
42. Lutz, J.-F.; Schmidt, B. V. K. J.; Pfeifer, S., Tailored Polymer Microstructures Prepared by Atom Transfer Radical Copolymerization of Styrene and *N*-substituted Maleimides. *Macromol. Rapid Commun.* **2011,** 32, (2), 127-135.
43. Pfeifer, S.; Lutz, J.-F., Development of a Library of *N*-Substituted Maleimides for the Local Functionalization of Linear Polymer Chains. *Chem. Eur. J.* **2008,** 14, (35), 10949-10957.
44. Ida, S.; Terashima, T.; Ouchi, M.; Sawamoto, M., Selective Radical Addition with a Designed Heterobifunctional Halide: A Primary Study toward Sequence-Controlled Polymerization upon Template Effect. *J. Am. Chem. Soc.* **2009,** 131, (31), 10808-10809.
45. Ida, S.; Ouchi, M.; Sawamoto, M., Designer Template Initiator for Sequence Regulated Polymerization: Systems Design for Substrate-Selective Metal-Catalyzed Radical Addition and Living Radical Polymerization. *Macromol. Rapid Commun.* **2011,** 32, (2), 209-214.
46. Hibi, Y.; Tokuoka, S.; Terashima, T.; Ouchi, M.; Sawamoto, M., Design of AB divinyl "template monomers" toward alternating sequence control in metal-catalyzed living radical polymerization. *Polym. Chem.* **2011,** 2, (2), 341-347.

47. Ouchi, M.; Nakano, M.; Nakanishi, T.; Sawamoto, M., Alternating Sequence Control for Carboxylic Acid and Hydroxy Pendant Groups by Controlled Radical Cyclopolymerization of a Divinyl Monomer Carrying a Cleavable Spacer. *Angew. Chem. Int. Ed.* **2016,** 55, (47), 14584-14589.
48. Gutekunst, W. R.; Hawker, C. J., A General Approach to Sequence-Controlled Polymers Using Macrocyclic Ring Opening Metathesis Polymerization. *J. Am. Chem. Soc.* **2015,** 137, (25), 8038-8041.
49. Zhang, J.; Matta, M. E.; Hillmyer, M. A., Synthesis of Sequence-Specific Vinyl Copolymers by Regioselective ROMP of Multiply Substituted Cyclooctenes. *ACS Macro Lett.* **2012,** 1, (12), 1383-1387.
50. Flory, P. J., Molecular Size Distribution in Linear Condensation Polymers1. *J. Am. Chem. Soc.* **1936,** 58, (10), 1877-1885.
51. Flory, P. J., Fundamental Principles of Condensation Polymerization. *Chem. Rev.* **1946,** 39, (1), 137-197.
52. Carothers, W. H., Polymers and polyfunctionality. *Trans. Faraday Soc.* **1936,** 32, (0), 39-49.
53. Sworen, J. C.; Smith, J. A.; Berg, J. M.; Wagener, K. B., Modeling Branched Polyethylene: Copolymers Possessing Precisely Placed Ethyl Branches. *J. Am. Chem. Soc.* **2004,** 126, (36), 11238-11246.
54. Berthet, M.-A.; Zarafshani, Z.; Pfeifer, S.; Lutz, J.-F., Facile Synthesis of Functional Periodic Copolymers: A Step toward Polymer-Based Molecular Arrays. *Macromolecules* **2010,** 43, (1), 44-50.
55. Yu, T.-B.; Bai, J. Z.; Guan, Z., Cycloaddition-Promoted Self-Assembly of a Polymer into Well-Defined β Sheets and Hierarchical Nanofibrils. *Angew. Chem. Int. Ed.* **2009,** 121, (6), 1117-1121.
56. Luo, K.; Yang, J.; Kopečková, P.; Kopeček, J., Biodegradable Multiblock Poly[*N*-(2-hydroxypropyl)methacrylamide] via Reversible Addition-Fragmentation Chain Transfer Polymerization and Click Chemistry. *Macromolecules* **2011,** 44, (8), 2481-2488.
57. Walker, C. N.; Sarapas, J. M.; Kung, V.; Hall, A. L.; Tew, G. N., Multiblock Copolymers by Thiol Addition Across Norbornene. *ACS Macro Lett.* **2014,** 3, (5), 453-457.
58. Vandenbergh, J.; Ramakers, G.; van Lokeren, L.; van Assche, G.; Junkers, T., Synthesis of degradable multi-segmented polymers via Michael-addition thiol-ene step-growth polymerization. *RSC Adv.* **2015,** 5, (100), 81920-81932.
59. Driessen, F.; Du Prez, F. E.; Espeel, P., Precision Multisegmented Macromolecular Lineups: A Display of Unique Control over Backbone Structure and Functionality. *ACS Macro Lett.* **2015,** 4, (6), 616-619.
60. Merrifield, R. B., Solid Phase Peptide Synthesis. I. The Synthesis of a Tetrapeptide. *J. Am. Chem. Soc.* **1963,** 85, (14), 2149-2154.
61. Fischer, E.; Fourneau, E., Über einige Derivate des Glykocolls. *Ber. Dtsch. Chem. Ges.* **1901,** 34, (2), 2868-2877.
62. Bergmann, M.; Zervas, L., Über ein allgemeines Verfahren der Peptid-Synthese. *Ber. Dtsch. Chem. Ges.* **1932,** 65, (7), 1192-1201.
63. Isidro-Llobet, A.; Álvarez, M.; Albericio, F., Amino Acid-Protecting Groups. *Chem. Rev.* **2009,** 109, (6), 2455-2504.
64. Kimmerlin, T.; Seebach, D., '100 years of peptide synthesis': ligation methods for peptide and protein synthesis with applications to β-peptide assemblies. *J. Pept. Res.* **2005,** 65, (2), 229-260.
65. Stawikowski, M.; Fields, G. B., Introduction to Peptide Synthesis. *Curr. Protoc. Protein Sci.* **2012,** 69, (1), 18.1.1-18.1.13.
66. Sheehan, J. C.; Hess, G. P., A New Method of Forming Peptide Bonds. *J. Am. Chem. Soc.* **1955,** 77, (4), 1067-1068.
67. Albericio, F.; Tulla-Puche, J., *The power of functional resins in organic synthesis*. WILEY-VCH Verlag GmbH & Co. KGaA: Weinheim, 2008.
68. Jin, S.; Holub, D. P.; Wustrow, D. J., Reductive cleavage of resin bound arylsulfonates. *Tetrahedron Lett.* **1998,** 39, (22), 3651-3654.
69. Yoo, D. J.; Greenberg, M. M., Synthesis of Oligonucleotides Containing 3'-Alkyl Carboxylic Acids Using Universal, Photolabile Solid Phase Synthesis Supports. *J. Org. Chem.* **1995,** 60, (11), 3358-3364.
70. Merrifield, R. B., Solid Phase Synthesis (Nobel Lecture). *Angew. Chem. Int. Ed.* **1985,** 24, (10), 799-810.

71. Stevens, C. M.; Watanabe, R., Amino Acid Derivatives. I. Carboallyloxy Derivatives of α-Amino Acids. *J. Am. Chem. Soc.* **1950,** 72, (2), 725-727.
72. Patchornik, A.; Amit, B.; Woodward, R. B., Photosensitive protecting groups. *J. Am. Chem. Soc.* **1970,** 92, (21), 6333-6335.
73. Bhushan, K. R., Light-directed maskless synthesis of peptide arrays using photolabile amino acid monomers. *Org. Biomol. Chem.* **2006,** 4, (10), 1857-1859.
74. Tatsu, Y.; Nishigaki, T.; Darszon, A.; Yumoto, N., A caged sperm-activating peptide that has a photocleavable protecting group on the backbone amide. *FEBS Lett.* **2002,** 525, (1-3), 20-24.
75. Pan, P.; Bayley, H., Caged cysteine and thiophosphoryl peptides. *FEBS Lett.* **1997,** 405, (1), 81-85.
76. Montalbetti, C. A. G. N.; Falque, V., Amide Bond Formation and Peptide Coupling. *Tetrahedron* **2005,** 61, (46), 10827-10852.
77. Castro, B.; Dormoy, J. R.; Evin, G.; Selve, C., Reactifs de couplage peptidique I (1) - l'hexafluorophosphate de benzotriazolyl *N*-oxytrisdimethylamino phosphonium (B.O.P.). *Tetrahedron Lett.* **1975,** 16, (14), 1219-1222.
78. Coste, J.; Le-Nguyen, D.; Castro, B., PyBOP®: A new peptide coupling reagent devoid of toxic by-product. *Tetrahedron Lett.* **1990,** 31, (2), 205-208.
79. Letsinger, R. L.; Mahadevan, V., Oligonucleotide Synthesis on a Polymer Support. *J. Am. Chem. Soc.* **1965,** 87, (15), 3526-3527.
80. Schuerch, C.; Frechet, J. M., Solid-phase synthesis of oligosaccharides. I. Preparation of the solid support. Poly[*p*-(1-propen-3-ol-1-yl)styrene]. *J. Am. Chem. Soc.* **1971,** 93, (2), 492-496.
81. Rose, K.; Vizzavona, J., Stepwise Solid-Phase Synthesis of Polyamides as Linkers. *J. Am. Chem. Soc.* **1999,** 121, (30), 7034-7038.
82. Bendavid, A.; Burns, C. J.; Field, L. D.; Hashimoto, K.; Ridley, D. D.; Samankumara Sandanayake, K. R. A.; Wieczorek, L., Solution- and Solid-Phase Synthesis of Components for Tethered Bilayer Membranes. *J. Org. Chem.* **2001,** 66, (11), 3709-3716.
83. Ponader, D.; Wojcik, F.; Beceren-Braun, F.; Dernedde, J.; Hartmann, L., Sequence-Defined Glycopolymer Segments Presenting Mannose: Synthesis and Lectin Binding Affinity. *Biomacromolecules* **2012,** 13, (6), 1845-1852.
84. Wojcik, F.; Mosca, S.; Hartmann, L., Solid-Phase Synthesis of Asymmetrically Branched Sequence-Defined Poly/Oligo(amidoamines). *J. Org. Chem.* **2012,** 77, (9), 4226-4234.
85. Baier, M.; Giesler, M.; Hartmann, L., Split-and-Combine Approach Towards Branched Precision Glycomacromolecules and Their Lectin Binding Behavior. *Chem. Eur. J.* **2018,** 24, (7), 1619-1630.
86. Ponader, D.; Maffre, P.; Aretz, J.; Pussak, D.; Ninnemann, N. M.; Schmidt, S.; Seeberger, P. H.; Rademacher, C.; Nienhaus, G. U.; Hartmann, L., Carbohydrate-Lectin Recognition of Sequence-Defined Heteromultivalent Glycooligomers. *J. Am. Chem. Soc.* **2014,** 136, (5), 2008-2016.
87. Wieczorek, S.; Vigne, S.; Masini, T.; Ponader, D.; Hartmann, L.; Hirsch, A. K. H.; Börner, H. G., Combinatorial Screening for Specific Drug Solubilizers with Switchable Release Profiles. *Macromol. Biosci.* **2015,** 15, (1), 82-89.
88. Klein, P. M.; Reinhard, S.; Lee, D.-J.; Muller, K.; Ponader, D.; Hartmann, L.; Wagner, E., Precise redox-sensitive cleavage sites for improved bioactivity of siRNA lipopolyplexes. *Nanoscale* **2016,** 8, (42), 18098-18104.
89. Freichel, T.; Eierhoff, S.; Snyder, N. L.; Hartmann, L., Toward Orthogonal Preparation of Sequence-Defined Monodisperse Heteromultivalent Glycomacromolecules on Solid Support Using Staudinger Ligation and Copper-Catalyzed Click Reactions. *J. Org. Chem.* **2017,** 82, (18), 9400-9409.
90. Igde, S.; Röblitz, S.; Müller, A.; Kolbe, K.; Boden, S.; Fessele, C.; Lindhorst, T. K.; Weber, M.; Hartmann, L., Linear Precision Glycomacromolecules with Varying Interligand Spacing and Linker Functionalities Binding to Concanavalin A and the Bacterial Lectin FimH. *Macromol. Biosci.* **2017,** 17, (12), 1700198.
91. Boden, S.; Wagner, K. G.; Karg, M.; Hartmann, L., Presenting Precision Glycomacromolecules on Gold Nanoparticles for Increased Lectin Binding. *Polymers* **2017,** 9, (12), 716.
92. Wojcik, F.; O'Brien, A. G.; Götze, S.; Seeberger, P. H.; Hartmann, L., Synthesis of Carbohydrate-Functionalised Sequence-Defined Oligo(amidoamine)s by Photochemical Thiol-Ene Coupling in a Continuous Flow Reactor. *Chem. Eur. J.* **2013,** 19, (9), 3090-3098.

93. Ponader, D. Synthesis of Sequence-defined Glycooligomers for Studying Multivalent Interactions. Freie Universität Berlin, 2014.
94. Leibfarth, F. A.; Johnson, J. A.; Jamison, T. F., Scalable synthesis of sequence-defined, unimolecular macromolecules by Flow-IEG. *Proc. Natl. Acad. Sci. U.S.A.* **2015,** 112, (34), 10617-10622.
95. Solleder, S. C.; Wetzel, K. S.; Meier, M. A. R., Dual side chain control in the synthesis of novel sequence-defined oligomers through the Ugi four-component reaction. *Polym. Chem.* **2015,** 6, (17), 3201-3204.
96. Trinh, T. T.; Oswald, L.; Chan-Seng, D.; Lutz, J.-F., Synthesis of Molecularly Encoded Oligomers Using a Chemoselective "AB + CD" Iterative Approach. *Macromol. Rapid Commun.* **2014,** 35, (2), 141-145.
97. Al Ouahabi, A.; Charles, L.; Lutz, J.-F., Synthesis of Non-Natural Sequence-Encoded Polymers Using Phosphoramidite Chemistry. *J. Am. Chem. Soc.* **2015,** 137, (16), 5629-5635.
98. Martens, S.; Van den Begin, J.; Madder, A.; Du Prez, F. E.; Espeel, P., Automated Synthesis of Monodisperse Oligomers, Featuring Sequence Control and Tailored Functionalization. *J. Am. Chem. Soc.* **2016,** 138, (43), 14182-14185.
99. Porel, M.; Alabi, C. A., Sequence-Defined Polymers via Orthogonal Allyl Acrylamide Building Blocks. *J. Am. Chem. Soc.* **2014,** 136, (38), 13162-13165.
100. Jiang, Y.; Golder, M. R.; Nguyen, H. V. T.; Wang, Y.; Zhong, M.; Barnes, J. C.; Ehrlich, D. J. C.; Johnson, J. A., Iterative Exponential Growth Synthesis and Assembly of Uniform Diblock Copolymers. *J. Am. Chem. Soc.* **2016,** 138, (30), 9369-9372.
101. Kolb, H. C.; Finn, M.; Sharpless, K. B., Click chemistry: diverse chemical function from a few good reactions. *Angew. Chem. Int. Ed.* **2001,** 40, (11), 2004-2021.
102. Barner-Kowollik, C.; Du Prez, F. E.; Espeel, P.; Hawker, C. J.; Junkers, T.; Schlaad, H.; Van Camp, W., "Clicking" Polymers or Just Efficient Linking: What Is the Difference? *Angew. Chem. Int. Ed.* **2011,** 50, (1), 60-62.
103. Huisgen, R.; Szeimies, G.; Möbius, L., 1.3-Dipolare Cycloadditionen, XXXII. Kinetik der Additionen organischer Azide an CC-Mehrfachbindungen. *Chem. Ber.* **1967,** 100, (8), 2494-2507.
104. Zhu, L.; Brassard, C. J.; Zhang, X.; Guha, P. M.; Clark, R. J., On the Mechanism of Copper(I)-Catalyzed Azide-Alkyne Cycloaddition. *Chem. Rec.* **2016,** 16, (3), 1501-1517.
105. Rodionov, V. O.; Fokin, V. V.; Finn, M. G., Mechanism of the Ligand-Free Cu^{I}-Catalyzed Azide-Alkyne Cycloaddition Reaction. *Angew. Chem. Int. Ed.* **2005,** 44, (15), 2210-2215.
106. Tornøe, C. W.; Christensen, C.; Meldal, M., Peptidotriazoles on Solid Phase: [1,2,3]-Triazoles by Regiospecific Copper(I)-Catalyzed 1,3-Dipolar Cycloadditions of Terminal Alkynes to Azides. *J. Org. Chem.* **2002,** 67, (9), 3057-3064.
107. Liang, L.; Astruc, D., The copper(I)-catalyzed alkyne-azide cycloaddition (CuAAC) "click" reaction and its applications. An overview. *Coord. Chem. Rev.* **2011,** 255, (23), 2933-2945.
108. Zhang, L.; Chen, X.; Xue, P.; Sun, H. H. Y.; Williams, I. D.; Sharpless, K. B.; Fokin, V. V.; Jia, G., Ruthenium-Catalyzed Cycloaddition of Alkynes and Organic Azides. *J. Am. Chem. Soc.* **2005,** 127, (46), 15998-15999.
109. Posner, T., Beiträge zur Kenntniss der ungesättigten Verbindungen. II. Ueber die Addition von Mercaptanen an ungesättigte Kohlenwasserstoffe. *Ber. Dtsch. Chem. Ges.* **1905,** 38, (1), 646-657.
110. Hoyle, C. E.; Lowe, A. B.; Bowman, C. N., Thiol-click chemistry: a multifaceted toolbox for small molecule and polymer synthesis. *Chem. Soc. Rev.* **2010,** 39, (4), 1355-1387.
111. Stenzel, M. H., Bioconjugation Using Thiols: Old Chemistry Rediscovered to Connect Polymers with Nature's Building Blocks. *ACS Macro Lett.* **2013,** 2, (1), 14-18.
112. Northrop, B. H.; Coffey, R. N., Thiol-Ene Click Chemistry: Computational and Kinetic Analysis of the Influence of Alkene Functionality. *J. Am. Chem. Soc.* **2012,** 134, (33), 13804-13817.
113. Nair, D. P.; Podgórski, M.; Chatani, S.; Gong, T.; Xi, W.; Fenoli, C. R.; Bowman, C. N., The Thiol-Michael Addition Click Reaction: A Powerful and Widely Used Tool in Materials Chemistry. *Chem. Mater.* **2014,** 26, (1), 724-744.
114. Uygun, M.; Tasdelen, M. A.; Yagci, Y., Influence of Type of Initiation on Thiol-Ene "Click" Chemistry. *Macromol. Chem. Phys.* **2010,** 211, (1), 103-110.
115. Cramer, N. B.; Scott, J. P.; Bowman, C. N., Photopolymerizations of Thiol-Ene Polymers without Photoinitiators. *Macromolecules* **2002,** 35, (14), 5361-5365.
116. ten Brummelhuis, N.; Diehl, C.; Schlaad, H., Thiol-Ene Modification of 1,2-Polybutadiene Using UV Light or Sunlight. *Macromolecules* **2008,** 41, (24), 9946-9947.

117. Sensfuß, S.; Friedrich, M.; Klemm, E., Untersuchungen zur Thiol/En-Polymerisation: elektronenspinresonanzspektroskopischer Nachweis spontaner Radikalbildung. *Makromol. Chem.* **1991,** 192, (12), 2895-2900.
118. Pryor, W. A.; Coco, J. H.; Daly, W. H.; Houk, K. N., Radical generation from polymolecular reactions of closed shell molecules. Molecule-assisted homolysis (MAH). Hydrogen atom transfer from a Diels-Alder adduct to an alkene. *J. Am. Chem. Soc.* **1974,** 96, (17), 5591-5593.
119. Cramer, N. B.; Reddy, S. K.; O'Brien, A. K.; Bowman, C. N., Thiol-Ene Photopolymerization Mechanism and Rate Limiting Step Changes for Various Vinyl Functional Group Chemistries. *Macromolecules* **2003,** 36, (21), 7964-7969.
120. Hoyle, C. E.; Bowman, C. N., Thiol-Ene Click Chemistry. *Angew. Chem. Int. Ed.* **2010,** 49, (9), 1540-1573.
121. Reddy, S. K.; Cramer, N. B.; Bowman, C. N., Thiol-Vinyl Mechanisms. 2. Kinetic Modeling of Ternary Thiol-Vinyl Photopolymerizations. *Macromolecules* **2006,** 39, (10), 3681-3687.
122. Lee, T. Y.; Smith, Z.; Reddy, S. K.; Cramer, N. B.; Bowman, C. N., Thiol-Allyl Ether-Methacrylate Ternary Systems. Polymerization Mechanism. *Macromolecules* **2007,** 40, (5), 1466-1472.
123. Lee, T. Y.; Carioscia, J.; Smith, Z.; Bowman, C. N., Thiol-Allyl Ether-Methacrylate Ternary Systems. Evolution Mechanism of Polymerization-Induced Shrinkage Stress and Mechanical Properties. *Macromolecules* **2007,** 40, (5), 1473-1479.
124. Chan, J. W.; Hoyle, C. E.; Lowe, A. B.; Bowman, M., Nucleophile-Initiated Thiol-Michael Reactions: Effect of Organocatalyst, Thiol, and Ene. *Macromolecules* **2010,** 43, (15), 6381-6388.
125. Moghaddam, F. M.; Bardajee, G. R.; Chadorneshine Veranlou, R. O., KF/Al2O3-Mediated Michael Addition of Thiols to Electron-Deficient Olefins. *Synth. Commun.* **2005,** 35, (18), 2427-2433.
126. Alleti, R.; Oh, W. S.; Perambuduru, M.; Ramana, C. V.; Prakash Reddy, V., Imidazolium-based polymer supported gadolinium triflate as a heterogeneous recyclable Lewis acid catalyst for Michael additions. *Tetrahedron Lett.* **2008,** 49, (21), 3466-3470.
127. Dwek, R. A., Glycobiology: Toward Understanding the Function of Sugars. *Chem. Rev.* **1996,** 96, (2), 683-720.
128. Rademacher, T. W.; Parekh, R. B.; Dwek, R. A., Glycobiology. *Annu. Rev. Biochem.* **1988,** 57, (1), 785-838.
129. Weymouth-Wilson, A. C., The role of carbohydrates in biologically active natural products. *Nat. Prod. Rep.* **1997,** 14, (2), 99-110.
130. Crocker, P. R.; Feizi, T., Carbohydrate recognition systems: functional triads in cell-cell interactions. *Curr. Opin. Struct. Biol.* **1996,** 6, (5), 679-691.
131. Linhardt, R. J.; Toida, T., Role of Glycosaminoglycans in Cellular Communication. *Acc. Chem. Res.* **2004,** 37, (7), 431-438.
132. Phillips, M.; Nudelman, E.; Gaeta, F.; Perez, M.; Singhal, A.; Hakomori, S.; Paulson, J., ELAM-1 mediates cell adhesion by recognition of a carbohydrate ligand, sialyl-Lex. *Science* **1990,** 250, (4984), 1130-1132.
133. Kruse, J.; Mailhammer, R.; Wernecke, H.; Faissner, A.; Sommer, I.; Goridis, C.; Schachner, M., Neural cell adhesion molecules and myelin-associated glycoprotein share a common carbohydrate moiety recognized by monoclonal antibodies L2 and HNK-1. *Nature* **1984,** 311, 153.
134. Rabinovich, G. A.; Baum, L. G.; Tinari, N.; Paganelli, R.; Natoli, C.; Liu, F.-T.; Iacobelli, S., Galectins and their ligands: amplifiers, silencers or tuners of the inflammatory response? *Trends Immunol.* **2002,** 23, (6), 313-320.
135. Stahl, P. D.; Ezekowitz, R. A. B., The mannose receptor is a pattern recognition receptor involved in host defense. *Curr. Opin. Immunol.* **1998,** 10, (1), 50-55.
136. Cambi, A.; Gijzen, K.; M. de Vries, I. J.; Torensma, R.; Joosten, B.; Adema, G. J.; Netea, M. G.; Kullberg, B.-J.; Romani, L.; Figdor, C. G., The C-type lectin DC-SIGN (CD209) is an antigen-uptake receptor for Candida albicans on dendritic cells. *Eur. J. Immunol.* **2003,** 33, (2), 532-538.
137. Cambi, A.; Koopman, M.; Figdor, C. G., How C-type lectins detect pathogens. *Cell. Microbiol.* **2005,** 7, (4), 481-488.
138. Eisen, D. P.; Minchinton, R. M., Impact of Mannose-Binding Lectin on Susceptibility to Infectious Diseases. *Clin. Infect. Dis.* **2003,** 37, (11), 1496-1505.

139. Appelmelk, B. J.; van Die, I.; van Vliet, S. J.; Vandenbroucke-Grauls, C. M. J. E.; Geijtenbeek, T. B. H.; van Kooyk, Y., Cutting Edge: Carbohydrate Profiling Identifies New Pathogens That Interact with Dendritic Cell-Specific ICAM-3-Grabbing Nonintegrin on Dendritic Cells. *J. Immunol.* **2003,** 170, (4), 1635-1639.
140. Yu, X.-Q.; Kanost, M. R., Manduca sexta lipopolysaccharide-specific immulectin-2 protects larvae from bacterial infection. *Devel. Comp. Immunol.* **2003,** 27, (3), 189-196.
141. Geijtenbeek, T. B. H.; Kwon, D. S.; Torensma, R.; van Vliet, S. J.; van Duijnhoven, G. C. F.; Middel, J.; Cornelissen, I. L. M. H. A.; Nottet, H. S. L. M.; KewalRamani, V. N.; Littman, D. R.; Figdor, C. G.; van Kooyk, Y., DC-SIGN, a Dendritic Cell-Specific HIV-1-Binding Protein that Enhances *trans*-Infection of T Cells. *Cell* **2000,** 100, (5), 587-597.
142. Feinberg, H.; Mitchell, D. A.; Drickamer, K.; Weis, W. I., Structural Basis for Selective Recognition of Oligosaccharides by DC-SIGN and DC-SIGNR. *Science* **2001,** 294, (5549), 2163-2166.
143. Werz, D. B.; Ranzinger, R.; Herget, S.; Adibekian, A.; von der Lieth, C.-W.; Seeberger, P. H., Exploring the Structural Diversity of Mammalian Carbohydrates ("Glycospace") by Statistical Databank Analysis. *ACS Chem. Biol.* **2007,** 2, (10), 685-691.
144. Gabius, H. J.; Siebert, H. C.; André, S.; Jiménez-Barbero, J.; Rüdiger, H., Chemical Biology of the Sugar Code. *ChemBioChem* **2004,** 5, (6), 740-764.
145. Vilaplana, F.; Gilbert, R. G., Characterization of branched polysaccharides using multiple-detection size separation techniques. *J. Sep. Sci.* **2010,** 33, (22), 3537-3554.
146. Roseman, S., Reflections on Glycobiology. *J. Biol. Chem.* **2001,** 276, (45), 41527-41542.
147. van den Berg, B. M.; Vink, H.; Spaan, J. A. E., The Endothelial Glycocalyx Protects Against Myocardial Edema. *Circ. Res.* **2003,** 92, (6), 592-594.
148. Mager, M. D.; LaPointe, V.; Stevens, M. M., Exploring and exploiting chemistry at the cell surface. *Nat. Chem.* **2011,** 3, (8), 582.
149. Tarbell, J. M.; Shi, Z.-D., Effect of the glycocalyx layer on transmission of interstitial flow shear stress to embedded cells. *Biomech. Model. Mechanobiol.* **2013,** 12, (1), 111-121.
150. Lis, H.; Sharon, N., Lectins: Carbohydrate-Specific Proteins That Mediate Cellular Recognition. *Chem. Rev.* **1998,** 98, (2), 637-674.
151. Rispens, T.; Heer, P. O.-d.; Derksen, N. I. L.; Wolbink, G.; van Schouwenburg, P. A.; Kruithof, S.; Aalberse, R. C., Nanomolar to sub-picomolar affinity measurements of antibody-antigen interactions and protein multimerizations: Fluorescence-assisted high-performance liquid chromatography. *Anal. Biochem.* **2013,** 437, (2), 118-122.
152. Tu, T.; Drăguşanu, M.; Petre, B.-A.; Rempel, D. L.; Przybylski, M.; Gross, M. L., Protein-Peptide Affinity Determination Using an H/D Exchange Dilution Strategy: Application to Antigen-Antibody Interactions. *J. Am. Soc. Mass Spectrom.* **2010,** 21, (10), 1660-1667.
153. Schwarz, F. P.; Puri, K. D.; Bhat, R. G.; Surolia, A., Thermodynamics of Monosaccharide Binding to Concanavalin A, Pea (Pisum sativum) Lectin, and Lentil (Lens culinaris) Lectin. *J. Biol. Chem.* **1993,** 268, (11), 7668-7677.
154. Mitchell, S. W., *Researches Upon the Venom of the Rattlesnake; With an Investigation of the Anatomy and Physiology of the Organs Concerned*. 1860.
155. Sumner, J. B.; Howell, S. F., Identification of Hemagglutinin of Jack Bean with Concanavalin A. *J. Bacteriol.* **1936,** 32, (2), 227-237.
156. Watkins, W. M.; Morgan, W. T. J., Neutralization of the Anti-H Agglutinin in Eel Serum by Simple Sugars. *Nature* **1952,** 169, 825.
157. Boyd, W. C.; Shapleigh, E., Specific Precipitating Activity of Plant Agglutinins (Lectins). *Science* **1954,** 119, (3091), 419-419.
158. Boyd, W. C.; Shapleigh, E., Separation of Individuals of Any Blood Group into Secretors and Non-Secretors by Use of a Plant Agglutinin (Lectin). *Blood* **1954,** 9, (12), 1195-1198.
159. Kilpatrick, D. C., Animal lectins: a historical introduction and overview. *Biochim. Biophys. Acta* **2002,** 1572, (2), 187-197.
160. Aub, J. C.; Tieslau, C.; Lankester, A., Reactions of Normal and Tumor Cell Surfaces to Enzymes, I. Wheat-Germ Lipase and Associated Mucopolysaccharides. *Proc. Natl. Acad. Sci. U.S.A.* **1963,** 50, (4), 613-619.
161. Aub, J. C.; Sanford, B. H.; Cote, M. N., Studies on reactivity of tumor and normal cells to a wheat germ agglutinin. *Proc. Natl. Acad. Sci. U.S.A.* **1965,** 54, (2), 396-399.

162. Bar-Shavit, Z.; Ofek, I.; Goldman, R.; Mirelman, D.; Sharon, N., Mannose residues on phagocytes as receptors for the attachment of Escherichia coli and Salmonella typhi. *Biochem. Biophys. Res. Commun.* **1977,** 78, (1), 455-460.
163. Sumner, J. B., The Globulins of the Jack Bean, Canavalia Ensiformis. *J. Biol. Chem.* **1919,** 37, (1), 137-142.
164. Edelman, G. M.; Cunningham, B. A.; Reeke, G. N.; Becker, J. W.; Waxdal, M. J.; Wang, J. L., The Covalent and Three-Dimensional Structure of Concanavalin A. *Proc. Natl. Acad. Sci. U.S.A.* **1972,** 69, (9), 2580-2584.
165. Naismith, J. H.; Emmerich, C.; Habash, J.; Harrop, S. J.; Helliwell, J. R.; Hunter, W. N.; Raftery, J.; Yariv, J., Refined Structure of Concanavalin A Complexed with Methyl α-D-Mannopyranoside at 2.0 Å Resolution and Comparison with the Saccharide-Free Structure. *Acta Crystallogr. Sect. D. Biol. Crystallogr.* **1994,** 50, (6), 847-858.
166. Rose, A. S.; Bradley, A. R.; Valasatava, Y.; Duarte, J. M.; Prli, A.; Rose, P. W., Web-based molecular graphics for large complexes. In *Proceedings of the 21st International Conference on Web3D Technology*, ACM: Anaheim, California, 2016; pp 185-186.
167. Rini, J. M., Lectin Structure. *Annu. Rev. Biophys. Biomol. Struct.* **1995,** 24, (1), 551-577.
168. Gabius, H.-J.; André, S.; Jiménez-Barbero, J.; Romero, A.; Solís, D., From lectin structure to functional glycomics: principles of the sugar code. *Trends Biochem. Sci.* **2011,** 36, (6), 298-313.
169. Gestwicki, J. E.; Cairo, C. W.; Strong, L. E.; Oetjen, K. A.; Kiessling, L. L., Influencing Receptor-Ligand Binding Mechanisms with Multivalent Ligand Architecture. *J. Am. Chem. Soc.* **2002,** 124, (50), 14922-14933.
170. Fasting, C.; Schalley, C. A.; Weber, M.; Seitz, O.; Hecht, S.; Koksch, B.; Dernedde, J.; Graf, C.; Knapp, E. W.; Haag, R., Multivalency as a Chemical Organization and Action Principle. *Angew. Chem. Int. Ed.* **2012,** 51, (42), 10472-10498.
171. Lee, Y. C.; Lee, R. T., Carbohydrate-Protein Interactions: Basis of Glycobiology. *Acc. Chem. Res.* **1995,** 28, (8), 321-327.
172. Lundquist, J. J.; Toone, E. J., The Cluster Glycoside Effect. *Chem. Rev.* **2002,** 102, (2), 555-578.
173. Kiessling, L. L.; Grim, J. C., Glycopolymer probes of signal transduction. *Chem. Soc. Rev.* **2013,** 42, (10), 4476-4491.
174. Mammen, M.; Choi, S.-K.; Whitesides, G. M., Polyvalent Interactions in Biological Systems: Implications for Design and Use of Multivalent Ligands and Inhibitors. *Angew. Chem. Int. Ed.* **1998,** 37, (20), 2754-2794.
175. Kiessling, L. L.; Gestwicki, J. E.; Strong, L. E., Synthetic Multivalent Ligands as Probes of Signal Transduction. *Angew. Chem. Int. Ed.* **2006,** 45, (15), 2348-2368.
176. Page, M. I.; Jencks, W. P., Entropic Contributions to Rate Accelerations in Enzymic and Intramolecular Reactions and the Chelate Effect. *Proc. Natl. Acad. Sci. U.S.A.* **1971,** 68, (8), 1678-1683.
177. Gargano, J. M.; Ngo, T.; Kim, J. Y.; Acheson, D. W. K.; Lees, W. J., Multivalent Inhibition of AB_5 Toxins. *J. Am. Chem. Soc.* **2001,** 123, (51), 12909-12910.
178. Hunter, C. A.; Tomas, S., Cooperativity, Partially Bound States, and Enthalpy-Entropy Compensation. *Chem. Biol.* **2003,** 10, (11), 1023-1032.
179. Weber, M.; Bujotzek, A.; Haag, R., Quantifying the rebinding effect in multivalent chemical ligand-receptor systems. *J. Chem. Phys.* **2012,** 137, (5), 054111.
180. Dam, T. K.; Brewer, C. F., Effects of Clustered Epitopes in Multivalent Ligand-Receptor Interactions. *Biochemistry* **2008,** 47, (33), 8470-8476.
181. Lees, W. J.; Spaltenstein, A.; Kingery-Wood, J. E.; Whitesides, G. M., Polyacrylamides Bearing Pendant α-Sialoside Groups Strongly Inhibit Agglutination of Erythrocytes by Influenza A Virus: Multivalency and Steric Stabilization of Particulate Biological Systems. *J. Med. Chem.* **1994,** 37, (20), 3419-3433.
182. Bojarova, P.; Kren, V., Sugared biomaterial binding lectins: achievements and perspectives. *Biomater. Sci.* **2016,** 4, (8), 1142-1160.
183. Ernst, B.; Magnani, J. L., From carbohydrate leads to glycomimetic drugs. *Nat. Rev. Drug Discov.* **2009,** 8, 661.
184. Fernández-Tejada, A.; Cañada F., J.; Jiménez-Barbero, J., Recent Developments in Synthetic Carbohydrate-Based Diagnostics, Vaccines, and Therapeutics. *Chem. Eur. J.* **2015,** 21, (30), 10616-10628.

185. Bhatia, S.; Camacho, L. C.; Haag, R., Pathogen Inhibition by Multivalent Ligand Architectures. *J. Am. Chem. Soc.* **2016,** 138, (28), 8654-8666.
186. DeMarco, M. L.; Woods, R. J., Structural glycobiology: A game of snakes and ladders. *Glycobiology* **2008,** 18, (6), 426-440.
187. Becer, C. R., The Glycopolymer Code: Synthesis of Glycopolymers and Multivalent Carbohydrate-Lectin Interactions. *Macromol. Rapid Commun.* **2012,** 33, (9), 742-752.
188. Roy, R.; Murphy, P. V.; Gabius, H.-J., Multivalent carbohydrate-lectin interactions: how synthetic chemistry enables insights into nanometric recognition. *Molecules* **2016,** 21, (5), 629.
189. André, S.; Pieters, R. J.; Vrasidas, I.; Kaltner, H.; Kuwabara, I.; Liu, F. T.; Liskamp, R. M. J.; Gabius, H. J., Wedgelike Glycodendrimers as Inhibitors of Binding of Mammalian Galectins to Glycoproteins, Lactose Maxiclusters, and Cell Surface Glycoconjugates. *ChemBioChem* **2001,** 2, (11), 822-830.
190. Wolfenden, M. L.; Cloninger, M. J., Carbohydrate-Functionalized Dendrimers To Investigate the Predictable Tunability of Multivalent Interactions. *Bioconjugate Chem.* **2006,** 17, (4), 958-966.
191. Muñoz, E. M.; Correa, J.; Riguera, R.; Fernández-Megia, E., Real-Time Evaluation of Binding Mechanisms in Multivalent Interactions: A Surface Plasmon Resonance Kinetic Approach. *J. Am. Chem. Soc.* **2013,** 135, (16), 5966-5969.
192. Gou, Y.; Geng, J.; Richards, S.-J.; Burns, J.; Becer, C. R.; Haddleton, D. M., A Detailed Study on Understanding Glycopolymer Library and Con A Interactions. *J. Polym. Sci. A* **2013,** 51, (12), 2588-2597.
193. Lavilla, C.; Yilmaz, G.; Uzunova, V.; Napier, R.; Becer, C. R.; Heise, A., Block-Sequence-Specific Glycopolypeptides with Selective Lectin Binding Properties. *Biomacromolecules* **2017,** 18, (6), 1928-1936.
194. Loka, R. S.; McConnell, M. S.; Nguyen, H. M., Studies of Highly-Ordered Heterodiantennary Mannose/Glucose-Functionalized Polymers and Concanavalin A Protein Interactions Using Isothermal Titration Calorimetry. *Biomacromolecules* **2015,** 16, (12), 4013-4021.
195. Nagao, M.; Fujiwara, Y.; Matsubara, T.; Hoshino, Y.; Sato, T.; Miura, Y., Design of Glycopolymers Carrying Sialyl Oligosaccharides for Controlling the Interaction with the Influenza Virus. *Biomacromolecules* **2017,** 18, (12), 4385-4392.
196. Chen, Y.; Lord, M. S.; Piloni, A.; Stenzel, M. H., Correlation between Molecular Weight and Branch Structure of Glycopolymers Stars and Their Binding to Lectins. *Macromolecules* **2015,** 48, (2), 346-357.
197. Xue, H.; Peng, L.; Dong, Y.; Zheng, Y.; Luan, Y.; Hu, X.; Chen, G.; Chen, H., Synthesis of star-glycopolymers by Cu(0)-mediated radical polymerisation in the absence and presence of oxygen. *RSC Adv.* **2017,** 7, (14), 8484-8490.
198. Kim, J. C.; Rho, Y.; Kim, G.; Kim, M.; Kim, H.; Kim, I. J.; Kim, J. R.; Ree, M., New self-assembled brush glycopolymers: synthesis, structure and properties. *Polym. Chem.* **2013,** 4, (7), 2260-2271.
199. Akasaka, T.; Matsuura, K.; Kobayashi, K., Transformation from Block-Type to Graft-Type Oligonucleotide-Glycopolymer Conjugates by Self-Organization with Half-Sliding Complementary Oligonucleotides and Their Lectin Recognition. *Bioconjugate Chem.* **2001,** 12, (5), 776-785.
200. Ordanini, S.; Varga, N.; Porkolab, V.; Thepaut, M.; Belvisi, L.; Bertaglia, A.; Palmioli, A.; Berzi, A.; Trabattoni, D.; Clerici, M.; Fieschi, F.; Bernardi, A., Designing nanomolar antagonists of DC-SIGN-mediated HIV infection: ligand presentation using molecular rods. *Chem. Commun.* **2015,** 51, (18), 3816-3819.
201. Hoshino, Y.; Nakamoto, M.; Miura, Y., Control of Protein-Binding Kinetics on Synthetic Polymer Nanoparticles by Tuning Flexibility and Inducing Conformation Changes of Polymer Chains. *J. Am. Chem. Soc.* **2012,** 134, (37), 15209-15212.
202. Huang, H.; Rodolis, M. T.; Bhatia, S. R.; Sampson, N. S., Sugars Require Rigid Multivalent Displays for Activation of Mouse Sperm Acrosomal Exocytosis. *Biochemistry* **2017,** 56, (22), 2779-2786.
203. Muñoz-Bonilla, A.; León, O.; Bordegé, V.; Sánchez-Chaves, M.; Fernández-García, M., Controlled block glycopolymers able to bind specific proteins. *J. Polym. Sci. A* **2013,** 51, (6), 1337-1347.

204. Abdu-Allah, H. H. M.; Watanabe, K.; Completo, G. C.; Sadagopan, M.; Hayashizaki, K.; Takaku, C.; Tamanaka, T.; Takematsu, H.; Kozutsumi, Y.; Paulson, J. C.; Tsubata, T.; Ando, H.; Ishida, H.; Kiso, M., CD22-Antagonists with nanomolar potency: The synergistic effect of hydrophobic groups at C-2 and C-9 of sialic acid scaffold. *Biorg. Med. Chem.* **2011,** 19, (6), 1966-1971.
205. Li, J.; Zacharek, S.; Chen, X.; Wang, J.; Zhang, W.; Janczuk, A.; Wang, P. G., Bacteria Targeted By Human Natural Antibodies Using α-Gal Conjugated Receptor-specific Glycopolymers. *Biorg. Med. Chem.* **1999,** 7, (8), 1549-1558.
206. Basuki, J. S.; Esser, L.; Duong, H. T. T.; Zhang, Q.; Wilson, P.; Whittaker, M. R.; Haddleton, D. M.; Boyer, C.; Davis, T. P., Magnetic nanoparticles with diblock glycopolymer shells give lectin concentration-dependent MRI signals and selective cell uptake. *Chem. Sci.* **2014,** 5, (2), 715-726.
207. Pussak, D.; Ponader, D.; Mosca, S.; Ruiz, S. V.; Hartmann, L.; Schmidt, S., Mechanical Carbohydrate Sensors Based on Soft Hydrogel Particles. *Angew. Chem. Int. Ed.* **2013,** 52, (23), 6084-6087.
208. Li, X.; Chen, G., Glycopolymer-based nanoparticles: synthesis and application. *Polym. Chem.* **2015,** 6, (9), 1417-1430.
209. Kumar, J.; Bousquet, A.; Stenzel, M. H., Thiol-alkyne Chemistry for the Preparation of Micelles with Glycopolymer Corona: Dendritic Surfaces versus Linear Glycopolymer in Their Ability to Bind to Lectins. *Macromol. Rapid Commun.* **2011,** 32, (20), 1620-1626.
210. Suriano, F.; Coulembier, O.; Degée, P.; Dubois, P., Carbohydrate-based amphiphilic diblock copolymers: Synthesis, characterization, and aqueous properties. *J. Polym. Sci. A* **2008,** 46, (11), 3662-3672.
211. Schaeffer, E.; Dehuyser, L.; Sigwalt, D.; Flacher, V.; Bernacchi, S.; Chaloin, O.; Remy, J.-S.; Mueller, C. G.; Baati, R.; Wagner, A., Dynamic Micelles of Mannoside Glycolipids are more Efficient than Polymers for Inhibiting HIV-1 *trans*-Infection. *Bioconjugate Chem.* **2013,** 24, (11), 1813-1823.
212. Wittmann, V.; Pieters, R. J., Bridging lectin binding sites by multivalent carbohydrates. *Chem. Soc. Rev.* **2013,** 42, (10), 4492-4503.
213. Abdouni, Y.; Yilmaz, G.; Becer, C. R., Sequence and Architectural Control in Glycopolymer Synthesis. *Macromol. Rapid Commun.* **2017,** 38, (24), 1700212.
214. Kanai, M.; Mortell, K. H.; Kiessling, L. L., Varying the Size of Multivalent Ligands: The Dependence of Concanavalin A Binding on Neoglycopolymer Length. *J. Am. Chem. Soc.* **1997,** 119, (41), 9931-9932.
215. Strong, L. E.; Kiessling, L. L., A General Synthetic Route to Defined, Biologically Active Multivalent Arrays. *J. Am. Chem. Soc.* **1999,** 121, (26), 6193-6196.
216. Chen, Y.; Chen, G.; Stenzel, M. H., Synthesis and Lectin Recognition of Glyco Star Polymers Prepared by "Clicking" Thiocarbohydrates onto a Reactive Scaffold. *Macromolecules* **2010,** 43, (19), 8109-8114.
217. Hartmann, M.; Lindhorst, T. K., The Bacterial Lectin FimH, a Target for Drug Discovery - Carbohydrate Inhibitors of Type 1 Fimbriae-Mediated Bacterial Adhesion. *Eur. J. Org. Chem.* **2011,** 2011, (20-21), 3583-3609.
218. Cairo, C. W.; Gestwicki, J. E.; Kanai, M.; Kiessling, L. L., Control of Multivalent Interactions by Binding Epitope Density. *J. Am. Chem. Soc.* **2002,** 124, (8), 1615-1619.
219. Ladmiral, V.; Mantovani, G.; Clarkson, G. J.; Cauet, S.; Irwin, J. L.; Haddleton, D. M., Synthesis of Neoglycopolymers by a Combination of "Click Chemistry" and Living Radical Polymerization. *J. Am. Chem. Soc.* **2006,** 128, (14), 4823-4830.
220. Hulme, E. C.; Trevethick, M. A., Ligand binding assays at equilibrium: validation and interpretation. *Br. J. Pharmacol.* **2010,** 161, (6), 1219-1237.
221. Dam, T. K.; Brewer, C. F., Thermodynamic Studies of Lectin-Carbohydrate Interactions by Isothermal Titration Calorimetry. *Chem. Rev.* **2002,** 102, (2), 387-430.
222. Christensen, T.; Toone, E. J., Calorimetric Evaluation of Protein-Carbohydrate Affinities. *Methods Enzymol.* **2003,** 362, 486-504.
223. Ratto, T. V.; Langry, K. C.; Rudd, R. E.; Balhorn, R. L.; Allen, M. J.; McElfresh, M. W., Force Spectroscopy of the Double-Tethered Concanavalin-A Mannose Bond. *Biophys. J.* **2004,** 86, (4), 2430-2437.
224. Touhami, A.; Hoffmann, B.; Vasella, A.; Denis, F. A.; Dufrêne, Y. F., Probing Specific Lectin-Carbohydrate Interactions Using Atomic Force Microscopy Imaging and Force Measurements. *Langmuir* **2003,** 19, (5), 1745-1751.

225. Zhang, X.; Yadavalli, V. K., Functionalized self-assembled monolayers for measuring single molecule lectin carbohydrate interactions. *Anal. Chim. Acta* **2009,** 649, (1), 1-7.
226. Roh, S.; Chung, T.; Lee, B., Overview of the Characteristics of Micro- and Nano-Structured Surface Plasmon Resonance Sensors. *Sensors* **2011,** 11, (2), 1565-1588.
227. Homola, J., Surface Plasmon Resonance Sensors for Detection of Chemical and Biological Species. *Chem. Rev.* **2008,** 108, (2), 462-493.
228. Schmidt, S.; Wang, H.; Pussak, D.; Mosca, S.; Hartmann, L., Probing multivalency in ligand-receptor-mediated adhesion of soft, biomimetic interfaces. *Beilstein J. Org. Chem.* **2015,** 11, 720-729.
229. Johnson, K. L.; Kendall, A.; Roberts, D., Surface energy and the contact of elastic solids. *Proc. Royal Soc. A* **1971,** 324, (1558), 301-313.
230. Wang, H.; Jacobi, F.; Waschke, J.; Hartmann, L.; Löwen, H.; Schmidt, S., Elastic Modulus Dependence on the Specific Adhesion of Hydrogels. *Adv. Funct. Mater.* **2017,** 27, (41), 1702040.
231. Mammen, M.; Dahmann, G.; Whitesides, G. M., Effective Inhibitors of Hemagglutination by Influenza Virus Synthesized from Polymers Having Active Ester Groups. Insight into Mechanism of Inhibition. *J. Med. Chem.* **1995,** 38, (21), 4179-4190.
232. Bates, F. S.; Hillmyer, M. A.; Lodge, T. P.; Bates, C. M.; Delaney, K. T.; Fredrickson, G. H., Multiblock Polymers: Panacea or Pandora's Box? *Science* **2012,** 336, (6080), 434-440.
233. D'Hooge, D. R.; Van Steenberge, P. H. M.; Derboven, P.; Reyniers, M.-F.; Marin, G. B., Model-based design of the polymer microstructure: bridging the gap between polymer chemistry and engineering. *Polym. Chem.* **2015,** 6, (40), 7081-7096.
234. Sun, J.; Zuckermann, R. N., Peptoid Polymers: A Highly Designable Bioinspired Material. *ACS Nano* **2013,** 7, (6), 4715-4732.
235. Rosales, A. M.; Segalman, R. A.; Zuckermann, R. N., Polypeptoids: a model system to study the effect of monomer sequence on polymer properties and self-assembly. *Soft Matter* **2013,** 9, (35), 8400-8414.
236. Trofimov, B. A.; Gusarova, N. K.; Arbuzova, S. N.; Ivanova, N. I.; Artem'ev, A. V.; Volkov, P. A.; Ushakov, I. A.; Malysheva, S. F.; Kuimov, V. A., Stereoselective free-radical addition of secondary phosphine selenides to aromatic acetylenes. *J. Organomet. Chem.* **2009,** 694, (5), 677-682.
237. Arbuzova, S. N.; Gusarova, N. K.; Trofimov, B. A., Nucleophilic and free-radical additions of phosphines and phosphine chalcogenides to alkenes and alkynes. *Arkivoc* **2006,** 2006, (5), 12-36.
238. Gaumont, A.-C.; Simon, A.; Denis, J.-M., Uncatalyzed hydrophosphination of multiple bonds by alkenyl- or alkynyl- phosphine-oxides; evidence for a P-H activation. *Tetrahedron Lett.* **1998,** 39, (9), 985-988.
239. Gao, X.-F.; Du, J.-J.; Liu, Z.; Guo, J., Visible-Light-Induced Specific Desulfurization of Cysteinyl Peptide and Glycopeptide in Aqueous Solution. *Org. Lett.* **2016,** 18, (5), 1166-1169.
240. Wang, Z.; Rejtar, T.; Zhou, Z. S.; Karger, B. L., Desulfurization of cysteine-containing peptides resulting from sample preparation for protein characterization by mass spectrometry. *Rapid Commun. Mass Spectrom.* **2010,** 24, (3), 267-275.
241. Wan, Q.; Danishefsky, S. J., Free-Radical-Based, Specific Desulfurization of Cysteine: A Powerful Advance in the Synthesis of Polypeptides and Glycopolypeptides. *Angew. Chem. Int. Ed.* **2007,** 46, (48), 9248-9252.
242. Bondalapati, S.; Jbara, M.; Brik, A., Expanding the chemical toolbox for the synthesis of large and uniquely modified proteins. *Nat. Chem.* **2016,** 8, 407.
243. Fernandez-Villamarin, M.; Sousa-Herves, A.; Correa, J.; Munoz, E. M.; Taboada, P.; Riguera, R.; Fernandez-Megia, E., The Effect of PEGylation on Multivalent Binding: A Surface Plasmon Resonance and Isothermal Titration Calorimetry Study with Structurally Diverse PEG-Dendritic GATG Copolymers. *ChemNanoMat* **2016,** 2, (5), 437-446.

5 Publications

5.1 Sequence-Controlled Glycopolymers via Step-Growth Polymerization of Precision Glycomacromolecules for Lectin Receptor Clustering

C. Gerke, M. F. Ebbesen, D. Jansen, S. Boden, T. Freichel and L. Hartmann

Biomacromolecules, **2017**, 18, (3), 787-796

[Impact Factor 2017: 5.738]

Contribution:

Collaborative design of structures and binding assays. Synthesis of all building blocks (except of the EDS building block needed for the macromonomers used during method development which was synthesized by a Bachelor student under my supervision and 2-azidoethyl-α-D-mannopyranoside), macromonomers (expect of the macromonomers used during method development which were synthesized by a Bachelor student under my supervision), and glycopolymers. Development of the polymerization method, supported by a supervised Bachelor student. Collaborative method development and independent measurement as well as evaluation of all LC-MS and GPC-RI-LS experiments. Evaluation of all NMR, UHR-MS and MALDI-TOF experiments. Performance and evaluation of the turbidity and precipitation assay. Independent performance and collaborative evaluation of SPR experiments. Collaborative writing of the manuscript.

Article

pubs.acs.org/Biomac

Sequence-Controlled Glycopolymers via Step-Growth Polymerization of Precision Glycomacromolecules for Lectin Receptor Clustering

Christoph Gerke,[†] Morten F. Ebbesen,[†] Dennis Jansen,[†] Sophia Boden,[†] Tanja Freichel,[†] and Laura Hartmann*[,†]

[†]Institute of Organic and Macromolecular Chemistry, Heinrich-Heine-University Düsseldorf, Universitätsstraße 1, 40225 Düsseldorf, Germany

Supporting Information

ABSTRACT: A versatile approach for the synthesis of sequence-controlled multiblock copolymers, using a combination of solid phase synthesis and step-growth polymerization by photoinduced thiol−ene coupling (TEC) is presented. Following this strategy, a series of sequence-controlled glycopolymers is derived from the polymerization of a hydrophilic spacer macromonomer and different glycomacromonomers bearing between one to five α-D-Mannose (Man) ligands. Through the solid phase assembly of the macromonomers, the number and positioning of spacer and sugar moieties is controlled and translates into the sequence-control of the final polymer. A maximum $\bar{M}_n$ of 16 kDa, corresponding to a $\bar{X}_n$ of 10, for the applied macromonomers is accessible with optimized polymerization conditions. The binding behavior of the resulting multiblock glycopolymers toward the model lectin Concanavalin A (ConA) is studied via turbidity assays and surface plasmon resonance (SPR) measurements, comparing the ability of precision glycomacromolecules and glycopolymers to bind to and cross-link ConA in dependence of the number of sugar moieties and overall molecular weight. The results show that there is a clear correlation between number of Man ligands and Con A binding and clustering, whereas the length of the glycooligomer- or polymer backbone seems to have no effect.

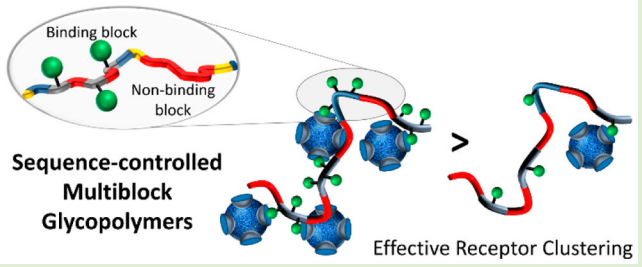

INTRODUCTION

Recently, the synthesis of sequence-controlled polymers, containing an ordered arrangement of functional monomers, has gained increasing attention. The control over the monomer sequence allows for the design of new polymeric materials with various applications from catalysis to medicine.[1] However, the synthesis of such precision polymers still remains a challenge. Different synthetic strategies have been applied to obtain monomer sequence control in oligomers and polymers such as controlled polymerization methods,[2,3] the use of special monomers,[4] iterative coupling protocols,[5] and solid phase synthesis.[6,7] Our approach is based on the use of solid phase peptide synthesis, which was originally developed by Merrifield in 1963 revealing a straightforward method of controlling the amino acid sequence of a peptide using a solid support.[8] In our group, we apply peptide coupling protocols to novel tailor-made building blocks generating monodisperse, sequence-defined oligomers.[9,10] For this purpose, the synthetic building blocks are equipped with a Fmoc-protected amine and a free carboxylic acid group. Besides that, they carry different functional side chain or main chain motifs giving access to a variety of so-called precision macromolecules.[9−16] Special focus has been devoted to the synthesis of precision glycomacromolecules carrying sugar ligands in the side chain and their evaluation as multivalent glycomimetics.[10−13,17] In this context, precision glycomacromolecules have great potential, as their design can be matched to accommodate specific receptor binding sites. Previous studies investigating the multivalent binding of glycomacromolecules to model lectin receptor ConA have shown that binding to the receptor can be enhanced by statistical effects where a higher number of sugar ligands on the macromolecular scaffolds increases the probability of binding to a receptor, e.g., by statistical rebinding events.[10,13,18] In addition, glycomacromolecules show the formation of intermolecular complexes where a single glycomacromolecule clusters several lectin receptors. Such receptor clustering behavior is of critical importance for several cell biological processes and enhanced bioactivity.[19−21] However, this requires comparatively large macromolecules, which is rather difficult to achieve with classic solid phase synthetic strategies. Therefore, we here extend on the previously introduced solid phase polymer synthesis and use precision glycomacromolecules as macromonomers to obtain higher molecular weight multiblock copolymers presenting, in an alternating fashion, blocks with sequence-defined density of sugar ligands and hydrophilic spacer blocks (Scheme 1). While the sugar carrying block should allow for effective binding to the receptor, the multiblock structure could enhance effective

Received: November 9, 2016
Revised: January 20, 2017
Published: January 24, 2017

DOI: 10.1021/acs.biomac.6b01657
Biomacromolecules 2017, 18, 787−796

Scheme 1. Schematic Presentation of the Solid Phase Synthesis of End-Functionalized Macromonomers Using Tailor-Made Building Blocks (Left)[10] and their Step-Growth Polymerization via Thiol−Ene Coupling (Right)[23]

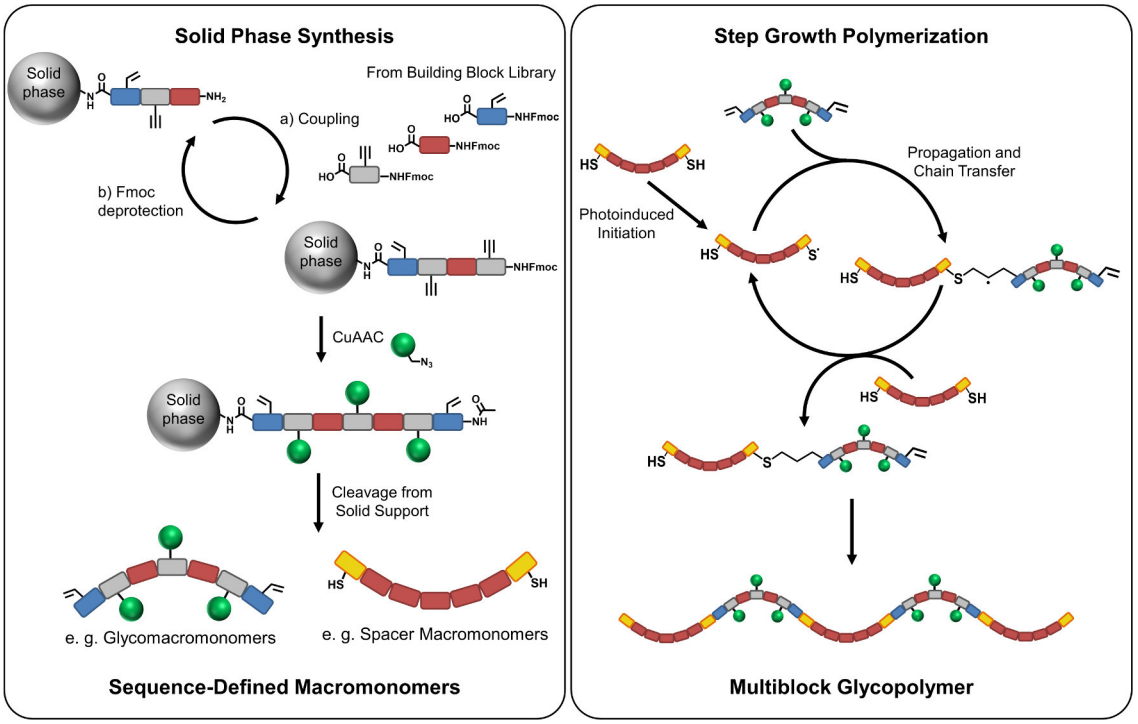

clustering of receptors due to an increased size and optimized ligand density of the polymer.

As polymerization reaction of the precision macromonomers, we used the click-type TEC by introducing reactive alkene and thiol end groups to either of two macromonomers. The resulting functionalized macromonomers are then polymerized in a step-growth fashion as an AA BB system, which is a polymerization method that leads to polymers with strictly alternating block sequences as already described by Carothers.[22] The combination of solid phase synthesis and step-growth polymerization therefore allows us to control the polymeric structure on two levels, first by controlling the monomer sequence within the blocks and second by a strictly alternating assembly of the two blocks. The final glycopolymers carry both amide and thioether linkages within the backbone from the two types of coupling methods, similar also to other sequence-controlled oligomers derived on solid phase.[7] In dependence of the building blocks used, the glycopolymers additionally carry ethylene glycol segments in the main chain and Man ligands in the side chain, similar to our previously reported glycomacromolecules (Scheme 1).[10]

A click-type coupling reaction was chosen in order to achieve high conversion and thereby reasonably large $\bar{X}_n$'s. In general, click reactions, predominantly copper mediated azide−alkyne cycloaddition (CuAAC) and TEC, are widely used in polymer chemistry, especially for cross-linking and post-functionalization, as also demonstrated in previous studies from our group.[11,14,23,24] However, there are only few examples where click reactions are used as polymerization method for the synthesis of sequence-controlled polymers.[2] The majority of these studies, regardless of whether CuAAC or TEC chemistry was applied, used low molecular weight monomers. Only the groups of Junkers[25] and Tew,[26] also using TEC, as well as the groups of Kopecek[27] and Lutz,[28] working with CuAAC coupling, presented first examples for the successful use of macromonomers obtaining multiblock copolymers.

Here, we now present the combination of solid phase polymer synthesis with TEC step-growth polymerization for straightforward access to sequence-controlled polymers and specifically sequence-controlled glycopolymers. Solid phase assembly of the macromonomers allows for the control, e.g., of the number of sugar ligands within one block, while the combination of two different macromonomers will lead to a high molecular weight alternating sequence of blocks, e.g., with or without sugar ligands. First, the influence of the different reaction parameters such as solvent, photoinitiator, reducing agent, and irradiation time will be investigated. Second, binding of the sequence-controlled glycopolymers as well as glycomacromonomers to model lectin ConA will be evaluated.

EXPERIMENTAL SECTION

Building Block Synthesis. Synthesis of building blocks DDS,[11] EDS,[14] and TDS[10] as well as the synthesis of 2-azidoethyl-α-D-Mannopyranoside[10] were reported earlier.

Oligomer Synthesis. The oligomers **1**−**7** were all synthesized via solid phase synthesis applying established protocols from our working group.[10,14] Obtained yields for the oligomers were between 45 and 81%, and the purities were larger 92% after cleavage from the resin and double precipitation from diethyl ether as determined by RP-HPLC (see Supporting Information).

Polymerization via TEC Coupling. The concentration of 2,2-dimethoxy-2-phenylacetophenone (DMPA) and tris(2-carboxyethyl)-phosphine hydrochloride (TCEP) were varied during the TEC coupling method development. The different reaction conditions are listed in Table 1. The preparation of the reagents and solvents, as well as the reaction procedures were not changed.

The oligomers were freshly freeze-dried and stock solutions of 40 mM in water were prepared. From the stock solutions, 250 μL of the thiol and the alkene bearing oligomers were transferred into a borosilicate glass HPLC vial without labels to prevent any kind of UV

DOI: 10.1021/acs.biomac.6b01657
Biomacromolecules 2017, 18, 787−796

absorption or reflection. The use of quartz glass was avoided to filter out highly energetic UV radiation below 300 nm. After the addition of both oligomers, the mixture was instantly freeze-dried again to remove the water and oxygen. The freeze-dried mixture of the two oligomers was flushed with argon and closed. DMSO and H_2O were degassed using the freeze−pump−thaw method. TCEP was freshly freeze-dried, and a stock solution of 50 mM in degassed DMSO was prepared. A DMPA stock solution of 100 mM in degassed DMSO was prepared without previous freeze-drying. From the stock solutions, required amounts were added to the vial with the freeze-dried oligomer mixture to obtain concentrations between 25 and 125 mM of DMPA and between 0.5 and 5 mM of TCEP, respectively. Additionally, degassed DMSO and degassed H_2O were added to obtain a total volume of 200 μL of a DMSO/H_2O mixture in a ratio 9/1, leading to a concentration of 50 mM of each oligomer. The vial was flushed with and kept under argon. The oligomers were completely dissolved, the vials were placed next to the UV lamp (distance of 7−10 cm) on a magnetic stirrer, and the mixture was stirred and irradiated for 1 h.

After 1 h of irradiation, the product was precipitated slowly in 10 mL of a mixture of ice cold diethyl ether/acetone with a volume ratio of 1/3. The obtained pallet was redissolved in 1 mL MeOH and reprecipitated in 10 mL ice cold diethyl ether. The pallets of glycopolymers had to be dissolved in 1 mL of MeOH with an additional drop of water. The pallet was redissolved again in 6 mL water and freeze-dried to give the final product.

Turbidity Assay/Ligand Concentration Dependent Assay. For the ligand concentration dependent assay, an adapted protocol from previous work by Kiessling et al. was used.[29] A ConA stock solution of approximately 20 μM was prepared in lectin binding buffer (LBB) (10 mM Hepes, 50 mM NaCl, 1 mM $MnCl_2$, 1 mM $CaCl_2$, pH 7.4). The exact concentration was determined by measuring the absorption of the ConA solution at 280 nm (ε 30150 L/(mol*cm)). For each ligand (glycomacromonomer or glycopolymer), a stock solution was prepared. Their concentration varied from 5 μM to 250 μM.

In a UV quartz cuvette, 5 μM of ConA in 2000 μL LBB were added and the measurement was started (100% of intensity for the clear solution). Subsequently, a certain amount of ligand (between 0.01 μM and 0.5 μM, V = 2 μL) was added to the cuvette, vigorously mixed using a Pasteur pipet, and the precipitate was allowed to form for 20 min. After 20 min, the concentration of ligand was further increased by the same amount. This was repeated until no further decrease in intensity was observed. The required ligand concentration for reaching the half-maximal turbidity (conc. $1/2T_{Max}$) measured was then determined from the curves for comparison of the different glycooligomer/-polymers. The measurement was repeated three times for each ligand (see SI), and the average value as well as the standard deviation were calculated.

Quantitative Precipitation Assay. The quantitative precipitation assay is a widely used assay in receptor/ligand interaction studies and was adapted from previous examples in literature.[30−33] For the quantitative precipitation assay, a ConA stock solution of approximately 30 μM was prepared in LBB. The exact concentration was determined by measuring the absorption of the ConA solution at 280 nm (ε 30150 L/(mol·cm)). Stock solutions of 500 μM, 50 μM and 5 μM were prepared in LBB for each ligand (glycomacromonomer or glycopolymer). As reaction vessels, 2 mL Eppendorf tubes were used. The total volume of the ConA/ligand mixture was 1 mL for all concentrations. In each Eppendorf tube, the ConA concentration amounts to 15 μM. The concentrations of ligand varied between 125 μM to 0.01 μM. After the addition of the ligand, the tubes were stored overnight, allowing the precipitant to form. The Eppendorf tubes were centrifuged for 5 min at 4400 rpm. The supernatant was removed, and the formed palette was carefully washed twice with 1 mL of cold LBB and centrifuged again under the same conditions. One milliliter of 0.05 M α-methyl-mannose solution in LBB was added to dissolve the palette. The ConA concentration of the solution was determined by measuring the UV absorption at 280 nm (ε 30150 L/(mol·cm)). The ligand concentration used to determine the ConA/ligand ratio in the precipitant (0.1, 0.5, 1.0, 2.5, and 5.0 μM) were measured three times and the average value as well as the standard deviation were calculated. The ConA/ligand ratio was found to have a linear regime for ligand concentrations from 0.5 μM to 2.5 μM allowing for the determination of an average ConA/ligand ratio in this concentration range. For the negative controls not containing sugar moieties, the assay was performed with one ligand concentration (5 μM) only.

Surface Plasmon Resonance (SPR). Ligand-ConA affinity experiments were performed using surface plasmon resonance (SPR) measurements, applying a direct binding assay with covalently bound ConA on a CM5 sensor chip (immobilization of 3085 RU). The assay was based on similar SPR assays performed by the groups of Fernandez-Megia and Riguera[20] as well as the group of Haddleton[34] also working with Man ligands and lectin.

LBB was used as the running buffer. Each ligand (glycomacromonomer or glycopolymer) was injected at different concentrations, ranging from 600 to 0.09 μM depending on the ligand. Each ligand was injected with six different concentrations (see SI for exact concentration values for each ligand). The flow rate was set to 30 μL/min, and the contact and dissociation times were 120 and 180 s, respectively. After ligand injection, the sensor chip was regenerated by injecting 0.8 M α-methyl-mannose in LBB buffer at a flow rate of 10 μL/min twice, to completely dissociate the bound ligand from the immobilized ConA. The equilibrium response 4 s before injection stop as a function of ligand concentration is fitted by using a steady state model, from which the dissociation constants K_D and K_A can be derived. Each ligand was measured three times to obtain standard deviations. As an internal reference, structure **6** was measured with a concentration of 6 μM in each measurement, showing good reproducibility within the series of glycomacromonomers and glycopolymers.

RESULTS AND DISCUSSION

Method Development of the Step-Growth Polymerization of Monodisperse Macromonomers by Photo-induced TEC. A medium pressure mercury UV lamp with a maximum intensity at 365 nm was used as the UV source. Macromonomers used for establishing TEC polymerization method contained five hydrophilic spacing building blocks (EDS) and either two terminal L-cysteine or alkene functionalized building blocks (DDS) (Scheme 2). Here we used single coupling and no additional purification of the macromonomers yielding both macromonomers with purities >92% as determined by RP-HPLC (structures were confirmed by ^{1}H NMR and HRMS, see SI). The impurities are mainly truncated sequences containing lower amounts of EDS, as determined by LC-MS measurements (see SI). If required, macromonomers can be obtained in higher purities by applying multiple coupling or additional purification after cleavage, e.g., by preparative HPLC. To ensure complete introduction of the reactive groups a double coupling of L-cysteine and DDS was performed. For TEC polymerization method development, the polymeric material was analyzed with GPC-RI-LS determining the molecular weight and dispersity and with MALDI-TOF-MS excluding interfering side-reactions. In all reactions both macromonomers were used in an equimolar ratio and high concentration (50 mM).

From the series of experiments varying solvent and irradiation time, the highest $\bar{M}_n$, as determined by GPC-RI-LS analysis, was observed when using dimethyl sulfoxide and water in a ratio of 9:1 and 60 min of irradiation. Next, in order to further increase $\bar{X}_n$, a screening of different photoinitiators was performed. A total of five photoinitiators, containing two benzophenone, two acetophenone, and one azo-based initiator, were tested. The initiators were chosen to include cleavage-type (Type I) and H-abstraction type (Type II) initiators from which one shows a maximum absorption slightly below and the other one close to the maximum intensity of the used UV lamp (365 nm). Best results were obtained when using the acetophenone based initiator DMPA, which is a Type I initiator with an absorption

DOI: 10.1021/acs.biomac.6b01657
Biomacromolecules 2017, 18, 787−796

Scheme 2. Polymerization of Precision Macromonomers 1 and 2 via Step-Growth TEC Resulting in the Sequence-Controlled Multiblock Copolymer 3

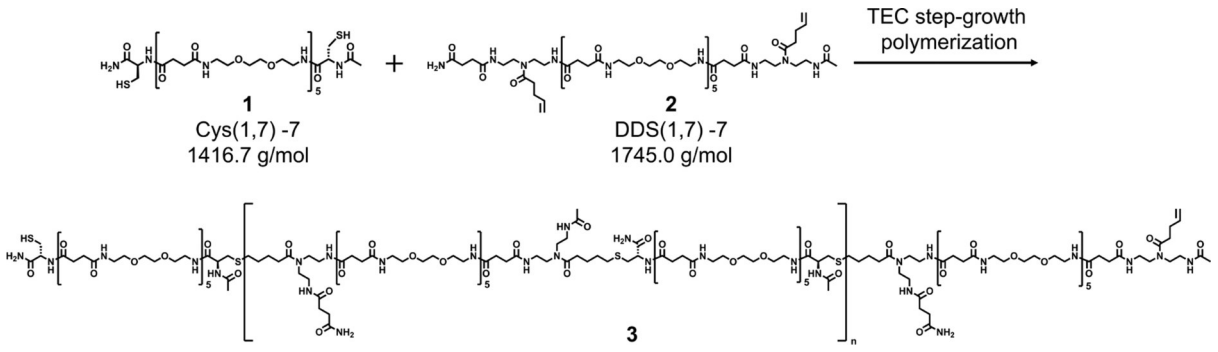

Table 1. Obtained $\bar{M}_w$, $\bar{M}_n$, $\bar{M}_w/\bar{M}_n$, and $\bar{X}_n$ after the Variation of the DMPA and TCEP Concentration in TEC Step-Growth Polymerization Reactions[a]

oligomer concentration [mM]	irradiation time [min]	DMPA [eq]	TCEP [eq]	$\bar{M}_w$ [kDa]	$\bar{M}_n$ [kDa]	$\bar{M}_w/\bar{M}_n$	$\bar{X}_n$
50	60	0	0.01	16.1	7.80	2.06	5
50	60	0.5	0	26.5	10.8	2.46	7
50	60	0.5	0.01	22.5	12.6	1.79	8
50	60	0.5	0.1	21.9	8.70	2.52	6
50	60	1.0	0	32.6	14.5	2.24	9
50	**60**	**1.0**	**0.01**	**29.0**	**16.0**	**1.81**	**10**
50	60	1.0	0.1	26.4	14.5	1.82	9
50	60	1.5	0	29.1	14.8	1.97	9
50	60	1.5	0.01	28.9	14.9	1.94	9
50	60	1.5	0.1	23.8	11.7	2.04	7

[a]The final reaction conditions are highlighted.

maximum of 250 nm, in agreement with previous results from the Yagci group.[35] Subsequently, DMPA was added to the reaction in different concentrations. An equimolar concentration of the photoinitiator (50 mM) showed highest $\bar{M}_n$ of 14−16 kDa which corresponds to a $\bar{X}_n$ of 9−10. A lower amount of DMPA of 0.5 equiv as well as a higher amount of 1.5 equiv lead to polymers with slightly lower $\bar{M}_n$ values of only 9−15 kDa. Without the addition of an initiator, only a poor $\bar{X}_n$ of about 5 was obtained, showing that the use of an initiator is essential in the performed reaction. All results are listed in Table 1.

Further, the influence of the addition of a reducing agent to the reaction mixture was evaluated. Due to the formation of disulfide bonds by oxidation, reactive end groups can be lost. There are different methods to prevent loss of reactive thiol groups due to oxidation, e.g., using thiolactone in situ generating a thiol after aminolysis.[7] For the reduction of disulfides, here we chose the addition of TCEP. There are two concurrent side reactions of TCEP, which can lead to the loss of reactive end groups and need to be evaluated. On the one hand, an irreversible hydrophosphination of the alkene moiety can occur under radical initiation, leading to the loss of reactive alkene groups.[36] Besides that, it is also possible that a thiyl radical, which is formed during the polymerization, reacts with the phosphine, forming a phosphine sulfide and alanine.[37] Both side reactions were observed by MALDI-TOF-MS analysis in first tests with high amounts of TCEP. An optimal amount of TCEP was determined by varying its concentration in the reaction mixture. Polymers with largest $\bar{M}_n$ were obtained when adding 0.01 equiv (0.5 mM) TCEP to the reaction mixture (Table 1). Additionally, the observed $\bar{M}_w/\bar{M}_n$ of final polymers was lower compared to reactions with higher and lower TCEP concentrations. Thus, the optimum amount of TCEP is sufficient to reduce formed disulfides but is still too low to significantly react with the alkene or thiyl groups. Hydrophosphination and desulfurization products were not observed by MALDI-TOF-MS analysis when using these conditions. However, during this analysis the presence of small amounts of remaining **1** with an intramolecular disulfide was determined. In ^{1}H NMR analysis of **3**, a total of 14% remaining alkene moieties which did not react during the polymerization was determined. In the reaction leading to **3**, a slightly higher amount of the alkene bearing macromonomer **2** was used as determined by ^{1}H NMR analysis of the product (**1** and **2** in the ratio of 1:1.07, see SI). This means some alkene groups remained in the product due to the mismatch in stoichiometry. Nevertheless, an extension of the irradiation time did not lead to further conversion. Potentially, a new building block containing a more reactive functional alkene group for photoinduced TEC could be investigated in future studies to obtain higher conversion and thus further increase $\bar{X}_n$. All polymerization experiments were repeated three times showing a variation of the $\bar{M}_n$ in a range of up to 2.5 kDa corresponding to a $\bar{X}_n$ between 1 and 2, when using the same reaction conditions in a series of experiments. The obtained $\bar{M}_w$, $\bar{M}_n$, and $\bar{M}_w/\bar{M}_n$ as well as the resulting $\bar{X}_n$ are listed in Table 1.

Application of the Developed TEC Method for the Synthesis of Sequence-Controlled Multiblock Glycopolymers. After establishing suitable polymerization protocols, a series of four different precision glycomacromolecules carrying Man to be used as macromonomers were synthesized following the previously established protocols.[10,13] In preliminary turbidity tests with trivalent glycomacromolecules, containing either two terminal DDS building blocks, two terminal L-cysteine residues, or no end-functionalization, it was observed that glycomacromolecules with either terminal alkene moieties or unfunction-

DOI: 10.1021/acs.biomac.6b01657
Biomacromolecules 2017, 18, 787−796

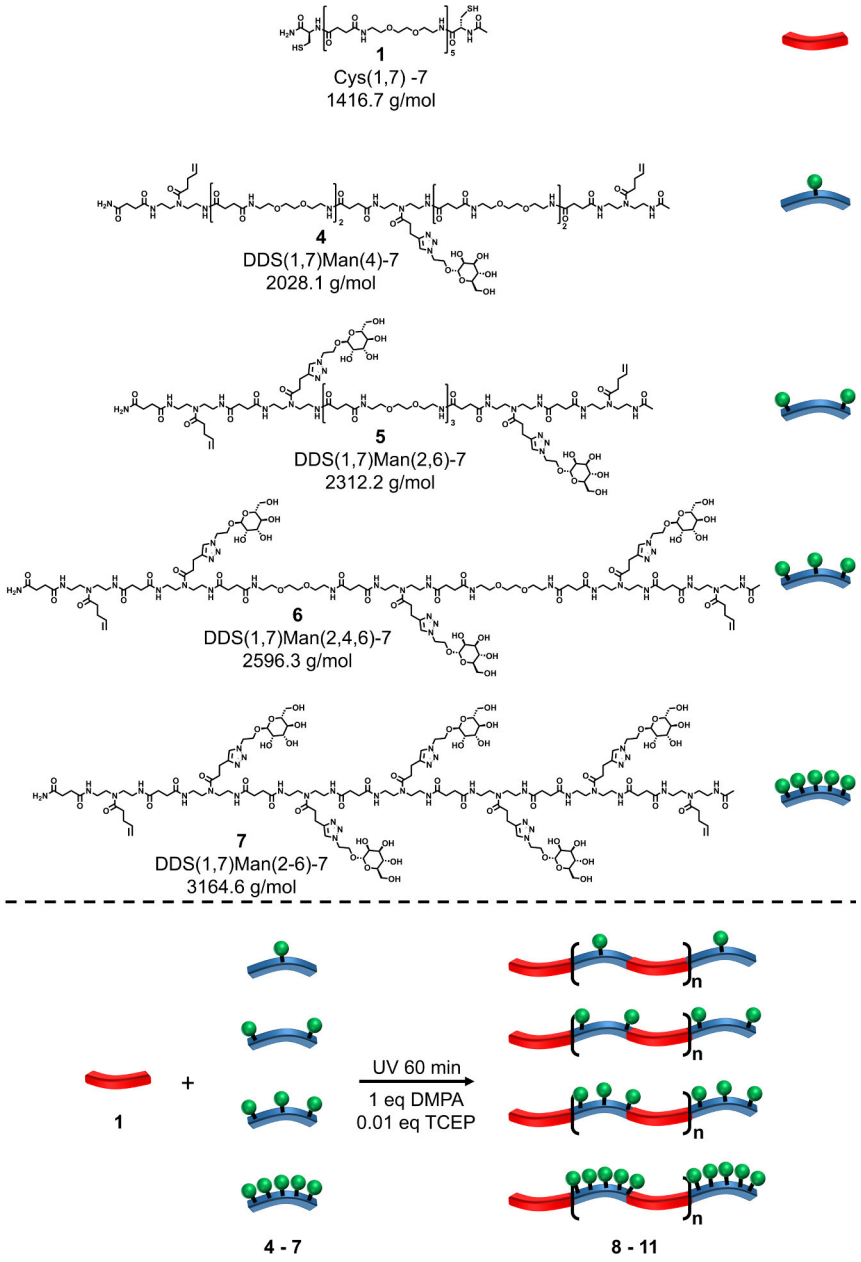

Figure 1. Structures of the glycomacromonomers **4**–**7** (top) and a schematic illustration of the formed multiblock glycopolymers **8**–**11** (bottom).

alized end groups show similar binding to ConA. In contrast to that, the glycomacromolecule with terminal L-cysteine residues showed a slightly higher cluster formation, potentially due to the conjunction of glycomacromolecules by the formation of disulfides. Therefore, all glycomacromolecules were synthesized with terminal DDS building blocks to allow for direct comparison of the macromonomer to the derived glycopolymer in later receptor binding studies.

The oligomers DDS(1,7)Man(4)-7 (**4**), DDS(1,7)Man(2,6)-7 (**5**), DDS(1,7)Man(2,4,6)-7 (**6**) and DDS(1,7)Man(2–6)-7 (**7**) were obtained with purities >92% after cleavage from the resin and a double precipitation from diethyl ether as determined by RP-HPLC and structures were confirmed by ^{1}H NMR and HRMS (see SI). Similar to the impurities determined in compounds **1** and **2**, the impurities are mainly truncated sequences with lower amounts of EDS or TDS (see SI). A double coupling of DDS was performed to ensure a complete introduction of the terminal alkene moieties for a successful polymerization. The structures of the glycomacromonomers are shown in Figure 1. All four glycomacromolecules were copolymerized with hydrophilic EDS-oligomer **1** under the previously established polymerization conditions giving final glycopolymers **8**–**11**. All polymers were analyzed by GPC-RI-LS, MALDI-TOF-MS, and ^{1}H NMR. The GPC data of glycopolymer **11** and the original macromonomers **1** and **7** is exemplarily presented in Figure 2. From GPC data of the purified glycopolymers after precipitation in cold diethyl ether, no remaining macromonomers were observed after polymerization.

All four Man-presenting glycopolymers **8**–**11** were obtained with the same $\overline{X}_n$ and $\overline{M}_w/\overline{M}_n$. The $\overline{X}_n$ of 8 for all glycopolymers was slightly lower as compared to the reaction optimization experiments with the spacer macromonomers ($\overline{X}_n$ of 10). This indicates that the reactivity of glycomacromonomers is lower, e.g., due to differences in polarity or accessibility of the functional

DOI: 10.1021/acs.biomac.6b01657
Biomacromolecules 2017, 18, 787–796

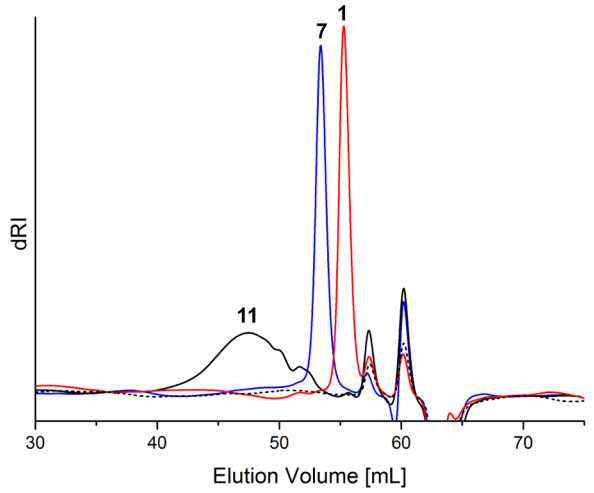

Figure 2. GPC-RI-LS data from the analysis of the glycopolymer **11** and its corresponding precursor macromonomers **1** and **7**. Columns: Suprema Lux (2 × 100 and 1000 Å). Buffer: 50 mM NaH_2PO_4, 150 mM NaCl, 250 ppm of NaN_3 (pH 7.2), 30% ACN. Flow: 1 mL/min.

end groups. In the polymerization of glycomacromonomers **5**−**7**, a slightly higher amount of the thiol bearing macromonomer **1** was used, as determined by ^{1}H NMR (**1** and **5**, **6**, **7** in the ratio of 1:0.88, 1:0.84, and 1:0.85, respectively; see SI). Because of this, the glycopolymers **9**−**11** show almost no remaining alkene moieties. In the polymerization leading to glycopolymer **8**, the ratio of the two monomers was almost equal; however, the determined remaining alkene moiety was 18% (**1** and **4** in the ratio of 1:0.94; see SI). In comparison to the remaining alkene moieties with about 14% for the polymer from reaction optimization, this value also suggests that the Man-bearing macromonomers are less reactive under these reaction conditions than the spacer macromonomers **1** and **2**. A schematic illustration of all multiblock glycopolymers is presented in Figure 1. Obtained $\bar{M}_w$, $\bar{M}_n$, $\bar{X}_n$, $\bar{M}_w/\bar{M}_n$ and the resulting amount of sugar moieties for all glycopolymers are listed in Table 2.

Table 2. Obtained $\bar{M}_w$, $\bar{M}_n$, $\bar{M}_w/\bar{M}_n$, and $\bar{X}_n$ and the Resulting Amount of Sugar Moieties (N) for the Glycopolymers 8−11 as well as their Precursor Glycomacromonomers

oligomer used	polymer	$\bar{M}_w$ [kDa]	$\bar{M}_n$ [kDa]	$\bar{M}_w/\bar{M}_n$	$\bar{X}_n$	N (sugar)
4	**8**	25.0	13.4	1.87	8	4
5	**9**	27.7	14.8	1.87	8	8
6	**10**	29.7	16.6	1.80	8	12
7	**11**	30.8	17.5	1.76	8	20

Binding Behavior of Glycomacromonomers and Glycopolymers toward ConA. The binding behavior of the glycomacromonomers as well as the glycopolymers to the lectin ConA were tested in a turbidity and precipitation assay and by SPR, performing a direct ligand binding assay. ConA is a plant lectin and widely used as model lectin to investigate ligand/receptor interactions of glycomimetics since it was the first lectin to be isolated, fully characterized, and commercially available.[38] It binds specifically to Man and does not have an affinity to galactose (Gal).[39] At a pH greater 7, it mainly exists in a homotetrameric form containing four identical Man binding subunits.[40] An interaction with multimeric carbohydrates or glycopolymers leads to clustering since the lectin acts as a cross-linker, known as the cluster glycoside effect.[19,41] When clustering occurs in solution, the formed cluster precipitates and the solution turns turbid. By different turbidity assays, the efficiency of the synthesized glycomacromonomers or glycopolymers in forming clusters with the lectin ConA can be determined. Besides the clustering potential, binding of glycopolymers to ConA can be further investigated using methods such as SPR,[10,20,32] isothermal titration calorimetry (ITC),[42] atomic force microscopy (AFM)[43] or soft colloidal probe−reflection interference contrast microscopy (SCP-RICM)[13,18] providing information on the binding affinity, kinetics and energies. Previously, a great number of studies investigating the cluster glycoside effect and multivalent interactions of synthetic glycomimetics, especially glycopolymers, has been published showing the influence, e.g., of total carbohydrate valency, epitope density, molecular weight, scaffold flexibility, and architecture of the glycopolymer on the resulting receptor binding properties.[10,13,18,29−31,44]

With the presented synthetic approach, we now have access to a series of ligands gradually varying the valency and going from lower molecular weight glycomacromonomers to higher molecular weight glycopolymers, each with similar degree of polymerization and dispersity. The contour length of the spacing block between the binding epitopes is about 140 Å for structures **5**−**7** and 200 Å for structure **4**. It can be expected that due to the flexibility of the backbone of the glycopolymers, they adapt coiled conformations, but still have enough spacing between the sugar functionalized blocks to potentially address several binding sites of ConA. Thus, the different spacing of sugar ligands during synthesis should translate into different sugar ligand densities for glycomacromolecules and−polymers in solution.

For the turbidity assay, a protocol from the work of the group of Kiessling[29] was adapted. In our study, the macromolecular ligands were titrated into the ConA solution in order to obtain the ligand concentration required for reaching the half-maximal turbidity (conc. $1/2T_{Max}$). The ligand concentration was increased stepwise via titration to a solution with a constant receptor concentration instead of preparing different receptor/ligand ratios in separate tubes. The ligand's potential to form clusters with ConA can be expressed as the reciprocal of the determined values ($1/(\text{conc. } 1/2T_{Max})$). In addition, by means of UV−vis measurements a quantitative precipitation assay was performed yielding the amount of glycooligomer-bound of ConA, and hence the stoichiometry of the glycooligomer or -polymer/ConA complex.[33] From both parameters, complementary information on the ConA clustering efficiency can be obtained. For the direct binding SPR assay, a similar procedure as described by the groups of Fernandez−Megia and Riguera was performed, using a sensor chip with covalently bound ConA onto which the glycomacromonomers and glycopolymers were injected in different concentrations.[20] From the direct binding experiments, K_D and K_A can be obtained. As negative control, the oligomeric and polymeric structures **2** and **3**, not containing sugar moieties, were tested for all three assays showing no binding to the lectin. Results from the three assays for all oligomeric and polymeric structures are shown in Figure 3.

From the obtained data for the cluster formation of mono-, di-, tri-, and pentavalent glycooligomers **4** to **7**, we were able to confirm preliminary findings on the lower limit of presented sugar ligands as well as the correlation of an increase in ConA clustering efficiency with an increasing Man valency.[10] A minimum of three sugar moieties were required for a clustering of the tetrameric lectin, as mono and divalent structures **4** and **5** did not show any precipitate formation in either of the performed assays. The increase from three to five Man moieties on an

DOI: 10.1021/acs.biomac.6b01657
Biomacromolecules 2017, 18, 787−796

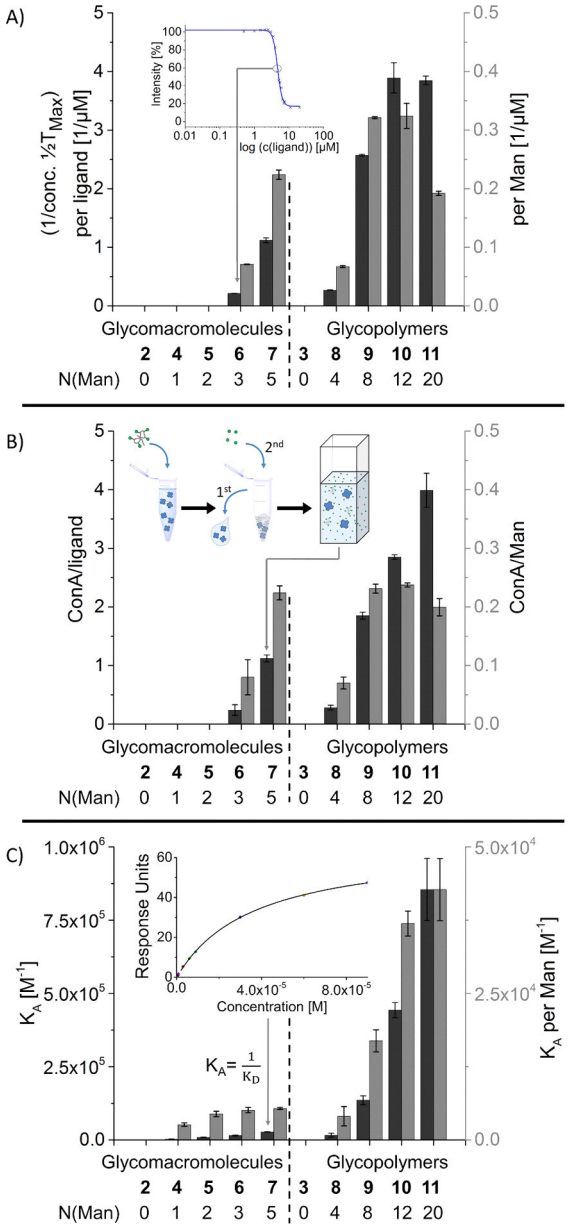

Figure 3. Results from turbidity assay (A) showing the reciprocal of half-maximal precipitation per ligand (black, left *y*-axis) and per Man (gray, right *y*-axis). Results from the quantitative precipitation assay (B) showing the amount of ConA bound per ligand (black, left *y*-axis) and per Man (gray, right *y*-axis). (C) Results from the SPR direct binding experiments showing the determined binding constant K_A per ligand (black, left *y*-axis) and per Man (gray, right *y*-axis).

oligomeric scaffold, compounds **6** and **7**, leads to a significant increase in cluster formation in both assays (Figure 3A,B, black bars).

Comparing the glycopolymers and glycomacromonomers, it seems that molecular weight of the structures does not influence the clustering but there is a strong dependency on the number of sugars presented on the scaffold. Values from both assays for glycopolymers **8** and **9** presenting on average 4 and 8 sugar ligands are in the same regime as for the tri- and pentavalent glycomacromonomers **6** and **7**. (Figure 3A,B, black bars).

The dependency of the Man valency on the ConA clustering can also be observed for the determined values from the quantitative precipitation assay for glycopolymers **8**–**11**. Here we see a steady increase in cluster formation with an increase in Man valency, where glycopolymers presenting more sugar ligands bind more ConA molecules in the formed precipitate (ConA/ligand) (Figure 3B, black bars). The lowest ConA/glycopolymer ratio was determined for the glycopolymer **8** presenting an average of 4 Man moieties, followed by the glycopolymers with an average of 8, 12, and 20 Man moieties **9**, **10**, and **11**, respectively.

The data of the turbidity assay shows a plateau in the efficiency of clustering ConA after reaching a certain Man valency. The obtained values for $1/(\text{conc. } 1/2T_{Max})$ were equal for the glycopolymers **10** and **11**, presenting 12 and 20 Man moieties, respectively (Figure 3A, black bars). Similar findings were previously reported for other glycopolymers binding to ConA, showing a maximum for the ligand concentration in the turbidity assay along with a steady increase of ConA/ligand ratio in a precipitation assay.[29−32] Indeed, the glycopolymer **10** with 12 Man moieties has a similar Man valency as the polymer reaching the maximum in a similar turbidity assay as presented by Kiessling and co-workers further supporting these findings.[29]

In order to evaluate the efficiency of glycomacromonomers and glycopolymers in terms of the presented Man moieties, values from all three assays were also normalized to the number of Man ligands per macromolecule/polymer (Figure 3A,B,C, gray bars). Interestingly, both assays based on the cluster formation reveal a maximum efficiency in cluster formation per Man ligand for glycopolymers **9** and **10** with 8−12 Man moieties. For the precipitation assay, glycomacromonomer **7** with 5 Man moieties already reaches the observed maximum ConA/Man value. Glycopolymer **11** with an average of 20 Man moieties even shows a decrease in clustering per Man unit in both assays. Again, these findings are in agreement with previous studies from the groups of Kiessling, Haddleton, and Stenzel, when normalizing their results to the number of Man ligands.[29−32] Such a maximum in cluster efficiency per Man ligand is often explained by the requirement of a certain Man density, rather than a Man valency, for the efficient clustering of ConA with glycopolymers.[32] Even if every repeating unit/monomer carries a sugar ligand, it is unlikely that all ligands will be involved in the cluster formation. Thus, a reduction in the ligand density, e.g., by introducing nonbinding ligands or increasing the spacing between the ligands, while maintaining the required number of binding ligands, should not alter the cluster efficiency.[29,30] When comparing our glycomacromonomers and glycopolymers, we even find that the spacing and size of the scaffold does not change the ability to form ConA clusters, as long as the valency is high enough. However, so far we do not have any information on the conformation of the glycopolymers in solution, and thus the density of accessible Man ligands which might be available for cluster formation.

In order to gain more insights into the availability of Man ligands for binding, we performed a direct binding assay determining the K_A of the glycomacromonomers and glycopolymers binding to immobilized ConA via SPR (Figure 3C). Again, we see a strong dependency of the binding on the valency of the ligands, with the glycopolymer with the highest valency **11** giving the highest K_A in this series. Ligands of the same valency, e.g., glycomacromonomer **6** with 3 Man ligands and glycopolymer **8** with an average of 4 Man ligands show very similar values for K_A despite their different contour length. When looking at K_A per Man ligand, we do not observe a decrease for the higher valent glycopolymers as we did for the cluster formation. Nevertheless,

DOI: 10.1021/acs.biomac.6b01657
Biomacromolecules 2017, 18, 787−796

the increase of K_A per Man ligand with increasing valency starts to stall for the higher valent glycopolymers.

Overall, it is difficult to directly compare the turbidity and direct binding assay, as different parameters of the measurement will also influence the ligand−receptor binding, e.g., the binding of glycopolymers to a surface-anchored ConA might lead to conformational changes, which would not be expected for binding in solution.[13,20] Nevertheless, all three assays show a similar trend, where we see a strong influence of the valency of the glycomacromonomers and glycopolymers but so far no influence of the overall size of the molecules with respect to K_A and ConA clustering. Furthermore, all three assays indicate that there is a maximum efficiency in clustering or binding when normalizing to the number of Man ligands, where a further increase in valency would not lead to a further increase in clustering or binding.

CONCLUSION

In summary, we were able to introduce a new strategy for the synthesis of sequence-controlled polymers combining solid phase synthesis and TEC. In a first step, two sets of macromonomers were obtained from the solid phase assembly of functional building blocks introducing either a hydrophilic spacer block with thiol end groups or sugar-presenting blocks with varying number of sugar ligands in the side chain and alkene end groups. Through TEC step-growth polymerization, multiblock copolymers were obtained with $\bar{M}_n$ of 16 kDa, corresponding to a $\bar{X}_n$ of 10. Thereby the monomer sequence of the macromonomers translates into sequence-controlled glycopolymers allowing for the variation of the number and positioning of sugar ligands. In a first binding study, precision glycomacromonomers and glycopolymers were investigated for their lectin clustering behavior showing a dependency on the number of sugar ligands on the clustering ability. For the glycopolymers with the highest ligand valencies studied in this series, the efficiency in forming clusters reached a maximum, which indicates, in conformity with previous studies from literature, that at a certain level of ligand valency a further increase in receptor clustering cannot simply be achieved by adding more sugars to the scaffold. In this study we could also show that when keeping the valency constant, further increase in clustering or direct binding of glycopolymers could not be achieved by increasing the size of the ligand-presenting scaffold. The presented multiblock glycopolymers combine blocks with precise positioning of binding ligands with nonbinding spacer blocks and thus give access to glycopolymers with a locally highly controlled valency as well as density of ligands. The local control of functionality along a polymer backbone is especially interesting for bioactive, biomimetic, and bioconjugate polymers more closely imitating monomer sequences of natural biopolymers but might also be applied for other classes of polymeric materials in the future.

ASSOCIATED CONTENT

Supporting Information

Information about used materials and analytical methods, as well as detailed analytical data of the compounds and data from the ConA binding assays are available. The Supporting Information is available free of charge on the ACS Publications website at DOI: 10.1021/acs.biomac.6b01657.

(PDF)

AUTHOR INFORMATION

Corresponding Author

*E-mail: laura.hartmann@hhu.de. Phone: +49 211 81-10360. Fax: +49 211 81-15840.

ORCID

Morten F. Ebbesen: 0000-0001-5416-7429

Laura Hartmann: 0000-0003-0115-6405

Author Contributions

All authors have given approval to the final version of the manuscript.

Notes

The authors declare no competing financial interest.

ACKNOWLEDGMENTS

We thank Jun.-Prof. Dr. Stephan Schmidt for valuable feedback on the data evaluation. We are grateful to Dr. Lothar Gremer and Prof. Dieter Willbold for kind donation of a CM5 chip. We also thank Sonja Coors for providing functionalized Man-ligands, Dr. Peter Tommes and Ralf Bürgel for performing HRMS and MALDI-TOF measurements, as well as Maria Beuer for performing NMR measurements. The authors gratefully acknowledge funding from the Boehringer-Ingelheim Foundation within the *Perspektivenprogramm* 'Plus3' and the Danish Council for Independent Research for support through the grant DFF-4005-00023.

ABBREVIATIONS

TEC, thiol−ene coupling; Man, α-D-Mannose; ConA, Concanavalin A; CuAAC, copper mediated azide−alkyne cycloaddition; DMPA, 2,2-dimethoxy-2-phenylacetophenone; TCEP, tris(2-carboxyethyl)phosphine hydrochloride; LBB, lectin binding buffer; SPR, surface plasmon resonance; ITC, isothermal titration calorimetry; AFM, atomic force microscopy; SCP-RICM, soft colloidal probe - reflection interference contrast microscopy; DDS, **D**ouble bond−**D**iethylenetriamine−**S**uccinic acid; TDS, **T**riple bond−**D**iethylenetriamine−**S**uccinic acid; EDS, **E**thylene glycol−**D**iamine−**S**uccinic acid

REFERENCES

(1) For general examples on sequence-controlled polymers see: (a) Lutz, J.-F.; Ouchi, M.; Liu, D. R.; Sawamoto, M. Sequence-Controlled Polymers. *Science* **2013**, *341* (6146), 1238149. (b) Rosales, A. M.; Segalman, R. A.; Zuckermann, R. N. Polypeptoids: a model system to study the effect of monomer sequence on polymer properties and self-assembly. *Soft Matter* **2013**, *9* (35), 8400−8414. (c) D'Hooge, D. R.; Van Steenberge, P. H. M.; Derboven, P.; Reyniers, M.-F.; Marin, G. B. Model-based design of the polymer microstructure: bridging the gap between polymer chemistry and engineering. *Polym. Chem.* **2015**, *6* (40), 7081−7096. (d) Bates, F. S.; Hillmyer, M. A.; Lodge, T. P.; Bates, C. M.; Delaney, K. T.; Fredrickson, G. H. Multiblock Polymers: Panacea or Pandora's Box? *Science* **2012**, *336* (6080), 434−440. (e) Sutthasupa, S.; Shiotsuki, M.; Sanda, F. Recent advances in ring-opening metathesis polymerization, and application to synthesis of functional materials. *Polym. J.* **2010**, *42* (12), 905−915.

(2) For recent examples on sequence-controlled polymers by controlled polymerization methods see: (a) Gutekunst, W. R.; Hawker, C. J. A General Approach to Sequence-Controlled Polymers Using Macrocyclic Ring Opening Metathesis Polymerization. *J. Am. Chem. Soc.* **2015**, *137* (25), 8038−8041. (b) Zhang, Q.; Collins, J.; Anastasaki, A.; Wallis, R.; Mitchell, D. A.; Becer, C. R.; Haddleton, D. M. Sequence-Controlled Multi-Block Glycopolymers to Inhibit DC-SIGN-gp120 Binding. *Angew. Chem., Int. Ed.* **2013**, *52* (16), 4435−4439. (c) Zhang, J.; Matta, M. E.; Hillmyer, M. A. Synthesis of Sequence-Specific Vinyl Copolymers by Regioselective ROMP of Multiply

DOI: 10.1021/acs.biomac.6b01657
Biomacromolecules 2017, 18, 787−796

Substituted Cyclooctenes. *ACS Macro Lett.* **2012**, *1* (12), 1383−1387. (d) Vandenbergh, J.; Reekmans, G.; Adriaensens, P.; Junkers, T. Synthesis of sequence controlled acrylate oligomers via consecutive RAFT monomer additions. *Chem. Commun.* **2013**, *49* (88), 10358−10360. (e) Satoh, K.; Ozawa, S.; Mizutani, M.; Nagai, K.; Kamigaito, M. Sequence-regulated vinyl copolymers by metal-catalysed step-growth radical polymerization. *Nat. Commun.* **2010**, *1*, 6. (f) Lutz, J.-F.; Schmidt, B. V. K. J.; Pfeifer, S. Tailored Polymer Microstructures Prepared by Atom Transfer Radical Copolymerization of Styrene and N-substituted Maleimides. *Macromol. Rapid Commun.* **2011**, *32* (2), 127−135. (g) Weiss, R. M.; Short, A. L.; Meyer, T. Y. Sequence-Controlled Copolymers Prepared via Entropy-Driven Ring-Opening Metathesis Polymerization. *ACS Macro Lett.* **2015**, *4* (9), 1039−1043.

(3) For recent examples on sequence-controlled polymers by click coupling see: (a) Driessen, F.; Du Prez, F. E.; Espeel, P. Precision Multisegmented Macromolecular Lineups: A Display of Unique Control over Backbone Structure and Functionality. *ACS Macro Lett.* **2015**, *4* (6), 616−619. (b) Lopez, G.; Ameduri, B.; Habas, J.-P. A Versatile Strategy to Synthesize Perfluoropolyether-Based Thermoplastic Fluoropolymers by Alkyne-Azide Step-Growth Polymerization. *Macromol. Rapid Commun.* **2016**, *37* (8), 711−717. (c) Xi, W.; Pattanayak, S.; Wang, C.; Fairbanks, B.; Gong, T.; Wagner, J.; Kloxin, C. J.; Bowman, C. N. Clickable Nucleic Acids: Sequence-Controlled Periodic Copolymer/Oligomer Synthesis by Orthogonal Thiol-X Reactions. *Angew. Chem., Int. Ed.* **2015**, *54* (48), 14462−14467. (d) Jiang, Y.; Golder, M. R.; Nguyen, H. V. T.; Wang, Y.; Zhong, M.; Barnes, J. C.; Ehrlich, D. J. C.; Johnson, J. A. Iterative Exponential Growth Synthesis and Assembly of Uniform Diblock Copolymers. *J. Am. Chem. Soc.* **2016**, *138* (30), 9369−9372.

(4) For recent examples on sequence-controlled polymers by the use of special monomers see: (a) Ouchi, M.; Nakano, M.; Nakanishi, T.; Sawamoto, M. Alternating Sequence Control for Carboxylic Acid and Hydroxy Pendant Groups by Controlled Radical Cyclopolymerization of a Divinyl Monomer Carrying a Cleavable Spacer. *Angew. Chem., Int. Ed.* **2016**, *55* (47), 14584−14589. (b) McKee, M. L.; Milnes, P. J.; Bath, J.; Stulz, E.; Turberfield, A. J.; O'Reilly, R. K. Multistep DNA-Templated Reactions for the Synthesis of Functional Sequence Controlled Oligomers. *Angew. Chem., Int. Ed.* **2010**, *49* (43), 7948−7951. (c) Ida, S.; Ouchi, M.; Sawamoto, M. Designer Template Initiator for Sequence Regulated Polymerization: Systems Design for Substrate-Selective Metal-Catalyzed Radical Addition and Living Radical Polymerization. *Macromol. Rapid Commun.* **2011**, *32* (2), 209−214.

(5) For recent examples on sequence-controlled polymers by iterative coupling see: (a) Leibfarth, F. A.; Johnson, J. A.; Jamison, T. F. Scalable synthesis of sequence-defined, unimolecular macromolecules by Flow-IEG. *Proc. Natl. Acad. Sci. U. S. A.* **2015**, *112* (34), 10617−10622. (b) Solleder, S. C.; Wetzel, K. S.; Meier, M. A. R. Dual side chain control in the synthesis of novel sequence-defined oligomers through the Ugi four-component reaction. *Polym. Chem.* **2015**, *6* (17), 3201−3204. (c) Porel, M.; Alabi, C. A. Sequence-Defined Polymers via Orthogonal Allyl Acrylamide Building Blocks. *J. Am. Chem. Soc.* **2014**, *136* (38), 13162−13165. (d) De Bo, G.; Kuschel, S.; Leigh, D. A.; Lewandowski, B.; Papmeyer, M.; Ward, J. W. Efficient Assembly of Threaded Molecular Machines for Sequence-Specific Synthesis. *J. Am. Chem. Soc.* **2014**, *136* (15), 5811−5814.

(6) For recent examples on sequence-controlled polymeres by solid phase synthesis see: (a) Al Ouahabi, A.; Charles, L.; Lutz, J.-F. Synthesis of Non-Natural Sequence-Encoded Polymers Using Phosphoramidite Chemistry. *J. Am. Chem. Soc.* **2015**, *137* (16), 5629−5635. (b) Trinh, T. T.; Oswald, L.; Chan-Seng, D.; Lutz, J.-F. Synthesis of Molecularly Encoded Oligomers Using a Chemoselective "AB + CD" Iterative Approach. *Macromol. Rapid Commun.* **2014**, *35* (2), 141−145.

(7) Martens, S.; Van den Begin, J.; Madder, A.; Du Prez, F. E.; Espeel, P. Automated Synthesis of Monodisperse Oligomers, Featuring Sequence Control and Tailored Functionalization. *J. Am. Chem. Soc.* **2016**, *138* (43), 14182−14185.

(8) Merrifield, R. B. Solid Phase Peptide Synthesis. I. The Synthesis of a Tetrapeptide. *J. Am. Chem. Soc.* **1963**, *85* (14), 2149−2154.

(9) Wojcik, F.; Mosca, S.; Hartmann, L. Solid-Phase Synthesis of Asymmetrically Branched Sequence-Defined Poly/Oligo-(amidoamines). *J. Org. Chem.* **2012**, *77* (9), 4226−4234.

(10) Ponader, D.; Wojcik, F.; Beceren-Braun, F.; Dernedde, J.; Hartmann, L. Sequence-Defined Glycopolymer Segments Presenting Mannose: Synthesis and Lectin Binding Affinity. *Biomacromolecules* **2012**, *13* (6), 1845−1852.

(11) Wojcik, F.; O'Brien, A. G.; Götze, S.; Seeberger, P. H.; Hartmann, L. Synthesis of Carbohydrate-Functionalised Sequence-Defined Oligo-(amidoamine)s by Photochemical Thiol-Ene Coupling in a Continuous Flow Reactor. *Chem. - Eur. J.* **2013**, *19* (9), 3090−3098.

(12) Ponader, D.; Igde, S.; Wehle, M.; Märker, K.; Santer, M.; Bléger, D.; Hartmann, L. Photoswitchable precision glycooligomers and their lectin binding. *Beilstein J. Org. Chem.* **2014**, *10* (1), 1603−1612.

(13) Ponader, D.; Maffre, P.; Aretz, J.; Pussak, D.; Ninnemann, N. M.; Schmidt, S.; Seeberger, P. H.; Rademacher, C.; Nienhaus, G. U.; Hartmann, L. Carbohydrate-Lectin Recognition of Sequence-Defined Heteromultivalent Glycooligomers. *J. Am. Chem. Soc.* **2014**, *136* (5), 2008−2016.

(14) Ebbesen, M. F.; Gerke, C.; Hartwig, P.; Hartmann, L. Biodegradable poly(amidoamine)s with uniform degradation fragments via sequence-controlled macromonomers. *Polym. Chem.* **2016**, *7* (48), 7086−7093.

(15) Mosca, S.; Dannehl, C.; Moginger, U.; Brezesinski, G.; Hartmann, L. β^{3R3}-Peptides: design and synthesis of novel peptidomimetics and their self-assembling properties at the air-water interface. *Org. Biomol. Chem.* **2013**, *11* (33), 5399−5403.

(16) Mosca, S.; Keller, J.; Azzouz, N.; Wagner, S.; Titz, A.; Seeberger, P. H.; Brezesinski, G.; Hartmann, L. Amphiphilic Cationic β^{3R3}-Peptides: Membrane Active Peptidomimetics and Their Potential as Antimicrobial Agents. *Biomacromolecules* **2014**, *15* (5), 1687−1695.

(17) Broecker, F.; Hanske, J.; Martin, C. E.; Baek, J. Y.; Wahlbrink, A.; Wojcik, F.; Hartmann, L.; Rademacher, C.; Anish, C.; Seeberger, P. H. Multivalent display of minimal Clostridium difficile glycan epitopes mimics antigenic properties of larger glycans. *Nat. Commun.* **2016**, *7*, 11224.

(18) Pussak, D.; Ponader, D.; Mosca, S.; Ruiz, S. V.; Hartmann, L.; Schmidt, S. Mechanical Carbohydrate Sensors Based on Soft Hydrogel Particles. *Angew. Chem., Int. Ed.* **2013**, *52* (23), 6084−6087.

(19) Lundquist, J. J.; Toone, E. J. The Cluster Glycoside Effect. *Chem. Rev.* **2002**, *102* (2), 555−578.

(20) Munoz, E. M.; Correa, J.; Fernandez-Megia, E.; Riguera, R. Probing the Relevance of Lectin Clustering for the Reliable Evaluation of Multivalent Carbohydrate Recognition. *J. Am. Chem. Soc.* **2009**, *131* (49), 17765−17767.

(21) For examples on receptor clustering see: (a) Mammen, M.; Choi, S.-K.; Whitesides, G. M. Polyvalent Interactions in Biological Systems: Implications for Design and Use of Multivalent Ligands and Inhibitors. *Angew. Chem., Int. Ed.* **1998**, *37* (20), 2754−2794. (b) Kiessling, L. L.; Gestwicki, J. E.; Strong, L. E. Synthetic Multivalent Ligands as Probes of Signal Transduction. *Angew. Chem., Int. Ed.* **2006**, *45* (15), 2348−2368.

(22) Carothers, W. H. Polymers and polyfunctionality. *Trans. Faraday Soc.* **1936**, *32* (0), 39−49.

(23) Hoyle, C. E.; Lowe, A. B.; Bowman, C. N. Thiol-click chemistry: a multifaceted toolbox for small molecule and polymer synthesis. *Chem. Soc. Rev.* **2010**, *39* (4), 1355−1387.

(24) For examples on click reactions in polymer chemistry see: (a) Ladmiral, V.; Mantovani, G.; Clarkson, G. J.; Cauet, S.; Irwin, J. L.; Haddleton, D. M. Synthesis of Neoglycopolymers by a Combination of "Click Chemistry" and Living Radical Polymerization. *J. Am. Chem. Soc.* **2006**, *128* (14), 4823−4830. (b) Qin, A.; Lam, J. W. Y.; Tang, B. Z. Click polymerization. *Chem. Soc. Rev.* **2010**, *39* (7), 2522−2544. (c) Gregory, A.; Stenzel, M. H. Complex polymer architectures via RAFT polymerization: From fundamental process to extending the scope using click chemistry and nature's building blocks. *Prog. Polym. Sci.* **2012**, *37* (1), 38−105. (d) Binder, W. H.; Sachsenhofer, R. 'Click' Chemistry in Polymer and Material Science: An Update. *Macromol. Rapid Commun.* **2008**, *29* (12−13), 952−981. (e) Lowe, A. B. Thiol-ene "click" reactions and recent applications in polymer and materials synthesis. *Polym. Chem.*

DOI: 10.1021/acs.biomac.6b01657
Biomacromolecules 2017, 18, 787−796

2010, *1* (1), 17−36. (f) Sun, J.; Schlaad, H. Thiol−Ene Clickable Polypeptides. *Macromolecules* **2010**, *43* (10), 4445−4448. (g) Brosnan, S. M.; Schlaad, H. Modification of polypeptide materials by Thiol-X chemistry. *Polymer* **2014**, *55* (22), 5511−5516.

(25) Vandenbergh, J.; Ramakers, G.; van Lokeren, L.; van Assche, G.; Junkers, T. Synthesis of degradable multi-segmented polymers via Michael-addition thiol-ene step-growth polymerization. *RSC Adv.* **2015**, *5* (100), 81920−81932.

(26) Walker, C. N.; Sarapas, J. M.; Kung, V.; Hall, A. L.; Tew, G. N. Multiblock Copolymers by Thiol Addition Across Norbornene. *ACS Macro Lett.* **2014**, *3* (5), 453−457.

(27) Luo, K.; Yang, J.; Kopečková, P.; Kopeček, J. Biodegradable Multiblock Poly[N-(2-hydroxypropyl)methacrylamide] via Reversible Addition−Fragmentation Chain Transfer Polymerization and Click Chemistry. *Macromolecules* **2011**, *44* (8), 2481−2488.

(28) Berthet, M.-A.; Zarafshani, Z.; Pfeifer, S.; Lutz, J.-F. Facile Synthesis of Functional Periodic Copolymers: A Step toward Polymer-Based Molecular Arrays. *Macromolecules* **2010**, *43* (1), 44−50.

(29) Gestwicki, J. E.; Cairo, C. W.; Strong, L. E.; Oetjen, K. A.; Kiessling, L. L. Influencing Receptor−Ligand Binding Mechanisms with Multivalent Ligand Architecture. *J. Am. Chem. Soc.* **2002**, *124* (50), 14922−14933.

(30) Gou, Y.; Geng, J.; Richards, S.-J.; Burns, J.; Remzi Becer, C.; Haddleton, D. M. A Detailed Study on Understanding Glycopolymer Library and Con A Interactions. *J. Polym. Sci., Part A: Polym. Chem.* **2013**, *51* (12), 2588−2597.

(31) Chen, Y.; Chen, G.; Stenzel, M. H. Synthesis and Lectin Recognition of Glyco Star Polymers Prepared by "Clicking" Thiocarbohydrates onto a Reactive Scaffold. *Macromolecules* **2010**, *43* (19), 8109−8114.

(32) Chen, Y.; Lord, M. S.; Piloni, A.; Stenzel, M. H. Correlation between Molecular Weight and Branch Structure of Glycopolymers Stars and Their Binding to Lectins. *Macromolecules* **2015**, *48* (2), 346−357.

(33) Bhattacharyya, L.; Khan, M. I.; Brewer, C. F. Interactions of concanavalin A with asparagine-linked glycopeptides: formation of homogeneous cross-linked lattices in mixed precipitation systems. *Biochemistry* **1988**, *27* (24), 8762−8767.

(34) Becer, C. R.; Gibson, M. I.; Geng, J.; Ilyas, R.; Wallis, R.; Mitchell, D. A.; Haddleton, D. M. High-Affinity Glycopolymer Binding to Human DC-SIGN and Disruption of DC-SIGN Interactions with HIV Envelope Glycoprotein. *J. Am. Chem. Soc.* **2010**, *132* (43), 15130−15132.

(35) Uygun, M.; Tasdelen, M. A.; Yagci, Y. Influence of Type of Initiation on Thiol−Ene "Click" Chemistry. *Macromol. Chem. Phys.* **2010**, *211* (1), 103−110.

(36) For previous reports on side reactions of TCEP (hydrophosphination) in thiol-ene see: (a) Trofimov, B. A.; Gusarova, N. K.; Arbuzova, S. N.; Ivanova, N. I.; Artem'ev, A. V.; Volkov, P. A.; Ushakov, I. A.; Malysheva, S. F.; Kuimov, V. A. Stereoselective free-radical addition of secondary phosphine selenides to aromatic acetylenes. *J. Organomet. Chem.* **2009**, *694* (5), 677−682. (b) Arbuzova, S. N.; Gusarova, N. K.; Trofimov, B. A. Nucleophilic and free-radical additions of phosphines and phosphine chalcogenides to alkenes and alkynes. *Arkivoc* **2006**, *5*, 12−36. (c) Gaumont, A.-C.; Simon, A.; Denis, J.-M. Uncatalyzed hydrophosphination of multiple bonds by alkenyl- or alkynyl-phosphine-oxides; evidence for a P-H activation. *Tetrahedron Lett.* **1998**, *39* (9), 985−988.

(37) For previous reports on side reactions of TCEP (phosphine sulfide and alanine) in thiol-ene see: (a) Gao, X.-F.; Du, J.-J.; Liu, Z.; Guo, J. Visible-Light-Induced Specific Desulfurization of Cysteinyl Peptide and Glycopeptide in Aqueous Solution. *Org. Lett.* **2016**, *18* (5), 1166−1169. (b) Wang, Z.; Rejtar, T.; Zhou, Z. S.; Karger, B. L. Desulfurization of cysteine-containing peptides resulting from sample preparation for protein characterization by mass spectrometry. *Rapid Commun. Mass Spectrom.* **2010**, *24* (3), 267−275. (c) Wan, Q.; Danishefsky, S. J. Free-Radical-Based, Specific Desulfurization of Cysteine: A Powerful Advance in the Synthesis of Polypeptides and Glycopolypeptides. *Angew. Chem., Int. Ed.* **2007**, *46* (48), 9248−9252.

(38) For information on ConA isolation and characterization see: (a) Sumner, J. B.; Howell, S. F. Identification of Hemagglutinin of Jack Bean with Concanavalin A. *J. Bacteriol.* **1936**, *32* (2), 227−237. (b) Edelman, G. M.; Cunningham, B. A.; Reeke, G. N.; Becker, J. W.; Waxdal, M. J.; Wang, J. L. The Covalent and Three-Dimensional Structure of Concanavalin A. *Proc. Natl. Acad. Sci. U. S. A.* **1972**, *69* (9), 2580−2584.

(39) Rotello, V.; Thayumanavan, S. *Molecular Recognition and Polymers: Control of Polymer Structure and Self-Assembly*; John Wiley & Sons: Hoboken, NJ, 2008.

(40) For information on ConA conformation see: (a) Gupta, D.; Dam, T. K.; Oscarson, S.; Brewer, C. F. Thermodynamics of Lectin-Carbohydrate Interactions: Binding of the core trimannoside of asparagine-linked carbohydrates and deoxy analogs to Concanavalin A. *J. Biol. Chem.* **1997**, *272* (10), 6388−6392. (b) Hardman, K. D.; Ainsworth, C. F. Structure of concanavalin A at 2.4-Ang resolution. *Biochemistry* **1972**, *11* (26), 4910−4919.

(41) Wittmann, V. Structural investigation of multivalent carbohydrate−protein interactions using synthetic biomolecules. *Curr. Opin. Chem. Biol.* **2013**, *17* (6), 982−989.

(42) For examples on the use of ITC in carbohydrate-ConA binding studies see: (a) Loka, R. S.; McConnell, M. S.; Nguyen, H. M. Studies of Highly-Ordered Heterodiantennary Mannose/Glucose-Functionalized Polymers and Concanavalin A Protein Interactions Using Isothermal Titration Calorimetry. *Biomacromolecules* **2015**, *16* (12), 4013−4021. (b) Wang, X.; Matei, E.; Gronenborn, A. M.; Ramström, O.; Yan, M. Direct Measurement of Glyconanoparticles and Lectin Interactions by Isothermal Titration Calorimetry. *Anal. Chem.* **2012**, *84* (10), 4248−4252.

(43) For examples on the use of AFM in carbohydrate-ConA binding studies see: (a) Senkara-Barwijuk, E.; Kobiela, T.; Lebed, K.; Lekka, M. Reaction pathway and free energy profile determined for specific recognition of oligosaccharide moiety of carboxypeptidase Y. *Biosens. Bioelectron.* **2012**, *36* (1), 103−109. (b) Ratto, T. V.; Langry, K. C.; Rudd, R. E.; Balhorn, R. L.; Allen, M. J.; McElfresh, M. W. Force Spectroscopy of the Double-Tethered Concanavalin-A Mannose Bond. *Biophys. J.* **2004**, *86* (4), 2430−2437.

(44) For further examples on the investigation of the cluster glycoside effect using synthetic glycomimetics see: (a) Kiessling, L. L.; Grim, J. C. Glycopolymer probes of signal transduction. *Chem. Soc. Rev.* **2013**, *42* (10), 4476−4491. (b) Kumar, J.; Bousquet, A.; Stenzel, M. H. Thiol-alkyne Chemistry for the Preparation of Micelles with Glycopolymer Corona: Dendritic Surfaces versus Linear Glycopolymer in Their Ability to Bind to Lectins. *Macromol. Rapid Commun.* **2011**, *32* (20), 1620−1626. (c) Richards, S.-J.; Jones, M. W.; Hunaban, M.; Haddleton, D. M.; Gibson, M. I. Probing Bacterial-Toxin Inhibition with Synthetic Glycopolymers Prepared by Tandem Post-Polymerization Modification: Role of Linker Length and Carbohydrate Density. *Angew. Chem., Int. Ed.* **2012**, *51* (31), 7812−7816. (d) Liu, S.; Kiick, K. L. Architecture Effects on the Binding of Cholera Toxin by Helical Glycopolypeptides. *Macromolecules* **2008**, *41* (3), 764−772. (e) Yilmaz, G.; Becer, C. R. Precision glycopolymers and their interactions with lectins. *Eur. Polym. J.* **2013**, *49* (10), 3046−3051.

DOI: 10.1021/acs.biomac.6b01657
Biomacromolecules 2017, 18, 787−796

Supporting Information

Sequence-Controlled Glycopolymers via Step-Growth Polymerization of Precision Glycomacromolecules for Lectin Receptor Clustering

Christoph Gerke, Morten F. Ebbesen, Dennis Jansen, Sophia Boden, Tanja Freichel, Laura Hartmann*

Institute of Organic and Macromolecular Chemistry, Heinrich-Heine-University Düsseldorf, Universitätsstraße 1, 40225 Düsseldorf, Germany

* Correspondence to Tel: +49 211 81-10360; Fax: +49 211 81-15840;
E-mail: laura.hartmann@hhu.de

Experimental Parts

Materials:

Dimethyl sulfoxide (DMSO) (≥ 99.9%), 2,2-dimethoxy-2-phenylacetophenone (DMPA) (99%), diethyl ether (with BHT as inhibitor, ≥ 99.8%), triisopropylsilane (TIPS) (98%), (+)-sodium-L-ascorbate (≥ 99.0%), manganese (II) chloride tetrahydrate (≥ 99%) and Concanavalin A from *Canavalia ensiformis* (Jack bean), Type IV (for the precipitation and turbidimetry assay), were all purchased from Sigma-Aldrich. N,N-Diisopropylethylamine (DIEA) (≥ 99%) and tris(2-carboxyethyl)phosphine hydrochloride (TCEP) (≥ 98%) were purchased from Carl Roth. Methanol (100%) and acetic anhydride (99.7%) were purchased from VWR BDH Prolabo Chemicals. Dimethylformamide (DMF) (99.8%, for peptide synthesis), piperidine (99%) and copper (II) sulfate (98%) were purchased from Acros Organics. Dichloromethane (DCM) (99.99%), sodium chloride (99.98%) and 4-(2-hydroxyethyl)-1-piperazineethanesulfonic acid (HEPES) (99%) were purchased from Fisher Scientific. Concanavalin A (for the SPR measurements) was purchased from LKT Laboratories. Calcium chloride (≥ 97%) was purchased from AppliChem. Trifluoroacetic acid (TFA) (99%) was purchased from Fluorochem. N-alpha-(9-Fluorenylmethyloxycarboxyl)-S-trityl-L-cysteine (Fmoc-L-Cys(Trt)-OH) (99.9%) was purchased from Iris Biotech. Tentagel S RAM (Rink Amide) resin (Capacity 0.23 mmol/g) was purchased from Rapp Polymere.

Instrumentation

Nuclear Magnetic Resonance spectroscopy (NMR)

^{1}H-NMR (600 MHz) spectra were recorded on a Bruker AVANCE III - 600. Chemical shifts of all NMR spectra were reported in delta (δ) expressed in parts per million (ppm). For ^{1}H-NMR the residual, non-deuterated solvent was used as internal standard (δ 4.79 ppm for D_2O). The following abbreviations are used to indicate the multiplicities: s, singlet, d, doublet; t, triplet; m multiplet.

Reversed Phase - High Pressure Liquid Chromatography - Mass Spectrometry (RP-HPLC-MS)

Measurements were performed on an Agilent 1260 Infinity instrument coupled to a variable wavelength detector (VWD) (set to 214 nm) and a 6120 Quadrupole LC/MS containing an Electrospray Ionization (ESI) source (operated in positive ionization mode in a m/z range of 200 to 2000). As HPLC column a Poroshell 120 EC-C18 (3.0×50 mm, 2.5 µm) RP column from Agilent was used. The mobile phases A and B were H_2O/ACN (95/5) and H_2O/ACN (5/95), respectively. Both mobile phases contained 0.1% of formic acid. Samples were analyzed at a flow rate of 0.4 mL/min using a linear gradient starting with 100% mobile phase A reaching 50% mobile phase B within 30 min. The temperature of the column compartment was set to 40 °C. UV and MS spectral analysis was done within the OpenLab ChemStation software for LC/MS from Agilent Technologies.

Ultra High Resolution - Mass Spectrometry (UHR-MS)
UHR-MS measurements were performed with a Bruker UHR-QTOF maXis 4G instrument with a direct inlet via syringe pump, an ESI source and a quadrupole followed by a Time Of Flight (QTOF) mass analyzer.

Matrix-Assisted Laser Desorption Ionization- Time Of Flight – Mass Spectrometry (MALDI-TOF-MS)
Compounds were analyzed using a Bruker MALDI-TOF Ultraflex I system with 2,5-dihydroxybenzoic acid (DHB) as matrix. The ratio of matrix to compound was 10:1. Spectra were acquired in both linear, for a m/z range of 1000-4000, and reflector mode for a m/z range 2000-20000. The reflector mode was calibrated using a protein mixture whereas the linear mode was not calibrated.

Gel Permeation Chromatography (GPC) analysis
GPC was performed using an Agilent 1200 series HPLC system equipped with three aqueous GPC columns from Polymer Standards Service (PSS) Mainz, Germany (Suprema Lux analytical 8 mm diameter, 5 µm particle size, precolumn of 50 mm, 2× 100 Å of 300 mm, 1000 Å of 300 mm). MilliQ water with 50 mM NaH_2PO_4, 150 mM NaCl, 250 ppm NaN_3 and of pH7 + 30% ACN, filtered through an inline 0.1 µm membrane filter, was used as GPC eluent with a flow rate of 1 mL/min. UV spectra were recorded on a Waters 486 Tunable Absorbance Detector. Multi-angle light scattering- and differential refractive index spectra were recorded using a miniDAWN TREOS and Optilab rEX, respectively, that were both from Wyatt Technologies EU. Data analysis was performed using the Astra 5 software using a measured dn/dc value of 0.156 mL/g for all the poly-/oligo(amidoamine)s.

Turbidimetry photometer.
Measurements were performed with a Tepper Turbidimetry Photometer containing a class 2 laser with a wavelength of 630-690 nm and an intensity of < 1 mW.

Surface Plasmon Resonance (SPR)
SPR measurements were performed with a Biacore X100 instrument from GE Healthcare Life Sciences. ConA was immobilized on a CM5 carboxymethyl dextran matrix sensor chip using 1-ethyl-3-(3-dimethylaminopropyl)carbodiimide (EDC) and N-hydroxysuccinimide (NHS) to 3085 response units (RU). The immobilization was performed in acetate buffer with pH 4.5. Sensorgrams were recorded with the Biacore X100 Control Software and evaluated with the Biacore X100 Evaluation Software.

UV-Vis photometer
UV measurements were performed with a SPECORD 210 PLUS UV-Vis photometer from Analytik Jena AG. The instrument was operated using Win ASPECT PLUS software. For ConA concentration determination, a Spectral Scan from 270-290 nm was performed. All measurements were performed in a 3.5 mL precision quartz glass cuvette from Carl Roth GmbH + Co. KG.

UV-lamp
A TQ150 Hg medium pressure UV lamp from Haraeus Nobellight GmbH with a quartz glass immersion and cooling tube from Peschl Ultraviolet GmbH was used for Thiol-Ene click reactions.

Freeze dryer
The final oligomers and polymers were freeze dried with an Alpha 1-4 LD plus instrument from Martin Christ Freeze Dryers GmbH. The Main Drying method was set to -42 °C and 0.1 mbar.

General Methods

Solid phase synthesis protocols

The batch sizes for synthesizing the oligomers using solid phase synthesis varied. The EDS spacing oligomers Cys(1,7)-7 (**1**) and DDS(1,7)-7 (**2**) were synthesized in a batch size of 0.3 mmol whereas the glycooligomers **4** - **7** were all synthesized in a batch size of 0.2 mmol. The amounts of reagents from following protocols correspond to the synthesis of 0.2 mmol of oligomer and can be multiplied by 1.5 for the synthesis of the oligomers that were synthesized in a batch size of 0.3 mmol.

Fmoc cleavage

The Fmoc protecting group of the resin as well as from the coupled building blocks or amino acid was cleaved by the addition of 10 mL of a solution of 25% piperidine in DMF. The deprotection was performed twice, the first time for 20 min and the second for 10 min. After that, the resin was washed thoroughly with DMF and DCM, seven times using 10 mL of each.

General coupling protocol

Commercially available Tentagel S RAM (Rink Amide) resin was used as resin for solid phase synthesis. First, 0.2 mmol (0.87 g) of resin were swollen in 10 mL of DCM for 20 min and subsequently washed four times with 10 mL of DMF. The Fmoc protecting group of the Tentagel S RAM resin was removed following the Fmoc cleavage protocol. A building block or amino acid was coupled to the resin using a mixture of 1 mmol (5 eq) of building block or amino acid and 1 mmol PyBOP (5 eq) dissolved in 4 mL DMF to which 2 mmol (2 eq) of DIEA were added. The mixture was shaken for 30 s under a nitrogen stream for activation and subsequently added to the resin. The resin with the coupling mixture was shaken for 1 h. After that, the resin was washed from excessive reagent 5 times with 10 mL of both, DMF and DCM. A double coupling, adding fresh building block and coupling reagents without prior deprotection of the Fmoc protective group, was performed each time L-cysteine or DDS was coupled.

Capping of N-terminal primary amine

After successful assembly of the desired number of building blocks on solid phase, the N-terminal site was capped with an acetyl group. Therefore, 10 mL acetic anhydride were shaken with the resin for 15 min.

General CuAAC protocol

To 0.2 mmol of resin loaded with the oligomeric structure, 0.8 mmol (4 eq) of acetyl protected 2-azidoethyl pyranoside per alkyne group, dissolved in 3 mL DMF was added.
20 mol% sodium ascorbate per alkyne group and 20 mol% $CuSO_4$ per alkyne group were dissolved in 1 mL water and also added to the resin. This mixture was shaken overnight and subsequently washed extensively with a 23 mM solution of sodium diethyldithiocarbamate in DMF, water, DMF and DCM.

On resin acetyl deprotection

In order to remove the acetyl protective groups of the 2-azidoethyl pyranoside moieties, 10 mL of a 0.2 M solution of sodium methanolate in methanol were added to the resin and shaken for 1 h. Subsequently the resin was washed 5 times with 10 mL of DMF and DCM.

Cleavage from solid phase

13 mL of a mixture of 95% TFA and 5% of TIPS were added to the resin and shaken for 1 h. The filtrate was poured into 120 mL cold diethyl ether. The resin was washed with an additional 5 mL of DCM which was also added to the cold ether. The resulting precipitate was centrifuged and the ether decanted. The crude product was dried over a stream of nitrogen, dissolved in 3 mL of methanol and precipitated again in 30 mL of cold diethyl ether. The precipitate was centrifuged and the ether decanted again. The pellet was dried over a stream of nitrogen, dissolved in 6 mL of water and lyophilized.

Additional Information about ConA Binding Studies
Ligand concentration dependent assay

Oligomeric structures (**2**+**4**-**7**):

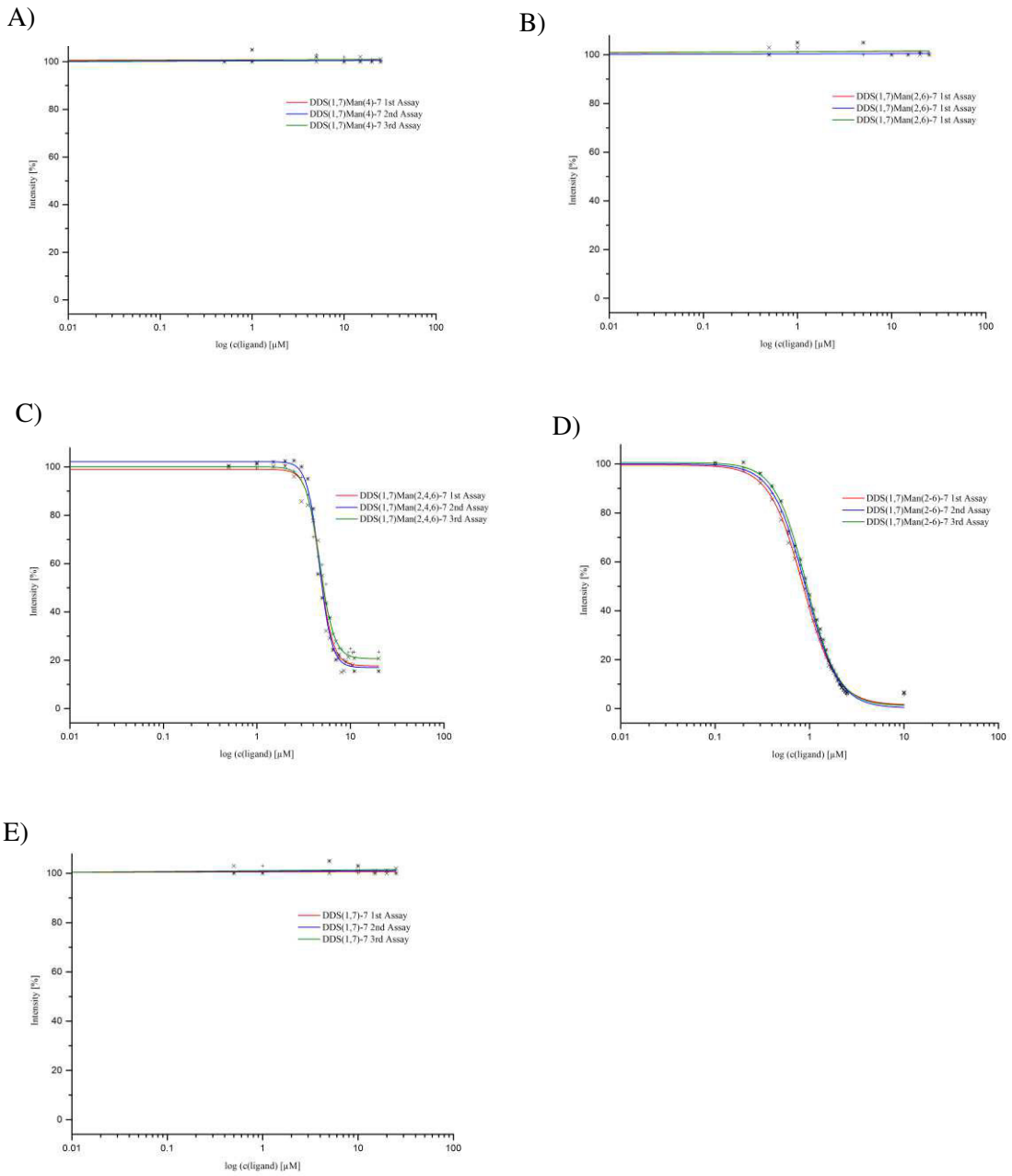

Figure S1: Obtained intensities from three ligand concentration dependent assays performed for oligomeric structures **2** as well as **4-7**. Data points were fitted either with a linear fit or with a Hill1 fit. A) DDS(1,7)Man(4)-7 (**4**), B) DDS(1,7)Man(2,6)-7 (**5**), C) DDS(1,7)Man(2,4,6)-7 (**6**), D) DDS(1,7)Man(2-6)-7 (**7**), E) DDS(1,7)-7 (**2**)

Polymeric structures (**3**+**8**-**11**):

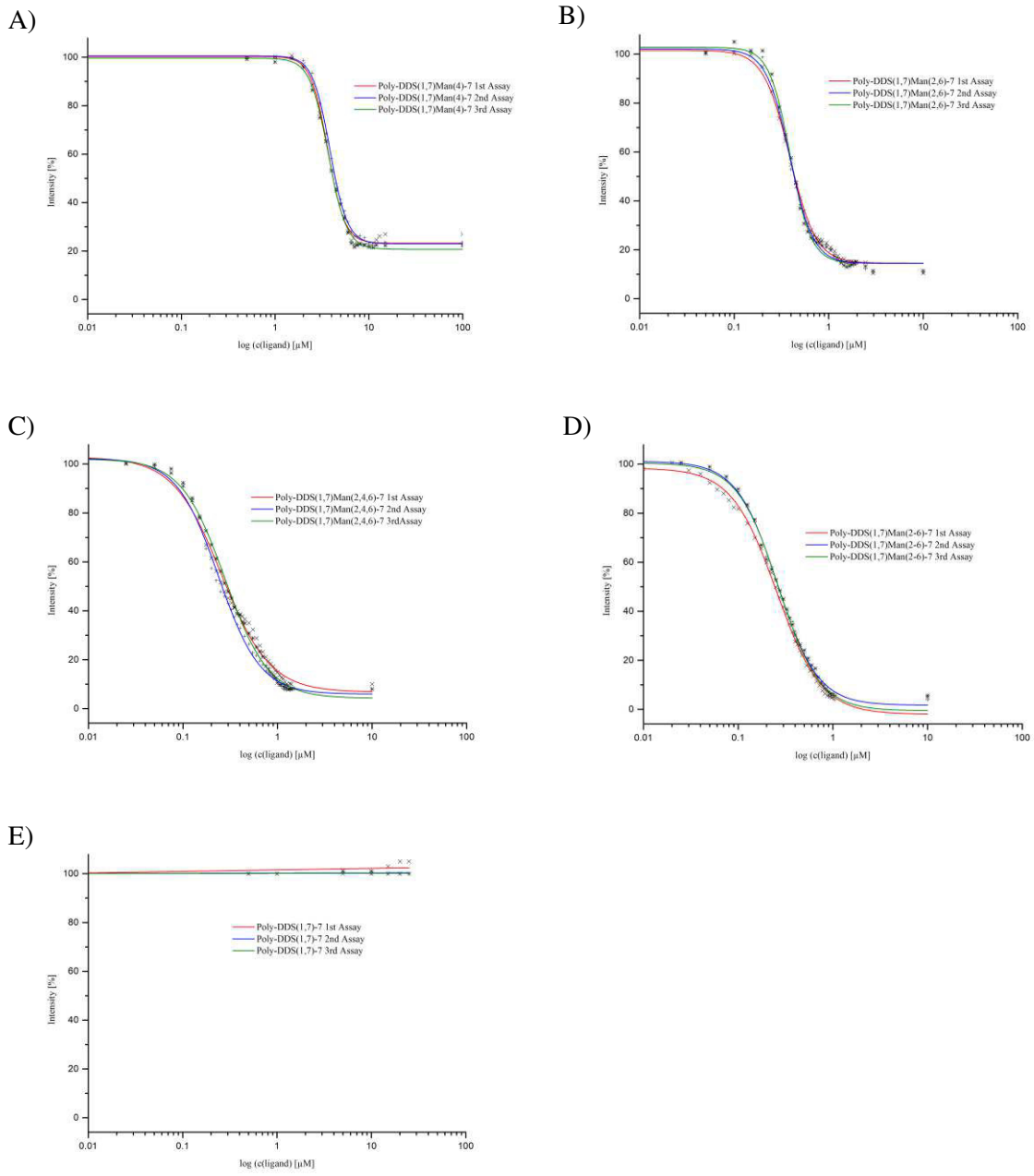

Figure S2: Obtained intensities from three ligand concentration dependent assays performed for polymeric structures **3** as well as **8-11**. Data points were fitted either with a linear fit or with a Hill1 fit. A) Poly-DDS(1,7)Man(4)-7 (**8**), B) Poly-DDS(1,7)Man(2,6)-7 (**9**), C) Poly-DDS(1,7)Man(2,4,6)-7 (**10**), D) Poly-DDS(1,7)Man(2-6)-7 (**11**), E) Poly-DDS(1,7)-7 (**3**)

Table S1: Results from the ligand concentration dependent turbidity assay calculated for the actual ligand concentration and the total mannose concentration

Entry	N(sugar)	Per Glycomonomer/polymer Conc. ½TMax [µM]	 1/(Conc. ½TMax) [1/µM]	Per Mannose 1/(Conc. ½TMax) [1/µM]
2	0	n. p.	n. p.	n. p.
4	1	n. p.	n. p.	n. p.
5	2	n. p.	n. p.	n. p.
6	3	4.69 ± 0.02 (± 0.45 %)	0.213 ± 0.001	0.0711 ± 0.0003
7	5	0.89 ± 0.03 (± 3.6 %)	1.12 ± 0.04	0.224 ± 0.008
3	0	n. p.	n. p.	n. p.
8	Ø 4	3.72 ± 0.09 (± 2.3 %)	0.269 ± 0.006	0.067 ± 0.002
9	Ø 8	0.389 ± 0.002 (± 0.51 %)	2.57 ± 0.01	0.321 ± 0.002
10	Ø 12	0.26 ± 0.02 (± 6.6 %)	3.89 ± 0.26	0.32 ± 0.02
11	Ø 20	0.260 ± 0.005 (± 1.9 %)	3.84 ± 0.07	0.192 ± 0.004

Quantitative precipitation assay

For structures DDS(1,7)Man(4)-7 (**4**), DDS(1,7)Man(2,6)-7 (**5**), DDS(1,7)-7 (**2**) and Poly-DDS(1,7)-7 (**3**), the assay was only performed with a concentration of 5 µM of ligand. None of the structures showed a formation of precipitate. The amount of ConA in the formed precipitate as a function of the glycooligomer/ -polymer concentrations are shown in Figures S3 and S4.

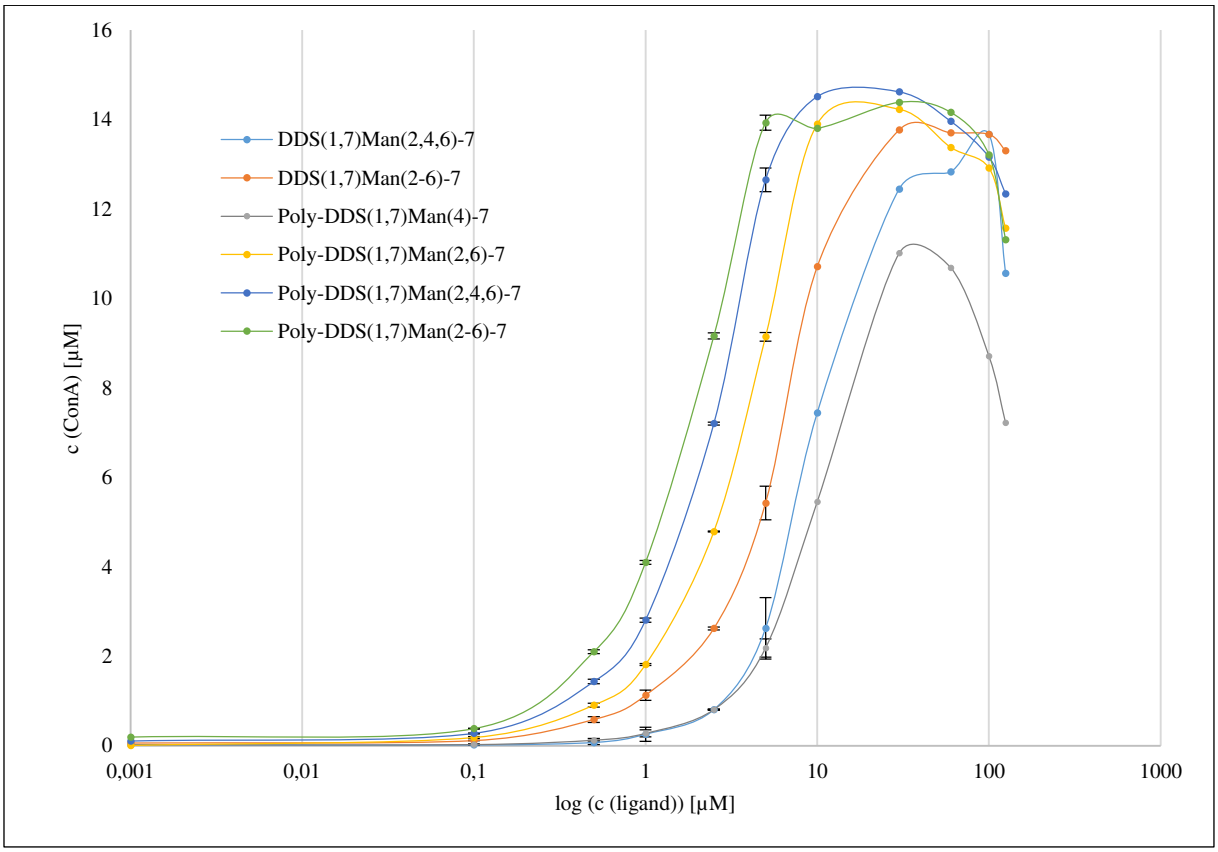

Figure S3: Obtained ConA amounts in formed precipitates with different concentrations of ligands DDS(1,7)Man(2,4,6)-7 (**6**), DDS(1,7)Man(2-6)-7 (**7**), Poly-DDS(1,7)Man(4)-7 (**8**), Poly-DDS(1,7)Man(2,6)-7 (**9**), Poly-DDS(1,7)Man(2,4,6)-7 (**10**) and Poly-DDS(1,7)Man(2-6)-7 (**11**).

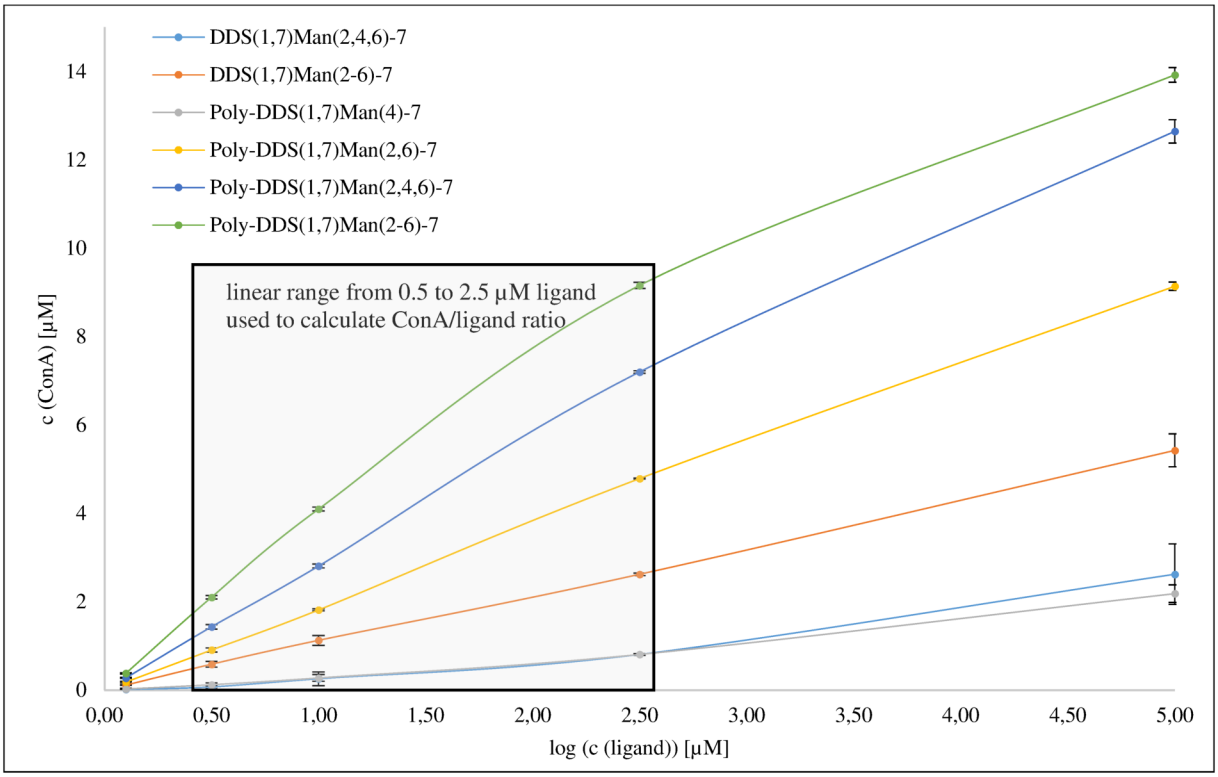

Figure S4: Linear range of the obtained data, used to calculate the ConA/ligand ratio in formed precipitate for ligands DDS(1,7)Man(2,4,6)-7 (**6**), DDS(1,7)Man(2-6)-7 (**7**), Poly-DDS(1,7)Man(4)-7 (**8**), Poly-DDS(1,7)Man(2,6)-7 (**9**), Poly-DDS(1,7)Man(2,4,6)-7 (**10**) and Poly-DDS(1,7)Man(2-6)-7 (**11**).

Table S2: Results from the quantitative precipitation assay calculated for the actual ligand concentration and the total mannose concentration

Entry	N(sugar)	Per Glycomonomer/polymer ConA/Ligand	Per Mannose ConA/Man
2	0	n. p.	n. p.
4	1	n. p.	n. p.
5	2	n. p.	n. p.
6	3	0.24 ± 0.09 (± 37 %)	0.08 ± 0.03
7	5	1.12 ± 0.06 (± 5.6 %)	0.22 ± 0.01
3	0	n. p.	n. p.
8	Ø 4	0.281 ± 0.04 (± 14 %)	0.07 ± 0.01
9	Ø 8	1.85 ± 0.06 (± 3.2 %)	0.231 ± 0.008
10	Ø 12	2.85 ± 0.04 (± 1.4 %)	0.238 ± 0.003
11	Ø 20	4.0 ± 0.3 (± 7.2 %)	0.20 ± 0.02

Surface Plasmon Resonance measurements

Oligomeric structures (**2**+**4**-**7**):

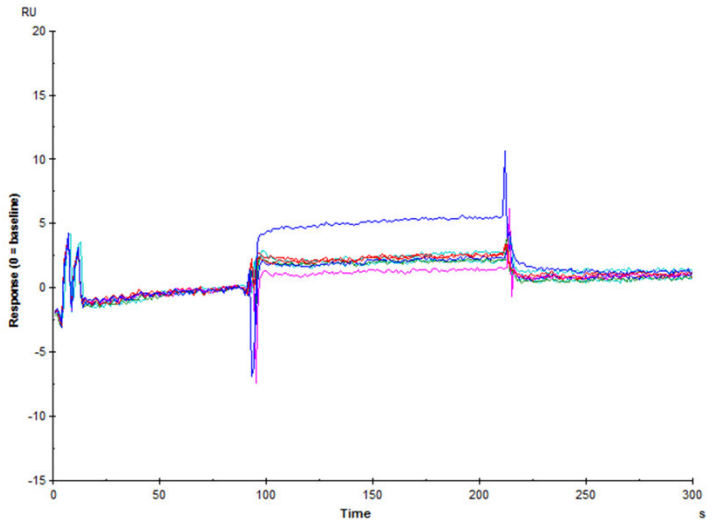

Figure S5: Sensorgrams of unfunctionalized macromonomer DDS(1,7)-7 (**2**) injected at different concentrations, showing no binding to the immobilized ConA sensor chip and sensorgram from measured reference trivalent glycomacromonomer DDS(1,7)Man(2,4,6)-7 (**6**) injected at 6 µM (blue). The unfunctionalized macromonomer was injected at concentrations of 0.6, 6, 60 and 600 µM.

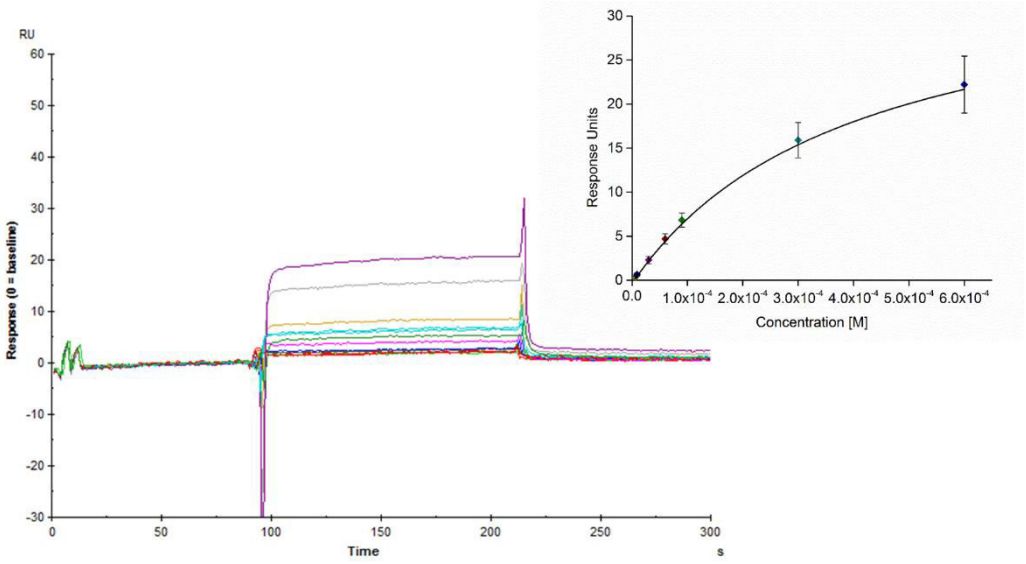

Figure S6: Sensorgrams and the equilibrium response as a function of concentration from glycomacromonomer DDS(1,7)Man(4)-7 (**4**) plotted using a steady state model. Experimental data from three consecutive measurements is plotted. The standard deviation is shown as error bar for each data point. The glycomacromonomer was injected at concentrations of 6, 9, 30, 60, 90, 300 and 600 µM.

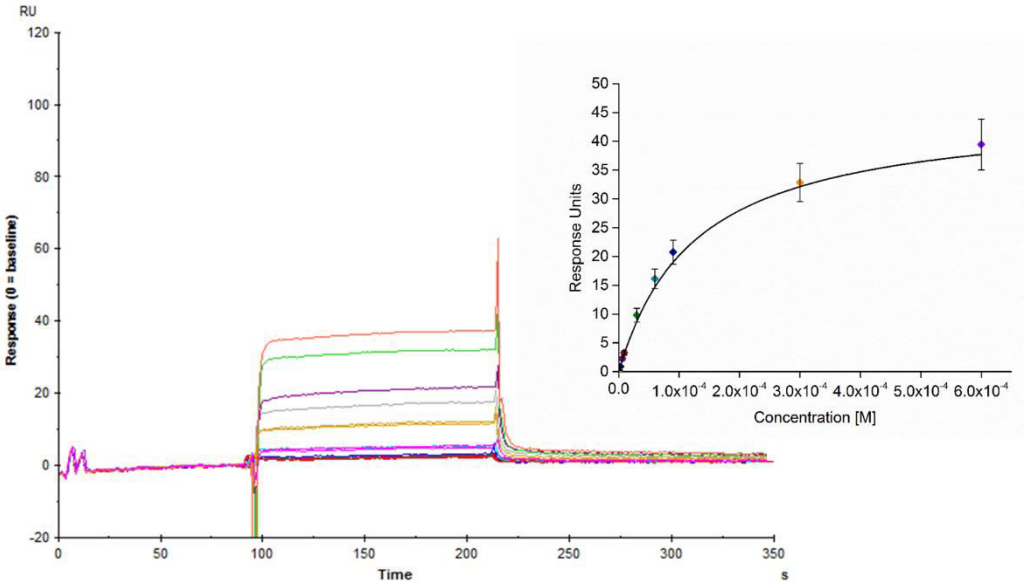

Figure S7: Sensorgrams and the equilibrium response as a function of concentration from glycomacromonomer DDS(1,7)Man(2,6)-7 (**5**) plotted using a steady state model. Experimental data from three consecutive measurements is plotted. The standard deviation is shown as error bar for each data point. The glycomacromonomer was injected at concentrations of 0.9, 3, 6, 9, 30, 60, 90, 300 and 600 µM.

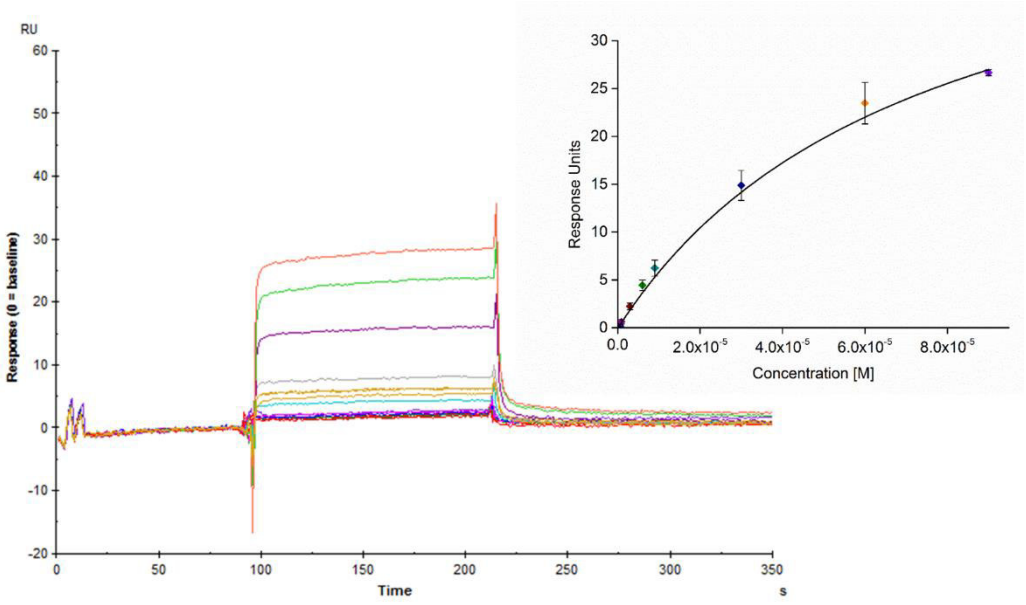

Figure S8: Sensorgrams and the equilibrium response as a function of concentration from glycomacromonomer DDS(1,7)Man(2,4,6)-7 (**6**) plotted using a steady state model. Experimental data from three consecutive measurements is plotted. The standard deviation is shown as error bar for each data point. The glycomacromonomer was injected at concentrations of 0.3, 0.6, 0.9, 3, 6, 9, 30, 60 and 90 µM.

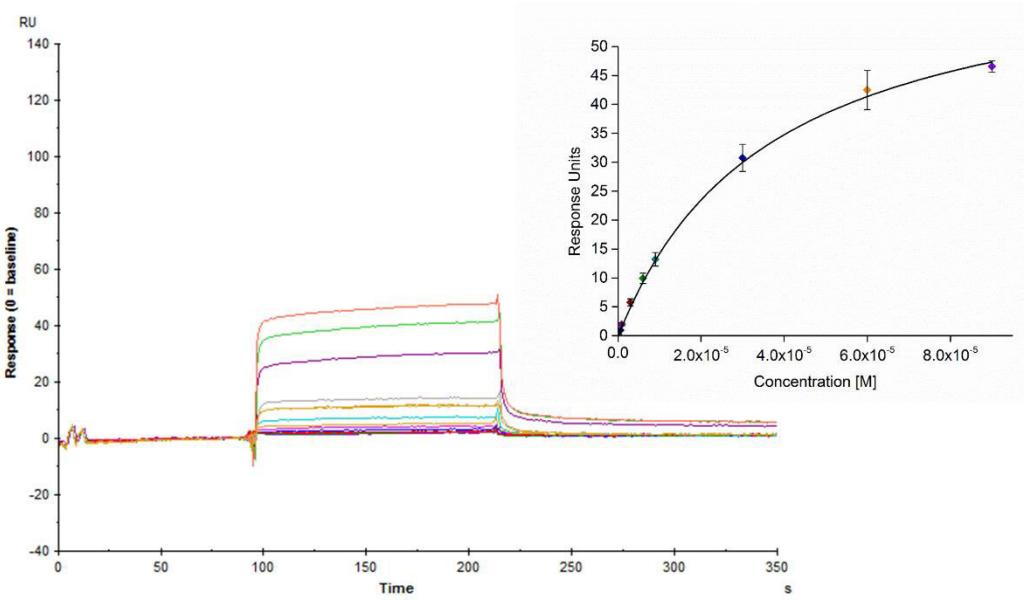

Figure S9: Sensorgrams and the equilibrium response as a function of concentration from glycomacromonomer DDS(1,7)Man(2-6)-7 (**7**) plotted using a steady state model. Experimental data from three consecutive measurements is plotted. The standard deviation is shown as error bar for each data point. The glycomacromonomer was injected at concentrations of 0.3, 0.6, 0.9, 3, 6, 9, 30, 60 and 90 µM.

Polymeric structures (**3**+**8**-**11**):

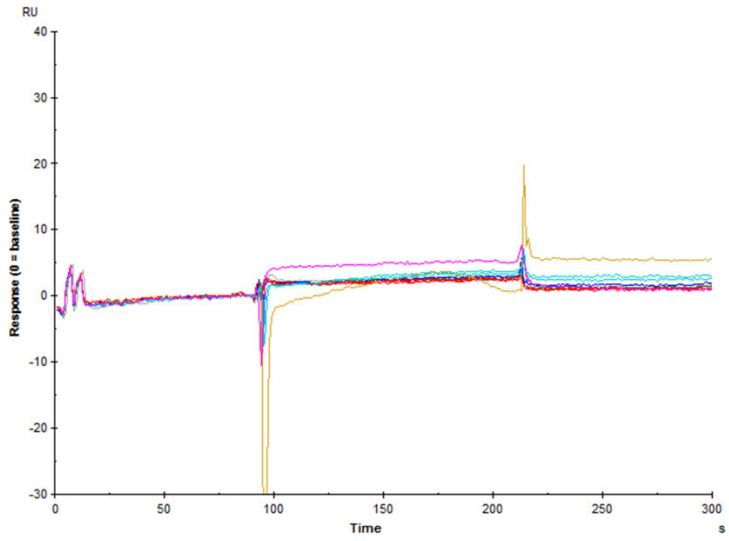

Figure S10: Sensorgrams of unfunctionalized macromonomer Poly-DDS(1,7)-7 (**3**) injected at different concentrations, showing no binding to the immobilized ConA sensor chip and sensorgram from measured reference trivalent glycomacromonomer DDS(1,7)Man(2,4,6)-7 (**6**) injected at 6 µM (pink). The unfunctionalized macromonomer was injected at concentrations of 0.09, 0.9, 9, and 90 µM.

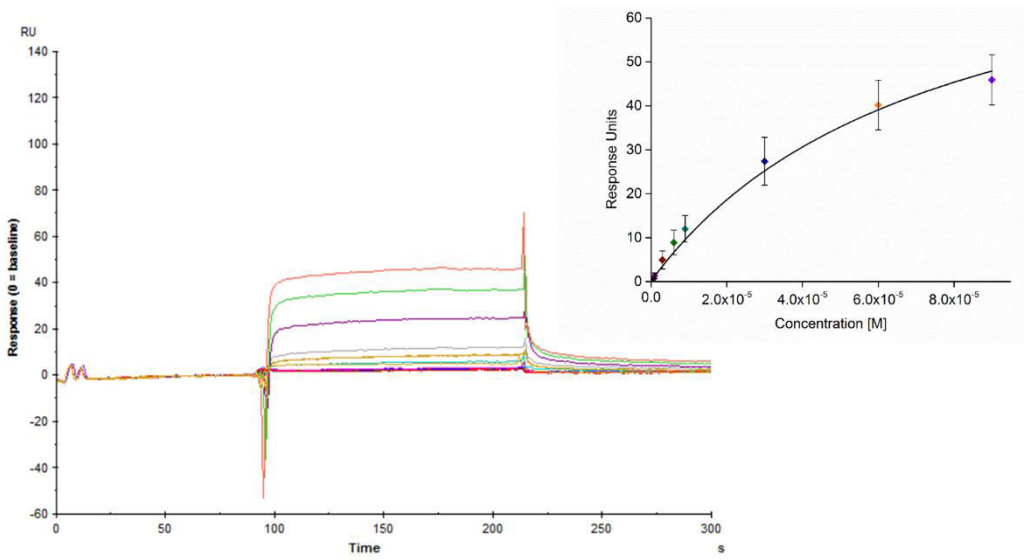

Figure S11: Sensorgrams and the equilibrium response as a function of concentration from glycomacromonomer Poly-DDS(1,7)Man(4)-7 (**8**) plotted using a steady state model. Experimental data from three consecutive measurements is plotted. The standard deviation is shown as error bar for each data point. The glycopolymer was injected at concentrations of 0.3, 0.6, 0.9, 3, 6, 9, 30, 60 and 90 µM.

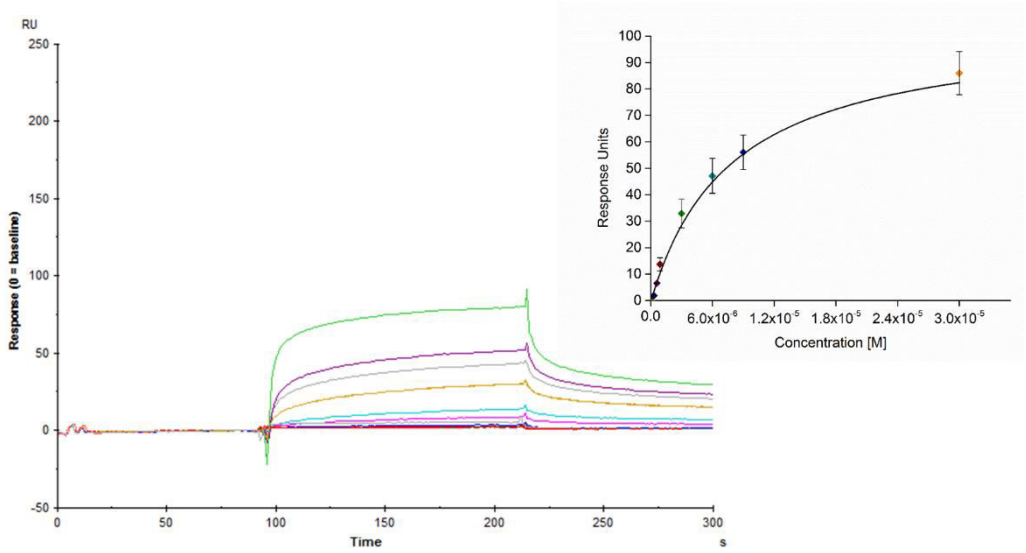

Figure S12: Sensorgrams and the equilibrium response as a function of concentration from glycomacromonomer Poly-DDS(1,7)Man(2,6)-7 (**9**) plotted using a steady state model. Experimental data from three consecutive measurements is plotted. The standard deviation is shown as error bar for each data point. The glycopolymer was injected at concentrations of 0.09, 0.3, 0.6, 0.9, 3, 6, 9 and 30 µM.

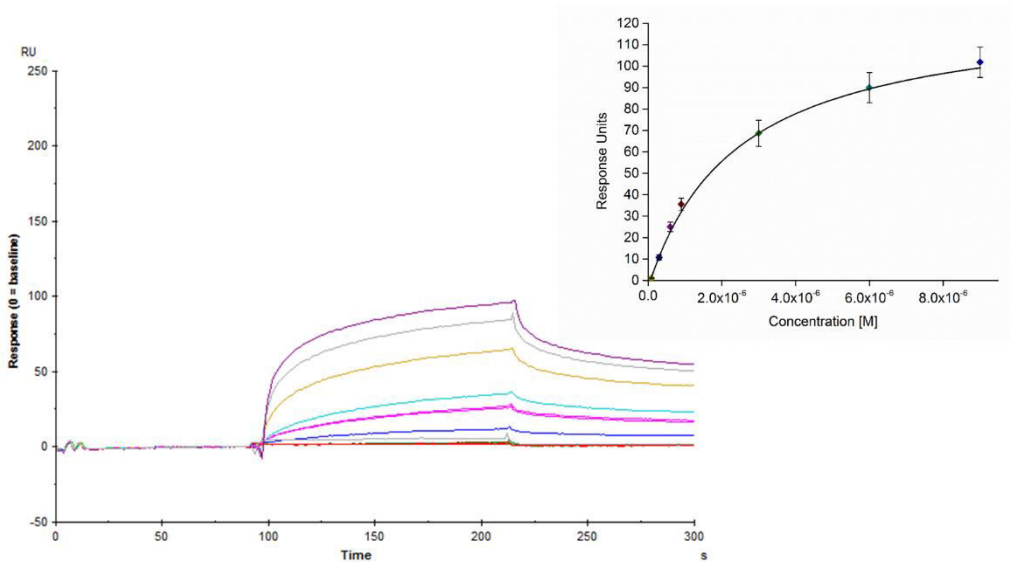

Figure S13: Sensorgrams and the equilibrium response as a function of concentration from glycomacromonomer Poly-DDS(1,7)Man(2,4,6)-7 (**10**) plotted using a steady state model. Experimental data from three consecutive measurements is plotted. The standard deviation is shown as error bar for each data point. The glycopolymer was injected at concentrations of 0.09, 0.3, 0.6, 0.9, 3, 6 and 9 µM.

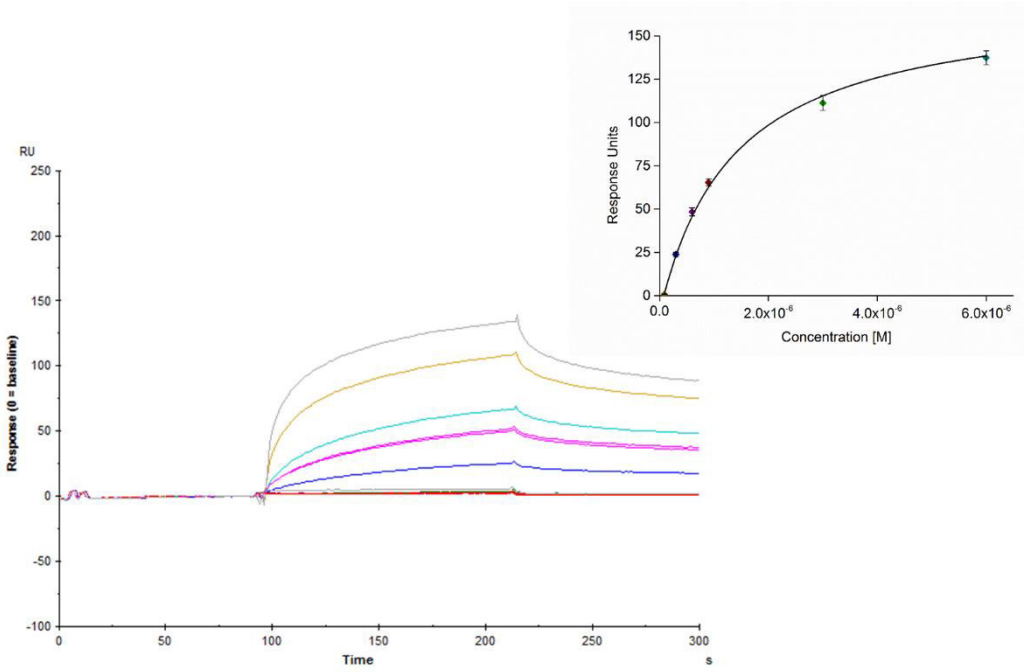

Figure S14: Sensorgrams and the equilibrium response as a function of concentration from glycomacromonomer Poly-DDS(1,7)Man(2-6)-7 (**11**) plotted using a steady state model. Experimental data from three consecutive measurements is plotted. The standard deviation is shown as error bar for each data point. The glycopolymer was injected at concentrations of 0.09, 0.3, 0.6, 0.9, 3 and 6 µM.

Table S3: Determined K_D values from the equilibrium response curves and the standard deviation from three consecutive measurements for oligomeric structures **2** and **4** – **7** for the actual ligand concentration and the total mannose concentration.

Entry	N(sugar)	Per Glycomonomer K_D [M]	Per Mannose K_D [M]
2	0	n. b.	n. b.
4	1	$3.82 * 10^{-4} \pm 4.09 * 10^{-5}$ (± 11 %)	$3.82 * 10^{-4} \pm 4.09 * 10^{-5}$ (± 11 %)
5	2	$1.12 * 10^{-4} \pm 1.13 * 10^{-5}$ (± 10 %)	$2.24 * 10^{-4} \pm 2.25 * 10^{-5}$ (± 10 %)
6	3	$6.54 * 10^{-5} \pm 6.09 * 10^{-6}$ (± 9.3 %)	$1.96 * 10^{-4} \pm 1.83 * 10^{-5}$ (± 9.3 %)
7	5	$3.72 * 10^{-5} \pm 1.28 * 10^{-6}$ (± 3.4 %)	$1.86 * 10^{-4} \pm 6.28 * 10^{-6}$ (± 3.4 %)

Table S4: K_A values calculated from the determined K_D for oligomeric structures **2** and **4** – **7** and the standard deviation from three consecutive measurements for the actual ligand concentration and the total mannose concentration.

Entry	N(sugar)	Per Glycomonomer K_A [1/M]	Per Mannose K_A [1/M]
2	0	n. b.	n. b.
4	1	$2.62 * 10^{3} \pm 3.02 * 10^{2}$ (± 11 %)	$2.62 * 10^{3} \pm 3.02 * 10^{2}$ (± 11 %)
5	2	$8.92 * 10^{3} \pm 9.11 * 10^{2}$ (± 10 %)	$4.46 * 10^{3} \pm 4.55 * 10^{2}$ (± 10 %)
6	3	$1.53 * 10^{4} \pm 1.40 * 10^{3}$ (± 9.1 %)	$5.10 * 10^{3} \pm 4.66 * 10^{2}$ (± 9.1 %)
7	5	$2.69 * 10^{4} \pm 9.01 * 10^{2}$ (± 3.3 %)	$5.38 * 10^{3} \pm 1.80 * 10^{2}$ (± 3.3 %)

Table S5: Determined K_D values from the equilibrium response curves and the standard deviation from three consecutive measurements for polymeric structures **3** and **8** – **11** for the actual ligand concentration and the total mannose concentration.

Entry	N(sugar)	Per Glycopolymer K_D [M]	Per Mannose K_D [M]
3	0	n. b.	n. b.
8	Ø 4	$6.17 * 10^{-5} \pm 1.79 * 10^{-5}$ (± 29 %)	$2.47 * 10^{-4} \pm 7.15 * 10^{-5}$ (± 29 %)
9	Ø 8	$7.39 * 10^{-6} \pm 7.59 * 10^{-7}$ (± 10 %)	$5.91 * 10^{-5} \pm 6.07 * 10^{-6}$ (± 10 %)
10	Ø 12	$2.26 * 10^{-6} \pm 1.31 * 10^{-7}$ (± 5.8 %)	$2.71 * 10^{-5} \pm 1.57 * 10^{-6}$ (± 5.8 %)
11	Ø 20	$1.17 * 10^{-6} \pm 1.43 * 10^{-7}$ (± 12 %)	$2.34 * 10^{-5} \pm 2.86 * 10^{-6}$ (± 12 %)

Table S6: K_A values calculated from the determined K_D for polymeric structures **3** and **8** – **11** and the standard deviation from three consecutive measurements for the actual ligand concentration and the total mannose concentration.

Entry	N(sugar)	Per Glycopolymer K_A [1/M]	Per Mannose K_A [1/M]
3	0	n. b.	n. b.
8	Ø 4	$1.62 * 10^{4} \pm 6.61 * 10^{3}$ (± 36 %)	$4.05 * 10^{3} \pm 1.65 * 10^{3}$ (± 36 %)
9	Ø 8	$1.35 * 10^{5} \pm 1.51 * 10^{4}$ (± 11 %)	$1.69 * 10^{4} \pm 1.89 * 10^{3}$ (± 11 %)
10	Ø 12	$4.43 * 10^{5} \pm 2.57 * 10^{4}$ (± 5.8 %)	$3.69 * 10^{4} \pm 2.14 * 10^{3}$ (± 5.8 %)
11	Ø 20	$8.55 * 10^{6} \pm 1.06 * 10^{5}$ (± 12 %)	$4.27 * 10^{4} \pm 5.30 * 10^{3}$ (± 12 %)

Analytical Data

Cys(1,7)-7 (1):

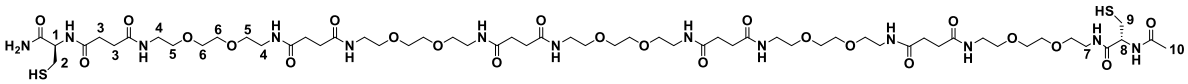

Compound **1** was obtained in a yield of 81%. In ^{1}H NMR an unidentified signal was detected with a chemical shift of δ 3.71 (s) ppm. ^{1}H NMR (600 MHz, D_2O): δ 4.49 (dd, *J* = 7.1, 5.1 Hz, 1H,1), 4.46 (t, *J* = 6.2 Hz, 1H, 8), 3.68 (s, 20H, 6), 3.62 (t, *J* = 5.5 Hz, 20H, 5), 3.46 – 3.42 (m, 2H, 7), 3.39 (t, *J* = 5.4 Hz, 18H, 4), 2.97 – 2.87 (m, 4H, 2 + 9), 2.66 – 2.53 (m, 20H, 3), 2.07 (s, 3H, 10) ppm. The assignment of the signals was verified by the implementation of ^{1}H-^{1}H-COSY experiments (data not shown).

HR-ESI-MS for $C_{58}H_{105}N_{13}O_{23}S_2$. (Exact monoisotopic mass 1415.6888): $[M+2H]^{2+}$ calcd. 708.8517, found 708.8510, mass accuracy -0.99 ppm.

RP-HPLC (linear gradient from 0 - 50% eluent B in 30 min at 40 °C): t_R = 10.0 min. Determined purity: 97% (addition of the area for **1**, 93%, the disulfide from **1**, t_R = 9.6 min 2%, and the dimer from **1** via disulfide, t_R = 11.7 min 2%).

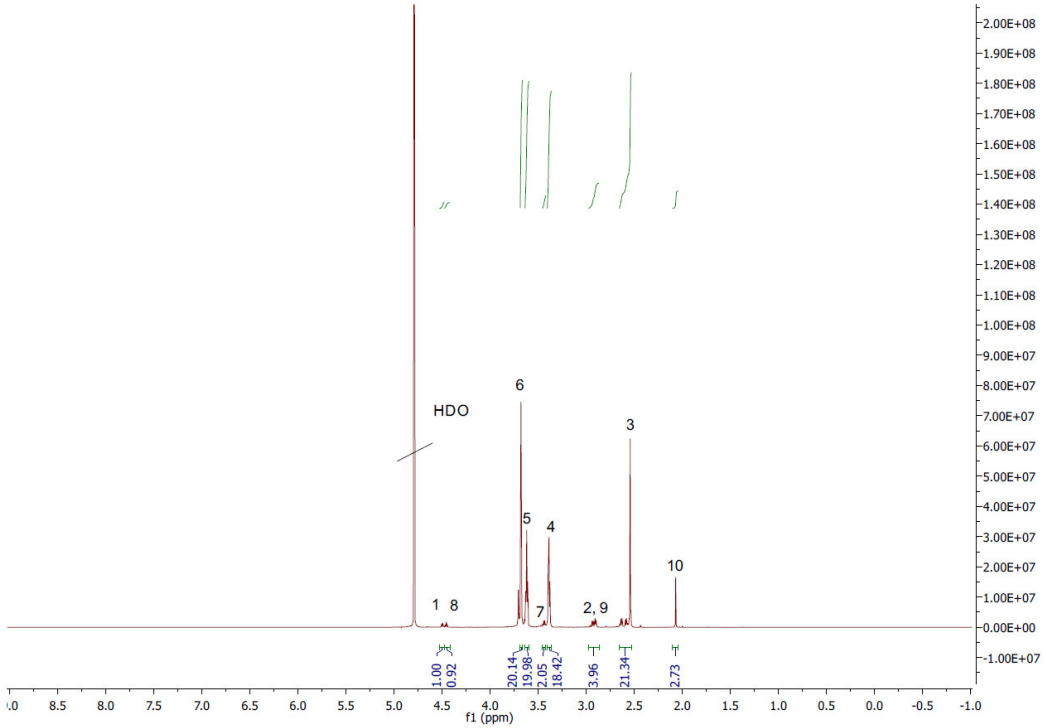

Figure S15: ^{1}H-NMR (600 MHz, D_2O) of compound **1.**

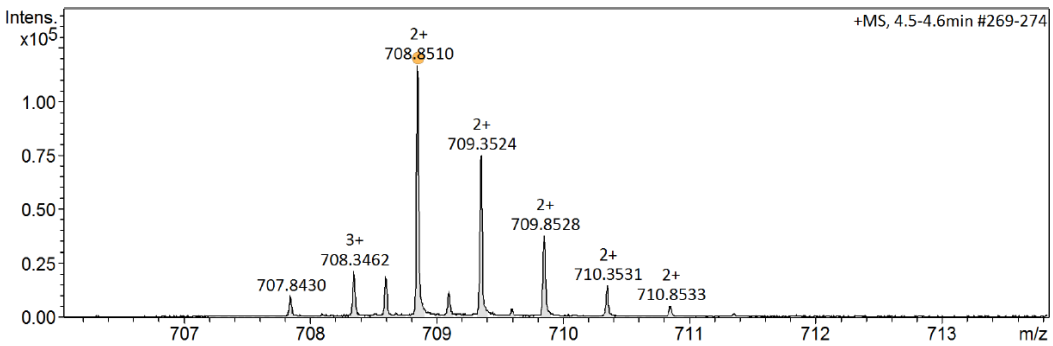

Figure S16: HR-MS (ESI$^+$ Q-TOF) of compound **1**.

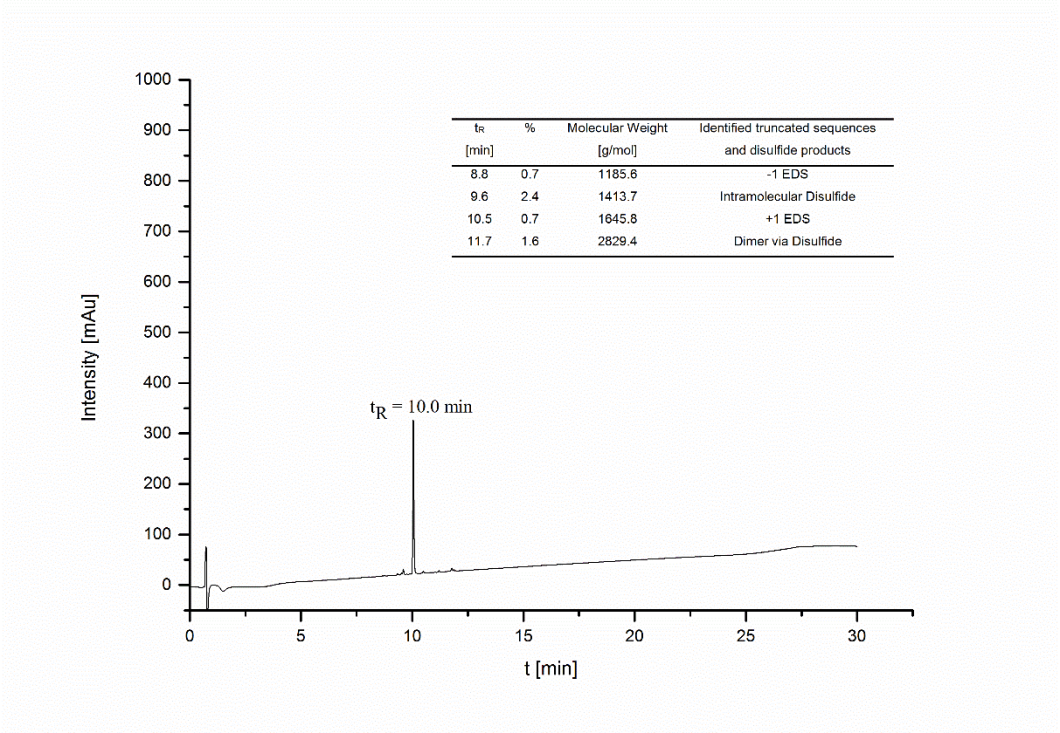

t_R [min]	%	Molecular Weight [g/mol]	Identified truncated sequences and disulfide products
8.8	0.7	1185.6	-1 EDS
9.6	2.4	1413.7	Intramolecular Disulfide
10.5	0.7	1645.8	+1 EDS
11.7	1.6	2829.4	Dimer via Disulfide

Figure S17: RP-HPLC analysis (linear gradient from 0 - 50% eluent B in 30 min at 40 °C) chromatogram of compound **1** with retention time. Identified truncated sequences and disulfide products are listed in the table with corresponding retention times, amounts and molecular weights.

DDS(1,7)-7 (2):

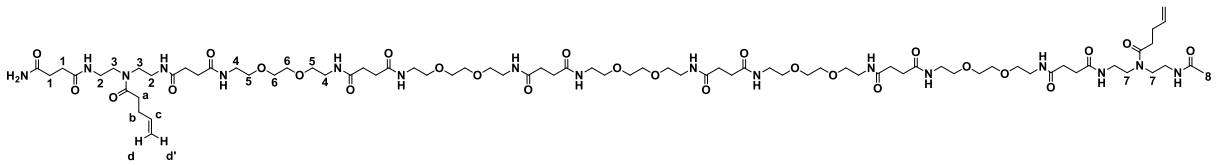

Compound **2** was obtained in a yield of 45%. For the acetyl group on the N-terminal end we observed two singlets with a ratio of 1:1 that we assign to two rotational isomers in equal amounts. The presence of rotational isomers was identified in ^{1}H-NMR experiments at higher temperatures (data not shown). ^{1}H NMR (600 MHz, D_2O): δ 5.93 – 5.84 (m, 2H, c), 5.13 – 5.07 (m, 2H, d), 5.07 – 5.03 (m, 2H, d‘), 3.69 (s, 20H, 6), 3.63 (t, *J* = 5.4 Hz, 20H, 5), 3.55 – 3.46 (m, 8H, 3+7), 3.43 – 3.34 (m, 28H, 2+4), 2.57 – 2.48 (m, 32H, 1+a), 2.37 – 2.30 (m, 4H, b), 1.98 + 1.96 (2s, 3H, 8) ppm. The assignment of the signals was verified by the implementation of ^{1}H-^{1}H-COSY experiments (data not shown).

HR-ESI-MS for $C_{78}H_{137}N_{17}O_{27}$ (Exact monoisotopic mass 1743.9870): $[M+3H]^{3+}$ calcd. 583.3363, found 582.3372, mass accuracy 1.55 ppm.

RP-HPLC (linear gradient from 0 - 50% eluent B in 30 min at 40 °C): t_R = 11.2 min. Determined purity: 92%.

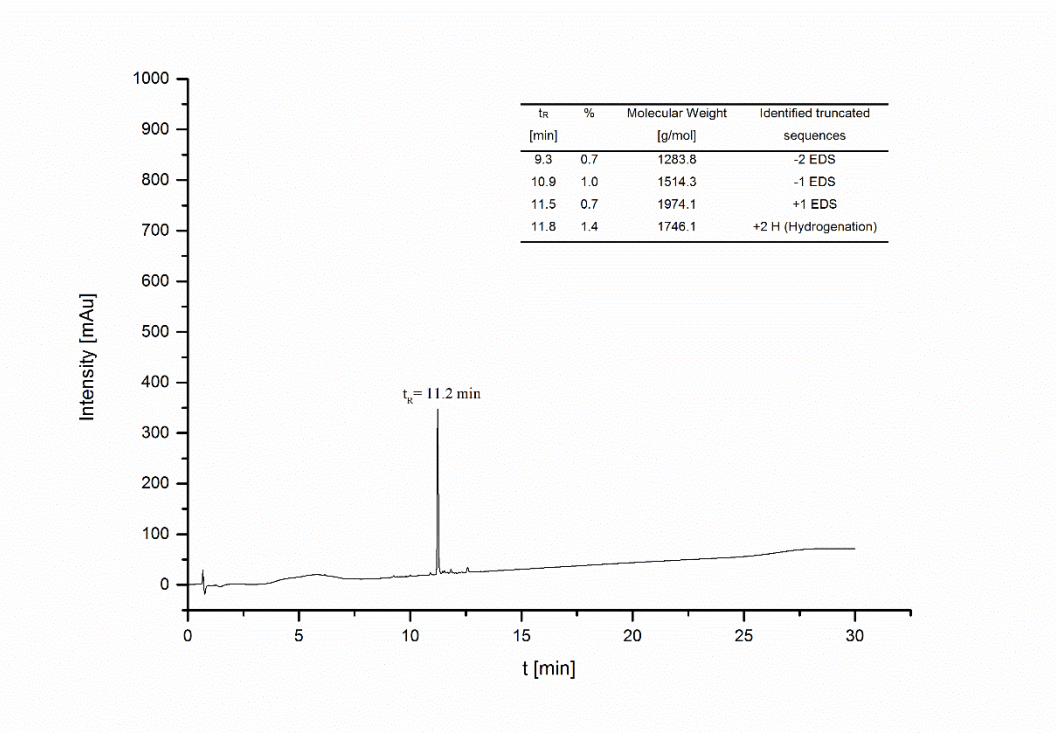

t_R [min]	%	Molecular Weight [g/mol]	Identified truncated sequences
9.3	0.7	1283.8	-2 EDS
10.9	1.0	1514.3	-1 EDS
11.5	0.7	1974.1	+1 EDS
11.8	1.4	1746.1	+2 H (Hydrogenation)

Figure S18: RP-HPLC analysis (linear gradient from 0 - 50% eluent B in 30 min at 40 °C) chromatogram of compound **2** with retention time. Identified truncated sequences are listed in the table with corresponding retention times, amounts and molecular weights.

DDS(1,7)Man(4)-7 (4):

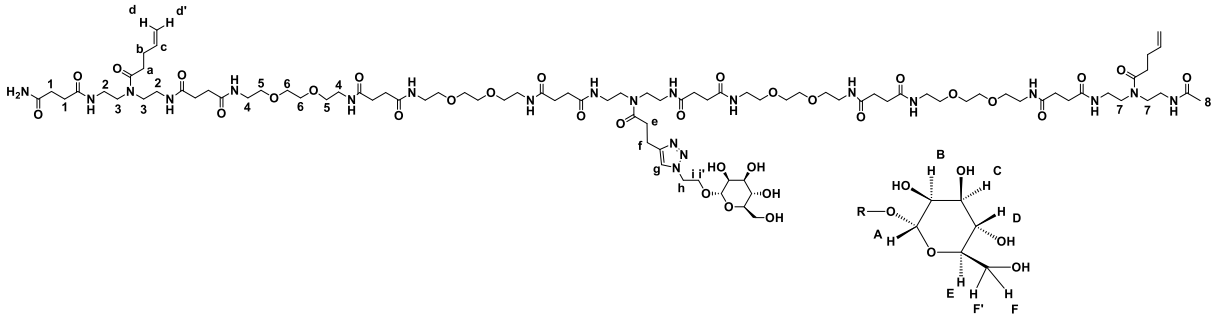

Compound **4** was obtained in a yield of 49%. The anomeric proton of Mannose (A) could not be examined in ^{1}H-NMR due to the overlaying signal from the residual solvent. An unidentified signal was detected with a chemical shift of δ 3.71 (s) ppm. For the acetyl group on the N-terminal end we observed two singlets with a ratio of 1:1 that we assign to two rotational isomers in equal amounts. The presence of rotational isomers was identified in ^{1}H-NMR experiments at higher temperatures (data not shown). ^{1}H NMR (600 MHz, D_2O): δ 7.98 (s, 1H, g), 5.92 – 5.83 (m, 2H, c), 5.12 – 5.06 (m, 2H, d), 5.06 – 5.02 (m, 2H, d'), 4.70 – 4.66 (m, 2H, h), 4.14 – 4.08 (m, 1H, i or i'), 3.96 – 3.91 (m, 1H, i or i'), 3.86 (dd, *J* = 3.4, 1.7 Hz, 1H, B), 3.75 (dd, *J* = 12.2, 2.3 Hz, 1H, F or F'), 3.71 – 3.64 (m, 19H, 6+C+D+F or F'), 3.63 – 3.59 (m, 16H, 5), 3.54 – 3.44 (m, 12H, 3+7), 3.43 – 3.31 (m, 28H, 2+4), 3.09 – 3.06 (m, 1H, E), 3.03 (t, *J* = 7.2 Hz, 2H, f), 2.82 (t, *J* = 7.3 Hz, 2H, e), 2.59 – 2.43 (m, 32H, 1+a), 2.35 – 2.29 (m, 4H, b), 1.98 + 1.95 (2s, 3H, 8) ppm. The assignment of the signals was verified by the implementation of ^{1}H-^{1}H-COSY experiments (data not shown).

HR-ESI-MS for $C_{89}H_{153}N_{21}O_{32}$ (exact monoisotopic mass 2028.0991): $[M+3H]^{3+}$ calcd. 677.0403, found 677.0402, mass accuracy -0.15 ppm.

RP-HPLC (linear gradient from 0 - 50% eluent B in 30 min at 40 °C): t_R = 10.7 min. Determined purity: 92%.

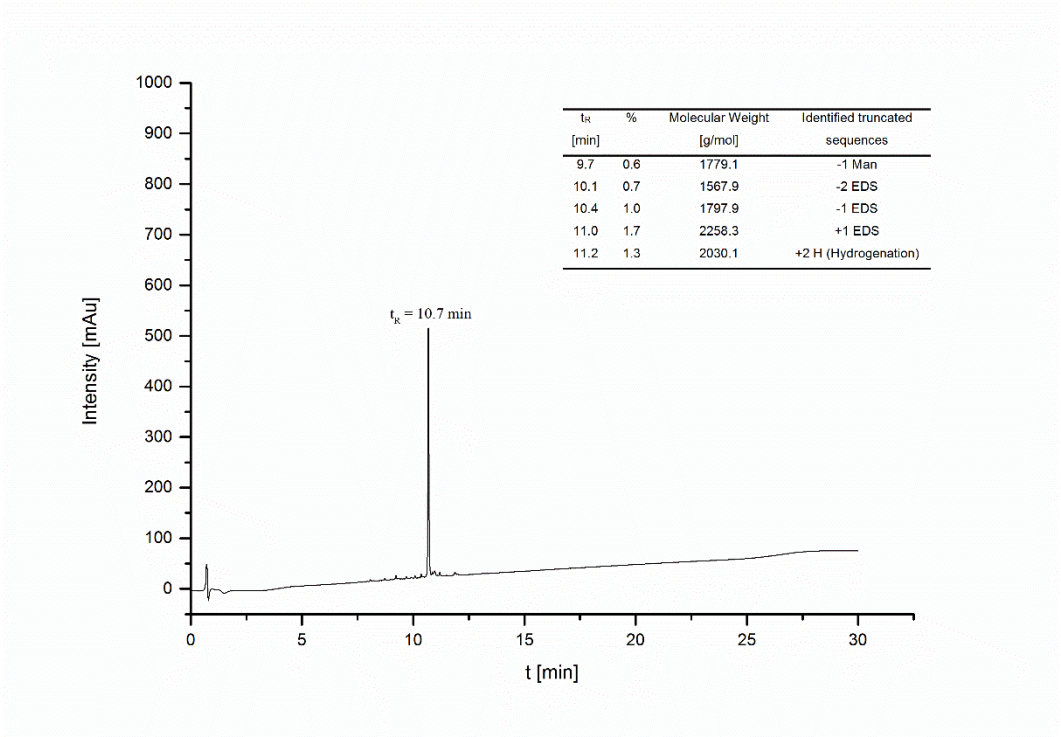

t_R [min]	%	Molecular Weight [g/mol]	Identified truncated sequences
9.7	0.6	1779.1	-1 Man
10.1	0.7	1567.9	-2 EDS
10.4	1.0	1797.9	-1 EDS
11.0	1.7	2258.3	+1 EDS
11.2	1.3	2030.1	+2 H (Hydrogenation)

Figure S19: RP-HPLC analysis (linear gradient from 0 - 50% eluent B in 30 min at 40 °C) chromatogram of compound **4** with retention time. Identified truncated sequences are listed in the table with corresponding retention times, amounts and molecular weights.

DDS(1,7)Man(2,6)-7 (5):

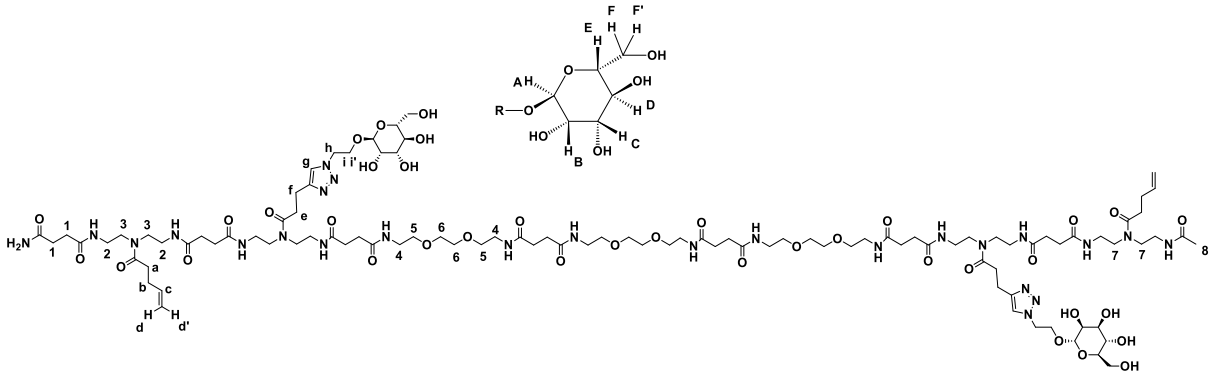

Compound **5** was obtained in a yield of 54%. The anomeric proton of Mannose (A) could not be examined in ^{1}H-NMR due to the overlaying signal from the residual solvent. An unidentified signal was detected with a chemical shift of δ 3.71 (s) ppm. For the acetyl group on the N-terminal end we observed two singlets with a ratio of 1:1 that we assign to two rotational isomers in equal amounts. The presence of rotational isomers was identified in ^{1}H-NMR experiments at higher temperatures (data not shown). ^{1}H NMR (600 MHz, D_2O): δ 8.01 (s, 2H, g), 5.91 – 5.82 (m, 2H, c), 5.10 – 5.05 (m, 2H, d), 5.04 – 5.00 (m, 2H, d‘), 4.72 – 4.65 (m, 4H, h), 4.14 – 4.07 (m, 2H, i or i‘), 3.97 – 3.91 (m, 2H, i or i‘), 3.86 (dd, *J* = 3.3, 1.7 Hz, 2H, B), 3.75 (dd, *J* = 12.2, 2.3 Hz, 2H, F or F‘), 3.71 – 3.63 (m, 18H, 6+C+D+F or F’), 3.63 – 3.59 (m, 12H, 5), 3.53 – 3.43 (m, 16H, 3+7), 3.41 – 3.31 (m, 28H, 2+4), 3.11 – 3.06 (m, 2H, E), 3.04 (t, *J* = 7.2 Hz, 4H, f), 2.82 (t, *J* = 7.2 Hz, 4H, e), 2.58 – 2.42 (m, 32H, 1+a), 2.34 – 2.28 (m, 4H, b), 1.97+1.95 (2s, 3H, 8) ppm. The assignment of the signals was achieved according to the structural similarities with compound **4**.

HR-ESI-MS for $C_{100}H_{169}N_{25}O_{37}$ (exact monoisotopic mass 2312.2111): $[M+3H]^{3+}$ calcd. 771.7443, found 771.7445, mass accuracy 0.26 ppm.

RP-HPLC (linear gradient from 0 - 50% eluent B in 30 min at 40 °C): t_R = 10.0 min. Determined purity: 92%.

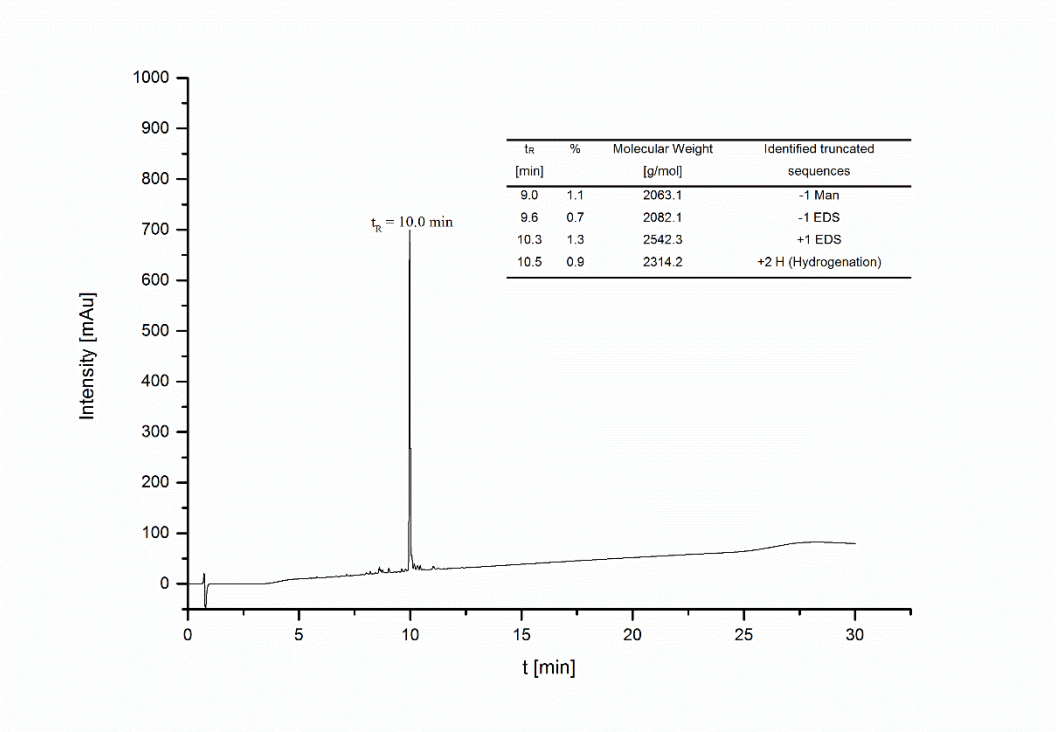

t_R [min]	%	Molecular Weight [g/mol]	Identified truncated sequences
9.0	1.1	2063.1	-1 Man
9.6	0.7	2082.1	-1 EDS
10.3	1.3	2542.3	+1 EDS
10.5	0.9	2314.2	+2 H (Hydrogenation)

Figure S20: RP-HPLC analysis (linear gradient from 0 - 50% eluent B in 30 min at 40 °C) chromatogram of compound **5** with retention time. Identified truncated sequences are listed in the table with corresponding retention times, amounts and molecular weights.

DDS(1,7)Man(2,4,6)-7 (6):

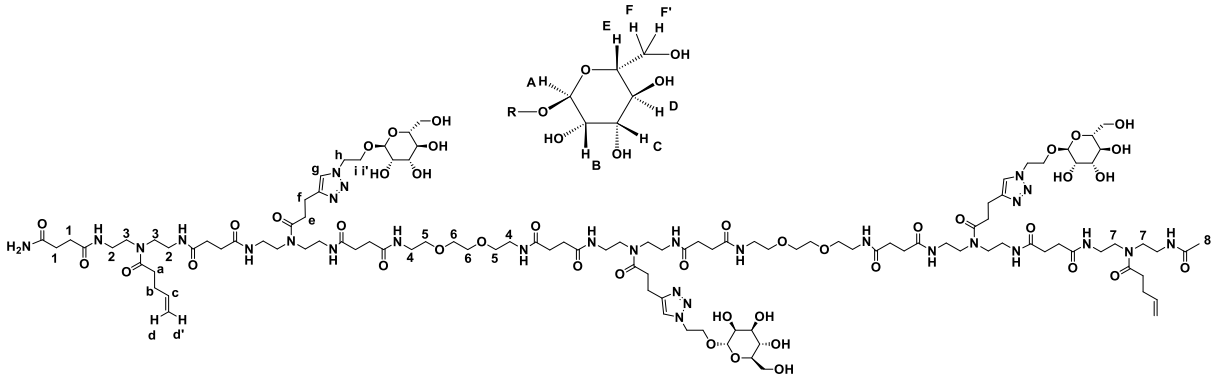

Compound **6** was obtained in a yield of 58%. The anomeric proton of Mannose (A) could not be examined in ^{1}H-NMR due to the overlaying signal from the residual solvent. An unidentified signal was detected with a chemical shift of δ 3.71 (s) ppm. For the acetyl group on the N-terminal end we observed two singlets with a ratio of 1:1 that we assign to two rotational isomers in equal amounts. The presence of rotational isomers was identified in ^{1}H-NMR experiments at higher temperatures (data not shown). ^{1}H NMR (600 MHz, D_2O): δ 8.03 (s, 3H, g), 5.90 – 5.81 (m, 2H, c), 5.10 – 5.04 (m, 2H, d), 5.04 – 5.00 (m, 2H, d‘), 4.72 – 4.67 (m, 6H, h), 4.15 – 4.07 (m, 3H, i or i‘), 3.97 – 9.91 (m, 3H, i or i‘), 3.87 – 3.84 (m, 3H, B), 3.75 (dd, *J* = 12.2, 2.3 Hz, 3H, F or F‘), 3.71 – 3.63 (m, 17H, 6+C+D+F or F’), 3.62 – 3.58 (m, 8H, 5), 3.53 – 3.42 (m, 20H, 3+7), 3.41 – 3.30 (m, 28H, 2+4), 3.14 – 3.07 (m, 3H, E), 3.04 (t, *J* = 7.2 Hz, 6H, f), 2.82 (t, *J* = 7.2 Hz, 6H, e), 2.57 – 2.41 (m, 32H, 1+a), 2.34 – 2.27 (m, 4H, b), 1.96+1.94 (2s, 3H, 8) ppm. The assignment of the signals was achieved according to the structural similarities with compound **4**.

HR-ESI-MS for $C_{111}H_{185}N_{29}O_{42}$ (exact monoisotopic mass 2596.3232): $[M+3H]^{3+}$ calcd. 866.4483, found 866.4476, mass accuracy -0.81 ppm.

RP-HPLC (linear gradient from 0 - 50% eluent B in 30 min at 40 °C): t_R = 9.4 min. Determined purity: 92%.

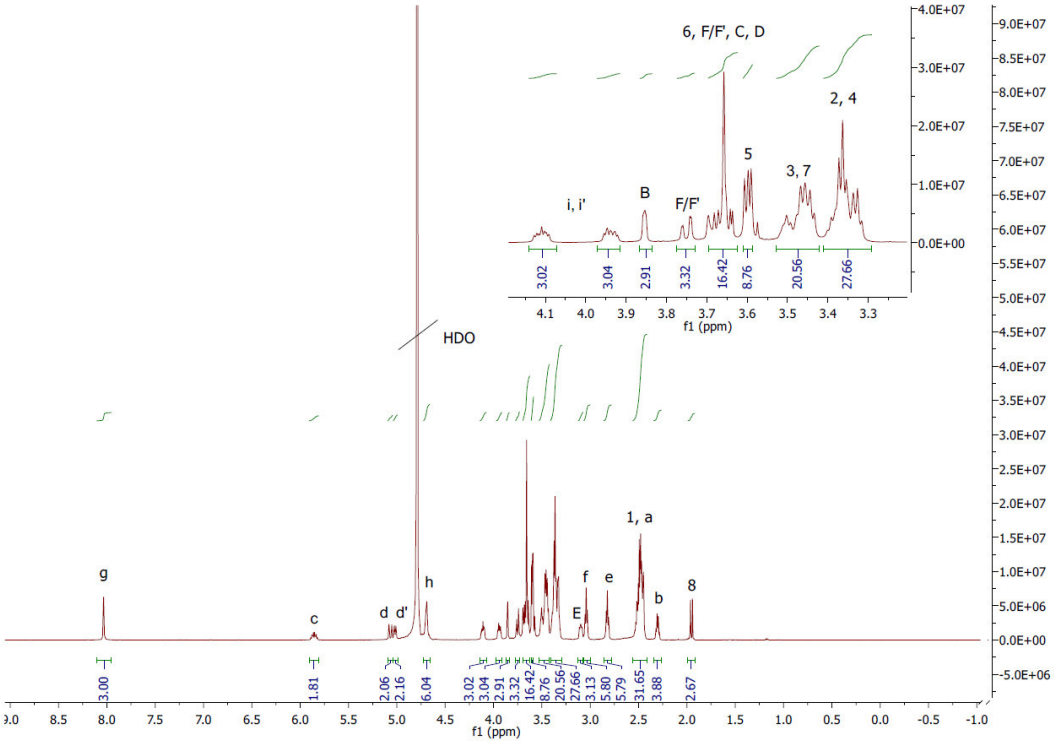

Figure S21: ^{1}H-NMR (600 MHz, D_2O) of compound **6.**

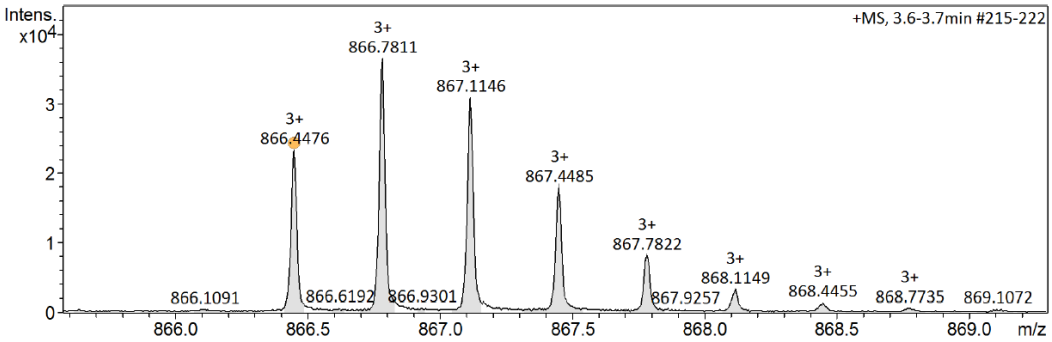

Figure S22: HR-MS (ESI$^+$ Q-TOF) of compound **6**.

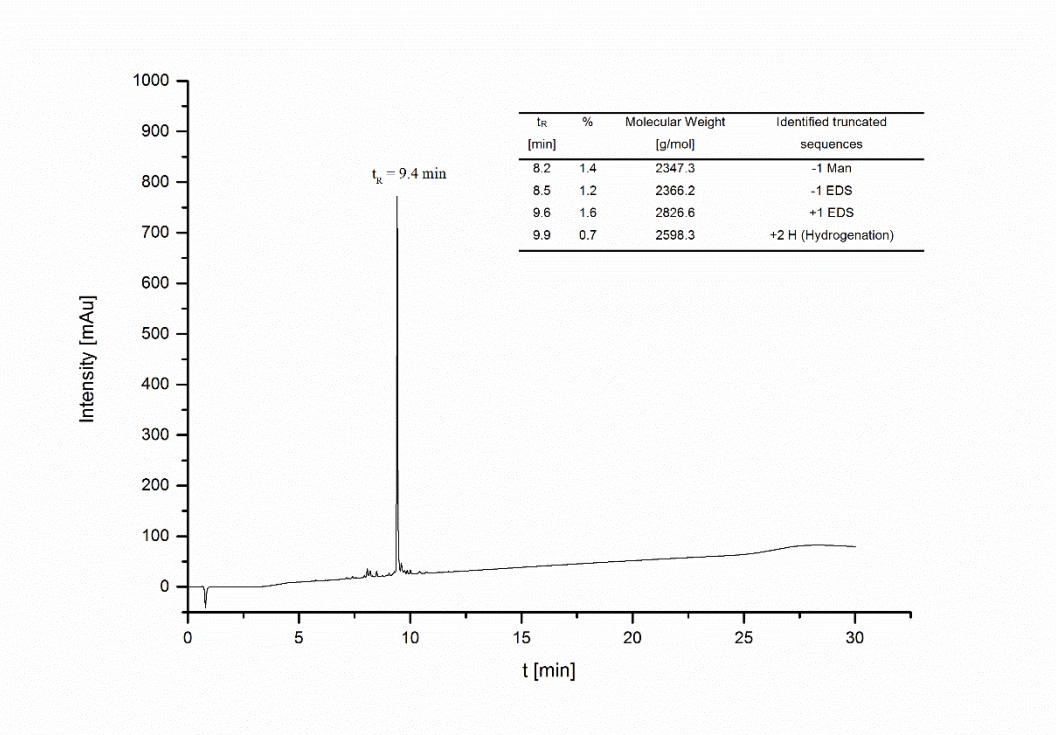

t_R [min]	%	Molecular Weight [g/mol]	Identified truncated sequences
8.2	1.4	2347.3	-1 Man
8.5	1.2	2366.2	-1 EDS
9.6	1.6	2826.6	+1 EDS
9.9	0.7	2598.3	+2 H (Hydrogenation)

Figure S23: RP-HPLC analysis (linear gradient from 0 - 50% eluent B in 30 min at 40 °C) chromatogram of compound **6** with retention time. Identified truncated sequences are listed in the table with corresponding retention times, amounts and molecular weights.

DDS(1,7)Man(2-6)-7 (7):

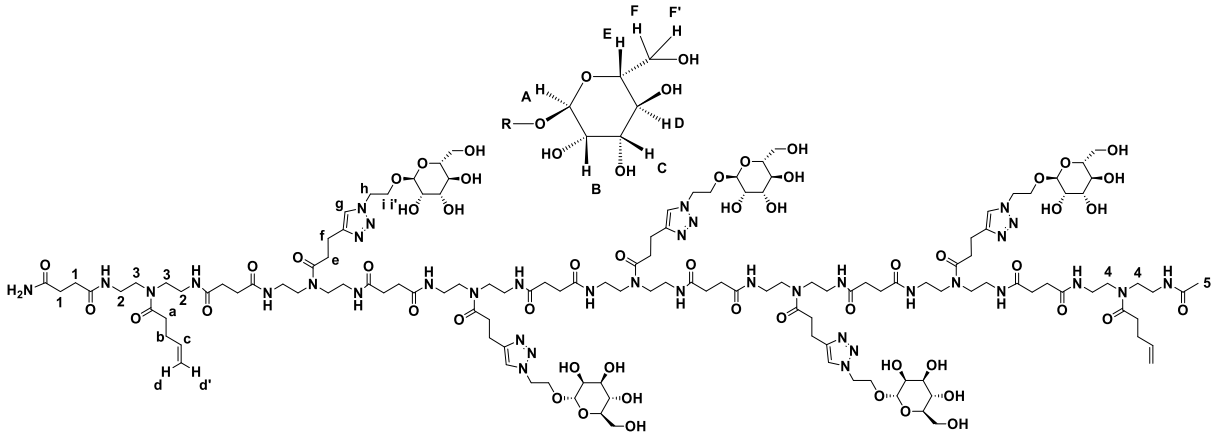

Compound **7** was obtained in a yield of 70%. The anomeric proton of Mannose (A) could not be examined in ^{1}H-NMR due to the overlaying signal from the residual solvent. An unidentified signal was detected with a chemical shift of δ 3.71 (s) ppm. For the acetyl group on the N-terminal end we observed two singlets with a ratio of 1:1 that we assign to two rotational isomers in equal amounts. The presence of rotational isomers was identified in ^{1}H-NMR experiments at higher temperatures (data not shown). ^{1}H NMR (600 MHz, D_2O): δ 8.03 (s, 5H, g), 5.90 – 5.81 (m, 2H, c), 5.09 – 5.03 (m, 2H, d), 5.03 – 4.99 (m, 2H, d‘), 4.72 – 4.65 (m, 10H, h), 4.14 – 4.06 (m, 5H, i or i‘), 3.97 – 3.90 (m, 5H, i or i‘), 3.87 – 3.83 (m, 5H, B), 3.77 – 3.72 (m, 5H, F or F’), 3.68 – 3.62 (m, 10H, C+F or F’), 3.59 (t, *J* = 9.7 Hz, 5H, D), 3.54 – 3.41 (m, 28H, 3+4), 3.40 – 3.27 (m, 28H, 2), 3.13 – 3.07 (m, 5H, E), 3.06 – 2.98 (m, 10H, f), 2.85 – 2.78 (m, 10H, e), 2.55 – 2.39 (m, 32H, 1+a), 2.33 – 2.26 (m, 4H, b), 1.96 +1.94 (2s, 3H, 5) ppm. The assignment of the signals was achieved according to the structural similarities with compound **4**.

HR-ESI-MS for $C_{133}H_{217}N_{37}O_{52}$ (exact monoisotopic mass 3164.5473): $[M+4H]^{4+}$ calcd. 792.1441, found 792.1449, mass accuracy 1.01 ppm.

RP-HPLC (linear gradient from 0 - 50% eluent B in 30 min at 40 °C): t_R = 8.5 min. Determined purity: 92%.

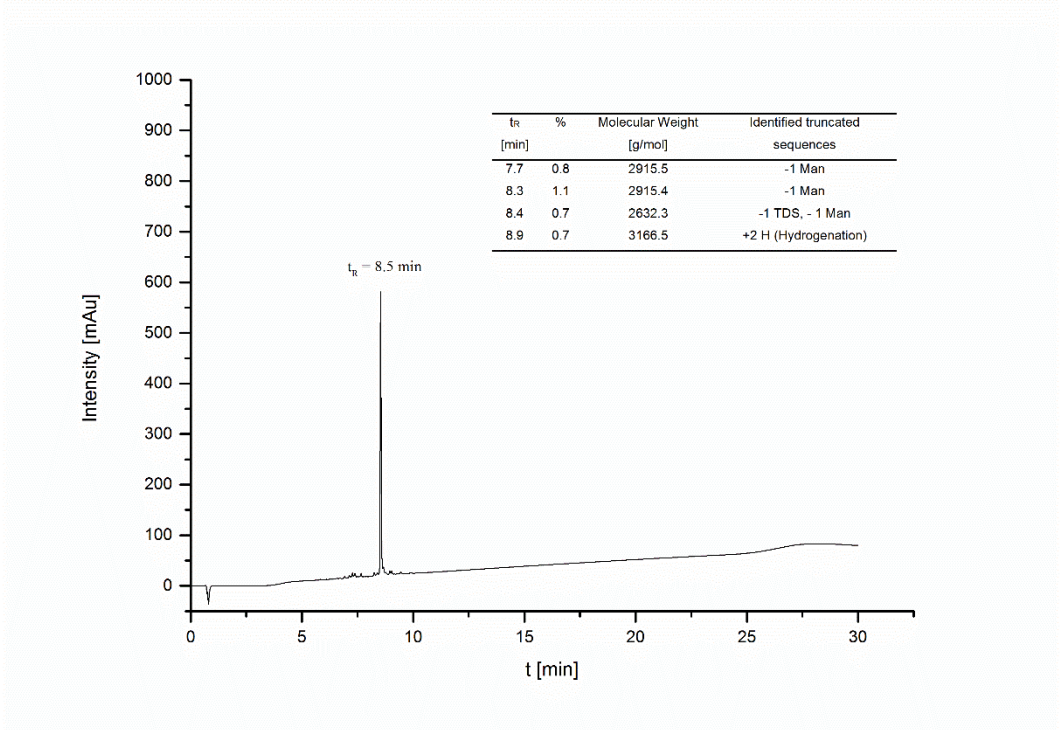

t_R [min]	%	Molecular Weight [g/mol]	Identified truncated sequences
7.7	0.8	2915.5	-1 Man
8.3	1.1	2915.4	-1 Man
8.4	0.7	2632.3	-1 TDS, - 1 Man
8.9	0.7	3166.5	+2 H (Hydrogenation)

Figure S24: RP-HPLC analysis (linear gradient from 0 - 50% eluent B in 30 min at 40 °C) chromatogram of compound **7** with retention time. Identified truncated sequences are listed in the table with corresponding retention times, amounts and molecular weights.

Poly-DDS(1,7)-7 (3):

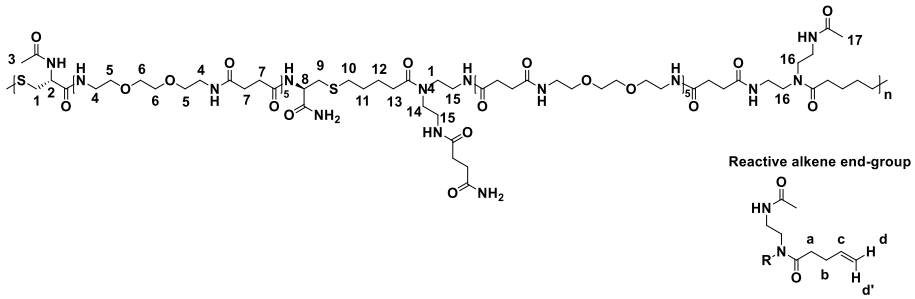

Polymer **3** was obtained in a yield of 70%. In ^{1}H-NMR two unidentified signals were detected with a chemical shift of δ 3.71 (s) and δ 2.65 (s) ppm. 14% of remaining functional alkene group were determined by ^{1}H-NMR. The ratio of macromonomer **1**:**2** was determined to be 1:1.07 by integration of the corresponding signals of the respective acetyl groups. Stated amounts of protons correspond to one repeating unit of the polymer. ^{1}H NMR (600 MHz, D_2O): δ 5.89 – 5.71 (m, end-group, c), 5.04 – 4.99 (m, end-group, d), 4.98 – 4.95 (m, end-group, d'), 4.41 – 4.36 (m, 2H, 2+8), 3.60 (s, 40H, 6), 3.54 (t, *J* = 5.4 Hz, 40H, 5), 3.46 – 3.37 (m, 8H, 14+16), 3.36 – 3.25 (m, 48H, 4+15), 2.98 – 2.74 (m, 4H, 1+9), 2.61 – 2.38 (m, 58H, 7+10), 2.36 – 2.30 (m, 4H, 13), 2.28 – 2.22 (m, end-group, b), 1.98 (s, 3H, 3), 1.90+1.88 (2s, 3H, 17), 1.61 – 1.47 (m, 8H, 11+12) ppm. The assignment of the signals was verified by the implementation of ^{1}H-^{1}H-COSY experiments (data not shown).

MALDI-TOF-MS in reflector mode in a *m/z* range from 1000 to 3000:
For remaining macromonomer **1** $C_{58}H_{105}N_{13}O_{23}S_2$. (Monoisotopic mass 1415.7 g/mol)**:** No signal detected.
For remaining macromonomer **2** $C_{78}H_{137}N_{17}O_{27}$ (Monoisotopic mass 1744.0 g/mol): [**2**+H]$^+$ calcd. 1745.0, found 1745.0, [**2**+Na]$^+$ calcd. 1767.0, found 1767.0.
For dimer **1-2** $C_{136}H_{242}N_{30}O_{50}S_2$ (Monoisotopic mass 3159.7 g/mol): [(**1-2**)+H]$^+$ calcd. 3160.7, found 3160.6, [(**1-2**)+Na]$^+$ calcd. 3182.7, found 3182.6.

MALDI-TOF-MS in linear mode in a *m/z* range from 2000 to 20000:
For dimer **1-2** $C_{136}H_{242}N_{30}O_{50}S_2$ (Monoisotopic mass 3159.7 g/mol): [(**1-2**)+Na]$^+$ calcd. 3182.7, found 3189.
For trimer **1-2-1** $C_{194}H_{347}N_{43}O_{73}S_4$ (Monoisotopic mass 4575.4 g/mol): [(**1-2-1**)+Na]$^+$ calcd. 4598.4, found 4604.
For trimer **2-1-2** $C_{214}H_{379}N_{47}O_{77}S_2$ (Monoisotopic mass 4903.7 g/mol): [(**2-1-2**)+Na]$^+$ calcd. 4926.7, found 4934.
For tetramer **2-1-2-1** $C_{272}H_{484}N_{60}O_{100}S_4$ (Monoisotopic mass 6319.4 g/mol): [(**2-1-2-1**)+Na]$^+$ calcd. 6342.4, found 6351.
For pentamer **1-2-1-2-1** $C_{330}H_{589}N_{73}O_{123}S_6$ (Monoisotopic mass 7735.1 g/mol): [(**1-2-1-2-1**)+Na]$^+$ calcd. 7758.1, found 7764.
For pentamer **2-1-2-1-2** $C_{350}H_{621}N_{77}O_{127}S_4$ (Monoisotopic mass 8063.4 g/mol): [(**2-1-2-1-2**)+Na]$^+$ calcd. 8086.4, found 8092.
For hexamer **2-1-2-1-2-1** $C_{408}H_{726}N_{90}O_{150}S_6$ (Monoisotopic mass 9479.1 g/mol): [(**2-1-2-1-2-1**)+Na]$^+$ calcd. 9502.1, found 9511.

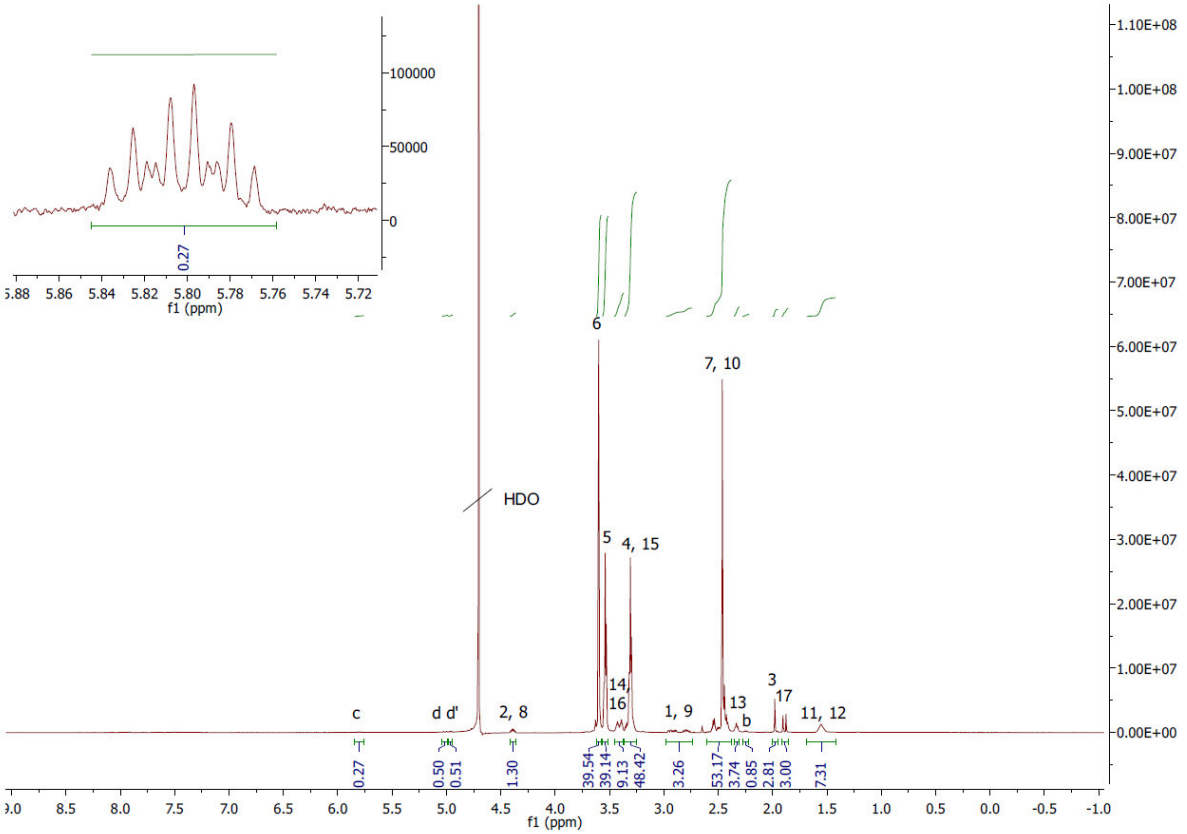

Figure S25: ^{1}H-NMR (600 MHz, D_2O) of compound **3** with an enlargement of the area from 5.9 to 5.7 ppm with the signal for proton c from the remaining reactive alkene group.

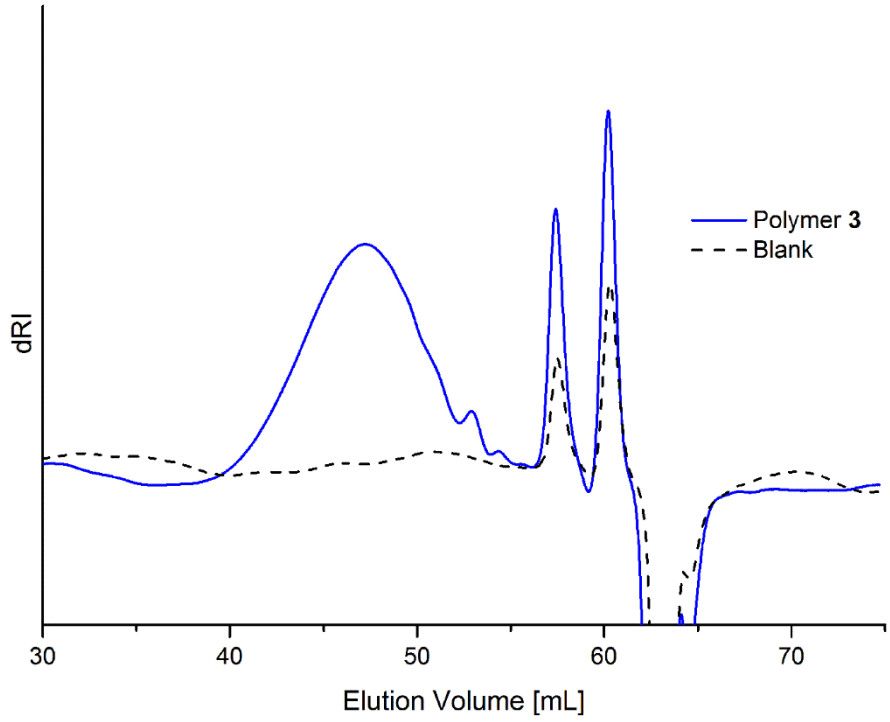

Figure S26: GPC-RI-LS of compound **3**. Columns: Suprema Lux (2x 100 Å and 1000 Å). Buffer: 50 mM NaH_2PO_4, 150 mM NaCl, 250 ppm NaN_3 (pH 7.2), 30% ACN. Flow rate: 1 mL/min.

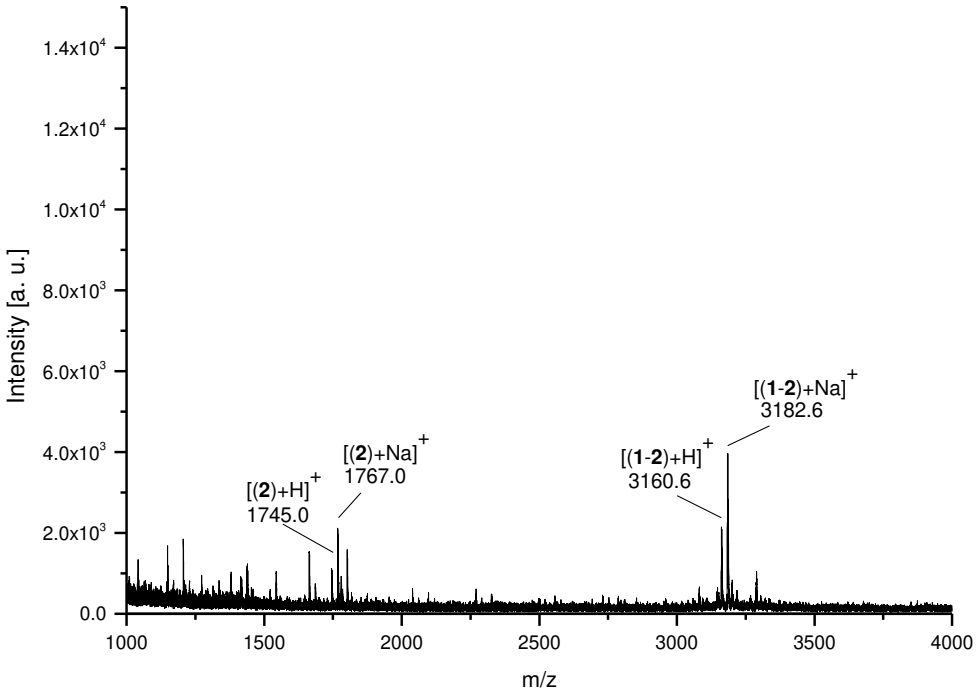

Figure S27: MALDI-TOF-MS of polymer **3** in reflector mode in a *m/z* range of 1000-4000 using DHB as matrix in a compound to matrix ratio of 1:10.

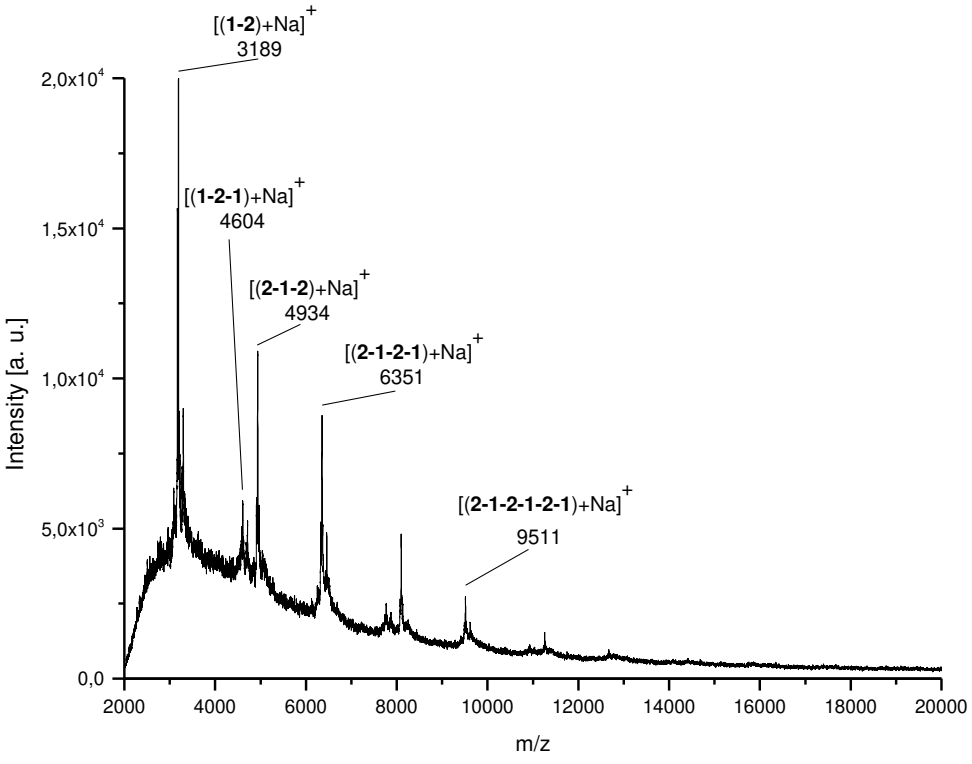

Figure S28: MALDI-TOF-MS of polymer **3** in linear mode in a m/z range of 2000-20000 using DHB as matrix in a compound to matrix ratio of 1:10.

Poly-DDS(1,7)Man(4)-7 (8):

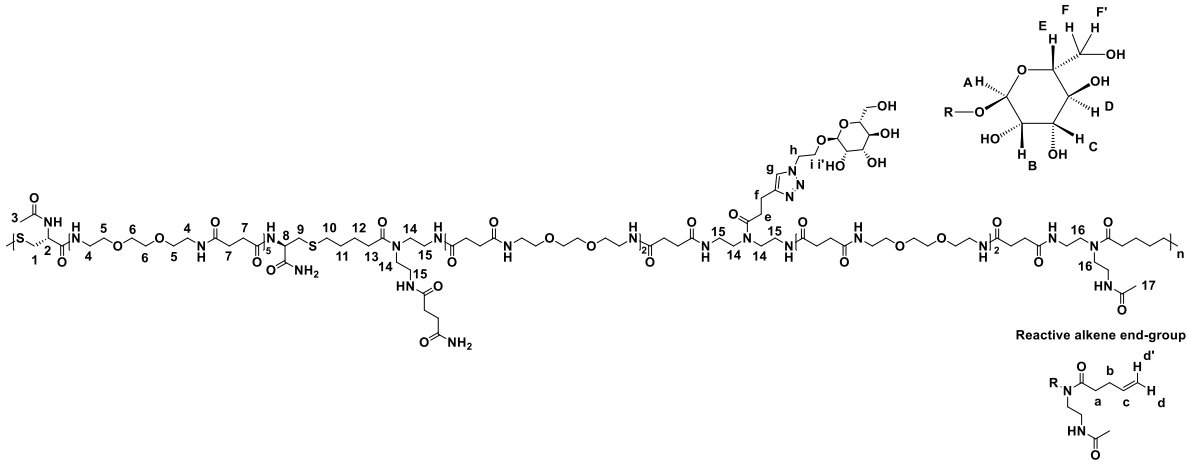

Glycopolymer **8** was obtained in a yield of 65%. The anomeric proton of Mannose (A) could not be examined in ^{1}H-NMR due to the overlaying signal from the residual solvent. Two unidentified signals were detected with a chemical shift of δ 3.71 (s) and δ 2.65 (s) ppm. 18% of remaining functional alkene group were determined from the ^{1}H-NMR. The ratio of macromonomer **1**:**4** was determined to be 1:0.94 by integration of the corresponding signals of the respective acetyl groups. Stated amounts of protons correspond to one repeating unit of the polymer. ^{1}H NMR (600 MHz, D_2O): δ 7.88 (s, 1H, g), 5.93 – 5.84 (m, end-group, c), 5.13 – 5.07 (m, end-group, d), 5.07 – 5.03 (m, end-group, d'), 4.67 – 4.61 (m, 2H, h), 4.51 – 4.44 (m, 2H, 2+8), 4.12 – 4.05 (m, 1H, i or i'), 3.95 – 3.90 (m, 1H, i or i'), 3.88 – 3.85 (m, 1H, B), 3.74 (dd, *J* = 12.3, 2.4 Hz, 1H, F or F'), 3.71 – 3.66 (m, 39H, 6+C+D+F or F'), 3.65 – 3.59 (m, 36H, 5), 3.55 – 3.45 (m, 12H, 14+16), 3.45 – 3.32 (m, 48H, 4+15), 3.08 – 2.84 (m, 7H, 1+9+E+f), 2.80 (t, *J* = 7.3 Hz, 2H, e), 2.66 – 2.46 (m, 52H, 7+10), 2.44 – 2.39 (m, 4H, 13), 2.36 – 2.30 (m, end-group, b), 2.07 (s, 3H, 3), 1.99 + 1.96 (2s, 3H, 17), 1.70 – 1.56 (m, 8H, 11+12) ppm. The assignment of the signals was performed according to the structural similarities with compound **1** and **4** as well as polymer **3**.

MALDI-TOF-MS in reflector mode in a *m/z* range from 1000 to 3000:
Remaining macromonomer **1** $C_{58}H_{105}N_{13}O_{23}S_2$. (Monoisotopic mass 1415.7 g/mol)**:** [**1**+H]$^+$ calcd. 1416.7, found 1416.7, [**1**+Na]$^+$ calcd. 1438.7, found 1438.8.
Disulfide from macromonomer **1** $C_{58}H_{103}N_{13}O_{23}S_2$. (Monoisotopic mass 1413.7 g/mol)**:** [(**1Disulfide**)+H]$^+$ calcd. 1414.7, found 1414.7.
Remaining macromonomer **4** $C_{89}H_{153}N_{21}O_{32}$ (Monoisotopic mass 2028.1 g/mol): No signal detected.
Dimer **1-4** $C_{147}H_{258}N_{34}O_{55}S_2$ (Monoisotopic mass 3443.8 g/mol): [(**1-4**)+H]$^+$ calcd. 3444.8, found 3444.7, [(**1-4**)+Na]$^+$ calcd. 3466.8, found 3466.7.

MALDI-TOF-MS in linear mode in a *m/z* range from 2000 to 20000:
For dimer **1-4** $C_{147}H_{258}N_{34}O_{55}S_2$ (Monoisotopic mass 3443.8 g/mol): [(**1-4**)+Na]$^+$ calcd. 3466.8, found 3474.
For trimer **1-4-1** $C_{205}H_{363}N_{43}O_{73}S_4$ (Monoisotopic mass 4859.5 g/mol): [(**1-4-1**)+Na]$^+$ calcd. 4882.5, found 4887.
For trimer **4-1-4** $C_{236}H_{411}N_{55}O_{87}S_2$ (Monoisotopic mass 5471.9 g/mol): [(**4-1-4**)+Na]$^+$ calcd. 5494.9, found 5505.
For tetramer **4-1-4-1** $C_{294}H_{516}N_{68}O_{110}S_4$ (Monoisotopic mass 6887.6 g/mol): [(**4-1-4-1**)+Na]$^+$ calcd. 6910.6, found 6919.
For pentamer **1-4-1-4-1** $C_{352}H_{621}N_{81}O_{133}S_6$ (Monoisotopic mass 8303.3 g/mol): [(**1-4-1-4-1**)+Na]$^+$ calcd. 8326.3, found 8335.
For pentamer **4-1-4-1-4** $C_{383}H_{669}N_{89}O_{142}S_4$ (Monoisotopic mass 8915.7 g/mol): [(**4-1-4-1-4**)+Na]$^+$ calcd. 8938.7, found 8949.
For hexamer **4-1-4-1-4-1** $C_{441}H_{774}N_{102}O_{165}S_6$ (Monoisotopic mass 10331.4 g/mol): [(**4-1-4-1-4-1**)+Na]$^+$ calcd. 10354.4, found. 10364.

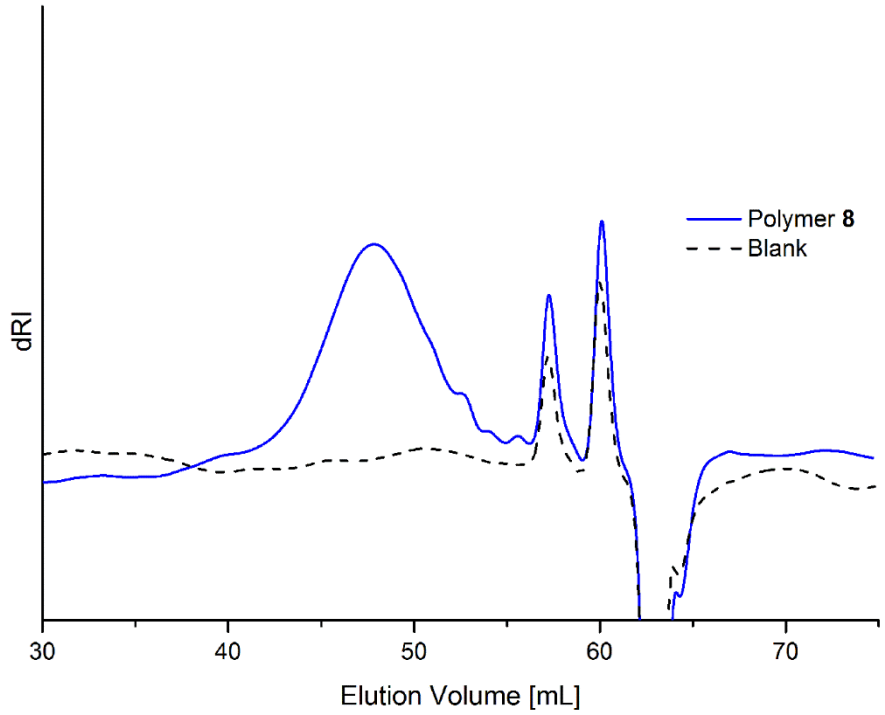

Figure S29: GPC-RI-LS of compound **8**. Columns: Suprema Lux (2x 100 Å and 1000 Å). Buffer: 50 mM NaH_2PO_4, 150 mM NaCl, 250 ppm NaN_3 (pH 7.2), 30% ACN. Flow rate: 1 mL/min.

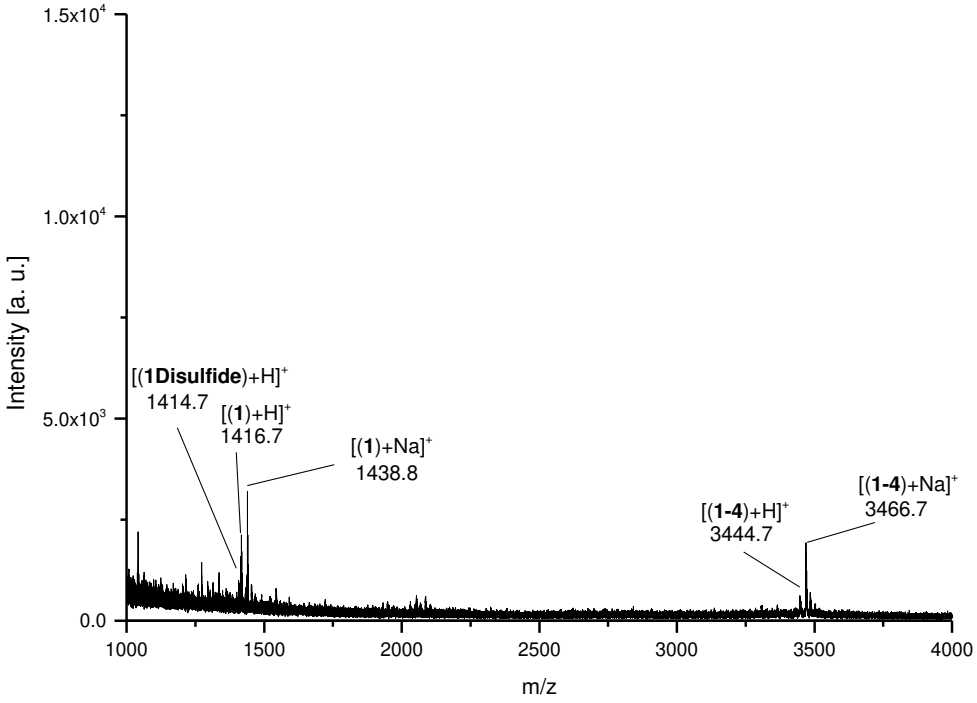

Figure S30: MALDI-TOF-MS of polymer **8** in reflector mode in a *m/z* range of 1000-4000 using DHB as matrix in a compound to matrix ratio of 1:10.

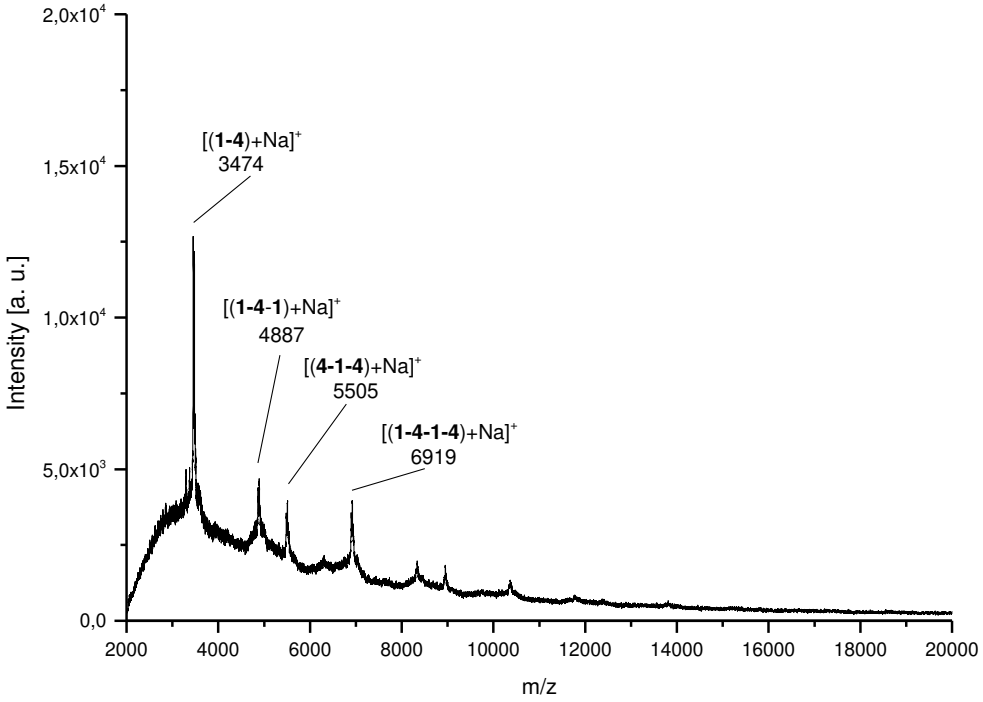

Figure S31: MALDI-TOF-MS of polymer **8** in linear mode in a m/z range of 2000-20000 using DHB as matrix in a compound to matrix ratio of 1:10.

Poly-DDS(1,7)Man(2,6)-7 (9):

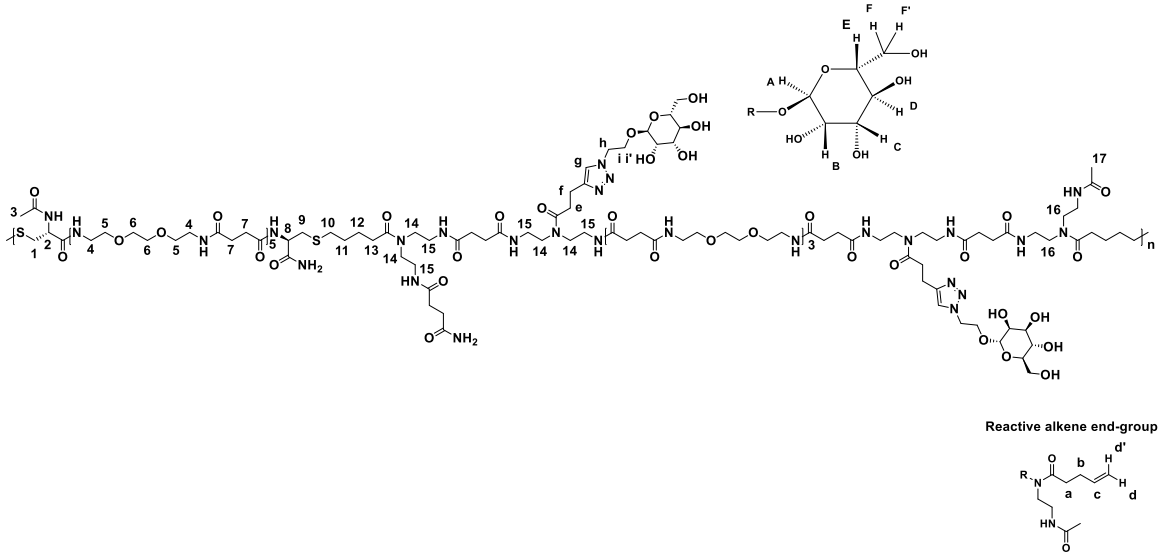

Glycopolymer **9** was obtained in a yield of 67%. The anomeric proton of Mannose (A) could not be examined in ^{1}H-NMR due to the overlaying signal from the residual solvent. Two unidentified signals were detected with a chemical shift of δ 3.71 (s) and δ 2.65 (s) ppm. 4% of remaining functional alkene group were determined from the ^{1}H-NMR. The ratio of macromonomer **1**:**5** was determined to be 1:0.88 by integration of the corresponding signals of the respective acetyl groups. Stated amounts of protons correspond to one repeating unit of the polymer. ^{1}H NMR (600 MHz, D_2O): δ 7.88 (s, 2H, g), 5.92 – 5.81 (m, end-group, c), 5.12 – 5.05 (m, end-group, d), 5.05 – 5.02 (m, end-group, d'), 4.69 – 4.59 (m, 4H, h), 4.51 – 4.44 (m, 1H, 2+8), 4.13 – 4.05 (m, 2H, i or i'), 3.96 – 3.90 (m, 2H, i or i'), 3.88 – 3.85 (m, 2H, B), 3.74 (dd, *J* = 12.2, 2.3 Hz, 2H, F or F'), 3.71 – 3.66 (m, 38H, 6+C+D+F or F'), 3.65 – 3.60 (m, 32H, 5), 3.55 – 3.45 (m, 16H, 14+16), 3.44 – 3.32 (m, 48H, 4+15), 3.08 – 2.83 (m, 10H, 1+9+E+f), 2.80 (t, *J* = 7.3 Hz, 4H, e), 2.70 – 2.44 (m, 52H, 7+10), 2.41 (t, *J* = 7.2 Hz, 4H, 13), 2.35 – 2.29 (m, end-group, b), 2.06 (s, 3H, 3), 1.98 + 1.96 (2s, 3H, 17), 1.74 – 1.53 (m, 8H, 11+12) ppm. The assignment of the signals was performed according to the structural similarities with compound **1** and **5** as well as polymer **3**.

MALDI-TOF-MS in reflector mode in a *m/z* range from 1000 to 3000:
Remaining macromonomer **1** $C_{58}H_{105}N_{13}O_{23}S_2$. (Monoisotopic mass 1415.7 g/mol)**:** [**1**+H]$^+$ calcd. 1416.7, found 1416.7, [**1**+Na]$^+$ calcd. 1438.7, found 1438.7.
Disulfide from macromonomer **1** $C_{58}H_{103}N_{13}O_{23}S_2$. (Monoisotopic mass 1413.7 g/mol)**:** [(**1Disulfide**)+Na]$^+$ calcd. 1436.7, found 1436.7.
Remaining macromonomer **5** $C_{100}H_{169}N_{25}O_{37}$ (Monoisotopic mass 2028.1 g/mol): No signal detected.
Dimer **1-5** $C_{158}H_{274}N_{38}O_{60}S_2$ (Monoisotopic mass 3727.9 g/mol): [(**1-5**)+Na]$^+$ calcd. 3750.9, found 3750.7.

MALDI-TOF-MS in linear mode in a *m/z* range from 2000 to 20000:
For dimer **1-5** $C_{158}H_{274}N_{38}O_{60}S_2$ (Monoisotopic mass 3727.9 g/mol): [(**1-5**)+Na]$^+$ calcd. 3750.9, found 3757.
For trimer **1-5-1** $C_{216}H_{379}N_{51}O_{83}S_4$ (Monoisotopic mass 5143.6 g/mol): [(**1-5-1**)+Na]$^+$ calcd. 5166.6, found 5173.
For trimer **5-1-5** $C_{258}H_{443}N_{63}O_{97}S_2$ (Monoisotopic mass 6040.1 g/mol): [(**5-1-5**)+Na]$^+$ calcd. 6063.1, found 6072.
For tetramer **5-1-5-1** $C_{316}H_{548}N_{76}O_{120}S_4$ (Monoisotopic mass 7455.8 g/mol): [(**5-1-5-1**)+Na]$^+$ calcd. 7478.8, found 7488.
For pentamer **1-5-1-5-1** $C_{374}H_{653}N_{89}O_{143}S_6$ (Monoisotopic mass 8871.5 g/mol): [(**1-5-1-5-1**)+Na]$^+$ calcd. 8894.5, found 8901.
For pentamer **5-1-5-1-5** $C_{416}H_{717}N_{101}O_{157}S_4$ (Monoisotopic mass 9768.0 g/mol): [(**5-1-5-1-5**)+Na]$^+$ calcd. 9791.0, found 9799.
For hexamer **5-1-5-1-5-1** $C_{474}H_{822}N_{114}O_{160}S_6$ (Monoisotopic mass 11183.7 g/mol): [(**5-1-5-1-5-1**)+Na]$^+$ calcd. 11206.7, found. 11215.7

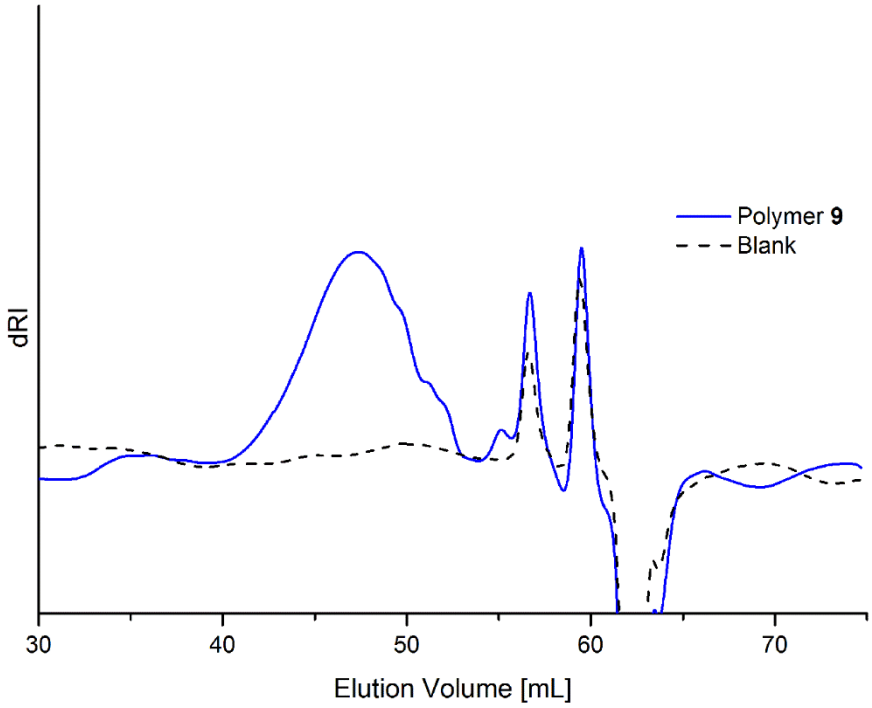

Figure S32: GPC-RI-LS of compound **9**. Columns: Suprema Lux (2x 100 Å and 1000 Å). Buffer: 50 mM NaH_2PO_4, 150 mM NaCl, 250 ppm NaN_3 (pH 7.2), 30% ACN. Flow rate: 1 mL/min.

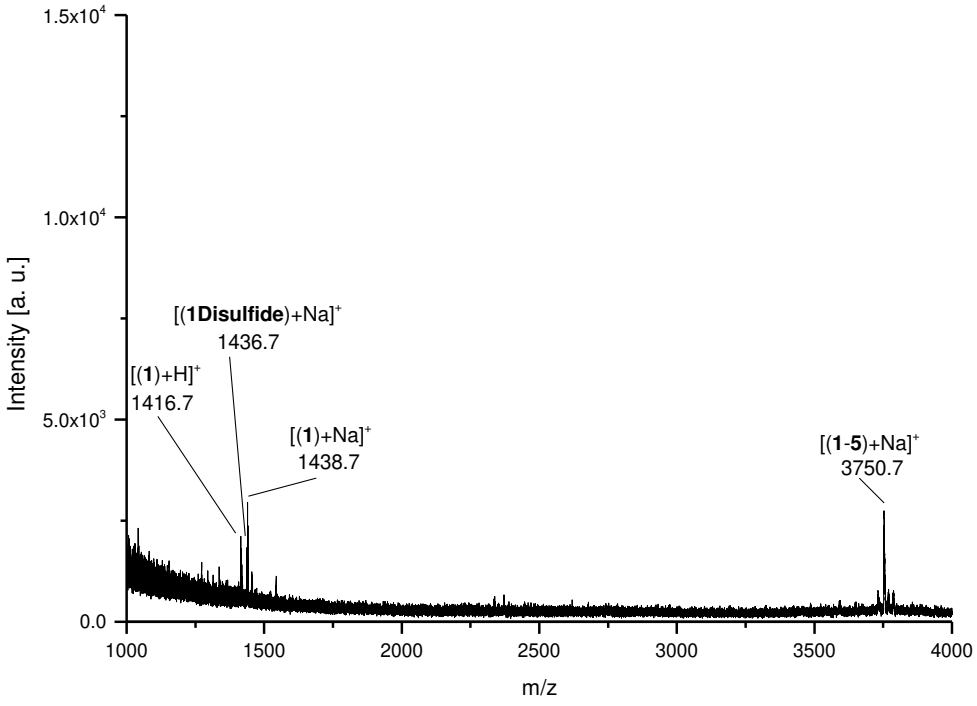

Figure S33: MALDI-TOF-MS of polymer **9** in reflector mode in a *m/z* range of 1000-4000 using DHB as matrix in a compound to matrix ratio of 1:10.

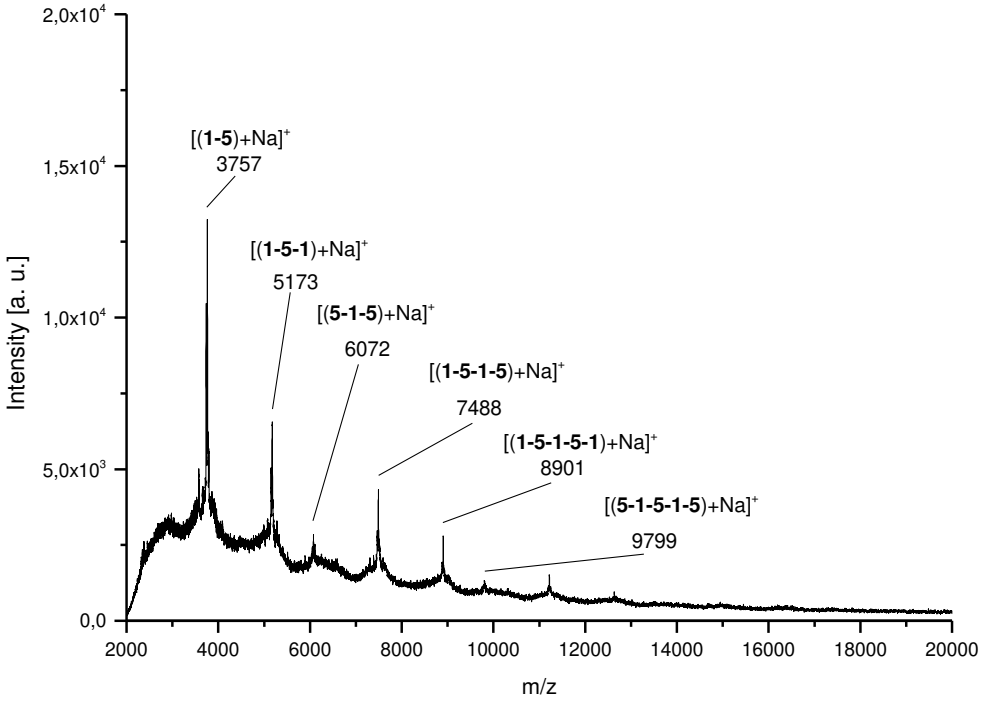

Figure S34: MALDI-TOF-MS of polymer **9** in linear mode in a m/z range of 2000-20000 using DHB as matrix in a compound to matrix ratio of 1:10.

Poly-DDS(1,7)Man(2,4,6)-7 (10):

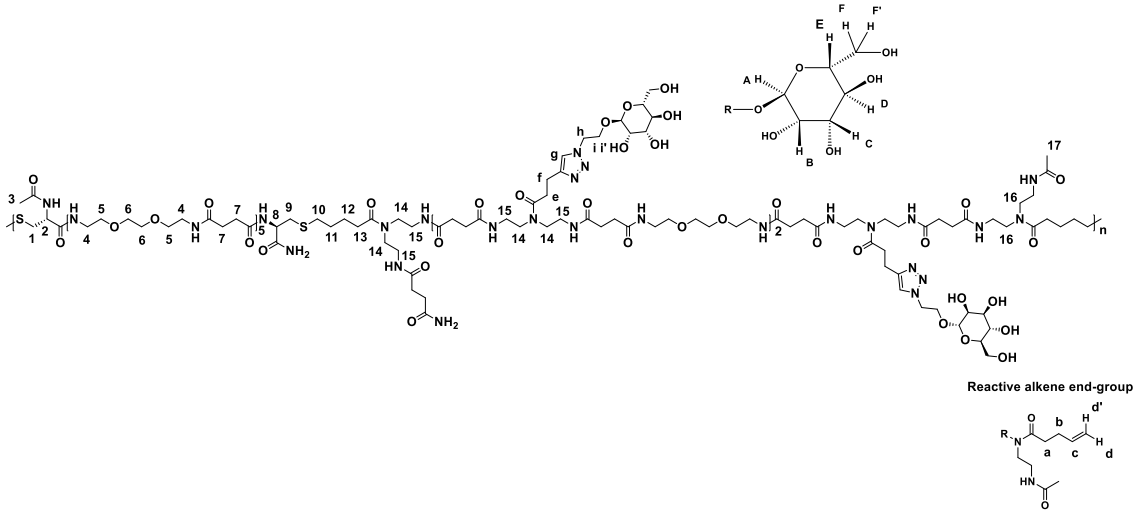

Glycopolymer **10** was obtained in a yield of 66%. The anomeric proton of Mannose (A) could not be examined in ^{1}H-NMR due to the overlaying signal from the residual solvent. Two unidentified signals were detected with a chemical shift of δ 3.71 (s) and δ 2.65 (s) ppm. 5% of remaining functional alkene group were determined from the ^{1}H-NMR. The ratio of macromonomer **1**:**6** was determined to be 1:0.84 by integration of the corresponding signals of the respective acetyl groups. Stated amounts of protons correspond to one repeating unit of the polymer. ^{1}H NMR (600 MHz, D_2O): δ 7.88 (s, 3H, g), 5.94 – 5.81 (m, end-group, c), 5.11 – 5.06 (m, end-group, d), 5.05 – 5.01 (m, end-group, d‘), 4.70 – 4.59 (m, 6H, h), 4.50 – 4.43 (m, 2H, 2+8), 4.13 – 4.05 (m, 3H, i or i‘), 3.95 – 3.89 (m, 3H, i or i’), 3.88 – 3.85 (m, 3H, B), 3.74 (dd, *J* = 12.3, 2.4 Hz, 3H, F or F’), 3.70 – 3.64 (m, 37H, 6+C+D+F or F’), 3.64 – 3.59 (m, 28H, 5), 3.54 – 3.44 (m, 20H, 14+16), 3.42 – 3.32 (m, 48H, 4+15), 3.08 – 2.83 (m, 13H, 1+9+E+f), 2.80 (t, *J* = 7.4 Hz, 6H, e), 2.67 – 2.44 (m, 52H, 7+10), 2.41 (t, *J* = 7.2 Hz, 4H, 13), 2.35 – 2.29 (m, end-group, b), 2.06 (s, 3H, 3), 1.98 + 1.96 (2s, 3H, 17), 1.70 – 1.56 (m, 8H, 11+12) ppm. The assignment of the signals was performed according to the structural similarities with compound **1** and **6** as well as polymer **3**.

MALDI-TOF-MS in reflector mode in a *m/z* range from 1000 to 3000:
Remaining macromonomer **1** $C_{58}H_{105}N_{13}O_{23}S_2$. (Monoisotopic mass 1415.7 g/mol)**:** [**1**+H]$^+$ calcd. 1416.7, found 1416.7, [**1**+Na]$^+$ calcd. 1438.7, found 1438.7.
Disulfide from macromonomer **1** $C_{58}H_{103}N_{13}O_{23}S_2$. (Monoisotopic mass 1413.7 g/mol)**:** [(**1Disulfide**)+H]$^+$ calcd. 1414.7, found 1414.7.
Remaining macromonomer **6** $C_{111}H_{185}N_{29}O_{37}$ (Monoisotopic mass 2596.3 g/mol): No signal detected.

MALDI-TOF-MS in linear mode in a *m/z* range from 2000 to 20000:
For dimer **1-6** $C_{169}H_{290}N_{42}O_{65}S_2$ (Monoisotopic mass 4012.0 g/mol): [(**1-6**)+Na]$^+$ calcd. 4025.0, found 4042.
For trimer **1-6-1** $C_{227}H_{395}N_{55}O_{88}S_4$ (Monoisotopic mass 5427.7 g/mol): [(**1-6-1**)+Na]$^+$ calcd. 5450.7, found 5458.
For tetramer **6-1-6-1** $C_{338}H_{580}N_{84}O_{130}S_4$ (Monoisotopic mass 8024.0 g/mol): [(**6-1-6-1**)+Na]$^+$ calcd. 8047.0, found 8056.
For pentamer **1-6-1-6-1** $C_{396}H_{685}N_{97}O_{153}S_6$ (Monoisotopic mass 9439.7 g/mol): [(**1-6-1-6-1**)+Na]$^+$ calcd. 9462.7, found 9468.

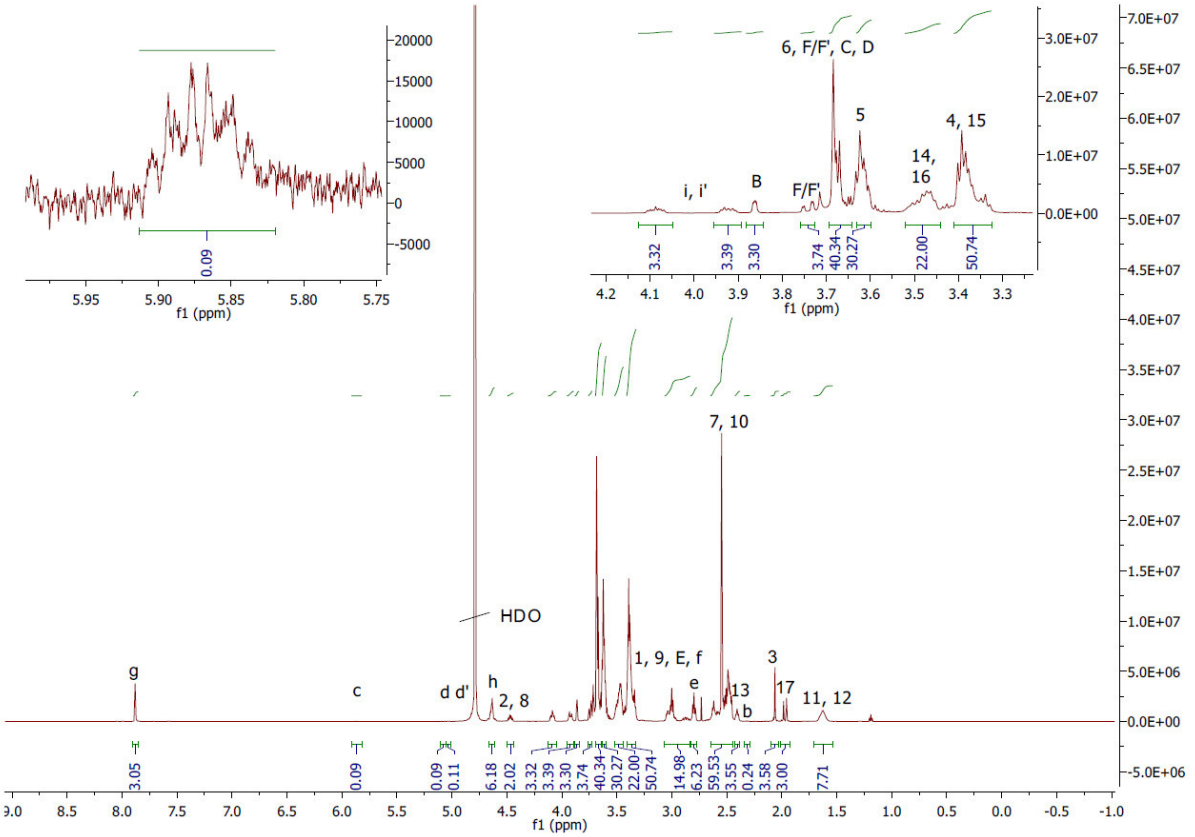

Figure S35: ^{1}H-NMR (600 MHz, D_2O) of compound **10** with an enlargement of the area from 6.0 to 5.8 ppm with the signal from the remaining proton c from the reactive alkene group and the area from 4.2 to 3.3 ppm.

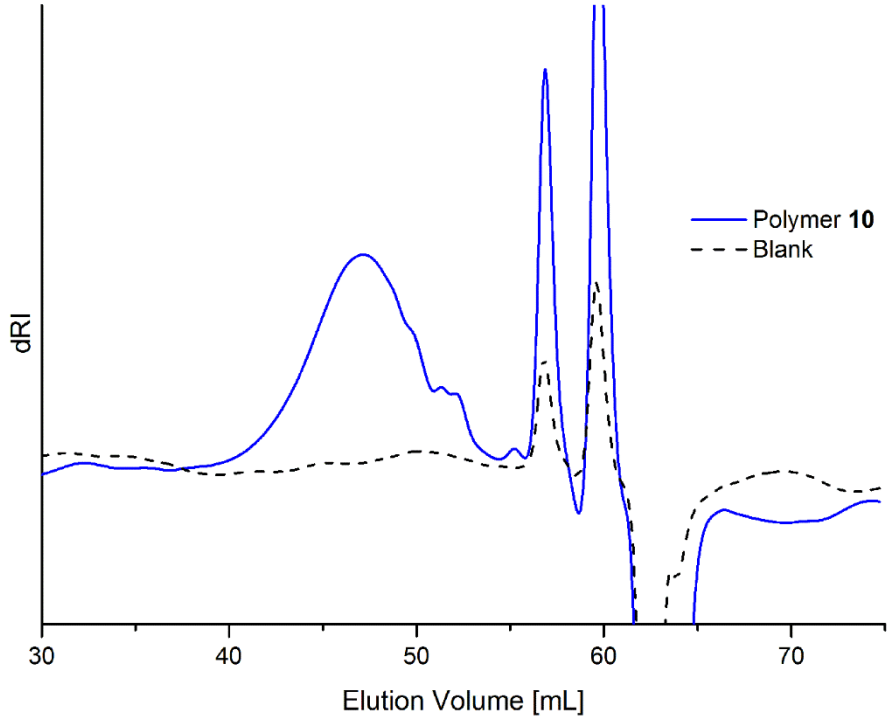

Figure S36: GPC-RI-LS of compound **10**. Columns: Suprema Lux (2x 100 Å and 1000 Å). Buffer: 50 mM NaH_2PO_4, 150 mM NaCl, 250 ppm NaN_3 (pH 7.2), 30% ACN. Flow rate: 1 mL/min.

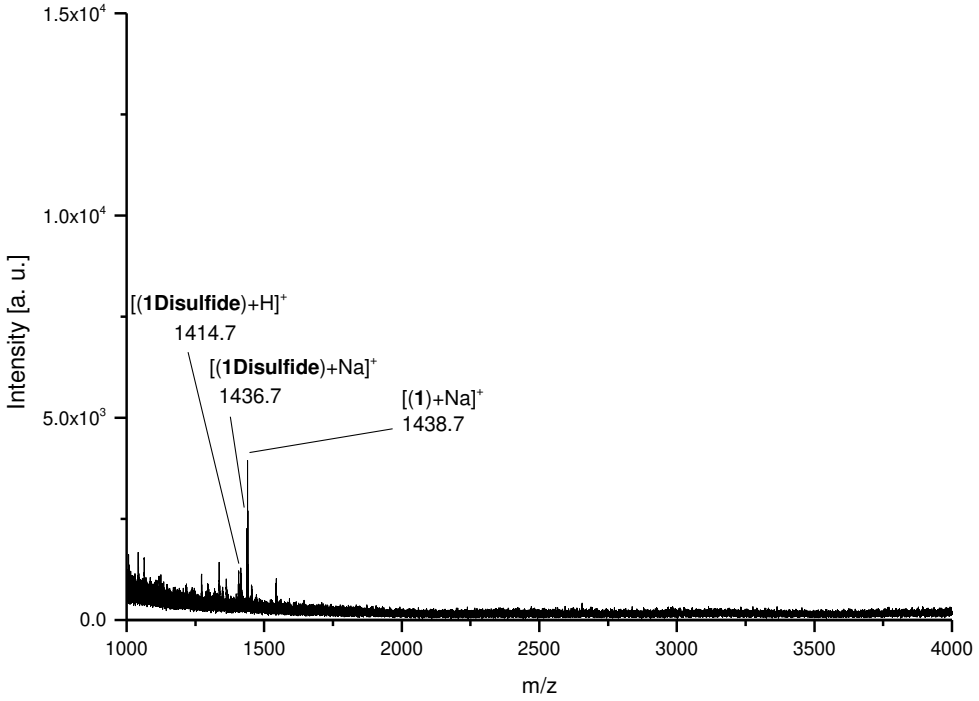

Figure S37 MALDI-TOF-MS of polymer **10** in reflector mode in a *m/z* range of 1000-4000 using DHB as matrix in a compound to matrix ratio of 1:10.

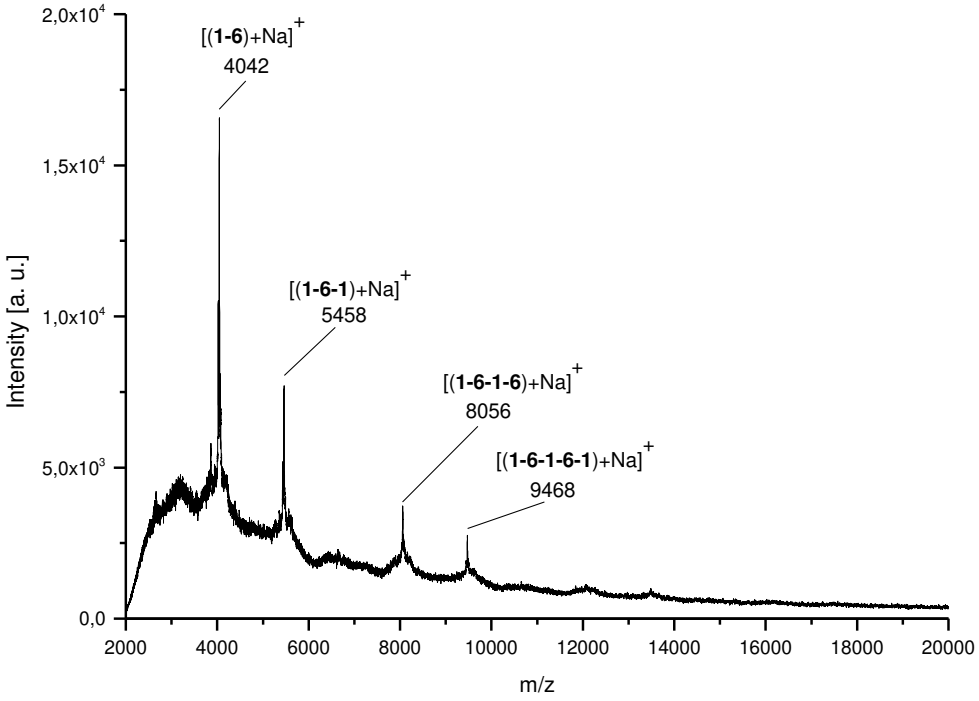

Figure S38: MALDI-TOF-MS of polymer **10** in linear mode in a m/z range of 2000-20000 using DHB as matrix in a compound to matrix ratio of 1:10.

Poly-DDS(1,7)Man(2-6)-7 (11):

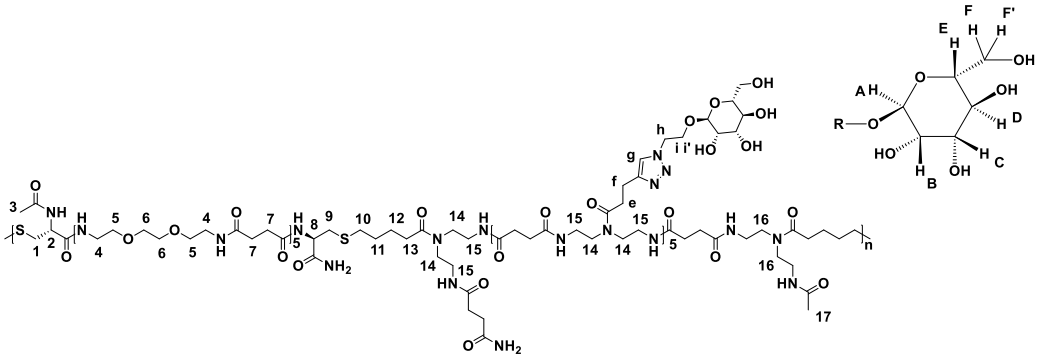

Glycopolymer **11** was obtained in a yield of 66%. The anomeric proton of Mannose (A) could not be examined in ^{1}H-NMR due to the overlaying signal from the residual solvent. Two unidentified signals were detected with a chemical shift of δ 3.71 (s) and δ 2.65 (s) ppm. No remaining functional alkene group was determined from the ^{1}H-NMR. The ratio of macromonomer **1**:**7** was determined to be 1:0.85 by integration of the corresponding signals of the respective acetyl groups. Stated amounts of protons correspond to one repeating unit of the polymer. ^{1}H NMR (600 MHz, D_2O): δ 7.87 (s, 5H, g), 4.68 – 4.58 (m, 10H, h), 4.51 – 4.43 (m, 2H, 2+8), 4.11 – 4.05 (m, 5H, i or i'), 3.94 – 3.89 (m, 5H, i or i'), 3.88 – 3.85 (m, 5H, B), 3.76 – 3.72 (m, 5H, F or F'), 3.70 – 3.64 (m, 35H, 6+C+D+F or F'), 3.64 – 3.58 (m, 20H, 5), 3.53 – 3.42 (m, 28H, 14+16), 3.41 – 3.30 (m, 48H, 4+15), 3.06 – 2.83 (m, 19H, 1+9+E+f), 2.81 – 2.76 (m, 10H, e), 2.67 – 2.37 (m, 56H, 7+10+13), 2.06 (s, 3H,3), 1.98 + 1.96 (2s, 3H, 17), 1.70 – 1.52 (m, 8H, 11+12) ppm. The assignment of the signals was performed according to the structural similarities with compound **1** and **7** as well as polymer **3**.

MALDI-TOF-MS in reflector mode in a *m/z* range from 1000 to 3000:
Remaining macromonomer **1** $C_{58}H_{105}N_{13}O_{23}S_2$. (Monoisotopic mass 1415.7 g/mol)**:** [**1**+H]$^+$ calcd. 1416.7, found 1416.7, [**1**+Na]$^+$ calcd. 1438.7, found 1438.7.
Disulfide from macromonomer **1** $C_{58}H_{103}N_{13}O_{23}S_2$. (Monoisotopic mass 1413.7 g/mol)**:** [(**1Disulfide**)+H]$^+$ calcd. 1414.7, found 1414.7.
Remaining macromonomer **7** $C_{133}H_{217}N_{37}O_{52}$ (Monoisotopic mass 3164.5 g/mol): No signal detected.

MALDI-TOF-MS in linear mode in a *m/z* range from 2000 to 20000:
For dimer **1-7** $C_{191}H_{322}N_{50}O_{75}S_2$ (Monoisotopic mass 4580.20 g/mol): [(**1-7**)+Na]$^+$ calcd. 4603.2, found 4610.
For trimer **1-7-1** $C_{249}H_{427}N_{63}O_{98}S_4$ (Monoisotopic mass 5995.9 g/mol): [(**1-7-1**)+Na]$^+$ calcd. 6018.9, found 6026.
For tetramer **7-1-7-1** $C_{382}H_{644}N_{100}O_{150}S_4$ (Monoisotopic mass 9160.4 g/mol): [(**7-1-7-1**)+Na]$^+$ calcd. 9183.4, found 9192.
For pentamer **1-7-1-7-1** $C_{440}H_{749}N_{113}O_{173}S_6$ (Monoisotopic mass 10576.1 g/mol): [(**1-7-1-7-1**)+Na]$^+$ calcd. 10599.1, found 10605.

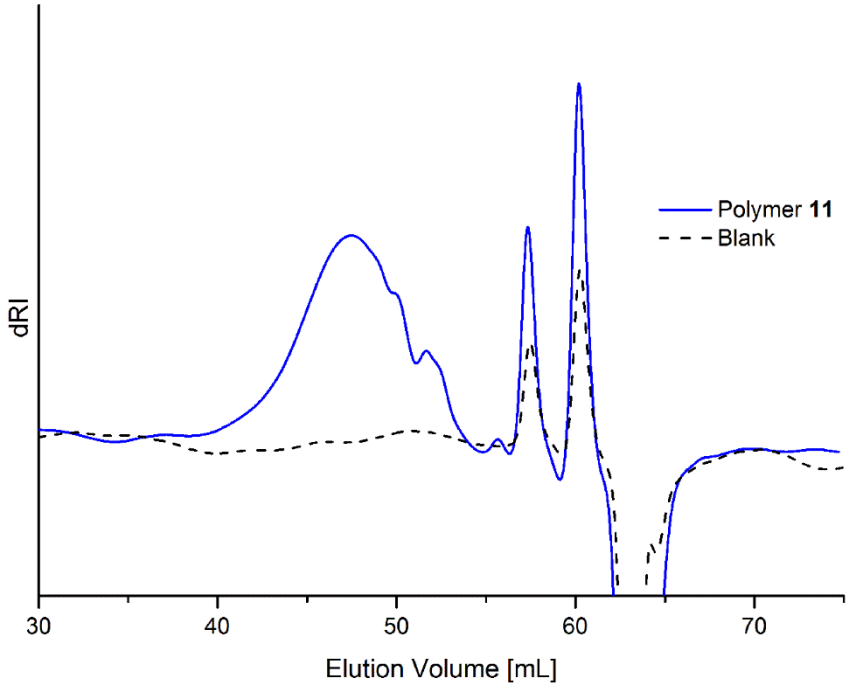

Figure S39: GPC-RI-LS of compound **11**. Columns: Suprema Lux (2x 100 Å and 1000 Å). Buffer: 50 mM NaH_2PO_4, 150 mM NaCl, 250 ppm NaN_3 (pH 7.2), 30% ACN. Flow rate: 1 mL/min.

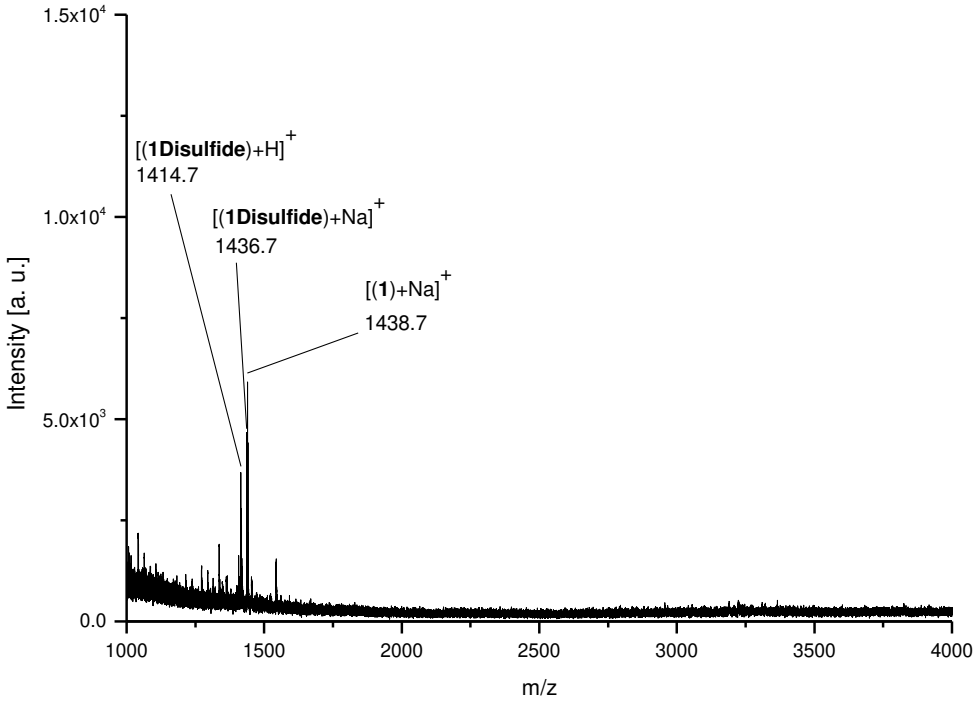

Figure S40: MALDI-TOF-MS of polymer **11** in reflector mode in a *m/z* range of 1000-4000 using DHB as matrix in a compound to matrix ratio of 1:10.

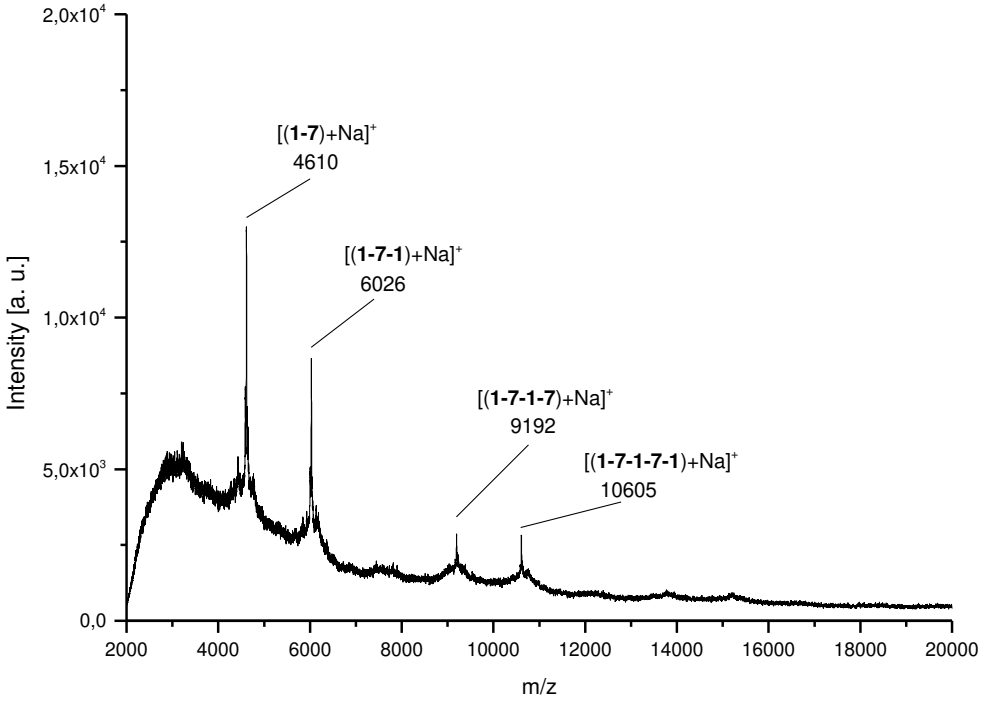

Figure S41: MALDI-TOF-MS of polymer **11** in linear mode in a m/z range of 2000-20000 using DHB as matrix in a compound to matrix ratio of 1:10.

5.2 Sequence-Controlled High Molecular Weight Glyco(oligoamide) – PEG Multiblock Copolymers as Ligands and Inhibitors in Lectin Binding

C. Gerke, F. Jacobi, L. E. Goodwin, F. Pieper, S. Schmidt, L. Hartmann

Macromolecules, **2018**, 51, (15), 5608−5619

[Impact Factor 2017: 5.914]

Contribution:

Collaborative design of structures and binding assays. Optimization of the NDS building block synthesis, supported by supervised students. Synthesis of building blocks, macromonomers, and glycopolymers. Experiments comparing different alkene reactivity. Optimization of polymerization procedure. Purification of glycopolymers. Measurement and evaluation of all LC-MS and GPC-RI-LS experiments. Evaluation of all NMR, UHR-MS and MALDI-TOF experiments. Performance and evaluation of SPR experiments. Collaborative writing of the manuscript.

Macromolecules

Article

Cite This: Macromolecules 2018, 51, 5608−5619

Sequence-Controlled High Molecular Weight Glyco(oligoamide)−PEG Multiblock Copolymers as Ligands and Inhibitors in Lectin Binding

Christoph Gerke, Fawad Jacobi, Laura E. Goodwin, Franziska Pieper, Stephan Schmidt, and Laura Hartmann*

Institute of Organic Chemistry and Macromolecular Chemistry, Heinrich-Heine-University Düsseldorf, Universitätsstraße 1, 40225 Düsseldorf, Germany

Supporting Information

ABSTRACT: A synthesis toward sequence-controlled multiblock glycopolymers, presenting a mannopyranoside (Man) glyco(oligoamide) block followed by a poly(ethylene glycol) (PEG) ($\bar{M}_n$ of 6 kDa) block, is shown. Therefore, monodisperse and sequence-defined glyco(oligoamide) macromonomers derived from solid phase synthesis (SPS) are polymerized with dithiol-functionalized PEG via thiol−ene coupling (TEC) in a step-growth fashion. For the polymerization, a novel building block introducing a norbornene moiety is developed which is used for end-functionalization of the glyco(oligoamide) macromonomers. As a highly reactive alkene moiety in photoinduced TEC, this gives access to $\bar{X}_n$ of up to 45. A total of 12 glyco(oligoamide)−PEG multiblock copolymers with maximum $\bar{M}_n$ of 200 kDa are obtained and subjected to a series of purification steps decreasing overall dispersity. In different binding studies toward model lectin Concanavalin A, despite their high number of Man ligands, we see rather weak binding of glycopolymers that we attribute to the introduction of higher molecular weight PEG blocks.

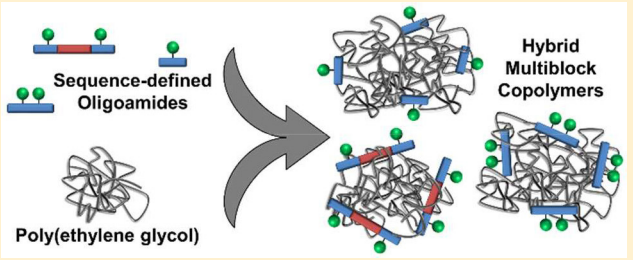

INTRODUCTION

The synthesis of well-defined polymeric materials, e.g., achieving narrow dispersity, monomer sequence, or a defined complex polymeric architecture, has gained increasing attention over the past decades.[1−6] Especially for the use of polymers as biomimetic materials, a well-defined structure is important as it allows for new insights into their structure−property relationships.[7−9] Despite the synthetic challenges, numerous approaches have been successfully established in the past years, from controlled polymerization methods[10−14] to the use of iterative coupling protocols in solution[15−21] or on solid support[22−25] to the use of specifically functionalized monomers.[26−28] In our group, we introduced an approach based on solid phase synthesis (SPS), as originally introduced by Merrifield,[29] to synthesize monodisperse, sequence-defined oligoamides or so-called precision macromolecules. In short, our synthetic strategy is based on the use of tailor-made building blocks carrying a free carboxylic acid and an Fmoc-protected amine terminus, thus allowing for stepwise assembly on solid support applying standard Fmoc coupling protocols.[30] Through choice of building block in every coupling step, we can control the monomer sequence of the final macromolecule introducing different main chain and side chain motifs as well as varying the architecture of the final construct, e.g., from linear to branched.[31−34] We are specifically interested in the synthesis and characterization of glycomacromolecules, oligoamides with pending sugar ligands at specific positions within the side chains.[33−35] The glycomacromolecules are applied as tools to study complex binding mechanisms in multivalent sugar−lectin interactions, which are of high importance in various biological processes such as cell−cell interactions or pathogen recognition.[33−35] In recent studies and in agreement with previous work from other groups looking at glycopolymers derived from classical polymerization methods, we found that both the number and the spacing of sugar ligands along the macromolecular scaffold strongly influence complex formation with lectins.[34−43] However, SPS is limited in terms of the overall chain length, where for longer chains purity and yield of the desired macromolecular structure decrease significantly.

In order to access higher molecular weight glycopolymers while maintaining sequence control, we introduced the polymerization of monodisperse macromonomers derived from SPS via photoinduced thiol−ene coupling (TEC), resulting in multiblock copolymers with two strictly alternating blocks of well-defined sequences.[36] Macromonomers were functionalized either with terminal cysteine moieties, introducing the required thiol functionality, or with tailor-made

Received: May 8, 2018
Revised: June 25, 2018
Published: July 18, 2018

DOI: 10.1021/acs.macromol.8b00982
Macromolecules 2018, 51, 5608−5619

Scheme 1. Schematic Depiction of Macromonomers O1−O6 and Resulting Multiblock Copolymers P1−P6 after Polymerization with PEG(SH)$_2$-6000 and Structures of Applied Building Blocks

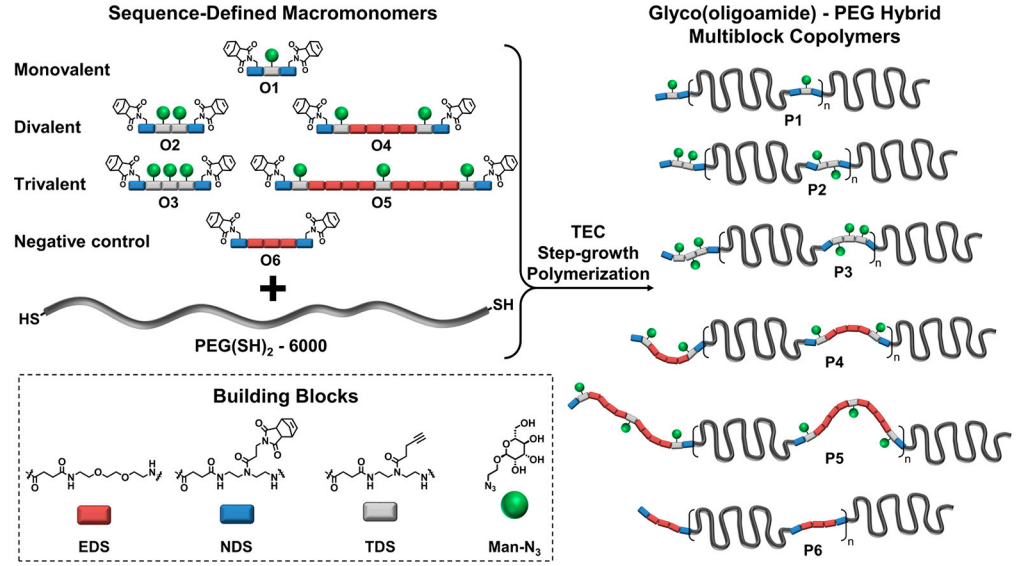

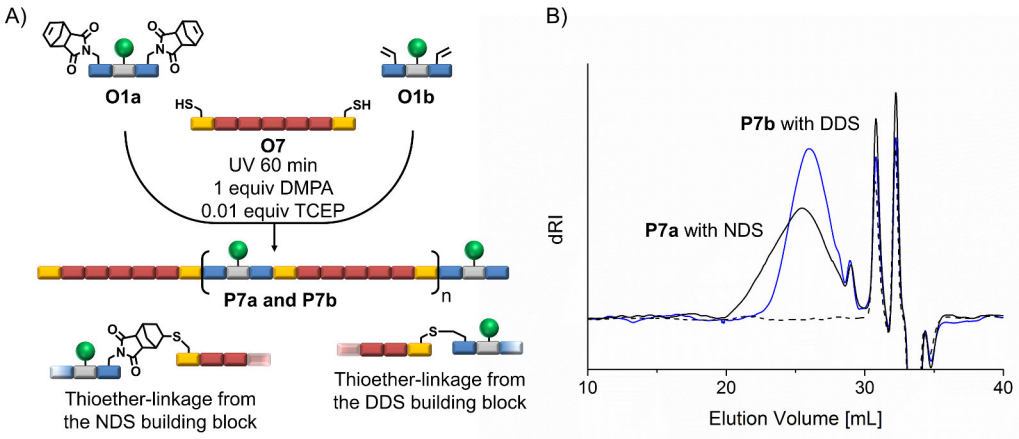

Figure 1. (A) Schematic overview of the polymerization of **O1a** and **O1b** with **O7** by TEC and their resulting polymers **P7a** and **P7b** with different thioether linkages resulting from the NDS and the DDS building blocks. (B) GPC-RI-LS elugrams from the glycopolymers **P7a** (black) and **P7b** (blue). Columns: Suprema Lux (2 × 100 and 1 × 1000 Å). Buffer: 50 mM NaH_2PO_4, 150 mM NaCl, 250 ppm of NaN_3 (pH 7.2), 30% ACN. Flow: 0.8 mL/min.

building blocks (DDS), introducing terminal alkene groups. Applying optimized thiol−ene reaction conditions, a first generation of sequence-controlled multiblock glycopolymers, containing α-D-mannopyranoside (Man) bearing binding and ethylene glycol-based nonbinding blocks in alternating fashion, was synthesized. Within the binding block, the number of Man ligands was varied from one to five while the nonbinding block was kept constant at a total of five ethylene glycol-based building blocks (EDS). Interestingly, for this first generation of multiblock glycopolymers we did not see an influence of the spacing on the resulting affinity toward model lectin Concanavalin A (Con A) but rather a pronounced effect of the overall number of Man ligands.[36]

In this work, we now extend on the concept of sequence-controlled multiblock glycopolymers, making use of the previously established polymerization method by thiol−ene polyaddition of sequence-defined macromonomers but using a higher molecular weight dithiol−poly(ethylene glycol) (PEG-$(SH)_2$) with a number-average molecular weight ($\bar{M}_n$) of 6000 Da as nonbinding spacer block. Furthermore, a novel building block (norbornene−diethylenetriamine−succinic acid, NDS) introducing a norbornene group as one of the most reactive alkene groups for thiol−ene coupling (TEC) was developed.[44] Thereby, sequence-controlled multiblock glycopolymers with high definition in the sugar ligand presenting block but overall higher molecular weight were targeted.

A schematic overview of the six macromonomers (**O1−O6**) as well as the resulting sequence-controlled glyco(oligoamide)−PEG hybrid multiblock copolymers (**P1−P6**) is shown in Scheme 1.

RESULTS AND DISCUSSION

Synthesis of a Novel Norbornene Bearing Building Block. To further improve the step-growth polymerization using TEC, a novel alkene bearing building block that can be used in SPS applying established coupling protocols was developed. The building block is a new component of our library of functional building blocks based on diethylenetriamine with a specific functional group on the centered secondary amine. The primary amines are functionalized by an

DOI: 10.1021/acs.macromol.8b00982
Macromolecules 2018, 51, 5608−5619

Scheme 2. Norbornene Building Block (NDS) Synthesis (Bottom) and the Synthesis of Its Precursors, the Protected Diethylenetriamine Key Intermediate 1 (Top), and the Norbornene Linker Acid Chloride 4 (Center)[a]

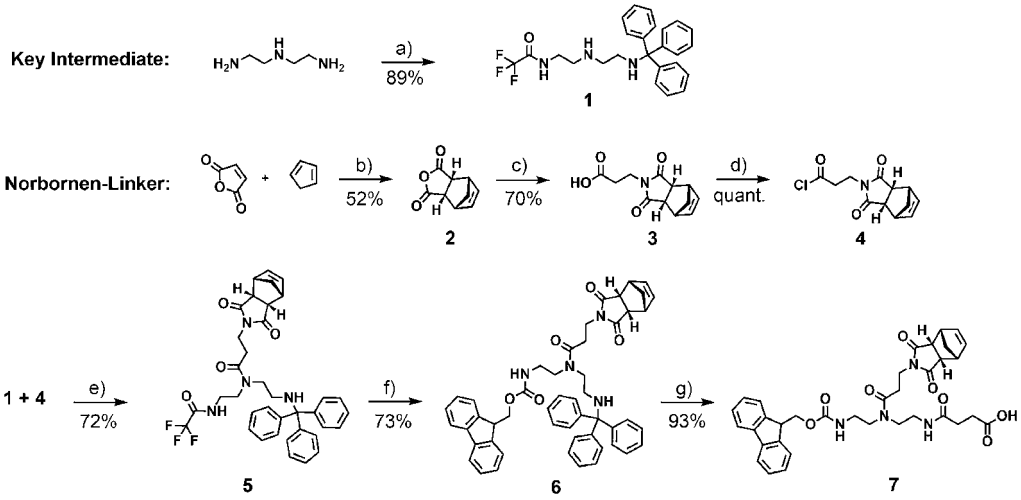

[a]Synthesis of key intermediate **1**: (a) TrtCl in DCM followed by EtOTFA in THF both at 0 °C. Synthesis of the norbornene linker **4**: (b) ethyl acetate and petroleum ether (60−80 °C) at 0 °C; (c) β-alanine and DABCO in toluene under reflux; (d) oxalyl chloride and cat. amounts of DMF in DCM at 0 °C. Synthesis of NDS **7**: (e) NEt_3 in DCM at 0 °C; (f) K_2CO_3 in water and methanol at 65 °C followed by FmocCl in THF and water at RT; (g) TFA and $^iPr_3SiH$ in DCM followed by succinic anhydride and NEt_3 in DCM both at RT.

Fmoc protection and a succinic acid group, similar to previously developed building blocks.[30,45] In contrast to the DDS building block previously used for thiol−ene chemistry[36] (Figure 1), the new NDS building block is equipped with a norbornene moiety in the side chain. Norbornenes have been described as one of the most reactive alkene groups for photoinduced thiol−ene click chemistry due to the high tension of the alkene bond within the ring structure.[44] A schematic overview of the synthesis of the norbornene building block is shown in Scheme 2. Synthesis followed previously established protocols, starting from the so-called key intermediate **1**.[30] In short, *N*-propionic acid-functionalized nadicimide (**3**) was chosen as norbornene linker which was coupled to the centered secondary amine of the key intermediate **1** after transformation into its acid chloride form **4**. Following established protocols[30] exchanging protection groups from intermediate **5**, first replacing the TFA group by an Fmoc group (**6**) and then the Trt group by a succinic acid group, the final NDS building block **7** was obtained in high purity (>98%) as confirmed by RP-HPLC, ^{1}H NMR, HRMS, and elementary analysis (for a detailed synthetic procedure as well as analytical data of the intermediates and product see the Supporting Information). In ^{1}H NMR spectra a broadening of signals and a presence of multiple signals for chemically equivalent protons were observed which we attribute to the presence of rotational isomers. Therefore, the ^{1}H NMR spectrum of **7** was recorded at 70 °C, showing signal sharpening and coalescence which also is in agreement with previous observations for similar building blocks.[33] The effect is not as pronounced compared to previous findings, but measurements at temperatures above 70 °C could not be conducted due to starting decomposition of the material (see the Supporting Information).

Coupling efficiency of NDS in SPS proved to be similar compared to other building blocks from our library when applying the same established coupling protocols using 5 equiv of the building block, 5 equiv of benzotriazol-1-yl-oxy-tris(pyrrolidino)phosphonium hexafluorophosphate (PyBOP) as coupling reagent, and 10 equiv of *N*,*N*-diisopropylethylamine (DIEA) (see Supporting Information). It was also possible to include NDS in the fully automated solid phase synthesis using a standard peptide synthesizer. In total, seven macromonomers **O1**−**O7** were synthesized in an automated fashion introducing norbornene end-groups (Scheme 1). Six of the macromonomers present Man ligands in varying valency from one to three and different spacing by introduction of additional EDS building blocks. Furthermore, an all EDS macromonomer was synthesized to be used as negative control in later binding studies. All macromonomers were obtained directly after cleavage from the resin with purities >93%. Main side products were identified as deletion sequences missing one or two building blocks. All macromonomers were further purified using preparative RP-HPLC to allow for a better stoichiometric control in later polyaddition reactions. Relative purities were determined by integration of UV signals in HPLC, and structures were confirmed by ^{1}H NMR and HRMS (see Supporting Information).

Comparison of Different Terminal Alkene Groups for the TEC Polymerization of Macromonomers. To prove the higher reactivity of the norbornene functionality on the novel NDS building block, a polymerization of a macromonomer with two terminal NDS moieties **O1a** was compared to macromonomer with two of the previously described DDS moieties **O1b**. Both macromonomers were polymerized with the same dithiol-terminated macromonomer **O7** using the same reaction conditions as previously optimized for the TEC polyaddition of similar macromonomers.[36] Macromonomers **O1a**, **O1b**, and **O7**, the resulting glycopolymers **P7a** and **P7b**, and the resulting thioether linkages from the NDS and DDS building blocks are schematically illustrated in Figure 1A. In short, polyaddition reaction was performed irradiating 10 μmol of each macromonomer for 60 min in the presence of 1 equiv of photoinitiator 2,2-dimethoxy-2-phenylacetophenone (DMPA) and 0.01 equiv of the reducing agent tris(2-carboxyethyl)phosphine hydrochloride (TCEP) in a mixture of DMSO and water with the ratio of 9/1 (total volume of

DOI: 10.1021/acs.macromol.8b00982
Macromolecules 2018, 51, 5608−5619

200 μL). Polymers **P7a** and **P7b** were isolated by multiple precipitation steps and analyzed using GPC-RI-LS, ^{1}H NMR, and MALDI-TOF analysis (see Supporting Information).

A degree of polymerization ($\bar{X}_n$) of 18 was achieved for oligomer **O1a** with terminal NDS moieties whereas only a $\bar{X}_n$ of 11 was achieved with **O1b** carrying the DDS moieties, indicating that with the norbornene building block the step-growth polymerization via TEC can be further improved toward higher $\bar{X}_n$. However, the dispersity of **P7a** was also significantly higher in comparison to polymer **P7b**, which according to Flory could be expected for polymerizations following a step-growth polymerization mechanism when reaching higher conversions.[46] Elugrams from GPC-RI-LS analysis of the glycopolymers **P7a** and **P7b** are shown in Figure 1B.

Synthesis of Glyco(oligoamide)−PEG Hybrid Multiblock Copolymers. For the polymerization of macromonomers **O1**−**O6** derived from SPS and PEG(SH)$_2$-6000 the reaction conditions had to be modified from previously optimized conditions. After only a few seconds of UV irradiation, the reaction mixture solidified due to the low solubility of the PEG-glyco-oligomer conjugates in DMSO/H_2O mixture with a ratio of 9/1 (50 mM of both monomers, 10 μmol in 200 μL), as used previously. Therefore, a ratio of 1/1 of DMSO/H_2O with a lower concentration of 25 mM for both monomers (20 μmol in a total of 800 μL) and a reaction temperature of 55 °C were applied, providing good solubility for both monomers as well as photoinitiator and reducing agent during the course of the reaction. The concentration of photoinitiator DMPA and reducing agent TCEP and a reaction time of 60 min were adapted from previous protocols. Each polymerization was performed twice independently to determine the reproducibility of the reaction. The final glyco(oligoamide)−PEG multiblock copolymers **P1**−**P6** were analyzed by GPC-RI-LS and ^{1}H NMR analysis (see Supporting Information). Analysis using MALDI-TOF was not successful. Determined molecular weights, dispersities, and degrees of polymerization are given in Table 1. Exemplarily structures of glyco(oligoamide) **O4**, the PEG(SH)$_2$-6000 macromonomer, and the resulting glycopolymer **P4** are illustrated in Scheme 3.

Measured $\bar{X}_n$ were significantly higher compared to those reported previously from the first series of multiblock glycopolymers.[36] This is especially true for **P1**−**P3** as well as **P6**, for which an average $\bar{X}_n$ of 45 was reached, resulting in 10-fold higher $\bar{M}_n$ compared to the previously synthesized glycopolymers. This could be related to the higher reactivity of the norbornene moiety in newly introduced NDS building block. Besides the norbornene group, the increased reaction temperature is also assumed to have a positive influence on the polymerization outcome, potentially increasing the diffusion rate of the monomers and preventing a strong increase in viscosity during the reaction. Indeed, when using lower reaction temperatures as in the case of **P7a**, $\bar{X}_n$ was found to be significantly lower (see achieved $\bar{X}_n$ for **P7a** in previous subsection). For glycopolymers **P4** and **P5**, $\bar{X}_n$ with an average value of 10 (not including the discordant value for batch 1 of **P4**) were found to be lower compared to the other glycopolymers **P1**−**P3** as well as **P6** and in a similar range as previously synthesized glycopolymers. However, achieved $\bar{M}_n$ are still significantly higher due to the use of the high molecular weight PEG(SH)$_2$-6000 macromonomer.

Furthermore, $\bar{X}_n$ for polymers **P1**−**P3**, obtained by polymerization of the short macromonomers **O1**−**O3** with PEG(SH)$_2$-6000, are significantly higher than for polymers **P4** and **P5**, derived from the longer macromonomers **O4** and **O5**. The highest $\bar{X}_n$ was achieved for **P1** from the shortest macromonomer **O1**. The size of the macromonomers seems to have an influence on the degree of polymerization, potentially due to the velocity of diffusion in the reaction mixture. Besides this, also other factors could influence the $\bar{X}_n$ such as differences in polarity or rigidity of the macromonomers **O1**−**O3** when compared to **O4** or **O5**, containing higher amounts of the EDS building block.

Table 1. Obtained $\bar{M}_w$, $\bar{M}_n$, $\bar{M}_w/\bar{M}_n$, and $\bar{X}_n$ for Polymers P1−P6 Determined by GPC-RI-LS Analysis (Each Polymerization Was Performed Twice)

macromonomer used	polymer	batch no.	$\bar{M}_w$[a] [kDa]	$\bar{M}_n$[a] [kDa]	$\bar{M}_w/\bar{M}_n$[a]	$\bar{X}_n$[b]
O1	**P1**	1	365.2	174.1	2.10	45
		2	360.2	162.5	2.22	42
O2	**P2**	1	375.1	183.9	2.04	44
		2	362.5	187.6	1.93	45
O3	**P3**	1	349.0	170.2	2.05	39
		2	329.1	130.5	2.52	30
O4	**P4**	1	488.8	305.0	1.60	66
		2	113.5	28.79	3.94	6
O5	**P5**	1	166.1	73.83	2.25	14
		2	157.5	61.05	2.58	11
O6	**P6**	1	366.1	238.5	1.54	60
		2	306.0	170.7	1.79	43

[a]Molecular weights and molecular weight distributions were determined using a GPC setup coupled to a RI and LS detector. The refractive index increment (dn/dc) was determined manually for the novel glyco(oligoamide)−PEG copolymers. [b]The $\bar{X}_n$ was calculated using the $\bar{M}_n$ and assuming that the ratio of glyco(oligoamide) and PEG(SH)$_2$-6000 in the final polymer is 1:1.

Unfortunately, reproducibility of the polymerizations was low with pronounced differences in the molecular weights and molecular weight distributions for different reactions using the same macromonomer (see Table 1). Here, especially the polymerization of macromonomer **O4** showed significant deviations within the two polymerizations as well as when compared to the polymerizations of the other macromonomers. The first polymerization of **O4** with PEG(SH)$_2$-6000 resulted in the largest polymer of all polymerizations with a $\bar{M}_n$ of approximately 240 kDa, which corresponds to a degree of polymerization of 60. For the second batch of the polymerization of **O4** the smallest $\bar{X}_n$ of this series was achieved.

Furthermore, elugrams of the final polymers showed multimodal distributions for most of the samples (see Figure 2A and Supporting Information). Besides the peak shape, it was also observed that the high molecular weight portion of the polymers show a slightly different slope when plotting the change in molecular weight against elution volume. Both these observations indicate a mixture of two different polymers assumingly due to formation of a side product. However, in ^{1}H NMR analysis, no further observations reinforcing our assumption were made, and MALDI-TOF analysis of the polymers was not successful. An exemplary GPC elugram of **P3** batch 2, showing the multimodal distribution and the difference in the slope of the molecular weight vs elution volume plot, is illustrated in Figure 2A. Therefore, in order to investigate potential side reactions during polyaddition reactions, several control experiments were performed.

DOI: 10.1021/acs.macromol.8b00982
Macromolecules 2018, 51, 5608−5619

Scheme 3. Step-Growth TEC Polymerization of Glyco(oligoamide) O4 with PEG(SH)$_2$-6000 and the Resulting Glyco(oligoamide)−PEG Multiblock Copolymer P4

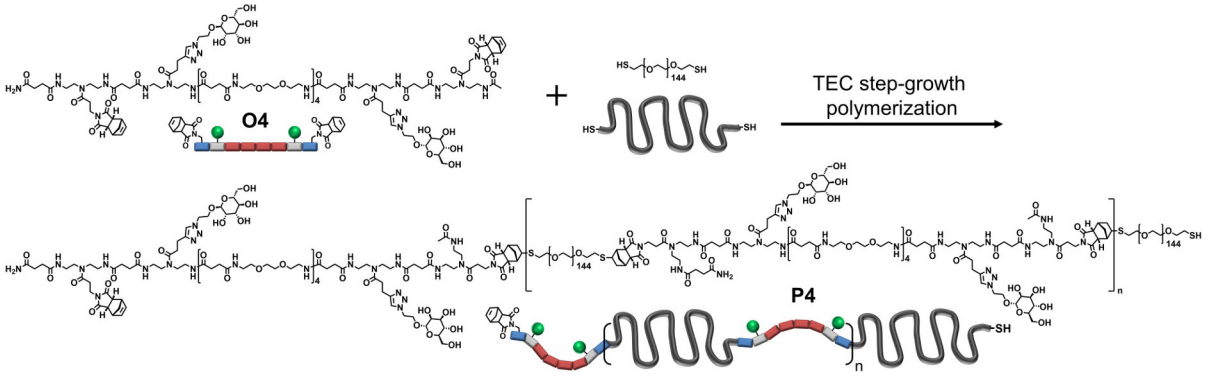

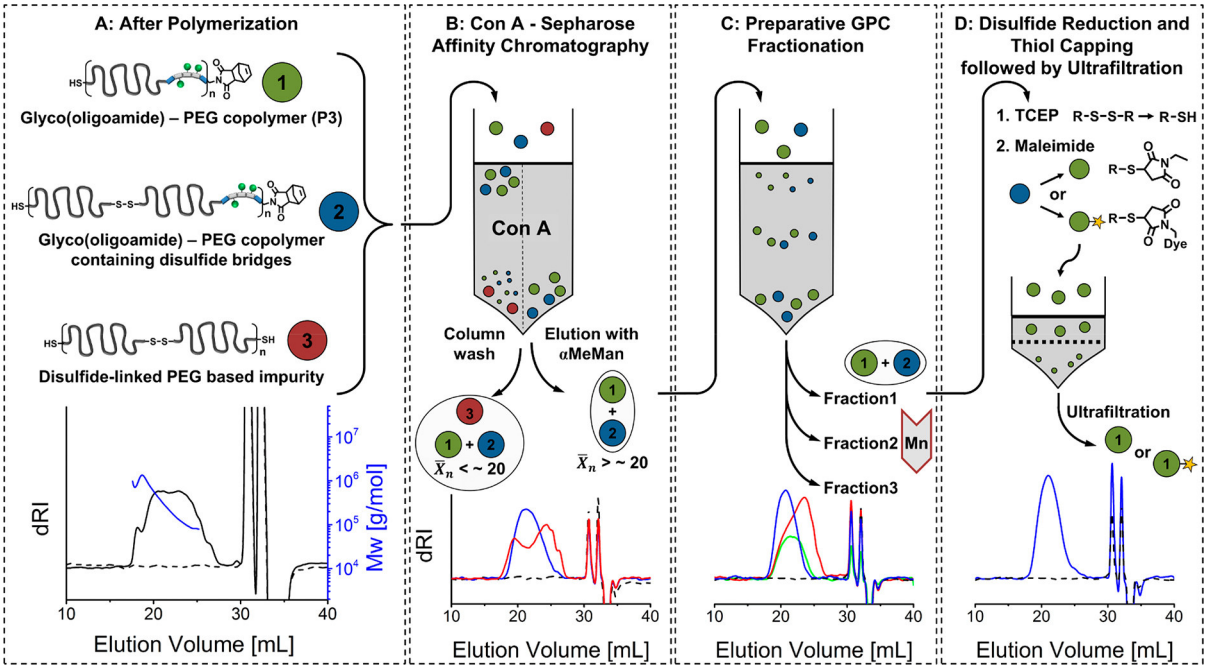

Figure 2. Overview of formed compounds using the example of the glyco(oligoamide)−PEG multiblock copolymer **P3** after synthesis as well as the separation of the two impurities applying different purification procedures. The purification procedures are illustrated schematically and the separation of a specific species is stated. Exemplary GPC-RI-LS elugrams after each purification step are shown. (A) Structure of desired product (1) as well as the two major side products (2 + 3) and GPC elugram (black) as well as the molecular weight plot (blue) for **P3**. (B) Illustration of purification by affinity chromatography and GPC elugram after washing (red) and elution (blue) process of **P3**. (C) Illustration of fractionation procedure by preparative GPC and GPC elugrams of the three separated fractions 1, 2, and 3 (blue, green, and red) of **P3**. (D) Illustration of disulfide reduction and thiol capping procedure and GPC elugram of the final purified glyco(oligoamide)−PEG multiblock copolymer **P3** (blue). GPC-RI-LS setup: columns: Suprema Lux (2 × 100 and 1 × 1000 Å); buffer: 50 mM NaH_2PO_4, 150 mM NaCl, 250 ppm of NaN_3 (pH 7.2), 30% ACN; flow: 0.8 mL/min.

Investigations of Potential Side Reactions in Step-Growth TEC Polymerization. During the TEC polymerization method development from previous work,[36] we found that functional groups of the macromonomers, e.g., the alcohol groups from the Man moieties, do not undergo side reactions. Consequently, we assume that potential side reactions can only occur with participation of the newly introduced NDS building block or the PEG(SH)$_2$-6000 macromonomer. An irradiation of the NDS bearing macromonomer **O1**, using the same polymerization conditions as used in the polymerizations of **P1**−**P6** without the addition of PEG(SH)$_2$-6000, was performed. As expected, only very small amounts of dimer and trimer were observed in GPC (see Supporting Information) since norbornene moieties have been shown to not undergo homopolymerization under the applied reaction conditions.[47]

The PEG(SH)$_2$-6000 macromonomer can theoretically undergo two different side reactions: First, an oxidation of the terminal thiol moieties to disulfides and thus a linkage of multiple PEG(SH)$_2$-6000 macromolecules are possible. To reduce such disulfides, the reducing agent TCEP was added to the reaction mixture. However, the amount might be too low to sufficiently reduce the disulfides of the high molecular weight PEG conjugates. Second, a radical transfer to the ethylene glycol of the PEG backbone can occur which could potentially lead to formation of a cross-linked network.[48] However, for the generation of radicals in the PEG backbone, usually higher amounts of radical initiators are required which

DOI: 10.1021/acs.macromol.8b00982
Macromolecules 2018, 51, 5608−5619

Table 2. Obtained $\bar{M}_n$ and $\bar{M}_w/\bar{M}_n$ for Oligoamide−PEG Copolymers P1−P6 after each Purification Step as Determined by GPC-RI-LS Analysis as well as Final $\bar{X}_n$ and Average Amount of Man Moieties (N) for the Final Structures

		affinity chromatography		preparative GPC fractionation			disulfide reduction and thiol capping			
macromonomer used	polymer	$\bar{M}_n$[a] [kDa]	$\bar{M}_w/\bar{M}_n$[a]	fraction	$\bar{M}_n$[a] [kDa]	$\bar{M}_w/\bar{M}_n$[a]	$\bar{M}_n$[a] [kDa]	$\bar{M}_w/\bar{M}_n$[a]	$\bar{X}_n$[b]	N (Man)
O1	**P1**	123.7	1.75	1	240.1	1.38	185.5	1.43	43	Ø 22
				2	127.5	1.70	130.8	1.55	32	Ø 16
				3	77.86	1.94				
O2	**P2**	123.5	1.81	1	235.2	1.35	195.2	1.39	44	Ø 44
				2	117.9	1.66	123.7	1.42	28	Ø 28
				3	66.74	2.04				
O3	**P3**	134.3	1.72	1	253.1	1.36	205.4	1.40	44	Ø 65
				2	143.0	1.62	153.8	1.51	33	Ø 49
				3	69.79	2.04				
O4	**P4**	114.3	1.72	1	222.1	1.34	152.7	1.43	31	Ø 31
				2	111.5	1.63	118.7	1.35	24	Ø 24
				3	64.24	1.95				
O5	**P5**	126.6	1.45	1	192.6	1.20	128.0	1.31	23	Ø 34
				2	135.8	1.29	102.7	1.33	19	Ø 28
				3	82.04	1.48	75.85	1.38	14	Ø 21
O6	**P6**						222.2	1.65	56	0

[a]Molecular weights and molecular weight distributions were determined using a GPC setup coupled to a RI and LS detector. The refractive index increment (dn/dc) was determined manually for glyco(oligoamide)−PEG copolymers. [b]The $\bar{X}_n$ was calculated using the $\bar{M}_n$ taking into account the determined ratio of oligoamide and PEG(SH)$_2$-6000 in the final polymer by ^{1}H NMR. See Supporting Information for the exact ratio in final copolymers.

is not the case for the used TEC polymerization conditions. Despite the fact that dithiol-PEGs are widely used in TEC reactions, in most studies no information about an ongoing side reaction is given or the oxidation is stated to be negligible.[49−52] In most cases the dithiol-PEGs are used to synthesize cross-linked hydrogels by TEC. Small amounts of disulfide bridges or cross-linking from the PEG chain in addition to the thioether bonds do not change the properties of the hydrogels, and a strict control of a sequence is not necessary. However, for our goal of synthesizing multiblock glyco(oligoamide)−PEG hybrid copolymers even small amounts of PEG-disulfides might strongly influence the final products.

Therefore, both possible side reactions were investigated by irradiating PEG(SH)$_2$-6000 without the presence of the norbornene bearing reaction partner varying the amount of reducing agent TCEP as well as photoinitiator DMPA. Furthermore, PEG-10000 without terminal thiol groups was irradiated using the TEC polymerization conditions (see Supporting Information for molecular weights, dispersities, and GPC elugrams for the control experiments).

We were able to show that the side product observed during TEC is most likely caused by formation of disulfide bonds of the PEG(SH)$_2$-6000. Only with increased amounts of reducing agent TCEP during TEC reaction, the formation of higher molecular weight compounds was significantly decreased. A decrease of the amount of DMPA did not have an effect on the homopolymerization of the PEG(SH)$_2$-6000, indicating that the side reaction does not depend on the amount of radicals and should be no cross-linking reaction. This is further supported by the obtained results of irradiating PEG-10000 without thiol moieties, which did not lead to the formation of any higher molecular weight compounds. To further support our assumption, the higher molecular weight PEG conjugates obtained in the control experiment (experiment using 0.01 equiv of TCEP and 1 equiv of DMPA) were incubated with TCEP to reduce the formed disulfides showing a reduction to the original $\bar{M}_n$, indicating complete cleavage of previously formed disulfide linkages.

To prevent the oxidation of the PEG thiol groups, polymerization was performed with higher amounts of the reducing agent TCEP (0.5 and 1 equiv). However, as already observed during previous method development, the degree of polymerization decreases significantly when further increasing the amount of TCEP caused by an occurring desulfurization reaction.[53,54] With the formation of terminal ethyl groups, which were determined by ^{1}H NMR (see Supporting Information), the reactive end-groups are lost, consequently resulting in the termination of the polymerization reaction.

Because of these findings, we assume that the large deviation between the different batches can be attributed to the ongoing side reaction, which is in some batches more pronounced compared to others e.g. due to different amounts of oxygen in the reaction.

Since an increase of the reducing agent TCEP is no option during polymerization, our next attempt was the separation of side products, isolating the targeted glyco(oligoamide)−PEG hybrid multiblock copolymers.

Purification of Glyco(oligoamide)−PEG Hybrid Multiblock Copolymers. From our control experiments, we assume that the major side product observed in the GPC analysis is based on PEG(SH)$_2$-6000 bridged by disulfides, with no or only very low amounts of glyco(oligoamide) blocks (disulfide-PEG impurity, Figure 2A). However, also glyco-

DOI: 10.1021/acs.macromol.8b00982
Macromolecules 2018, 51, 5608−5619

(oligoamide)−PEG copolymers containing higher amounts of PEG due to disulfide formation are possible (disulfide−copolymer impurity, Figure 2A). In order to isolate the desired glyco(oligoamide)−PEG copolymers and potentially decrease overall dispersity of the samples, a series of purification steps were performed. In short, first, disulfide−PEG impurities were removed via affinity chromatography. Second, fractionation via preparative GPC was performed, and third, reductive cleavage, maleimide capping, and purification via dialysis gave final glyco(oligoamide)−PEG multiblock copolymers (see Figure 2).

In the first step, affinity chromatography using Sepharose 4B resin containing immobilized Con A was performed (see Figure 2B). Multiblock glycopolymers with high Man valency will bind to the column material, whereas PEG and structures with low Man valency will be eluted off the column. Glycopolymers **P1**−**P5** from the two batches were pooled, dissolved in lectin binding buffer (LBB) (10 mM Hepes, 50 mM NaCl, 1 mM $MnCl_2$, 1 mM $CaCl_2$, pH 7.4), and applied to the Con A Sepharose 4B column. Polymer **P6**, not presenting Man moieties, could not be purified with the Con A Sepharose column. After extensive washing with LBB, glycopolymers bound to the column material were eluted using a solution of methyl-α-D-mannopyranoside (αMeMan) in LBB (0.1 M for **P1**, **P2**, **P4** and 0.2 M for **P3**, **P5**). After desalting by ultrafiltration and freeze-drying, polymer fractions from the washing as well as the elution procedure were analyzed by GPC-RI-LS and ^{1}H NMR analysis. GPC traces from the washing fractions of glycopolymers **P1**−**P5** showed two separated peaks, indicating a higher and a lower molecular weight polymer with low binding avidity to the Con A Sepharose column (see Supporting Information). The first signal (elution volume 17−22 mL) is assumed to be PEG-based homopolymer whereas the second peak (elution volume 22−27 mL) is low molecular weight glyco(oligoamide)−PEG copolymer with an insufficient Man valency to withstand the washing procedure of the Con A Sepharose column. ^{1}H NMR analysis gives glyco(oligoamide):PEG ratios of 0.7:1 for the washing fractions, additionally supporting this assumption. The amount of the PEG homopolymer is approximately 30% (integration of the GPC traces), which is in correspondence with the determined ratios of glyco(oligoamide) and PEG by ^{1}H NMR analysis in the isolated polymer mixture. GPC elugrams of glycopolymers after the elution procedure show unimodal distributions for all samples (see Supporting Information). An almost equimolar ratio of glyco(oligoamide) and PEG was determined by ^{1}H NMR analysis (0.95:1), indicating that the removal of PEG homopolymer was successful. Number-average molecular weights and dispersities of the purified glycopolymers are listed in Table 2 (column 1: affinity chromatography).

In the second step of purification, glycopolymers **P1**−**P5** were subjected to preparative GPC and fractionated into three samples. Negative control **P6** was not purified by preparative GPC. Fractions were desalted by ultrafiltration and freeze-dried before further GPC-RI-LS and ^{1}H NMR analysis. A successful decrease in dispersity of approximately 0.3 was achieved for the highest molecular weight fraction 1 of all glycopolymers. No improvement of the dispersities was observed for fractions 2 and 3 of glycopolymers **P1**−**P4** (see Supporting Information for GPC elugrams). Number-average molecular weights and dispersities for different fractions of **P1**−**P5** are listed in Table 2 (column 2: preparative GPC fractionation). Only fractions with dispersities lower 1.7 were used for further studies.

^{1}H NMR analysis of glycopolymers after these two purification procedures still indicates the presence of disulfide bonds, as the amount of $PEG(SH)_2$-6000 is always slightly higher than the amount of glyco(oligoamide). This is especially pronounced for higher molecular weight structures (fraction 1) of all glycopolymers. Therefore, following previously used protocols,[55] disulfides were reduced by incubating glycopolymers **P1**−**P5** as well as negative control **P6** for 48 h with high excess of TCEP (50 equiv) in degassed water. After the incubation, the reducing agent was removed by ultrafiltration, and terminal thiol groups were capped by reaction with *N*-ethylmaleimide (NEM) in high access (50 equiv) to prevent successive oxidation. Such reaction is also highly interesting for the introduction of a functional end-group to the glycopolymers such as a fluorophore or drug. To demonstrate this, parts of fraction 2 of **P2** as well as **P3** were functionalized with Alexa Fluor 488 C_5 maleimide using a slightly lower excess (15 equiv) as for the functionalization with NEM (see Supporting Information). Smaller fragments from the reductive treatment and capping reaction were removed from the samples by ultrafiltration with high molecular weight cut off membranes (MWCO 50 kDa and 100 kDa, depending on the sample; see Supporting Information). Determined molecular weights, dispersities, and degree of polymerization as well as the average Man valencies are listed in Table 2 (column 3: disulfide reduction and thiol capping).

For glycopolymers (fraction 1 of **P1**−**P4** as well as fractions 1−3 of **P5** and **P6**) purified using membranes with MWCO of 50 kDa after reductive treatment and capping, we observed a reduction in molecular weight but no change in dispersity. A further decrease in dispersity can be achieved when membranes with higher MWCO are used (as for fraction 2 of **P1**−**P4**), however, also resulting in substantial loss of material (about one-third of the material in comparison to yields after the previous step of purification).

For this final set of glyco(oligoamide)−PEG multiblock copolymers, we looked in more detail at the structural information accessible from the GPC-LS experiments. By plotting the R_g as a function of the molecular weight, information on the conformation of the polymer in solution can be derived from the resulting slope of the curve. For comparison, a PEG sample with a molecular weight of 100 kDa with an expected random coil conformation was measured. Calculated slopes for the conformation plots were slightly higher for structures **P1**−**P5** (average of 0.3) compared to the slope of PEG-100000 (0.23) (see Supporting Information), indicating that the glyco(oligoamide)−PEG multiblock copolymers also adapt a coiled conformation in solution but are less compact compared to PEG. For the negative control **P6** containing no sugar ligands in the oligoamide segment, a lower slope was determined (0.19). Thus, this data suggests that multiblock glycopolymers also adapt coiled conformation in solution but that sugar moieties seem to reduce intramolecular interaction, resulting in a less compact conformation compared to pure PEG. Without the presence of the sugar moieties, introduction of oligoamide segments seems to have the opposite effect, promoting intramolecular interactions e.g. via hydrogen bonding, leading to a slightly more compact structure in comparison to pure PEG.

DOI: 10.1021/acs.macromol.8b00982
Macromolecules 2018, 51, 5608−5619

Table 3. Determined Binding Constants K_A per Ligand and Normalized per Man Moiety in M^{-1} from SPR Direct Binding Assay as well as the Adhesion Reduction in % from SCP−Adhesion Assay Are Given for Final Oligoamide−PEG Copolymers P1−P6; Schematic Illustration of each Copolymer, the Number-Average Molecular Weight ($\bar{M}_n$), Molecular Weight Distribution ($\bar{M}_w/\bar{M}_n$), and the Resulting Average Man Valency (N)

Glycopolymer	Schematic illustration	N (Man)	$\bar{M}_n$[a] [kDa]	$\bar{M}_w/\bar{M}_n$[a]	K_A[b] Per Ligand [$\times 10^3$ M^{-1}]	K_A[b] Per Man [M^{-1}]	Adhesion Reduction[c] [%]
P1 F1		Ø 22	185.5	1.43	n.d.[d]	n.d.[d]	19.7 ± 3.3
P1 F2		Ø 16	130.8	1.55	n.d.[d]	n.d.[d]	n.m.[e]
P2 F1		Ø 44	195.2	1.39	18.3 ± 2.1	41.5 ± 4.8	39.6 ± 3.2
P2 F2		Ø 28	123.7	1.42	n.d.[d]	n.d.[d]	n.m.[e]
P3 F1		Ø 65	205.4	1.40	48.1 ± 3.9	74.0 ± 5.9	42.5 ± 3.9
P3 F2		Ø 49	153.8	1.51	30.5 ± 1.9	62.2 ± 3.9	n.m.[e]
P4 F1		Ø 31	152.7	1.43	21.2 ± 2.9	68.5 ± 9.3	30.1 ± 2.0
P4 F2		Ø 24	118.7	1.35	n.d.[d]	n.d.[d]	n.m.[e]
P5 F1		Ø 34	128.0	1.31	30.4 ± 1.7	89.3 ± 4.9	33.2 ± 3.7
P5 F2		Ø 28	102.7	1.33	28.4 ± 2.7	102 ± 9.6	28.7 ± 4.1
P5 F3		Ø 21	75.85	1.38	30.7 ± 2.7	146 ± 13	26.0 ± 4.3
P6	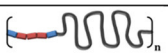	0	222.2	1.65	n.b.[f]	n.b.[f]	2.8 ± 2.4

[a] $\bar{M}_n$ and $\bar{M}_w/\bar{M}_n$ were determined using a GPC setup coupled to a RI and LS detector. The refractive index increment (dn/dc) was determined manually for glyco(oligoamide)−PEG copolymers. [b] Errors in K_A refer to the standard deviation from two independent experiments performing a duplicate determination for all oligoamide−PEG multiblock copolymers included in the SPR assay. [c] Errors in adhesion reduction refer to the standard deviation from three independent experiments for all oligoamide−PEG multiblock copolymers included in the SCP−adhesion assay. [d] Not determined (n.d.) as less than four binding events were observed for the five concentrations injected for this sample (see Supporting Information for details on SPR experiment and evaluation). [e] Not measured (n.m.). [f] No binding (n.b.).

Con A Binding Affinity and Adhesion Reduction of the Glyco(oligoamide)e−PEG Hybrid Multiblock Copolymers. In previous studies investigating the lectin binding of glycopolymers, we and others have found that a highly dense presentation of carbohydrate ligands along a polymeric backbone is not always beneficial for effective binding to a lectin receptor. In such highly functionalized polymers, not every sugar ligand can contribute to the binding, especially for multivalent binding events such as clustering of lectin receptors. Closely positioned ligands could even sterically interfere and thus negatively influence the binding event.[36−39,56,57] With this new series of multiblock glycopolymers now introducing higher molecular weight non-glycofunctionalized blocks through the introduction of the PEG(SH)$_2$-6000, we extend the spacing between the sugar ligand presenting blocks of the copolymer. Valency of the overall glycopolymer is varied both by the introduction of a defined number of sugar ligands within the glycofunctionalized block during solid phase assembly as well as through the resulting degree of polymerization after polyaddition reaction. Furthermore, for the di- and trivalent glycofunctionalized blocks, shorter and longer spacings are realized by addition of spacing building blocks (EDS) during solid phase assembly (Scheme 1). Overall, multiblock glycopolymers with similar degrees of polymerization ($\bar{X}_n$) and number-average molecular weights ($\bar{M}_n$) but different Man valencies, e.g. fractions 1 of structures **P1**−**P3**, but also structures with similar Man valencies but different molecular weights, e.g. fractions 1 of structure **P1** and fraction 3 of **P5**, are available for lectin binding studies using Con A as well established model lectin.[58,59] To allow for a comparison with our previous studies, we performed a similar direct binding assay using surface plasmon resonance (SPR) and immobilized Con A in its predominantly tetrameric form in LBB.[60,61] Following their binding to the Con A-functionalized chip surface, dissociation and binding constants K_D and K_A of multiblock glycopolymers were determined. Specifically, fractions 1 and 2 for each glycopolymer **P1**−**P4** as well as fractions 1, 2, and 3 for **P5** and the negative control **P6** were injected at five different concentrations between 0.25 and 20 μM in single cycle experiments. Each sample was measured four times. However, to our surprise, all structures showed dissociation constants K_D significantly above the highest concentration injected (see Supporting Information for K_D and R_{max} values), although for multiblock glycopolymers with low molecular weight spacers from previous study[36] K_D values below 20 μM were determined. Here, a structure of this first series of multiblock glycopolymers was included in the SPR measurements, and the K_D from previous SPR measurements[36] was reproduced showing the comparability of these studies. Binding affinities, stated in Table 3 as binding constants K_A (reciprocal value of K_D), of multiblock glycopolymers from the current series seem to be significantly lower in comparison to our first generation of multiblock glycopolymers,[36] although most of the structures present a higher Man valency. Besides low K_A values, also the fast association and especially dissociation indicate a weak interaction with the immobilized lectin, although no values for k_{on} and k_{off} were determined (see Supporting Information).

Overall, the results of this lectin binding study with multiblock glycopolymers show that the introduction of a higher molecular weight PEG chain into the glycopolymer structure and thereby reduction in overall ligand density as well as increase of steric repulsion has a negative effect on the binding affinity as determined by the direct binding assay. These results are in agreement with findings of the group of Fernandez-Megia[62] which showed that a PEGylation of their

DOI: 10.1021/acs.macromol.8b00982
Macromolecules 2018, 51, 5608−5619

glycodendrimers resulted in a reduction in lectin binding affinity. Potentially, this finding can be attributed to the coiled structure of the glyco(oligoamide)−PEG multiblock copolymers as was determined by GPC analysis. The PEG chains may shield Man moieties sitting on the inside of such a coil from interacting with the lectin receptor, which becomes more evident when normalizing the determined K_A values to the number of Man moieties (see Table 3). The relative contribution in binding of one Man moiety is higher for glyco(oligoamide)−PEG multiblock copolymers with lower molecular weights and lower PEG content, e.g., when comparing the three fractions of **P5**. Furthermore, previous studies looking at the binding of Man-functionalized PEG microgels[56] indicated that the conformational flexibility of the PEG chains might lead to negative entropic contributions upon binding to the receptor which could also occur for the multiblock copolymers. Thus, our results for the glyco(oligoamide)−PEG multiblock copolymers indicate that when decreasing the ligand density below a certain threshold, lowered accessibility and potential entropic contributions could decrease binding probability.

Another related structural feature that seems to play a key role in this direct binding assay is the molecular weight and overall size of the glyco(oligoamide)−PEG hybrid copolymers. When comparing for example the binding affinities of fractions 1 from **P2** and **P4**, both presenting two Man moieties in their binding block, we can see very similar K_A values despite the fact that fraction 1 of **P2** contains a significantly higher average Man valency. Also when comparing the three fractions of **P5**, an effect of the molecular weight can be observed. All three structures show similar binding constants, although the average Man valency decreases constantly from fractions 1 to 3. Since their molecular weight decreases along with the average valency, it could be reasoned that reduction in binding by decrease in valency is compensated by more favorable binding of lower weight polymers with reduced steric repulsion, leading in the end to similar affinities for all three structures. Similar observations of molecular weight influence on lectin binding were made previously e.g. by the groups of Stenzel,[37] Haddleton,[38] and Kiessling[39] also seeing a decrease in binding affinity toward Con A when increasing molecular weight of glycopolymers with similar valency.

When looking at the influence of the ligand presenting blocks within the glycopolymers, we observe highest binding affinities for the fractions 1 and 2 of **P3** as well as fractions 1, 2, and 3 of **P5**, carrying three Man moieties in their glycofunctionalized blocks. For fraction 1 of **P2** and **P4**, presenting two Man in the binding block, the determined values for K_A were smaller than for the other five structures despite having a similar or even a higher overall average Man valency, especially compared to the three fractions of **P5**. Comparing fraction 2 of **P4** with fraction 2 of **P5**, not only their average Man valencies but also their $\bar{M}_n$ as well as R_g are similar, indicating an affinity increasing effect when raising the amount of Man moieties within the binding block. A higher local concentration of Man ligands within the glycofunctionalized block might enhance statistical probability of binding to a receptor. Thus, when such a trivalent glycooligomer block is exposed and available for binding, it has a higher chance in binding than its divalent counterpart.

In addition to the direct binding assay, we also performed an adhesion reduction assay for selected multiblock glycopolymers. The assay is based on the so-called soft colloidal probe (SCP) adhesion, in which the adhesion energy of a Man-functionalized PEG microparticle on a Con A-functionalized glass surface is determined.[34,63] More in detail, the mechanical deformation of the SCPs upon their adhesion to the surface is detected and evaluated using the Johnson−Kendall−Roberts model.[64] Determination of the SCP mechanical deformation was done by evaluating the interference pattern formed by illuminating the planar Con A surface and adhered SCP with monochromatic light using reflection interference contrast microscopy (RICM). To perform an adhesion reduction assay, the adhesion of a Man-functionalized SCP on a Con A-functionalized glass slide was inhibited with 22 μM of glycopolymers **P1**−**P5** as well as the negative control **P6**. The decrease in SCP adhesion upon addition of this fixed concentration of glycopolymer normalized to the SCP adhesion without the presence of inhibitor in % is given in Table 3. The negative control **P6** did not show a reduction of the SCPs adhesion. The highest adhesion reduction was achieved for the glycopolymer presenting the highest amount of Man moieties (fraction 1 of **P3**), which was also the structure with the highest binding in the SPR direct binding assay. In general, for the adhesion reduction assay we can observe a strong dependency on the Man valency. The higher the Man valency, the better the potential of the multiblock glycopolymers to reduce the SCP adhesion to the Con A surface. This also means that fraction 1 of **P1** and fraction 3 of **P5**, both carrying a similar average amount of Man moieties (22 and 21 moieties, respectively), are able to reduce the SCP adhesion to a similar degree, although they exhibited different direct binding properties in the SPR study. When comparing the three fractions of **P5**, a decrease in adhesion reduction with decreasing Man valency as well as decreasing molecular weight can be observed. Thus, the molecular weight of the glycomimetic seems to contribute differently in an adhesion reduction assay than a direct binding situation.

CONCLUSION

Sequence-controlled multiblock copolymers by combining SPS and step-growth polymerization via photoinduced TEC with further increased $\bar{M}_n$ as well as $\bar{X}_n$ were realized, on the one hand, by using PEG(SH)$_2$-6000 macromonomers and, on the other, by applying norbornene end-groups. Norbornene moieties were introduced during SPS via a novel functional building block (NDS).

During polymerization, formation of a major side product was observed which is attributed to the oxidation of the PEG(SH)$_2$-6000 macromonomers resulting in their linkage via disulfide bonds. We were able to successfully remove this side product by affinity chromatography using a Sepharose column with immobilized Con A. For further improvement of dispersity, samples were fractionated by preparative GPC, and as last purification step, disulfide bonds within the sequence were reduced by incubation in reducing agent TCEP and liberated thiols subsequently capped with different maleimide derivatives preventing oxidation to disulfides.

A total of 12 glyco(oligoamide)−PEG multiblock copolymers were synthesized with dispersities below 1.55 after purification and a variation in their average Man amounts ranging from 65 to 16 moieties. All glycopolymers were subsequently applied in a direct binding as well as an adhesion reduction assay, investigating their interactions with model lectin Con A. We observed surprisingly low binding affinities for all glycopolymers which we attribute to the introduction of

DOI: 10.1021/acs.macromol.8b00982
Macromolecules 2018, 51, 5608−5619

the PEG blocks resulting in a decrease in ligand density as well as an increase in overall molecular weight, which increases steric repulsion. Both parameters have been shown to potentially decrease binding affinity of glycopolymers. This indicates that introducing a high molecular weight PEG as nonbinding spacing block has a negative influence on the binding to the Con A receptors. In contrast to the finding from the direct binding assay, results from the adhesion reduction assay exclusively show a correlation between the overall average Man valency and adhesion reduction whereas molecular weight or Man valency within a binding block does not seem to influence their ability to inhibit Man−Con A interactions.

Overall, combination of precision macromolecules derived from SPS and polymers from classical polymerization reactions via photoinduced TEC gives access to a large variety of multiblock copolymers with varying degrees of sequence control. We believe this is not only relevant for the synthesis of glycopolymers but can also be applied to other functional macromolecules and extends the overall realm of sequence-controlled, multifunctional polymers.

■ ASSOCIATED CONTENT

Supporting Information

The Supporting Information is available free of charge on the ACS Publications website at DOI: 10.1021/acs.macromol.8b00982.

Information about used materials and analytical methods; detailed synthetic procedures and analytical data of the NDS building block, the glyco-oligomers, and glycopolymers including control experiments and purification steps as well as data from the Con A binding and adhesion reduction assays (PDF)

■ AUTHOR INFORMATION

Corresponding Author

*(L.H.) E-mail: laura.hartmann@hhu.de; Ph +49 211 81-10360; Fax +49 211 81-15840.

ORCID

Laura Hartmann: 0000-0003-0115-6405

Notes

The authors declare no competing financial interest.

■ ACKNOWLEDGMENTS

We thank Mischa Baier and Julia Becker for their contributions during the NDS building block synthesis as well as Sophia Boden, Tanja Freichel, and Markus Giesler for their support during SPR analysis and data evaluation. We also thank Dr. Peter Tommes and Ralf Bürgel for performing HRMS and MALDI-TOF measurements as well as Maria Beuer for performing NMR measurements. The authors gratefully acknowledge support from the Boehringer-Ingelheim Foundation within the Perspektivenprogramm "Plus3" and the DFG for large equipment grant (INST 208/735-1).

■ ABBREVIATIONS

Man, α-D-mannopyranoside; TEC, thiol−ene coupling; SPS, solid phase synthesis; PEG, poly(ethylene glycol); Con A, Concanavalin A; DMPA, 2,2-dimethoxy-2-phenylacetophenone; TCEP, tris(2-carboxyethyl)phosphine hydrochloride; NEM, *N*-ethylmaleimide; LBB, lectin binding buffer; SPR, surface plasmon resonance; SCP−RICM, soft colloidal probe−reflection interference contrast microscopy; DDS, double bond−diethylenetriamine−succinic acid; NDS, norbornene−diethylenetriamine−succinic acid; TDS, triple bond−diethylenetriamine−succinic acid; EDS, ethylene glycol−diamine−succinic acid.

■ REFERENCES

(1) Grubbs, R. B.; Grubbs, R. H. 50th Anniversary Perspective: Living Polymerization—Emphasizing the Molecule in Macromolecules. *Macromolecules* **2017**, *50* (18), 6979−6997.

(2) Lutz, J. F. Defining the Field of Sequence-Controlled Polymers. *Macromol. Rapid Commun.* **2017**, *38* (24), 1700582.

(3) Martens, S.; Holloway, J. O.; Du Prez, F. E. Click and Click-Inspired Chemistry for the Design of Sequence-Controlled Polymers. *Macromol. Rapid Commun.* **2017**, *38* (24), 1700469.

(4) Solleder, S. C.; Schneider, R. V.; Wetzel, K. S.; Boukis, A. C.; Meier, M. A. R. Recent Progress in the Design of Monodisperse, Sequence-Defined Macromolecules. *Macromol. Rapid Commun.* **2017**, *38* (9), 1600711.

(5) Lutz, J.-F.; Ouchi, M.; Liu, D. R.; Sawamoto, M. Sequence-Controlled Polymers. *Science* **2013**, *341*, 1238149 6146.

(6) Ouchi, M.; Sawamoto, M. 50th Anniversary Perspective: Metal-Catalyzed Living Radical Polymerization: Discovery and Perspective. *Macromolecules* **2017**, *50* (7), 2603−2614.

(7) Huang, J.; Turner, S. R. Recent advances in alternating copolymers: The synthesis, modification, and applications of precision polymers. *Polymer* **2017**, *116*, 572−586.

(8) Abdouni, Y.; Yilmaz, G.; Becer, C. R. Sequence and Architectural Control in Glycopolymer Synthesis. *Macromol. Rapid Commun.* **2017**, *38* (24), 1700212.

(9) Grate, J. W.; Mo, K. F.; Daily, M. D. Triazine-Based Sequence-Defined Polymers with Side-Chain Diversity and Backbone−Backbone Interaction Motifs. *Angew. Chem., Int. Ed.* **2016**, *55* (12), 3925−3930.

(10) Ouchi, M.; Sawamoto, M. Sequence-controlled polymers via reversible-deactivation radical polymerization. *Polym. J.* **2018**, *50*, 83.

(11) Pan, X.; Tasdelen, M. A.; Laun, J.; Junkers, T.; Yagci, Y.; Matyjaszewski, K. Photomediated controlled radical polymerization. *Prog. Polym. Sci.* **2016**, *62*, 73−125.

(12) Gutekunst, W. R.; Hawker, C. J. A General Approach to Sequence-Controlled Polymers Using Macrocyclic Ring Opening Metathesis Polymerization. *J. Am. Chem. Soc.* **2015**, *137* (25), 8038−8041.

(13) Zhang, J.; Matta, M. E.; Hillmyer, M. A. Synthesis of Sequence-Specific Vinyl Copolymers by Regioselective ROMP of Multiply Substituted Cyclooctenes. *ACS Macro Lett.* **2012**, *1* (12), 1383−1387.

(14) Engelis, N. G.; Anastasaki, A.; Whitfield, R.; Jones, G. R.; Liarou, E.; Nikolaou, V.; Nurumbetov, G.; Haddleton, D. M. Sequence-Controlled Methacrylic Multiblock Copolymers: Expanding the Scope of Sulfur-Free RAFT. *Macromolecules* **2018**, *51* (2), 336−342.

(15) Porel, M.; Thornlow, D. N.; Artim, C. M.; Alabi, C. A. Sequence-Defined Backbone Modifications Regulate Antibacterial Activity of OligoTEAs. *ACS Chem. Biol.* **2017**, *12* (3), 715−723.

(16) Porel, M.; Brown, J. S.; Alabi, C. A. Sequence-Defined Oligothioetheramides. *Synlett* **2015**, *26* (05), 565−571.

(17) Jiang, Y.; Golder, M. R.; Nguyen, H. V. T.; Wang, Y.; Zhong, M.; Barnes, J. C.; Ehrlich, D. J. C.; Johnson, J. A. Iterative Exponential Growth Synthesis and Assembly of Uniform Diblock Copolymers. *J. Am. Chem. Soc.* **2016**, *138* (30), 9369−9372.

(18) Leibfarth, F. A.; Johnson, J. A.; Jamison, T. F. Scalable synthesis of sequence-defined, unimolecular macromolecules by Flow-IEG. *Proc. Natl. Acad. Sci. U. S. A.* **2015**, *112* (34), 10617−10622.

(19) Driessen, F.; Du Prez, F. E.; Espeel, P. Precision Multisegmented Macromolecular Lineups: A Display of Unique Control over Backbone Structure and Functionality. *ACS Macro Lett.* **2015**, *4* (6), 616−619.

DOI: 10.1021/acs.macromol.8b00982
Macromolecules 2018, 51, 5608−5619

(20) Wu, Y.-H.; Zhang, J.; Du, F.-S.; Li, Z.-C. Dual Sequence Control of Uniform Macromolecules through Consecutive Single Addition by Selective Passerini Reaction. *ACS Macro Lett.* **2017**, *6* (12), 1398−1403.
(21) Amrane, M. I.; Chouikhi, D.; Badi, N.; Lutz, J. F. Synthesis of Well-Defined Polystyrene Rink Amide Soluble Supports and Their Use in Peptide Synthesis. *Macromol. Chem. Phys.* **2014**, *215* (20), 1984−1990.
(22) Martens, S.; Van den Begin, J.; Madder, A.; Du Prez, F. E.; Espeel, P. Automated Synthesis of Monodisperse Oligomers, Featuring Sequence Control and Tailored Functionalization. *J. Am. Chem. Soc.* **2016**, *138* (43), 14182−14185.
(23) Telitel, S.; Petit, B. E.; Poyer, S.; Charles, L.; Lutz, J.-F. Sequence-coded ATRP macroinitiators. *Polym. Chem.* **2017**, *8* (34), 4988−4991.
(24) Al Ouahabi, A.; Charles, L.; Lutz, J.-F. Synthesis of Non-Natural Sequence-Encoded Polymers Using Phosphoramidite Chemistry. *J. Am. Chem. Soc.* **2015**, *137* (16), 5629−5635.
(25) Edwardson, T. G. W.; Carneiro, K. M. M.; Serpell, C. J.; Sleiman, H. F. An Efficient and Modular Route to Sequence-Defined Polymers Appended to DNA. *Angew. Chem., Int. Ed.* **2014**, *53* (18), 4567−4571.
(26) De Bo, G.; Kuschel, S.; Leigh, D. A.; Lewandowski, B.; Papmeyer, M.; Ward, J. W. Efficient Assembly of Threaded Molecular Machines for Sequence-Specific Synthesis. *J. Am. Chem. Soc.* **2014**, *136* (15), 5811−5814.
(27) Ouchi, M.; Nakano, M.; Nakanishi, T.; Sawamoto, M. Alternating Sequence Control for Carboxylic Acid and Hydroxy Pendant Groups by Controlled Radical Cyclopolymerization of a Divinyl Monomer Carrying a Cleavable Spacer. *Angew. Chem., Int. Ed.* **2016**, *55* (47), 14584−14589.
(28) Ida, S.; Ouchi, M.; Sawamoto, M. Designer Template Initiator for Sequence Regulated Polymerization: Systems Design for Substrate-Selective Metal-Catalyzed Radical Addition and Living Radical Polymerization. *Macromol. Rapid Commun.* **2011**, *32* (2), 209−214.
(29) Merrifield, R. B. Solid Phase Peptide Synthesis. I. The Synthesis of a Tetrapeptide. *J. Am. Chem. Soc.* **1963**, *85* (14), 2149−2154.
(30) Ponader, D.; Wojcik, F.; Beceren-Braun, F.; Dernedde, J.; Hartmann, L. Sequence-Defined Glycopolymer Segments Presenting Mannose: Synthesis and Lectin Binding Affinity. *Biomacromolecules* **2012**, *13* (6), 1845−1852.
(31) Wojcik, F.; Mosca, S.; Hartmann, L. Solid-Phase Synthesis of Asymmetrically Branched Sequence-Defined Poly/Oligo-(amidoamines). *J. Org. Chem.* **2012**, *77* (9), 4226−4234.
(32) Ebbesen, M. F.; Gerke, C.; Hartwig, P.; Hartmann, L. Biodegradable poly(amidoamine)s with uniform degradation fragments via sequence-controlled macromonomers. *Polym. Chem.* **2016**, *7* (46), 7086−7093.
(33) Baier, M.; Giesler, M.; Hartmann, L. Split-and-Combine Approach Towards Branched Precision Glycomacromolecules and Their Lectin Binding Behavior. *Chem. - Eur. J.* **2018**, *24* (7), 1619−1630.
(34) Ponader, D.; Maffre, P.; Aretz, J.; Pussak, D.; Ninnemann, N. M.; Schmidt, S.; Seeberger, P. H.; Rademacher, C.; Nienhaus, G. U.; Hartmann, L. Carbohydrate-Lectin Recognition of Sequence-Defined Heteromultivalent Glycooligomers. *J. Am. Chem. Soc.* **2014**, *136* (5), 2008−2016.
(35) Igde, S.; Röblitz, S.; Müller, A.; Kolbe, K.; Boden, S.; Fessele, C.; Lindhorst, T. K.; Weber, M.; Hartmann, L. Linear Precision Glycomacromolecules with Varying Interligand Spacing and Linker Functionalities Binding to Concanavalin A and the Bacterial Lectin FimH. *Macromol. Biosci.* **2017**, *17* (12), 1700198.
(36) Gerke, C.; Ebbesen, M. F.; Jansen, D.; Boden, S.; Freichel, T.; Hartmann, L. Sequence-Controlled Glycopolymers via Step-Growth Polymerization of Precision Glycomacromolecules for Lectin Receptor Clustering. *Biomacromolecules* **2017**, *18* (3), 787−796.
(37) Chen, Y.; Lord, M. S.; Piloni, A.; Stenzel, M. H. Correlation between Molecular Weight and Branch Structure of Glycopolymers Stars and Their Binding to Lectins. *Macromolecules* **2015**, *48* (2), 346−357.
(38) Gou, Y.; Geng, J.; Richards, S.-J.; Burns, J.; Remzi Becer, C.; Haddleton, D. M. A Detailed Study on Understanding Glycopolymer Library and Con A Interactions. *J. Polym. Sci., Part A: Polym. Chem.* **2013**, *51* (12), 2588−2597.
(39) Gestwicki, J. E.; Cairo, C. W.; Strong, L. E.; Oetjen, K. A.; Kiessling, L. L. Influencing Receptor−Ligand Binding Mechanisms with Multivalent Ligand Architecture. *J. Am. Chem. Soc.* **2002**, *124* (50), 14922−14933.
(40) Loka, R. S.; McConnell, M. S.; Nguyen, H. M. Studies of Highly-Ordered Heterodiantennary Mannose/Glucose-Functionalized Polymers and Concanavalin A Protein Interactions Using Isothermal Titration Calorimetry. *Biomacromolecules* **2015**, *16* (12), 4013−4021.
(41) Nagao, M.; Fujiwara, Y.; Matsubara, T.; Hoshino, Y.; Sato, T.; Miura, Y. Design of Glycopolymers Carrying Sialyl Oligosaccharides for Controlling the Interaction with the Influenza Virus. *Biomacromolecules* **2017**, *18* (12), 4385−4392.
(42) Lavilla, C.; Yilmaz, G.; Uzunova, V.; Napier, R.; Becer, C. R.; Heise, A. Block-Sequence-Specific Glycopolypeptides with Selective Lectin Binding Properties. *Biomacromolecules* **2017**, *18* (6), 1928−1936.
(43) Yilmaz, G.; Uzunova, V.; Hartweg, M.; Beyer, V.; Napier, R.; Becer, C. R. The effect of linker length on ConA and DC-SIGN binding of S-glucosyl functionalized poly(2-oxazoline)s. *Polym. Chem.* **2018**, *9* (5), 611−618.
(44) Northrop, B. H.; Coffey, R. N. Thiol−Ene Click Chemistry: Computational and Kinetic Analysis of the Influence of Alkene Functionality. *J. Am. Chem. Soc.* **2012**, *134* (33), 13804−13817.
(45) Wojcik, F.; O'Brien, A. G.; Götze, S.; Seeberger, P. H.; Hartmann, L. Synthesis of Carbohydrate-Functionalised Sequence-Defined Oligo(amidoamine)s by Photochemical Thiol-Ene Coupling in a Continuous Flow Reactor. *Chem. - Eur. J.* **2013**, *19* (9), 3090−3098.
(46) Flory, P. J. Fundamental Principles of Condensation Polymerization. *Chem. Rev.* **1946**, *39* (1), 137−197.
(47) Fairbanks, B. D.; Schwartz, M. P.; Halevi, A. E.; Nuttelman, C. R.; Bowman, C. N.; Anseth, K. S. A Versatile Synthetic Extracellular Matrix Mimic via Thiol-Norbornene Photopolymerization. *Adv. Mater.* **2009**, *21* (48), 5005−5010.
(48) Lee, W.; Choi, D.; Lee, Y.; Kim, D.-N.; Park, J.; Koh, W.-G. Preparation of micropatterned hydrogel substrate via surface graft polymerization combined with photolithography for biosensor application. *Sens. Actuators, B* **2008**, *129* (2), 841−849.
(49) Fairbanks, B. D.; Love, D. M.; Bowman, C. N. Efficient Polymer-Polymer Conjugation via Thiol-ene Click Reaction. *Macromol. Chem. Phys.* **2017**, *218* (18), 1700073.
(50) McCall, J. D.; Anseth, K. S. Thiol−Ene Photopolymerizations Provide a Facile Method To Encapsulate Proteins and Maintain Their Bioactivity. *Biomacromolecules* **2012**, *13* (8), 2410−2417.
(51) Sawicki, L. A.; Kloxin, A. M. Design of thiol-ene photoclick hydrogels using facile techniques for cell culture applications. *Biomater. Sci.* **2014**, *2* (11), 1612−1626.
(52) Tan, V. T. G.; Nguyen, D. H. T.; Utama, R. H.; Kahram, M.; Ercole, F.; Quinn, J. F.; Whittaker, M. R.; Davis, T. P.; Gooding, J. J. Modular photo-induced RAFT polymerised hydrogels via thiol-ene click chemistry for 3D cell culturing. *Polym. Chem.* **2017**, *8* (39), 6123−6133.
(53) Wan, Q.; Danishefsky, S. J. Free-Radical-Based, Specific Desulfurization of Cysteine: A Powerful Advance in the Synthesis of Polypeptides and Glycopolypeptides. *Angew. Chem., Int. Ed.* **2007**, *46* (48), 9248−9252.
(54) Bondalapati, S.; Jbara, M.; Brik, A. Expanding the chemical toolbox for the synthesis of large and uniquely modified proteins. *Nat. Chem.* **2016**, *8*, 407.
(55) Boden, S.; Wagner, K. G.; Karg, M.; Hartmann, L. Presenting Precision Glycomacromolecules on Gold Nanoparticles for Increased Lectin Binding. *Polymers* **2017**, *9* (12), 716.

DOI: 10.1021/acs.macromol.8b00982
Macromolecules 2018, 51, 5608−5619

(56) Schmidt, S.; Wang, H.; Pussak, D.; Mosca, S.; Hartmann, L. Probing multivalency in ligand−receptor-mediated adhesion of soft, biomimetic interfaces. *Beilstein J. Org. Chem.* **2015**, *11*, 720−729.
(57) Bhatia, S.; Camacho, L. C.; Haag, R. Pathogen Inhibition by Multivalent Ligand Architectures. *J. Am. Chem. Soc.* **2016**, *138* (28), 8654−8666.
(58) Sumner, J. B.; Howell, S. F. Identification of Hemagglutinin of Jack Bean with Concanavalin A. *J. Bacteriol.* **1936**, *32* (2), 227−237.
(59) Edelman, G. M.; Cunningham, B. A.; Reeke, G. N.; Becker, J. W.; Waxdal, M. J.; Wang, J. L. The Covalent and Three-Dimensional Structure of Concanavalin A. *Proc. Natl. Acad. Sci. U. S. A.* **1972**, *69* (9), 2580−2584.
(60) Hardman, K. D.; Ainsworth, C. F. Structure of concanavalin A at 2.4-Ang resolution. *Biochemistry* **1972**, *11* (26), 4910−4919.
(61) Gupta, D.; Dam, T. K.; Oscarson, S.; Brewer, C. F. Thermodynamics of Lectin-Carbohydrate Interactions: Binding of the core trimannoside of asparagine-linked carbohydrates and deoxy analogs to concanavalin a. *J. Biol. Chem.* **1997**, *272* (10), 6388−6392.
(62) Fernandez-Villamarin, M.; Sousa-Herves, A.; Correa, J.; Munoz, E. M.; Taboada, P.; Riguera, R.; Fernandez-Megia, E. The Effect of PEGylation on Multivalent Binding: A Surface Plasmon Resonance and Isothermal Titration Calorimetry Study with Structurally Diverse PEG-Dendritic GATG Copolymers. *ChemNanoMat* **2016**, *2* (5), 437−446.
(63) Pussak, D.; Ponader, D.; Mosca, S.; Ruiz, S. V.; Hartmann, L.; Schmidt, S. Mechanical Carbohydrate Sensors Based on Soft Hydrogel Particles. *Angew. Chem., Int. Ed.* **2013**, *52* (23), 6084−6087.
(64) Johnson, K. L.; Kendall, A.; Roberts, D. Surface energy and the contact of elastic solids. *Proc. R. Soc. London, Ser. A* **1971**, *324* (1558), 301−313.

DOI: 10.1021/acs.macromol.8b00982
Macromolecules 2018, 51, 5608−5619

Supporting Information

Sequence-controlled high molecular weight glycooligoamide – PEG multiblock copolymers as ligands and inhibitors in lectin binding

Christoph Gerke, Fawad Jacobi, Laura E. Goodwin, Franziska Pieper, Stephan Schmidt, Laura Hartmann*

Institute of Organic and Macromolecular Chemistry, Heinrich-Heine University Düsseldorf, Universitätsstraße 1, 40225 Düsseldorf, Germany

* Correspondence to Tel: +49 211 81-10360; Fax: +49 211 81-15840;
E-mail: laura.hartmann@hhu.de

Materials:

Dimethyl sulfoxide (DMSO) (≥ 99.9%), 2,2-dimethoxy-2-phenylacetophenone (DMPA) (99%), diethyl ether (with BHT as inhibitor, ≥ 99.8%), triisopropylsilane (TIPS) (98%), (+)-sodium-L-ascorbate (≥ 99.0%), manganese (II) chloride tetrahydrate (≥ 99%), sodium diethyldithiocarbamate trihydrate (≥ 99%), acetic acid (99.8%), conc. hydrochloric acid (p.a.), 1,4-diazabicyclo[2.2.2]octane (DABCO) (≥ 99%), 3-aminopropionic acid (≥ 99%) and *N*-ethylmaleimide (NEM) (≥ 98%) were all purchased from Sigma-Aldrich. *N,N*-Diisopropylethylamine (DIEA) (≥ 99%) and tris(2-carboxyethyl)phosphine hydrochloride (TCEP) (≥ 98%) were purchased by Carl Roth. Methanol (100%) and acetic anhydride (99.7%) were purchased from VWR BDH Prolabo Chemicals. Dimethylformamide (DMF) (99.8%, for peptide synthesis), piperidine (99%), copper (II) sulfate (98%), cyclopentadiene (95%) trityl chloride (Trt-Cl) (98%), maleic anhydride (99%), succinic anhydride (99%) and methyl-α-D-mannopyranoside (αMeMan) (≥ 99%) were purchased Acros Organics. Dichloromethane (DCM) (99.99%), sodium chloride (99.98%), 4-(2-hydroxyethyl)-1-piperazineethanesulfonic acid (HEPES) (99%), tetrahydrofuran (THF) (analytical reagent grade), ethyl acetate (analytical reagent grade), sodium hydrogen carbonate (analytical reagent grade), toluene (analytical reagent grade), triethylamine (≥ 99%) and Alexa Fluor™ 488 C_5 maleimide were purchased from Fisher Scientific. Tentagel S RAM (Rink Amide) resin (Capacity 0.23 mmol/g) and poly(ethylene glycol) dithiol MW 6000 Dalton were purchased from Rapp Polymere. Calcium chloride (≥ 97%), potassium carbonate (99%) and citric acid monohydrate (for analysis) were purchased from AppliChem. Oxalyl chloride (98%) and sodium methoxide (98%) were purchased from Alfa Aesar. Trifluoroacetic acid (TFA) (99%) and benzotriazol-1-yl-oxy-tris-(pyrrolidino)-phosphonium hexafluorophosphate (PyBOP) were purchased from Fluorochem. Concanavalin A was purchased from LKT Laboratories. Sodium sulfate (anhydrous) was purchased from Caelo. *N*-alpha-(9-Fluorenylmethyloxycarboxyl)-S-trityl-L-cysteine (Fmoc-L-Cys(Trt)-OH) (99.9%) was purchased from Iris Biotech. 9-Fluorenylmethoxycarbonyl chloride (FmocCl) (98%) was purchased from ChemPur. AG® 1-X8 Anion Exchange Resin, analytical grade, 100–200 mesh, acetate form was purchased from Bio Rad. Con A Sepharose 4B was purchased from GE Healthcare Life Sciences. Vivaspin 6 and 20 ultrafiltration concentrators with MWCO of 5, 50 and 100 kDa were purchased from VWR. Water was purified with a Milli-Q system (Millipore) obtaining a final resistivity of 18 MΩcm.

Instrumentation

Nuclear Magnetic Resonance spectroscopy (NMR)

^{1}H-NMR (600 MHz) and ^{13}C-NMR (151 MHz) spectra were recorded on a Bruker AVANCE III - 600. Chemical shifts of all NMR spectra were reported in delta (δ) expressed in parts per million (ppm). The signal of residual solvent was used as internal standard (For ^{1}H-NMR: δ 4.79 ppm for D_2O, δ 7.26 ppm for $CDCl_3$, δ 2.50 ppm for DMSO-d_6 and for ^{13}C-NMR δ 77.16 ppm for $CDCl_3$, δ 39.52 ppm for DMSO-d_6). The following abbreviations are used to indicate the multiplicities: s, singlet; d, doublet; dd, doublet of doublets; dt, doublet of triplets; t, triplet; m multiplet. All measurements were performed at 25°C if not stated otherwise.

Reversed Phase - High Pressure Liquid Chromatography - Mass Spectrometry (RP-HPLC-MS)

Measurements were performed on an Agilent 1260 Infinity instrument coupled to a variable wavelength detector (VWD) (set to 214 nm) and a 6120 Quadrupole LC/MS containing an Electrospray ionization (ESI) source (operated in positive ionization mode in a m/z range of 200 to 2000). As HPLC column a MZ-Aqua Perfect C18 (3.0×50 mm, 3 µm) RP Column from MZ Analysetechnik was used. The mobile phases A and B were H_2O/ACN (95/5) and H_2O/ACN (5/95), respectively. Both mobile phases contained 0.1% of formic acid. The flow rate was set to 0.4 mL/min. NDS intermediates **5** and **6** as well as final NDS **7** were analyzed using a liner gradient starting with 80% mobile phase A reaching 80% mobile phase B within 30 min. Oligoamides **O1** – **O7** and NDS intermediate **3** were analyzed using a linear gradient starting with 100% mobile phase A reaching 50% mobile phase B within 30 min. The temperature of the column compartment was set to 25 °C. UV and MS spectral analysis was done within the OpenLab ChemStation software for LC/MS from Agilent Technologies.

Preparative Reversed Phase – High Pressure Liquid Chromatography (Preparative RP-HPLC)

For the purification of the glycooligomers an Agilent 1260 Infinity instrument coupled to a variable wavelength detector (VWD) (set to 214 nm) and an automated fraction collector (FC) was used. For the purification of the glycooligomers as RP-HPLC column a CAPCELL PAK C18 (20×250 mm, 5 µm) was used. The mobile phases A and B were H_2O and ACN, respectively. Both mobile phases contained 0.1% of formic acid. The flow rate was set to 20 ml/min. The gradient was varied for each compound and is stated in the analytical data for each compound.

Ultra High Resolution - Mass Spectrometry (UHR-MS)

UHR-MS measurements were performed with a Bruker UHR-QTOF maXis 4G instrument with a direct inlet via syringe pump, an ESI source and a quadrupole followed by a Time Of Flight (QTOF) mass analyzer.

Matrix-Assisted Laser Desorption Ionization- Time Of Flight – Mass Spectrometry (MALDI-TOF-MS)

Compounds were analyzed using a Bruker MALDI-TOF Ultraflex I system with 2,5-dihydroxybenzoic acid (DHB) as matrix. The ratio of matrix to compound were 10:1 and 1:1. Spectra were acquired in both linear, for a m/z range of 1000-4000, and reflector mode for a m/z range 2000-20000. The reflector mode was calibrated using a protein mixture whereas the linear mode was not calibrated.

Gel Permeation Chromatography (GPC) analysis

GPC was performed using an Agilent 1200 series HPLC system equipped with three aqueous GPC columns from Polymer Standards Service (PSS) Mainz, Germany (Suprema Lux analytical 8 mm diameter, 5 µm particle size, precolumn of 50 mm, 2× 100 Å of 300 mm, 1000 Å of 300 mm). MilliQ water with 50 mM NaH_2PO_4, 150 mM NaCl, 250 ppm NaN_3 and of pH7 + 30% ACN, filtered through an inline 0.1 µm membrane filter, was used as GPC eluent with a flow rate of 1 mL/min. UV spectra were recorded on a Waters 486 Tunable Absorbance Detector. Multi-angle light scattering- and differential refractive index spectra were recorded using a miniDAWN TREOS and Optilab rEX, respectively, that were both from Wyatt Technologies EU. Data analysis was performed using the Astra 5 software using measured dn/dc values of 0.111 mL/g for poly(ethylene glycol) samples, 0.130 mL/g for oligoamide – PEG hybrid copolymers (**P1** – **P6**) and 0.156 mL/g for the poly(amidoamine) **P7**. All dn/dc values were determined prior to the analysis of the samples.

UV-Vis photometer

UV measurements were performed with a SPECORD 210 PLUS UV-Vis photometer from Analytik Jena AG. The instrument was operated using Win ASPECT PLUS software. For determination of the fulvene-piperidine adduct, a Spectral Scan from 290-310 nm was performed. All measurements were performed in a 3.5 mL precision quartz glass cuvette from Carl Roth GmbH + Co. KG.

UV-lamp

A TQ150 Hg medium pressure UV lamp from Haraeus Nobellight GmbH with a quartz glass immersion and cooling tube from Peschl Ultraviolet GmbH was used for Thiol-Ene click reactions.

Freeze dryer

The final oligomers and polymers were freeze dried with an Alpha 1-4 LD plus instrument from Martin Christ Freeze Dryers GmbH. The Main Drying method was set to -42 °C and 0.1 mbar.

Peptide Synthesizer

Oligomers **O2** – **O7** were synthesized on an automated peptide synthesizer CS136X from CS Bio.

Building block synthesis

Synthesis of building blocks DDS[2], EDS[3] and TDS[4] as well as the synthesis of 2-azidoethyl-α-D-Mannopyranoside[4] were reported earlier.

Synthesis and characterization of the NDS building block

Key Intermediate synthesis

2,2,2-trifluoro-*N*-(2-((2-(tritylamino)ethyl)amino)ethyl)acetamide (**1**) was synthesized according to a previously published method.[4]

Synthesis of (3aR,4S,7R,7aS)-3a,4,7,7a-tetrahydro-4,7-methanoisobenzofuran-1,3-dione (2)

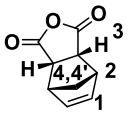

The reaction of cyclopentadiene and maleic anhydride was performed according to a protocol from literature.[5] 50 mL of dicyclopentadiene were freshly distilled. The temperature of the oil-bath was set to 180 °C and the transition temperature should not exceed 45 °C. The collector flask with cyclopentadiene was cooled with an ice bath to prevent dimerization. The freshly distilled cyclopentadiene has to be applied directly in the following reaction step. 24.18 g (245 mmol) maleic anhydride were dissolved in 80 mL ethyl acetate followed by an addition of 60 mL petroleum ether (60-80 °C). The solution was cooled with an ice bath to 0 °C. 33 mL (380 mmol) cyclopentadiene in 25 mL petroleum ether were added in three portions using a dropping funnel. The mixture was stirred for another 10 min. Compound **2** crystallized in the reaction mixture and the crystals were filtered under vacuum and dried under high vacuum. 21.3 g (130 mmol, 53%) of compound **2** were isolated as white crystals. The *endo* norbornene product was formed exclusively as confirmed by ^{1}H-NMR.

^{1}H-NMR (600 MHz, $CDCl_3$): δ 6.43 – 6.08 (m, 2H, 1), 3.59 – 3.53 (m, 2H, 3), 3.47 – 3.42 (m, 2H, 2), 1.75 – 1.69 (m, 1H, 4 or 4'), 1.57 – 1.52 (m, 1H, 4 or 4') ppm.

^{13}C-NMR (151 MHz, $CDCl_3$): δ 171.5, 135.5, 52.7, 47.1, 46.1 ppm.

HR-ESI-MS for $C_9H_8O_3$ (Exact monoisotopic mass 164.0473 g/mol): $[M+H]^+$ calcd. 165.0546, found 165.0546, mass accuracy 0.00 ppm.

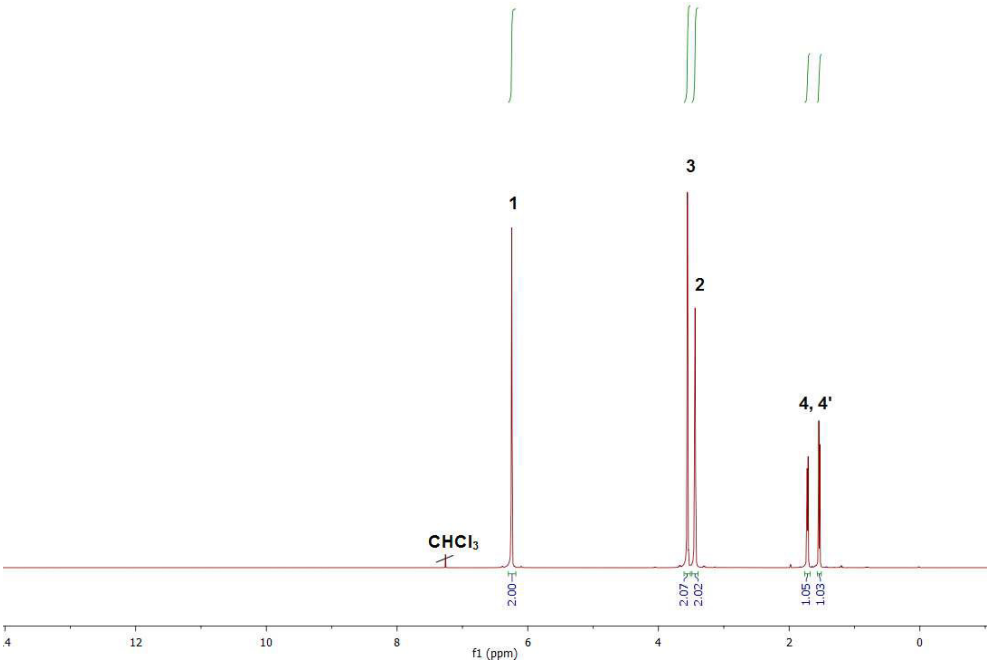

Figure S1: ^{1}H-NMR (600 MHz, $CDCl_3$) of compound **2**.

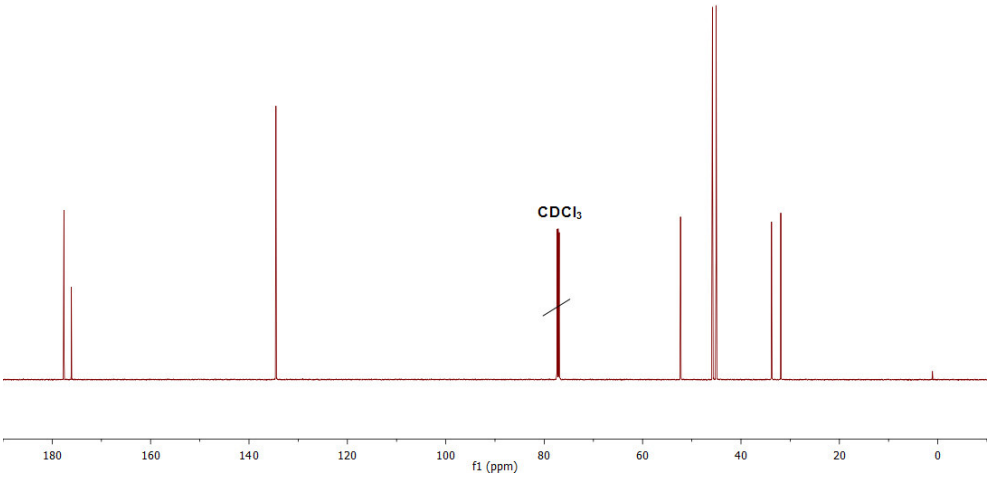

Figure S2: ^{13}C-NMR (151 MHz, $CDCl_3$) of compound **2**.

Synthesis of 3-((3aR,4S,7R,7aS)-1,3-dioxo-1,3,3a,4,7,7a-hexahydro-2H-4,7-methanoisoindol-2-yl)propanoic acid (3)

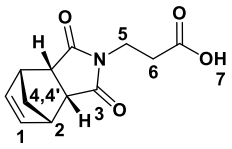

The reaction of **2** and 3-aminopropionic acid (ß-alanine) was performed according to the published protocol from Zhang et al.[6] The protocol was changed and 1,4-diazabicyclo[2.2.2]octan (DABCO) was used as base instead of triethylamine (TEA). The amount of base used remained equal. Reaction mixture was refluxed for only 7 h instead of 12 h.

Compound **2** (16.4 g, 100 mmol), 3-aminopropionic acid (11.6 g, 130 mmol), and 1,4-diazabicyclo[2.2.2]octan (DABCO) (1.5 mg, 13 mmol) were dissolved in 60 mL toluene. The mixture was refluxed for 7 h using a Dean-Stark apparatus. After refluxing, the reaction solution was cooled and concentrated under reduced pressure. The crude solid was dissolved in chloroform (300 mL) and washed using acidic water (pH = 1) (3 × 200 mL). After drying the chloroform phase with anhydrous Na_2SO_4, the chloroform was removed under reduced pressure giving 16.5 g (70%) of compound **3** as white solid.

^{1}H-NMR (600 MHz, $CDCl_3$): δ 10.56 (s, 1H, 7), 6.06 (t, *J* = 2.0 Hz, 2H, 1), 3.62 (t, *J* = 7.5 Hz, 2H, 5), 3.39 – 3.33 (m, 2H, 2), 3.27 – 3.22 (m, 2H, 3), 2.51 (t, *J* = 7.5 Hz, 2H, 6), 1.70 (dt, *J* = 8.8, 1.7 Hz, 1H, 4 or 4'), 1.51 (dt, *J* = 8.8, 1.5 Hz, 1H, 4 or 4') ppm.

^{13}C-NMR (151 MHz, $CDCl_3$): δ 177.6, 176.1, 134.5, 52.3, 45.8, 45.1, 33.8, 31.9 ppm.

HR-ESI-MS for $C_{12}H_{13}NO_4$ (Exact monoisotopic mass 235.0845 g/mol): $[M+H]^+$ calcd. 236.0917; found 235.0917; mass accuracy 0.00 ppm.

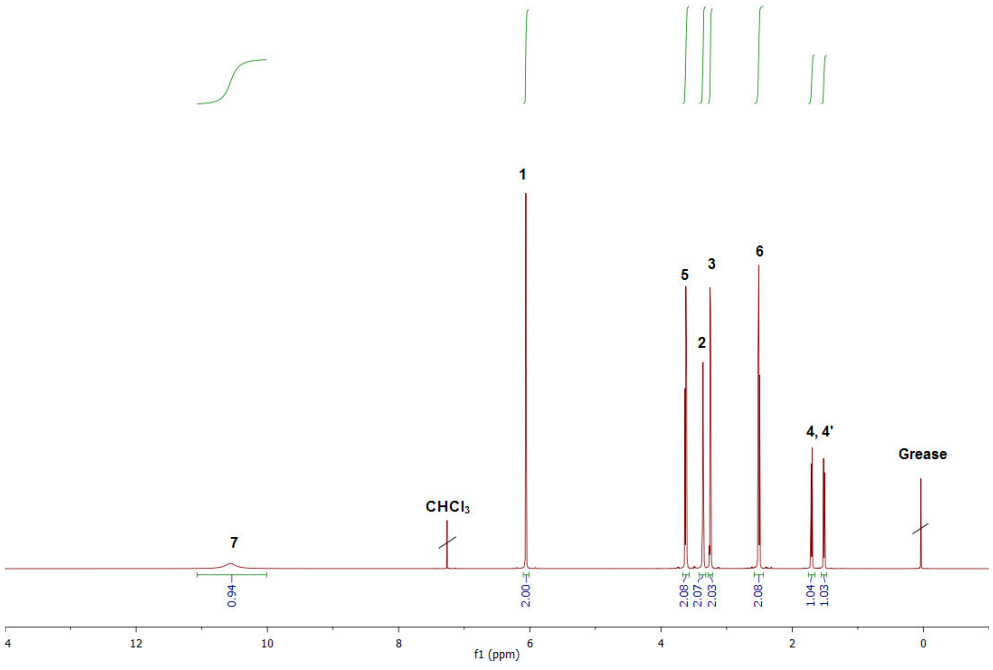

Figure S3: ^{1}H-NMR (600 MHz, $CDCl_3$) of compound **3**.

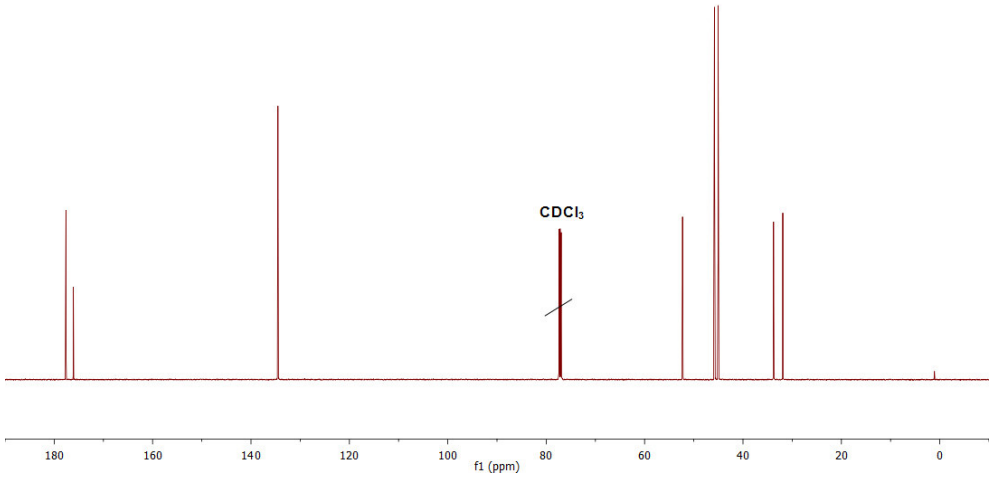

Figure S4: ^{13}C-NMR (151 MHz, $CDCl_3$) of compound **2**.

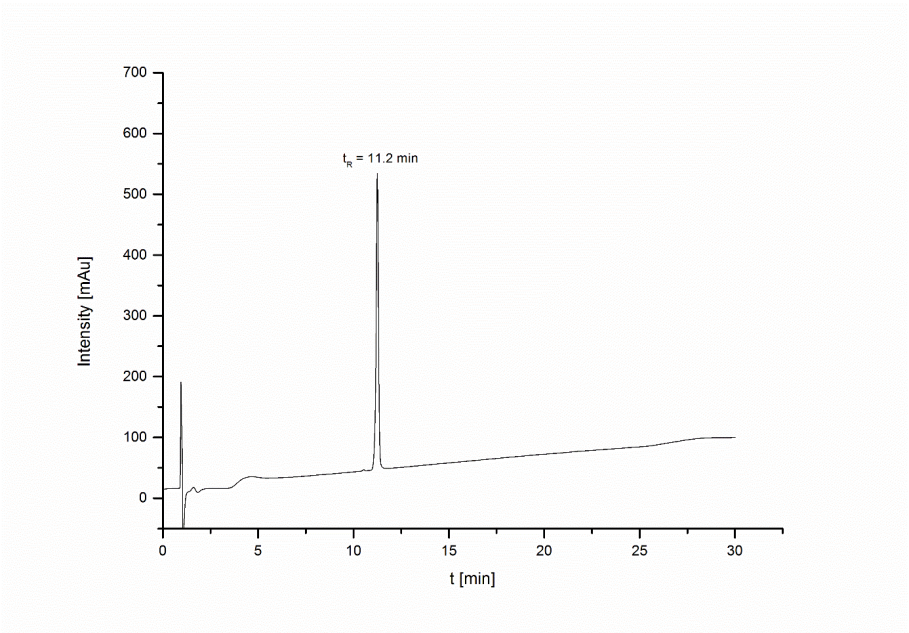

Figure S5: RP-HPLC analysis (linear gradient from 0 - 50% eluent B in 30 min at 25 °C) chromatogram of compound **2.**

Synthesis of 3-((3aR,4S,7R,7aS)-1,3-dioxo-1,3,3a,4,7,7a-hexahydro-2H-4,7-methanoisoindol-2-yl)propanoyl chloride (4)

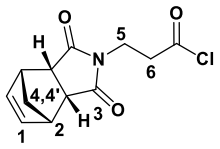

To a solution of **3** (12.8 g, 54.4 mmol) in 100 mL DCM and 0.1vol% DMF at 0°C, oxalyl chloride (7 ml, 10.36 g, 81.6 mmol) was added dropwise and the reaction was stirred for an additional 2h at room temperature. The solvent and the remaining oxalyl chloride were removed under reduced pressure giving a yellow solid. Product **4** was obtained in quantitative yield (13.8 g, 54.4 mmol) and used in the next reaction step without further purification.

^{1}H-NMR (600 MHz, $CDCl_3$): δ 6.07 (t, *J* = 1.9 Hz, 2H, 1), 3.65 (t, *J* = 7.0 Hz, 2H, 5), 3.41 – 3.33 (m, 2H, 2), 3.27 – 3.22 (m, 2H, 3), 3.06 (t, *J* = 7.0 Hz, 2H, 6), 1.72 (dt, *J* = 8.8, 1.7 Hz, 1H, 4 or 4'), 1.52 (dt, *J* = 8.9, 1.5 Hz, 1H, 4 or 4') ppm.

^{13}C-NMR (151 MHz, $CDCl_3$): δ 177.12, 171.29, 134.58, 52.33, 45.81, 45.10, 44.22, 33.58 ppm.

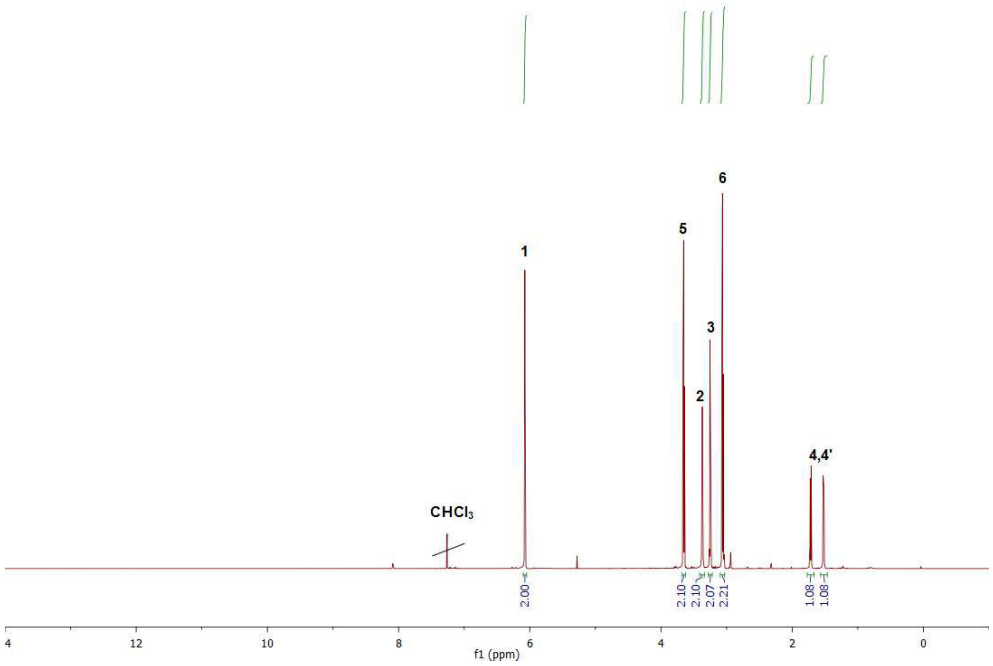

Figure S6: ^{1}H-NMR (600 MHz, $CDCl_3$) of compound **4**.

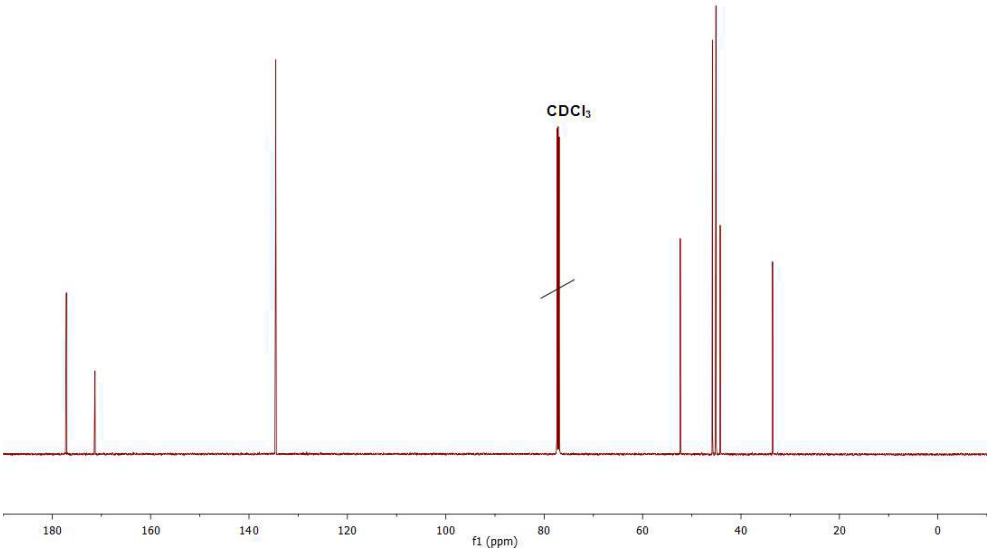

Figure S7: ^{13}C-NMR (151 MHz, $CDCl_3$) of compound **4**.

Synthesis of 3-((3aR,4S,7R,7aS)-1,3-dioxo-1,3,3a,4,7,7a-hexahydro-2H-4,7-methanoisoindol-2-yl)-*N*-(2-(2,2,2-trifluoroacetamido)ethyl)-*N*-(2-(tritylamino)ethyl)propanamide (5)

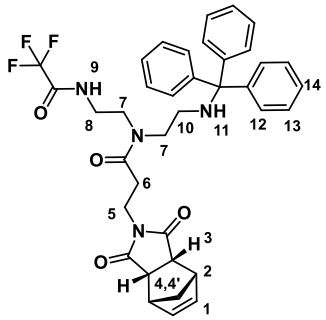

Compound **1** (20.0 g, 45.3 mmol) and triethylamine (12.5 mL, 9.1 g, 90 mmol) in DCM (350 mL) were cooled to 0°C under inert atmosphere. The norbornen linker chloride **4** (13.8 g, 54.4 mmol) was dissolved in 50 mL DCM and added dropwise to the reaction mixture. The mixture was stirred for an additional 3 hours at room temperature and was subsequently washed three times with sat. $NaHCO_3$ (250 ml). The DCM was dried with Na_2SO_4 and concentrated under reduced pressure. The crude product was dried under high vacuum and crystallized from methanol giving **5** (21.5 g, 32.6 mmol, 72%) as a white solid.

^{1}H-NMR (600 MHz, $CDCl_3$): δ 8.07 – 7.99 (m, 1H, 9), 7.44 – 7.37 (m, 6H, 12), 7.34 – 7.27 (m, 6H, 13), 7.24 – 7.15 (m, 3H, 14), 6.11 – 6.04 (m, 2H, 1), 3.67 (t, *J* = 7.3 Hz, 2H, 5), 3.51 – 3.31 (m, 9H, 2+7+8+11), 3.29 – 3.21 (m, 2H, 3), 2.69 (t, *J* = 7.3 Hz, 2H, 6), 2.35 – 2.22 (m, 2H, 10), 1.72 (dt, *J* = 8.9, 1.7 Hz, 1H, 4 or 4'), 1.53 (dt, *J* = 8.8, 1.5 Hz, 1H, 4 or 4') ppm.

^{13}C-NMR (151 MHz, DMSO-d_6): δ 177.20, 170.26, 169.24, 156.74 – 155.91 (m), 145.98, 134.29, 128.27, 127.71, 126.06, 116.81, 114.90, 70.34, 70.25, 51.53, 47.76, 46.67, 45.66, 45.15, 44.32, 43.58, 42.40, 42.00, 37.68, 37.08, 34.05, 30.67, 30.01 ppm.

RP-HPLC (linear gradient from 20 - 80% eluent B in 30 min at 25 °C): t_R = 17.4 min. Determined purity: > 98%.

HR-ESI-MS for $C_{37}H_{37}F_3N_4O_4$ (Exact monoisotopic mass 658.2767 g/mol): $[M+H]^+$ calcd. 659.2840; found 659.2851; mass accuracy 1.67 ppm.

Elemental analysis calcd (%) for $C_{37}H_{37}F_3N_4O_4$: C 67.47, H 5.66, N 8.51; found: C 67.29, H 5.75, N 8.28.

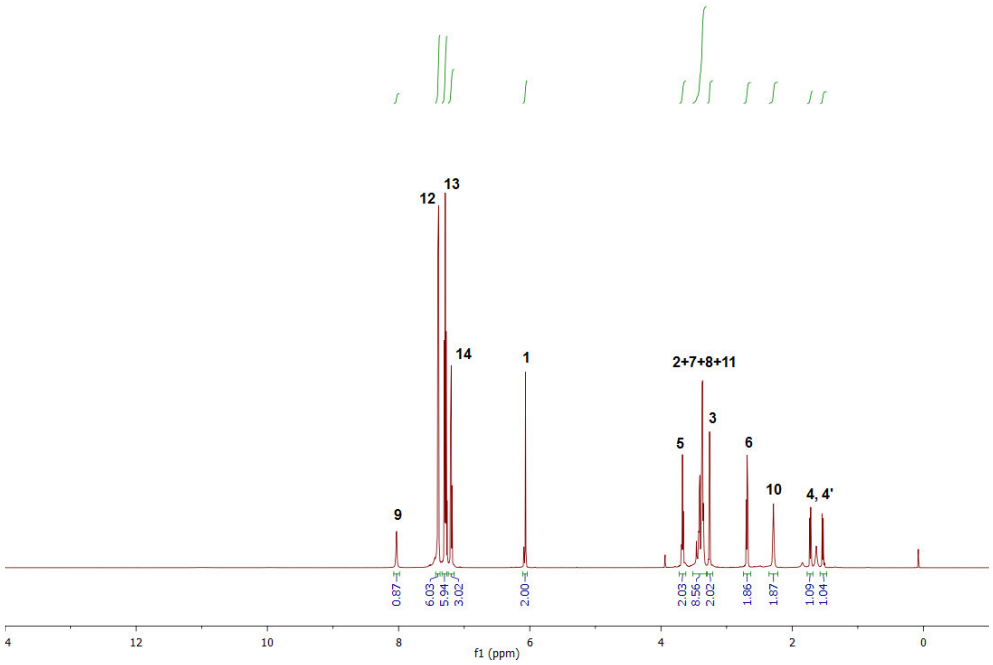

Figure S8: ^{1}H-NMR (600 MHz, $CDCl_3$) of compound **5**.

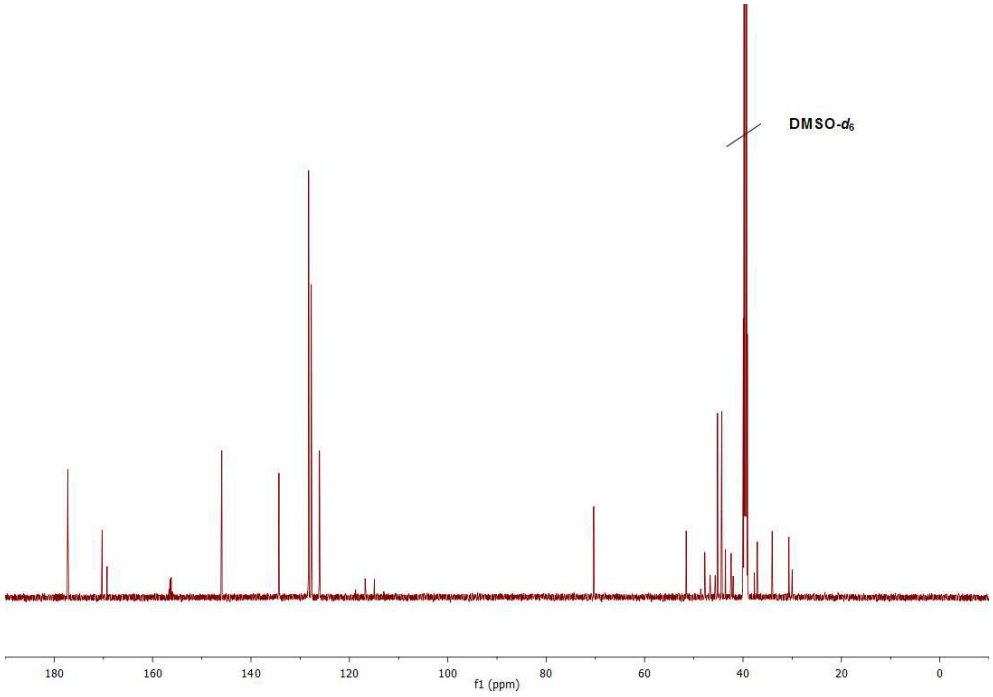

Figure S9: ^{13}C-NMR (151 MHz, DMSO-d_6) of compound **5**.

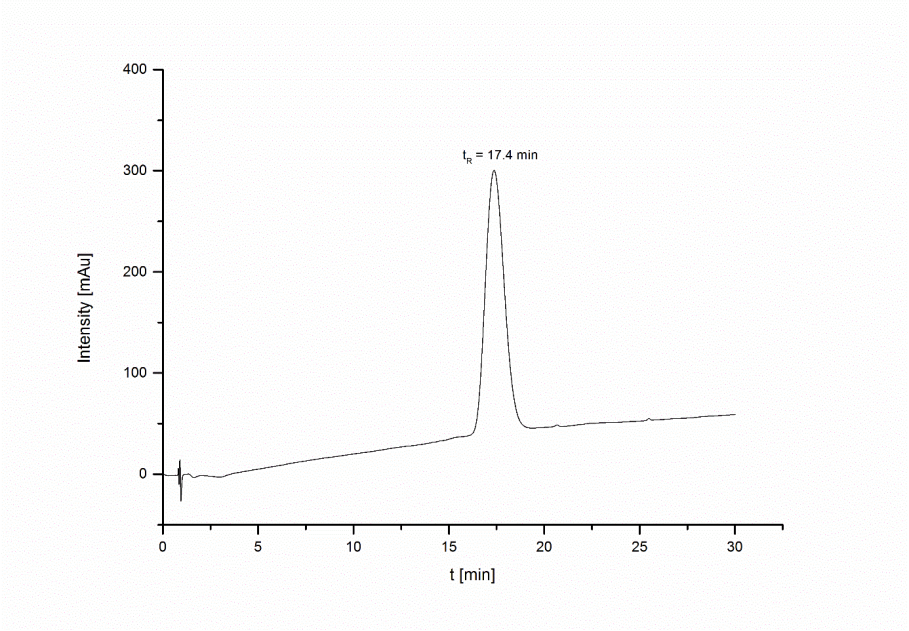

Figure S10: RP-HPLC analysis (linear gradient from 20 - 80% eluent B in 30 min at 25 °C) chromatogram of compound **5** ..

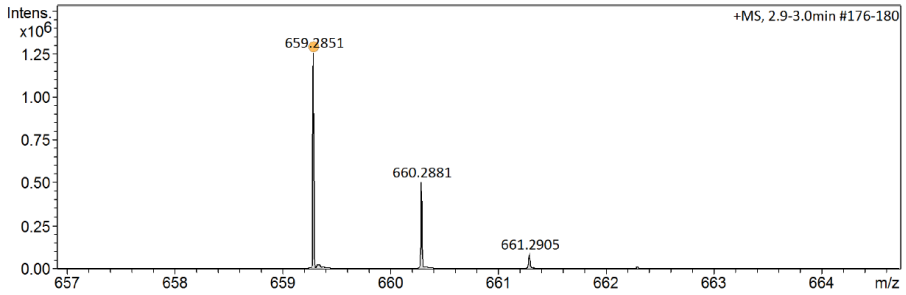

Figure S11: HR-MS (ESI$^+$ Q-TOF) of compound **5**.

Synthesis of (9H-fluoren-9-yl)methyl (2-(3-((3aR,4S,7R,7aS)-1,3-dioxo-1,3,3a,4,7,7a-hexahydro-2H-4,7-methanoisoindol-2-yl)-*N*-(2-(tritylamino)ethyl)propanamido)ethyl)carbamate (6)

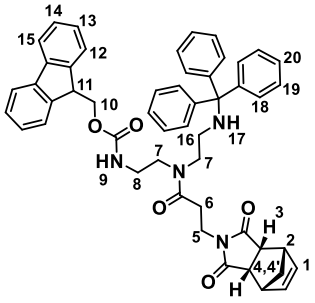

Product **5** (20 g, 30.4 mmol) was dissolved in 400 mL methanol and heated to 65°C (85°C water bath). K_2CO_3 (29 g, 168 mmol) was dissolved in 40 mL water and added to the solution (MeOH/H2O 9/1). The reaction mixture was stirred for 30 min at 70°C. Reaction time and temperature have to be applied exactly to prevent formation of a rearranged side product as stated in previous work.[7] Methanol and water were removed under reduced pressure and the product was dried under high vacuum.

The introduction of the Fmoc-protective group was performed without further purification. The crude product was dissolved in 150 mL THF and 130 mL water, giving a biphasic system. FmocCl (9.44 g, 30.4 mmol) was added and the reaction mixture was stirred overnight. Subsequently THF was removed under reduced pressure and the crude product subsequently dissolved in 300 mL EtOAc. The organic layer was washed with sat. $NaHCO_3$ (3 x 250 mL). The organic phase was dried with Na_2SO_4 and EtOAc was removed under reduced pressure. The product was dried under high vacuum and crystallized in EtOAc and slight amounts of petroleum ether (40-60°C). The white crystals of product **6** (17.4 g, 22.2 mmol, 73%) were filtered and dried under high vacuum.

^{1}H-NMR (600 MHz, $CDCl_3$): δ 7.75 (d, *J* = 7.6 Hz, 2H, 15), 7.65 – 7.50 (m, 2H, 12), 7.46 – 7.33 (m, 8H, 13+18), 7.33 – 7.24 (m, 8H, 14+19), 7.23 – 7.12 (m, 3H, 20), 6.15 – 6.01 (m, 2H, 1), 5.60 – 4.94 (m, 1H, 9), 4.53 – 4.29 (m, 2H, 10), 4.20 (t, *J* = 7.3 Hz, 1H, 11), 3.78 – 3.61 (m, 2H, 5), 3.55 – 2.84 (m, 11H, 2+3+7+8+17), 2.79 – 2.46 (m, 2H, 6), 2.44 – 2.19 (m, 2H, 16), 1.74 – 1.68 (m, 1H, 4 or 4'), 1.57 – 1.48 (m, 1H, 4 or 4') ppm. Signals for residue ethyl acetate were observed with chemical shifts of δ 4.12 (q, 2H), 2.05 (s, 3H), 1.26 (t, 3H) ppm.

^{13}C-NMR (151 MHz, DMSO-d_6): 177.26, 169.95, 169.39, 156.26, 156.11, 146.06, 145.93, 143.88, 142.56, 140.73, 139.41, 137.42, 134.32, 128.92, 128.28, 127.71, 127.58, 127.28, 127.03, 126.06, 125.09, 121.38, 120.08, 109.75, 70.34, 70.26, 65.44, 65.22, 51.52, 48.07, 47.34, 46.75, 45.55, 45.16, 44.62, 44.34, 42.37, 41.98, 38.63, 38.11, 34.13, 30.68, 30.09 ppm. Signals for residue ethyl acetate were observed with chemical shifts of δ 59.76, 20.76, 14.09 ppm.

RP-HPLC (linear gradient from 20 - 80% eluent B in 30 min at 25 °C): t_R = 23.3 min. Determined purity: > 98%.

HR-ESI-MS for $C_{50}H_{48}N_4O_5$ (Exact monoisotopic mass 784.3625 g/mol): $[M+H]^+$ calcd. 785.3697; found 785.3696; mass accuracy -0.13 ppm.

Elemental analysis calcd (%) for $C_{50}H_{48}N_4O_5$: C 76.51, H 6.16, N 7.14; found: C 76.34, H 6.13, N 7.09.

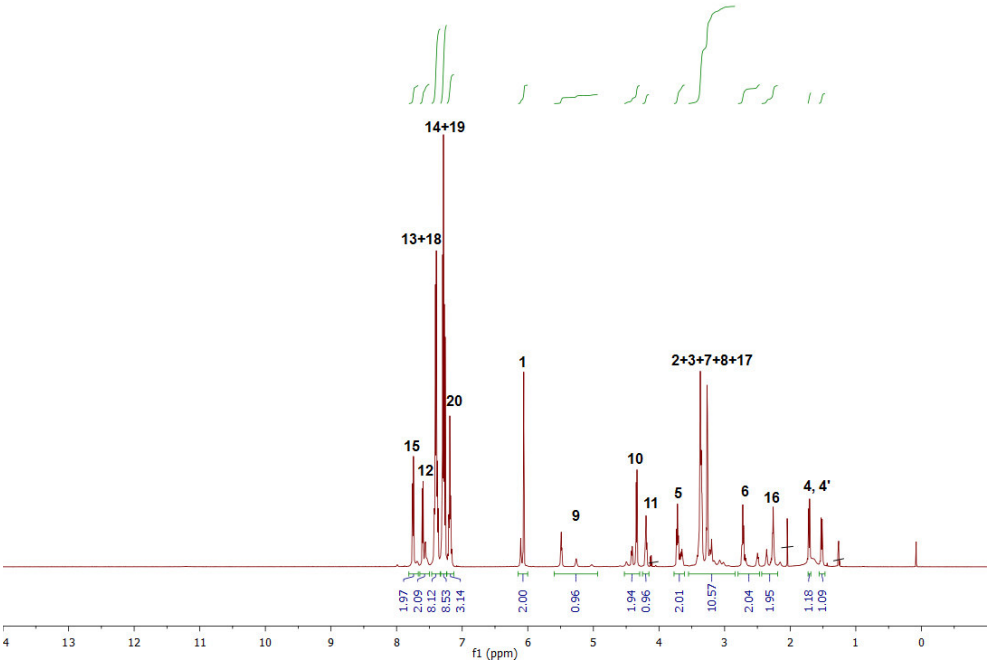

Figure S12: ^{1}H-NMR (600 MHz, $CDCl_3$) of compound **6**.

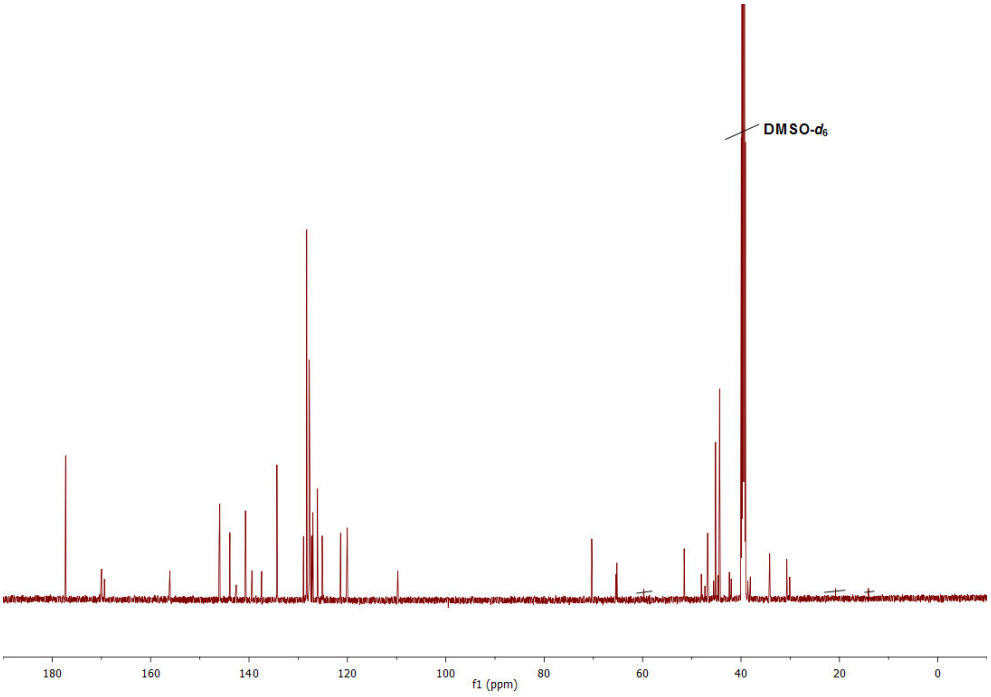

Figure S13: ^{13}C-NMR (151 MHz, DMSO-d_6) of compound **6**.

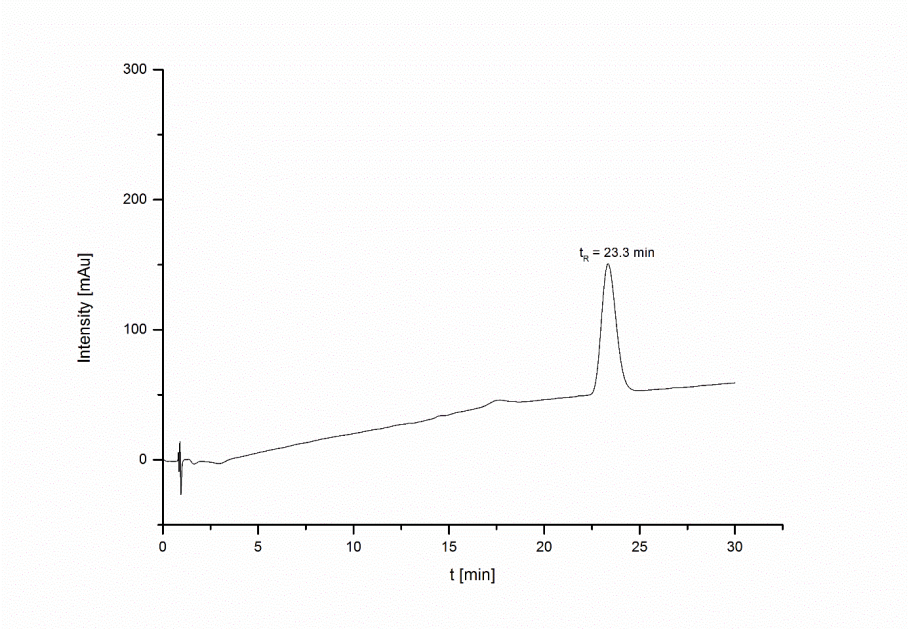

Figure S14: RP-HPLC analysis (linear gradient from 20 - 80% eluent B in 30 min at 25 °C) chromatogram of compound **6**.

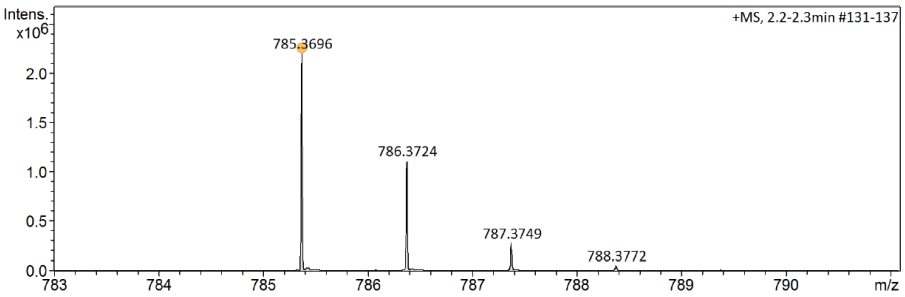

Figure S15: HR-MS (ESI$^+$ Q-TOF) of compound **6**.

Synthesis of 7-(3-((3aR,4S,7R,7aS)-1,3-dioxo-1,3,3a,4,7,7a-hexahydro-2H-4,7-methanoisoindol-2-yl)propanoyl)-1-(9H-fluoren-9-yl)-3,11-dioxo-2-oxa-4,7,10-triazatetradecan-14-oic acid (7)

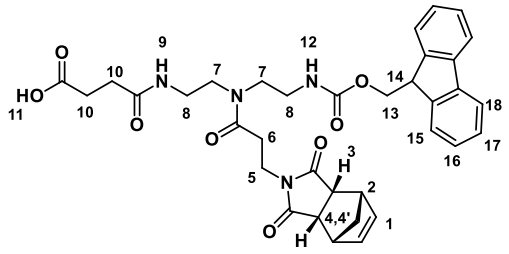

Product **6** (17.4 g, 22.2 mmol) was dissolved in 280 mL DCM and triisopropylsilane (13.6 ml, 10.6 g, 66.6 mmol) were added. The reaction mixture was cooled to 0°C and TFA (15 ml, total of 5vol%) was added dropwise to the reaction mixture. The reaction was stirred for 30 min and the reaction mixture was concentrated under reduced pressure. 200 mL of toluene were added twice to coevaporate TFA. The crude product was dissolved in 45 mL DCM and slowly poured into 450 mL cold diethyl ether to precipitate the product. The product was centrifuged and the ether decanted.

The introduction of the succinyl group was performed without further purification. The crude product and succinic anhydride (2.44 g, 24.4 mmol) were dissolved in 360 mL DCM. Triethylamine (9.28 ml, 6.74 g, 66.6 mmol) was slowly added to the solution and the reaction mixture was stirred for 1h at room temperature. The reaction mixture was washed twice with 200 mL of 10% citric acid and the organic phase was dried with Na_2SO_4. DCM was evaporated under reduced pressure and product **7** was dried under high vacuum. Product **7** (13.2 g, 20.5 mmol, 93%) crystallized as white solid from ethyl acetate and small amounts of petroleum ether.

Protons for the two amides 9 and 12 give two signals each with intensities of 0.5 that we assign to two rotational isomers in equal amounts. NMR experiments at higher temperatures show coalescence and signal sharpening. The effect is exemplarily shown for the signals from the Fmoc residue as well as the amide signals in the area of chemical shifts from δ 8.2 – 7.0 ppm. ^{1}H-NMR (600 MHz, DMSO-d_6): δ 12.06 (s, 1H, 11), 8.01 (t, J = 5.9 Hz, 0.5H, 9), 7.93 – 7.84 (m, 2.5H, 9+18), 7.68 (dd, J = 7.7, 3.4 Hz, 2H, 15), 7.45 (t, J = 6.0 Hz, 0.5H, 12), 7.43 – 7.38 (m, 2H, 17), 7.37 – 7.29 (m, 2.5H, 12+16), 6.18 – 5.96 (m, 2H, 1), 4.30 (t, J = 6.9 Hz, 2H, 13), 4.25 – 4.18 (m, 1H, 14), 3.44 – 3.37 (m, 2H, 5), 3.31 – 3.05 (m, 12H, 2+3+7+8), 2.42 (dt, J = 7.0, 2.4 Hz, 2H, 6), 2.39 – 2.25 (m, 4H, 10), 1.61 – 1.46 (m, 2H, 4+4') ppm. Signals for residual ethyl acetate were observed with chemical shifts of δ 4.03 (q, 2H), 1.99 (s, 3H), 1.17 (t, 3H) ppm.

^{13}C-NMR (151 MHz, DMSO-d_6): δ 177.24, 173.84, 171.46, 171.11, 169.69, 156.22, 143.90, 140.73, 134.31, 128.92, 127.60, 127.06, 125.11, 120.11, 65.50, 65.34, 51.52, 46.99, 46.72, 45.14, 44.34, 34.03, 30.12, 29.91, 29.17, 29.05 ppm. Signals for residue ethyl acetate were observed with chemical shifts of δ 170.33, 59.76, 20.76, 14.09 ppm.

RP-HPLC (linear gradient from 20 - 80% eluent B in 30 min at 25 °C): t_R = 14.4 min. Determined purity: > 98%.

HR-ESI-MS for $C_{35}H_{38}N_4O_8$ (Exact monoisotopic mass 642.2690 g/mol): $[M+H]^+$ calcd. 643.2762; found 643.2766; mass accuracy 0.62 ppm.

Elemental analysis calcd (%) for $C_{35}H_{38}N_4O_8$: C 65.41, H 5.96, N 8.72; found: C 65.10, H 6.24, N 8.41.

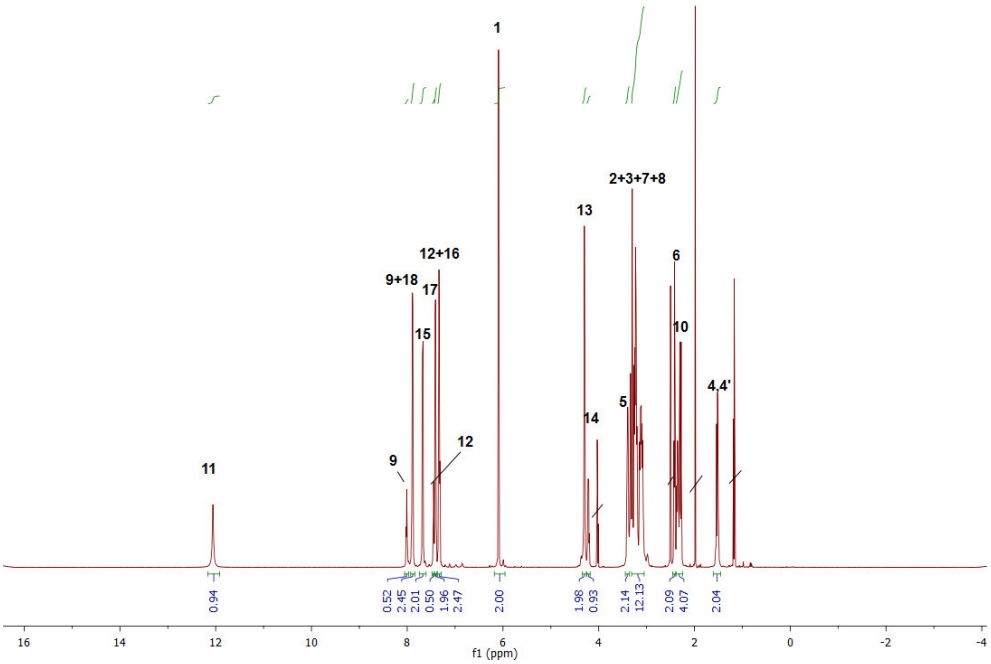

Figure S16: ^{1}H-NMR (600 MHz, DMSO-d_6) of compound **7**.

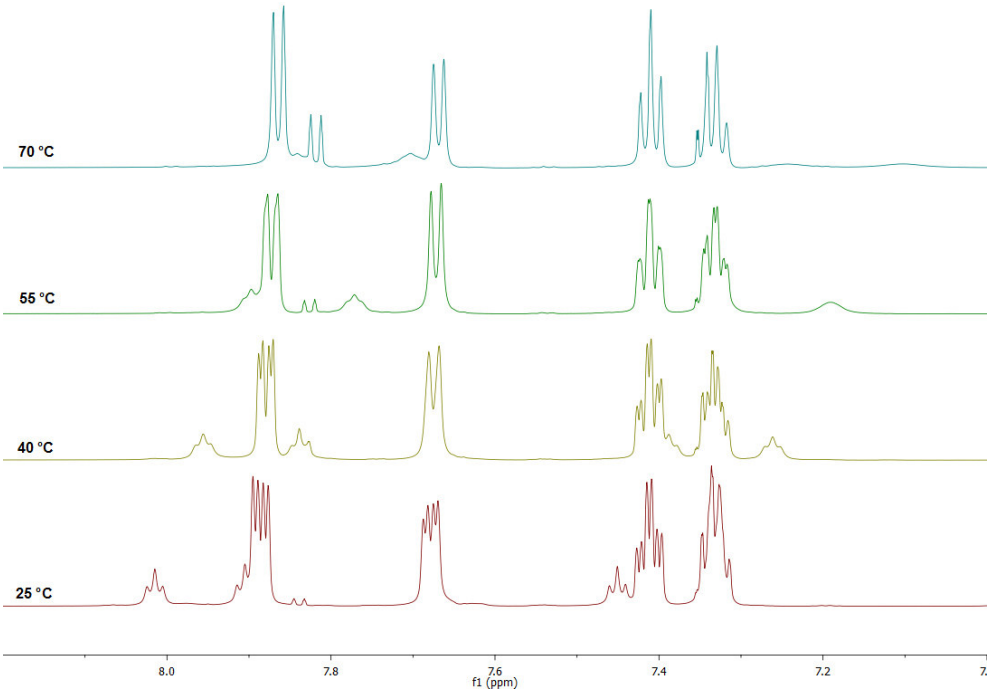

Figure S17: ^{1}H-NMR (600 MHz, DMSO-d_6) from δ 8.2 – 7.0 ppm at 25, 40, 55 and 70 °C of compound **7**.

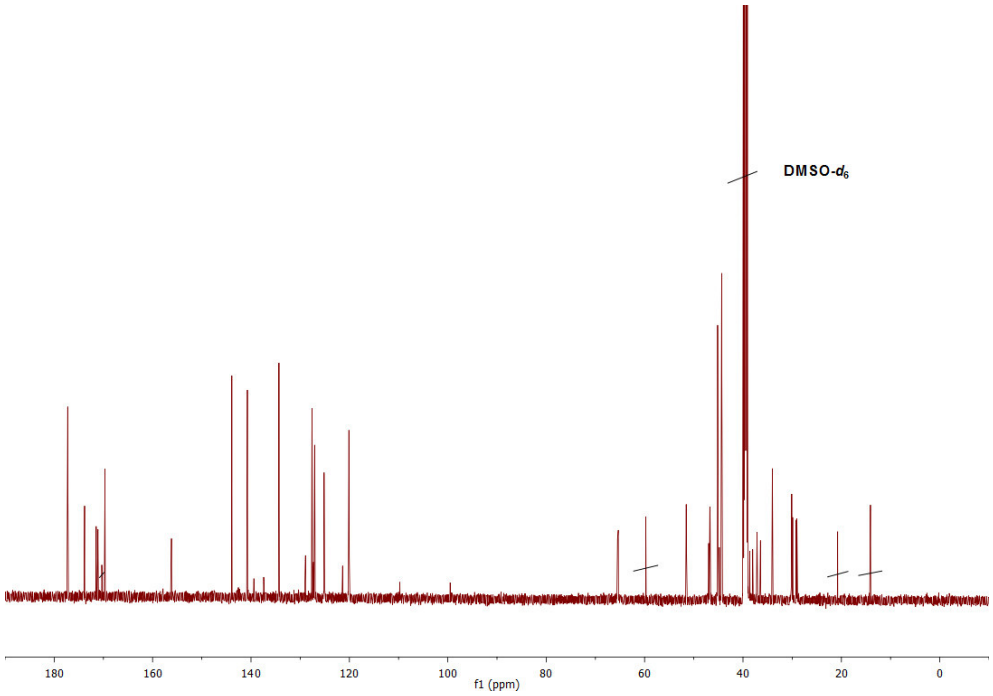

Figure S18: ^{13}C-NMR (151 MHz, DMSO-d_6) of compound **7**.

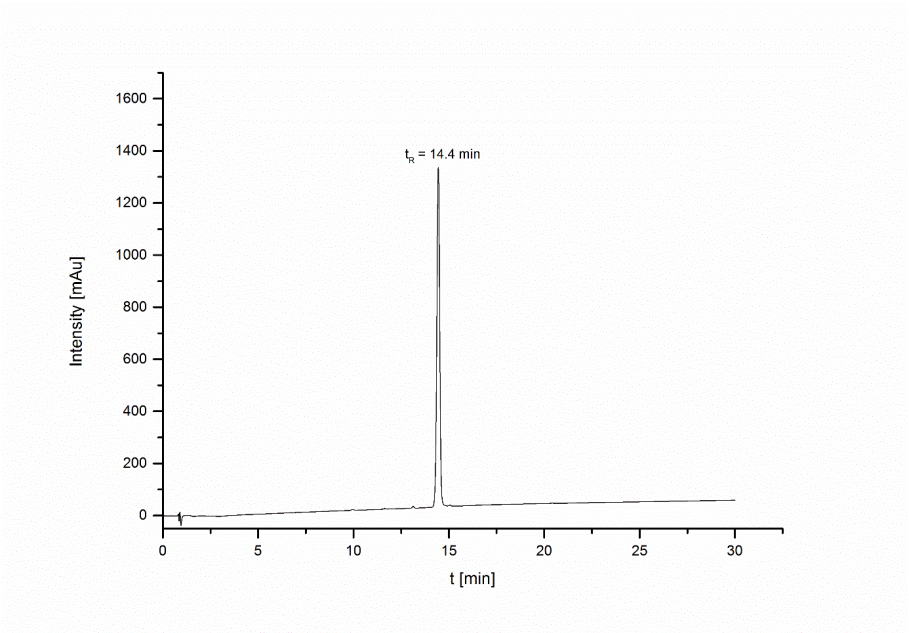

Figure S19: RP-HPLC analysis (linear gradient from 20 - 80% eluent B in 30 min at 25 °C) chromatogram of compound **7**.

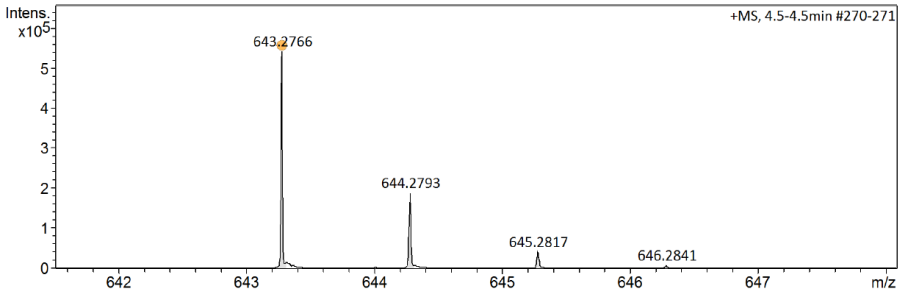

Figure S20: HR-MS (ESI$^+$ Q-TOF) of compound **7**.

Coupling efficiency of final NDS:

The coupling efficiency of a coupling step can be determined by quantification of the released Fmoc moiety from a previously coupled building block. The amount of cleaved Fmoc can be photometrically quantified (fulvene-piperidine adduct) and is an established procedure to determine the resin capacity. The determined value for the fulvene-piperidine adduct is directly proportional to the amount of previously coupled building block and the resulting decrease in resin capacity [%] corresponds to the coupling efficiency for each coupling step. A test sequence (50 µmol batch size), consisting of two EDS building blocks, followed by the novel NDS building block and a further EDS building block was synthesized using a Tentagel S Ram (Rink Amide) resin (capacity of 0.22 mmol/g). The coupling procedure was performed in a 10 mL syringe reactor. 5 equiv of the coupling reagent PyBOP as well as the building block and 10 equiv of DIEA were used. The exact coupling protocol used for SPS by hand was established in previous work.[4, 8] After each coupling step, approximately 10 mg of resin with Fmoc protected building block were taken from the batch to determine the resin capacity and thus the coupling efficiency. The resin was put into a 2 mL Eppendorf tube and 800 µL of DMF were added and agitated for 15 min to swell the resin. Subsequently 200 µL of piperidine were added and the tube with the resin was agitated for an additional 15 min. 100 µL of the cleavage solution were transferred into a quartz cuvette (1 cm) and diluted with 900 µL DMF. The absorbance at 301 nm was measured to determine the amount of released Fmoc as the formed fulvene-piperidine adduct. Each sample was measured three times. To calculate the resin capacity (in mmol/g), the extinction coefficient 7800 mL/mmol*cm was used. Finally, the purity of the test oligomer (acetylated N-terminus) was determined by RP-HPLC measurements.

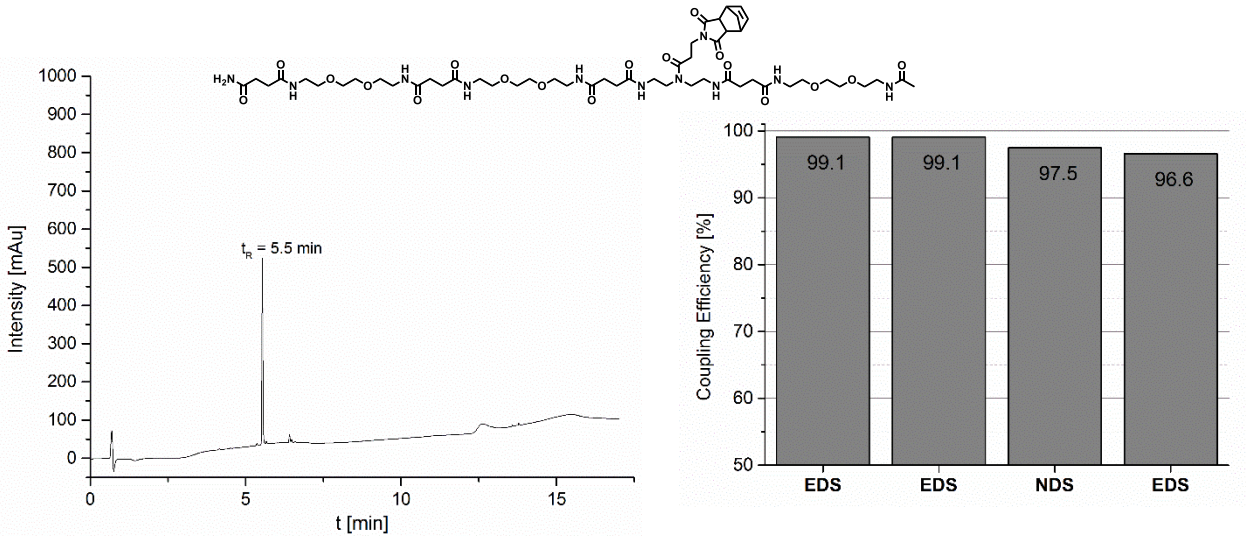

Figure S21: Left: RP-HPLC analysis (linear gradient from 0 - 50% eluent B in 10 min at 40 °C) chromatogram of a test compound $(EDS)_2$-NDS-EDS synthesized to determine the coupling efficiency of NDS. Right: Coupling efficiencies for each coupling step compared to the previous step in %.

Synthesis and characterization of glycooligoamides

Solid phase synthesis protocols

Glycooligomers **O1** – **O7** were synthesized applying established protocols.[4, 8] The used batch size was 0.3 mmol for all structures and the synthesis was performed using an automated peptide synthesizer. The mannose functionalization of oligomers **O1** - **O5** was performed in a 25 mL syringe reactor.

Preswell of the resin (On automated synthesizer)

Commercially available Tentagel S RAM (Rink Amide) resin (Capacity of 0.25 mmol/g) was used as resin for solid phase synthesis. First, 0.3 mmol (1.2 g) of resin were swollen in 15 mL of DCM for 30 min and subsequently washed three times with 15 mL of DMF for 1 min. The Fmoc protection group of the Tentagel S RAM resin was removed following the Fmoc cleavage protocol.

Fmoc cleavage (On automated synthesizer)

The Fmoc protecting group of the resin as well as from the coupled building blocks or amino acid was cleaved by the addition of 18 mL of a solution of 25% piperidine in DMF. The deprotection was performed three times for 10 min. After the first and second deprotection, the resin was washed once with 16 mL DMF for 1 min. After the third deprotection, the resin was washed thoroughly with DMF, 10 times using 16 mL.

General coupling protocol (On automated synthesizer)

Coupling reagent, base and building blocks or amino acids were prepared in separate vessels on the automated peptide synthesizer. All reagents were dissolved or diluted in DMF. Building blocks and amino acids were supplied at a concentration of 0.6 M, the coupling reagent PyBOP at a concentration of 0.5 M and DIEA at 1 M. For the coupling, 3 mL of the dissolved building block or amino acid (1.8 mmol, 6 eq.), 3.5 mL of dissolved PyBOP (1.8 mmol, 6 eq) and 3 mL of DIEA solution (3 mmol, 10 eq.) were transferred to the activation vessel and the reaction mixture was activated under nitrogen stream for 1 min. After activation, the mixture (total of 9.5 mL) was transferred to the reaction vessel with the resin and shaken for 1 h. After that, the resin was washed from excessive reagent 6 times with 15 mL DMF. A double coupling, adding fresh building block and coupling reagents without prior deprotection of the Fmoc protective group, was performed for structures **3** and **4** starting with the sixth building block or amino acid to ensure a complete coupling.

Capping of N-terminal primary amine (On automated synthesizer)

After successful assembly of the desired number of building blocks on solid phase, the N-terminal site was capped with an acetyl group. Therefore, 15 mL acetic anhydride were shaken with the resin for 30 min and the resin was washed three times with 15 mL DMF and DCM, respectively.

General CuAAC protocol (In a syringe reactor)

To 0.3 mmol of resin loaded with the oligomeric structure, 1.2 mmol (4 eq) of acetyl protected 2-azidoethyl pyranoside per alkyne group dissolved in 6 mL DMF, was added. 20 mol% sodium ascorbate per alkyne group and 20 mol% $CuSO_4$ per alkyne group were dissolved in 2 mL water and also added to the resin. This mixture was shaken overnight and subsequently washed extensively with a 23 mM solution of sodium diethyldithiocarbamate in DMF, DCM, DMF and water.

On resin acetyl deprotection (In a syringe reactor)

In order to remove the acetyl protective groups of the 2-azidoethyl pyranoside moieties, 10 mL of an ice-cold 0.1 M solution of sodium methanolate in methanol were added to the resin and shaken for 1 h. The deprotection was performed in an ice/water bath at 0°C. Subsequently, the resin was washed 5 times with 10 mL of DMF and DCM.

Cleavage from solid phase (In a syringe reactor)

13 mL of a mixture of 95% TFA and 5% of TIPS were added to the resin and shaken for 1 h. The filtrate was poured into 120 mL cold diethyl ether. The resin was washed with an additional 5 mL of DCM which was also added to the cold ether. The resulting precipitate was centrifuged and the ether decanted. The crude product was dried under a stream of nitrogen, dissolved in 3 mL of methanol and precipitated again in 30 mL of cold diethyl ether. The precipitate was centrifuged and the ether decanted again. The pellet was dried over a stream of nitrogen, dissolved in 6 mL of water and lyophilized.

TFA removal (In a syringe reactor)

Trifluoroacetate was removed according to the described procedure from Cintrat, Fay and co-workers.[9] 4 g of anion exchange resin was transferred to a 20 mL syringe reactor and washed three times with 13 mL of 1.6 N acetic acid and three times with 13 mL of 0.16 N acetic acid. The oligomers **O1** – **O7** were dissolved in 12 mL water each and transferred to a syringe reactor with conditioned anion exchange resin. The syringe reactor was shaken for 1 h, the oligomer solution was recovered in a flask and the resin was washed three times with 13 mL water. The solutions were pooled and the water removed under reduced pressure. The remaining oligomer was dissolved with 5 mL water and freeze-dried.

Analytical Data

NDS(1,3)Man(2)-3 (O1a):

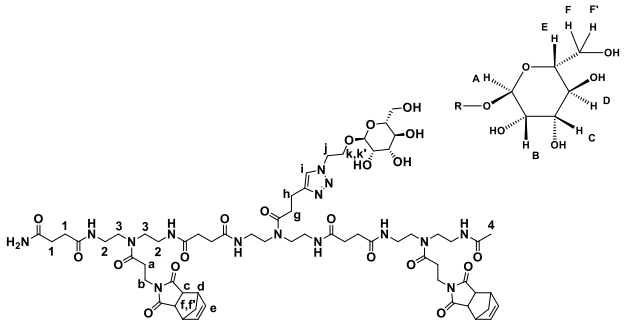

Compound **O1a** was obtained in a yield of 69% (258.0 mg) after purification by preparative HPLC. The anomeric proton of Mannose (A) could not be examined in ^{1}H-NMR due to interference with the signal from the residual solvent. For the acetyl group on the N-terminal end we observed two singlets with a ratio of 1:1 that we assign to two rotational isomers in equal amounts. The presence of rotational isomers was identified in ^{1}H-NMR experiments at higher temperatures (data not shown). ^{1}H-NMR (600 MHz, D_2O): δ 7.88 (s, 1H, i), 6.14 – 6.11 (m, 4H, e), 4.69 – 4.60 (m, 2H, j), 4.13 – 4.06 (m, 1H, k or k'), 3.97 – 3.90 (m, 1H, k or k'), 3.88 – 3.84 (m, 1H, B), 3.77 – 3.72 (m, 1H, F or F'), 3.70 – 3.55 (m, 7H, F or F'+C+D+b), 3.52 – 3.31 (m, 32H, 2+3+b+c), 3.07 – 3.02 (m, 1H, E), 3.00 (t, *J* = 7.3 Hz, 2H, h), 2.84 – 2.77 (m, 2H, g), 2.60 – 2.42 (m, 16H, 1+a), 1.99 + 1.97 (2s, 3H, 4), 1.76 – 1.68 (m, 2H, f or f'), 1.66 – 1.59 (m, 2H, f or f') ppm. The assignment of the signals was verified by the implementation of ^{1}H-^{1}H-COSY experiments (data not shown).

HR-ESI-MS for $C_{63}H_{91}N_{15}O_{20}$ (Exact monoisotopic mass 1377.6565 g/mol): $[M+2H]^{2+}$ calcd. 689.8355, found 689.8364, mass accuracy 1.30 ppm.

RP-HPLC (linear gradient from 0 - 50% eluent B in 30 min at 25 °C): t_R = 14.7 min. Determined purity: > 99%.

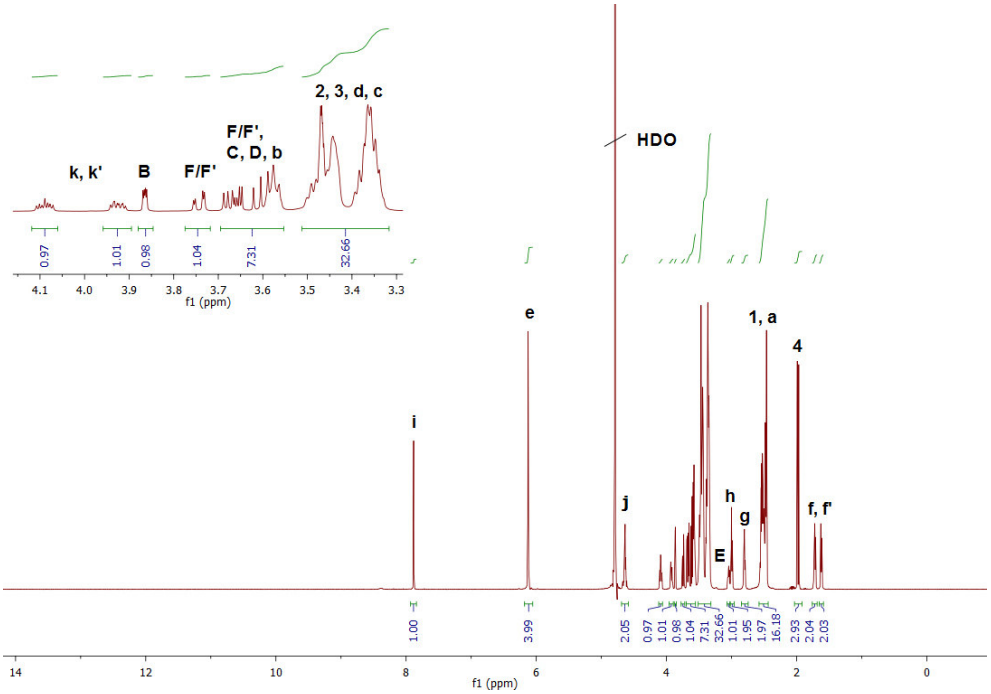

Figure S22: ^{1}H-NMR (600 MHz, D_2O) of **O1a** enlarging the area from δ 3.3 to 4.2 ppm.

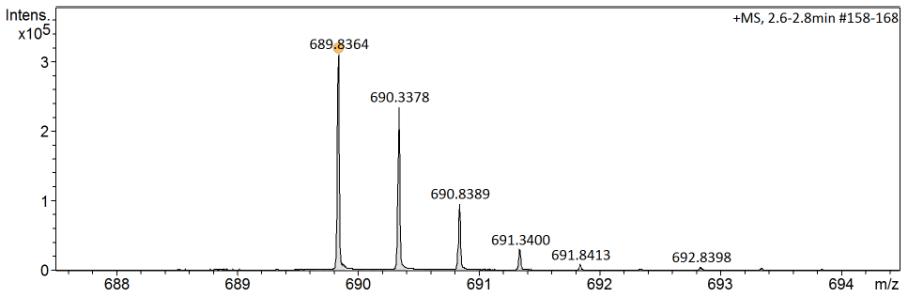

Figure S23: HR-MS (ESI$^+$ Q-TOF) of **O1a**.

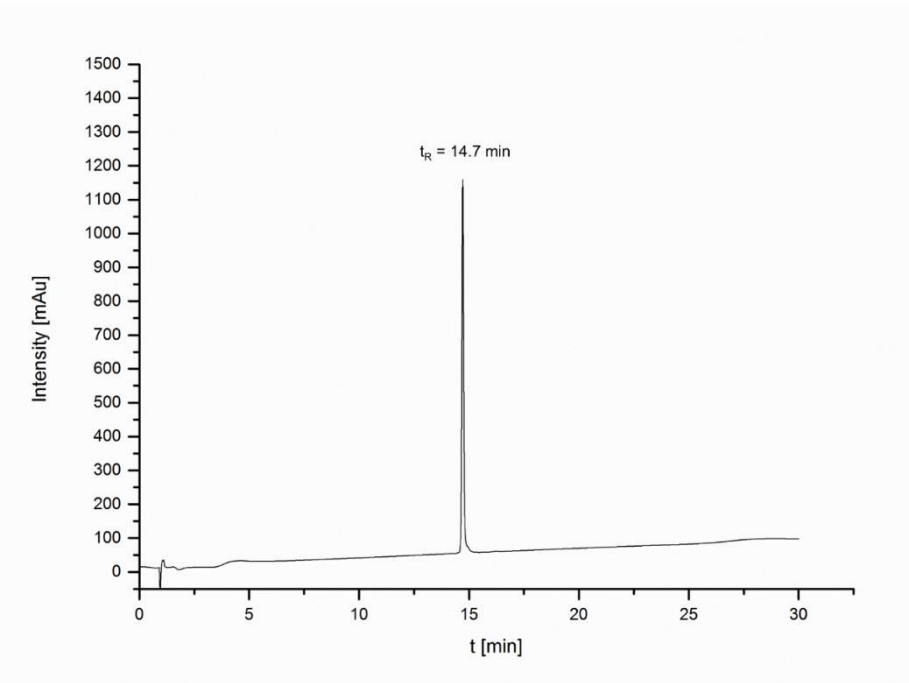

Figure S24: RP-HPLC analysis (linear gradient from 0 - 50% eluent B in 30 min at 25 °C) chromatogram of **O1a**.

DDS(1,3)Man(2)-3 (O1b):

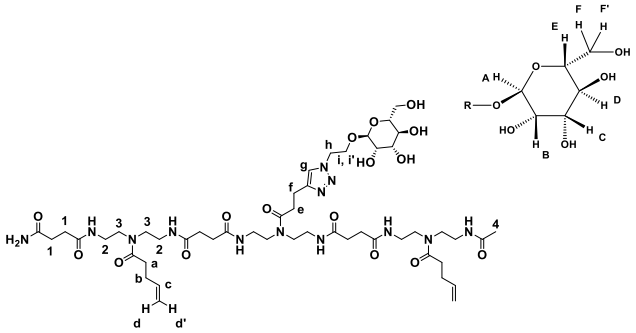

Compound **O1b** was obtained in a yield of 60% (133.0 mg) after purification by preparative HPLC. The anomeric proton of Mannose (A) could not be examined in ^{1}H-NMR due to interference with the signal from the residual solvent. For the acetyl group on the N-terminal end we observed two singlets with a ratio of 1:1 that we assign to two rotational isomers in equal amounts. The presence of rotational isomers was identified in ^{1}H-NMR experiments at higher temperatures (data not shown). ^{1}H-NMR (600 MHz, D_2O): δ 7.88 (s, 1H, g), 5.95 – 5.81 (m, 2H, c), 5.14 – 4.99 (m, 4H, d+d'), 4.68 – 4.58 (m, 2H, h), 4.14 – 4.04 (m, 1H, i or i'), 3.96 – 3.89 (m, 1H, i or i'), 3.88 – 3.84 (m, 1H, B), 3.78 – 3.71 (m, 1H, F or F'), 3.70 – 3.57 (m, 3H, F or F'+C+D), 3.55 – 3.44 (m, 12H, 3), 3.43 – 3.32 (m, 12H, 2), 3.06 – 3.02 (m, 1H, E), 3.00 (t, *J* = 7.3 Hz, 2H, f), 2.79 (t, *J* = 7.3 Hz, 2H, e), 2.56 – 2.44 (m, 16H, 1+a), 2.36 – 2.28 (m, 4H, b), 1.98+1.95 (2s, 3H, 4) ppm. The assignment of the signals was verified by the implementation of ^{1}H-^{1}H-COSY experiments (data not shown).

HR-ESI-MS for $C_{49}H_{81}N_{13}O_{16}$ (exact monoisotopic mass 1107.5924 g/mol): $[M+2H]^{2+}$ calcd. 554.8035, found 554.8037, mass accuracy 0.36 ppm.

RP-HPLC (linear gradient from 0 - 50% eluent B in 30 min at 25 °C): t_R = 12.2 min. Determined purity: > 99%.

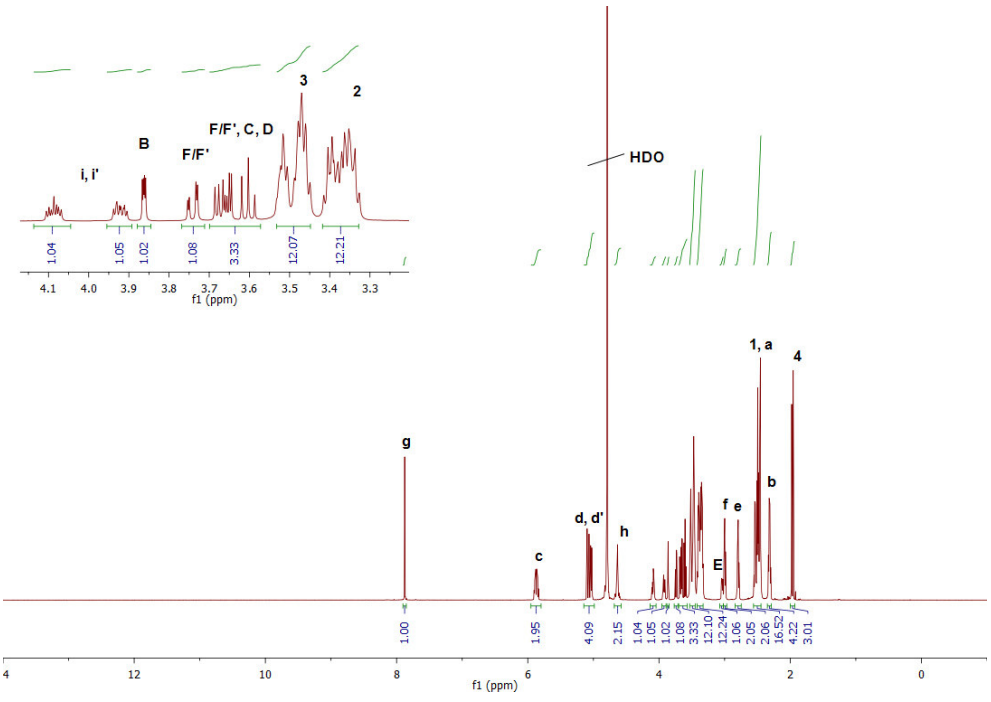

Figure S25: ^{1}H-NMR (600 MHz, D_2O) of **O1b** enlarging the area from δ 3.3 to 4.2 ppm.

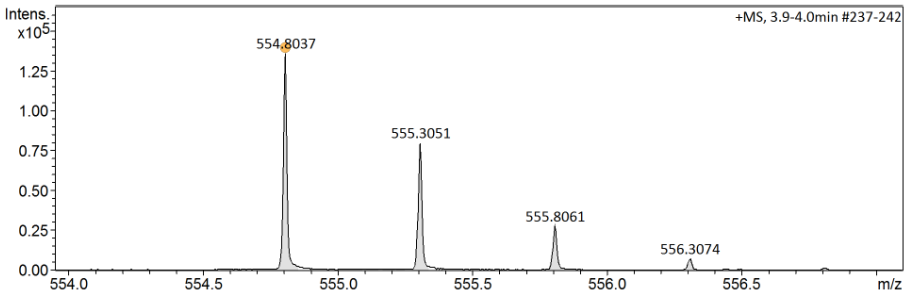

Figure S26: HR-MS (ESI$^+$ Q-TOF) of **O1b**.

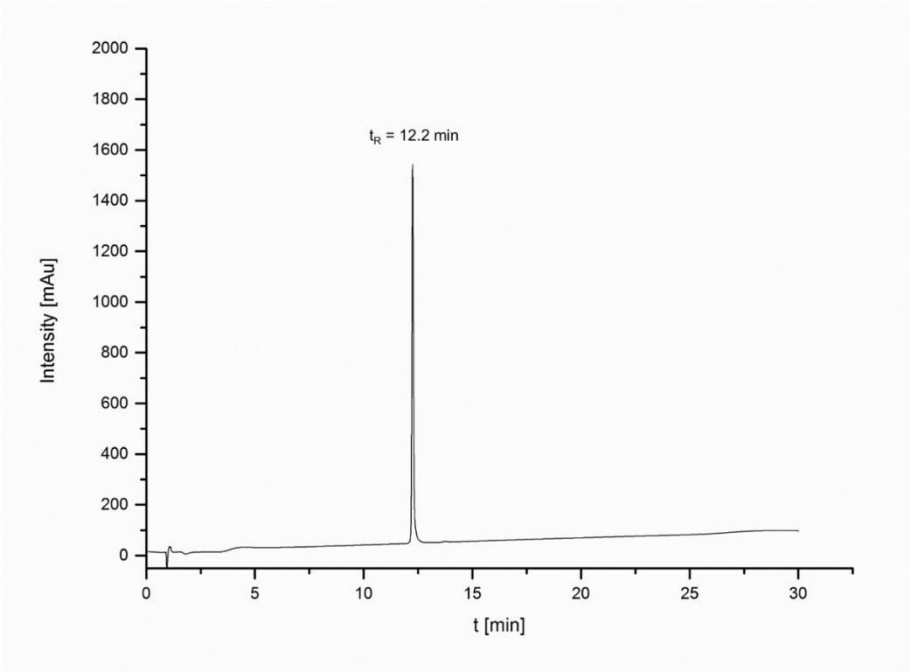

Figure S27: RP-HPLC analysis (linear gradient from 0 - 50% eluent B in 30 min at 25 °C) chromatogram of **O1b**.

NDS(1,4)Man(2,3)-4 (O2):

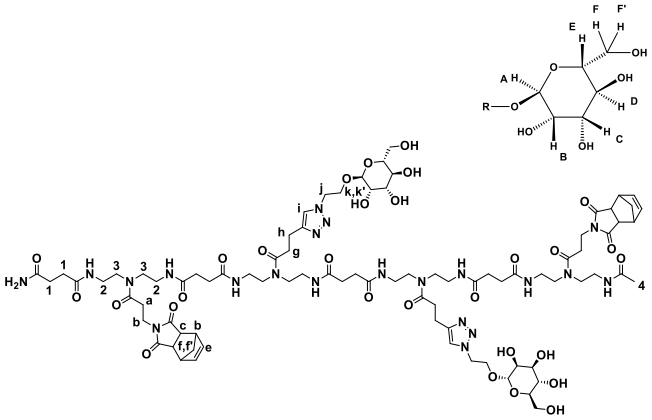

Compound **O2** was obtained in a yield of 50% (287.4 mg) after purification by preparative HPLC. The anomeric proton of Mannose (A) could not be examined in ^{1}H-NMR due to interference with the signal from the residual solvent. For the acetyl group on the N-terminal end we observed two singlets with a ratio of 1:1 that we assign to two rotational isomers in equal amounts. The presence of rotational isomers was identified in ^{1}H-NMR experiments at higher temperatures (data not shown). ^{1}H-NMR (600 MHz, D_2O): δ 7.87 (s, 2H, i), 6.13 – 6.11 (m, 4H, e), 4.65 – 4.61 (m, 4H, j), 4.12 – 4.06 (m, 2H, k or k'), 3.95 – 3.90 (m, 2H, k or k'), 3.88 – 3.85 (m, 2H, B), 3.76 – 3.72 (m, 2H, F or F'), 3.69 – 3.55 (m, 9H, F or F'+C+D+b), 3.50 – 3.31 (m, 40H, 2+3+d+c), 3.06 – 3.02 (m, 2H, E), 2.99 (t, *J* = 7.3 Hz, 4H, h), 2.82 – 2.77 (m, 4H, g), 2.59 – 2.40 (m, 20H, 1+a), 1.99 + 1.97 (2s, 2H, 4), 1.75 – 1.69 (m, 2H, f or f'), 1.64 – 1.59 (m, 2H, f or f') ppm. The assignment of the signals was achieved according to the structural similarities with compound **O1**.

HR-ESI-MS for $C_{84}H_{125}N_{21}O_{29}$ (exact monoisotopic mass 1891.8952 g/mol): $[M+2H]^{2+}$ calcd. 946.9549, found 946.9544, mass accuracy -0.53 ppm.

RP-HPLC (linear gradient from 0 - 50% eluent B in 30 min at 25 °C): t_R = 14.2 min. Determined purity: > 99%.

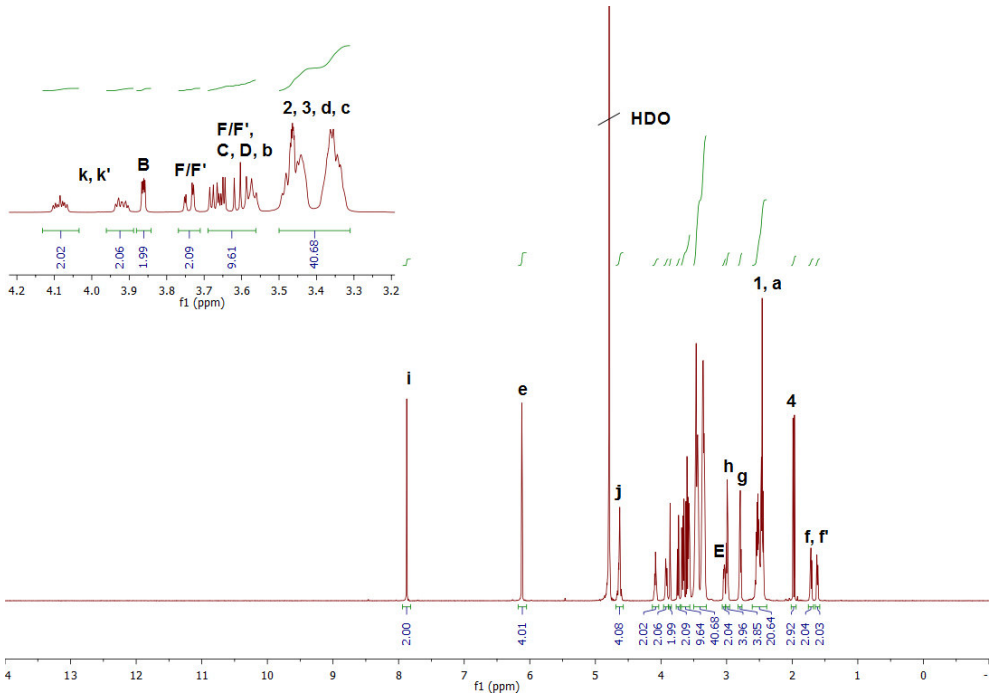

Figure S28: ^{1}H-NMR (600 MHz, D_2O) of **O2** enlarging the area from δ 3.3 to 4.2 ppm.

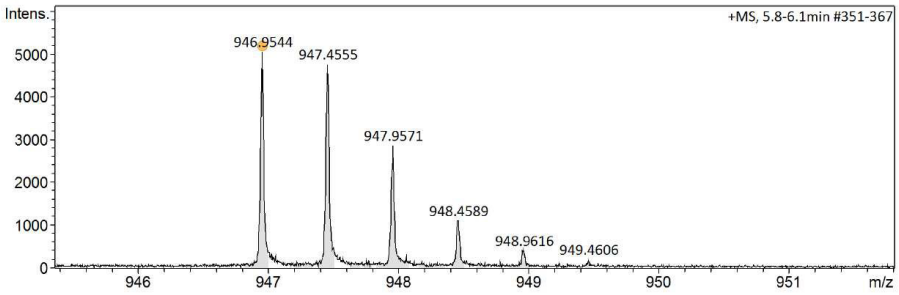

Figure S29: HR-MS (ESI$^+$ Q-TOF) of **O2**.

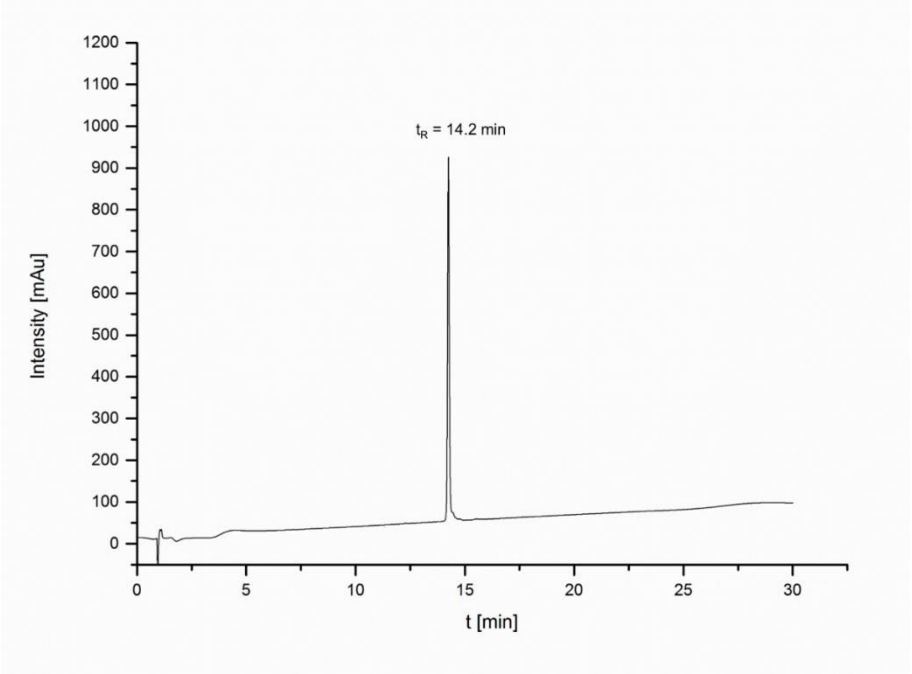

Figure S30: RP-HPLC analysis (linear gradient from 0 - 50% eluent B in 30 min at 25 °C) chromatogram of **O2**.

NDS(1,5)Man(2,3,4)-5 (O3):

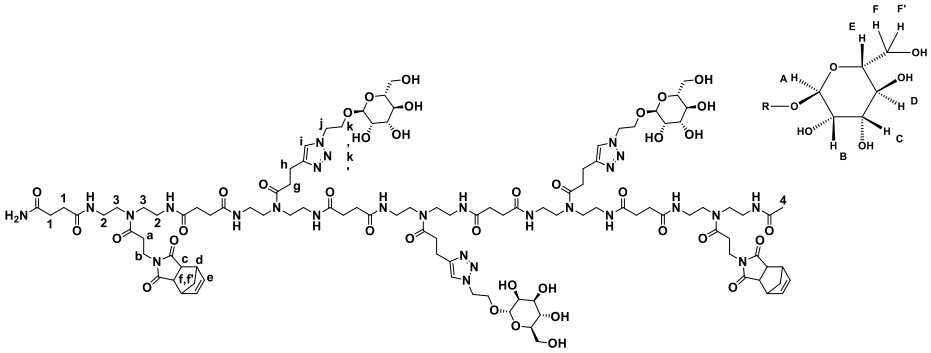

Compound **O3** was obtained in a yield of 51% (370.9 mg) after purification by preparative HPLC. The anomeric proton of Mannose (A) could not be examined in ^{1}H-NMR due to interference with the signal from the residual solvent. For the acetyl group on the N-terminal end we observed two singlets with a ratio of 1:1 that we assign to two rotational isomers in equal amounts. The presence of rotational isomers was identified in ^{1}H-NMR experiments at higher temperatures (data not shown). ^{1}H-NMR (600 MHz, D_2O): δ 7.89 – 7.86 (m, 3H, i), 6.15 – 6.09 (m, 4H, e), 4.66 – 4.60 (m, 6H, j), 4.12 – 4.05 (m, 3H, k or k'), 3.95 – 3.89 (m, 3H, k or k'), 3.88 – 3.84 (m, 3H, B), 3.77 – 3.71 (m, 3H, F or F'), 3.69 – 3.55 (m, 13H, F or F'+C+D+b), 3.51 – 3.31 (m, 48H, 2+3+d+c), 3.06 – 3.02 (m, 3H, E), 3.01 – 2.96 (m, 6H, h), 2.83 – 2.75 (m, 6H, g), 2.62 – 2.37 (m, 24H, 1+a), 1.99 + 1.96 (2s, 3H, 4), 1.75 – 1.67 (m, 2H, f or f'), 1.65 – 1.57 (m, 2H, f or f') ppm. The assignment of the signals was achieved according to the structural similarities with compound **O1**.

HR-ESI-MS for $C_{105}H_{159}N_{27}O_{38}$ (exact monoisotopic mass 2406.1339 g/mol): $[M+3H]^{3+}$ calcd. 803.0519, found 803.0515, mass accuracy -0.50 ppm.

RP-HPLC (linear gradient from 0 - 50% eluent B in 30 min at 25 °C): t_R = 13.9 min. Determined purity: > 99%.

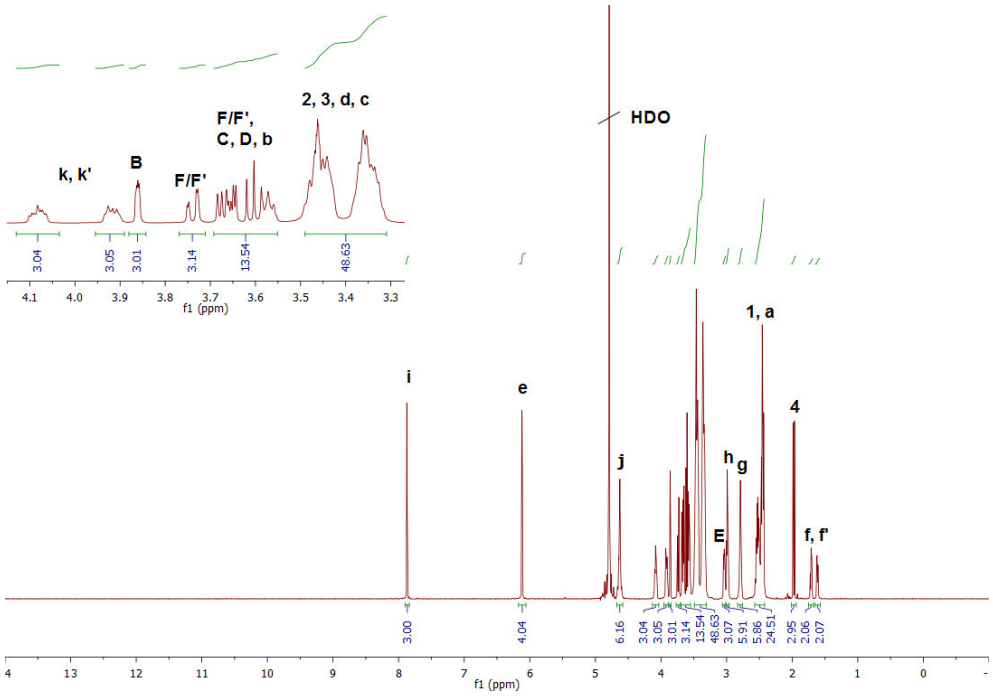

Figure S31: ^{1}H-NMR (600 MHz, D_2O) of **O3** enlarging the area from δ 3.3 to 4.2 ppm.

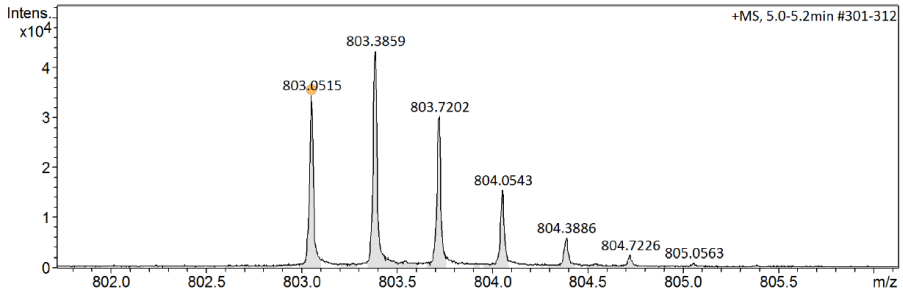

Figure S32: HR-MS (ESI$^+$ Q-TOF) of **O3.**

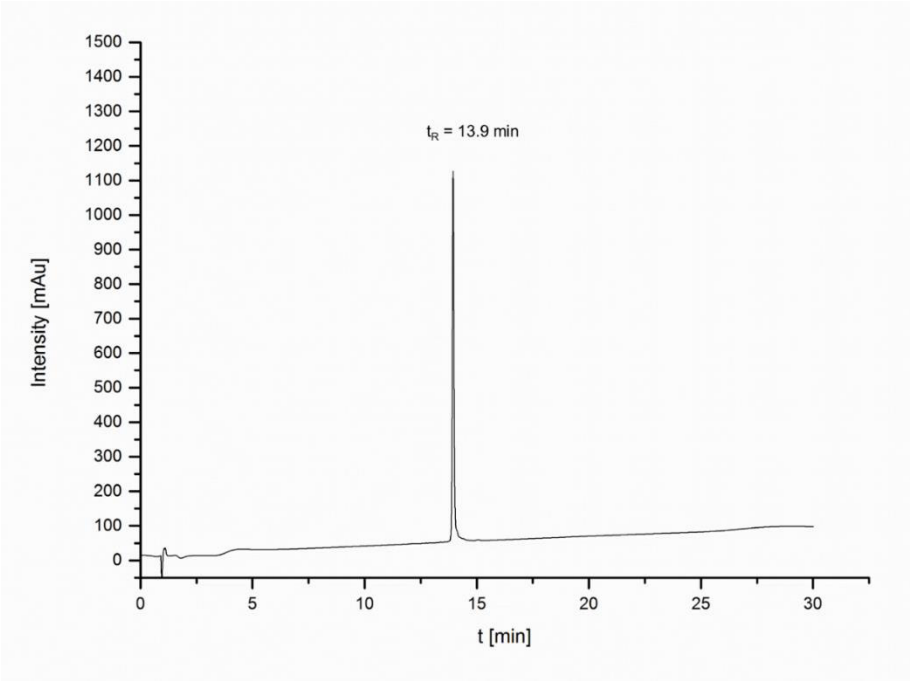

Figure S33: RP-HPLC analysis (linear gradient from 0 - 50% eluent B in 30 min at 25 °C) chromatogram of **O3**.

NDS(1,8)Man(2,7)-8 (O4):

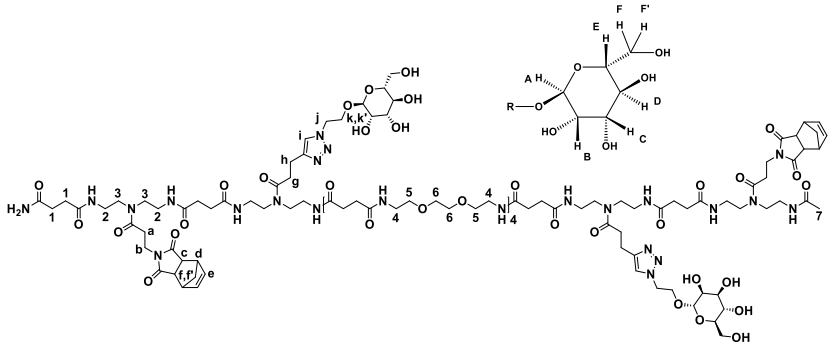

Compound **O4** was obtained in a yield of 56% (474.7 mg) after purification by preparative HPLC. The anomeric proton of Mannose (A) could not be examined in ^{1}H-NMR due to interference with the signal from the residual solvent. For the acetyl group on the N-terminal end we observed two singlets with a ratio of 1:1 that we assign to two rotational isomers in equal amounts. The presence of rotational isomers was identified in ^{1}H-NMR experiments at higher temperatures (data not shown). ^{1}H-NMR (600 MHz, D_2O): δ 7.88 (s, 2H, i), 6.14 – 6.11 (m, 4H, e), 4.67 – 4.61 (m, 4H, j), 4.12 – 4.05 (m, 2H, k or k'), 3.96 – 3.89 (m, 2H, k or k'), 3.88 – 3.84 (m, 2H, B), 3.77 – 3.72 (m, 2H, F or F'), 3.71 – 3.55 (m, 42H, 6+5+F or F'+C+D+b), 3.53 – 3.31 (m, 56H, 2+3+4+d+c), 3.06 – 3.02 (m, 2H, E), 3.00 (t, *J* = 7.3 Hz, 4H, h), 2.85 – 2.76 (m, 4H, g), 2.59 – 2.44 (m, 36H, 1+a), 1.99 + 1.97 (2s, 3H, 7), 1.75 – 1.68 (m, 2H, f or f'), 1.65 – 1.59 (m, 2H, f or f'). The assignment of the signals was verified by the implementation of ^{1}H-^{1}H-COSY experiments (data not shown).

HR-ESI-MS for $C_{124}H_{197}N_{29}O_{45}$ (exact monoisotopic mass 2812.4018 g/mol): $[M+4H]^{4+}$ calcd. 704.1077, found 704.1070, mass accuracy -0.99 ppm.

RP-HPLC (linear gradient from 0 - 50% eluent B in 30 min at 25 °C): t_R = 15.0 min. Determined purity: > 99%.

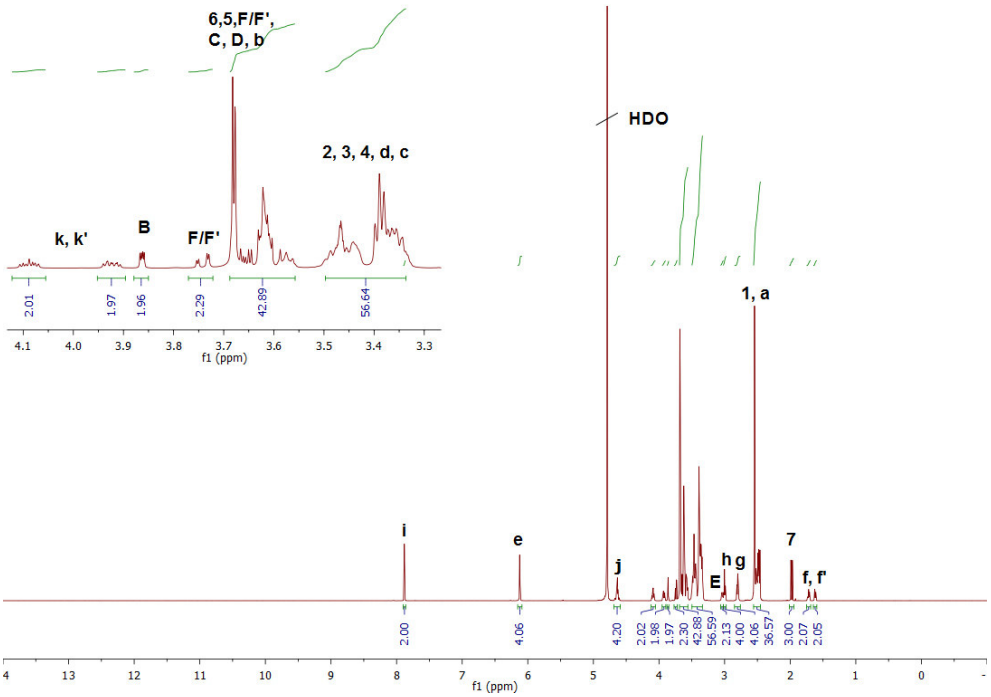

Figure S34: ^{1}H-NMR (600 MHz, D_2O) of **O4** enlarging the area from δ 3.3 to 4.2 ppm.

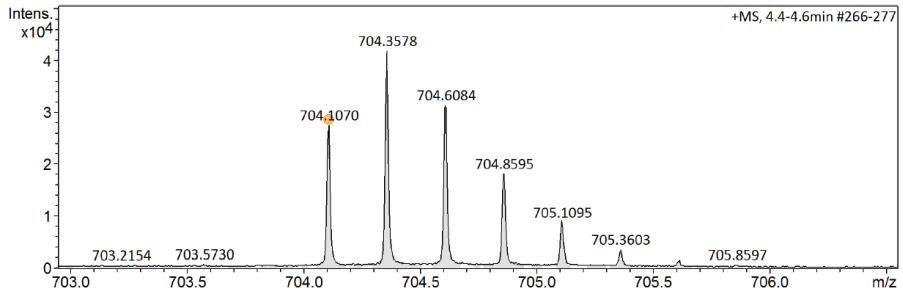

Figure S35: HR-MS (ESI$^+$ Q-TOF) of **O4**.

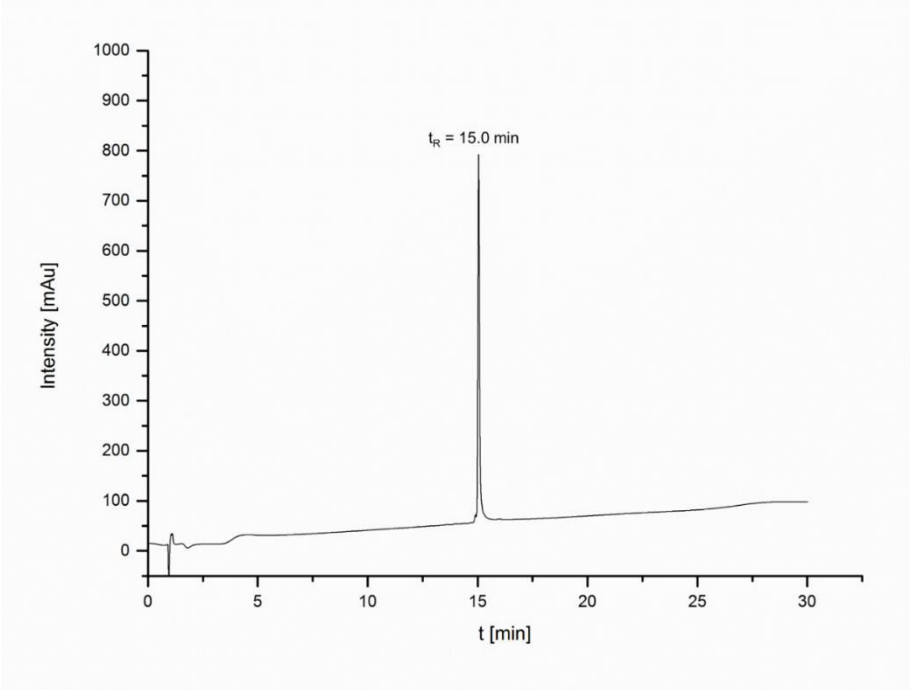

Figure S36: RP-HPLC analysis (linear gradient from 0 - 50% eluent B in 30 min at 25 °C) chromatogram of **O4**.

NDS(1,13)Man(2,7,12)-13 (O5):

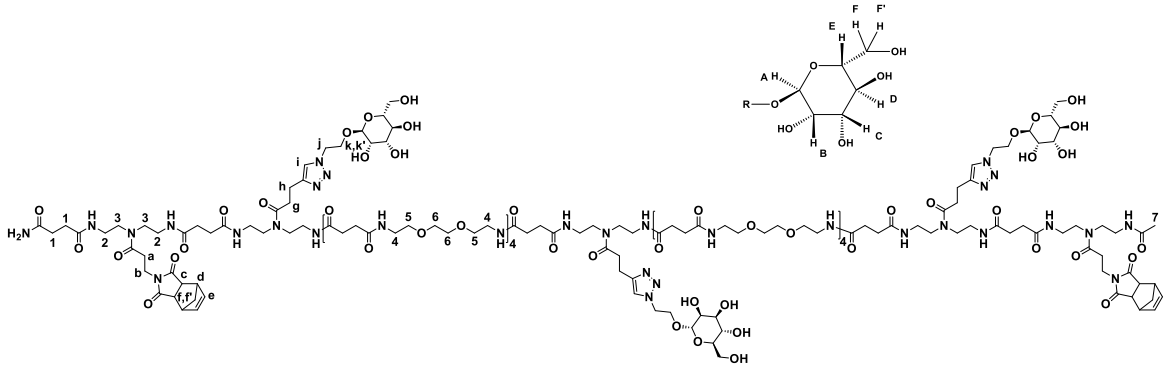

Compound **O5** was obtained in a yield of 48% (606.4 mg) after purification by preparative HPLC. The anomeric proton of Mannose (A) could not be examined in ^{1}H-NMR due to interference with the signal from the residual solvent. For the acetyl group on the N-terminal end we observed two singlets with a ratio of 1:1 that we assign to two rotational isomers in equal amounts. The presence of rotational isomers was identified in ^{1}H-NMR experiments at higher temperatures (data not shown). ^{1}H-NMR (600 MHz, D_2O): δ 7.88 (s, 3H, i), 6.16 – 6.09 (m, 4H, e), 4.69 – 4.59 (m, 6H, j), 4.13 – 4.05 (m, 3H, k or k'), 3.97 – 3.90 (m, 3H, k or k'), 3.88 – 3.84 (m, 3H, B), 3.77 – 3.72 (m, 3H, F or F'), 3.71 – 3.55 (m, 78H, 6+5+F or F'+C+D+b), 3.51 – 3.32 (m, 80H, 2+3+4+d+c), 3.06 – 3.02 (m, 3H, E), 3.00 (t, *J* = 7.2 Hz, 6H, h), 2.80 (t, *J* = 7.4 Hz, 6H, g), 2.58 – 2.45 (m, 56H, 1+a), 1.99 + 1.97 (2s, 3H, 7), 1.74 – 1.70 (m, 2H, f or f'), 1.64 – 1.60 (m, 2H, f or f') ppm. The assignment of the signals was achieved according to the structural similarities with compound **O4**.

HR-ESI-MS for $C_{185}H_{303}N_{43}O_{70}$ (exact monoisotopic mass 4247.1472 g/mol): $[M+4H]^{4+}$ calcd. 1062.7941, found 1062.7940, mass accuracy -0.09 ppm.

RP-HPLC (linear gradient from 0 - 50% eluent B in 30 min at 25 °C): t_R = 15.2 min. Determined purity: > 99%.

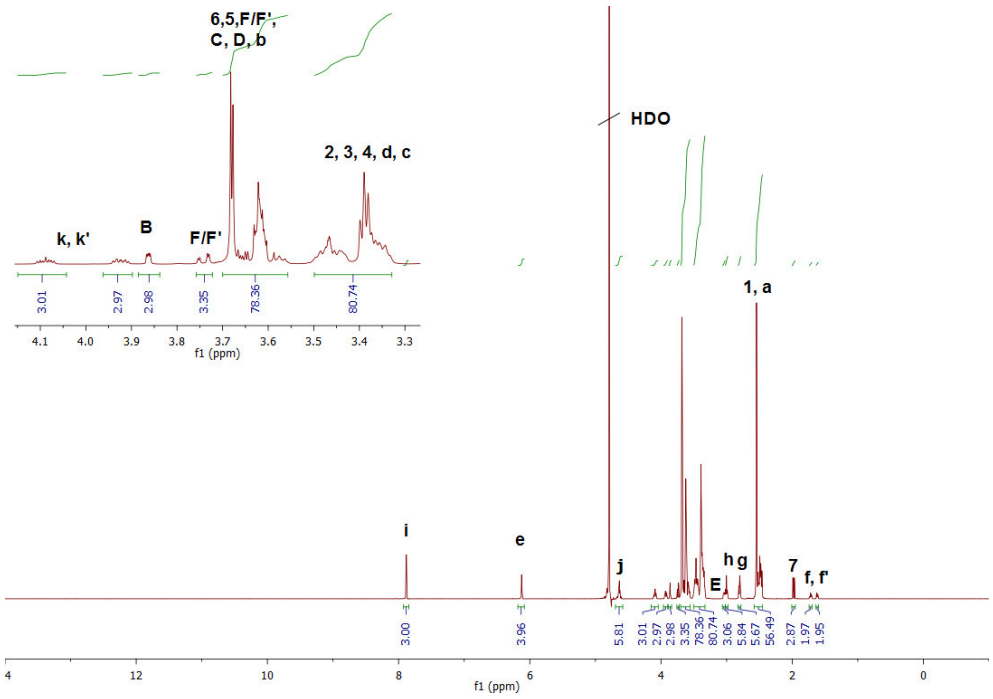

Figure S37: ^{1}H-NMR (600 MHz, D_2O) of **O5** enlarging the area from δ 3.3 to 4.2 ppm.

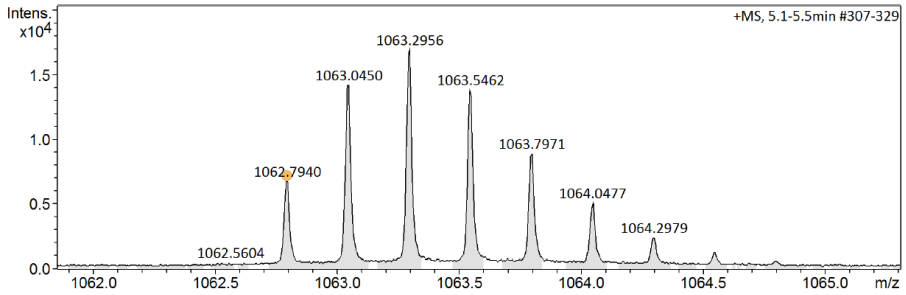

Figure S38: HR-MS (ESI$^+$ Q-TOF) of **O5.**

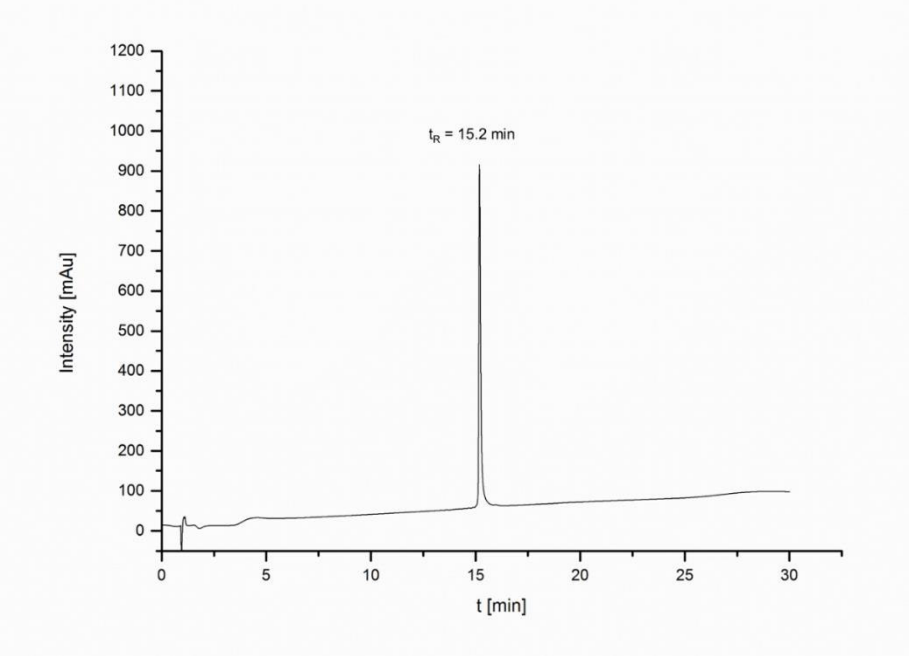

Figure S39: RP-HPLC analysis (linear gradient from 0 - 50% eluent B in 30 min at 25 °C) chromatogram of **O5**.

NDS(1,5)-5 (O6):

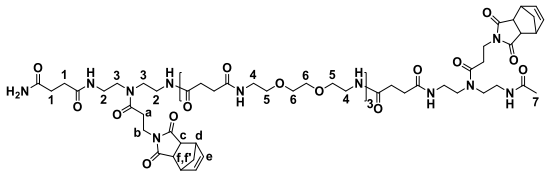

Compound **O6** was obtained in a yield of 57% (266.82 mg) after purification by preparative HPLC. For the acetyl group on the N-terminal end we observed two singlets with a ratio of 1:1 that we assign to two rotational isomers in equal amounts. The presence of rotational isomers was identified in ^{1}H-NMR experiments at higher temperatures (data not shown). ^{1}H-NMR (600 MHz, D_2O): δ 6.14 (s, 4H, e), 3.69 (s, 12H, 6), 3.65 – 3.56 (m, 16H, 5+b), 3.51 – 3.32 (m, 36H, 2+3+4+d+c), 2.60 – 2.47 (m, 24H, 1+a), 1.99 + 1.97 (2s, 3H, 7), 1.76 – 1.70 (m, 2H, f or f'), 1.65 – 1.61 (m, 2H, f or f') ppm. The assignment of the signals was verified by the implementation of ^{1}H-^{1}H-COSY experiments (data not shown).

HR-ESI-MS for $C_{72}H_{111}N_{15}O_{23}$ (exact monoisotopic mass 1553.7977 g/mol): $[M+2H]^{2+}$ calcd. 777.9061, found 777.9067, mass accuracy 0.77 ppm.

RP-HPLC (linear gradient from 0 - 50% eluent B in 30 min at 25 °C): t_R = 16.0 min. Determined purity: > 99%.

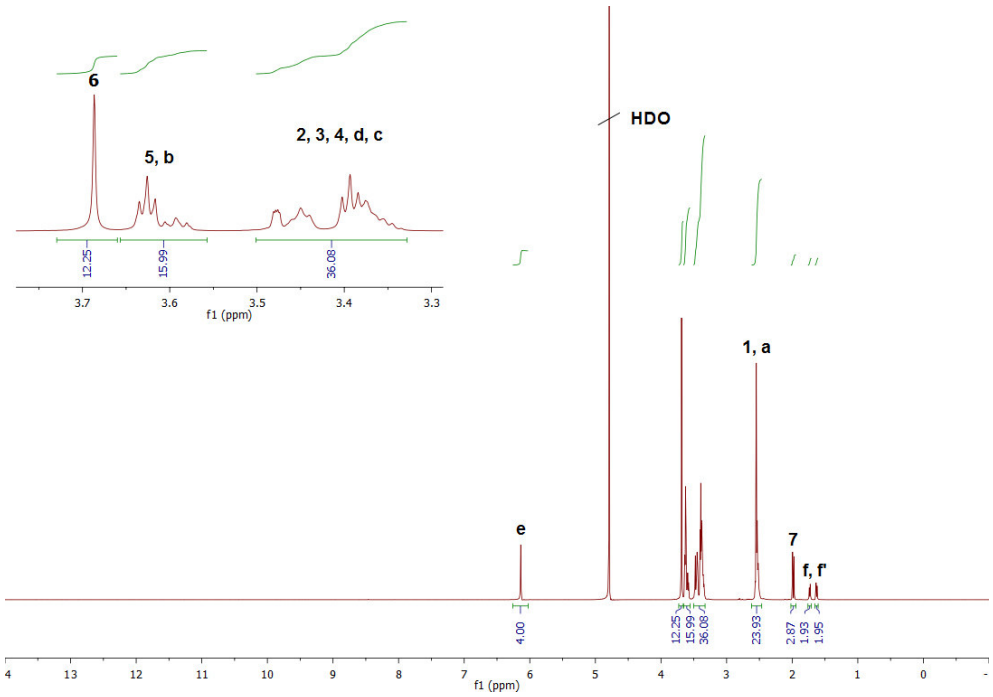

Figure S40: ^{1}H-NMR (600 MHz, D_2O) of **O6** enlarging the area from δ 3.3 to 3.8 ppm.

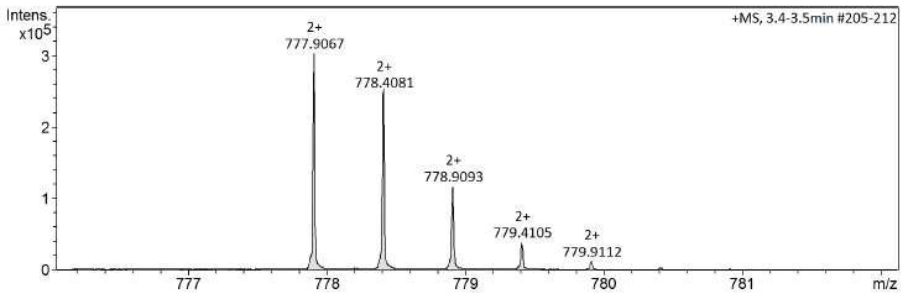

Figure S41: HR-MS (ESI$^+$ Q-TOF) of **O6.**

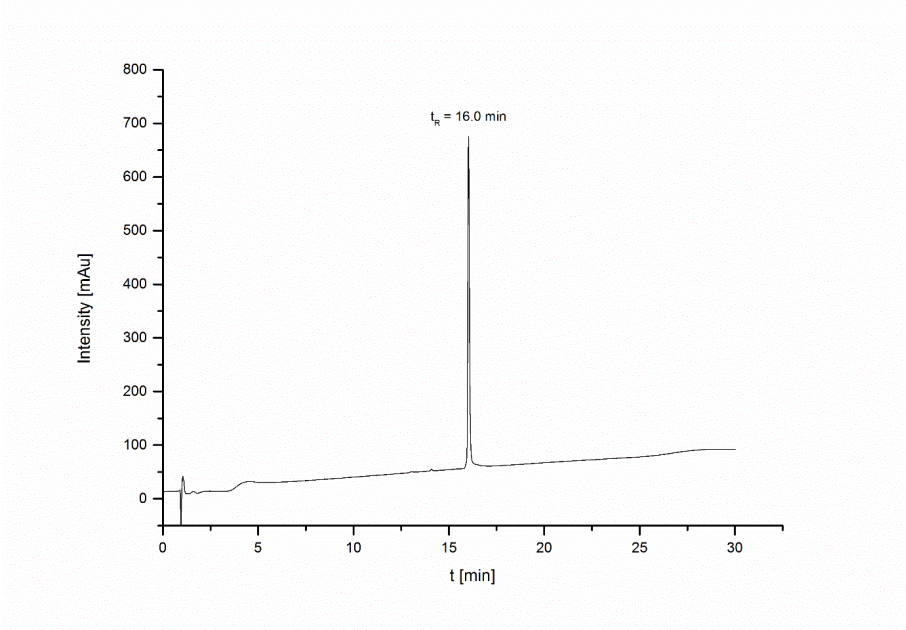

Figure S42: RP-HPLC analysis (linear gradient from 0 - 50% eluent B in 30 min at 25 °C) chromatogram of **O6**.

Cys(1,7)-7 (O7):

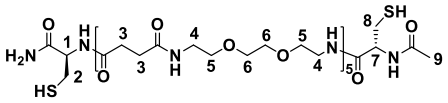

Compound **O7** was obtained in a yield of 68% (266.82 mg) after purification by preparative HPLC.

^{1}H-NMR (600 MHz, D_2O): δ 4.58 – 4.40 (m, 2H, 1+7), 3.71 – 3.67 (m, 20H, 6), 3.66 – 3.61 (m, 20H, 5), 3.47 – 3.37 (m, 20H, 4), 2.99 – 2.85 (m, 4H, 2+8), 2.67 – 2.52 (m, 20H, 3), 2.08 (s, 3H, 9) ppm. The assignment of the signals was verified by the implementation of ^{1}H-^{1}H-COSY experiments (data not shown).

HR-ESI-MS for $C_{58}H_{105}N_{13}O_{23}S_2$. (Exact monoisotopic mass 1415.6888 g/mol): $[M+2H]^{2+}$ calcd. 708.8517, found 708.8510, mass accuracy -0.99 ppm.

RP-HPLC (linear gradient from 0 - 50% eluent B in 30 min at 25 °C): t_R = 13.0 min. Determined purity: > 98% (addition of the area for **O7**, 96%, the disulfide from **O7**, t_R = 12.8 min 2%, and the dimer from **O7** via disulfide, t_R = 14.5 min 0.5%).

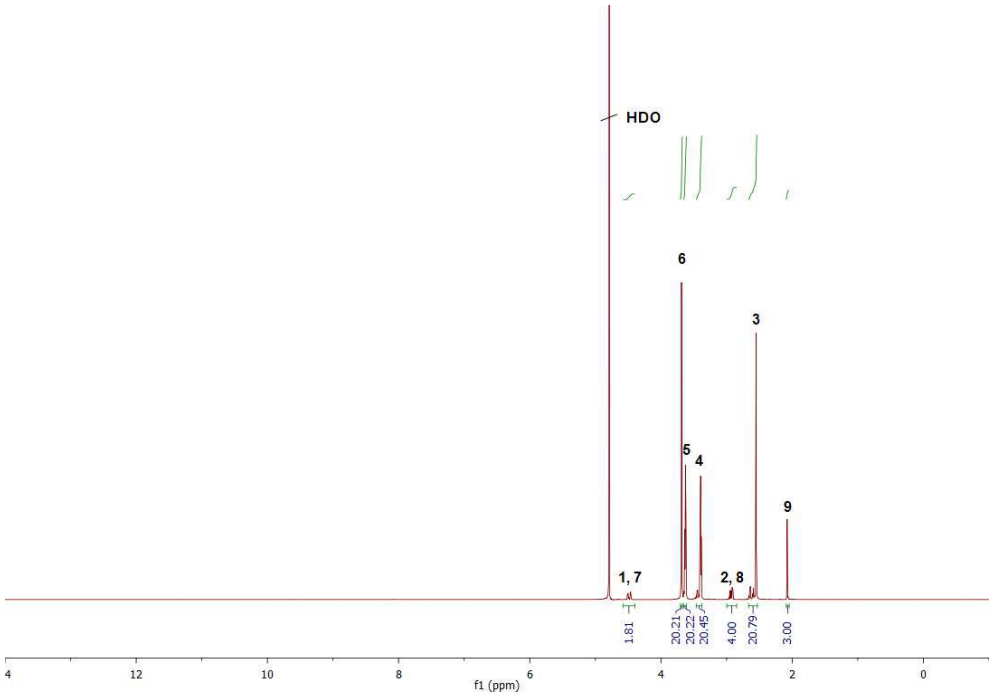

Figure S43: ^{1}H-NMR (600 MHz, D_2O) of **O7**.

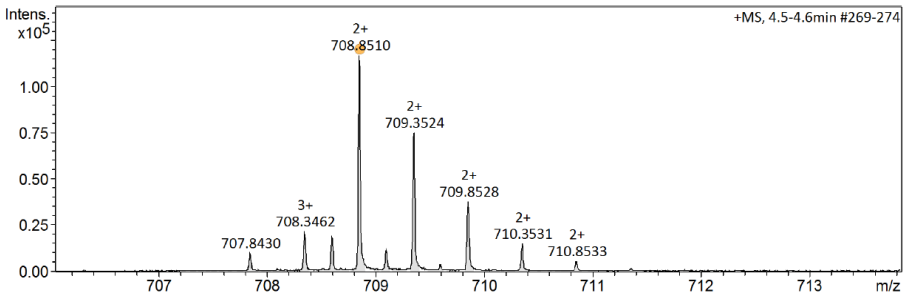

Figure S44: HR-MS (ESI$^+$ Q-TOF) of **O7.**

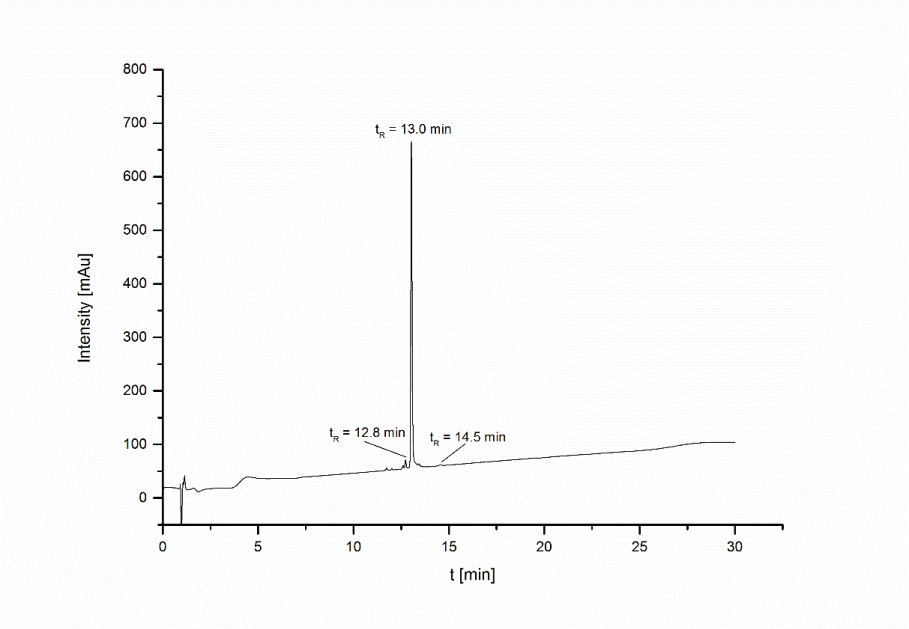

Figure S45: RP-HPLC analysis (linear gradient from 0 - 50% eluent B in 30 min at 25 °C) chromatogram of **O7** with its retention time as well as the intramolecular disulfide of **O7** (t_R = 12.8 min) and the dimer **O7** (t_R = 14.5 min) via disulfide linkage.

Characterization of dithiol-poly(ethylene glycol)

PEG(SH)$_2$-6000 from RAPP Polymere:

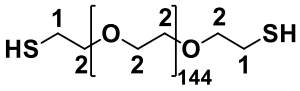

^{1}H-NMR (600 MHz, D_2O): δ 3.72 (s, 576H, 2), 2.75 (t, J = 6.2 Hz, 4H, 1) ppm.

GPC-RI-LS (Columns: Suprema Lux (2 X 100 and 1 X 1000 Å). Buffer: 50 mM NaH_2PO_4, 150 mM NaCl, 250 ppm of NaN_3 (pH 7.2), 30% ACN. Flow: 0.8 mL/min.). Elution volume: 26.8 mL. Determined $\bar{M}_n$: 6390 g/mol. Used dn/dc: 0.11 as determined using a PEG 100 kDa sample. A signal for a formed dimer by disulfide formation was also determined by GPC analysis.

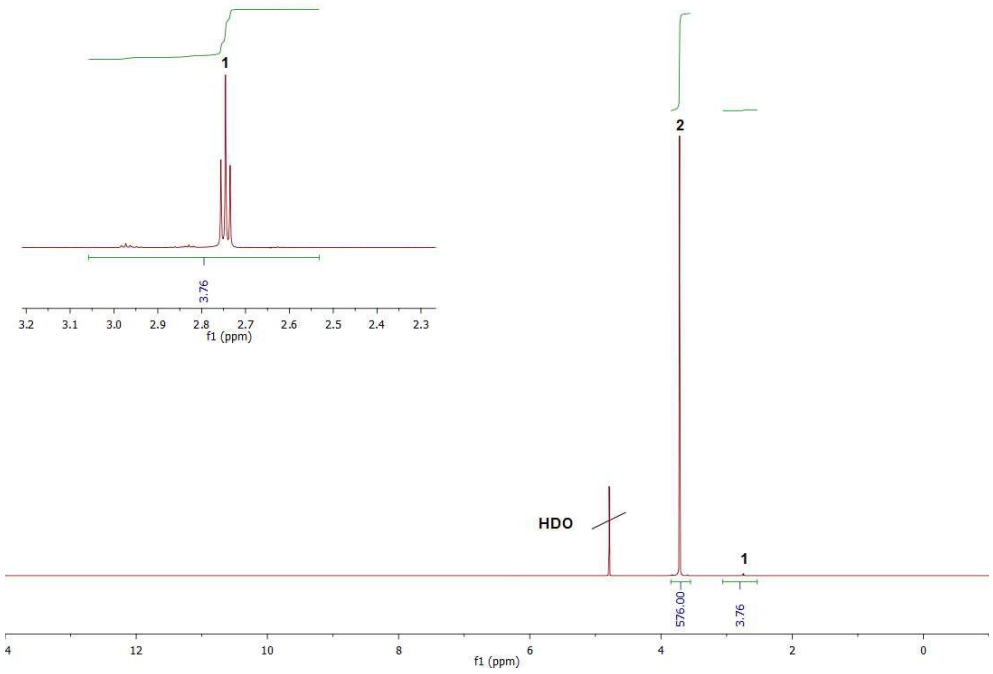

Figure S46: ^{1}H-NMR (600 MHz, D_2O) of PEG(SH)$_2$-6000 enlarging the area from δ 2.3 to 3.2 ppm.

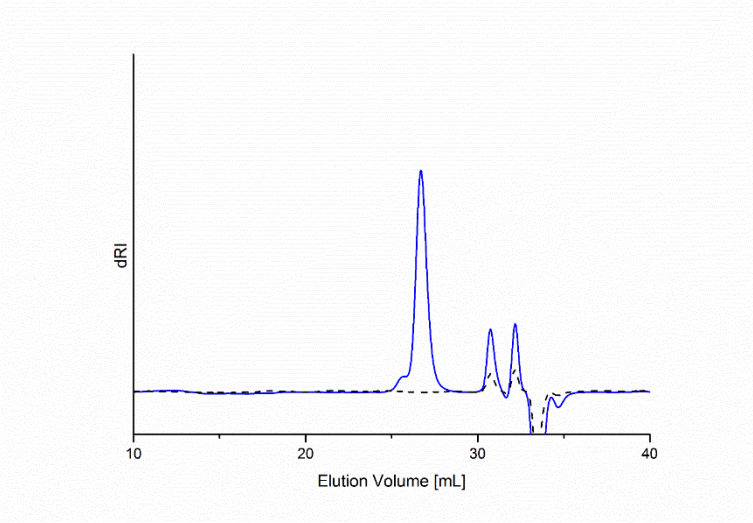

Figure S47: GPC-RI-LS of PEG(SH)$_2$-6000. Columns: Suprema Lux (2x 100 Å and 1000 Å). Buffer: 50 mM NaH_2PO_4, 150 mM NaCl, 250 ppm NaN_3 (pH 7.2), 30% ACN. Flow rate: 0.8 mL/min.

Polymerization via TEC coupling

For the comparison of the reactivity of the norbornene and the vinyl moiety in TEC (Polymerization of **O1a** and **O1b** with **O7**), the polymerization was conducted according to the previously published polymerization procedure.[8]

For the polymerization of the glycooligoamides **O1** – **O6** with $PEG(SH)_2$-6000, 20 µmol of $PEG(SH)_2$-6000 were weighed into borosilicate glass microwave vials without label to prevent UV absorption or reflection. Stock solutions (57.1 mM in water) of freshly freeze-dried oligomers were prepared. From the stock solutions, 350 µL of the glycooligoamides (**O1** – **O6**) were transferred into a microwave vial together with an adequate amount of $PEG(SH)_2$-6000. After the addition of both macromonomers an additional 200 µl of H_2O were added to dissolve both compounds. Subsequently the mixture was freeze-dried to remove water and oxygen. The freeze-dried mixture of the glycooligoamide and $PEG(SH)_2$-6000 was flushed with argon and closed. DMSO and H_2O were degassed using the freeze-pump-thaw method. Stock solutions of tris(2-carboxyethyl)-phosphine hydrochloride (TCEP) and dimethoxy-2-phenylacetphenone (DMPA) with concentrations of 50 mM in degassed H_2O as well as 100 mM in degassed DMSO, respectively, were prepared. 4 µL (0.25mM final concentration) of the TCEP stock and 200 µL (25 mM final concentration) of the DMAP stock were added to the freeze-dried macromonomers. An additional 396 µL of H_2O as well as 200 µL of DMSO were added, resulting in a total of 800 µL of a 1/1 mixture of DMSO/H_2O. Thus the final reactions mixture is composed of 25 mM of both macromonomers and 0.01 equiv of TCEP and 1 equiv of DMPA. After the addition of all reagents a magnetic stirring bar was added and the microwave vials were flushed with argon and subsequently closed tightly. All reagents were dissolved completely and the vials were placed on the magnetic stirring plate next to the UV lamp (distance of 7 – 10 cm). The reaction mixtures were heated to 55°C and irradiated for 1 h under stirring. After 1 h of irradiation, the product was slowly precipitated in 10 mL of an ice cold diethyl ether/acetone mixture with a volume ratio of 1/3. The obtained pallet was redissolved in 5 mL MeOH and a drop of water and reprecipitated in 30 mL ice cold diethyl ether. After evaporation of the diethyl ether under nitrogen stream, the pallet was redissolved in 6 mL water and freeze-dried to give the final product.

Data from the investigation of potential side-reactions in step-growth TEC polymerization

Irradiation of macromonomers separately using optimized TEC conditions as well as different concentration of DMPA and TCEP

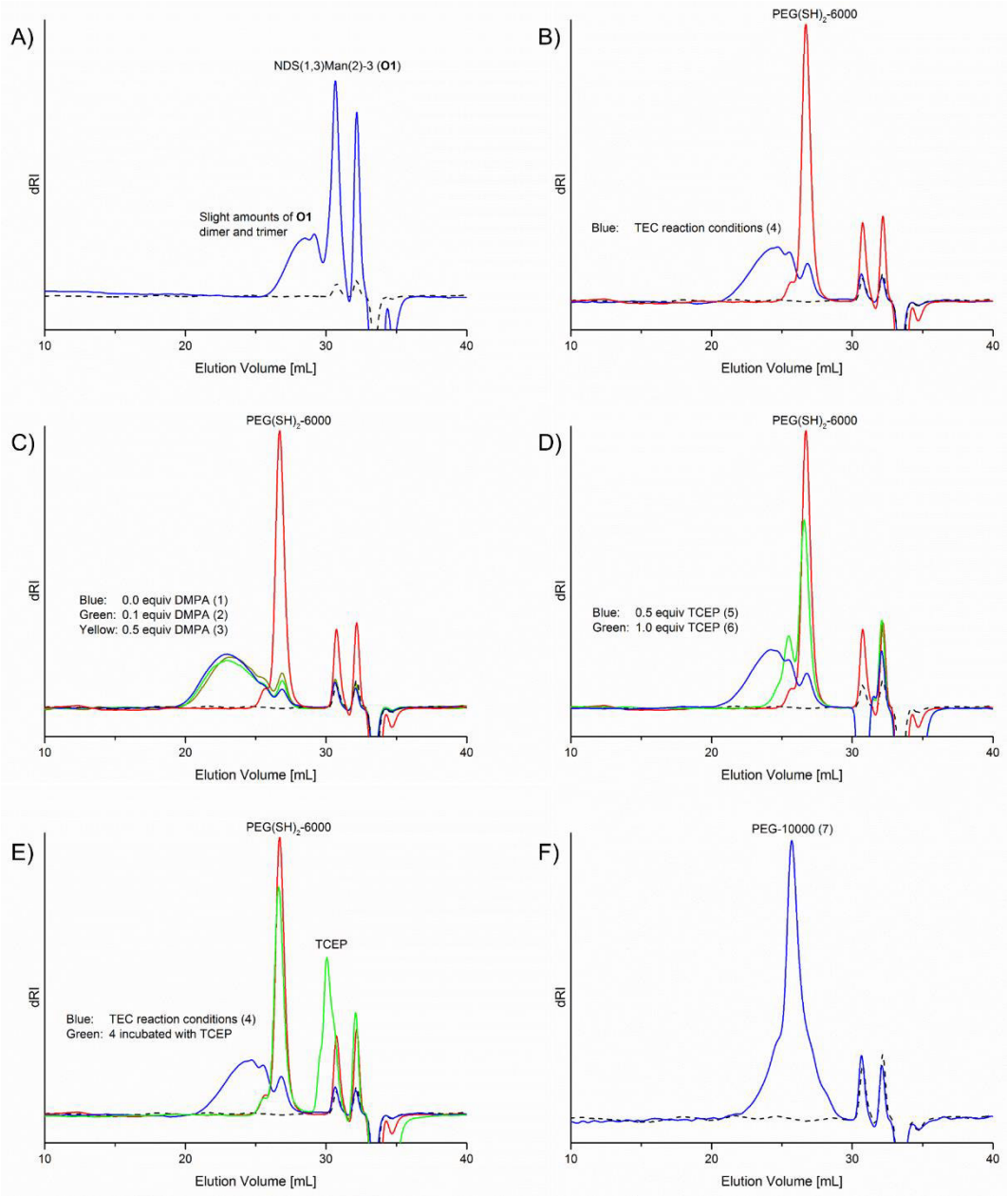

Figure S48: GPC elugrams of performed control experiments. A) Irradiation of structure **O1** using optimized TEC conditions without the presence of $PEG(SH)_2$-6000. B) Irradiation of $PEG(SH)_2$-6000 using optimized TEC conditions without the presence of a NDS carrying oligomer (blue (4)) and $PEG(SH)_2$-6000 without irradiation (red). C) Irradiation of $PEG(SH)_2$-6000 without the presence of a NDS carrying oligomer with 0.0 (blue (1)), 0.1 (green (2)) and 0.5 equiv DMPA (yellow (3)) as well as $PEG(SH)_2$-6000 without irradiation (red). D) Irradiation of $PEG(SH)_2$-6000 without the presence of a NDS carrying oligomer with 0.5 (blue (5)) and 1.0 equiv TCEP (green (6)) as well as $PEG(SH)_2$-6000 without irradiation (red). E) Irradiation of $PEG(SH)_2$-6000 using optimized TEC conditions without the presence of a NDS carrying oligomer (blue), the same sample after incubation with high excess of TCEP (green) and $PEG(SH)_2$-6000 without irradiation (red). F) Irradiation of PEG-10kDa using optimized TEC conditions without the presence of a NDS carrying oligomer (blue (7)).

Table S1: Used amounts of TCEP and DMPA as well as obtained $\bar{M}_w$, $\bar{M}_n$ and $\bar{M}_w/\bar{M}_n$ for performed control experiments determined by GPC-RI-LS analysis.

PEG	Experiment No.	TCEP [equiv]	DMPA [equiv]	$\bar{M}_w$ [kDa]	$\bar{M}_n$ [kDa]	$\bar{M}_w/\bar{M}_n$
$PEG(SH)_2$-6000	1	0.01	0	53.2	29.0	1.8
	2	0.01	0.1	60.6	31.6	1.9
	3	0.01	0.5	63.6	33.0	1.9
	4	0.01	1	38.1	22.7	1.7
	5	0.5	1	36.2	23.3	1.6
	6	1	1	10.2	8.9	1.1
PEG-10000	7	0.01	1	15.8	10.6	1.5

Polymerization of O2 and $PEG(SH)_2$-6000 using higher amounts of TCEP

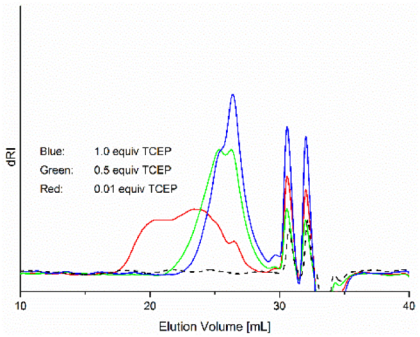

Figure S49: GPC elugrams for preformed TEC polymerization using higher amounts of TCEP (0.5 (green) and 1.0 equiv (blue)) compared to the optimized amount of 0.01 equiv TCEP (red).

Mechanism of the desulfurization of $PEG(SH)_2$-6000 according to the group of Brik[1] and the formation of the terminal ethyl group.

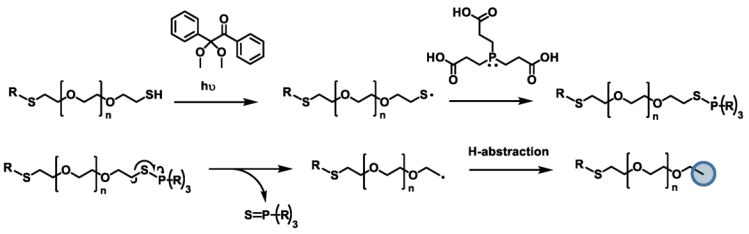

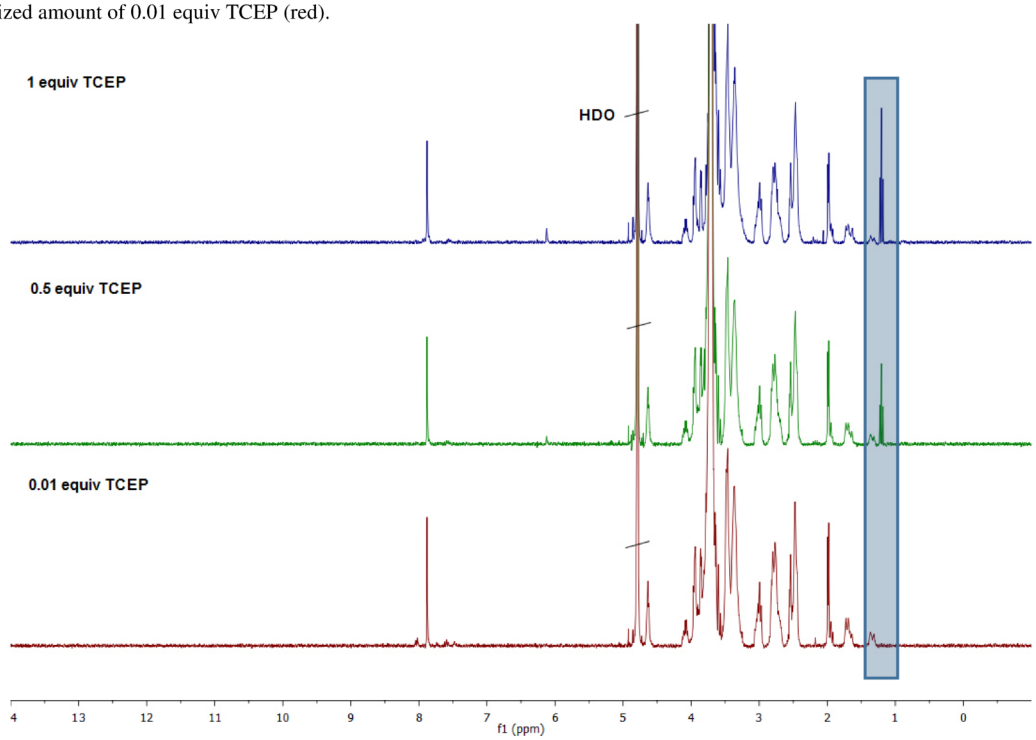

Figure S50: ^{1}H-NMR (300 MHz, D_2O) for preformed TEC polymerization using higher amounts of TCEP (0.5 (green) and 1.0 equiv (blue)) compared to the optimized amount of 0.01 equiv TCEP (red). Signals for the formed ethyl group at 1.2 ppm after desulfurization are highlighted (blue square).

Glycooligoamide – PEG multiblock copolymer purification procedures

Con A Sepharose affinity chromatography

The affinity chromatography purification procedure was performed for glycooligoamide – PEG multiblock copolymers **P1** – **P5**. For all polymers batches 1 and 2 were pooled.

30 mL of Concanavalin A (Con A) Sepharose™ 4B resin (containing 13 mg/mL Con A) in 0.1 M acetate buffer at pH 6.0 with 20% ethanol was pipetted into a glass chromatography column (1.7 cm diameter). The column material was covered with glass wool and conditioned with 180 mL (6 column volumes) lectin binding buffer (LBB) (10 mM Hepes, 50 mM NaCl, 1 mM $MnCl_2$, 1 mM $CaCl_2$, pH 7.4). Each glycopolymer (pooled batches 1 and 2 of **P1** – **P5**) was dissolved in 5 mL of LBB and applied to the column. The column was washed with 160 mL LBB and 20 mL fractions were collected. Subsequently, the bound glycopolymers were eluted using 160 mL of αMeMan (0.1 M for **P1**, **P2** and **P4** and 0.2 M for **P3** and **P5**) in LBB and 20 mL fractions were collected. The column was washed with 150 mL Hepes buffer (10 mM Hepes, 50 mM NaCl, pH 7.4) followed by 150 mL Hepes buffer (pH 8.5) and reconditioned for next use by 150 mLHepes buffer (pH 7.4) followed by 150 mL LBB. The fractions 1 – 5 from the washing procedure and fractions 1 – 6 of the glycopolymer elution procedure were combined and salts as well as αMeMan were removed by ultrafiltration using Vivaspin 6 centrifugal concentrators with a MWCO of 5000 Da. The glycopolymers were recovered from the Vivaspin concentrators and freeze-dried.

Preparative GPC fractionation

The fractionation procedure by preparative GPC was performed for glycooligoamide – PEG multiblock copolymers **P1** – **P5**.

For the fractionation of the glycopolymers an Agilent 1260 Infinity instrument coupled to a variable wavelength detector (VWD) (Set to 214 nm) and an automated fraction collector (FC) was used. As size-exclusion column a GPC HiLoad 16/600 Superdex 200 pg column from GE Healthcare was used. As mobile phase a buffer of MilliQ water with 50 mM NaH_2PO_4 and 150 mM NaCl. The flow rate was set to 1 ml/min and 100 min isocratic runs were performed for all polymers. Starting from 30 min of each run, 5 min fractions were collected until the end of the run. Individually selected fractions were combined, salts were removed by ultrafiltration using Vivaspin 6 centrifugal concentrators with a MWCO of 5000 Da and subsequently freeze-dried, resulting in three fractions for each glycooligoamide – PEG hybrid multiblock copolymer **P1** – **P5**.

Disulfide reduction and capping of terminal thiol-groups

The disulfide reduction and thiol capping was performed for fraction 1 and 2 of glycooligoamide – PEG multiblock copolymers **P1** – **P4**, faction 1 – 3 of **P5** as well as for **P6**.

For reduction of disulfide linkages in the glycooligoamide – PEG multiblock copolymers, the glycopolymers were incubated for 48 h with an access of 50 equiv TCEP calculated with the $\bar{M}_n$ of the corresponding glycopolymer. The final concentration of the glycopolymers was 2.5 mg/mL and the reduction was performed in degassed H_2O under argon. After the incubation of 48 h, TCEP was removed by ultrafiltration using Vivaspin concentrators with MWCO of 50 or 100 kDa (See **Tables S2** – **S7**). The collected glycopolymers were washed with degassed H_2O to prevent reoxidation of the generated thiols, recovered from the Vivaspin concentrators and freeze-dried. The liberated thiols were capped with *N*-ethylmaleimide (NEM) by adding 50 equiv of the maleimide in degassed Hepes buffer (10 mM, pH 7.2) under argon for 12 h and the capped glycooligoamide – PEG copolymers were again purified by ultrafiltration (using the same Vivaspin concentrators as after the disulfide reduction) to remove Hepes as well as excess of NEM, subsequently recovered and freeze-dried. The liberated thiols of two samples, fraction 2 of **P2** and **P3**, were capped using Alexa Fluor™ 488 C_5 maleimide. The capping with the fluorophore was performed with an excess of 15 equiv of maleimide using the same reaction conditions and purification steps as for the functionalization with NEM.

Characterization of glycooligoamide – PEG hybrid multiblock copolymers

Poly-NDS(1,3)Man(2)-3 (P1):

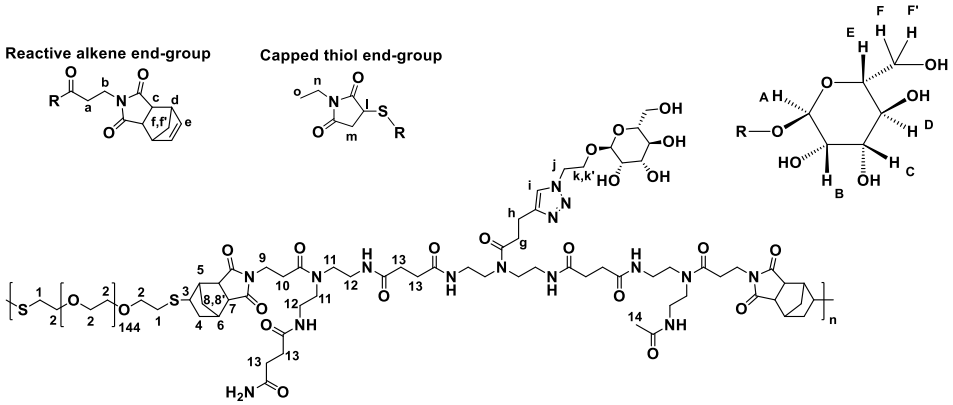

Obtained yields for glycooligoamide – PEG multiblock copolymer **P1** after the synthesis as well as each purification step are listed in Table S2.

Table S2: Determined yields for each reaction and purification step, remaining amount of reactive alkene end-groups, ratio of oligoamide and PEG, amount of NEM functionalization as well as the slope of the conformational plot and radius of gyration of the final multiblock copolymer **P1**.

Reaction step	Info	Yield [mg]	Yield [%]	MWCO [kDa]	Remaining Alkene [%]	Ratio **O1**:PEG	NEM Funct. [%]	Confor. Plot	R_g [nm]
Synthesis	Batch 1	101.6	69	-	-	-	-	-	-
	Batch 2	104.3	71	-	-	-	-	-	-
Affinity Chromatography	Washing	101.7	49[a)]	5	-	-	-	-	-
	Elution	44.9	22[a)]	5	-	-	-	-	-
Preparative GPC	Fraction 1	10.3	5.0[a)]	5	1.3	0.90:1	-	-	-
	Fraction 2	11.7	5.7[a)]	5	2.0	0.97:1	-	-	-
	Fraction 3	7.3	3.5[a)]	5	-	-	-	-	-
Disulfide reduction and thiol capping	Fraction 1	9.3	4.5[a)]	50	1.3	0.90:1	4.7	0.33	19.0
	Fraction 2	4.5	2.1[a)]	100	1.5	0.94:1	1.5	0.32	15.5
	Fraction 3	-	-	-	-	-	-	-	-

a) Theoretical yield in % calculated using the sum of batch 1 and batch 2, which were pooled prior to the purification steps.

The anomeric proton of Mannose (A) could not be examined in ^{1}H-NMR due to the overlaying signal from the residual solvent. Signals with chemical shift of δ 8.07 – 8.01 (m), 7.77 – 7.72 (m) and 7.66 – 7.56 (m) ppm are assumed to be recombination products with DMPA radicals. Stated amounts of protons correspond to one repeating unit of the polymer. ^{1}H-NMR (600 MHz, D_2O): δ 7.89 (s, 1H, i), 6.13 (s, end-group, e), 4.68 – 4.61 (m, 2H, j), 4.14 – 4.06 (m, 1H, k or k'), 3.96 – 3.90 (m, 1H, k or k'), 3.88 – 3.85 (m, 1H, B), 3.85 – 3.56 (m, 586H, 2+5+9+F+F'+C+D), 3.54 – 3.23 (m, 28H, 7+11+12), 3.07 – 3.03 (m, 1H, E), 3.00 (t, J = 7.3 Hz, 2H, h), 2.92 – 2.66 (m, 14H, 1+3+6+10+g), 2.59 – 2.41 (m, 12H, 13), 2.02 – 1.92 (m, 5H, 14+8 or 8'), 1.77 – 1.60 (m, 4H, 4), 1.43 – 1.27 (m, 2H, 8 or 8'), 1.23 – 1.10 (m, ethyl group from the NEM-functionalization, o) ppm. The assignment of the signals was performed according to the structural similarities with compound **O1** and PEG(SH)$_2$-6000.

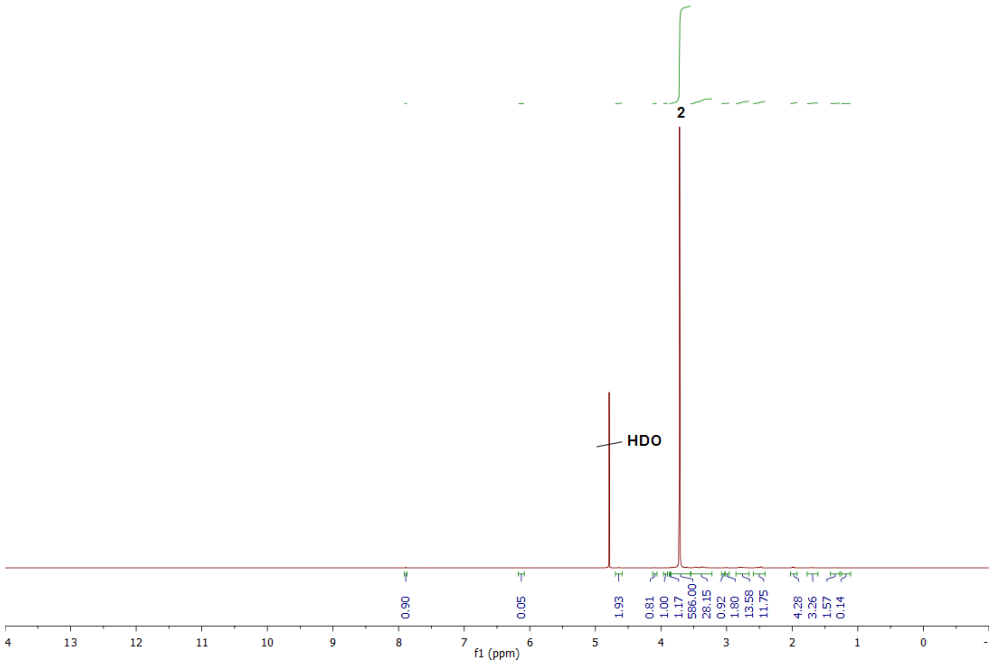

Figure S51: ^{1}H-NMR (600 MHz, D_2O) of fraction 1 from **P1** showing the intense signal for the PEG backbone.

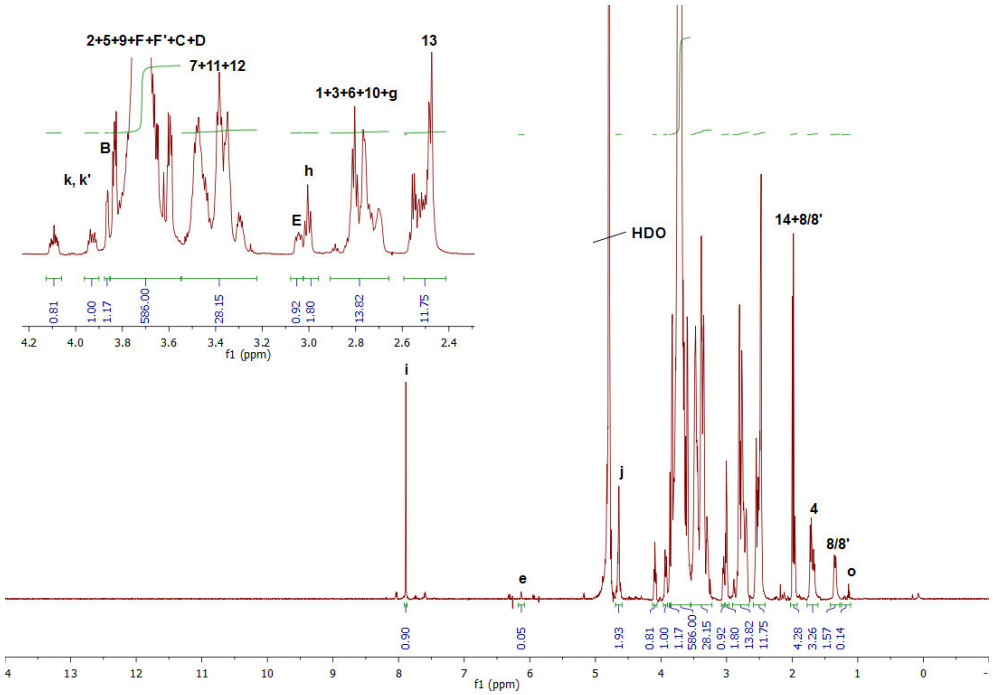

Figure S52: ^{1}H-NMR (600 MHz, D_2O) of fraction 1 from **P1** showing the signals for the glycooligoamide enlarging the area from δ 4.2 to 2.4 ppm.

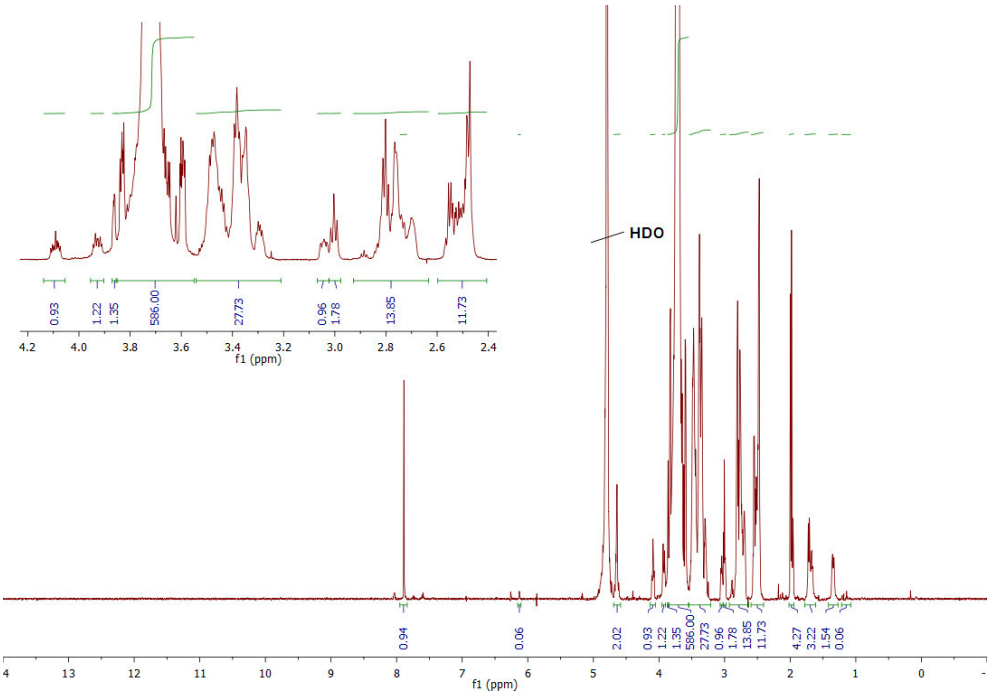

Figure S53: ^{1}H-NMR (600 MHz, D_2O) of fraction 2 from **P1** showing the signals for the glycooligoamide enlarging the area from δ 4.2 to 2.4 ppm.

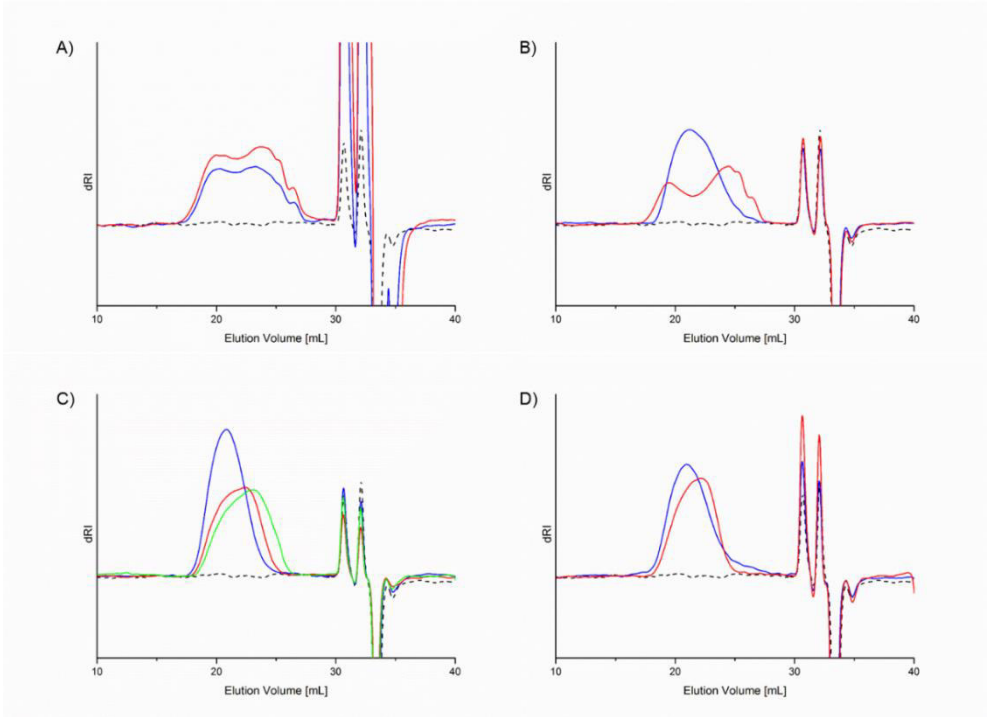

Figure S54: GPC-RI-LS elugrams of **P1** at different steps during the synthesis and purification. A) From the two batches (batch 1 (blue) and batch 2 (red)). B) From the purification by affinity chromatography after the washing (red) and the elution (blue) process. C) From the purification by preparative GPC of the three separated fractions 1 (blue), 2 (red) and 3 (green). D) From the disulfide reduction and thiol capping procedure of fraction 1 (blue) and 2 (red). Columns: Suprema Lux (2 X 100 and 1 X 1000 Å). Buffer: 50 mM NaH_2PO_4, 150 mM NaCl, 250 ppm of NaN_3 (pH 7.2), 30% ACN. Flow: 0.8 mL/min.

Poly-NDS(1,4)Man(2,3)-4 (P2):

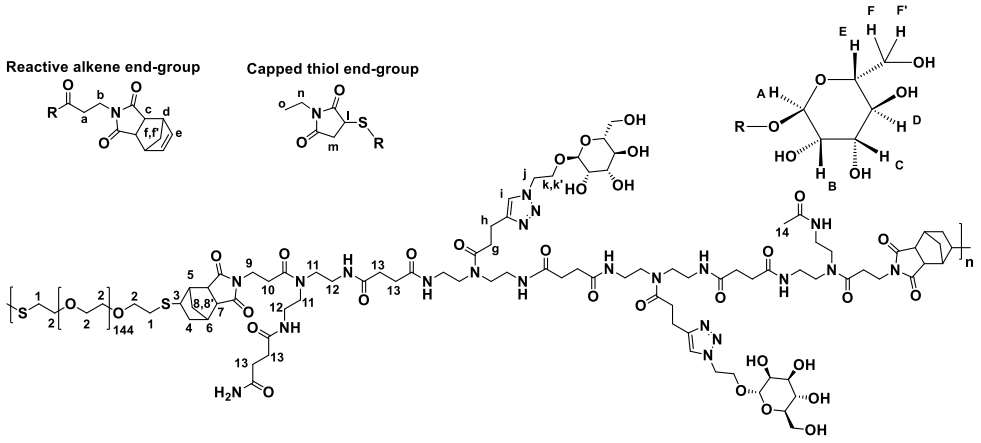

Obtained yields for glycooligoamide – PEG multiblock copolymer **P2** after the synthesis as well as each purification step are listed in Table S3.

Table S3: Determined yields for each reaction and purification step, remaining amount of reactive alkene end-groups, ratio of oligoamide and PEG, amount of NEM functionalization as well as the slope of the conformational plot and radius of gyration of the final multiblock copolymer **P2**.

Reaction step	Info	Yield [mg]	Yield [%]	MWCO [kDa]	Remaining Alkene [%]	Ratio **O2**:PEG	NEM Funct. [%]	Confor. Plot	R_g [nm]
Synthesis	Batch 1	90.5	57	-	-	-	-	-	-
	Batch 2	78.1	49	-	-	-	-	-	-
Affinity Chromatography	Washing	72.7	43[a)]	5	-	-	-	-	-
	Elution	58.9	35[a)]	5	-	-	-	-	-
Preparative GPC	Fraction 1	11.7	6.9[a)]	5	n.d.[b)]	0.90:1	-	-	-
	Fraction 2	13.6	8.1[a)]	5	1.3	0.95:1	-	-	-
	Fraction 3	12.7	7.5[a)]	5	-	-	-	-	-
Disulfide reduction and thiol capping	Fraction 1	8.4	5.0[a)]	50	1.0	0.91:1	2.8	0.28	22.0
	Fraction 2	2.8	1.7[a)]	100	1.0	0.92:1	1.3	0.31	16.8
	Fraction 3	-	-		-	-	-	-	-

a) Theoretical yield in % calculated using the sum of batch 1 and batch 2, which were pooled prior to the purification steps.
b) No signal for remaining alkene end-groups determined.

The anomeric proton of Mannose (A) could not be examined in ^{1}H-NMR due to the overlaying signal from the residual solvent. Signals with chemical shift of δ 8.07 – 8.01 (m), 7.77 – 7.72 (m) and 7.66 – 7.56 (m) ppm are assumed to be recombination products with DMPA radicals. Stated amounts of protons correspond to one repeating unit of the polymer. ^{1}H-NMR (600 MHz, D_2O): δ 7.88 (s, 2H, i), 6.12 (s, end-group, e), 4.69 – 4.59 (m, 4H, j), 4.14 – 4.05 (m, 2H, k or k'), 3.95 – 3.90 (m, 2H, k or k'), 3.87 – 3.85 (m, 2H, B), 3.85 – 3.56 (m, 590H, 2+5+9+F+F'+C+D), 3.55 – 3.22 (m, 36H, 7+11+12), 3.07 – 3.02 (m, 2H, E), 3.00 (t, J = 7.3 Hz, 4H, h), 2.91 – 2.66 (m, 16H, 1+3+6+10+g), 2.61 – 2.39 (m, 16H, 13), 2.04 – 1.91 (m, 5H, 14+8 or 8'), 1.76 – 1.63 (m, 4H, 4), 1.40 – 1.29 (m, 2H, 8 or 8'), 1.23 – 1.07 (m, ethyl group from the NEM-functionalization, o) ppm. The assignment of the signals was performed according to the structural similarities with compound **O2** and PEG(SH)$_2$-6000.

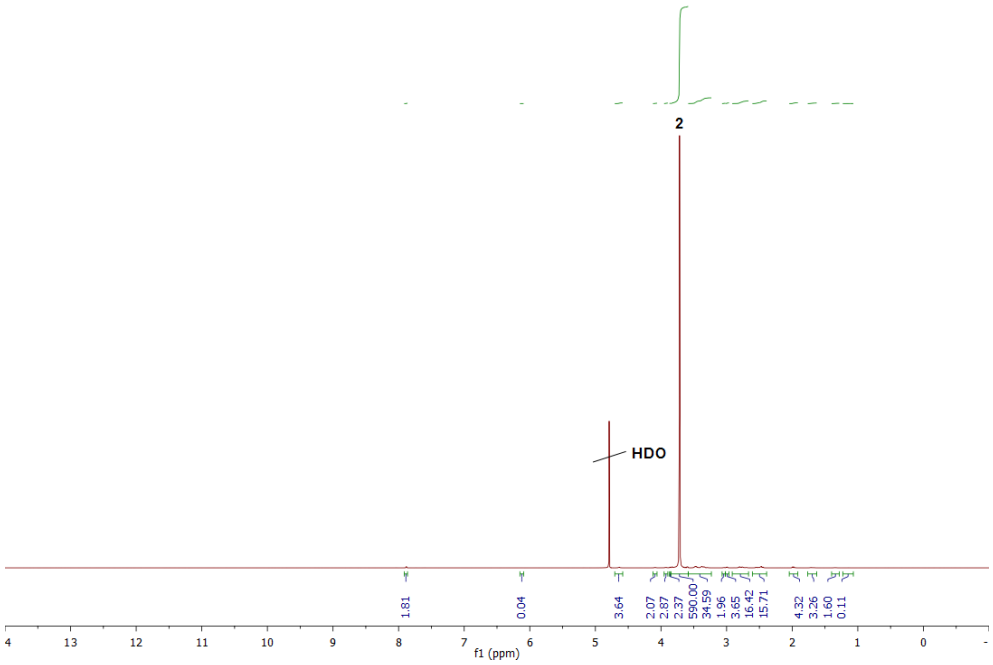

Figure S55: ^{1}H-NMR (600 MHz, D_2O) of fraction 1 from **P2** showing the intense signal for the PEG backbone.

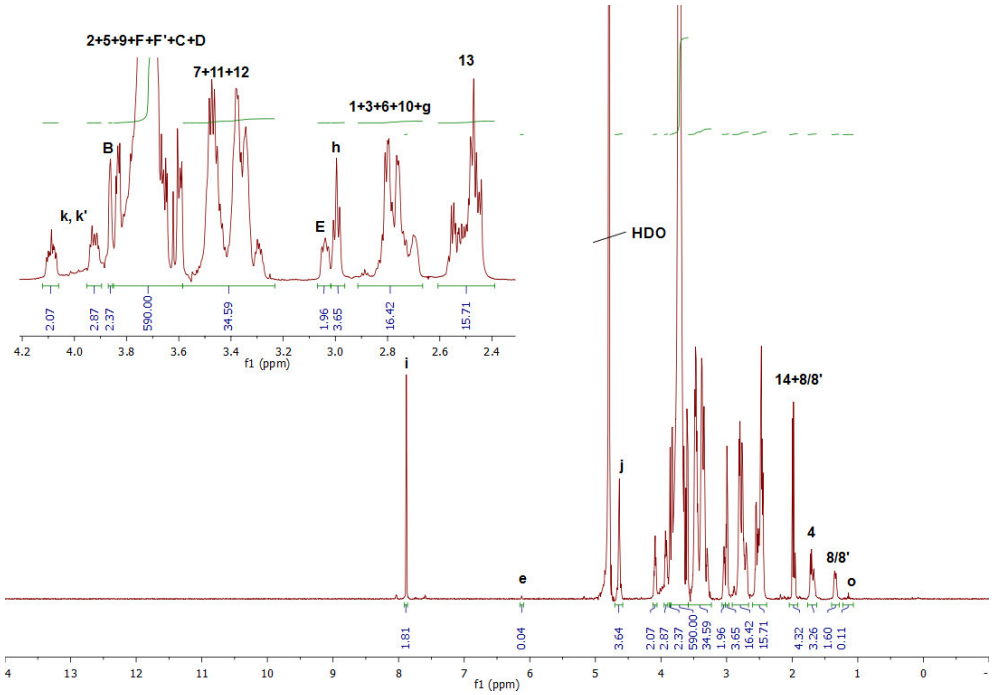

Figure S56: ^{1}H-NMR (600 MHz, D_2O) of fraction 1 from **P2** showing the signals for the glycooligoamide enlarging the area from δ 4.2 to 2.4 ppm.

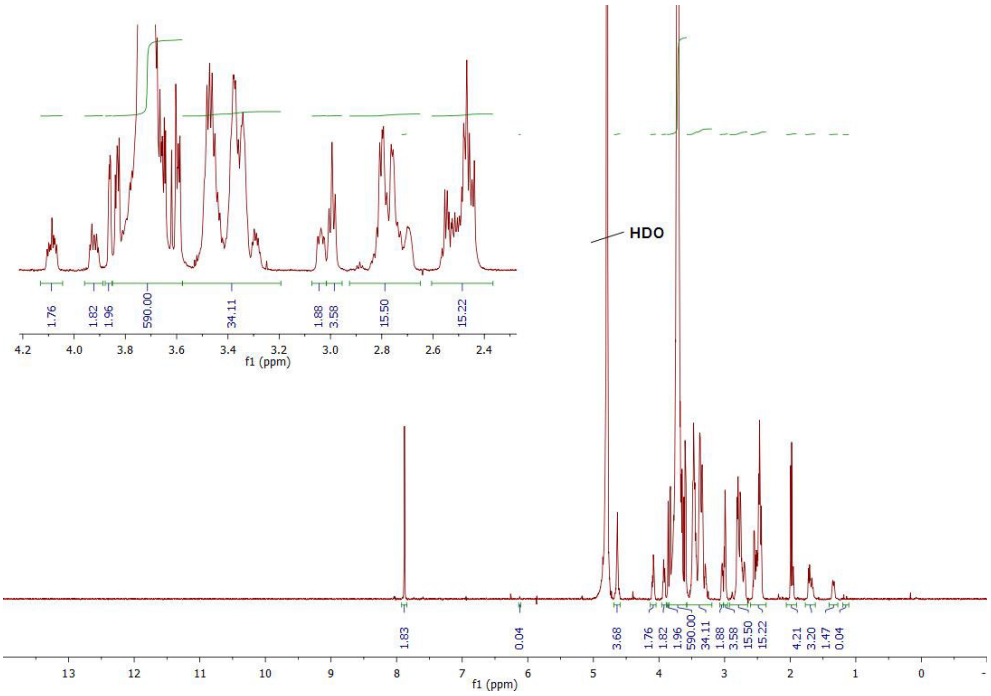

Figure S57: ^{1}H-NMR (600 MHz, D_2O) of fraction 2 from **P2** showing the signals for the glycooligoamide enlarging the area from δ 4.2 to 2.4 ppm.

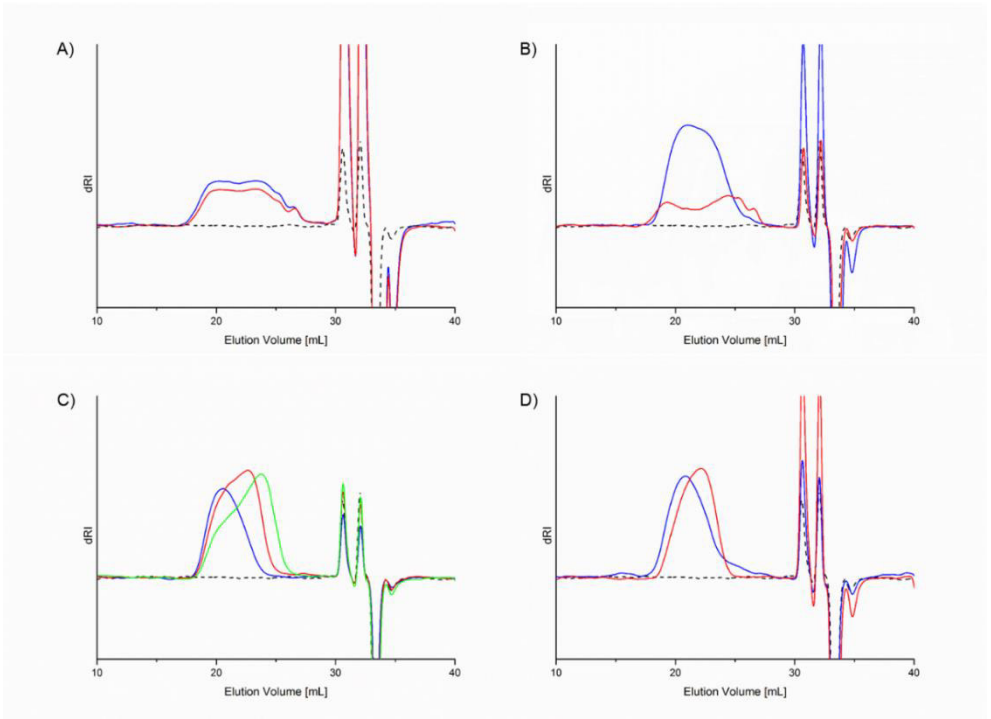

Figure S58: GPC-RI-LS elugrams of **P2** at different steps during the synthesis and purification. A) From the two batches (batch 1 (blue) and batch 2 (red)). B) From the purification by affinity chromatography after the washing (red) and the elution (blue) process. C) From the purification by preparative GPC of the three separated fractions 1 (blue), 2 (red) and 3 (green). D) From the disulfide reduction and thiol capping procedure of fraction 1 (blue) and 2 (red). Columns: Suprema Lux (2 X 100 and 1 X 1000 Å). Buffer: 50 mM NaH_2PO_4, 150 mM NaCl, 250 ppm of NaN_3 (pH 7.2), 30% ACN. Flow: 0.8 mL/min.

Poly-NDS(1,5)Man(2,3,4)-5 (P3):

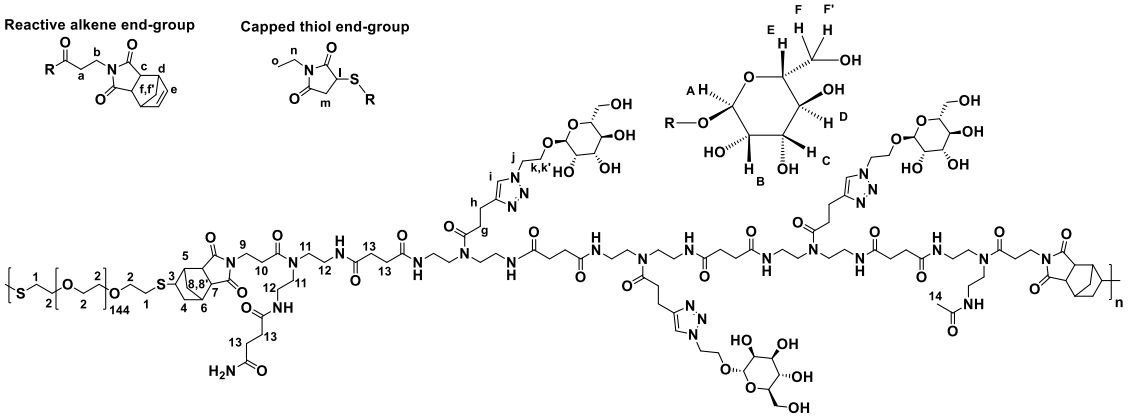

Obtained yields for glycooligoamide – PEG multiblock copolymer **P3** after the synthesis as well as each purification step are listed in Table S4.

Table S4: Determined yields for each reaction and purification step, remaining amount of reactive alkene end-groups, ratio of oligoamide and PEG, amount of NEM functionalization as well as the slope of the conformational plot and radius of gyration of the final multiblock copolymer **P3**.

Reaction step	Info	Yield [mg]	Yield [%]	MWCO [kDa]	Remaining Alkene [%]	Ratio **O3**:PEG	NEM Funct. [%]	Confor. Plot	R_g [nm]
Synthesis	Batch 1	116.7	69	-	-	-	-	-	-
	Batch 2	108.6	64	-	-	-	-	-	-
Affinity Chromatography	Washing	83.3	37[a)]	5	-	-	-	-	-
	Elution	55.6	25[a)]	5	-	-	-	-	-
Preparative GPC	Fraction 1	10.3	4.6[a)]	5	2.0	0.94:1	-	-	-
	Fraction 2	15.1	6.7[a)]	5	2.5	1:1	-	-	-
	Fraction 3	10.7	4.8[a)]	5	-	-	-	-	-
Disulfide reduction and thiol capping	Fraction 1	9.6	4.3[a)]	50	2.0	0.91:1	7.7	0.28	22.7
	Fraction 2	3.5	1.6[a)]	100	2.3	0.92:1	2.3	0.27	19.8
	Fraction 3	-	-	-	-	-	-	-	-

a) Theoretical yield in % calculated using the sum of batch 1 and batch 2, which were pooled prior to the purification steps.

The anomeric proton of Mannose (A) could not be examined in ^{1}H-NMR due to the overlaying signal from the residual solvent. Signals with chemical shift of δ 8.07 – 8.01 (m), 7.77 – 7.72 (m) and 7.66 – 7.56 (m) ppm are assumed to be recombination products with DMPA radicals. Stated amounts of protons correspond to one repeating unit of the polymer. ^{1}H-NMR (600 MHz, D_2O): δ 7.90 – 7.85 (m, 3H, i), 6.14 – 6.09 (s, end-group, e), 4.69 – 4.57 (m, 6H, j), 4.14 – 4.03 (m, 3H, k or k'), 3.96 – 3.89 (m, 3H, k or k'), 3.88 – 3.85 (m, 3H, B), 3.85 – 3.58 (m, 594H, 2+5+9+F+F'+C+D), 3.55 – 3.20 (m, 44H, 7+11+12), 3.07 – 3.02 (m, 3H, E), 3.01 – 2.95 (m, 6H, h), 2.91 – 2.65 (m, 18H, 1+3+6+10+g), 2.60 – 2.36 (m, 20H, 13), 2.05 – 1.89 (m, 5H, 14+8 or 8'), 1.79 – 1.57 (m, 4H, 4), 1.44 – 1.25 (m, 2H, 8 or 8'), 1.23 – 1.07 (m, ethyl group from the NEM-functionalization, o) ppm. The assignment of the signals was performed according to the structural similarities with compound **O3** and PEG(SH)$_2$-6000.

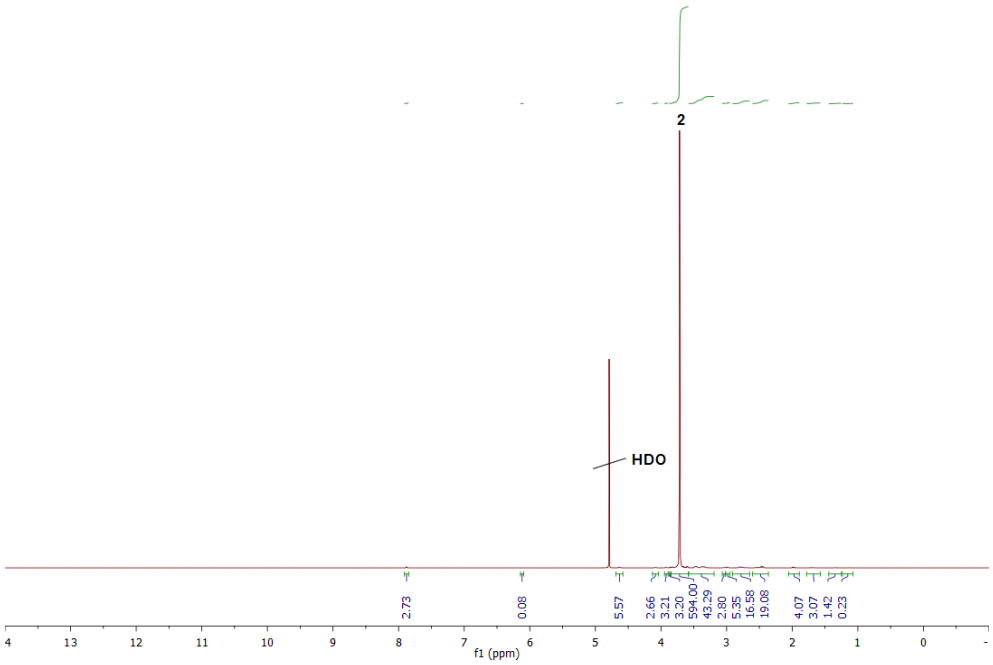

Figure S59: ^{1}H-NMR (600 MHz, D_2O) of fraction 1 from **P3** showing the intense signal for the PEG backbone.

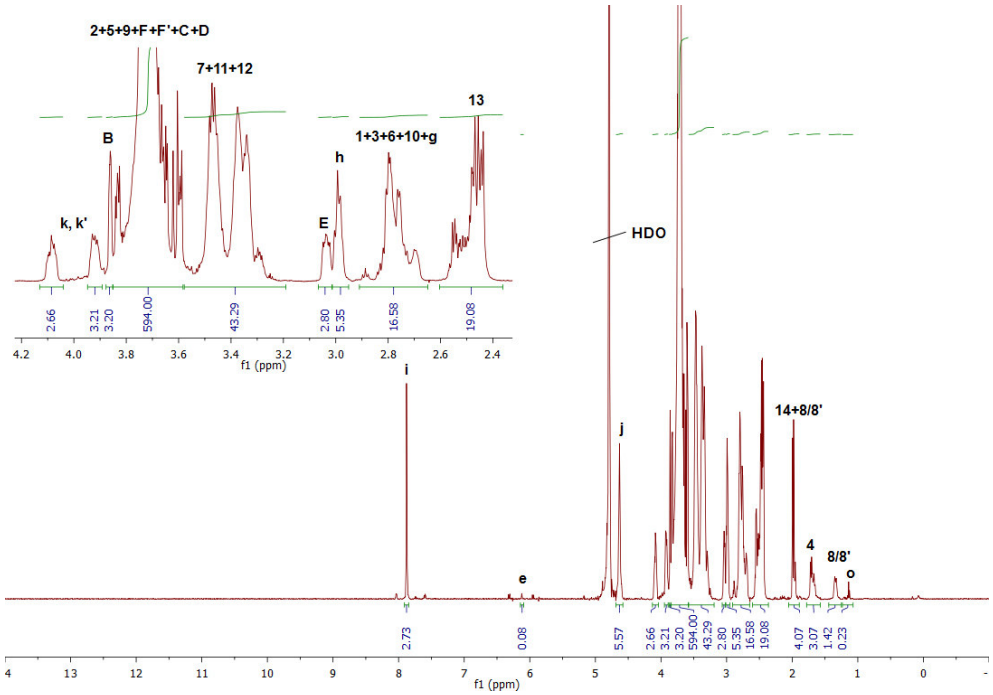

Figure S60: ^{1}H-NMR (600 MHz, D_2O) of fraction 1 from **P3** showing the signals for the glycooligoamide enlarging the area from δ 4.2 to 2.4 ppm.

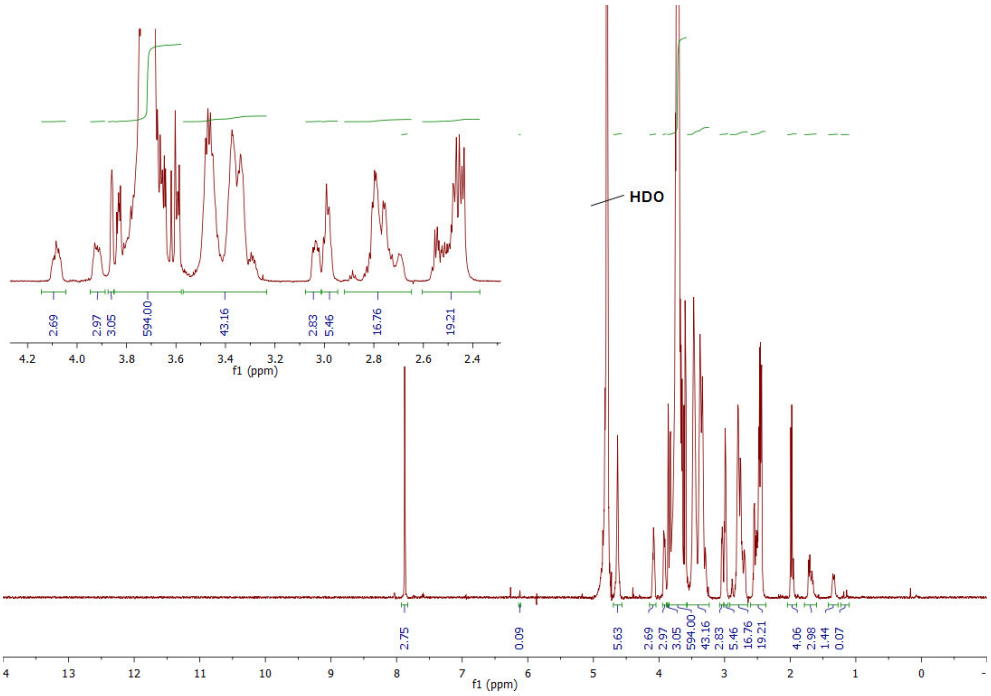

Figure S61: ^{1}H-NMR (600 MHz, D_2O) of fraction 2 from **P3** showing the signals for the glycooligoamide enlarging the area from δ 4.2 to 2.4 ppm.

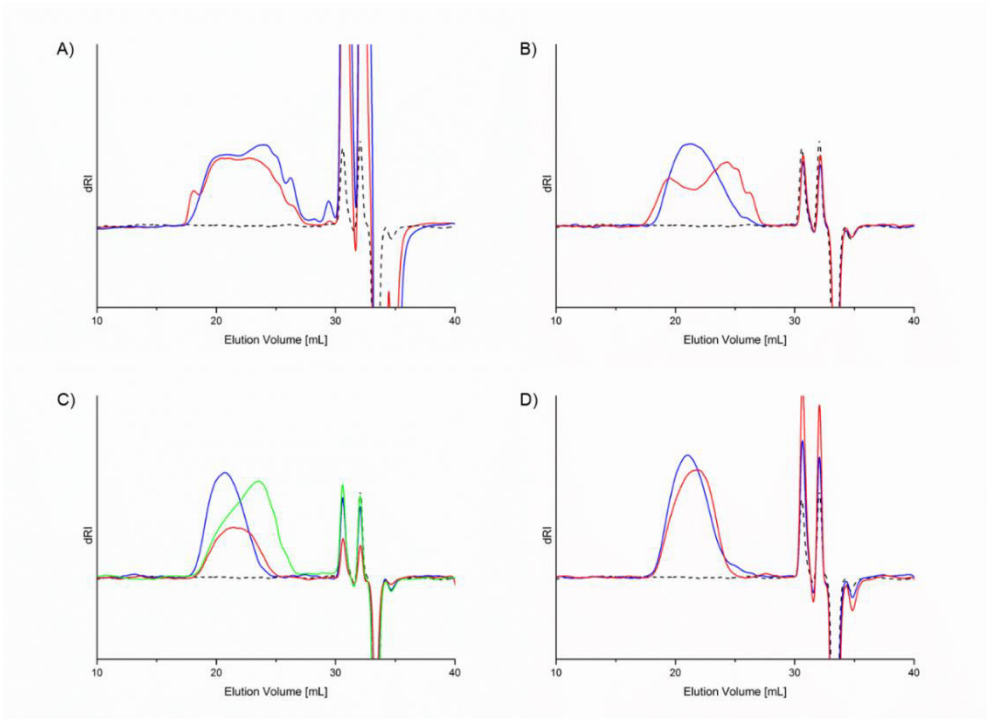

Figure S62: GPC-RI-LS elugrams of **P3** at different steps during the synthesis and purification. A) From the two batches (batch 1 (blue) and batch 2 (red)). B) From the purification by affinity chromatography after the washing (red) and the elution (blue) process. C) From the purification by preparative GPC of the three separated fractions 1 (blue), 2 (red) and 3 (green). D) From the disulfide reduction and thiol capping procedure of fraction 1 (blue) and 2 (red). Columns: Suprema Lux (2 X 100 and 1 X 1000 Å). Buffer: 50 mM NaH_2PO_4, 150 mM NaCl, 250 ppm of NaN_3 (pH 7.2), 30% ACN. Flow: 0.8 mL/min.

Poly-NDS(1,8)Man(2,7)-8 (P4):

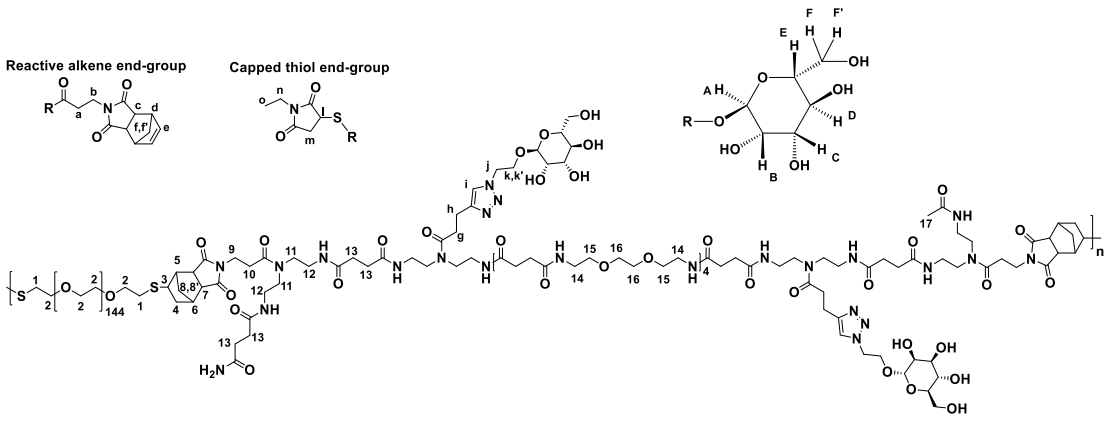

Obtained yields for glycooligoamide – PEG multiblock copolymer **P4** after the synthesis as well as each purification step are listed in Table S5.

Table S5: Determined yields for each reaction and purification step, remaining amount of reactive alkene end-groups, ratio of oligoamide and PEG, amount of NEM functionalization as well as the slope of the conformational plot and radius of gyration of the final multiblock copolymer **P4**.

Reaction step	Info	Yield [mg]	Yield [%]	MWCO [kDa]	Remaining Alkene [%]	Ratio **O4**:PEG	NEM Funct. [%]	Confor. Plot	R_g [nm]
Synthesis	Batch 1	132.5	75	-	-	-	-	-	-
	Batch 2	108.6	62	-	-	-	-	-	-
Affinity Chromatography	Washing	98.9	41[a)]	5	-	-	-	-	-
	Elution	48.0	20[a)]	5	-	-	-	-	-
Preparative GPC	Fraction 1	11.3	4.7[a)]	5	5.0	0.95:1	-	-	-
	Fraction 2	9.4	3.9[a)]	5	7.3	1.06:1	-	-	-
	Fraction 3	10.6	4.4[a)]	5	-	-	-	-	-
Disulfide reduction and thiol capping	Fraction 1	10.7	4.4[a)]	50	4.8	0.91:1	15	0.32	16.6
	Fraction 2	5.3	2.2[a)]	100	5.0	0.92:1	4.3	0.35	15.1
	Fraction 3	-	-	-	-	-	-	-	-

a) Theoretical yield in % calculated using the sum of batch 1 and batch 2, which were pooled prior to the purification steps.

The anomeric proton of Mannose (A) could not be examined in ^{1}H-NMR due to the overlaying signal from the residual solvent. Signals with chemical shift of δ 8.07 – 8.01 (m), 7.77 – 7.72 (m) and 7.66 – 7.56 (m) ppm are assumed to be recombination products with DMPA radicals. Stated amounts of protons correspond to one repeating unit of the polymer. ^{1}H-NMR (600 MHz, D_2O): δ 7.89 (s, 2H, i), 6.14 – 6.11 (m, end-group, e), 4.69 – 4.60 (m, 4H, j), 4.14 – 4.05 (m, 2H, k or k'), 3.96 – 3.89 (m, 2H, k or k'), 3.87 – 3.85 (m, 2H, B), 3.85 – 3.55 (m, 622H, 2+5+9+15+16+F+F'+C+D), 3.53 – 3.26 (m, 52H, 7+11+12+14), 3.08 – 3.02 (m, 2H, E), 3.00 (t, J = 7.3 Hz, 4H, h), 2.93 – 2.60 (m, 16H, 1+3+6+10+g), 2.59 – 2.41 (m, 32H, 13), 2.05 – 1.90 (m, 5H, 17+8 or 8'), 1.81 – 1.52 (m, 4H, 4), 1.42 – 1.25 (m, 2H, 8 or 8'), 1.23 – 1.07 (m, ethyl group from the NEM-functionalization, o) ppm. The assignment of the signals was performed according to the structural similarities with compound **O4** and PEG(SH)$_2$-6000.

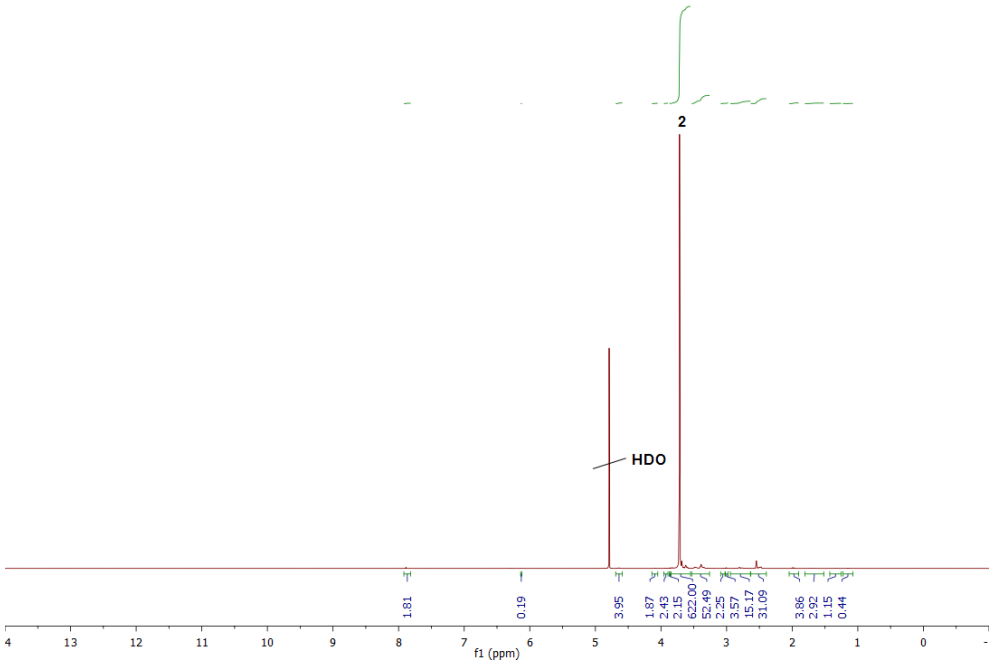

Figure S63: ^{1}H-NMR (600 MHz, D_2O) of fraction 1 from **P4** showing the intense signal for the PEG backbone.

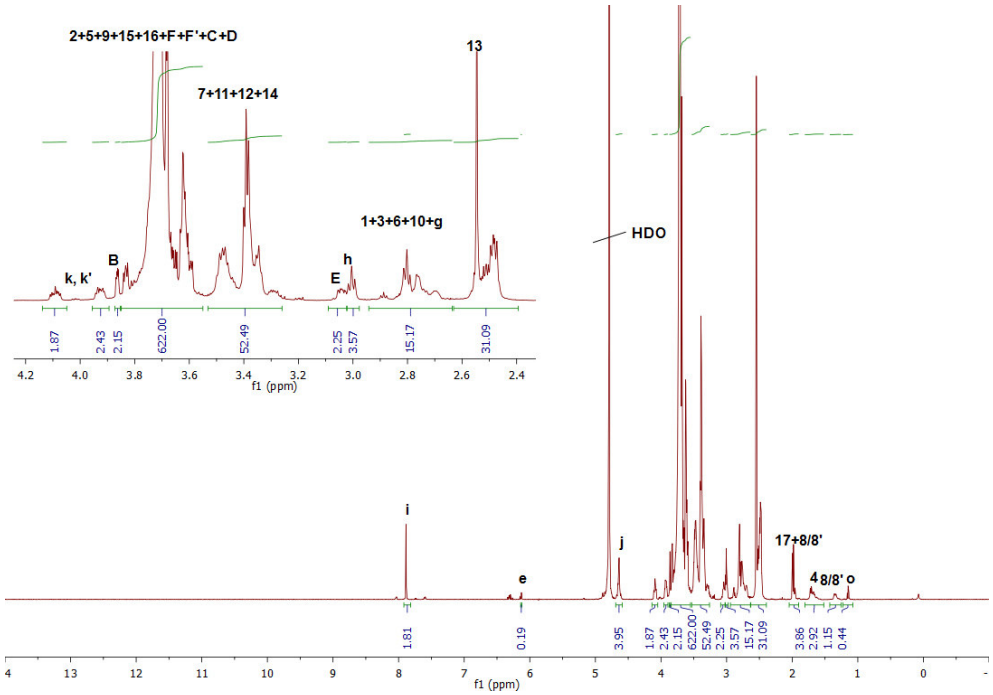

Figure S64: ^{1}H-NMR (600 MHz, D_2O) of fraction 1 from **P4** showing the signals for the glycooligoamide enlarging the area from δ 4.2 to 2.4 ppm.

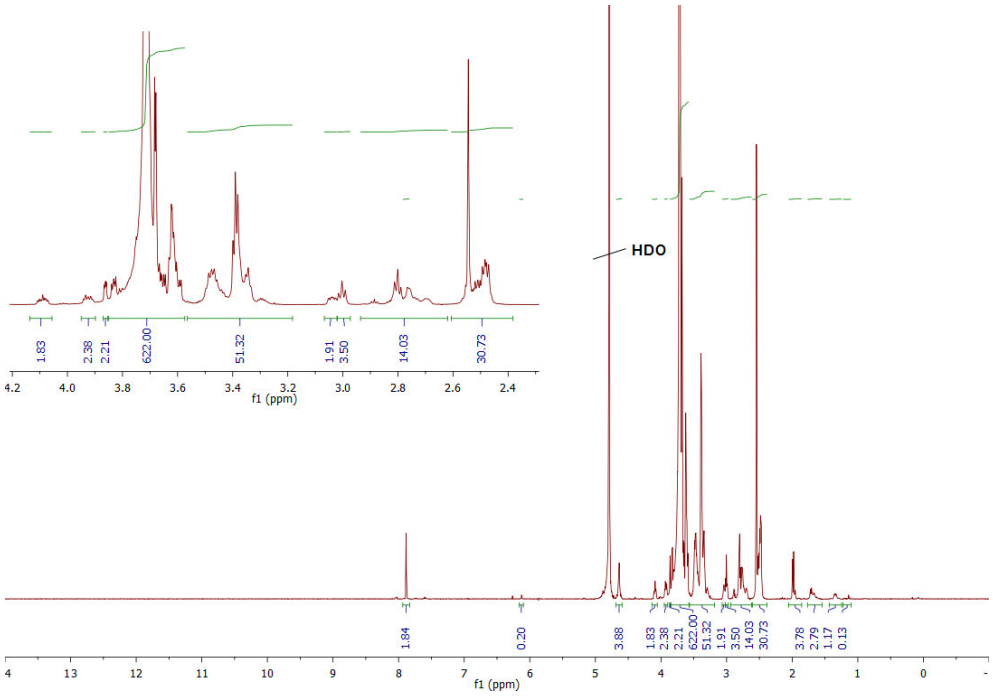

Figure S65: ^{1}H-NMR (600 MHz, D_2O) of fraction 2 from **P4** showing the signals for the glycooligoamide enlarging the area from δ 4.2 to 2.4 ppm.

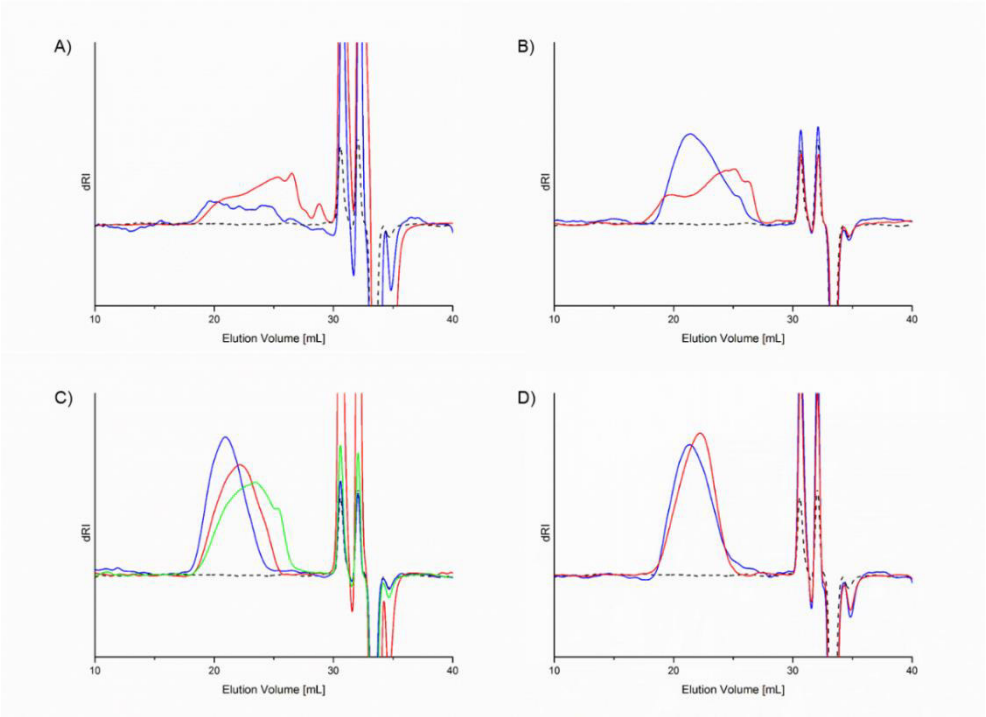

Figure S66: GPC-RI-LS elugrams of **P4** at different steps during the synthesis and purification. A) From the two batches (batch 1 (blue) and batch 2 (red)). B) From the purification by affinity chromatography after the washing (red) and the elution (blue) process. C) From the purification by preparative GPC of the three separated fractions 1 (blue), 2 (red) and 3 (green). D) From the disulfide reduction and thiol capping procedure of fraction 1 (blue) and 2 (red). Columns: Suprema Lux (2 X 100 and 1 X 1000 Å). Buffer: 50 mM NaH_2PO_4, 150 mM NaCl, 250 ppm of NaN_3 (pH 7.2), 30% ACN. Flow: 0.8 mL/min.

Poly-NDS(1,13)Man(2,7,12)-13 (P5):

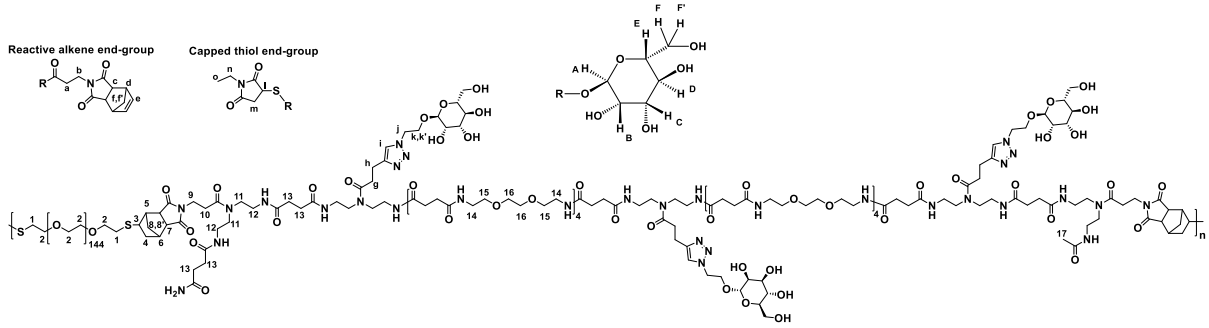

Obtained yields for glycooligoamide – PEG multiblock copolymer **P5** after the synthesis as well as each purification step are listed in Table S6.

Table S6: Determined yields for each reaction and purification step, remaining amount of reactive alkene end-groups, ratio of oligoamide and PEG, amount of NEM functionalization as well as the slope of the conformational plot and radius of gyration of the final multiblock copolymer **P5**.

Reaction step	Info	Yield [mg]	Yield [%]	MWCO [kDa]	Remaining Alkene [%]	Ratio **O5**:PEG	NEM Funct. [%]	Confor. Plot	R_g [nm]
Synthesis	Batch 1	121.8	59	-	-	-	-	-	-
	Batch 2	139.1	68	-	-	-	-	-	-
Affinity Chromatography	Washing	142.0	54[a)]	5	-	-	-	-	-
	Elution	56.0	21[a)]	5	-	-	-	-	-
Preparative GPC	Fraction 1	11.4	4.4[a)]	5	n.d.[b)]	0.92:1	-	-	-
	Fraction 2	12.9	4.9[a)]	5	n.d.[b)]	0.97:1	-	-	-
	Fraction 3	11.4	4.4[a)]	5	n.d.[b)]	0.99:1	-	-	-
Disulfide reduction and thiol capping	Fraction 1	8.7	3.3[a)]	50	0.8	0.92:1	9.3	0.39	16.6
	Fraction 2	11.1	4.3[a)]	50	1.0	0.96:1	8.0	0.35	15.0
	Fraction 3	9.8	3.8[a)]	50	1.5	1.01:1	5.7	0.31	13.5

a) Theoretical yield in % calculated using the sum of batch 1 and batch 2, which were pooled prior to the purification steps.
b) No signal for remaining alkene end-groups determined.

The anomeric proton of Mannose (A) could not be examined in ^{1}H-NMR due to the overlaying signal from residual solvent. Signals with chemical shift of δ 8.07 – 8.01 (m), 7.77 – 7.72 (m) and 7.66 – 7.56 (m) ppm are assumed to be recombination products with DMPA radicals. Stated amounts of protons correspond to one repeating unit of the polymer. ^{1}H-NMR (600 MHz, D_2O): δ 7.92 – 7.81 (m, 3H, i), 6.13 (s, end-group, e), 4.70 – 4.57 (m, 6H, j), 4.12 – 4.05 (m, 3H, k or k'), 3.96 – 3.90 (m, 3H, k or k'), 3.88 – 3.85 (m, 3H, B), 3.85 – 3.55 (m, 658H, 2+5+9+15+16+F+F'+C+D), 3.54 – 3.17 (m, 76H, 7+11+12+14), 3.07 – 3.02 (m, 3H, E), 3.01 (t, J = 7.3 Hz, 6H, h), 2.95 – 2.63 (m, 18H, 1+3+6+10+g), 2.61 – 2.36 (m, 52H, 13), 2.10 – 1.81 (m, 5H, 17+8 or 8'), 1.79 – 1.60 (m, 4H, 4), 1.41 – 1.27 (m, 2H, 8 or 8'), 1.22 – 1.09 (m, ethyl group from the NEM-functionalization, o) ppm. The assignment of the signals was performed according to the structural similarities with compound **O5** and PEG(SH)$_2$-6000.

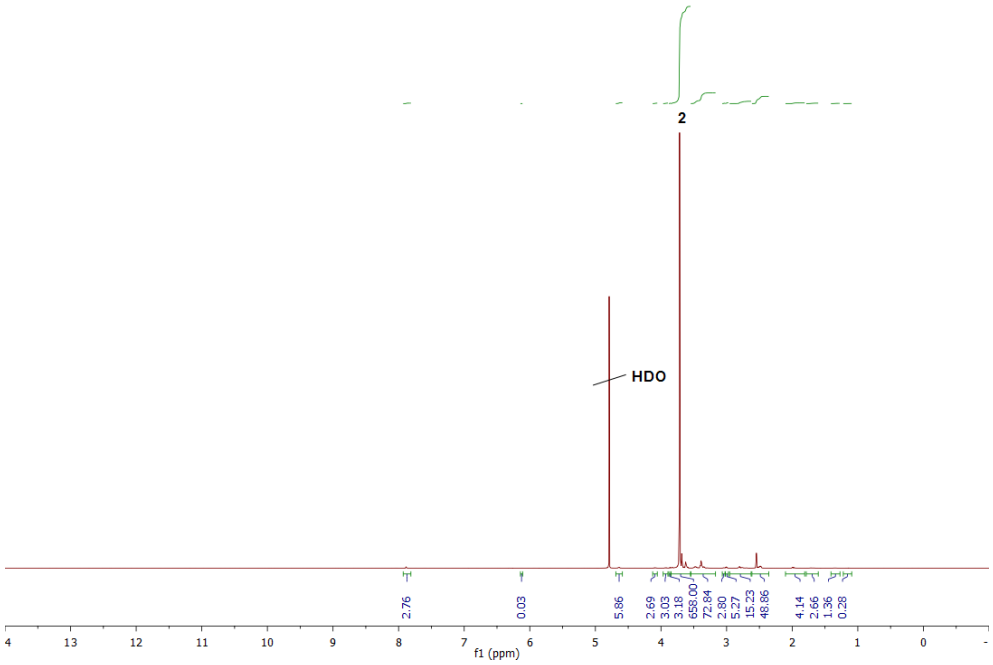

Figure S67: ^{1}H-NMR (600 MHz, D_2O) of fraction 1 from **P5** showing the intense signal for the PEG backbone.

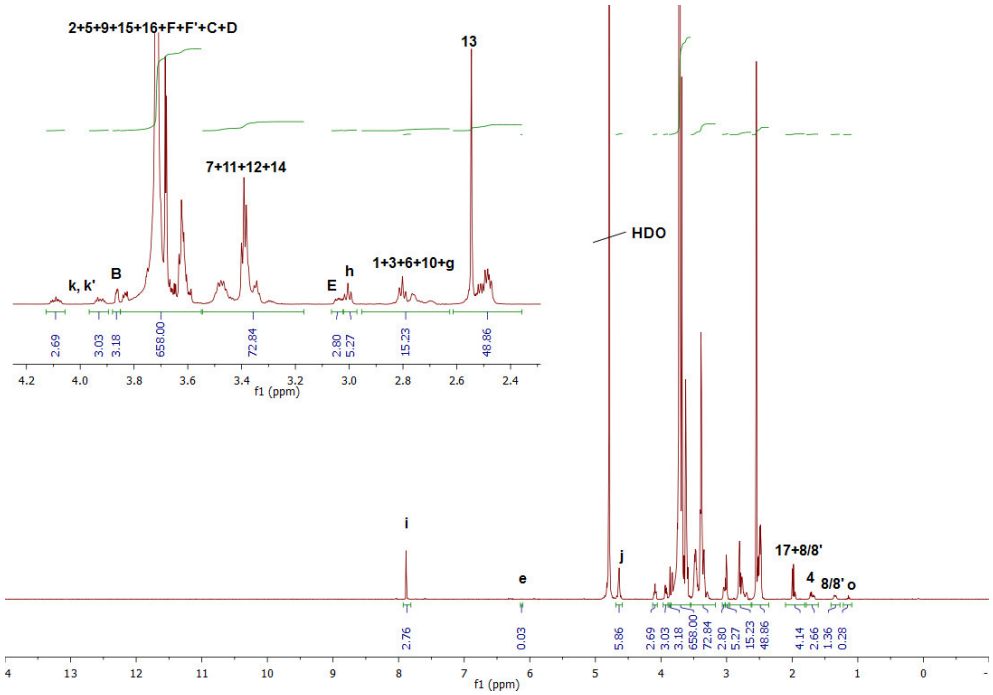

Figure S68: ^{1}H-NMR (600 MHz, D_2O) of fraction 1 from **P5** showing the signals for the glycooligoamide enlarging the area from δ 4.2 to 2.4 ppm.

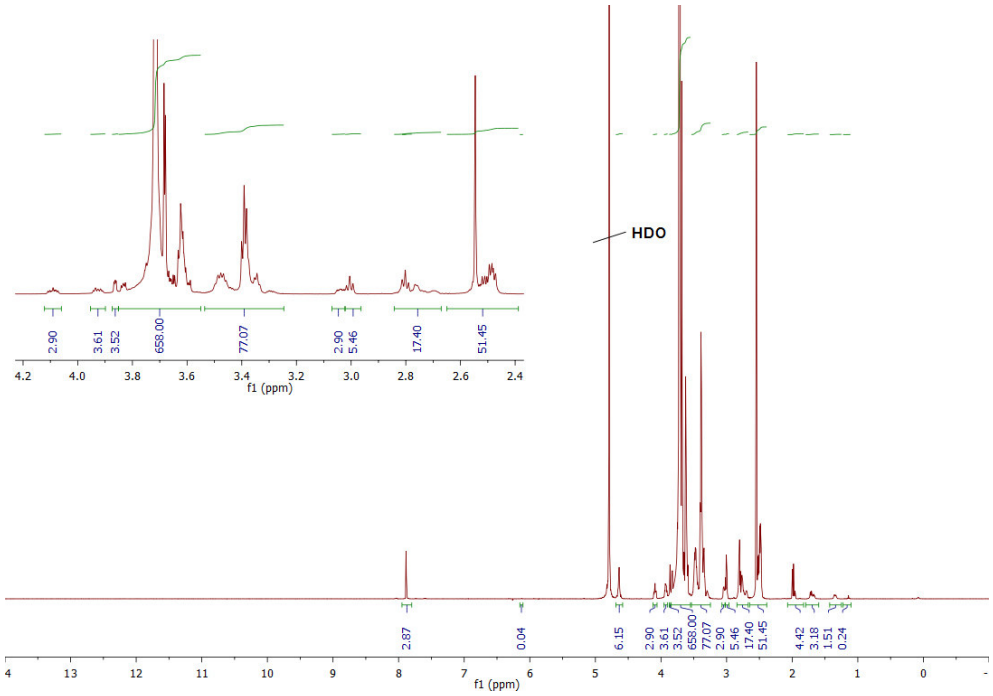

Figure S69: ^{1}H-NMR (600 MHz, D_2O) of fraction 2 from **P5** showing the signals for the glycooligoamide enlarging the area from δ 4.2 to 2.4 ppm.

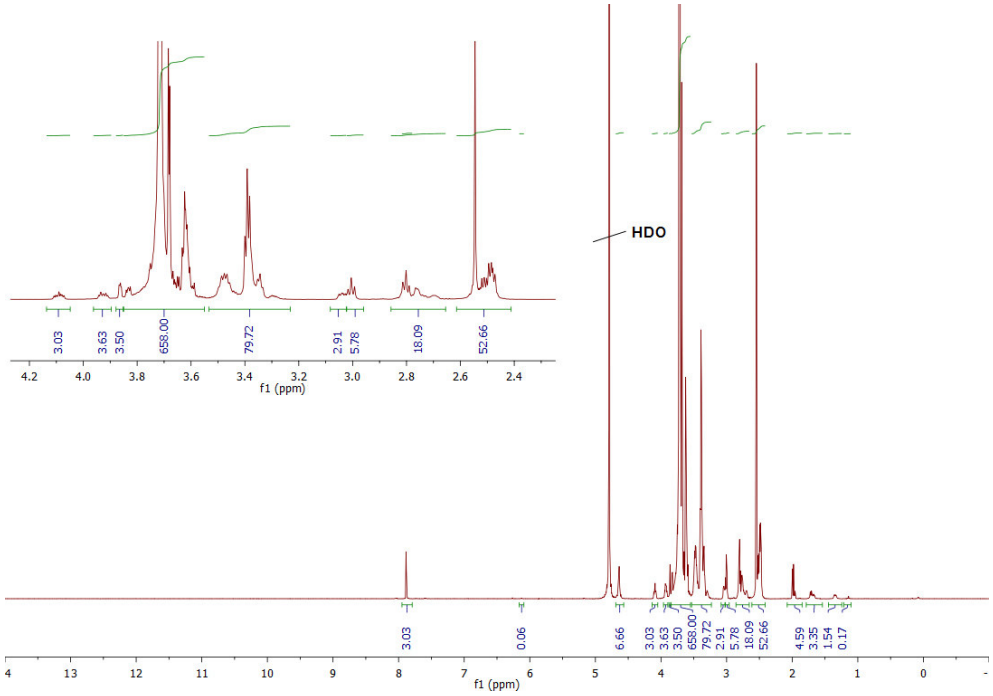

Figure S70: ^{1}H-NMR (600 MHz, D_2O) of fraction 3 from **P5** showing the signals for the glycooligoamide enlarging the area from δ 4.2 to 2.4 ppm.

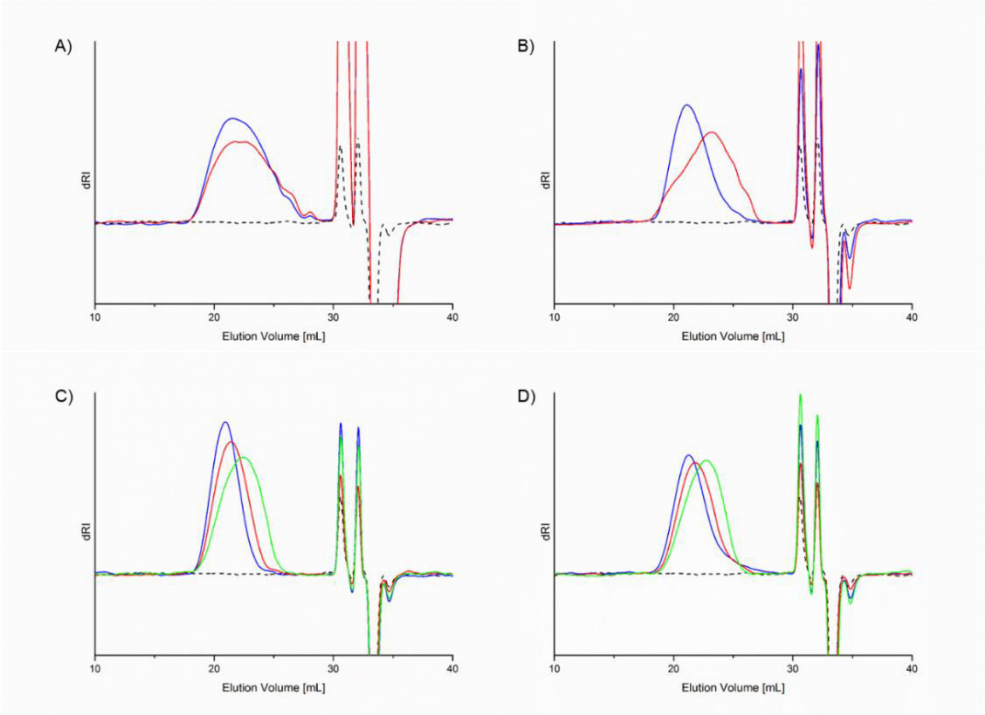

Figure S71: GPC-RI-LS elugrams of **P5** at different steps during the synthesis and purification. A) From the two batches (batch 1 (blue) and batch 2 (red)). B) From the purification by affinity chromatography after the washing (red) and the elution (blue) process. C) From the purification by preparative GPC of the three separated fractions 1 (blue), 2 (red) and 3 (green). D) From the disulfide reduction and thiol capping procedure of fraction 1 (blue), 2 (red) and 3 (green). Columns: Suprema Lux (2 X 100 and 1 X 1000 Å). Buffer: 50 mM NaH_2PO_4, 150 mM NaCl, 250 ppm of NaN_3 (pH 7.2), 30% ACN. Flow: 0.8 mL/min.

Poly-NDS(1,5)-5 (P6):

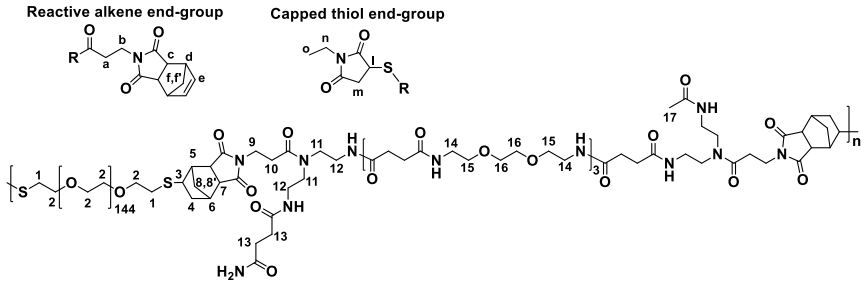

Obtained yields for glycooligoamide – PEG multiblock copolymer **P6** after the synthesis as well as each purification step are listed in Table S7.

Table S7: Determined yields for each reaction step, remaining amount of reactive alkene end-groups, ratio of oligoamide and PEG, amount of NEM functionalization as well as the slope of the conformational plot and radius of gyration of the final multiblock copolymer **P6**.

Reaction step	Info	Yield [mg]	Yield [%]	MWCO	Remaining Alkene [%]	Ratio **O6**:PEG	NEM Funct. [%]	Confor. Plot	R_g [nm]
Synthesis	Batch 1	96.2	63	-	n.d.[b)]	0.97:1	-	-	-
	Batch 2	82.9	55	-	-	-	-	-	-
Disulfide reduction and thiol capping		9.87	99	50	1.3	0.96:1	1.3	0.19	30.0

a) No signal for remaining alkene end-groups determined.

Signals with chemical shift of δ 8.07 – 8.01 (m), 7.77 – 7.72 (m) and 7.66 – 7.56 (m) ppm are assumed to be recombination products with DMPA radicals. Stated amounts of protons correspond to one repeating unit of the polymer. ^{1}H-NMR (600 MHz, D_2O): δ 6.15 – 6.13 (m, end-group, e), 3.90 – 3.55 (m, 606H, 2+5+9+15+16), 3.54 – 3.26 (m, 32H, 7+11+12+14), 2.95 – 2.66 (m, 12H, 1+3+6+10), 2.61 – 2.42 (m, 20H, 13), 2.06 – 1.91 (m, 4H, 17+8 or 8'), 1.83 – 1.59 (m, 4H, 4), 1.45 – 1.28 (m, 2H, 8 or 8'), 1.24 – 1.03 (m, ethyl group from the NEM-functionalization, o) ppm. The assignment of the signals was performed according to the structural similarities with compound **O6** and PEG$(SH)_2$-6000.

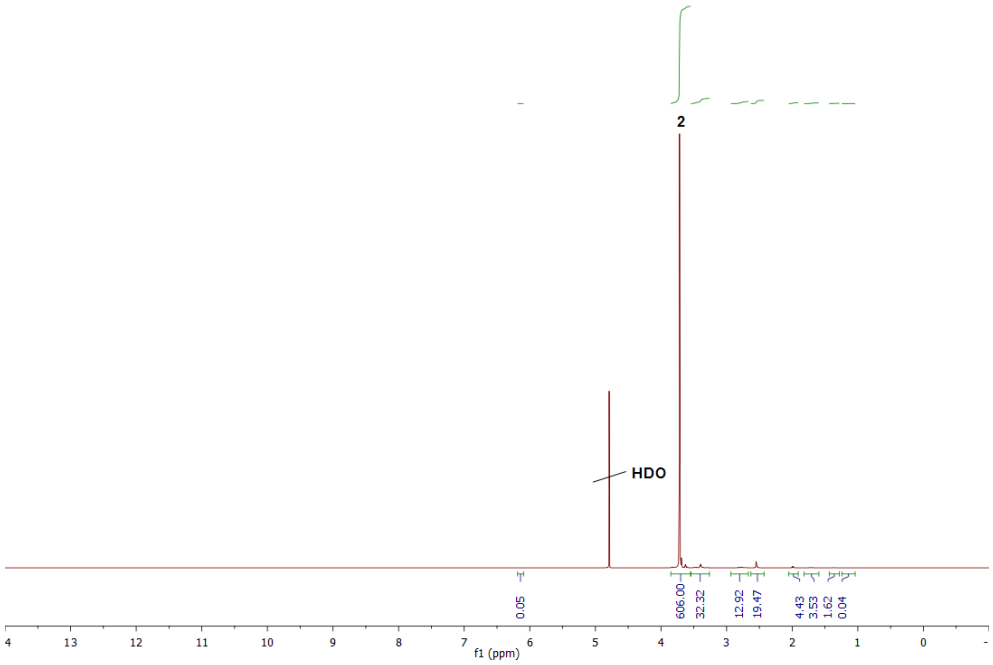

Figure S72: ^{1}H-NMR (600 MHz, D_2O) of **P6** showing the intense signal for the PEG backbone.

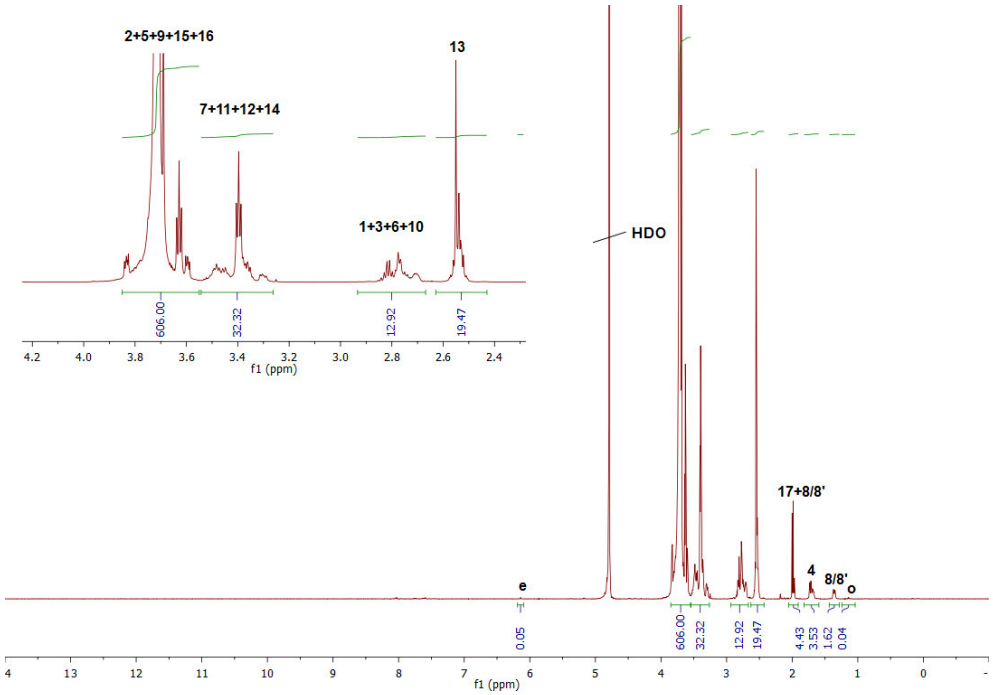

Figure S73: ^{1}H-NMR (600 MHz, D_2O) of **P6** showing the signals for the oligoamide enlarging the area from δ 4.2 to 2.4 ppm.

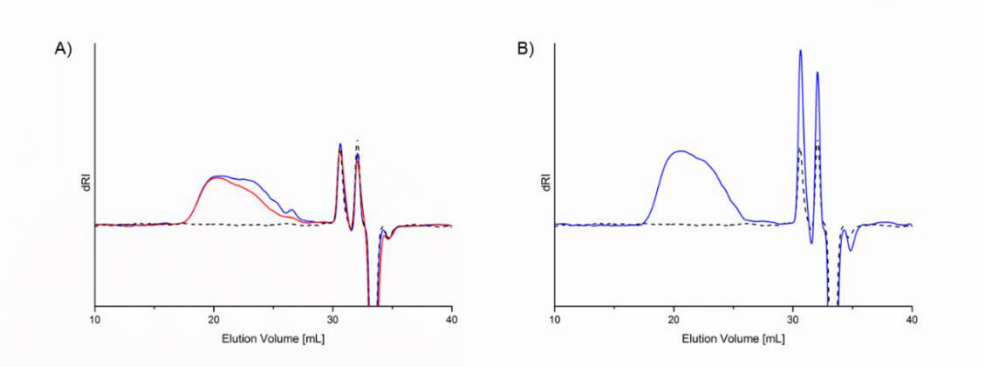

Figure S74: GPC-RI-LS elugrams of **P6** at different steps during the synthesis and purification. A) From the two batches (batch 1 (blue) and batch 2 (red)). B) From the disulfide reduction and thiol capping procedure of batch 2 (blue). Columns: Suprema Lux (2 X 100 and 1 X 1000 Å). Buffer: 50 mM NaH_2PO_4, 150 mM NaCl, 250 ppm of NaN_3 (pH 7.2), 30% ACN. Flow: 0.8 mL/min.

Poly-NDS(1,4)Man(2,3)-4-AlexaFluor (P2+Alexa):

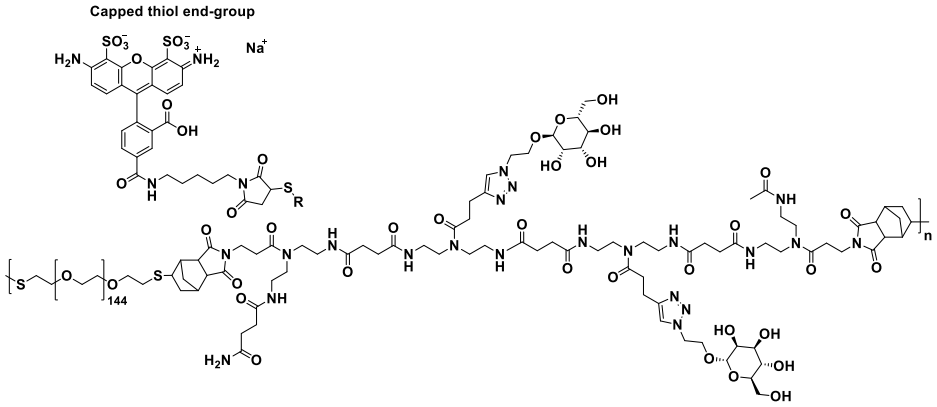

For assignment of the signals of one repeating unit of the Alexa Fluor 488 functionalized polymer **P2**, see analytical data for the NEM functionalized polymer **P2**. Only specific signals for the Alexa Fluor fluorophore are stated. ^{1}H-NMR (600 MHz, D_2O): δ 7.28 – 7.21 (m, AlexaFluor), 7.03 – 6.94 (m, AlexaFluor), 1.23 – 1.15 (m, AlexaFluor) ppm.

GPC-RI-LS (Columns: Suprema Lux (2 X 100 and 1 X 1000 Å). Buffer: 50 mM NaH_2PO_4, 150 mM NaCl, 250 ppm of NaN_3 (pH 7.2), 30% ACN. Flow: 0.8 mL/min.). Elution volume: 22.5 – 31 mL.
Determined $\bar{M}_w$ 152.8 kDa, $\bar{M}_n$ 93.81 kDa and $\bar{M}_w/\bar{M}_n$ 1.63.

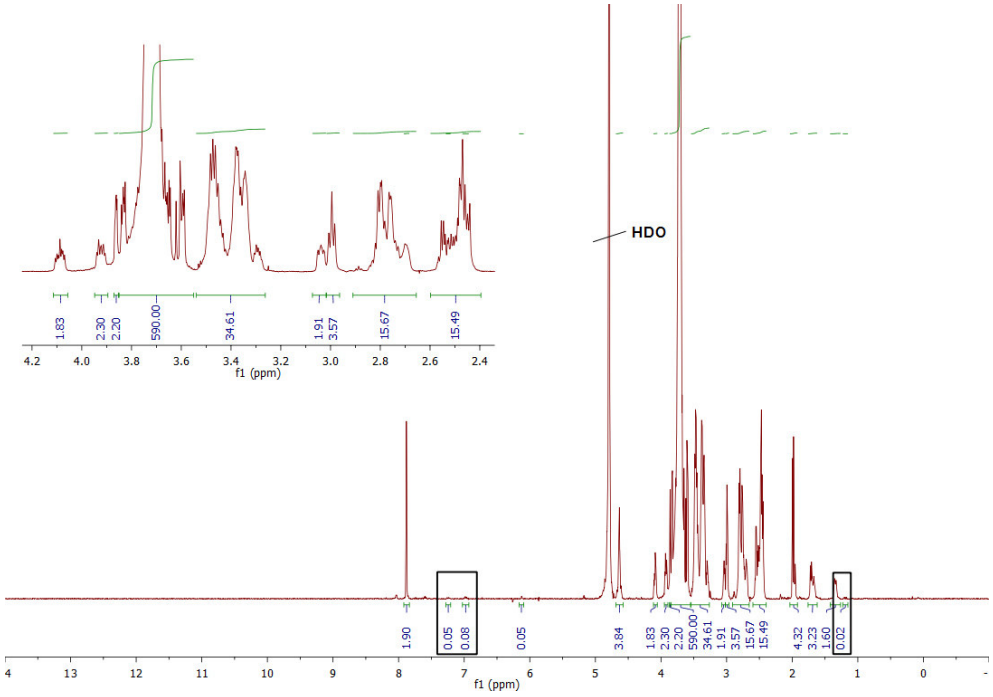

Figure S75: ^{1}H-NMR (600 MHz, D_2O) of fraction 2 from **P2** functionalized with Alex Fluor 488 showing the signals for the glycooligoamide enlarging the area from δ 4.2 to 2.4 ppm as well as the highlighted signals for the fluorophore.

Poly-NDS(1,5)Man(2,3,4)-5-AlexaFluor (P3+Alexa):

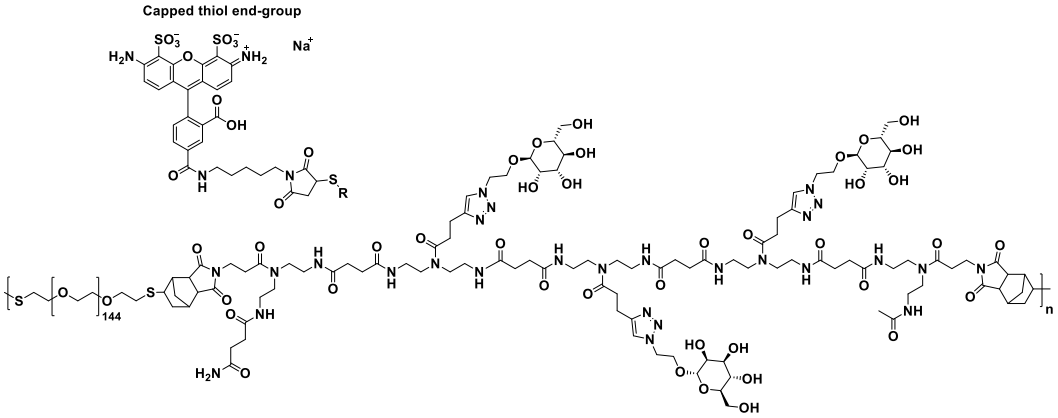

For assignment of the signals of one repeating unit of the Alexa Fluor 488 functionalized polymer **P3**, see analytical data for the NEM functionalized polymer **P3**. Only specific signals for the Alexa Fluor fluorophore are stated. ^{1}H-NMR (600 MHz, D_2O): δ 7.29 – 7.19 (m, AlexaFluor), 7.02 – 6.94 (m, AlexaFluor), 1.23 – 1.15 (m, AlexaFluor) ppm.

GPC-RI-LS (Columns: Suprema Lux (2 X 100 and 1 X 1000 Å). Buffer: 50 mM NaH_2PO_4, 150 mM NaCl, 250 ppm of NaN_3 (pH 7.2), 30% ACN. Flow: 0.8 mL/min.). Elution volume: 22.5 – 31 mL.
Determined $\bar{M}_w$ 208.5 kDa, $\bar{M}_n$ 118.5 kDa and $\bar{M}_w/\bar{M}_n$ 1.76.

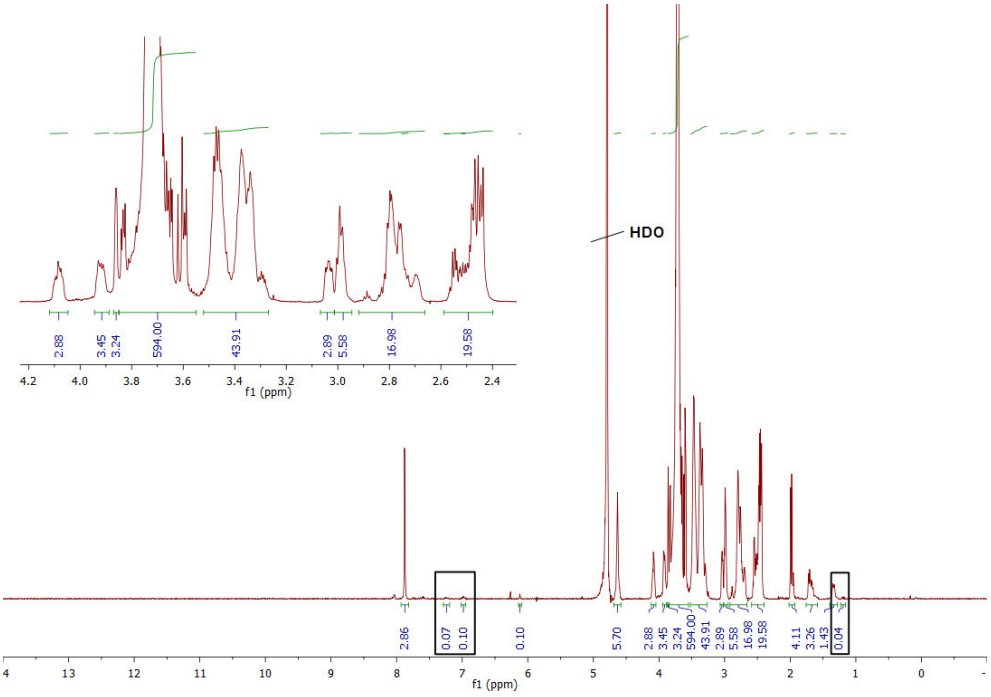

Figure S76: ^{1}H-NMR (600 MHz, D_2O) of fraction 2 from **P3** functionalized with Alex Fluor 488 showing the signals for the glycooligoamide enlarging the area from δ 4.2 to 2.4 ppm as well as the highlighted signals for the fluorophore.

Poly-NDS(1,3)Man(2)-3+Cys(1,7)-7 (P7a):

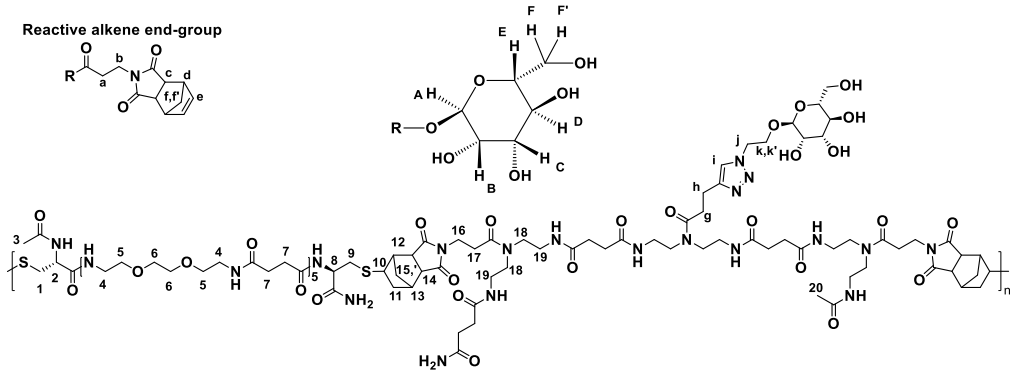

Glycopolymer **P7a** was obtained in a yield of 64%. The anomeric proton of Mannose (A) could not be examined in ^{1}H-NMR due to the overlaying signal from the residual solvent. 7.5% of remaining functional alkene group were determined from the ^{1}H-NMR. The triplet with a chemical shift of δ 1.19 ppm (t, J = 7.1 Hz) indicates a desulfurization caused by a side reaction with TCEP. Signals with chemical shift of δ 8.07 – 8.01 (m), 7.77 – 7.72 (m) and 7.66 – 7.56 (m) ppm are assumed to be recombination products with DMPA radicals. Stated amounts of protons correspond to one repeating unit of the polymer. ^{1}H-NMR (300 MHz, D_2O): δ 7.88 (s, 1H, i), 6.12 (s, end-group, e), 4.67 – 4.59 (m, 2H, j), 4.52 – 4.40 (m, 2H, 2+8), 4.16 – 4.03 (m, 1H, k or k'), 3.98 – 3.88 (m, 1H, k or k'), 3.88 – 3.84 (m, 1H, B), 3.79 – 3.55 (m, 50H, 5+6+12+16+F+F'+C+D), 3.53 – 3.27 (m, 48H, 4+14+18+19), 3.15 – 2.65 (m, 17H, 1+9+10+13+17+E+g+h), 2.65 – 2.44 (m, 32H, 7), 2.10 – 2.02 (m, 3H, 3), 2.01 – 1.88 (m, 5H, 10+15 or 15'), 1.79 – 1.58 (m, 4H, 11), 1.46 – 1.25 (m, 2H, 15 or 15') ppm. The assignment of the signals was performed according to the structural similarities with compound **O1a** and **O7**.

MALDI-TOF-MS in reflector mode in a *m/z* range from 1000 to 4000:
Disulfide from macromonomer **O7** $C_{58}H_{103}N_{13}O_{23}S_2$. (Monoisotopic mass 1413.7 g/mol)**:** [(**O7Disulfide**)+Na]$^+$ calcd. 1436.7, found 1436.6.
For dimer **O1a-O7** $C_{121}H_{196}N_{28}O_{43}S_2$ (Monoisotopic mass 2793.3 g/mol): [(**O1a-O7**)+Na]$^+$ calcd. 2816.3, found 2816.2.

MALDI-TOF-MS in linear mode in a *m/z* range from 2000 to 20000 with exemplary assignments for dimer, the two different trimers as well as the tetramer:
For dimer **O1a-O7** $C_{121}H_{196}N_{28}O_{43}S_2$ (Monoisotopic mass 2793.3 g/mol): [(**O1a-O7**)+Na]$^+$ calcd. 2816.3, found 2818.
For trimer **O1a-O7-O1a** $C_{184}H_{287}N_{43}O_{63}S_2$ (Monoisotopic mass 4171.0 g/mol): [(**O1a-O7-O1a**)+Na]$^+$ calcd. 4194.0, found 4200.
For trimer **O7-O1a-O7** $C_{179}H_{301}N_{41}O_{66}S_4$ (Monoisotopic mass 4201.0 g/mol): [(**O7-O1a-O7**)+Na]$^+$ calcd. 4232.0, found 4235.
For tetramer **O7-O1a-O7-O1a** $C_{242}H_{392}N_{56}O_{86}S_4$ (Monoisotopic mass 5586.7 g/mol): [(**O7-O1a-O7-O1a**)+Na]$^+$ calcd. 5609.7, found 5616.

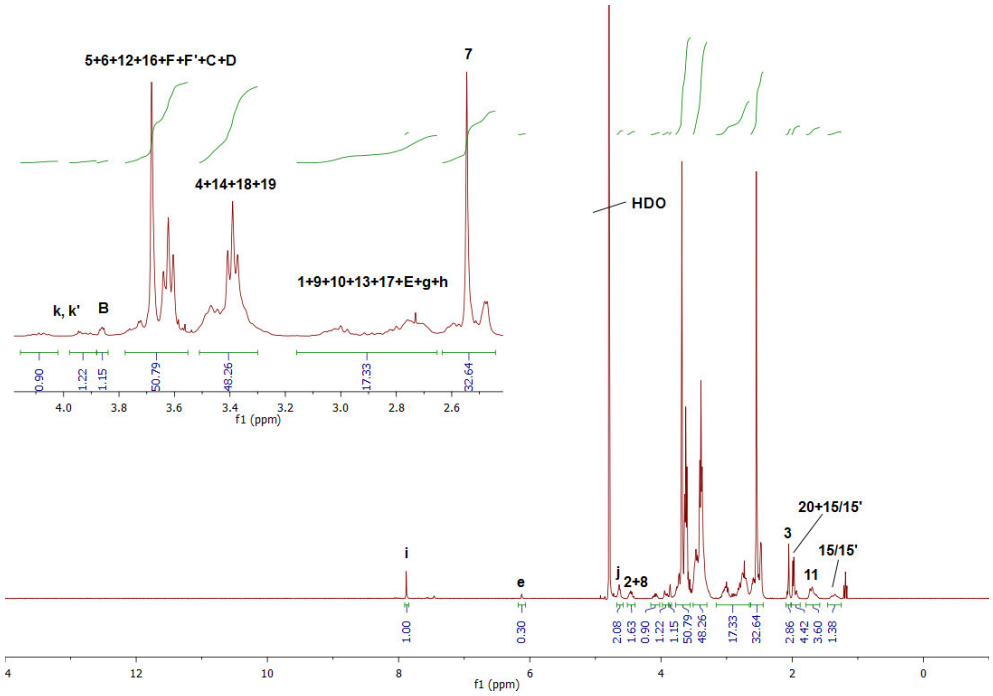

Figure S77: ^{1}H-NMR (300 MHz, D_2O) of **P7a** showing the signals for the glycooligoamide enlarging the area from δ 4.2 to 2.4 ppm.

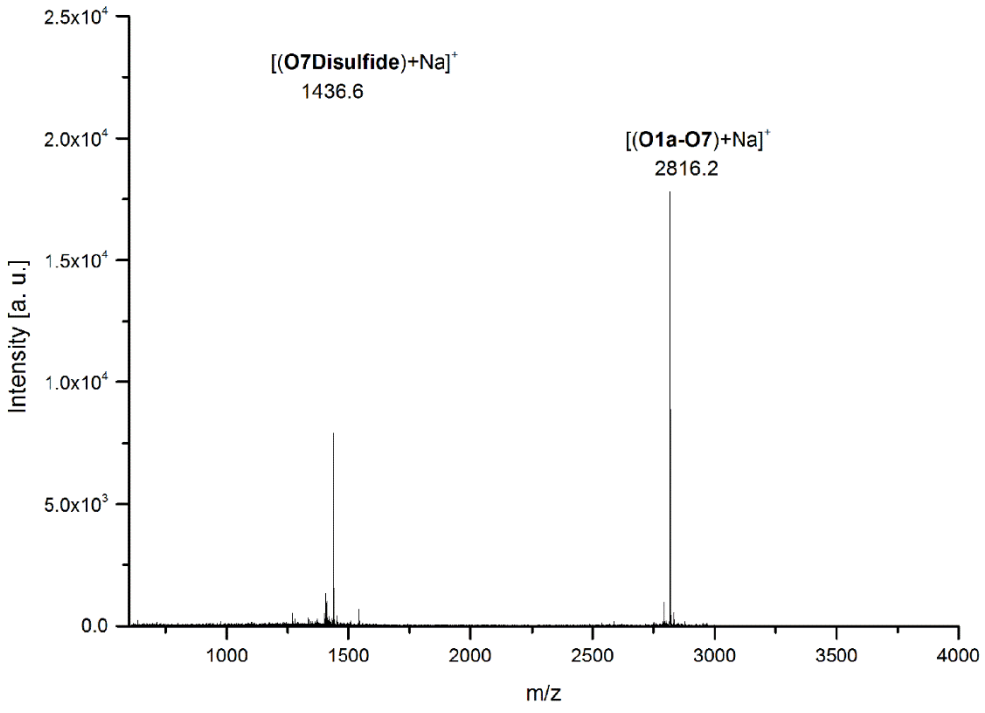

Figure S78: MALDI-TOF-MS of polymer **P7a** in reflector mode in a *m/z* range of 1000-4000 using DHB as matrix in a compound to matrix ratio of 1:1.

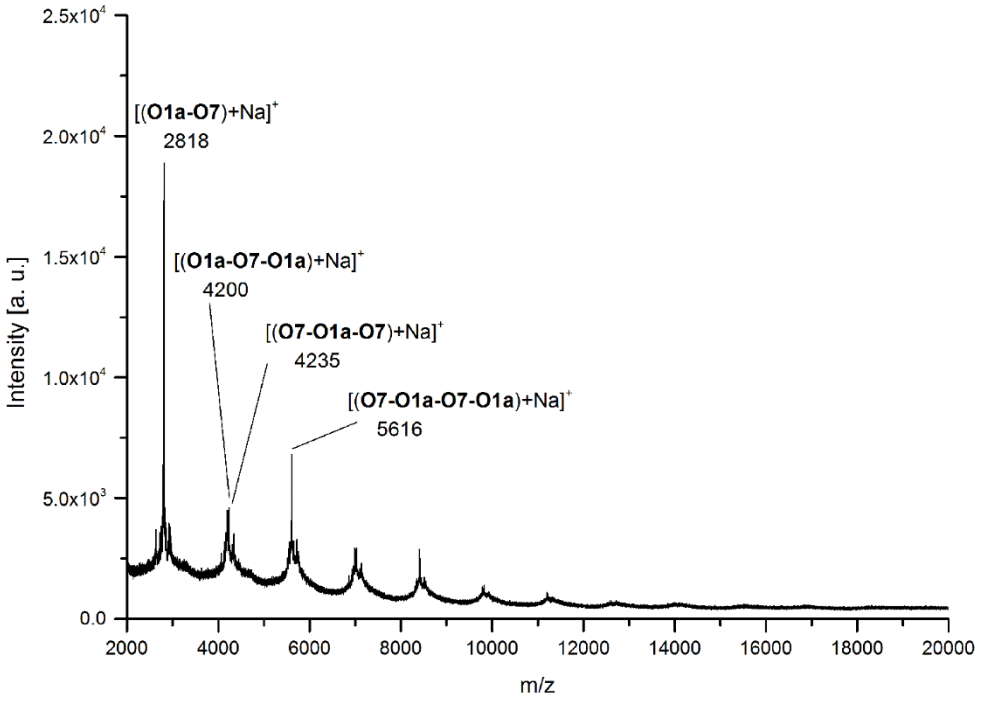

Figure S79: MALDI-TOF-MS of polymer **P7a** in linear mode in a m/z range of 2000-20000 using DHB as matrix in a compound to matrix ratio of 1:10.

Poly-DDS(1,3)Man(2)-3+Cys(1,7)-7 (P7b):

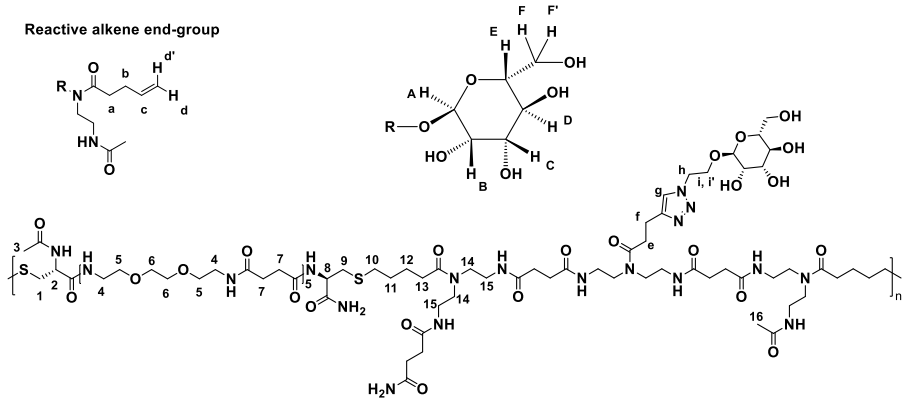

Glycopolymer **P7b** was obtained in a yield of 77%. The anomeric proton of Mannose (A) could not be examined in ^{1}H-NMR due to the overlaying signal from the residual solvent. 10% of remaining functional alkene group were determined from the ^{1}H-NMR. The triplet with a chemical shift of δ 1.19 ppm (t, J = 7.1 Hz) indicates a desulfurization caused by a side reaction with TCEP. Signals with chemical shift of δ 8.07 – 8.01 (m), 7.77 – 7.72 (m) and 7.66 – 7.56 (m) ppm are assumed to be recombination products with DMPA radicals. Stated amounts of protons correspond to one repeating unit of the polymer. ^{1}H-NMR (300 MHz, D_2O): δ 7.88 (s, 1H, g), 5.95 – 5.79 (m, end-group, c), 5.15 – 4.98 (m, end-group, d+d'), 4.69 – 4.60 (m, 2H, h), 4.53 – 4.42 (m, 2H, 2+8), 4.15 – 4.03 (m, 1H, i or i'), 3.97 – 3.88 (m, 1H, i or i'), 3.88 – 3.84 (m, 1H, B), 3.80 – 3.56 (m, 44H, 5+6+F+F'+C+D), 3.55 – 3.30 (m, 44H, 4+14+15), 3.13 – 2.71 (m, 9H, 1+9+E+f+e), 2.70 – 2.24 (m, 40H, 7+10+13), 2.06 (s, 3H, 3), 2.01 – 1.92 (m, 3H, 16), 1.63 (s, 8H, 11+12) ppm. The assignment of the signals was performed according to the structural similarities with compound **O1b** and **O7**.

MALDI-TOF-MS in reflector mode in a *m/z* range from 1000 to 4000:
Remaining macromonomer **O1b** $C_{49}H_{81}N_{13}O_{16.}$ (Monoisotopic mass 1107.6 g/mol)**:** [**O1a**+Na]$^+$ calcd. 1130.6, found 1130.6.
Disulfide from macromonomer **O7** $C_{58}H_{103}N_{13}O_{23}S_{2.}$ (Monoisotopic mass 1413.7 g/mol)**:** [(**O7Disulfide**)+Na]$^+$ calcd. 1436.7, found 1436.6.
For dimer **O1b-O7** $C_{107}H_{186}N_{26}O_{39}S_2$ (Monoisotopic mass 2523.3 g/mol): [(**O1b-O7**)+Na]$^+$ calcd. 2546.3, found 2546.2.

MALDI-TOF-MS in linear mode in a *m/z* range from 2000 to 20000 with exemplary assignments for dimer, the two different trimers as well as the tetramer:
For dimer **O1b-O7** $C_{107}H_{186}N_{26}O_{39}S_2$ (Monoisotopic mass 2523.3 g/mol): [(**O1b-O7**)+Na]$^+$ calcd. 2546.3, found 2548.
For trimer **O1b-O7-O1b** $C_{156}H_{267}N_{39}O_{55}S_2$ (Monoisotopic mass 3630.9 g/mol): [(**O1b-O7-O1b**)+Na]$^+$ calcd. 3653.9, found 3658.
For trimer **O7-O1b-O7** $C_{165}H_{291}N_{39}O_{62}S_4$ (Monoisotopic mass 3939.0 g/mol): [(**O7-O1b-O7**)+Na]$^+$ calcd. 3962.0, found 3966.
For tetramer **O7-O1b-O7-O1b** $C_{214}H_{372}N_{52}O_{78}S_4$ (Monoisotopic mass 5046.6 g/mol): [(**O7-O1b-O7-O1b**)+Na]$^+$ calcd. 5069.6, found 5075.

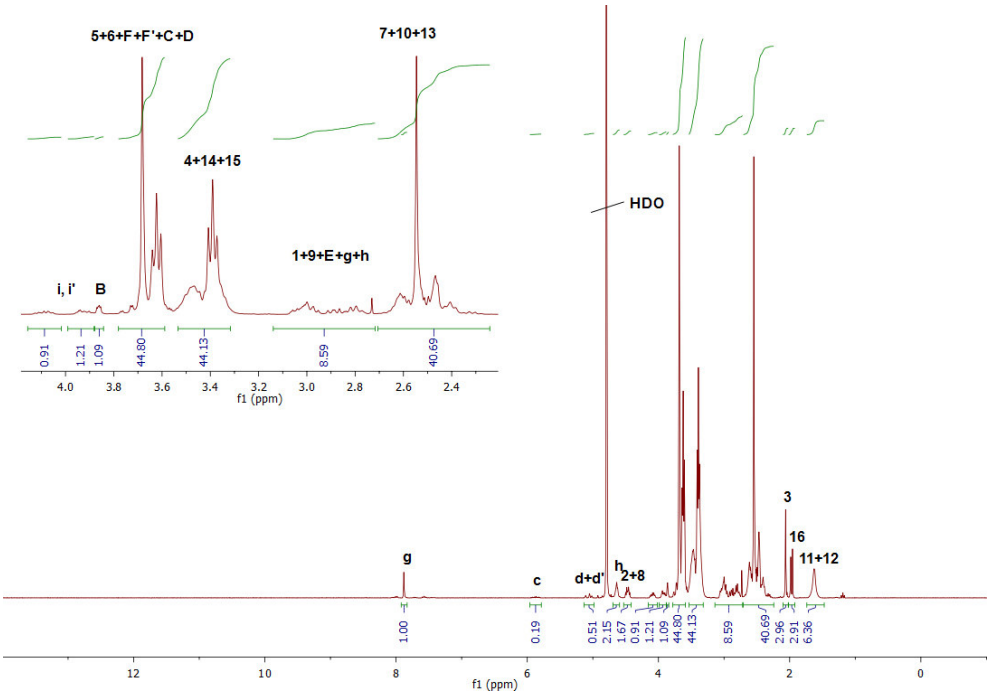

Figure S80: ^{1}H-NMR (300 MHz, D_2O) of **P7b** showing the signals for the glycooligoamide enlarging the area from δ 4.2 to 2.4 ppm.

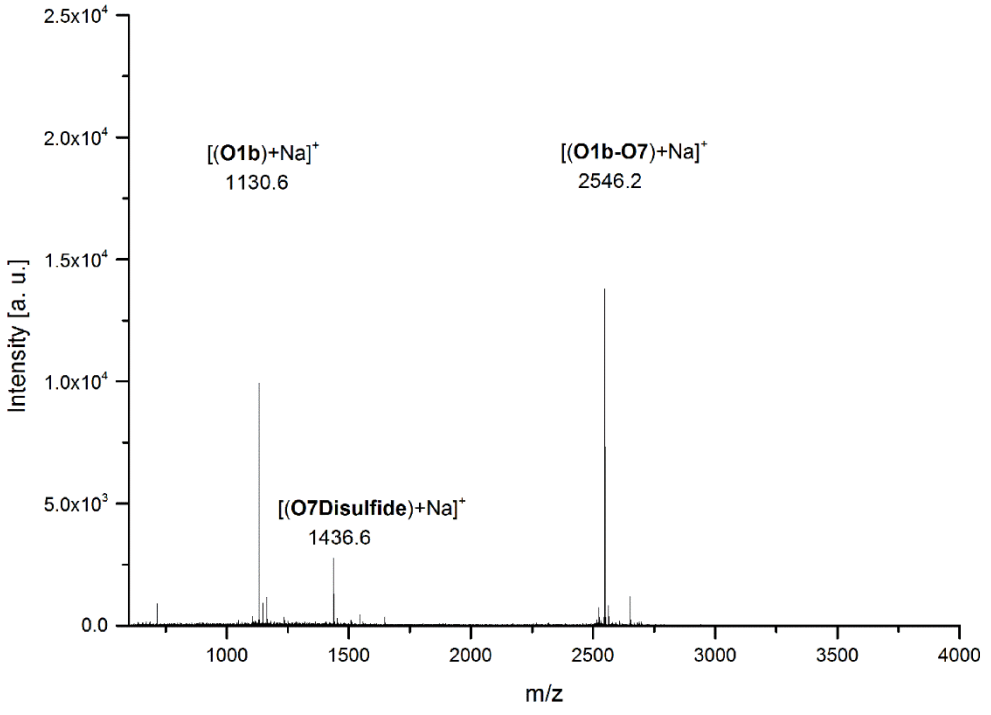

Figure S81: MALDI-TOF-MS of polymer **P7b** in reflector mode in a *m/z* range of 1000-4000 using DHB as matrix in a compound to matrix ratio of 1:1.

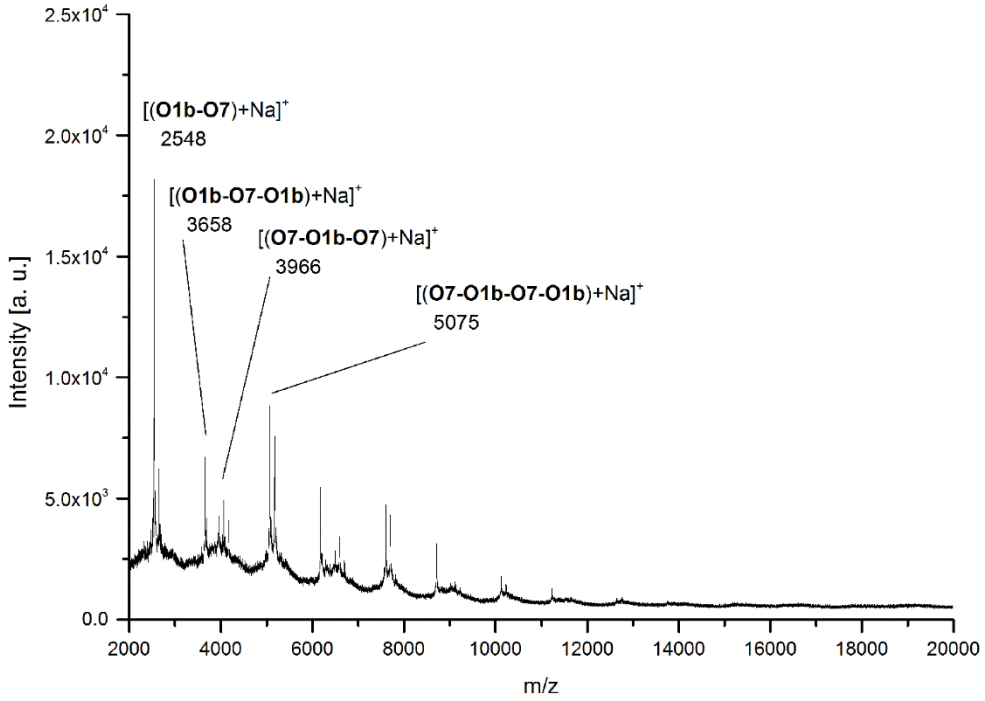

Figure S82: MALDI-TOF-MS of polymer **P7b** in linear mode in a m/z range of 2000-20000 using DHB as matrix in a compound to matrix ratio of 1:10.

Additional information about Con A binding studies

Surface Plasmon Resonance direct binding assay

For the investigation of binding affinities of the glycooligoamide – PEG multiblock copolymers towards ConA, a direct binding surface plasmon resonance assay with covalently immobilized Con A on a CM5 carboxymethyl dextran matrix sensor chip was performed which was based on the assay performed in previous studies by our group.[8] Con A was immobilized using 1-ethyl-3-(3-dimethylaminopropyl)carbodiimide (EDC) and *N*-hydroxysuccinimide (NHS) to 3145 response units (RU). The immobilization was performed in acetate buffer (pH 4.5). The measurements were performed with a Biacore X100 instrument from GE Healthcare Life Sciences and sensorgrams were recorded with the Biacore X100 Control Software and evaluated with the Biacore X100 Evaluation Software.

As running buffer, LBB was used. Fraction 1 and 2 of glycooligoamide – PEG copolymers **P1** – **P4** as well as fraction 1, 2 and 3 of **P5** and the negative control **P6** were all injected at concentration of 20.0, 6.67, 2.22, 0.74 and 0.25 µM, respectively. The flow rate was set to 15 µL/min and the contact and dissociation time were 360 and 600 sec, respectively. In contrast to the previously performed SPR direct binding assay, single cycle experiments were performed, not regenerating the sensor chip after each ligands injection but after the injection of all concentrations. Regeneration of the sensor chip was performed by injection of 0.8 M αMeMan in LBB buffer at a flow rate of 10 µl/min and with a contact time of 30 sec. The regeneration step was performed twice to ensure complete dissociation of bound glycooligoamide – PEG copolymer.

For all analyzed glycooligoamide – PEG copolymers, K_D values were above the highest concentration injected. Unfortunately, it was not possible to inject higher concentration since only low amounts of final glycopolymers were isolated after the multiple purification steps. Besides the low concentrations, the SPR sensorgrams showed strong baseline drifts and unstable binding during the association phase for some of the analyzed structures. The drifts and unstable association seem to be related to the presence of the $PEG(SH)_2$-6000 blocks within the structures. Similar sensorgrams were presented by the group of Fernandez-Megia also working with PEGylated glycomimetics.[10] However, in their study a multi cycle SPR direct binding assay was performed and thus the baseline drift was not as pronounced as for the sensorgrams derived in this assay. Due to the baseline drift, sensorgrams were evaluated manually by determining the increase in RU values from the baseline just before an injection to the reached steady state after the injection of a multiblock glycopolymer, which are then plotted against the corresponding concentration. All structures show a rapid dissociation and thus a complete regeneration of the surface after an injection, which is required for the performed manual evaluation. The resulting saturation curve was fitted using a steady state model giving the dissociation constant K_D and K_A values (reciprocal value of K_D). The manual data evaluation was only performed for structures showing a binding event for at least four of the injected concentrations (structures with less than four determined binding events are stated as n.d. in **Table S8**). The negative control **P6** showed low binding to the Con A immobilized surface which is attributed to interactions of the PEG blocks, since no interaction was observed for an oligoamide based negative control in previous studies.[8]

Table S8: Manually determined RU of the reached equilibrium response after the injection of 20.0 – 0.25 µM of each glycooligoamide – PEG multiblock copolymer as well as the R_{max} and resulting calculated K_D and K_A (per ligand and per Man) values.

#P	F	Steady state response per injected ligand concentration[a] [RU]					R_{max}[a] [RU]	K_D[a] [×10^{-6} M]	K_A[a] Per ligand [×10^{3} M^{-1}]	K_A[a] Per Man [M^{-1}]
		20.0 µM	6.67 µM	2.22 µM	0.74 µM	0.25 µM				
P1	1	29.1 ± 0.3	10.8 ± 0.1	3.2 ± 0.2	-	-	-	n.d.[b]	n.d.[b]	n.d.[b]
	2	24.4 ± 2.0	8.3 ± 0.8	1.7 ± 0.4	-	-	-	n.d.[b]	n.d.[b]	n.d.[b]
P2	1	43.7 ± 1.2	17.9 ± 0.4	6.2 ± 0.2	1.9 ± 0.3	-	165.0 ± 17.2	55.5 ± 6.6	18.3 ± 2.1	41.5 ± 4.8
	2	28.0 ± 0.3	10.0 ± 0.3	2.7 ± 0.7	-	-	-	n.d.[b]	n.d.[b]	n.d.[b]
P3	1	55.4 ± 1.4	25.9 ± 0.6	12.6 ± 0.5	4.8 ± 0.2	2.4±0.1	112.9 ± 7.3	20.9 ± 1.7	48.1 ± 3.9	74.0 ± 5.9
	2	47.1 ± 1.2	20.5 ± 1.2	8.5 ± 0.3	3.5 ± 0.4	-	124.3 ± 2.0	33.0 ± 2.0	30.5 ± 1.9	62.2 ± 3.9
P4	1	38.4 ± 1.8	16.0 ± 0.3	6.0 ± 0.8	1.4 ± 0.4	-	130.4 ± 10.2	48.0 ± 6.4	21.2 ± 2.9	68.5 ± 9.3
	2	28.9 ± 1.3	10.1 ± 0.4	4.3 ± 0.3	-	-	-	n.d.[b]	n.d.[b]	n.d.[b]
P5	1	35.8 ± 0.9	15.7 ± 0.4	6.5 ± 0.6	1.7 ± 0.3	-	94.9 ± 3.7	33.0 ± 1.8	30.4 ± 1.7	89.3 ± 4.9
	2	32.6 ± 0.5	14.4 ± 0.4	5.8 ± 0.4	0.7 ± 0.1	-	90.3 ± 4.5	35.5 ± 3.4	28.4 ± 2.7	102 ± 9.6
	3	29.7 ± 1.2	13.2 ± 0.4	5.4 ± 0.3	1.2 ± 0.2	-	78.8 ± 7.5	32.9 ± 2.9	30.7 ± 2.7	146 ± 13
P6	-	27.7 ± 0.7	9.1 ± 0.3	2.2 ± 0.3	-	-	-	n.b.[c]	n.b.[c]	n.b.[c]

a) Errors in RU, R_{max}, K_D as well as K_A refer to the standard deviation from two independent experiments performing a duplicate determination for all oligoamide – PEG multiblock copolymers included in the SPR assay. b) Not determined (n.d.) as less than four binding events were observed for the five concentrations injected for this sample. c) No binding (n.b.).

Poly-NDS(1,3)Man(2)-3 (P1):

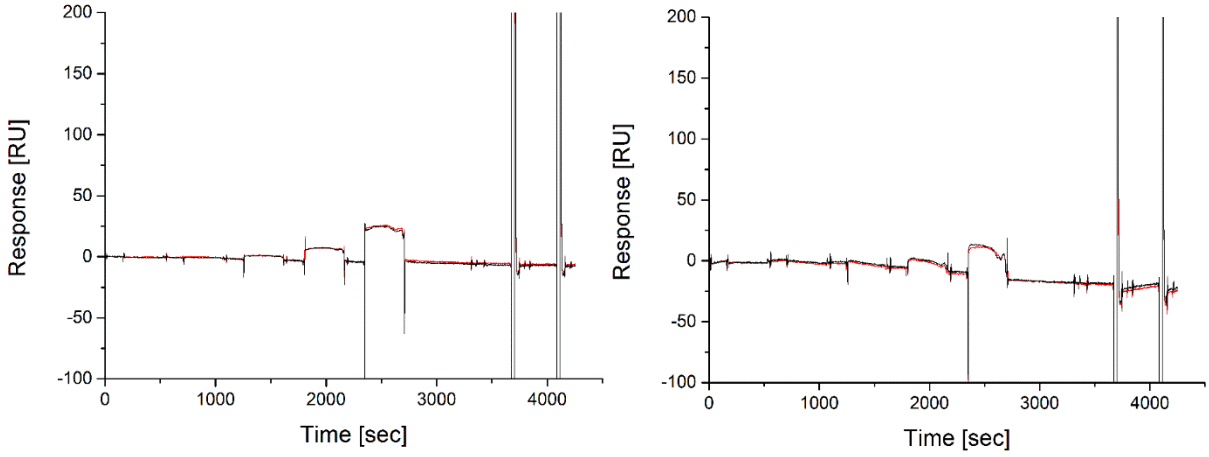

Figure S83: Exemplary sensorgrams of a duplicate measurement from fraction 1 (left) and fraction 2 (right) of **P1** which were injected at concentrations 0.25, 0.74, 2.22, 6.67 and 20.0 µM.

Poly-NDS(1,4)Man(2,3)-4 (P2):

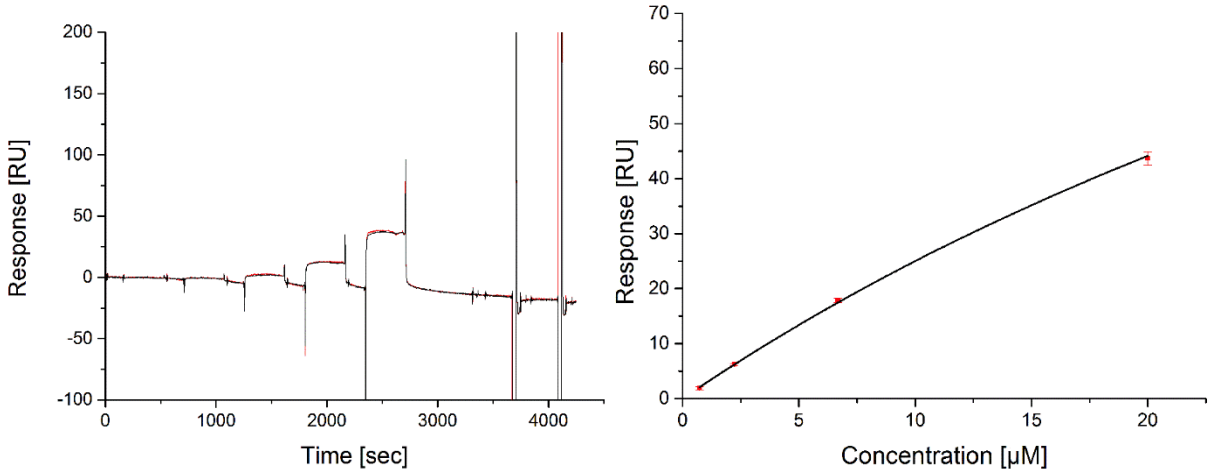

Figure S84: Exemplary sensorgrams of a duplicate measurement (left) and the equilibrium response as a function of concentration from fraction 1 of **P2** plotted using a steady state model (right). Experimental data from four consecutive measurements is plotted. The standard deviation is shown as error bar for each data point. Fraction 1 of **P2** was injected at concentrations of 0.25, 0.74, 2.22, 6.67 and 20.0 µM.

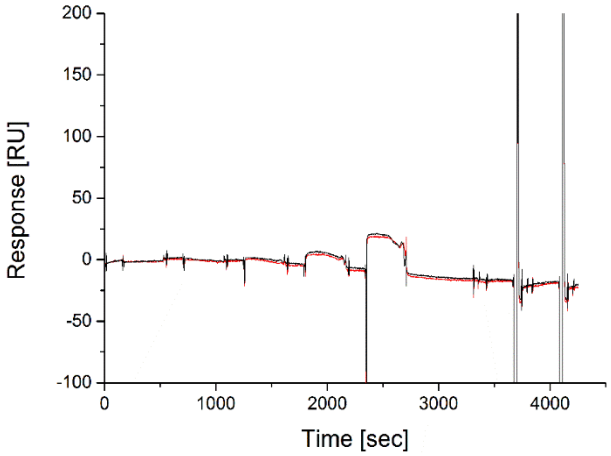

Figure S85: Exemplary sensorgrams of a duplicate measurement from fraction 2 of **P2** which was injected at concentrations 0.25, 0.74, 2.22, 6.67 and 20.0 µM.

Poly-NDS(1,5)Man(2,3,4)-5 (P3):

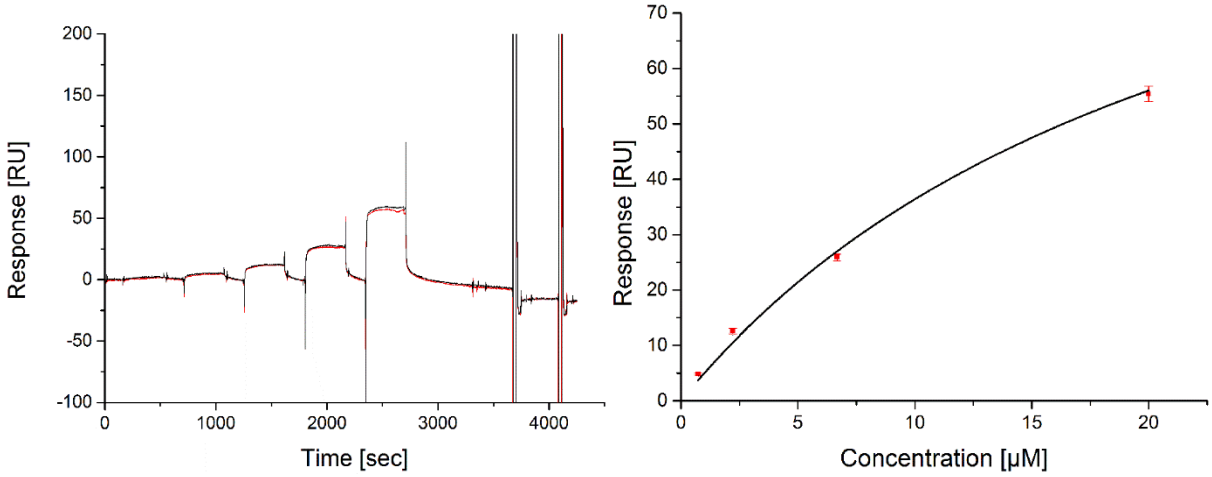

Figure S86: Exemplary sensorgrams of a duplicate measurement (left) and the equilibrium response as a function of concentration from fraction 1 of **P3** plotted using a steady state model (right). Experimental data from four consecutive measurements is plotted. The standard deviation is shown as error bar for each data point. Fraction 1 of **P3** was injected at concentrations of 0.25, 0.74, 2.22, 6.67 and 20.0 µM.

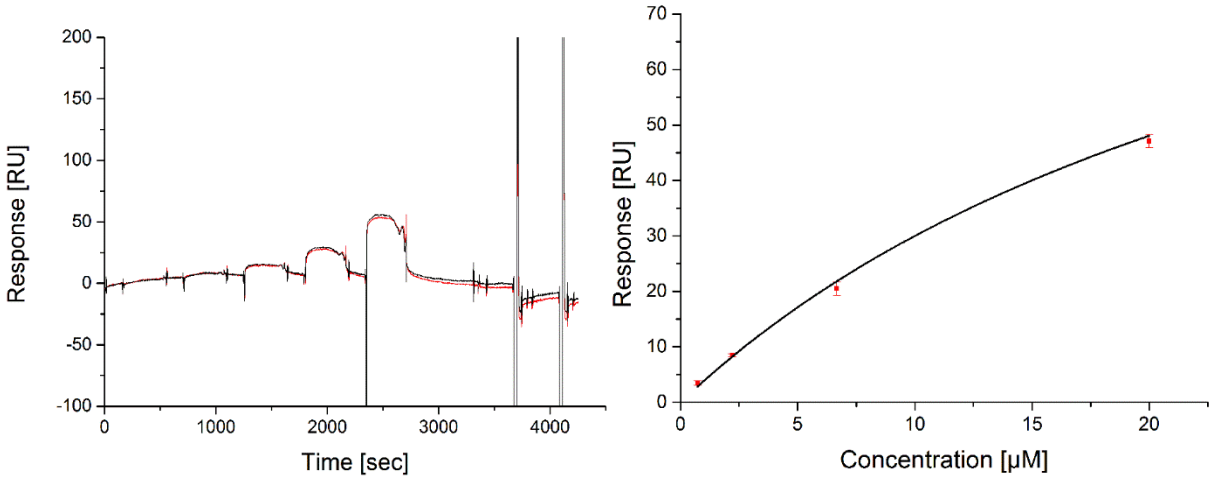

Figure S87: Exemplary sensorgrams of a duplicate measurement (left) and the equilibrium response as a function of concentration from fraction 2 of **P3** plotted using a steady state model (right). Experimental data from four consecutive measurements is plotted. The standard deviation is shown as error bar for each data point. Fraction 2 of **P3** was injected at concentrations of 0.25, 0.74, 2.22, 6.67 and 20.0 µM.

Poly-NDS(1,8)Man(2,7)-8 (P4):

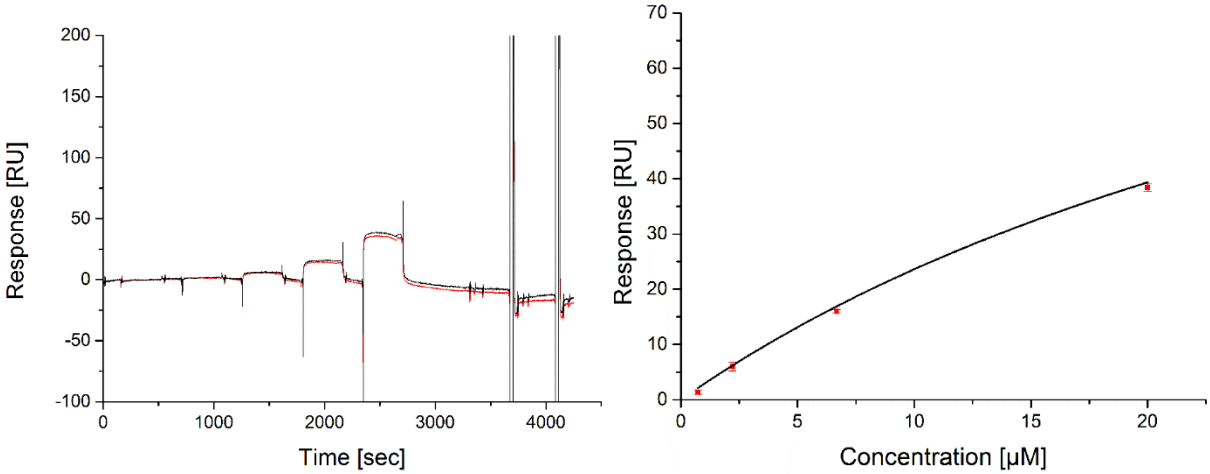

Figure S88: Exemplary sensorgrams of a duplicate measurement (left) and the equilibrium response as a function of concentration from fraction 1 of **P4** plotted using a steady state model (right). Experimental data from four consecutive measurements is plotted. The standard deviation is shown as error bar for each data point. Fraction 1 of **P4** was injected at concentrations of 0.25, 0.74, 2.22, 6.67 and 20.0 µM.

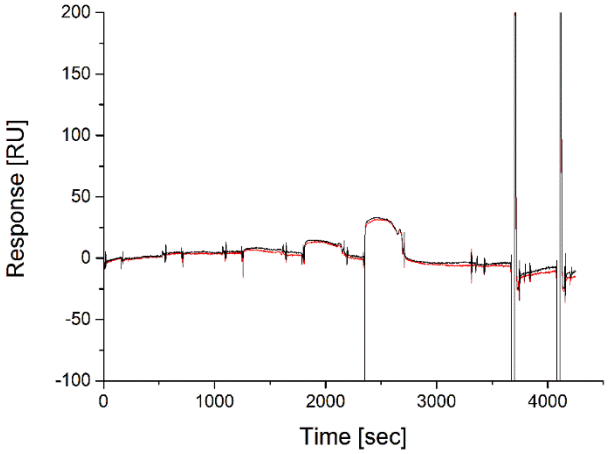

Figure S89: Exemplary sensorgrams of a duplicate measurement from fraction 2 of **P4** which was injected at concentrations 0.25, 0.74, 2.22, 6.67 and 20.0 µM.

Poly-NDS(1,13)Man(2,7,12)-13 (P5):

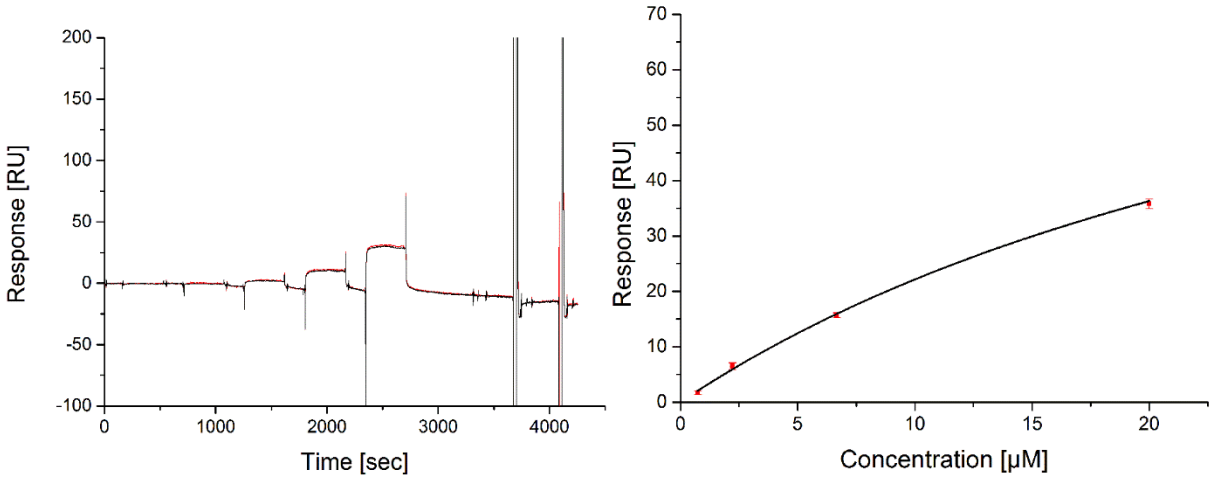

Figure S90: Exemplary sensorgrams of a duplicate measurement (left) and the equilibrium response as a function of concentration from fraction 1 of **P5** plotted using a steady state model (right). Experimental data from four consecutive measurements is plotted. The standard deviation is shown as error bar for each data point. Fraction 1 of **P5** was injected at concentrations of 0.25, 0.74, 2.22, 6.67 and 20.0 µM.

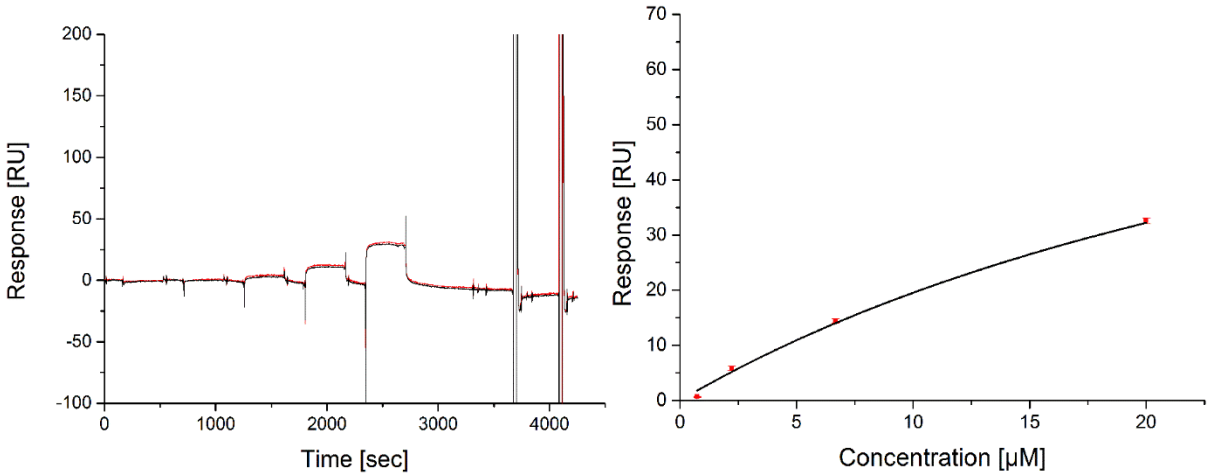

Figure S91: Exemplary sensorgrams of a duplicate measurement (left) and the equilibrium response as a function of concentration from fraction 2 of **P5** plotted using a steady state model (right). Experimental data from four consecutive measurements is plotted. The standard deviation is shown as error bar for each data point. Fraction 2 of **P5** was injected at concentrations of 0.25, 0.74, 2.22, 6.67 and 20.0 µM.

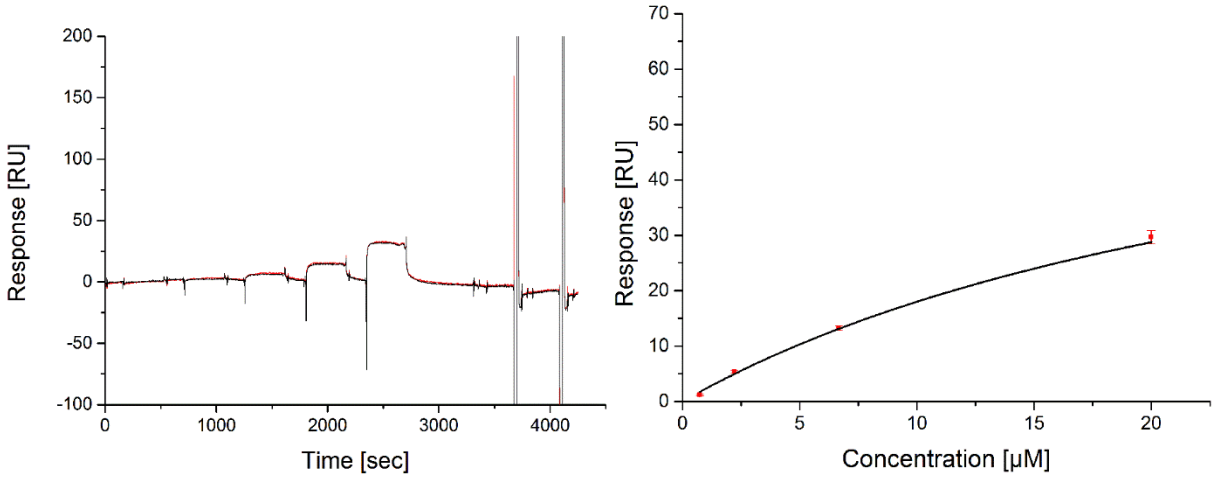

Figure S92: Exemplary sensorgrams of a duplicate measurement (left) and the equilibrium response as a function of concentration from fraction 3 of **P5** plotted using a steady state model (right). Experimental data from four consecutive measurements is plotted. The standard deviation is shown as error bar for each data point. Fraction 3 of **P5** was injected at concentrations of 0.25, 0.74, 2.22, 6.67 and 20.0 µM.

Poly-NDS(1,3)-3 (P6):

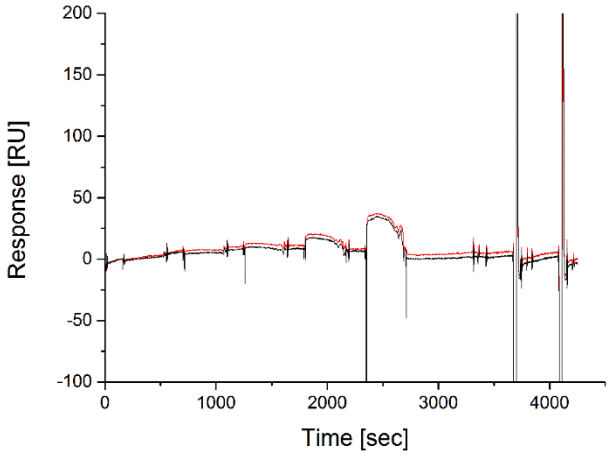

Figure S93: Exemplary sensorgrams of a duplicate measurement from **P6** which was injected at concentrations 0.25, 0.74, 2.22, 6.67 and 20.0 µM.

Soft Colloidal Probe – Reflection Interference Contrast Microscopy adhesion reduction assay

Immobilization of Con A to glass surface

Con A was bound to the glass surface by physical absorption. Briefly, IBIDI glass slides were cleaned and activated by UV ozone cleaner for 30 min. Immediately the Con A solution (0.2 mg/mL, prepared one day in advance) in LBB buffer pH 7.4 was added (190 µL for each vial). The slide was placed on a shaker for 60 min followed by solution exchange. Therefore, each slide was placed twice in beakers containing 150 mL LBB for 60 sec each time. Subsequently, the solution was exchanged a last time by removing the solvent with an Eppendorf pipette and immediately adding 190 µL of the measuring solution into the vial.

SCP – RICM measurements

RICM was performed on an IX 73 inverted microscope from Olympus to obtain the contact area between the SCPs and the glass coverslip surfaces. For illumination, an Hg-vapour arc lamp was used with a green monochromator (546 nm). An UPlanFL N 60×/0.90 dry objective from Olympus and an uEye digital camera from IDS Imaging Development Systems GmbH were used to image the RICM patterns. To conduct the JKR measurements of the adhesion energies, both the contact radius and the particle radius were measured. Images with RICM patterns were read out using self-written image analysis software, contact areas and particle profiles were evaluated using scripted peak finding algorithms from IgorPro Wavemetrics. For further information about the calculation of the surface adhesion of the SCPs see previously published work.[11, 12]

General procedure of the SCP – adhesion assay

To the protein functionalized glass slides covered with measurement solution, 10 µL SCP dispersion (approximately 1 mg/mL) were added. After 30 min, the SCPs were studied by an inverted reflection interference microscope to determine the contact area between the SCPs and the glass slides. For each sample, 20 SCPs interference patterns were recorded and the measurements were repeated two more times on other glass surfaces.

Next, 100 µL of a stock solution (66 µM prepared in LBB) of fraction 1 of glycooligoamide – PEG copolymers **P1** – **P4** as well as fraction 1, 2 and 3 of **P5** and the negative control **P6** were added to the measurement vial to give a 22 µM inhibitor concentration. After reaching an equilibrium at 60 min, the contact area of the SCPs were determined again and the reduction to the previously determined surface adhesion was calculated giving the adhesion reduction in % for each of the oligoamide – PEG copolymers included in the assay.

Table S9: Determined surface adhesions of Man-functionalized SCP to three independent Con A functionalized glass slides prior to inhibition and after inhibition with 22 µM of each glycooligoamide – PEG multiblock copolymer as well as the remaining surface adhesion after inhibition in %, the average of the three measurements and the resulting adhesion reduction in %.

Polymer	F.	Glass slide	Surface adhesion [µJ/m^2]		Remaining adhesion [%]	Average[b)] [%]	Adhesion reduction[b)] [%]
			Not inhibited[a)]	22 µM of inhibitor[a)]			
		1	279 ± 7	213 ± 4	76.3		
P1	1	2	244 ± 6	206 ± 11	84.4	80.3 ± 3.3	19.7 ± 3.3
		3	255 ± 10	204 ± 10	80.0		
		1	273 ± 8	163 ± 5	59.7		
P2	1	2	273 ± 13	155 ± 7	56.8	60.4 ± 3.2	39.6 ± 3.2
		3	260 ± 10	168 ± 11	64.6		
		1	245 ± 7	148 ± 8	60.4		
P3	1	2	265 ± 8	159 ± 14	60.0	57.5 ± 3.9	42.5 ± 3.9
		3	294 ± 7	153 ± 13	52.0		
		1	281 ± 7	199 ± 7	70.8		
P4	1	2	272 ± 6	195 ± 8	71.7	69.9 ± 2.0	30.1 ± 2.0
		3	258 ± 8	173 ± 8	67.1		
		1	279 ± 7	200 ± 7	71.7		
	1	2	229 ± 6	151 ± 7	65.9	66.8 ± 3.7	33.2 ± 3.7
		3	261 ± 6	164 ± 11	62.8		
		1	293 ± 9	205 ± 7	70.0		
P5	2	2	228 ± 6	153 ± 6	67.1	71.3 ± 4.1	28.7 ± 4.1
		3	238 ± 9	183 ± 9	76.9		
		1	282 ± 6	206 ± 7	73.0		
	3	2	208 ± 6	144 ± 9	69.2	74.0 ± 4.3	26.0 ± 4.3
		3	221 ± 8	176 ± 10	79.6		
		1	294 ± 9	278 ± 10	94.6		
P6	-	2	232 ± 8	233 ± 10	100.4	97.2 ± 2.4	2.8 ± 2.4
		3	231 ± 12	223 ± 7	96.5		

a) Errors in the surface adhesion of the SCP at non inhibited and inhibited stated refer to the standard deviation from 20 separately analyzed SCPs. b) Errors in the average value of the reduction of the surface adhesion as well as the adhesion reduction refer to the standard deviation from three independent experiments for all oligoamide – PEG multiblock copolymers included in the SCP – adhesion assay.

1. Bondalapati, S.; Jbara, M.; Brik, A., Expanding the chemical toolbox for the synthesis of large and uniquely modified proteins. *Nat. Chem.* **2016,** 8, 407.
2. Wojcik, F.; O'Brien, A. G.; Götze, S.; Seeberger, P. H.; Hartmann, L., Synthesis of Carbohydrate-Functionalised Sequence-Defined Oligoamides by Photochemical Thiol-Ene Coupling in a Continuous Flow Reactor. *Chem. Eur. J.* **2013,** 19, (9), 3090-3098.
3. Ebbesen, M. F.; Gerke, C.; Hartwig, P.; Hartmann, L., Biodegradable poly(amidoamine)s with uniform degradation fragments via sequence-controlled macromonomers. *Polym. Chem.* **2016,** 7, (46), 7086-7093.
4. Ponader, D.; Wojcik, F.; Beceren-Braun, F.; Dernedde, J.; Hartmann, L., Sequence-Defined Glycopolymer Segments Presenting Mannose: Synthesis and Lectin Binding Affinity. *Biomacromolecules* **2012,** 13, (6), 1845-1852.
5. Hunig, S.; Markl, G.; Sauer, J., *Integriertes Organisches Praktikum*. Verl. Chemie Weinheim; NY: 1979.
6. Zhang, K.; Zha, Y.; Peng, B.; Chen, Y.; Tew, G. N., Metallo-Supramolecular Cyclic Polymers. *J. Am. Chem. Soc.* **2013,** 135, (43), 15994-15997.
7. Baier, M.; Giesler, M.; Hartmann, L., Split-and-Combine Approach Towards Branched Precision Glycomacromolecules and Their Lectin Binding Behavior. *Chem. Eur. J.* 24, (7), 1619-1630.
8. Gerke, C.; Ebbesen, M. F.; Jansen, D.; Boden, S.; Freichel, T.; Hartmann, L., Sequence-Controlled Glycopolymers via Step-Growth Polymerization of Precision Glycomacromolecules for Lectin Receptor Clustering. *Biomacromolecules* **2017,** 18, (3), 787-796.
9. Roux, S.; Zékri, E.; Rousseau, B.; Paternostre, M.; Cintrat, J.-C.; Fay, N., Elimination and exchange of trifluoroacetate counter-ion from cationic peptides: a critical evaluation of different approaches. *J. Pept. Sci.* **2008,** 14, (3), 354-359.
10. Fernandez-Villamarin, M.; Sousa-Herves, A.; Correa, J.; Munoz, E. M.; Taboada, P.; Riguera, R.; Fernandez-Megia, E., The Effect of PEGylation on Multivalent Binding: A Surface Plasmon Resonance and Isothermal Titration Calorimetry Study with Structurally Diverse PEG-Dendritic GATG Copolymers. *ChemNanoMat* **2016,** 2, (5), 437-446.
11. Pussak, D.; Ponader, D.; Mosca, S.; Ruiz, S. V.; Hartmann, L.; Schmidt, S., Mechanical Carbohydrate Sensors Based on Soft Hydrogel Particles. *Angew. Chem. Int. Ed.* **2013,** 52, (23), 6084-6087.
12. Wang, H.; Jacobi, F.; Waschke, J.; Hartmann, L.; Löwen, H.; Schmidt, S., Elastic Modulus Dependence on the Specific Adhesion of Hydrogels. *Adv. Funct. Mater.* **2017,** 27, (41), 1702040.

5.3 Enabling Directional Sequence-Control via Step-Growth Polymerization of Heterofunctionalized Precision Macromonomers

C. Gerke, P. Siegfeld, K. Schaper, L. Hartmann

Macromolecular Rapid Communications, **2019**, 40, (3), 1800735

[Impact Factor 2017: 4.265]

Contribution:

Collaborative design of structures. Synthesis of building blocks (except of the photolabile protecting group), macromonomers, and polymers. Introduction of the photolabile protecting group. Two-step polymerization procedure (except of the first irradiation) and polymer purification. Measurement and evaluation of all LC-MS and GPC-RI-LS experiments. Evaluation of all NMR, UHR-MS and MALDI-TOF experiments. Collaborative writing of the manuscript.

Macromolecular Rapid Communications
www.mrc-journal.de

Enabling Directional Sequence-Control via Step-Growth Polymerization of Heterofunctionalized Precision Macromonomers

*Christoph Gerke, Patrick Siegfeld, Klaus Schaper, and Laura Hartmann**

The synthesis of periodic copolymers with a regularly recurring sequence in one direction along the polymeric backbone is presented, applying a step-growth polymerization of heterofunctionalized precision macromonomers derived from solid phase synthesis (SPS) via photoinduced thiol-ene coupling (TEC). Heterofunctional macromonomers with monomer sequence-control of the AB type present a terminal alkene and a terminal thiol group carrying a photolabile protecting group to avoid uncontrolled polymerization by self-initiation. As protecting group, 3,4-methylenebisoxy-6-nitrobenzyl is attached onto the thiol via its bromide derivative directly on solid support. The protected heterofunctionalized macromonomer is polymerized in a two-step procedure, first cleaving the photolabile group and subsequent polymerization of the macromonomer via TEC, giving a high molecular weight polymer with $\bar{M}_n$ of 23.8 kDa corresponding to a $\bar{X}_n$ of 10 with one directional sequence-control due to their consistent head-to-tail linkage.

Synthesizing polymers with a defined monomer arrangement is an ongoing objective in polymer science, potentially leading to new functional polymers and materials.[1–3] Indeed, over the last decade, different methods have been developed to access sequence-control in polymers, for example, by the repetitive addition of multiple monomers in controlled polymerizations,[4–6] the use of specific arranged or functionalized monomers,[7–9] or the exploitation of different monomer reactivities.[10–12] However, sequence-defined compounds which are monodisperse with a defined monomer sequence, thereby exhibiting highest definition accessible, are obtained by iterative coupling methods such as solid phase synthesis (SPS) or approaches using soluble supporting materials.[13–17] Previously, we have demonstrated the use of SPS to access monodisperse, sequence-defined oligoamides with specifically tuned backbone properties or architectures as well as precisely positioned functional side chain motifs.[18–22] During SPS, based on the classical solid phase peptides synthesis introduced by Merrifield,[23] we perform iterative coupling and deprotection steps of tailor-made building blocks on a solid support. Building blocks are equipped with an Fmoc-protected amine and a carboxylic acid group allowing for straightforward use of well-established peptide coupling procedures as well as for the introduction of conventional amino acids within the oligoamide sequence and full automation of the overall synthesis by using a standard peptide synthesizer.[18,24] A major drawback of solid phase synthesis is that the accessible molecular weights are significantly lower compared to polymers obtained from other polymerization methods. To overcome this limitation, we recently showed the use of sequence-defined macromonomers derived from SPS in photoinduced thiol-ene click (TEC) polyaddition reaction giving access to sequence-controlled multiblock copolymers.[25,26] An AA/BB approach was chosen where one macromonomer was functionalized with terminal thiol groups and the second macromonomer with terminal alkene groups giving no control over the orientation of the macromonomers upon placement within the polymeric chain.[25,26] Since an incorporation of the macromonomers in a definite direction within the final polymer is thereby not achieved, so far only symmetrical macromonomers were used, which therefore did not affect the sequence-control in the final polymers (see **Figure 1**, left). In contrast to an AA/BB approach, a directional sequence-control can be achieved when applying an AB approach polymerizing one heterofunctionalized macromonomer, due to its head-to-tail linkage (see Figure 1, right). The implementation of an AB approach is especially interesting for the synthesis of high molecular weight biomimetic polymers containing a bioactive sequence of nonsymmetrical nature. A multiple presentation of an active sequence after its polymerization can enhance the overall activity of the resulting polymer, for example, when clustering several proteins through interactions with the polymer.[25–29] Including additional directional control in the polymer could then be explored in terms of a more controlled arrangement of proteins in such clusters. An important inspiration for directional control in polymers comes from the proteins, where the monomer sequence triggers the overall structure and thereby often function of the molecule. Thus also for synthetic polymers, for example, self-assembling or single-chain particle systems, the direction of the assembling blocks or functional

C. Gerke, P. Siegfeld, Dr. K. Schaper, Prof. L. Hartmann
Institute of Organic Chemistry and Macromolecular Chemistry
Universitätsstraße 1, Heinrich-Heine-University Düsseldorf
40225 Düsseldorf, Germany
E-mail: laura.hartmann@hhu.de

The ORCID identification number(s) for the author(s) of this article can be found under https://doi.org/10.1002/marc.201800735.

DOI: 10.1002/marc.201800735

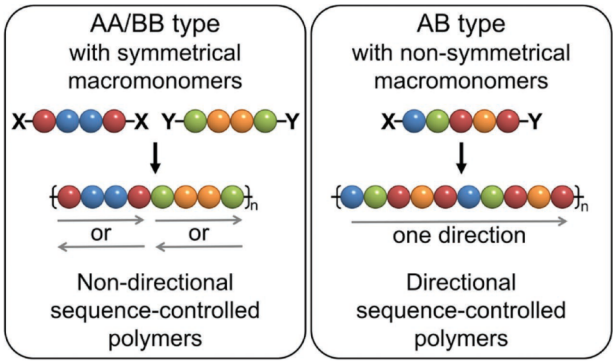

Figure 1. Overview of the different outcomes using symmetrical macromonomers in an AA/BB step-growth polymerization approach (left) as well as when using nonsymmetrical macromonomers in an AB approach (right).

groups can be expected to give access to selective supramolecular structure formation.[30–32] A more practical challenge when using an AA/BB approach is the realization of equimolar amounts of the reactive end-groups which is crucial to obtain high molecular weights in step-growth polymerization. However, first attempts to use an AB approach with macromonomers, carrying a terminal thiol as well as a terminal alkene moiety, showed uncontrolled polymerization immediately after cleaving the macromonomers from the solid support. We believe polymerization proceeds following self-initiation, a well-known problem when performing TEC assumed to be caused by a molecule-assisted homolysis after interaction of the thiol and alkene moiety.[33–37]

Here, we now present an approach using an AB system introducing a nitrobenzyl-based photolabile protecting group for the reactive thiol end-group which can be specifically removed prior to the polymerization, thereby overcoming previously stated obstacles both in terms of the directional control when working with nonsymmetrical macromonomers due to their strict head-to-tail linkage (see Figure 1, right) as well as uncontrolled self-initiation. Nitrobenzyl protecting groups are commonly used in peptide synthesis, providing excellent orthogonality toward other protecting groups and ensuring a quantitative cleavage under mild conditions.[38,39] Besides that, they are also used as caged compounds mainly in biophysical and biochemical studies, temporarily deactivating a biologically active compound by their introduction. After UV irradiation and the resulting removal of the nitrobenzyl group, the biological activity is restored which is generally performed directly in the organism.[40,41] By changing the substituents of the nitrobenzyl group, the required wavelength for its cleavage can be varied and various derivatives were successfully developed over the years.[41,42] We deliberately chose a 3,4-methylenebisoxy-6-nitrobenzyl (MBNB) derivative which, attached to alcohols or carboxylic acids, exhibits one of the highest absorption coefficients at 365 nm among similar nitrobenzyl derivatives.[43,44] The medium pressure mercury (Hg) lamp used for the photoinduced TEC polymerization step shows a strong emission band in the same range and therefore in situ liberation of the thiol and a direct polymerization via TEC should be possible.

The MBNB moiety was coupled to the thiol group on solid support via its bromide derivative (see **Figure 2**A), performing a nucleophilic substitution reaction with the thiolate under basic conditions resulting in the MBNB thioether. A similar introduction of a nitrobenzyl using its bromide derivative onto a thiol moiety was already performed by the group of Barner–Kowollik[45,46] and Dong;[47] however, so far only in solution and not on solid support. For the optimization of the reaction conditions on solid support, oligomer **1** consisting of two ethylene glycol-based building blocks (EDS) followed by the trityl protected amino acid L-cysteine (Cys(Trt); see Figure 2A) was synthesized applying previously established coupling protocols (0.15 mmol batch size).[18,25] The Fmoc protecting group of the terminal Cys was removed and the primary amine was acetylated as shown in Figure 2B. Next, the

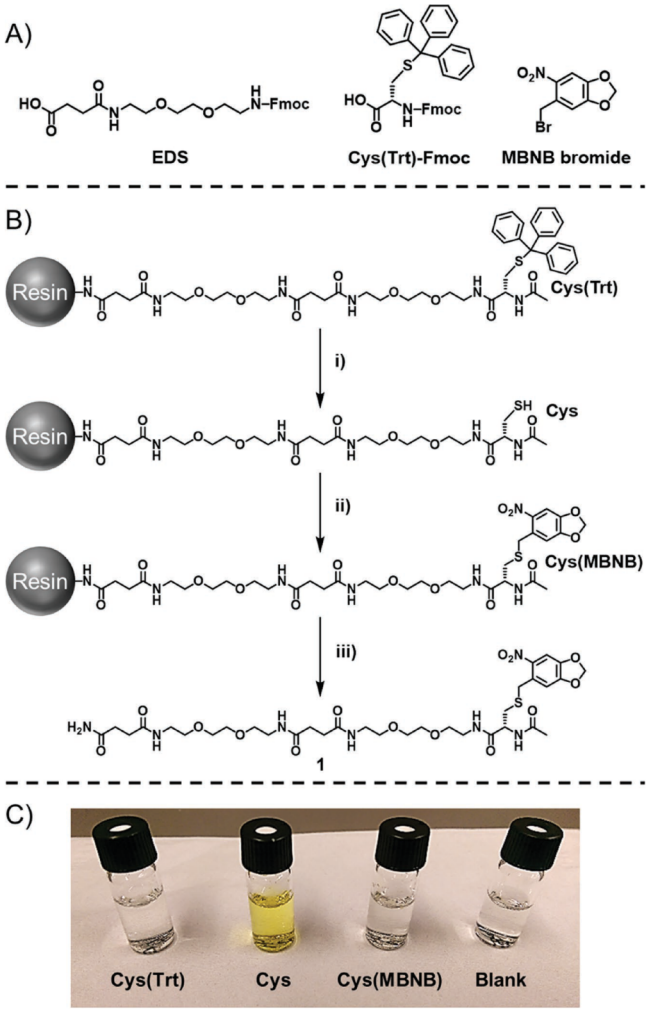

Figure 2. A) Structures of applied building blocks including 3,4-methylenebisoxy-6-nitrobenzyl (MBNB) protecting group. B) Synthesis of oligomer **1** i) Trt cleavage using 5% TFA and 5% tri-isopropylsilane (TIPS) in DCM twice for 30 min, ii) introduction of MBNB group applying 2 equiv. TCEP in DMF/H_2O (1/1) for 2 h followed by 5 equiv. of MBNB bromide with 5 equiv. DIEA in DCM for 2 h, iii) cleavage of **1** from the solid support using 95% TFA and 5% TIPS. C) On-resin Ellman's test showing successful exchange of protecting groups.

Trt protecting group was released applying acid conditions using 5% trifluoroacetic acid (TFA). Although a Rink Amide Linker was used to anchor the compound onto the solid support, usually requiring 95% of TFA for quantitative cleavage, slight loss of oligomer was observed during the Trt group removal resulting in lower yields in comparison to previously published oligoamides derived from SPS.[25] Following the Trt cleavage, resin-bound oligomer was incubated with reducing agent tris(2-carboxyethyl)phosphine hydrochloride (TCEP) to reduce potentially formed disulfide bonds. To prevent a subsequent oxidation of the thiols, the resin was rapidly washed with degassed solvents and the MBNB bromide, dissolved in dichloromethane (DCM), was added to the resin in the presence of *N,N*-diisopropylethylamine (DIEA) as base. In this coupling step, different equivalents of the photolabile MBNB group and DIEA as well as different reaction times were evaluated, showing quantitative coupling already with 5 equiv. of MBNB and DIEA and a reaction time of 2 h. A complete overview of the reaction steps is given in Figure 2B. After cleavage of the resin and precipitation from diethyl ether, oligomer **1** was isolated already in high purity (>95% as determined by integration of UV-signals HPLC analysis) and further purified by preparative HPLC (see Supporting Information for analytical data of **1**). Successful exchange of the Cys protecting group was further monitored by an qualitative on-resin Ellman's test[48,49] as shown in Figure 2C.

After the successful introduction of the MBNB group onto a terminal thiol moiety on solid support, a first heterofunctionalized macromonomer (0.3 mmol batch size) for later step-growth polymerization was synthesized. Besides the terminal Cys, an NDS building block was introduced on the other chain end carrying a norbornene functionality as highly reactive alkene moiety in TEC.[26] As building blocks, the hydrophilic spacer unit EDS as well as amino acids (L-glycine [Gly], L-histidine [His], L-leucine [Leu], L-phenylalanine [Phe], L-serine [Ser], and L-lysine [Lys]) were used to build-up a monomer sequence displaying, from one chain end to the other, the initials of the contributing authors of this project (**Figure 3**D). Thereby, the directional placement of the macromonomer in the later polymer chain is highlighted. The final structure of the protected macromonomer with a total of 14 monomer units is shown in Figure 3C.

Following the procedure established for oligomer **1**, synthesis of the macromonomer was first performed introducing the Cys residue as final building block during solid phase assembly (see Supporting Information for macromonomer **2**). However, partial cleavage of the Boc and tBu protecting groups of Lys, His, and Ser side chains was observed as well as coupling of the released alcohol and amine moieties during the nucleophilic substitution of the MBNB bromide as determined by LC-MS analysis (see Supporting Information). Therefore, in a second approach (0.3 mmol batch size), the Cys moiety was coupled as first monomer unit onto the solid support immediately followed by the protecting group exchange introducing the MBNB group (see Figure 3A). Introduction of the photolabile protecting group was successful and resulted in similar purities as oligomer **1**. After Fmoc cleavage, the rest of the macromonomer including terminal NDS building block was assembled following previously established coupling protocols, resulting in macromonomer **3** as shown in Figure 3B,C. After cleavage from resin and precipitation from diethyl ether, macromonomer **3** was isolated with 85% purity (as determined by the integration of UV signals in HPLC analysis) and further purified by preparative HPLC giving the final product with 98% purity (as determined by the integration of UV signals in HPLC analysis, see Supporting Information).

To evaluate cleavage of the MBNB protecting group, oligomer **1** (3.5 µmol) was irradiated directly in an NMR tube at 385 nm using a UV-LED lamp as well as at 365 nm using a medium pressure Hg UV lamp and cleavage was monitored by ^{1}H NMR spectroscopy and LC-MS (see Supporting Information). For the cleavage test, DMSO-d_6 as well as D_2O were used since the polymerization reaction is performed in

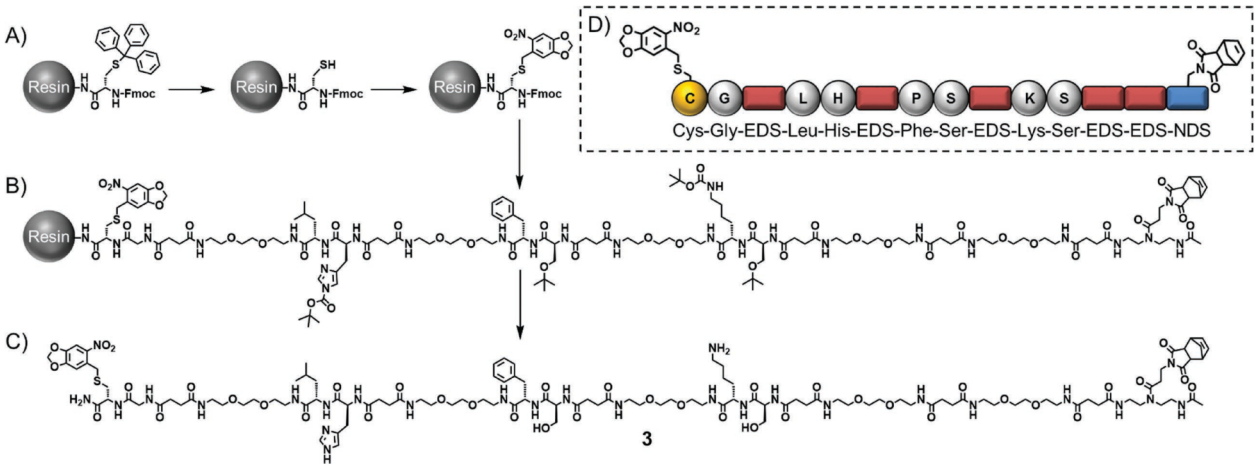

Figure 3. Synthesis of AB type macromonomer **3**: A) exchange of protecting groups; B) solid phase synthesis using EDS, Fmoc amino acids, and NDS; C) final structure of heterofunctionalized macromonomer **3** with terminal Cys(MBNB) and norbornene moiety after cleavage from solid support; and D) schematic illustration of macromonomer **3** highlighting the directional monomer sequence giving the initials of the corresponding authors (we used L-phenylalanine (Phe) instead of L-proline (Pro) to introduce the letter P).

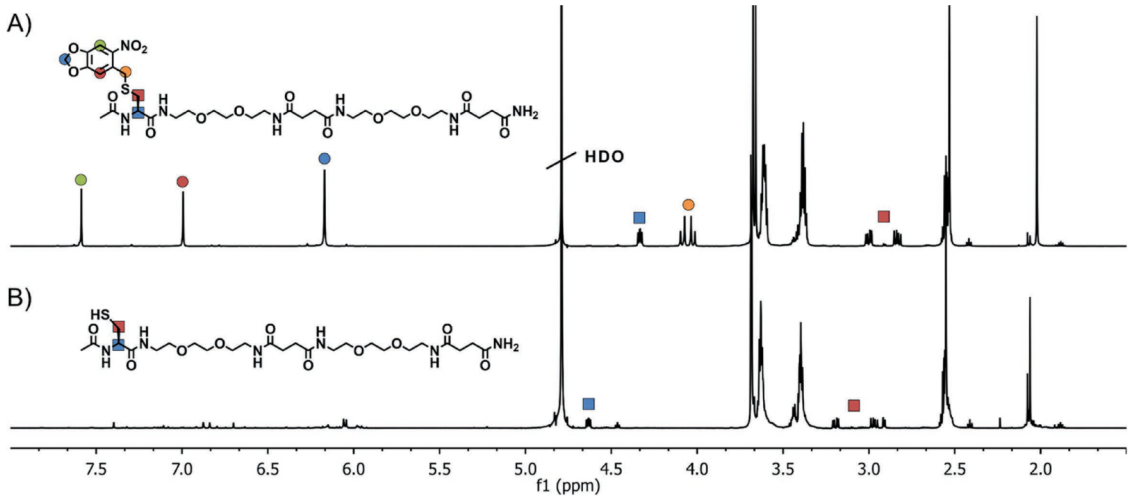

Figure 4. ^{1}H NMR (600 MHz) spectra in D_2O of A) oligomer **1** prior to the UV irradiation with highlighted signals of the MBNB protecting group as well as the Cys moiety, and B) after 90 min of UV irradiation showing the complete removal of the MBNB group and shift of the Cys protons after cleavage. Between 7.5 and 6.0 ppm signals for nitroso cleaving products are detected and multiple signals for the Cys protons are observed due to disulfide formation.

a water/DMSO mixture.[25] **Figure 4** shows ^{1}H NMR spectra before and after irradiation of oligomer **1** in D_2O. The MBNB group was successfully cleaved in both solvents and by both lamps as additionally observed by LC-MS analysis only showing a signal for oligomer **1** with the liberated thiol as well as its dimer due to disulfide formation. Further signals are low molecular weight compounds which are assumed to be different nitroso cleavage products (see Supporting Information). Surprisingly, cleavage of the MBNB group using the reaction setup for the polymerization[25] was not possible, most likely due to insufficient penetration depth of the light into the vessel and the reaction medium. Furthermore, the significantly higher concentration (50 mM) of oligomer **1** compared to the test reaction could have an effect.

A direct in situ liberation of the thiol followed by the TEC polymerization within the same setup was therefore not possible and polymerization of macromonomer **3** was performed in a two-step procedure (10 µmol batch size). First, the MBNB protecting group was removed and after a rapid disulfide reduction and purification step, the macromonomer was subsequently polymerized in step-growth fashion, as shown in **Figure 5**A.

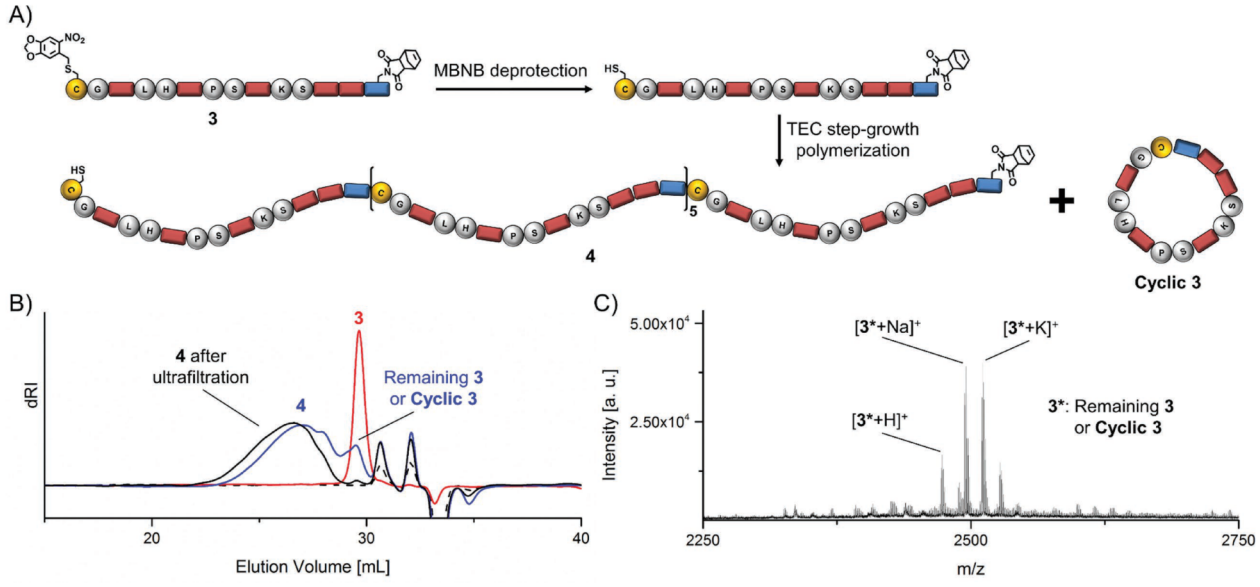

Figure 5. Polymerization of macromonomer: A) deprotection of terminal Cys group followed by TEC polyaddition reaction (the five structural repeating units stated on the brackets in the final polymer **4** refer to the $\overline{X}_n$ achieved in the polymerization and does not imply the formation of a uniform end product), B) GPC-RI-LS elugrams of macromonomer **3** (red) and polymer **4** before (blue) and after its purification via ultrafiltration (black) (columns: Suprema Lux [2 × 100 and 1 × 1000 Å]; buffer: 50 mM NaH_2PO_4, 150 mM NaCl, 250 ppm NaN_3 (pH 7.2), 30% ACN; flow: 0.8 mL min^{-1}), and C) MALDI-TOF spectrum (m/z range 2250–2750) showing the signals for remaining macromonomer **3** or its cyclic form.

Prior to the polymerization, the MBNB group of macromonomer **3** (10 µmol) was cleaved by irradiation in an NMR tube using a UV-LED lamp and D_2O as solvent. Successful cleavage was monitored by ^{1}H NMR analysis until quantitative deprotection was confirmed. Due to pronounced disulfide formation during the MBNB cleavage, macromonomer **3** with free thiol groups was incubated with reducing agent TCEP (2 equiv.) overnight. The excess of TCEP as well as low molecular weight nitroso compounds were removed by ultrafiltration with a molecular weight cutoff (MWCO) membrane of 2 kDa. Subsequently, macromonomer **3** was polymerized applying previously optimized reaction conditions for TEC polyaddition.[25] After irradiation, the formed periodic copolymer **4** was isolated and purified by precipitation from a mixture of diethyl ether/acetone (ratio of 1/3) and analyzed by GPC-RI-LS (see Figure 5B), ^{1}H NMR, and MALDI-TOF (see Supporting Information). The achieved number average molecular weight ($\bar{M}_n$) of polymer **4** was 18.2 kDa as determined by GPC, corresponding to a degree of polymerization ($\bar{X}_n$) of 7, which lies in a similar range compared to previously synthesized sequence-controlled polymers using the AA/BB approach.[25] As determined by ^{1}H NMR analysis, the reaction was not driven to completion as about 25% of the remaining norbornene end-group were detected (see Supporting Information). This is also seen in remaining non-polymerized macromonomer after polymerization as observed in GPC as well as MALDI-TOF analysis (see Figure 5B,C). However, due to a different elution volume in GPC analysis of this fraction compared to the initial macromonomer **3** (see Figure 5B) as well as an expected oxidation of the free thiol of **3**, we assume that a cyclic side-product is formed from an intramolecular TEC reaction of one macromonomer (see Figure 5). By increasing the amount of the macromonomer in the reaction mixture, it should be possible to increase $\bar{M}_n$ and reduce intramolecular cyclization. Especially, intramolecular cyclization is known to be concentration dependent and can most likely be reduced by adjusting the macromonomer concentration.[50,51] To isolate only higher molecular weight fractions of the periodic copolymer **4**, we performed ultrafiltration using an MWCO of 10 kDa, giving final polymer fraction with $\bar{M}_n$ of 23.8 kDa ($\bar{X}_n$ of 10) as determined by GPC (see Figure 5B). Besides the removal of the low molecular weight fractions including the cyclic by-product, the molecular weight of the high molecular weight chains slightly increased due to a further polymerization via self-initiated TEC since both reactive end-groups are still present in the polymer. Remaining end-groups as determined by ^{1}H NMR (see Supporting Information) are similar to polymer sample prior to purification further supporting our assumption that an intramolecular cyclization reaction occurs.

We successfully introduced an AB approach for the TEC polyaddition reaction of sequence-controlled macromonomers derived from solid phase polymer synthesis now giving access to periodic copolymers with control over the direction of monomer sequences along the polymeric backbone. Therefore, a photolabile 3,4-methylenebisoxy-6-nitrobenzyl protecting group was introduced onto a thiol end-group of the macromonomer during solid phase assembly accompanied by a terminal norbornene group at the opposite chain end. Subsequent cleavage of the macromonomer from support, release of the thiol protecting group, and TEC step-growth polymerization resulted in a sequence-controlled polymer with a periodically repeating monomer sequence in one direction and $\bar{M}_n$ of 23.8 kDa after purification via ultrafiltration.

Overall, this approach gives access to high molecular weight periodic copolymers with high levels of control in terms of the monomer sequence within the repeating blocks and now also control over the direction of nonsymmetrical sequenced blocks along the polymer chain. Thus, this approach is a next step toward obtaining sequence-definition well known for biomacromolecules such as the proteins also for synthetic polymers, potentially enabling new properties, for example, in terms of their self-assembly or bioactivity.

Supporting Information

Supporting Information is available from the Wiley Online Library or from the author.

Acknowledgements

The authors thank Dr. Peter Tommes and Ralf Bürgel for performing HRMS and MALDI-TOF measurements, as well as Maria Beuer for performing NMR measurements. The authors gratefully acknowledge support from the Boehringer-Ingelheim Foundation within the *Perspektivenprogramm* "Plus3" and the DFG for large equipment grant (INST 208/735-1).

Conflict of Interest

The authors declare no conflict of interest.

Keywords

nitrobenzyl protecting groups, sequence-controlled polymers, solid-phase synthesis, thiol-ene

Received: October 1, 2018
Revised: October 31, 2018
Published online:

[1] J. F. Lutz, *Macromol. Rapid Commun.* **2017**, *38*, 1700582.
[2] S. Martens, J. O. Holloway, F. E. Du Prez, *Macromol. Rapid Commun.* **2017**, *38*, 1700469.
[3] S. C. Solleder, R. V. Schneider, K. S. Wetzel, A. C. Boukis, M. A. R. Meier, *Macromol. Rapid Commun.* **2017**, *38*, 1600711.
[4] Q. Zhang, J. Collins, A. Anastasaki, R. Wallis, D. A. Mitchell, C. R. Becer, D. M. Haddleton, *Angew. Chem. Int. Ed.* **2013**, *52*, 4435.
[5] Y. Matsuo, R. Konno, T. Ishizone, R. Goseki, A. Hirao, *Polymers* **2013**, *5*, 1012.
[6] Y. Chen, M. S. Lord, A. Piloni, M. H. Stenzel, *Macromolecules* **2015**, *48*, 346.
[7] M. Ouchi, M. Nakano, T. Nakanishi, M. Sawamoto, *Angew. Chem. Int. Ed.* **2016**, *55*, 14584.
[8] W. R. Gutekunst, C. J. Hawker, *J. Am. Chem. Soc.* **2015**, *137*, 8038.

[9] J. Zhang, M. E. Matta, M. A. Hillmyer, *ACS Macro Lett.* **2012**, *1*, 1383.
[10] J.-F. Lutz, B. V. K. J. Schmidt, S. Pfeifer, *Macromol. Rapid Commun.* **2011**, *32*, 127.
[11] S. Pfeifer, J. F. Lutz, *Chem. Eur. J.* **2008**, *14*, 10949.
[12] E. Rieger, A. Alkan, A. Manhart, M. Wagner, F. R. Wurm, *Macromol. Rapid Commun.* **2016**, *37*, 833.
[13] S. Martens, J. Van den Begin, A. Madder, F. E. Du Prez, P. Espeel, *J. Am. Chem. Soc.* **2016**, *138*, 14182.
[14] T. T. Trinh, L. Oswald, D. Chan-Seng, J.-F. Lutz, *Macromol. Rapid Commun.* **2014**, *35*, 141.
[15] A. Al Ouahabi, L. Charles, J.-F. Lutz, *J. Am. Chem. Soc.* **2015**, *137*, 5629.
[16] M. Porel, C. A. Alabi, *J. Am. Chem. Soc.* **2014**, *136*, 13162.
[17] Y. Jiang, M. R. Golder, H. V. T. Nguyen, Y. Wang, M. Zhong, J. C. Barnes, D. J. C. Ehrlich, J. A. Johnson, *J. Am. Chem. Soc.* **2016**, *138*, 9369.
[18] D. Ponader, F. Wojcik, F. Beceren-Braun, J. Dernedde, L. Hartmann, *Biomacromolecules* **2012**, *13*, 1845.
[19] S. Igde, S. Röblitz, A. Müller, K. Kolbe, S. Boden, C. Fessele, T. K. Lindhorst, M. Weber, L. Hartmann, *Macromol. Biosci.* **2017**, *17*, 1700198.
[20] D. Ponader, P. Maffre, J. Aretz, D. Pussak, N. M. Ninnemann, S. Schmidt, P. H. Seeberger, C. Rademacher, G. U. Nienhaus, L. Hartmann, *J. Am. Chem. Soc.* **2014**, *136*, 2008.
[21] F. Wojcik, S. Mosca, L. Hartmann, *J. Org. Chem.* **2012**, *77*, 4226.
[22] M. Baier, M. Giesler, L. Hartmann, *Chem. Eur. J.* **2018**, *24*, 1619.
[23] R. B. Merrifield, *J. Am. Chem. Soc.* **1963**, *85*, 2149.
[24] M. F. Ebbesen, C. Gerke, P. Hartwig, L. Hartmann, *Polym. Chem.* **2016**, *7*, 7086.
[25] C. Gerke, M. F. Ebbesen, D. Jansen, S. Boden, T. Freichel, L. Hartmann, *Biomacromolecules* **2017**, *18*, 787.
[26] C. Gerke, F. Jacobi, L. E. Goodwin, F. Pieper, S. Schmidt, L. Hartmann, *Macromolecules* **2018**, *51*, 5608.
[27] J. E. Gestwicki, C. W. Cairo, L. E. Strong, K. A. Oetjen, L. L. Kiessling, *J. Am. Chem. Soc.* **2002**, *124*, 14922.
[28] L. L. Kiessling, J. C. Grim, *Chem. Soc. Rev.* **2013**, *42*, 4476.
[29] Y. Gou, J. Geng, S.-J. Richards, J. Burns, C. Remzi Becer, D. M. Haddleton, *J. Polym. Sci. Part A Polym. Chem.* **2013**, *51*, 2588.
[30] E. Elacqua, K. B. Manning, D. S. Lye, S. K. Pomarico, F. Morgia, M. Weck, *J. Am. Chem. Soc.* **2017**, *139*, 12240.
[31] G. Yilmaz, V. Uzunova, R. Napier, C. R. Becer, *Biomacromolecules* **2018**, *19*, 3040.
[32] M. Zamfir, P. Theato, J.-F. Lutz, *Polym. Chem.* **2012**, *3*, 1796.
[33] W. A. Pryor, J. H. Coco, W. H. Daly, K. N. Houk, *J. Am. Chem. Soc.* **1974**, *96*, 5591.
[34] O. Nuyken, T. Völkel, *Die Makromol. Chem. Rapid Comm.* **1990**, *11*, 365.
[35] S. Sensfuß, M. Friedrich, E. Klemm, *Die Makromol. Chem.* **1991**, *192*, 2895.
[36] U. Biermann, W. Butte, R. Koch, P. A. Fokou, O. Türünç, M. A. R. Meier, J. O. Metzger, *Chem. Eur. J.* **2012**, *18*, 8201.
[37] U. Biermann, J. O. Metzger, *Eur. J. Org. Chem.* **2018**, *2018*, 730.
[38] C. G. Bochet, *J. Chem. Soc. Perkin Trans.1* **2002**, 125, https://doi.org/10.1039/B009522M.
[39] P. Klán, T. Šolomek, C. G. Bochet, A. Blanc, R. Givens, M. Rubina, V. Popik, A. Kostikov, J. Wirz, *Chem. Rev.* **2013**, *113*, 119.
[40] G. Mayer, A. Heckel, *Angew. Chem. Int. Ed.* **2006**, *45*, 4900.
[41] M. J. Hansen, W. A. Velema, M. M. Lerch, W. Szymanski, B. L. Feringa, *Chem. Soc. Rev.* **2015**, *44*, 3358.
[42] F. Bley, K. Schaper, H. Görner, *Photochem. Photobiol.* **2008**, *84*, 162.
[43] A. Blanc, C. G. Bochet, *Org. Lett.* **2007**, *9*, 2649.
[44] K. Schaper, M. Etinski, T. Fleig, *Photochem. Photobiol.* **2009**, *85*, 1075.
[45] G. Delaittre, T. Pauloehrl, M. Bastmeyer, C. Barner-Kowollik, *Macromolecules* **2012**, *45*, 1792.
[46] T. Pauloehrl, G. Delaittre, M. Bastmeyer, C. Barner-Kowollik, *Polym. Chem.* **2012**, *3*, 1740.
[47] G. Liu, C.-M. Dong, *Biomacromolecules* **2012**, *13*, 1573.
[48] G. L. Ellman, *Arch. Biochem. Biophys.* **1959**, *82*, 70.
[49] J. P. Badyal, A. M. Cameron, N. R. Cameron, D. M. Coe, R. Cox, B. G. Davis, L. J. Oates, G. Oye, P. G. Steel, *Tetrahedron Lett.* **2001**, *42*, 8531.
[50] C. J. White, A. K. Yudin, *Nat. Chem.* **2011**, *3*, 509.
[51] T. F. A. de Greef, G. Ercolani, G. B. W. L. Ligthart, E. W. Meijer, R. P. Sijbesma, *J. Am. Chem. Soc.* **2008**, *130*, 13755.

Supporting Information

for *Macromol. Rapid Commun.,* DOI: 10.1002/marc.201800735

Enabling Directional Sequence-Control via Step-Growth Polymerization of Heterofunctionalized Precision Macromonomers

Christoph Gerke, Patrick Siegfeld, Klaus Schaper, and Laura Hartmann*

Supporting Information

Enabling Directional Sequence-Control via Step-Growth Polymerization of Heterofunctionalized Precision Macromonomers

Christoph Gerke, Patrick Siegfeld, Klaus Schaper, Laura Hartmann*

Institute of Organic and Macromolecular Chemistry, Heinrich-Heine University Düsseldorf, Universitätsstraße 1, 40225 Düsseldorf, Germany

* Correspondence to Tel: +49 211 81-10360; Fax: +49 211 81-15840;

E-mail: laura.hartmann@hhu.de

Materials:

Dimethyl sulfoxide (DMSO) (≥ 99.9%), 2,2-dimethoxy-2-phenylacetophenone (DMPA) (99%), diethyl ether (with BHT as inhibitor, ≥ 99.8%), triisopropylsilane (TIPS) (98%) and acetic acid (99.8%) were all purchased from Sigma-Aldrich. *N*,*N*-Diisopropylethylamine (DIEA) (≥ 99%) and tris(2-carboxyethyl)phosphine hydrochloride (TCEP) (≥ 98%) were purchased by Carl Roth. Methanol (100%) and acetic anhydride (99.7%) were purchased from VWR BDH Prolabo Chemicals. Dimethylformamide (DMF) (99.8%, for peptide synthesis) and piperidine (99%) were purchased Acros Organics. Dichloromethane (DCM) (99.99%) and sodium chloride (99.98%) were purchased from Fisher Scientific. Tentagel S RAM (Rink Amide) resin (Capacity 0.25 mmol/g) was purchased from Rapp Polymere. Trifluoroacetic acid (TFA) (99%) and (Benzotriazol-1-yloxy)tripyrrolidinophosphonium hexafluorophosphate (PyBOP) were purchased from Fluorochem. *N*-α-(9-Fluorenylmethyloxycarbonyl)-L-glycine (Fmoc-L-Gly-OH) (99.9%), *N*-α-(9-fluorenylmethyloxycarbonyl)-L-leucine (Fmoc-L-Leu-OH) (99.8%), *N*-α-(9-fluorenylmethyloxycarbonyl)-*N*-im-(t-butyloxycarbonyl)-L-histidine cyclohexylamine (Fmoc-L-His(Boc)-OH*CHA) (98.9%), *N*-α-(9-fluorenylmethyloxycarbonyl)-L-phenylalanine (Fmoc-L-Phe-OH) (99.9%), *N*-α-(9-fluorenylmethyloxycarbonyl)-*N*-ε-t-butyloxycarbonyl-L-lysine (Fmoc-L-Lys(Boc)-OH) (99.9%), *N*-α-(9-fluorenylmethyloxycarbonyl)-*O*-t-butyl-L-serine (Fmoc-L-Ser(tBu)-OH) (99.9%), *N*-α-(9-fluorenylmethyloxycarboxyl)-*S*-trityl-L-cysteine (Fmoc-L-Cys(Trt)-OH) (99.9%) were purchased from Iris Biotech. AG ® 1-X8 Anion Exchange Resin, analytical grade, 100–200 mesh, acetate form was purchased from Bio Rad. Vivaspin 6 and 20 ultrafiltration concentrators with MWCO of 2kDa and 10 kDa were purchased from VWR. Water was purified with a Milli-Q system (Millipore) obtaining a final resistivity of 18 MΩcm.

Instrumentation

Peptide Synthesizer

The majority of the sequence of macromonomers **2** and **3** was synthesized on an automated peptide synthesizer CS136X from CS Bio.

Nuclear Magnetic Resonance spectroscopy (NMR)

^{1}H NMR (600 MHz) spectra was recorded on a Bruker AVANCE III - 600. Chemical shifts of all NMR spectra were reported in delta (δ) expressed in parts per million (ppm). The signal of residual solvent was used as internal standard (δ 4.79 ppm for D_2O and δ 2.50 ppm for DMSO-d_6). The following abbreviations are used to indicate the multiplicities: s, singlet; d, doublet; dd, doublet of doublets; m multiplet. All measurements were performed at 25 °C if not stated otherwise.

Reversed Phase - High Pressure Liquid Chromatography - Mass Spectrometry (RP-HPLC-MS)

Measurements were performed on an Agilent 1260 Infinity instrument coupled to a variable wavelength detector (VWD) (set to 214 nm) and a 6120 Quadrupole LC/MS containing an Electrospray ionization (ESI) source (operated in positive ionization mode in an *m/z* range of 200 to 2000). As HPLC column a MZ-Aqua Perfect C18 (3.0×50 mm, 3 µm) RP Column from MZ Analysetechnik was used. The mobile phases A and B were H_2O/ACN (95/5) and H_2O/ACN (5/95), respectively. Both mobile phases contained 0.1% of formic acid. Samples were analyzed at a flow rate of 0.4 mL/min using a linear gradient starting with 100% mobile phase A reaching 50% mobile phase B within 30 min. The temperature of the column compartment was set to 25 °C. UV and MS spectral analysis was done within the OpenLab ChemStation software for LC/MS from Agilent Technologies.

Preparative Reversed Phase – High Pressure Liquid Chromatography (Preparative RP-HPLC)

For the purification of the glycooligomers an Agilent 1260 Infinity instrument coupled to a variable wavelength detector (VWD) (set to 214 nm) and an automated fraction collector (FC) was used. For the purification of the glycooligomers as RP-HPLC column a CAPCELL PAK C18 (20×250 mm, 5 µm) was used. The mobile phases A and B were H_2O and ACN, respectively. The flow rate was set to 20 ml/min.

Ultra High Resolution - Mass Spectrometry (UHR-MS)

UHR-MS measurements were performed with a Bruker UHR-QTOF maXis 4G instrument with a direct inlet via syringe pump, an ESI source and a quadrupole followed by a Time Of Flight (QTOF) mass analyzer.

Matrix-Assisted Laser Desorption Ionization- Time Of Flight – Mass Spectrometry (MALDI-TOF-MS)

MALDI-TOF-MS analysis was performed using a Bruker MALDI-TOF Ultraflex I system with 2,5-dihydroxybenzoic acid (DHB) as matrix. The ratio of matrix to compound was 10:1. Spectra were acquired in both linear, for an *m/z* range of 1000-4000, and reflector mode for an *m/z* range 2000-20000. The reflector mode was calibrated using a protein mixture whereas the linear mode was not calibrated.

Gel Permeation Chromatography (GPC) analysis

GPC was performed using an Agilent 1200 series HPLC system equipped with three aqueous GPC columns from Polymer Standards Service (PSS) Mainz, Germany (Suprema Lux analytical 8 mm diameter, 5 µm particle size, precolumn of 50 mm, 2× 100 Å of 300 mm, 1000 Å of 300 mm). MilliQ water with 50 mM NaH_2PO_4, 150 mM NaCl, 250 ppm NaN_3 and of pH 7 + 30% ACN, filtered through an inline 0.1 µm membrane filter, was used as GPC eluent with a flow rate of 0.8 mL/min. Multi-angle light scattering- and differential refractive index spectra were recorded using a miniDAWN TREOS and Optilab rEX, respectively, that were both from Wyatt Technologies EU. Data analysis was performed using the Astra 5 software using a measured dn/dc value of 0.156 mL/g for all the poly/oligoamides.

UV-lamp for cleavage of photolabile protecting group

For cleavage experiments of the photolabile protecting group, a LUMOS 43 from Atlas Photonics with an UV-LED and NMR tube holder was used. A wavelength of 385 nm was adjusted.

UV-lamp for polymerization

A TQ150 Hg medium pressure UV lamp from Haraeus Nobellight GmbH with a quartz glass immersion and cooling tube from Peschl Ultraviolet GmbH was used for thiol-ene click reactions.

Freeze dryer

The final oligomers and polymers were freeze dried with an Alpha 1-4 LD plus instrument from Martin Christ Freeze Dryers GmbH. The Main Drying method was set to -42 °C and 0.1 mbar.

Synthetic procedures

3,4-Methylenebisoxy-6-nitrobenzyl-1-bromid synthesis

The nitrobenzyl derivative, 3,4-methylenebisoxy-6-nitrobenzyl (MBNB) bromide, was synthesized according to a previously published procedures.[1]

Building block synthesis

Synthesis of building blocks DDS[2], EDS[3] and NDS[4] were reported earlier.

Solid phase synthesis protocols

Oligomer **1** and macromonomers **2** and **3** were synthesized in a batch size of 0.15 and 0.3 mmol, respectively. Oligomer **1** as well as the coupling of the Cys moiety and the introduction of the photolabile protecting group were performed by hand coupling in a syringe reactor (15 mL for oligomer **1** and 25 mL for macromonomers **2** and **3**). The remaining amino acids and building blocks of macromonomers **2** and **3** were coupled using an automated peptide synthesizer.

As resin a commercially available Tentagel S RAM (Rink Amide) resin with a capacity of 0.25 mmol/g was used. The general procedures for the solid phase synthesis were reported earlier.[4, 5] All oligoamides were purified using an anion exchange resin as described by Cintrat, Fay and co-workers[6] followed by preparative HPLC.

MBNB protecting group removal

For the MBNB cleavage experiments, 3.5 µmol of oligomer **1** were dissolved in 700 µL deuterated DMSO or water, transferred into a NMR tube and irradiated for 90 min with an UV-LED (385 nm) or an medium pressure mercury UV (365 nm) lamp. A ^{1}H NMR spectrum was recorded prior as well as after UV irradiation to monitor the MBNB cleavage. From the test experiment in D_2O using the UV-LED lamp, the MBNB cleavage was additionally monitored by LC-MS.

Two-step polymerization procedure of macromonomer 3

In the two-step polymerization procedure of macromonomer **3**, first 10 µmol of **3** were dissolved in 700 µL D_2O, transferred to an NMR tube and irradiated for a total of 5 h using the UV-LED lamp. Subsequently, the material was collected and incubated with a solution of TCEP (2 equiv) overnight to reduce formed disulfide linkages. After the disulfide reduction, excessive reducing agent as well as low molecular weight nitroso compounds were removed by ultrafiltration (MWCO 2 kDa). Macromonomer **3** with the liberated thiol group was rapidly washed with degassed water to prevent subsequent oxidation to disulfides and freeze-dried in the polymerization reaction vessel. The following polymerization was performed with previously optimized reaction conditions.[5] Briefly, the freshly freeze-dried macromonomer **3** (10 µmol) was irradiated for 60 min using the medium pressure Hg lamp under the presence of 1 equiv of the photoinitiator DMPA as well as 0.01 equiv of the reducing agent TCEP in 200 µL of a DMSO/H_2O mixture (9/1).

Analytical data

EDS-EDS-Cys(MBNB) (Oligomer 1):

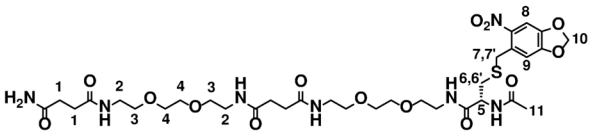

Oligomer **1** was obtained in a yield of 38% (45.9 mg) after purification by preparative HPLC.

^{1}H NMR (600 MHz, D_2O): δ 7.65 (s, 1H, 8), 7.03 (s, 1H, 9), 6.18 (s, 2H, 10), 4.32 (dd, *J* = 8.0, 5.8 Hz, 1H, 5), 4.14 (d, *J* = 13.9 Hz, 1H, 7 or 7'), 4.06 (d, *J* = 13.8 Hz, 1H, 7 or 7'), 3.72 – 3.64 (m, 8H, 4), 3.64 – 3.58 (m, 8H, 3), 3.45 – 3.33 (m, 8H, 2), 3.03 (dd, *J* = 14.1, 5.8 Hz, 1H, 6 or 6'), 2.85 (dd, *J* = 14.1, 8.1 Hz, 1H, 6 or 6'), 2.61 – 2.49 (m, 8H, 1), 2.02 (s, 3H, 11) ppm. The assignment of the signals was verified by the implementation of ^{1}H-^{1}H-COSY experiments (data not shown).

HR-ESI-MS for $C_{33}H_{51}N_7O_{14}S$ (exact monoisotopic mass 801.3215 g/mol): $[M+H]^+$ calcd. 802.3287, found 802.3289, mass accuracy 0.25 ppm.

RP-HPLC (linear gradient from 0 - 50% eluent B in 30 min at 25 °C): t_R = 17.3 min. Determined purity: > 99%.

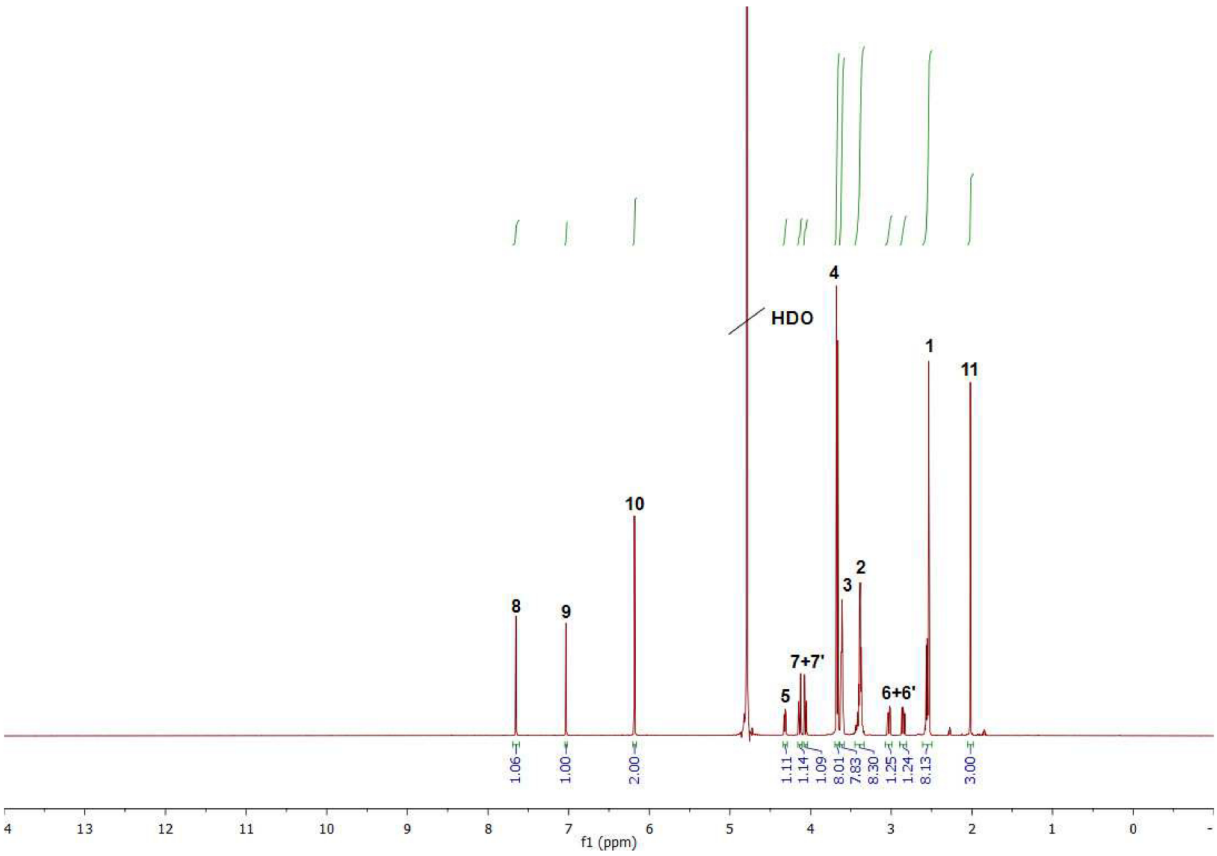

Figure S1: ^{1}H NMR (600 MHz, D_2O) of oligomer **1**.

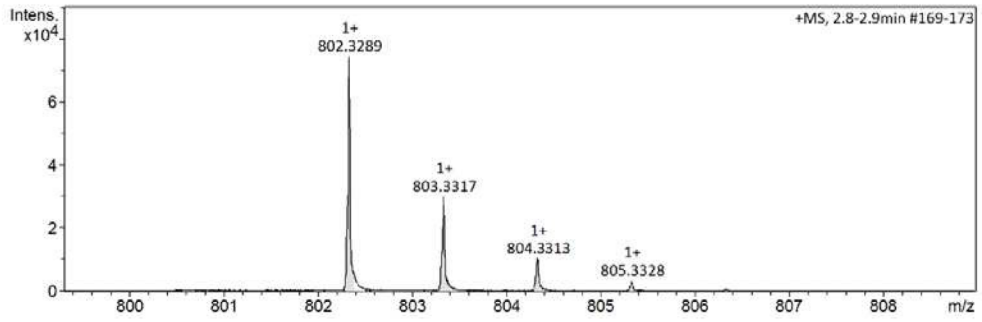

Figure S2: HR-MS (ESI$^+$ Q-TOF) of oligomer **1**.

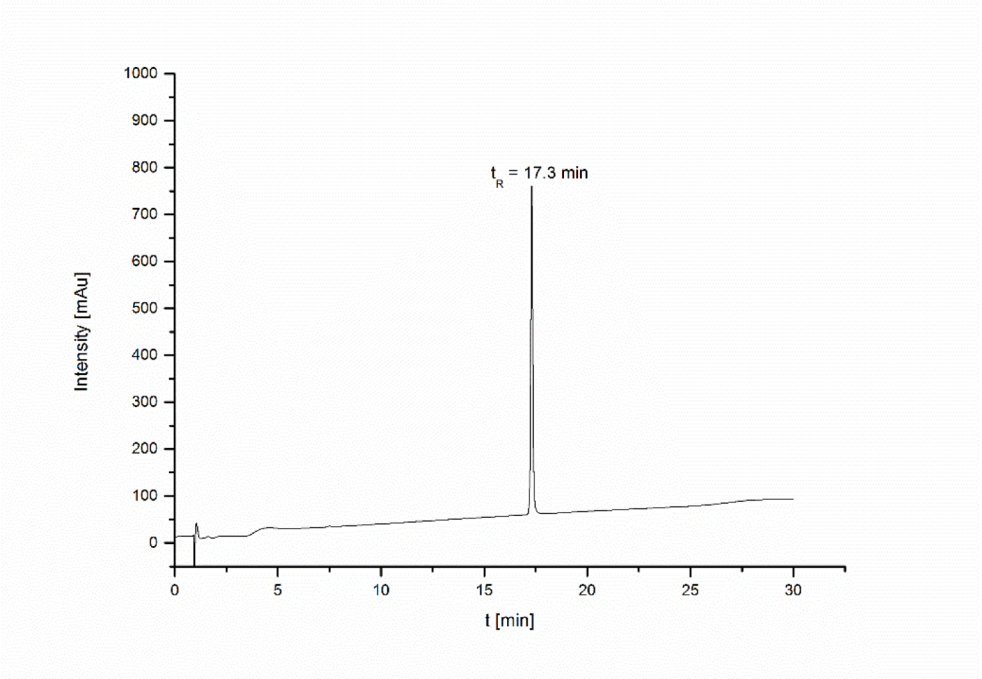

Figure S3: RP-HPLC analysis (linear gradient from 0 - 50% eluent B in 30 min at 25 °C) chromatogram of oligomer **1** with retention time.

NDS-EDS-SK-EDS-SP-EDS-HL-G-Cys(MBNB) (Macromonomer 2):

The first approach of synthesizing the heterofunctionalized macromonomer (macromonomer **2**), starting with the alkene carrying NDS block, followed by the EDS building blocks as well as amino acids and finally terminating the sequence with the Cys moiety (see Figure S4), was not possible due to partial cleavage of the Boc and tBu protecting groups of the Lys, His and Ser moieties. Aside the thiol of the Cys moiety, the liberated amine and alcohol groups also underwent nucleophilic substitution reaction with the MBNB bromide, leading to several MBNB functionalized side products as well as high amounts of unfunctionalized compound, as observed by LCMS analysis (see Figure S5).

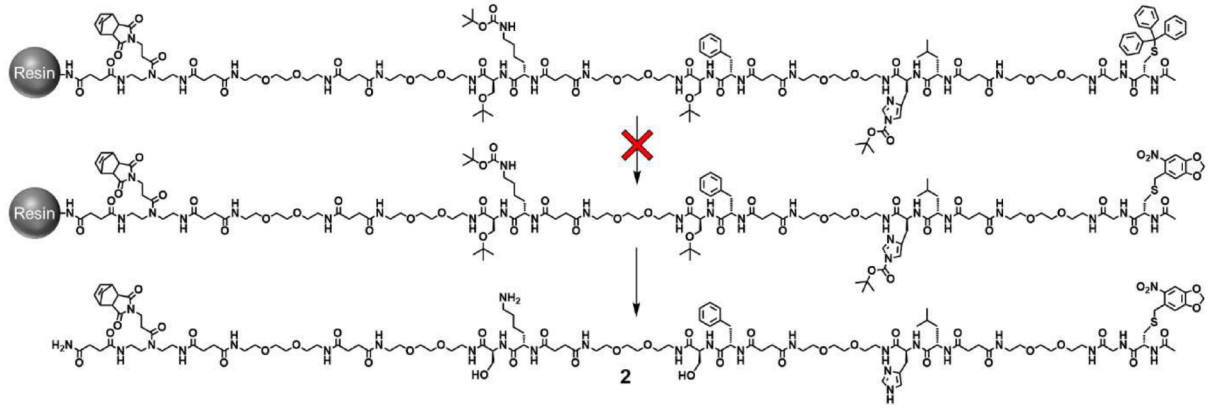

Figure S4: Overview of the synthetic approach to synthesize macromonomer **2**, starting with the NDS and terminating with the Cys(Trt) moiety (top), followed by the protecting group exchange from the Trt to the MBNB group (center) and the final cleavage from the resin (bottom).

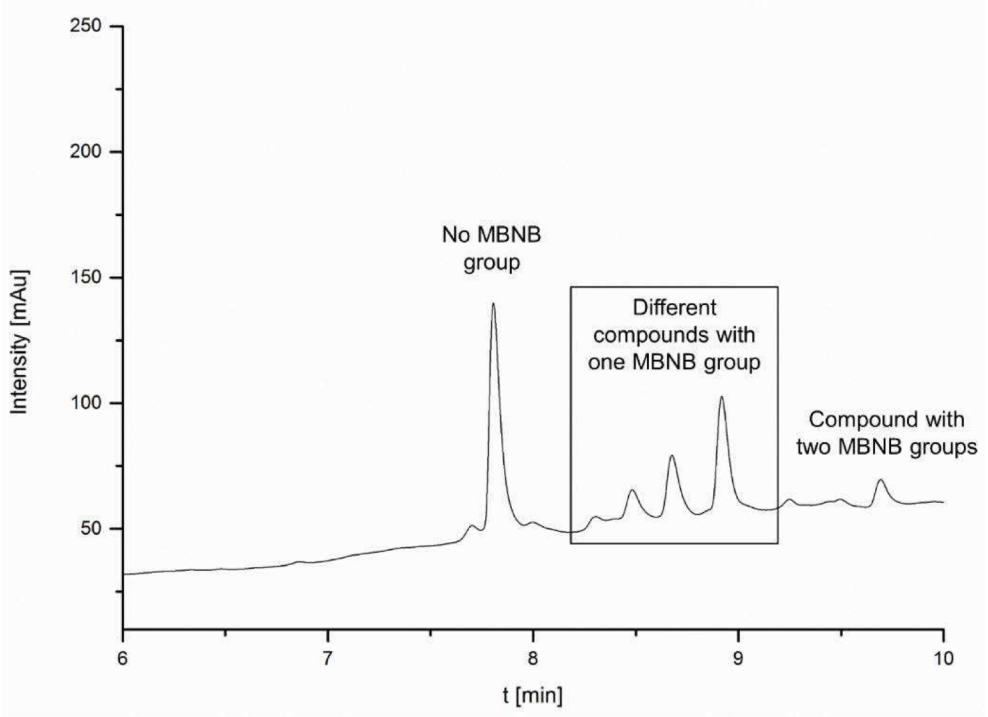

Figure S5: Minute 6 till 10 of the RP-HPLC analysis (linear gradient from 0 - 50% eluent B in 10 min at 25 °C) chromatogram of macromonomer **2** with assigned signals; first corresponding to the unfunctionalized compound without an MBNB group, following three signals corresponding to different compound with one MBNB group as well as last signal corresponding to a compound carrying two MBNB groups.

Cys(MBNB)G-EDS-LH-EDS-PS-EDS-KS-EDS-EDS-NDS (Macromonomer 3):

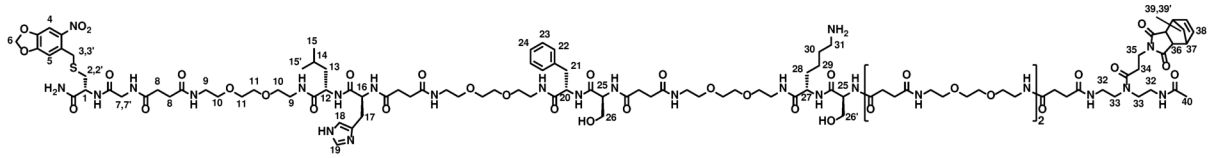

Macromonomer **3** was obtained in a yield of 13% (103.0 mg) after purification by preparative HPLC. For the acetyl group on the N-terminal end we observed two singlets with a ratio of 1:1 that we assign to two rotational isomers in equal amounts. The presence of rotational isomers was identified by ^{1}H NMR experiments at higher temperatures (data not shown). ^{1}H NMR (600 MHz, D_2O): δ 7.71 – 7.66 (m, 1H, 19), 7.62 (s, 1H, 4), 7.38 – 7.33 (m, 2H, 24), 7.32 – 7.27 (m, 1H, 23), 7.27 – 7.23 (m, 2H, 22), 7.01 (s, 1H, 5), 6.94 (s, 1H, 18), 6.16 (s, 2H, 6), 6.13 (s, 2H, 38), 4.61 – 4.52 (m, 2H, 16+20), 4.44 – 4.38 (m, 2H, 25), 4.36 (dd, *J* = 9.0, 5.0 Hz, 1H, 1), 4.32 (dd, *J* = 9.5, 5.2 Hz, 1H, 12), 4.27 (dd, *J* = 10.3, 5.0 Hz, 1H, 27), 4.11 (d, *J* = 13.8 Hz, 1H, 3 or 3'), 4.05 (d, *J* = 13.8 Hz, 1H, 3 or 3'), 3.94 – 3.91 (m, 2H, 26 or 26'), 3.91 – 3.87 (m, 1H, 7 or 7'), 3.86 – 3.81 (m, 1H, 7 or 7'), 3.79 – 3.73 (m, 2H, 26 or 26'), 3.70 – 3.49 (m, 42H, 10+11+35), 3.49 – 3.24 (m, 32H, 9+32+33+36+37), 3.17 – 2.84 (m, 8H, 2+2'+17+21+31), 2.64 – 2.47 (m, 26H, 8+34), 1.99 + 1.97 (2s, 3H, 40), 1.93 – 1.31 (m, 11H, 13+14+28+29+30+39+39'), 0.88 (d, *J* = 6.6 Hz, 3H, 15 or 15'), 0.81 (d, *J* = 6.5 Hz, 3H, 15 or 15') ppm. The assignment of the signals was verified by the implementation of ^{1}H-^{1}H-COSY experiments (data not shown).

HR-ESI-MS for $C_{118}H_{183}N_{27}O_{40}S$ (exact monoisotopic mass 2650.2836 g/mol): $[M+3H]^{3+}$ calcd. 884.4352, found 884.4355, mass accuracy 0.34 ppm.

RP-HPLC (linear gradient from 0 - 50% eluent B in 30 min at 25 °C): t_R = 18.4 min. Determined purity: > 98%.

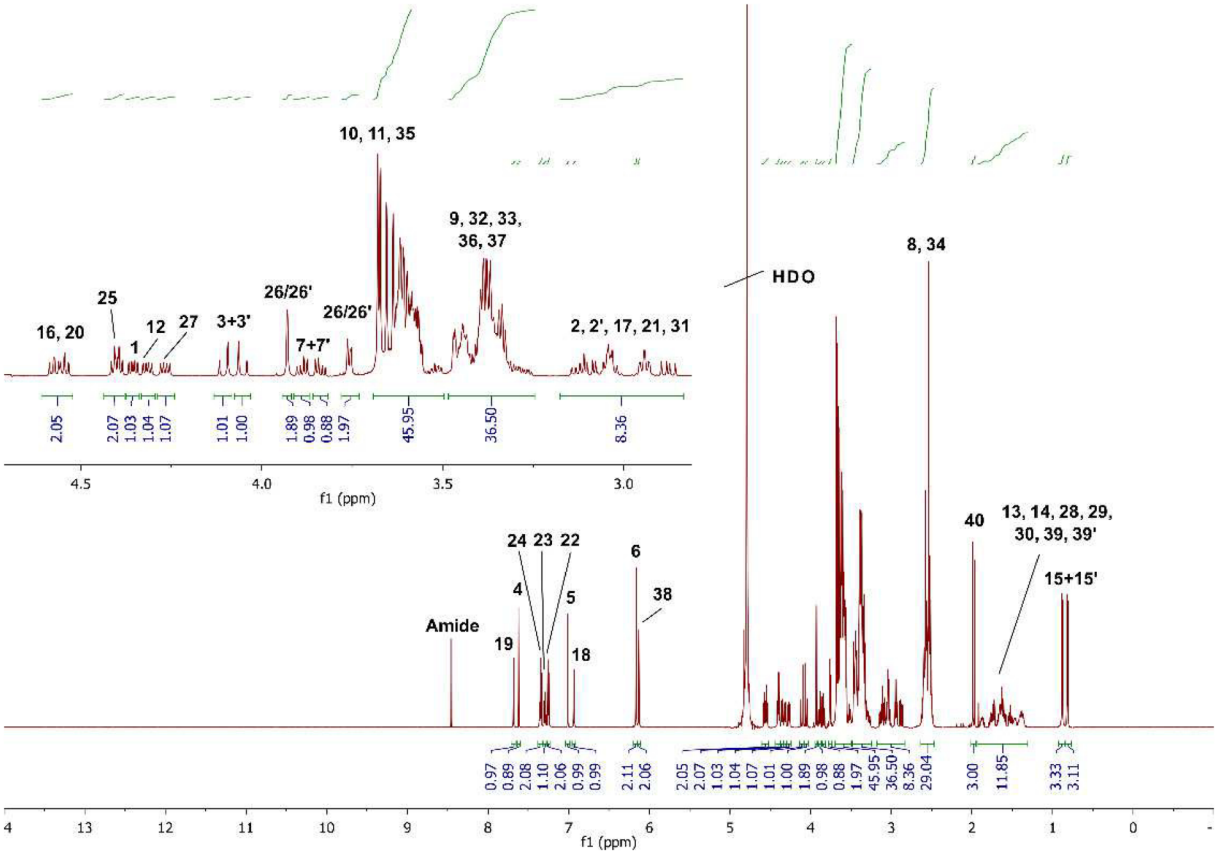

Figure S6: ^{1}H NMR (600 MHz, D_2O) of macromonomer **3** with an enlargement of the area from δ 2.8 to 4.7 ppm.

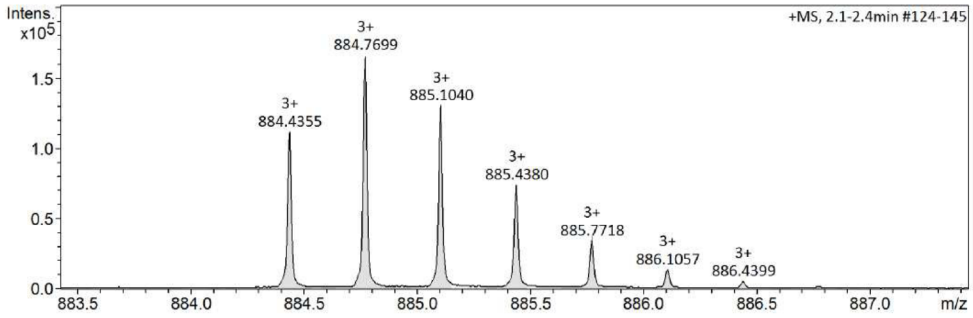

Figure S7: HR-MS (ESI$^+$ Q-TOF) of macromonomer **3**.

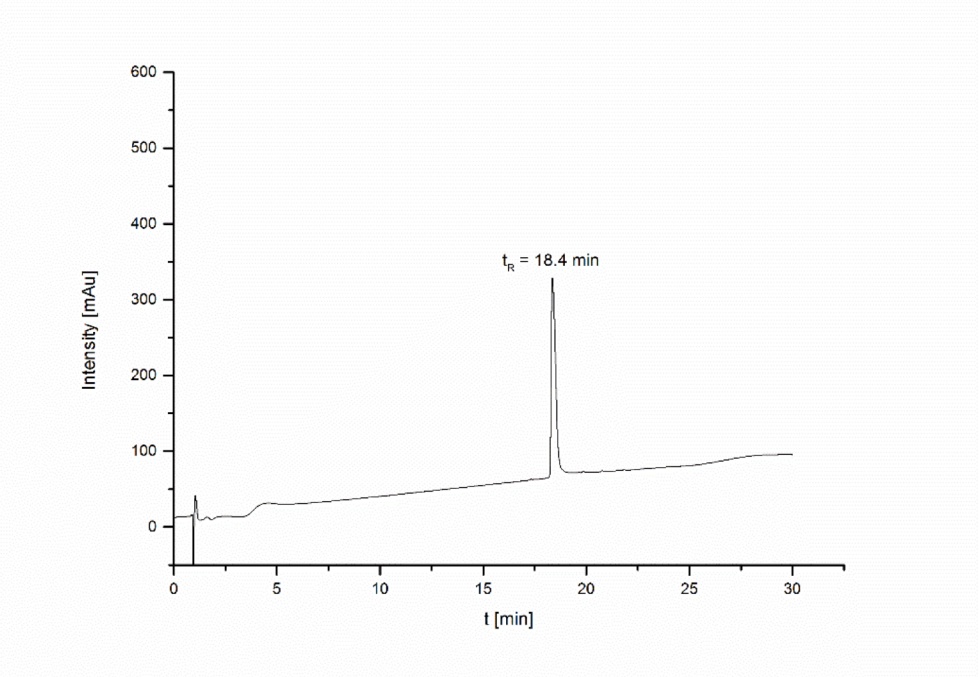

Figure S8: RP-HPLC analysis (linear gradient from 0 - 50% eluent B in 30 min at 25 °C) chromatogram of macromonomer **3** with retention time.

3,4-Methylenebisoxy-6-nitrobenzyl (MBNB) cleavage test

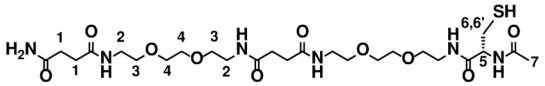

Cleavage test in D_2O using the LUMOS 43 UV-LED (385 nm):

Due to disulfide formation of the free thiol groups, multiple signals were observed, especially for the protons of the Cys moiety (5 and 6+6'). Signals with chemical shift between δ 7.5 and 5.5 ppm are assumed to be nitroso cleavage products. ^{1}H NMR (600 MHz, D_2O): δ 4.66 – 4.44 (m, 1H, 5), 3.74 – 3.54 (m, 16H, 3+4), 3.49 – 3.30 (m, 8H, 2), 3.25 – 2.86 (m, 2H, 6+6'), 2.63 – 2.47 (m, 8H, 1), 2.15 – 1.95 (m, 3H, 7) ppm.

RP-HPLC (linear gradient from 0 - 50% eluent B in 30 min at 25 °C): t_R = 10.0 min for oligomer **1** with the free thiol and t_R = 12.0 min for the dimer of oligomer **1** via a disulfide linkage. The disulfide was unambiguously determined after its reduction by incubation with the reducing agent TCEP (black chromatogram). Further signals are low molecular weight compounds with *m/z* below 200 and were therefore not detected by MS. The low molecular weight compounds are assumed to be nitroso cleavage products.

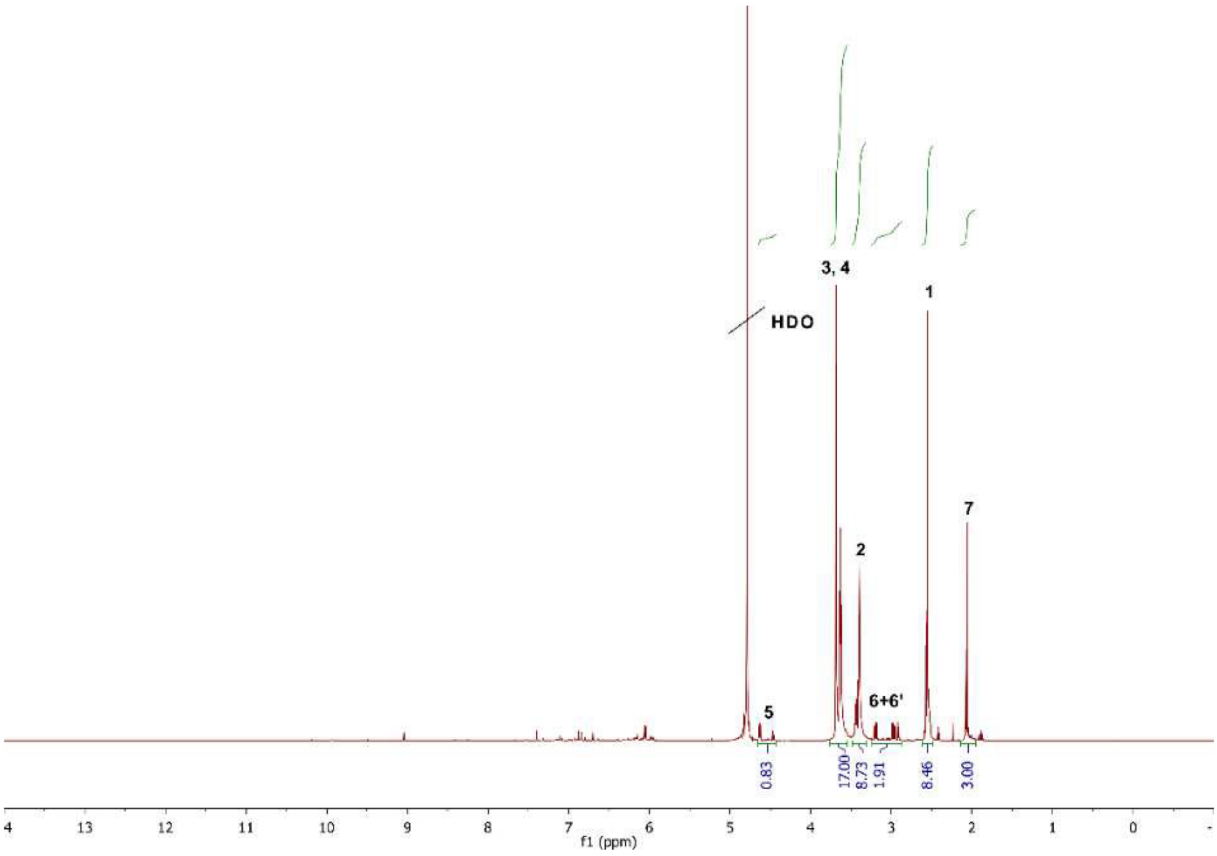

Figure S9: ^{1}H NMR (600 MHz, D_2O) of oligomer **1** after MBNB cleavage test in D_2O using the Lumos 43 with an UV-LED (385 nm).

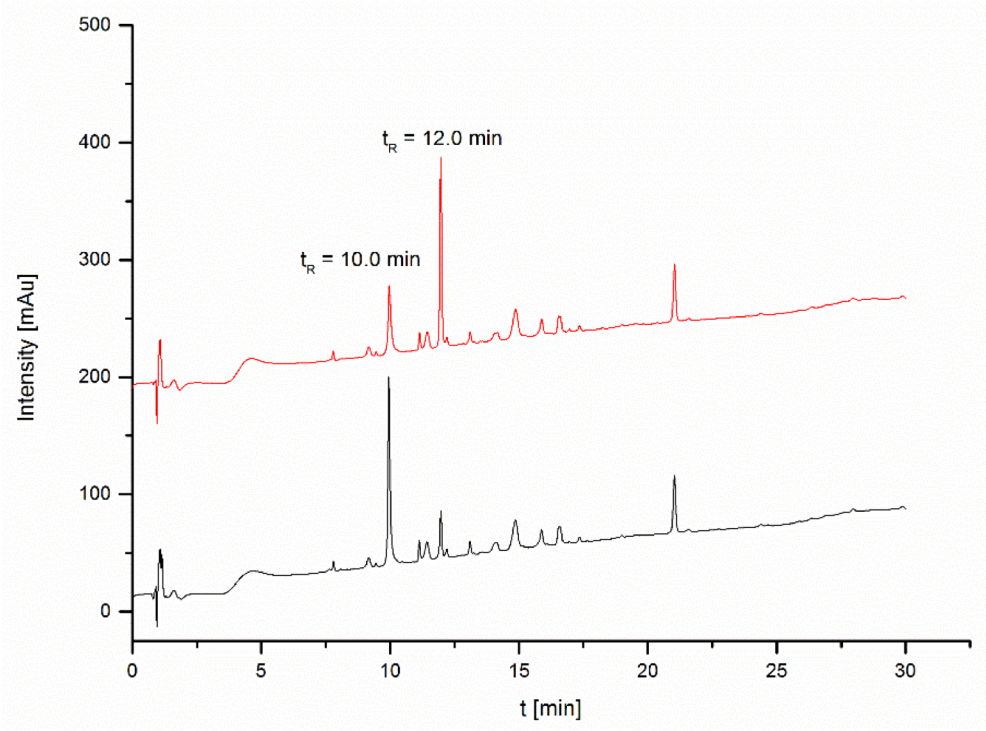

Figure S10: RP-HPLC analysis (linear gradient from 0 - 50% eluent B in 30 min at 25 °C) chromatogram of oligomer **1** after the MBNB group cleavage test performed in D_2O using the Lumos 43 with an UV-LED (385 nm) showing in red the reaction mixture of oligomer **1** directly after the cleavage (retention time of 10.0 min for oligomer **1** with the liberated thiol as well as retention time of 12.0 min for its dimer due to a disulfide formation). Shown in black is chromatogram of the mixture after the incubation of the cleavage mixture of oligomer **1** in 2 equiv TCEP solution overnight.

Cleavage test in DMSO using the LUMOS 43 UV-LED (385 nm):

^{1}H NMR analysis prior to the cleavage in DMSO-d_6:
Observed signals for protons of amides in DMSO were not assigned. ^{1}H NMR (600 MHz, DMSO-d_6): δ 8.21 – 8.07 (m, 2H, Amide), 7.91 – 7.82 (m, 3H, Amide), 7.65 (s, 1H, 8), 7.26 (s, 1H, Amide), 7.16 (s, 1H, 9), 6.71 (s, 1H, Amide), 6.27 – 6.20 (m, 2H, 10), 4.48 – 4.41 (m, 1H, 5), 4.03 – 3.94 (m, 2H, 7+7'), 3.52 – 3.47 (m, 8H, 4), 3.43 – 3.36 (m, 8H, 3), 3.23 – 3.15 (m, 8H, 2), 2.70 (dd, J = 13.5, 6.0 Hz, 1H, 6 or 6'), 2.55 (dd, J = 13.5, 8.1 Hz, 1H, 6 or 6'), 2.32 – 2.25 (m, 8H, 1), 1.84 (s, 3H, 11) ppm.

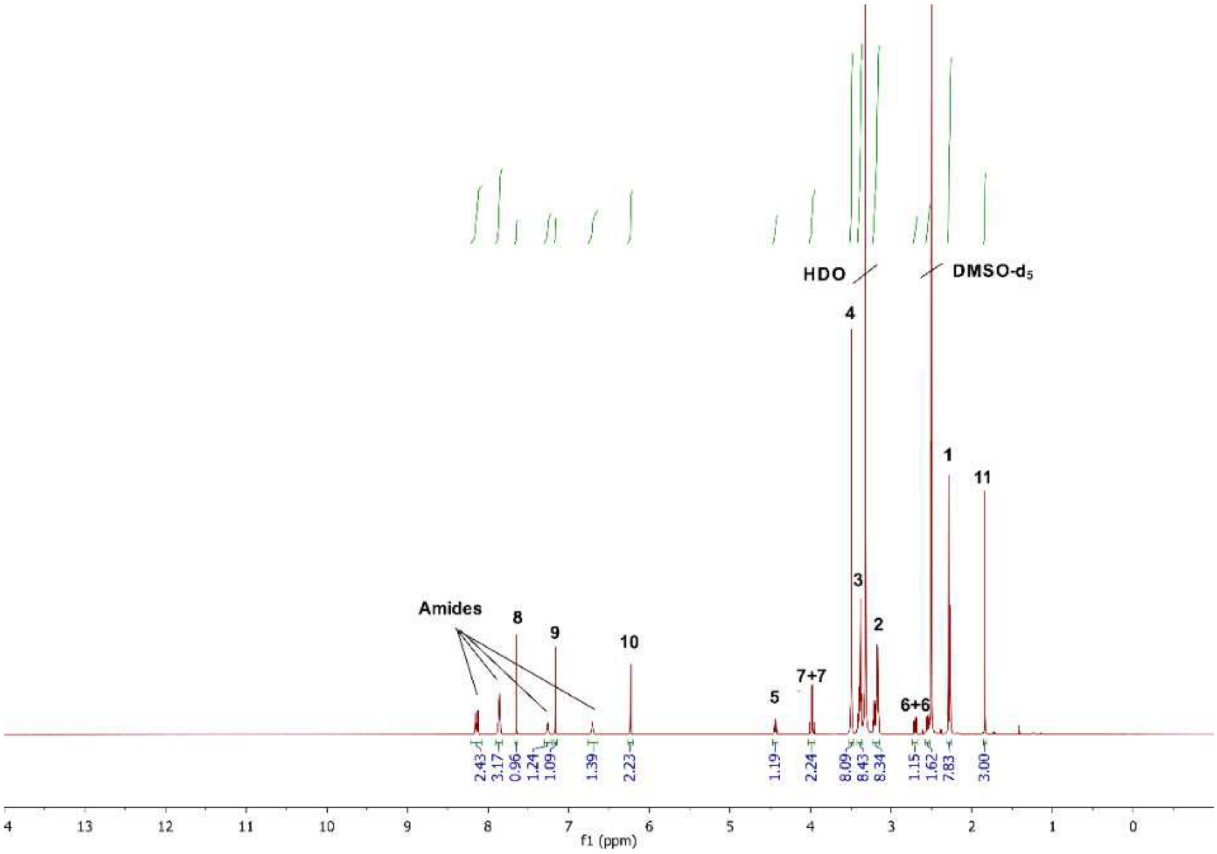

Figure S11: ^{1}H NMR (600 MHz, DMSO-d_6) of oligomer **1** prior to the MBNB cleavage test.

^{1}H NMR analysis after the cleavage in DMSO-d_6:
Signals with chemical shift between δ 7.5 and 5.5 ppm which were not assigned as amides are assumed to be nitroso cleavage products. ^{1}H NMR (600 MHz, D_2O): δ 8.24 – 8.01 (m, 2H, Amide), 7.92 – 7.81 (m, 3H, Amide), 7.26 (s, 1H, Amide), 6.71 (s, 1H, Amide), 4.54 – 4.42 (m, 1H, 5), 3.54 – 3.45 (m, 8H, 4), 3.43 – 3.35 (m, 8H, 3), 3.24 – 3.13 (m, 8H, 2), 3.05 (dd, *J* = 13.5, 5.3 Hz, 1H, 6 or 6'), 2.82 (dd, *J* = 13.4, 8.9 Hz, 1H, 6 or 6'), 2.35 – 2.22 (m, 8H, 1), 1.91 – 1.80 (m, 3H, 7) ppm.

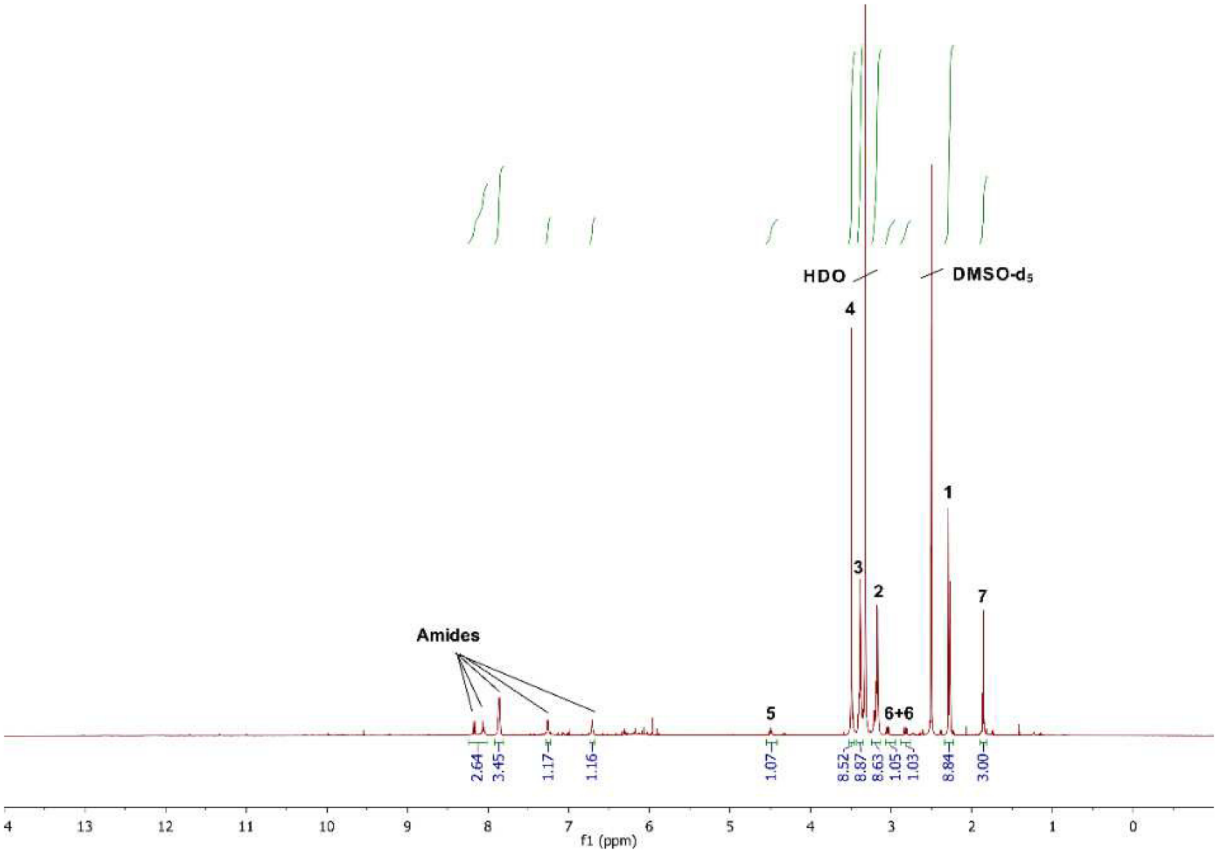

Figure S12: ^{1}H NMR (600 MHz, DMSO-d_6) of oligomer **1** after MBNB cleavage test in DMSO-d_6 using the Lumos 43 with an UV-LED (385 nm).

Cleavage test in D_2O using the medium pressure mercury UV lamp (365 nm):

Due to disulfide formation of the free thiol groups, multiple signals were observed, especially for the protons of the Cys moiety (5 and 6+6'). Signals with chemical shift between δ 7.5 and 5.5 ppm are assumed to be nitroso cleavage products. ^{1}H NMR (600 MHz, D_2O): δ 4.65 – 4.45 (m, 1H, 5), 3.71 – 3.58 (m, 16H), 3+4, 3.45 – 3.35 (m, 8H, 2), 3.23 – 2.93 (m, 2H, 6+6'), 2.60 – 2.50 (m, 8H, 1), 2.12 – 1.99 (m, 3H, 7) ppm.

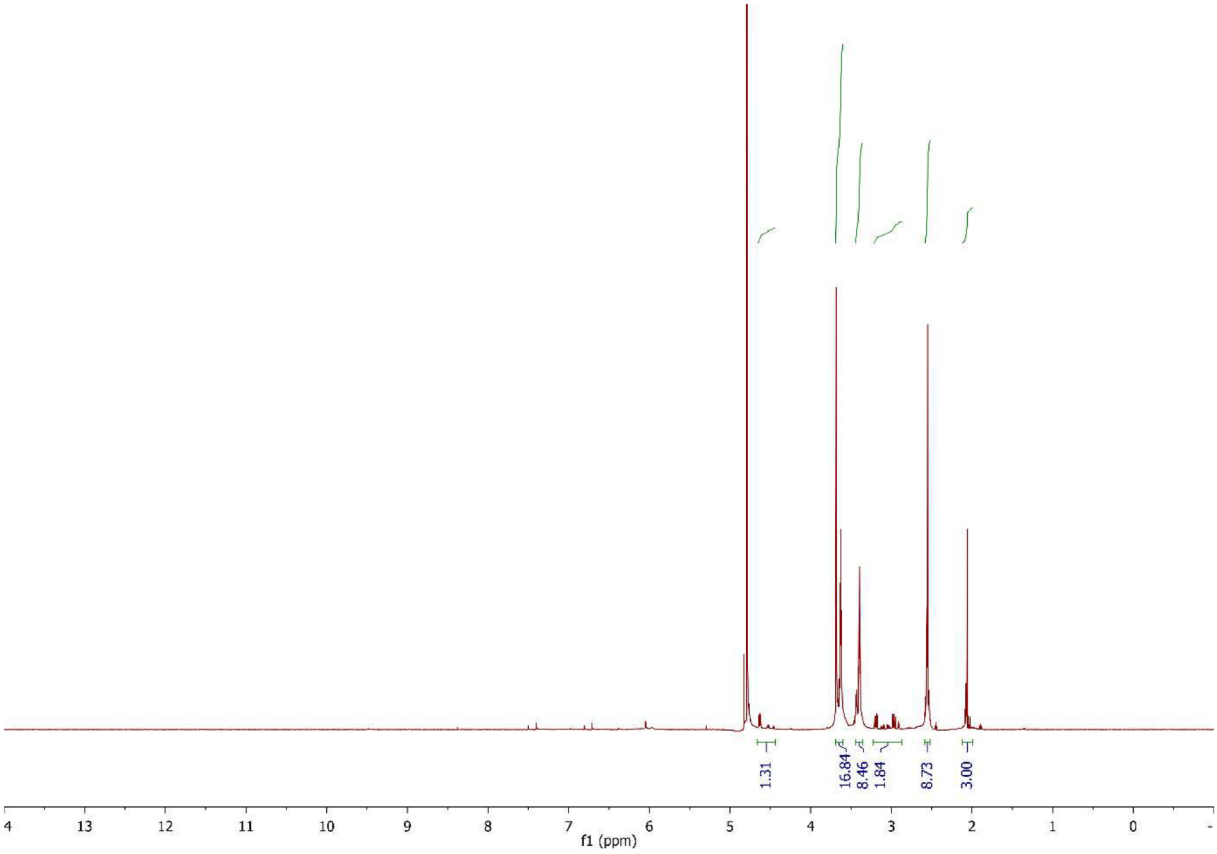

Figure S13: ^{1}H NMR (600 MHz, D_2O) of oligomer **1** after MBNB cleavage test in D_2O using the medium pressure mercury UV lamp (365 nm).

Poly(CG-EDS-LH-EDS-PS-EDS-KS-EDS-EDS-NDS) (Polymer 4):

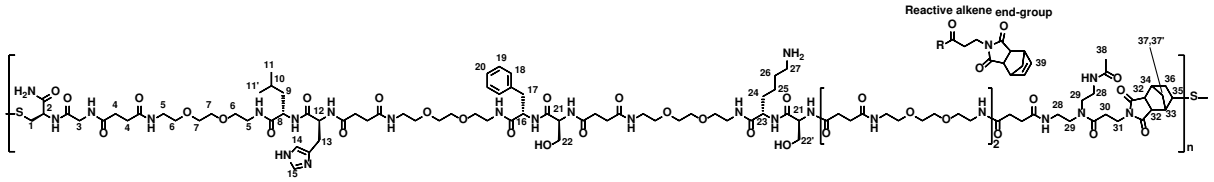

Isolated polymer directly after the polymerization:

Polymer **4** was obtained in a yield of 86% (22.2 mg). 25% of remaining reactive alkene end-group were determined. Signals with chemical shift of δ 8.07 – 7.99 (m), 7.98 – 7.91 (m) and 7.62 – 7.47 (m) ppm are assumed to be recombination products with DMPA radicals. Signals with chemical shift of δ 2.25 – 2.07 (m) were not able to be assigned. Stated amounts of protons correspond to one repeating unit of the polymer. ^{1}H NMR (600 MHz, D_2O): δ 8.63 (s, 1H, 15), 7.42 – 7.09 (m, 6H, 14+18+19+20), 6.13 (s, 1H, end-group, 39), 4.71 – 4.63 (m, 1H, 12), 4.61 – 4.54 (m, 1H, 16), 4.52 – 4.46 (m, 1H, 2), 4.44 – 4.36 (m, 2H, 21), 4.35 – 4.26 (m, 2H, 8+23), 4.03 – 3.92 (m, 2H, 22 or 22'), 3.92 – 3.81 (m, 2H, 3), 3.80 – 3.73 (m, 2H, 22 or 22'), 3.72 – 3.53 (m, 43H, 6+7+31+33), 3.52 – 3.24 (m, 30H, 5+28+29+32), 3.22 – 2.66 (m, 10H, 1+13+17+27+34+35), 2.65 – 2.43 (m, 26H, 4+30), 2.01 – 1.95 (m, 3H, 38), 1.93 – 1.25 (m, 12H, 9+10+24+25+26+36+37+37'), 0.99 – 0.88 (m, 3H, 11 or 11'), 0.88 – 0.77 (m, 3H, 11 or 11') ppm. The assignment of the signals was performed according to the structural similarities with compound **3** as well as the implementation of ^{1}H-^{1}H-COSY experiments (data not shown).

GPC-RI-LS: $\bar{M}_w$ 25.4 kDa, $\bar{M}_n$ 18.2 kDa, $\bar{M}_w/\bar{M}_n$ 1.5.

MALDI-TOF-MS in reflector mode in an *m/z* range from 1000 to 4000:
For remaining macromonomer **3** or its cyclic from $C_{110}H_{178}N_{26}O_{36}S$ (Monoisotopic mass 2471.3 g/mol)**:** [**3**+H]$^+$ calcd. 2472.3, found 2472.2; [**3**+Na]$^+$ calcd. 2494.3, found 2494.3; [**3**+K]$^+$ calcd. 2510.2, found 2510.3.

MALDI-TOF-MS in linear mode in an *m/z* range from 2000 to 20000 with exemplary assignments for remaining monomer **3** or its cyclic form, the dimer as well as trimer:
For remaining monomer **3** or its cyclic form $C_{110}H_{178}N_{26}O_{36}S$ (Monoisotopic mass 2471.3 g/mol): [**2**+Na]$^+$ calcd. 2494.3, found 2495.
For dimer **3-3** $C_{220}H_{356}N_{52}O_{72}S_2$ (Monoisotopic mass 4942.5 g/mol): [(**3-3**)+Na]$^+$ calcd. 4965.5, found 4972.
For trimer **3-3-3** $C_{330}H_{534}N_{78}O_{108}S_3$ (Monoisotopic mass 7413.8 g/mol): [(**3-3-3**)+Na]$^+$ calcd. 7436.8, found 7461.

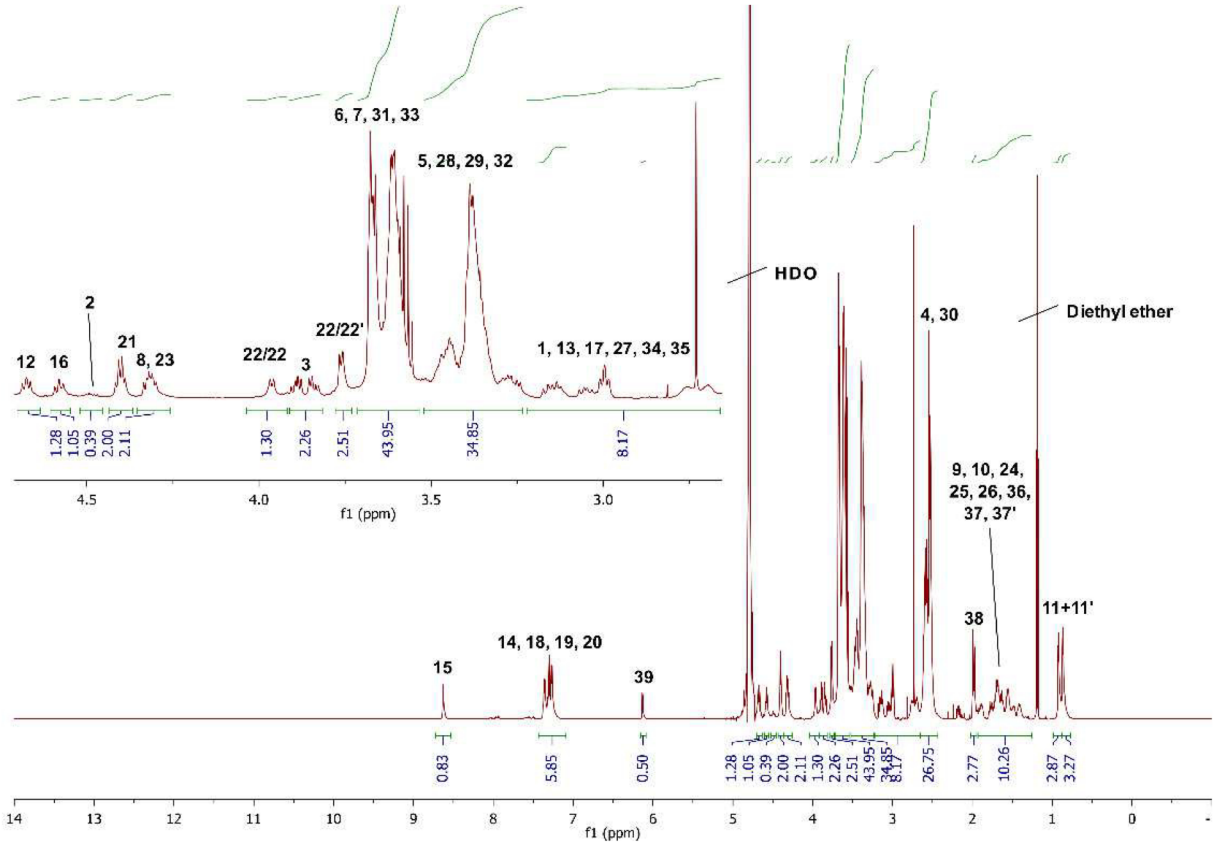

Figure S14: ^{1}H NMR (600 MHz, D_2O) of polymer **4** with an enlargement of the area from δ 2.8 to 4.7 ppm.

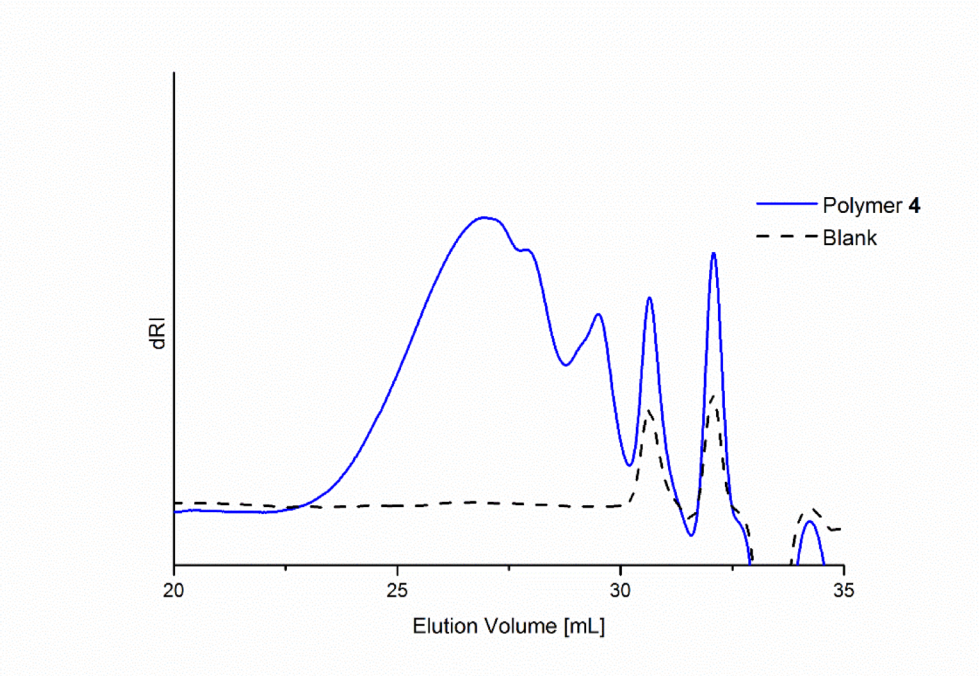

Figure S15: GPC-RI-LS of polymer **4**. Columns: Suprema Lux (2x 100 Å and 1000 Å). Buffer: 50 mM NaH_2PO_4, 150 mM NaCl, 250 ppm NaN_3 (pH 7.2), 30% ACN. Flow rate: 0.8 mL/min.

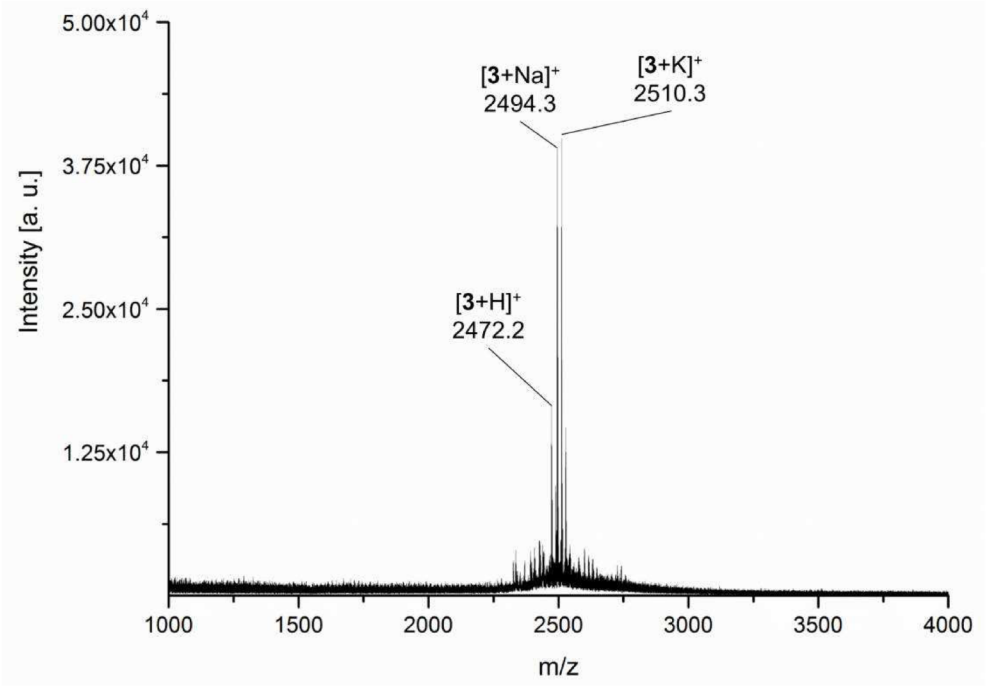

Figure S16: MALDI-TOF-MS of polymer **4** in reflector mode in an *m/z* range of 1000-4000 using DHB as matrix in a compound to matrix ratio of 1:10.

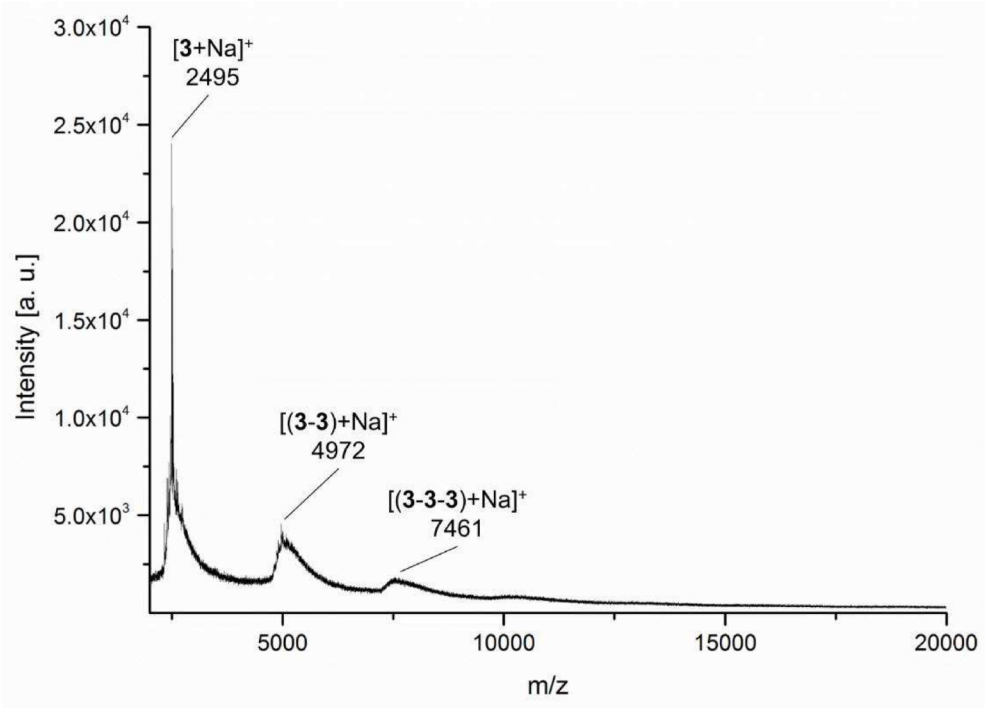

Figure S 17 MALDI-TOF-MS of polymer **4** in linear mode in an *m/z* range of 2000-20000 using DHB as matrix in a compound to matrix ratio of 1:10.

After the removal of low molecular weight compounds by ultrafiltration:

After its purification by ultrafiltration using a Vivaspin 20 centrifugal concentrators with a MWCO of 10 kDa, polymer **4** was obtained in a yield of 31% (9.08 mg). 20% of remaining reactive alkene end-group were determined. Signals with chemical shift of δ 7.89 – 7.85 (m), 7.58 – 7.53 (m) and 7.51 – 7.46 (m) ppm are assumed to be recombination products with DMPA radicals. Signals with chemical shift of δ 2.25 – 2.07 (m) were not able to be assigned. Stated amounts of protons correspond to one repeating unit of the polymer. ^{1}H NMR (600 MHz, D_2O): δ 8.14 – 7.84 (m, 1H, 15), 7.45 – 7.13 (m, 5H, 18+19+20), 7.06 (s, 1H, 14), 6.13 (s, end-group, 39), 4.63 – 4.54 (m, 2H, 12+16), 4.53 – 4.44 (m, 1H 2), 4.44 – 4.36 (m, 2H, 21), 4.35 – 4.22 (m, 2H, 8+23), 4.02 – 3.92 (m, 2H, 22 or 22'), 3.92 – 3.81 (m, 2H, 3), 3.78 – 3.73 (m, 2H, 22 or 22'), 3.71 – 3.50 (m, 43H, 6+7+31+33), 3.50 – 3.19 (m, 30H, 5+28+29+32), 3.18 – 2.66 (m, 10H, 1+13+17+27+34+35), 2.65 – 2.35 (m, 26H, 4+30), 2.04 – 1.96 (m, 3H, 38), 1.94 – 1.26 (m, 12H, 9+10+24+25+26+36+37+37'), 0.96 – 0.87 (m, 3H, 11 or 11'), 0.86 – 0.78 (m, 3H, 11 or 11') ppm.

GPC-RI-LS: $\bar{M}_w$ 35.6 kDa, $\bar{M}_n$ 23.8 kDa, $\bar{M}_w/\bar{M}_n$ 1.5.

MALDI-TOF analysis of the purified polymer **4** was not possible.

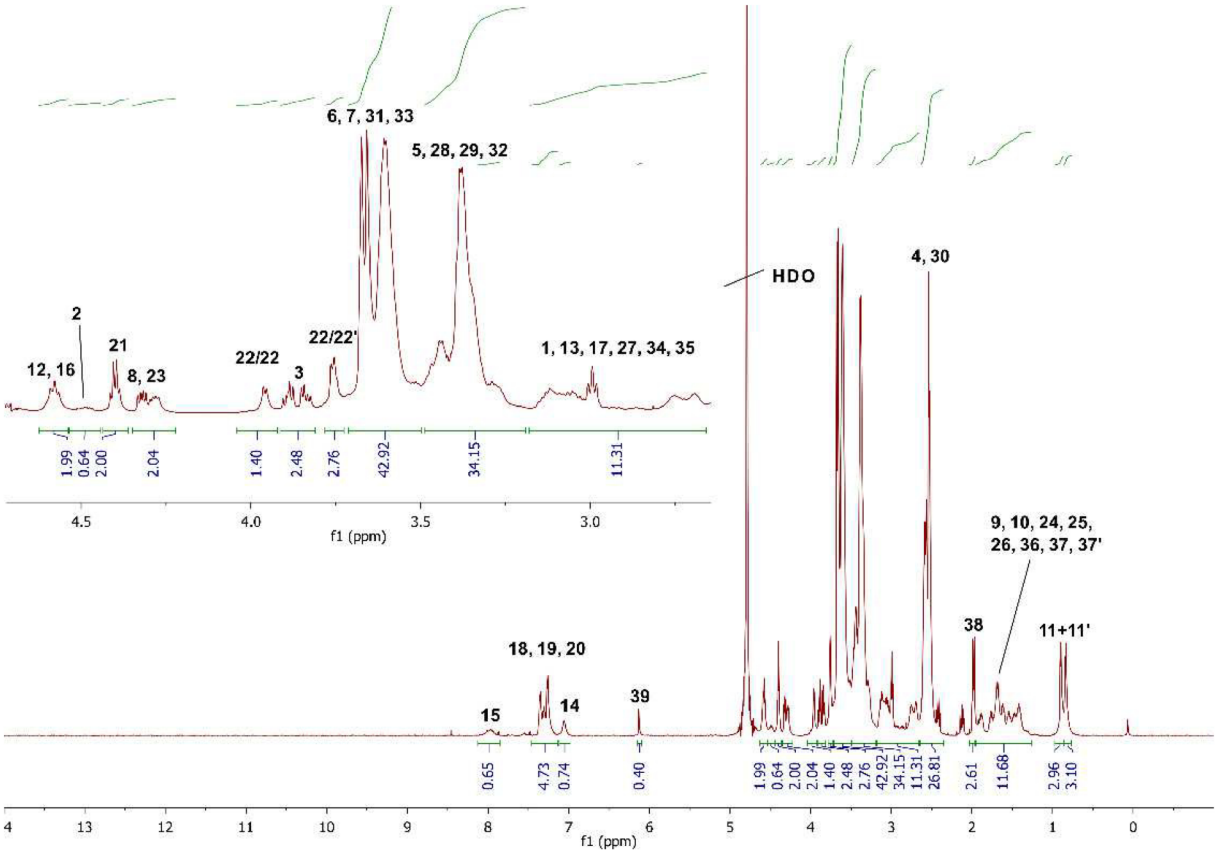

Figure S18: ^{1}H NMR (600 MHz, D_2O) of polymer **4** after ultrafiltration using a MWCO of 10 kDa with an enlargement of the area from δ 2.8 to 4.7 ppm.

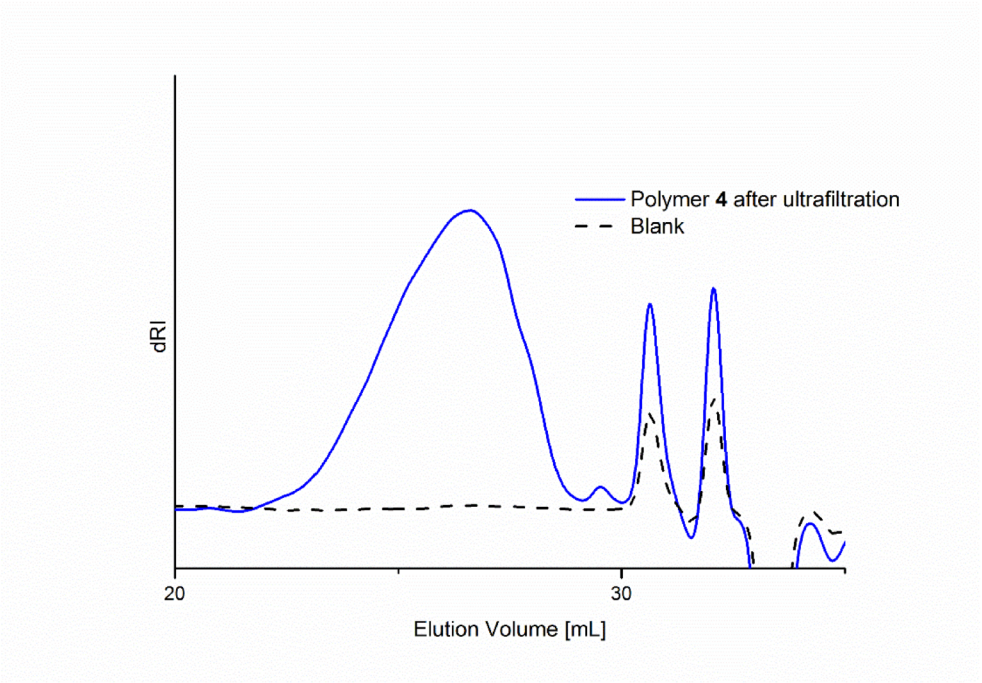

Figure S19: GPC-RI-LS of polymer **4** after ultrafiltration using a MWCO of 10 kDa. Columns: Suprema Lux (2x 100 Å and 1000 Å). Buffer: 50 mM NaH_2PO_4, 150 mM NaCl, 250 ppm NaN_3 (pH 7.2), 30% ACN. Flow rate: 0.8 mL/min.

References

[1] E. Hafizoglu, "Synthese und Charakterisierung von photochemisch aktiven Bichromophoren", 2014.
[2] F. Wojcik, A. G. O'Brien, S. Götze, P. H. Seeberger, L. Hartmann, *Chem. Eur. J.* **2013**, *19*, 3090.
[3] M. F. Ebbesen, C. Gerke, P. Hartwig, L. Hartmann, *Polym. Chem.* **2016**, *7*, 7086.
[4] C. Gerke, F. Jacobi, L. E. Goodwin, F. Pieper, S. Schmidt, L. Hartmann, *Macromolecules* **2018**, *51*, 5608.
[5] C. Gerke, M. F. Ebbesen, D. Jansen, S. Boden, T. Freichel, L. Hartmann, *Biomacromolecules* **2017**, *18*, 787.
[6] S. Roux, E. Zékri, B. Rousseau, M. Paternostre, J.-C. Cintrat, N. Fay, *Journal of Peptide Science* **2008**, *14*, 354.

6 Appendix

6.1 List of abbreviations

General abbreviations

Abbreviation	*Definition*
calcd.	Calculated
CRD	carbohydrate recognition domain
DNA	deoxyribonucleic acid
e.g.	exempli gratia (for example)
et al.	et alteri (and others)
LBB	lectin binding buffer
MAH	molecule-assisted homolysis
MWCO	molecular weight cut off
RNA	ribonucleic acid
rpm	rounds per minute
RT	room temperature
RU	response unit
UV	ultraviolet
UV-LED	ultraviolet light emitting diode
vs.	versus

Chemicals

Abbreviation	*Trivial or IUPAC name*
ACN	acetonitrile
Alloc	allyloxycarbonyl
BOP	benzotriazol-1-yl-oxy-tris-(dimethylamino)-phosphonium hexafluorophosphate
Ca^{2+}	divalent calcium cation
$CaCl_2$	calcium chloride
$CDCl_3$	deuterated chloroform
Con A	Concanavalin A
Cu	copper
$CuSO_4$	copper sulfate
D_2O	deuterium oxide
DABCO	1,4-diazabicyclo[2.2.2]octane
DCC	*N,N'*-dicyclohexylcarbodiimide
DCM	dichloromethane
DHB	2,5-dihydroxybenzoic acid
DIC	*N,N'*-diisopropylcarbodiimide
DIEA	*N,N*-diisopropylethylamine
DMF	dimethylformamide
DMPA	2,2-dimethoxy-2-phenylacetophenone
DMSO	dimethyl sulfoxide
DMSO-d_6	deuterated dimethyl sulfoxide
DMT	dimethoxytrityl
DVB	divinylbenzene
EDC	1-ethyl-3-(3- dimethylaminopropyl)carbodiimide
EtOAc	ethyl acetate
EtOTFA	ethyl trifluoroacetate
Fmoc	fluorenylmethyloxycarbonyl
FmocCl	fluorenylmethyloxycarbonyl chloride
Fmoc-L-Cys(Trt)-OH	*N*-α-(9-fluorenylmethyloxycarboxyl)-*S*-trityl-L-cysteine
Fmoc-L-Gly-OH	*N*-α-(9-fluorenylmethyloxycarbonyl)-L-glycine

Fmoc-L-His(Boc)-OH*CHA	*N*-α-(9-fluorenylmethyloxycarbonyl)-*N*-im-(t-butyloxycarbonyl)-L-histidine cyclohexylamine
Fmoc-L-Leu-OH	*N*-α-(9-fluorenylmethyloxycarbonyl)-L-leucine
Fmoc-L-Lys(Boc)-OH	*N*-α-(9-fluorenylmethyloxycarbonyl)-*N*-ε-t-butyloxycarbonyl-L-lysine
Fmoc-L-Phe-OH	*N*-α-(9-fluorenylmethyloxycarbonyl)-L-phenylalanine
Fmoc-L-Ser(tBu)-OH	*N*-α-(9-fluorenylmethyloxycarbonyl)-*O*-t-butyl-L-serine
H_2O	water
HEPES	4-(2-hydroxyethyl)-1-piperazineethanesulfonic acid
HF	hydrofluoric acid
Hg	mercury
HOBt	hydroxybenzotriazole
$^{i}Pr_3SiH$	triisopropyl silane
K_2CO_3	potassium carbonate
MBNB	3,4-methylenebisoxy-6-nitrobenzyl
MeOH	methanol
Mn^{2+}	divalent manganese cation
$MnCl_2$	manganese(II) chloride
Na_2SO_4	sodium sulfate
NaCl	sodium chloride
NaH_2PO_4	sodium dihydrogen phosphate
$NaHCO_3$	sodium hydrogen carbonate
NaN_3	sodium azide
NEM	*N*-ethylmaleimide
NEt_3	triethylamine
NHS	*N*-hydroxysuccinimide
PEG	poly(ethylene glycol)
$PEG(SH)_2$	dithiol-poly(ethylene glycol)
$PEG(SH)_2$-6000	dithiol-poly(ethylene glycol) with a $\bar{M}_n$ of 6000 Da
PEG-100000	poly(ethylene glycol) with a $\bar{M}_n$ of 100000 Da
PyBOP	benzotriazol-1-yl-oxy-tris-(pyrrolidino)-phosphonium hexafluorophosphate
t-Boc / Boc	*tert*-butyloxycarbonyl
tBu	*tert*-butyl
TCEP	tris(2-carboxyethyl)phosphine hydrochloride
TEA	triethylamine
TFA	trifluoroacetic acid
THF	tetrahydrofuran
TIPS	triisopropylsilane
Trt	trityl
TrtCl	trityl chloride
WGA	wheat germ agglutinin

Building blocks

Abbreviation	*Definition*
ADS	Alloc – Diethylenetriamine – Succinic acid
BADS	Benzyl Azide – Diethylenetriamine – Succinic acid
BDS	Boc – Diethylenetriamine – Succinic acid
DDS	Double bond − Diethylenetriamine − Succinic acid
EDS	Ethylene glycol – Diamine – Succinic acid
MDS	Methyl succinyl – Diethylenetriamine − Succinic acid
NDS	Norbornene – Diethylenetriamine − Succinic acid
ODS	Octyl – Diamine – Succinic acid
SDS	Short – Diamine – Succinic acid
TDS	Triple bond − Diethylenetriamine − Succinic acid

Monosaccharides

Abbreviation	*Trivial name*
αMeMan	methyl-α-D-mannopyranoside
Fuc	α-L-fucose
Gal	D-galactose
Gal*N*Ac	D-*N*-acetylgalactosamine
Glc	α-D-glucopyranoside / D-glucose
GlcA	D-glucuronic acid
Glc*N*Ac	*N*-acetylglucosamine
IdoA	α-L-iduronic acid
Man	α-D-mannopyranoside / D-mannose
Neu5Ac	*N*-acetylneuraminic acid
Xyl	D-xylose

Amino acids

One letter code / Three letter code	*Trivial name*
C / Cys	L-cysteine
F / Phe	L-phenylalanine
G / Gly	L-glycine
H / His	L-histidine
K / Lys	L-lysine
L / Leu	L-leucine
P / Pro	L-proline
S / Ser	L-serine

Methods and instruments

Abbreviation	*Definition*
^{13}C	carbon wit 13 atomic mass units
^{1}H	hydrogen with 1 atomic mass unit
ATRP	atom transfer radical polymerization
COSY	correlation spectroscopy
CRP	controlled radical polymerization
CuAAC	copper (I) mediated azide-alkyne cycloaddition
ESI	electrospray ionization
ESI^+	electrospray ionization in positive operating mode
FC	fraction collector
GPC-RI-LS	gel permeation chromatography – refractive index –light scattering
HPLC	high pressure liquid chromatography
HR-ESI-MS	high resolution – electrospray ionization – mass spectrometry
IEG	iterative exponential growth
ITC	isothermal titration calorimetry
JKR	Johnson−Kendall−Roberts model
LC-MS / LC/MS	liquid chromatography – mass spectrometry
MALDI-TOF	matrix-assisted laser desorption ionization – time of flight
NMP	nitroxide mediated polymerization
NMR	nuclear magnetic resonance
Q-TOF	quadrupole – time of flight
RAFT	reversible addition-fragmentation chain transfer
RICM	reflection interference contrast microscopy
ROMP	ring opening metathesis polymerization
ROP	ring opening polymerization
RP-HPLC	reverse phase – high pressure liquid chromatography
SCP	soft colloidal probe

SCP-RICM	soft colloidal probe − reflection interference contrast microscopy
SFRP	stable free radical polymerization
SM-AFM	single molecule atomic force microscopy
SPPS	solid phase peptide synthesis
SPR	surface plasmon resonance
SPS	solid phase synthesis
TEC	thiol-ene click / thiol-ene coupling
UHR-MS	ultra high resolution – mass spectrometry
VWD	variable wavelength detector

Measurement parameters, units and symbols

Abbreviation	*Definition*
%	percent
°C	degrees Celsius
µJ/m^2	microjoule per square meter
µL	microliter
µL/min	microliter per minute
µM	micromolar (micromole per liter)
µm	micrometer
µmol	micromole
1/(conc. ½T_{Max})	reciprocal value of conc. ½T_{Max}
Å	ångström (10^{-10} meter)
a. u.	arbitrary unit
cm	centimeter
conc. ½T_{Max}	concentration required for reaching the half-maximal turbidity
d	doublet
Da	dalton
dd	doublet of doublets
*d*n/*d*c	refractive index increment
*d*RI	refractive index change
dt	doublet of triplets
equiv /eq	equivalent
ε	molar attenuation coefficient
g	gram
h	hour
Hz	hertz
IC_{50}	half maximum inhibitory concentration
J	coupling constant
K_A	binding constants
K_D	dissociation constant
k_{CT}	chain transfer rate constant
k_i	rate of precipitation
k_{off}	dissociation rate constants
k_{on}	association rate constants
k_p	propagation rate constant
kDa	kilodalton
L/(mol·cm)	liter per mole centimeter
M	molar (mole per liter)
m	multiplet
m/z	mass per charge ratio
mAu	milliabsorption units
mbar	millibar
mg	milligram
mg/mL	milligram per milliliter
MHz	megahertz

min	minute
mL	milliliter
mL/g	milliliter per gram
mL/min	milliliter per minute
mm	millimeter
mM	millimolar (millimole per liter)
mmol	millimole
mmol/g	millimole per gram
$\bar{M}_n$	number average molecular weight
mol%	mole percent
MW	Molecular weight
mW	milliwatt
$\bar{M}_w$	mass average molecular weight
$\bar{M}_w/\bar{M}_n$	molecular weight distribution
MΩcm	megaohm centimeter
N	normality / equivalent concentration
N (Man)	number of α-D-mannopyranoside moieties
n.b.	no binding
n.d.	not determined
n.m.	not measured
n.p.	no precipitation
nm	nanometer
Ø	average
pg	picogram
ppm	parts per million
R_h	hydrodynamic radius
R_g	radius of gyration
R_{max}	maximal response
$R_{max}/2$	half maximal response
s (NMR)	singlet
s (time unit)	second
t	triplet
$t_{½}$	time needed reaching half maximal precipitation
t_R	retention time
vol%	volume percent
$\bar{X}_n$	degree of polymerization
δ	chemical shift
ΔG	Gibbs free energy change
ΔH	molar enthalpy change
ΔS	entropy change

6.2 List of figures

6.3 List of schemes

7 Acknowledgments

First, I would like to express my special thanks and appreciation to Prof. Dr. Laura Hartmann for giving me the opportunity to obtain my Ph.D. degree in her working group at the Heinrich-Heine-University Düsseldorf. Besides that, I would also like to thank her for the interesting project, the opportunity to attend scientific conferences and her countless great ideas, fruitful discussions, advice and especially motivation throughout the time working on the project. I wish her all the best for her future research and hope for many more successful Ph.D. students in her working group to come.

I would also like to thank Priv.-Doz. Dr. Klaus Schaper for his interesting inputs in this project thereby pushing forwards the research and for agreeing to be the second supervisor of this thesis.

Furthermore, I would like to thank Jun.-Prof. Dr. Stephan Schmidt gratefully for always taking time to discuss scientific issues and perform measurements as well as for his help during data evaluation and his numerous corrections of manuscripts.

I also want to thank the whole staff of the working group, particularly senior scientist Dr. Monir Tabatabai for her corrections of all experimental parts but especially for her open ear and great support at all hours as well as lab technician Stephanie Scheelen and secretaries Michaela Kitza and Viola Schürmanns for their continuous help providing me with anything needed in lab and office, for their help with organizational issues and for their loving personalities. Furthermore, I thank Maria Breuer for performing NMR as well as Dr. Peter Tommes and Ralf Bürgel for performing HRMS and MALDI-TOF measurements.

I want to express my special thanks to Dr. Morten Frendø Ebbesen, from whom I have learned so much in the first months. Without him and his help, I wouldn't have got started with the project in the same way. Besides that, I want to thank him for the great times in and outside the lab and for becoming such a good friend!

I truly appreciate the hard work, sweat and long evenings in the lab of all my undergraduate and graduate students that helped in this project and therefore gratefully thank Alexander Banger, Leon Cappel, Dennis Jansen, Laura Goodwin, Franziska Pieper, Julia Becker and Theresa Seiler for their scientific contributions and fun in the lab.

I want to thank all my lab partners during the last years, Dr. Sinaida Igde, Markus Giesler, Tanja Paul, Peter Pasch and Sophia Boden. Thank you all for the great memories with a lot of laughter, joy and long talks, also outside the lab. My special thanks are for Sophia who accompanied me for almost the whole time in the same lab and was the best lab partner someone can ask for. Also, thank you for the great scientific inputs, help with corrections, SPR measurements and much more. Besides that, I want to especially thank Peter for becoming such a good friend also outside the lab and the great times together.

I thank all former and current group members of the Hartmann Group for being the best group one can imagine. Thanks to Dr. Hanqing Wang, Alberto Camaleño de la Calle, Dana Itskalov, Mischa Baier, Fawad Jacobi, Alexander Strzelczyk, Florian Malotke, Tanja Freichel, Katharina Bücher, Sebastian Bauer, Tanja Freichel, Lukas Fischer, Philipp Reuther, Dr. Stephen Hill, Kira Neuhaus, Özgür Capar, Serap Üclü, Hendrik Wöhlk, Florian Trilling, Lars Krüger, Fadi Shamout, Josip Stipanovic, Patrick Konietzny, Miriam Hoffmann and Genescha Olgar. I am thankful that I got to know each and every one of you and that I was able to be part of the group. I will never forget the great memories from barbecue nights, team events, Christmas and summer parties and especially the “class trips”. Special thanks to Dana, Philipp, Alex, Alberto, Özgür and Stephen for their help correcting manuscripts and the thesis, Lukas with his help during the GPC measurements and Tanja and Markus during the SPR measurements. Furthermore, I would like to especially thank my office partner Mischa for the great support, long discussion in the office and help throughout the last years. I will never forget our trip together with Fawad to the ACS meeting. Thanks for the great memories to the both of you.

Finally, but most importantly, I would like to express my deepest gratitude to my family, especially my parents Annette and Christian as well as Carsten and Christina, my brothers Peter and Claudius and my girlfriend and best friend Elena! Thanks for being great listeners, motivators and for giving me strength but especially for letting me choose my own way and supporting me with everything that goes with it.